

# CURRENT ANALYTICAL TRENDS IN DRUG TESTING IN CLINICAL AND FORENSIC TOXICOLOGY

EDITED BY: Eugenia Gallardo, Mário Barroso, Marta Concheiro-Guisan  
and Ana de-Castro-Ríos

PUBLISHED IN: Frontiers in Chemistry





# frontiers

## Frontiers eBook Copyright Statement

The copyright in the text of individual articles in this eBook is the property of their respective authors or their respective institutions or funders. The copyright in graphics and images within each article may be subject to copyright of other parties. In both cases this is subject to a license granted to Frontiers.

The compilation of articles constituting this eBook is the property of Frontiers.

Each article within this eBook, and the eBook itself, are published under the most recent version of the Creative Commons CC-BY licence.

The version current at the date of publication of this eBook is CC-BY 4.0. If the CC-BY licence is updated, the licence granted by Frontiers is automatically updated to the new version.

When exercising any right under the CC-BY licence, Frontiers must be attributed as the original publisher of the article or eBook, as applicable.

Authors have the responsibility of ensuring that any graphics or other materials which are the property of others may be included in the CC-BY licence, but this should be checked before relying on the CC-BY licence to reproduce those materials. Any copyright notices relating to those materials must be complied with.

Copyright and source acknowledgement notices may not be removed and must be displayed in any copy, derivative work or partial copy which includes the elements in question.

All copyright, and all rights therein, are protected by national and international copyright laws. The above represents a summary only. For further information please read Frontiers' Conditions for Website Use and Copyright Statement, and the applicable CC-BY licence.

ISSN 1664-8714

ISBN 978-2-88966-894-6

DOI 10.3389/978-2-88966-894-6

## About Frontiers

Frontiers is more than just an open-access publisher of scholarly articles: it is a pioneering approach to the world of academia, radically improving the way scholarly research is managed. The grand vision of Frontiers is a world where all people have an equal opportunity to seek, share and generate knowledge. Frontiers provides immediate and permanent online open access to all its publications, but this alone is not enough to realize our grand goals.

## Frontiers Journal Series

The Frontiers Journal Series is a multi-tier and interdisciplinary set of open-access, online journals, promising a paradigm shift from the current review, selection and dissemination processes in academic publishing. All Frontiers journals are driven by researchers for researchers; therefore, they constitute a service to the scholarly community. At the same time, the Frontiers Journal Series operates on a revolutionary invention, the tiered publishing system, initially addressing specific communities of scholars, and gradually climbing up to broader public understanding, thus serving the interests of the lay society, too.

## Dedication to Quality

Each Frontiers article is a landmark of the highest quality, thanks to genuinely collaborative interactions between authors and review editors, who include some of the world's best academicians. Research must be certified by peers before entering a stream of knowledge that may eventually reach the public - and shape society; therefore, Frontiers only applies the most rigorous and unbiased reviews. Frontiers revolutionizes research publishing by freely delivering the most outstanding research, evaluated with no bias from both the academic and social point of view. By applying the most advanced information technologies, Frontiers is catapulting scholarly publishing into a new generation.

## What are Frontiers Research Topics?

Frontiers Research Topics are very popular trademarks of the Frontiers Journals Series: they are collections of at least ten articles, all centered on a particular subject. With their unique mix of varied contributions from Original Research to Review Articles, Frontiers Research Topics unify the most influential researchers, the latest key findings and historical advances in a hot research area! Find out more on how to host your own Frontiers Research Topic or contribute to one as an author by contacting the Frontiers Editorial Office: [frontiersin.org/about/contact](https://frontiersin.org/about/contact)

# CURRENT ANALYTICAL TRENDS IN DRUG TESTING IN CLINICAL AND FORENSIC TOXICOLOGY

Topic Editors:

**Eugenia Gallardo**, Universidade da Beira Interior, Portugal

**Mário Barroso**, Portuguese National Institute of Legal Medicine and Forensic Sciences, Portugal

**Marta Concheiro-Guisan**, John Jay College of Criminal Justice, United States

**Ana de-Castro-Ríos**, University of Santiago de Compostela, Spain

**Citation:** Gallardo, E., Barroso, M., Concheiro-Guisan, M., de-Castro-Ríos, A., eds. (2021). Current Analytical Trends in Drug Testing in Clinical and Forensic Toxicology. Lausanne: Frontiers Media SA. doi: 10.3389/978-2-88966-894-6

# Table of Contents

- 04 Editorial: Current Analytical Trends in Drug Testing in Clinical and Forensic Toxicology**  
Eugenia Gallardo, Mário Barroso, Marta Concheiro-Guisan and Ana de-Castro-Ríos
- 07 Can X-Ray Powder Diffraction Be a Suitable Forensic Method for Illicit Drug Identification?**  
Bronislav Jurásek, Vilém Bartůňek, Štěpán Huber, Patrik Fagan, Vladimír Setnička, František Králík, Wim Dehaen, Daniel Svozil and Martin Kuchař
- 17 High-Throughput Qualitative and Quantitative Drug Checking by MALDI HRMS**  
Timothée Joye, Christèle Widmer, Roxane Morger Mégevand, Serge Longère, Marc Augsburg and Aurélien Thomas
- 26 Driving Under the Influence of Drugs: A Single Parallel Monitoring-Based Quantification Approach on Whole Blood**  
Timothée Joye, Katell Rocher, Julien Déglon, Jonathan Sidibé, Bernard Favrat, Marc Augsburg and Aurélien Thomas
- 36 Fast Hollow Fiber Liquid-Phase Microextraction as a Greener Alternative for the Determination of N,N-Dimethyltryptamine and Harmala Alkaloids in Human Urine**  
Gabriela de Oliveira Silveira, Felipe Rebello Lourenço, Vitor Bruno and Mauricio Yonamine
- 49 Extended Stability Evaluation of Selected Cathinones**  
Heather L. Ciallella, Lexus R. Rutter, Lorna A. Nisbet and Karen S. Scott
- 60 Detection of a New Tert-Leucinate Synthetic Cannabinoid 5F-MDMB-PICA and Its Metabolites in Human Hair: Application to Authentic Cases**  
Yan Shi, Liying Zhou, Le Li, Mengxi Liu, Huosheng Qiang, Min Shen, Baohua Shen, Hang Chen, Olaf H. Drummer, Wanhui Liu, Hejian Wu and Ping Xiang
- 71 Metabolic Profile of Four Selected Cathinones in Microsome Incubations: Identification of Phase I and II Metabolites by Liquid Chromatography High Resolution Mass Spectrometry**  
Beatriz T. Lopes, Maria João Caldeira, Helena Gaspar and Alexandra M. M. Antunes
- 84 Challenges and Strategies of Chemical Analysis of Drugs of Abuse and Explosives by Mass Spectrometry**  
Ahsan Habib, Lei Bi, Huanhuan Hong and Luhong Wen
- 115 Analytical Characterization of 3-MeO-PCP and 3-MMC in Seized Products and Biosamples: The Role of LC-HRAM-Orbitrap-MS and Solid Deposition GC-FTIR**  
Giampietro Frison, Flavio ancanaro, Samuela Frasson, Laura Quadretti, Michele Agnati, Francesca Vlassich, Giuseppe Gagliardi, Tania Maria Grazia Salerno, Paola Donato and Luigi Mondello
- 131 Evaluation of Illicit Drug Consumption by Wastewater Analysis Using Polar Organic Chemical Integrative Sampler as a Monitoring Tool**  
Roberta Zilles Hahn, Carlos Augusto do Nascimento and Rafael Linden





# Editorial: Current Analytical Trends in Drug Testing in Clinical and Forensic Toxicology

Eugenia Gallardo<sup>1\*</sup>, Mário Barroso<sup>2\*</sup>, Marta Concheiro-Guisan<sup>3\*</sup> and Ana de-Castro-Ríos<sup>4\*</sup>

<sup>1</sup> Health Sciences Research Center, Faculty of Health Sciences, University of Beira Interior, Covilhã, Portugal, <sup>2</sup> Instituto Nacional de Medicina Legal e Ciências Forenses (INMLCF), Lisbon, Portugal, <sup>3</sup> John Jay College of Criminal Justice, New York, NY, United States, <sup>4</sup> Institute of Forensic Sciences "Luis Concheiro", University of Santiago de Compostela, Santiago de Compostela, Spain

**Keywords:** drugs of abuse, chromatographic techniques, drug testing, clinical and forensic toxicology, trends in bioanalysis, novel analytical approaches, new psychoactive substance

## OPEN ACCESS

### Edited and reviewed by:

Huangxian Ju,  
Nanjing University, China

### \*Correspondence:

Eugenia Gallardo  
egallardo@fcsaude.ubi.pt  
Mário Barroso  
mario.j.barroso@inmlcf.mj.pt  
Marta Concheiro-Guisan  
mconcheiro-guisan@jjay.cuny.edu  
Ana de-Castro-Ríos  
ana.decastro@usc.es

### Specialty section:

This article was submitted to  
Analytical Chemistry,  
a section of the journal  
Frontiers in Chemistry

**Received:** 27 February 2021

**Accepted:** 14 April 2021

**Published:** 07 May 2021

### Citation:

Gallardo E, Barroso M,  
Concheiro-Guisan M and  
de-Castro-Ríos A (2021) Editorial:  
Current Analytical Trends in Drug  
Testing in Clinical and Forensic  
Toxicology. *Front. Chem.* 9:673397.  
doi: 10.3389/fchem.2021.673397

## Editorial on the Research Topic

### Current Analytical Trends in Drug Testing in Clinical and Forensic Toxicology

The articles included in this collection cover novel analytical approaches, including chromatographic and spectrometric methods, and sample preparation techniques for the investigation and analysis of several classes of compounds. These compounds include novel psychoactive substances (NPS) as well as other drugs and substances within the scope of clinical and forensic toxicology, and other fields, such as doping control.

Current trends in bioanalysis require the constant development of novel analytical tools, which includes efficient sample collection procedures and adequate sample preparation protocols in order to maximize compound detection, even at trace levels. Taking into account that the number of substances possibly present in a sample are increasing, efficient multi-analyte methods are usually necessary. The detection of NPS, including synthetic cathinones and synthetic cannabinoids, is becoming more and more important as several reports of acute intoxications and deaths are often being issued. Therefore, developing new analytical methods and strategies help scientists efficiently face those challenges, allowing laboratories to be one-step ahead.

In this topic collection, four publications focus on the investigation of different critical aspects of NPS. These studies provide new tools for the identification of new NPS derivatives and metabolites (Frison et al.; Lopes et al.), investigate the stability of synthetic cathinones in biological samples and storage solvents (Ciallella et al.) or explore the detectability of synthetic cannabinoids in hair samples (Shi et al.). Frison et al. described the analytical characterization, following two non-fatal intoxication cases, of 3-methylmethcathinone (3-MMC) and 3-methoxyphencyclidine (3-MeO-PCP) in seized products, and the investigation of 3-MeO-PCP and metabolites in biological samples. Three different analytical approaches were employed to identify 3-MMC and 3-MeO-PCP in seized materials, including gas chromatography-mass spectrometry (GC-MS) with electron impact ionization, liquid chromatography-high-resolution accurate-mass Orbitrap

mass spectrometry (LC-HRAM-Orbitrap-MS), and solid deposition gas chromatography-Fourier transform infrared spectroscopy (sd-GC-FTIR). The role of the two latter techniques in attaining full structural characterization of the psychoactive drugs and related metabolites, in both non-biological and biological samples, was highlighted. The novelty of Frison et al. work lies in this aspect of the employment of LC-HRAM-Orbitrap-MS and sd-GC-FTIR instrumentation to identify and characterize new psychoactive substances in the absence of reference standards in different types of samples. Lopes et al. also employed high resolution mass spectrometry (HRMS) for the identification of new metabolites of synthetic cathinones. In particular, they identified the phase I and II metabolites of 4'-methyl-N,N-dimethylcathinone (4-MDMC), 4'-methyl-N,N-diethylcathinone (4-MDEC), 4'-chloro- $\alpha$ -pyrrolidinovalerophenone (4Cl-PVP) and 4'-chloroethylcathinone (4-CEC). The metabolites herein identified are expected to play an important role not only because they act as potential selective biomarkers of the intake of the studied synthetic cathinones, but also because their potential adverse effects may be better understood. In addition, those causative agents may be linked to toxicities, thereby helping understanding and treating non-fatal intoxications. This study highlights the critical role of high resolution mass spectrometry in the investigation of the toxicity of NPS. Ciallella et al. studied the stability of four Schedule I synthetic cathinones, namely mephedrone, naphyrone, MDPV, and  $\alpha$ -PVP. Indeed, stability is a critical parameter for toxicology laboratories. Understanding the variability in the analyte concentrations due to stability issues has an impact in the subsequent interpretation of concentration data derived from biological sample analysis. In this research, Ciallella et al. were able to analyze these cathinone derivatives employing solid phase extraction of blood and urine samples, and analyzing the compounds by GC-MS. The results of this study provided a comprehensive overview of the stability of these compounds in biological matrices over an extended period, including the evaluation of an alternative preservative and the inclusion of solvent-based working solutions. Shi et al. developed and validated a novel target analytical method for the determination of the synthetic cannabinoid 5F-MDMB-PICA and five metabolites in hair samples by liquid chromatography-tandem mass spectrometry (LC-MSMS). This new synthetic cannabinoid has been used in the form of "spice-like" herbal incenses or in electronic cigarette oil, and this study provides critical data for the interpretation of hair testing for this type of substances. The sensitivity of LC-MSMS allowed the authors of this study to achieve limits of detection at low pg/mg level in hair.

This topic collection also covers new challenges and strategies of analytical methods. Jurásek et al. investigated the potential of X-ray powder diffraction (XRPD) for rapid and simple identification of drugs of abuse in seized material. In this work, the authors proved that XRPD could be used to unambiguously identify 7 selected psychoactive substances (including 5 NPS) in different street sample mixtures, and proposed this technique as a complement to Infrared and Raman spectroscopies, the most common techniques used for this purpose, when unequivocal

drug identification with these techniques is hindered by drug or additives native fluorescence or matrix complexity. Joye, Widmer et al. used matrix-assisted laser desorption/ionization (MALDI) high-resolution mass spectrometric (HRMS) technologies, which have been used to analyze the samples seized in the black market. The authors highlight the potential of MALDI-HRMS as high-throughput analytical strategy in toxicology laboratories, which significantly accelerates the detection and quantification of several drugs of abuse. The developed approach showed qualitative and quantitative results comparable to those obtained using LC-MS and GC-MS, reducing the analytical procedure by six times. With the development of bioinformatics tools and shared online libraries, new drugs of abuse that appear in the markets are easily identified and determined. In a second manuscript, Joye, Rocher et al. also used liquid chromatography hyphenated with Orbitrap high-resolution mass spectrometry with parallel reaction monitoring (PRM) for the quantification of the major classes of psychoactive substances present in the context of driving under the influence of drugs (DUID), such as cannabinoids, cocaine and its metabolites, amphetamines, opiates and opioids, and the major benzodiazepines and z-drugs, achieving the required sensitivity for DUID cases using a sample amount as low as 0.1 mL of whole blood. In addition to high resolution, Orbitrap-based PRM acquires all the selected precursor ions, avoiding *a priori* knowledge of the fragments of interest for method development, which represents an advantage over classical multiple reaction monitoring (MRM). Habib et al. reviewed the strategies for chemical analysis of drugs of abuse and explosives, using mass spectrometry-based approaches. Several new ionization sources were revisited and the mechanisms of ion formation following their use were addressed for illicit drugs and explosives. The authors concluded presenting the main challenges that the future holds regarding the analysis of non-volatile compounds in what concerns ionization procedures.

Greener sample preparation techniques, like hollow fiber liquid-phase microextraction, are also presented in this collection, namely by de Oliveira Silveira et al., to determine the main markers of Ayahuasca consumption in urine specimens. This alternative and eco-friendly sample preparation approach was fully validated, showing excellent limits of detection and quantification (1-5 ng/mL), reproducibility, reduced matrix effect interferences, and outstanding recoveries (above 80%).

Finally, new approaches to determine drug use via wastewater analysis were reviewed by Zilles Hahn et al. The authors addressed new insights about wastewater-based epidemiology (WBE) as a useful tool to detect in real time illicit drug use by a population. Also, the most important biomarkers of drugs of abuse consumption in wastewater and the fundamentals of polar organic chemical integrative sampling (POCIS) in WBE were discussed and compared with other strategies.

In summary, this collection covers Research Topics representative of the recent trends and advances in drug testing and new compound identification in biological specimens, with focus on the development of novel analytical approaches,

new chromatographic and spectrometric techniques, and sample preparation procedures, including miniaturized and environmentally friendly methodologies.

## AUTHOR CONTRIBUTIONS

All authors listed have made a substantial, direct and intellectual contribution to the work, and approved it for publication.

**Conflict of Interest:** The authors declare that the research was conducted in the absence of any commercial or financial relationships that could be construed as a potential conflict of interest.

*Copyright © 2021 Gallardo, Barroso, Concheiro-Guisan and de-Castro-Ríos. This is an open-access article distributed under the terms of the Creative Commons Attribution License (CC BY). The use, distribution or reproduction in other forums is permitted, provided the original author(s) and the copyright owner(s) are credited and that the original publication in this journal is cited, in accordance with accepted academic practice. No use, distribution or reproduction is permitted which does not comply with these terms.*



# Can X-Ray Powder Diffraction Be a Suitable Forensic Method for Illicit Drug Identification?

Bronislav Jurásek<sup>1\*</sup>, Vilém Bartůňek<sup>2</sup>, Štěpán Huber<sup>2</sup>, Patrik Fagan<sup>3</sup>, Vladimír Setnička<sup>3</sup>, František Králík<sup>3</sup>, Wim Dehaen<sup>4</sup>, Daniel Svozil<sup>4</sup> and Martin Kuchař<sup>1\*</sup>

<sup>1</sup> Forensic Laboratory of Biologically Active Substances, Department of Chemistry of Natural Compounds, University of Chemistry and Technology Prague, Prague, Czechia, <sup>2</sup> Department of Inorganic Chemistry, University of Chemistry and Technology Prague, Prague, Czechia, <sup>3</sup> Department of Analytical Chemistry, University of Chemistry and Technology Prague, Prague, Czechia, <sup>4</sup> CZ-OPENSCREEN: National Infrastructure for Chemical Biology, Department of Informatics and Chemistry, Faculty of Chemical Technology, University of Chemistry and Technology Prague, Prague, Czechia

## OPEN ACCESS

### Edited by:

Ana de-Castro-Ríos,  
University of Santiago de  
Compostela, Spain

### Reviewed by:

Juan Manuel Lázaro-Martínez,  
University of Buenos Aires, Argentina  
Anthony Martin Thomas Bell,  
Sheffield Hallam University,  
United Kingdom

### \*Correspondence:

Bronislav Jurásek  
jurasekb@vscht.cz  
Martin Kuchař  
kuchara@vscht.cz

### Specialty section:

This article was submitted to  
Analytical Chemistry,  
a section of the journal  
Frontiers in Chemistry

Received: 02 March 2020

Accepted: 14 May 2020

Published: 23 June 2020

### Citation:

Jurásek B, Bartůňek V, Huber Š,  
Fagan P, Setnička V, Králík F,  
Dehaen W, Svozil D and Kuchař M  
(2020) Can X-Ray Powder Diffraction  
Be a Suitable Forensic Method for  
Illicit Drug Identification?  
Front. Chem. 8:499.  
doi: 10.3389/fchem.2020.00499

New psychoactive substances (NPSs) are associated with a significant number of intoxications. With the number of readily available forms of these drugs rising every year, there are even risks for the general public. Consequently, there is a high demand for methods sufficiently sensitive to detect NPSs in samples found at the crime scene. Infrared (IR) and Raman spectroscopies are commonly used for such detection, but they have limitations; for example, fluorescence in Raman can overlay the signal and when the sample is a mixture sometimes neither Raman nor IR is able to identify the compounds. Here, we investigate the potential of X-ray powder diffraction (XRPD) to analyse samples seized on the black market. A series of psychoactive substances (heroin, cocaine, mephedrone, ephylone, butylone, JWH-073, and naphyrone) was measured. Comparison of their diffraction patterns with those of the respective standards showed that XRPD was able to identify each of the substances. The same samples were analyzed using IR and Raman, which in both cases were not able to detect the compounds in all of the samples. These results suggest that XRPD could be a valuable addition to the range of forensic tools used to detect these compounds in illicit drug samples.

**Keywords:** new psychoactive substances, X-ray powder diffraction, drug detection, infrared spectroscopy, Raman spectroscopy

## INTRODUCTION

The pharmacophore is the part of the chemical structure that is responsible for the biological effect of the substance. Thus, if the structure of a chemical entity is modified without affecting the pharmacophore, this substance will very likely retain the biological effects of the starting compound. These findings are widely used in drug design; however, the pharmacophore theory has also begun to be used in the illicit drug scene over the last decade. If the structure of an illicit drug is modified while retaining its pharmacophore, the newly prepared entity will not be covered by the current legislation, while its effects will very likely be similar to the already banned unaltered substance. These substances [called new psychoactive substances (NPSs) or designer drugs] are being monitored by the European Monitoring Centre for Drugs and Drug Addiction

(EMCDDA). The latest EMCDDA annual drug market report mentions about 730 different NPSs. Although the annual growth of these substances has decreased over the last 2 years (about 1 new substance per week), according to the latest EMCDDA report there are ~400 NPSs appearing on the market regardless of any regulations (European Monitoring Centre for Drugs Drug Addiction, 2018; European Monitoring Centre for Drugs Drug Addiction Europol, 2019). The increase of both substances that are completely new on the market and those that occur on the market regardless of any legal regulations already exerts considerable pressure on the analytical teams monitoring these compounds. Moreover, psychoactive substances are often sold as blends, which complicates their detection further. Hence, there is a significant demand for the development of easy, fast and reliable field detection methods for psychoactive substances (European Monitoring Centre for Drugs Drug Addiction, 2018; European Monitoring Centre for Drugs Drug Addiction Europol, 2019).

United Nations Office on Drugs and Crime (UNODC) has published (UNODC - United Nations Office on Drugs Crime, 2013) a study that has gathered data on the methods used for the identification of NPSs from 60 countries (Popovic et al., 2019). According to the respondents, the mostly used group of methods belong to the chemical analysis techniques [i.e., gas chromatography—mass spectrometry (GC-MS), liquid chromatography—mass spectrometry (LC-MS), high performance liquid chromatography (HPLC), vibrational spectroscopies—Fourier transform infrared spectroscopy (FTIR) and Raman spectroscopy, and nuclear magnetic resonance (NMR)]. While GC and LC enable separation of the analytes and thus may provide both qualitative and quantitative analysis, NMR is especially valuable due to its potential to elucidate unknown structures in the samples. However, all of these instrumentations have to be used wisely, with regard to their individual strengths and limitations (complex mixtures renders the NMR and FTIR spectra too complex, while isomers may complicate the use of GC-MS or LC-MS techniques; UNODC - United Nations Office on Drugs Crime, 2013).

The choice of analytical instrumentation is often limited by the type of the sample. Biological samples such as blood (Mercieca et al., 2018), hair (Kyriakou et al., 2017; Salomone et al., 2017; Fabresse et al., 2019), or urine (Meyer et al., 2016; Vikingsson et al., 2017; Mercieca et al., 2018) are a relatively complex matrix for analysis. Therefore, considerable effort has been invested into development of separation methods coupled with mass detection, which are, together with immunochemical methods (Cannaert et al., 2018; Maryška et al., 2018), currently the main techniques for NPS identification in biological matrices. Furthermore, the sensitivity of current techniques and the knowledge of psychoactive substance metabolisms (Vikingsson et al., 2015, 2017; Šícho et al., 2019) allow their detection also in local wastewater (González-Mariño et al., 2013; Rosi-Marshall et al., 2015; Croft et al., 2020) (e.g., festivals, prisons) and thus offer valuable data on the prevalence (Mastroianni et al., 2016; Croft et al., 2020) of individual substances in society.

Substances of certain groups (e.g., cannabinoids) are often distributed to the end user applied on another medium, such as dried herbal leaves (Ciolino, 2015; Namera et al., 2015) (e.g.,

damiana) or on paper and, as such, smuggled into prisons in letters or books (Metternich et al., 2019; Hvozdozovich et al., 2020). Although after appropriate sample treatment a wide selection of techniques can be used for the analysis, LC-MS seems to be the most prevalent one (UNODC - United Nations Office on Drugs Crime, 2013). Mass spectrometry seems to be also used to analyse seized psychoactive substances in its powder form even though such samples can be analyzed by any of the aforementioned methods. Although a tandem of separation technique with a mass detector appears to be the universal method (Pasin et al., 2017), it requires an experienced operator for its use and maintenance, on top of the often required standards. This renders the analyses expensive (Pasin et al., 2017). Therefore, from the perspective of price efficiency, there is still a significant demand for less resource intensive yet reliable analytical alternatives.

Infrared (IR) and Raman spectroscopies belong to the other most common choices for the analysis of solid illicit street drug samples as they generally enable a fast and relatively cheap analysis (Stewart et al., 2012; Jones et al., 2016; Maheux et al., 2016; Apirakkan et al., 2018; Pereira et al., 2018). Their application does not demand a complicated sample preparation and commercially available portable spectrometers offer the possibility of *in situ* measurements (Correia et al., 2018; Yu et al., 2018). However, these methods also have some limitations. In case of Raman spectroscopy, a high level of fluorescence caused either by an active substance or by an additive may complicate the interpretation of the spectra. Furthermore, in the case of complex mixtures (e.g., heroin street samples generally do not contain more than 30% of the active substance) (Fabresse et al., 2019), the interpretation of the IR and Raman spectra may be very difficult due to interfering bands of various adulterants.

Hence, we investigated the potential of X-ray powder diffraction (XRPD) in the analysis of solid samples seized on the black market. XRPD, a widely used analytical technique in the pharmaceutical industry, has been used in several forensic cases involving analyses of soils (Kotrly, 2006), where it offered fruitful results for the investigation, so it is an already established analytical technique in forensic sciences (Thatcher and Briner, 1986). Although it has a relatively wide possibilities of its use in forensics, including analyses of explosives (Thatcher and Briner, 1986; Kotrly, 2006), fibers (Thatcher and Briner, 1986) or illicit drugs including some of the cutting agents (Folen, 1975; Thatcher and Briner, 1986), its use has been rather neglected in this field. Moreover, the situation in the field of psychoactive substances has changed dramatically with the NPSs entering the drug market in recent years. XRPD represents a simple, non-destructive technique enabling the reliable identification of either pure solid substances or their street sample mixtures. Moreover, it might also be able to distinguish inorganic compounds (e.g., gypsum) that might be often life threatening when injected. XRPD may serve as a suitable complementary method to vibrational spectroscopy for the analysis of various seized street drug samples that may especially help in cases where fluorescence or the varied composition of the analyzed samples hinder the routine identification by Raman or IR spectroscopies. However, the scope of XRPD is limited solely to use on solid samples. In our previous work we have shown on a series of cathinones that



this method can not only distinguish between structurally similar NPSs, but that it can also identify substances in mixtures (Jurásek et al., 2019). In this work, we analyzed cocaine, heroin, and 5 NPS street samples with their respective standards by XRPD and the results were compared with the commonly used IR and Raman spectroscopy measurements.

## EXPERIMENTAL SECTION

### Analyzed Samples

The origin and specifications of all the analyzed samples are given in **Table 1**. The real samples, which were collected with standard ethical procedure, were provided as a part of the seizures performed by the Police of the Czech Republic, while the standards (purity of all the used standards were higher than 98%) were acquired from different sources (**Table 1**). Samples 5F-ADB I. and II. were provided as a part of seizures performed by the Police of the Czech Republic, while the samples 5F-ADB IV., V., and VI. were obtained from a commercial vendor in the framework of a darknet study. Sample 5F-ADB III. was prepared in house.

### X-Ray Powder Diffraction

The sample crystals were crushed with a microscope slide on a silicon pod (see **Supplementary Figure 1**) and, thus, a narrow surface was created. For the remeasurement, JWH-073 samples were ground extensively in the agate mortar to show the differences in relative intensities.

The XRPD data were collected with a Bruker 2nd generation D2 Phaser powder diffractometer (Bruker AXS, Germany) at room temperature with parafocusing Bragg-Brentano geometry using CuK $\alpha$  radiation ( $\lambda = 1.5418$  Å,  $U = 30$  kV,  $I = 10$  mA). The data were scanned with an ultrafast LYNXEYE XE detector over the angular range of 5 to 60 °2 $\theta$  with a step size of 0.019 °2 $\theta$  and a counting time of 1 s per step. The software HIGHSCORE PLUS 3.0e (PANalytical, Almelo, Netherlands) was employed to fit the background using a polynomial method, to smooth the data and to eliminate the K $\alpha$ 2 component. The top of the smoothed peaks was used to determine the peak positions and intensities. Determination of peak positions was made by an in-build algorithm in the HIGHSCORE PLUS 3.0e. Thus, processed diffraction patterns were subjected to the pattern searching procedure within PDF4+ database via the HighScore software.

To compare similarity of XRPD diffractograms quantitatively, a cross-correlation score was used. To accentuate peaks and attenuate background noise and minor pollutant effects, we prepare the normalized patterns by squaring them (Equations 1, 2) and only then calculating their cross-correlation (Equations 3, 4). With  $f'(\theta)$  as the normalized XRPD diffractogram of a known standard and  $g'(\theta)$  as the normalized XRPD diffractogram of a measured sample, we calculate a cross-correlation score  $CCS_{fg}$  as defined below (Equation 5):

$$\text{Squared XRPD pattern of standard: } f(\theta) = f'^2(\theta) \quad (1)$$

$$\text{Squared XRPD pattern of sample: } g(\theta) = g'^2(\theta) \quad (2)$$

$$\text{Cross - correlation: } C_{fg}(\tau) \triangleq \int_{-\infty}^{\infty} \overline{f(\theta)} g(\theta + \tau) d\theta \quad (3)$$

$$\text{Auto - correlation: } C_{ff}(\tau) \triangleq \int_{-\infty}^{\infty} \overline{f(\theta)} f(\theta + \tau) d\theta \quad (4)$$

$$\text{Cross - correlation score: } CCS_{fg} \triangleq \frac{\int_{-\infty}^{\infty} C_{fg}(\tau) d\tau}{\int_{-\infty}^{\infty} C_{ff}(\tau) d\tau} \quad (5)$$

A discrete calculation method for  $CCS_{fg}$ , directly using ASC files, was implemented as a Python script (available at <https://github.com/dehaenw/cross-correlation>).

### Optical Microscopy

Crystal shapes were visualized by confocal microscope Olympus Lext OLS 3100 without any additional image processing.

### Infrared and Raman Spectroscopy

The IR spectra of the standards and real samples were measured on a FT-IR Nicolet iS50 spectrometer (Thermo Scientific, USA) with a Tungsten-halogen MIR radiation source, KBr beam splitter and DLaTGS detector. All the samples were in the form of a powder and they were analyzed by the ATR technique with a diamond crystal. The spectra were recorded in a spectral region of 4,000–400  $\text{cm}^{-1}$  with a resolution of 4  $\text{cm}^{-1}$  and they are presented as an average of 256 scans. The spectral background was collected before every sample measurement.

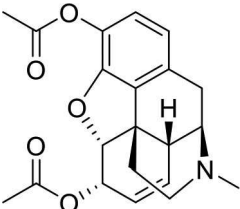
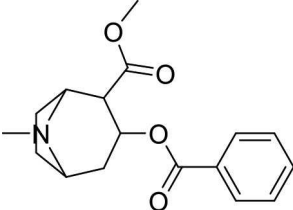
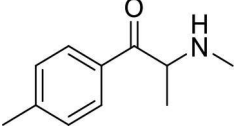
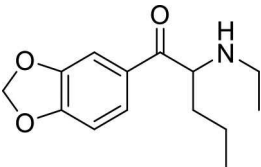
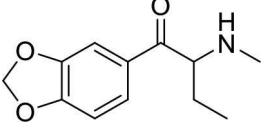
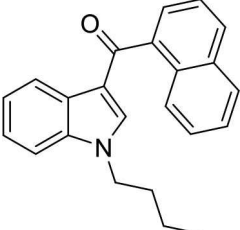
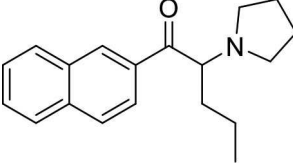
The Raman spectra were acquired on a DXR SmartRaman spectrometer (Thermo Scientific, USA) equipped with two lasers (excitation wavelengths 532 and 780 nm). In the case of the 532 nm laser, a diffraction grid comprised of 900 lines per mm, a laser power of 5 mW and 10 accumulations each of 10 s exposure time were used. A diffraction grid with 400 lines per mm, a laser power of 65 mW and 10 accumulations each of 10 s exposure time were used for the measurements with the 780 nm laser. The spectra were recorded in a spectral region of 400–3,000  $\text{cm}^{-1}$  with a resolution of 2.4–4.4  $\text{cm}^{-1}$  and all the samples were analyzed in glass vials. The spectra were processed with the correction of fluorescence (6th order polynomial).

## RESULTS AND DISCUSSION

### X-Ray Powder Diffraction

We have demonstrated in our previous work (Jurásek et al., 2019) that XRPD can effectively distinguish between particular

**TABLE 1** | Overview of the tested samples and standards.

Sample name	Chemical name	Structure	Origin
Heroin seized	(5 $\alpha$ ,6 $\alpha$ )-7,8-didehydro-4,5-epoxy-17-methylmorphinan-3,6-diol diacetate		Sample was seized by the Police of the Czech Republic.
Heroin standard			Standard was purified in our laboratory.
Cocaine seize	methyl (1S,3S,4R,5R)-3-benzoyloxy-8-methyl-8-azabicyclo[3.2.1]octane-4-carboxylate		Sample was seized by Police of the Czech Republic.
Cocaine standard			Standard purchased from Fagron a.s.
Mephedrone seized	2-(methylamino)-1-(4-methylphenyl)propan-1-one		Sample was seized by Police of the Czech Republic.
Mephedrone standard			Standard was purchased from Alfarma s.r.o.
Ephylone seized	1-(1,3-Benzodioxol-5-yl)-2-(ethylamino)pentan-1-one		Sample was seized by Police of the Czech Republic.
Ephylone standard			Sample was purified in our laboratory.
Butylone seized	1-(1,3-benzodioxol-5-yl)-2-(methylamino)butan-1-one		Sample was seized by Police of the Czech Republic.
Butylone standard			Standard was purchased from Alfarma s.r.o.
JWH-073 seized	Naphthalen-1-yl-(1-butylindol-3-yl)methanone		Sample was seized by Police of the Czech Republic.
JWH-073 standard			Standard was purchased from Alfarma s.r.o.
2-naphyrone seized	1-(naphthalen-2-yl)-2-(pyrrolidin-1-yl)pentan-1-one		Samples were seized by Police of the Czech Republic.
2-naphyrone standard			Standard was purchased from Alfarma s.r.o.

chemical entities even with similar chemical structures, which is essential in the forensic analysis of NPSs. However, most of the tested standards were prepared in our laboratory and the results were not extensively compared with authentic samples that might occur on the drug market (Jurásek et al., 2019). Therefore, in the current study, we analyzed 7 samples of psychoactive substances (cocaine, heroin, and 5 NPSs) that

were seized on the black market and the acquired results were compared with the diffraction patterns of the respective standards (**Figure 1**).

PDF4+ is a commercially available database that contains more than 410 000 diffraction patterns. Although this database does not contain most NPSs, this database contains diffraction patterns of heroin and cocaine. Such a big amount of

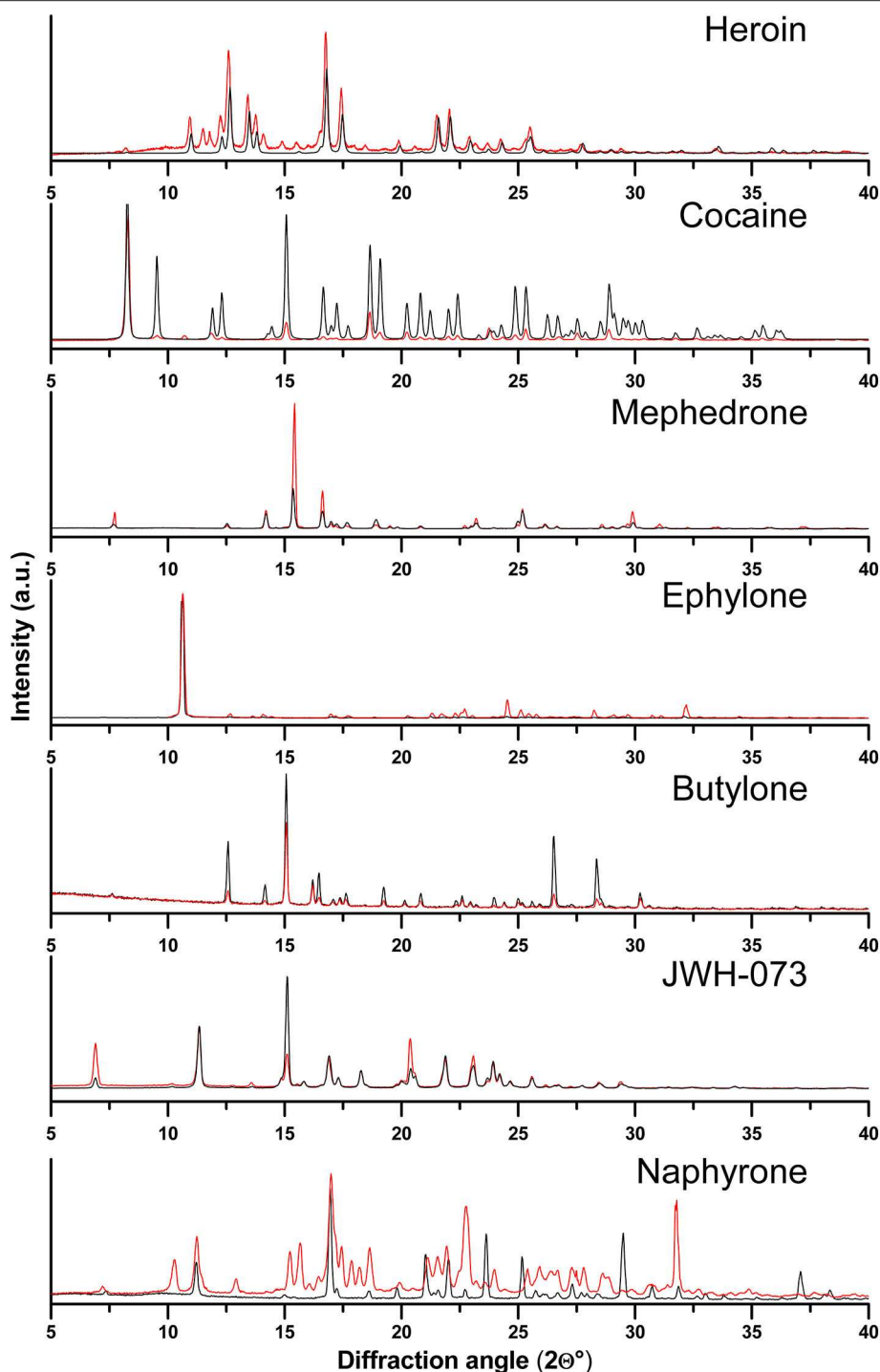


**FIGURE 1** | Diffraction patterns of heroin, cocaine, mephedrone, ephylone, butylone, JWH-073, and naphyrone samples. The red line marks the seized samples and the black marks the standards.

patterns in this database made us wonder if it would be possible to use it for identification of street samples of heroin and cocaine. The results were quite impressive, as we were able to identify both cocaine and heroin in street mixtures

(see non-modified search data in the **Supplementary Data**) using this commercial database. However, we were unable to assign the cutting agents, as this database mostly does not contain their respective patterns. Because there is no



suitable database of illicit substances yet, street samples of NPSs were just compared with the diffraction patterns of their respective standards.

JWH-073 was identified by XRPD (**Figure 1**) in one of the seized materials despite the observation that relative intensities in

the diffraction pattern differed considerably. The most intensive peak of the standard sample was  $15.1^\circ 2\theta$  whereas in the seized sample it was  $21.5^\circ 2\theta$ . However, these differences in the relative intensities might be caused by different crystal shapes. To confirm that the standard and seized sample had different

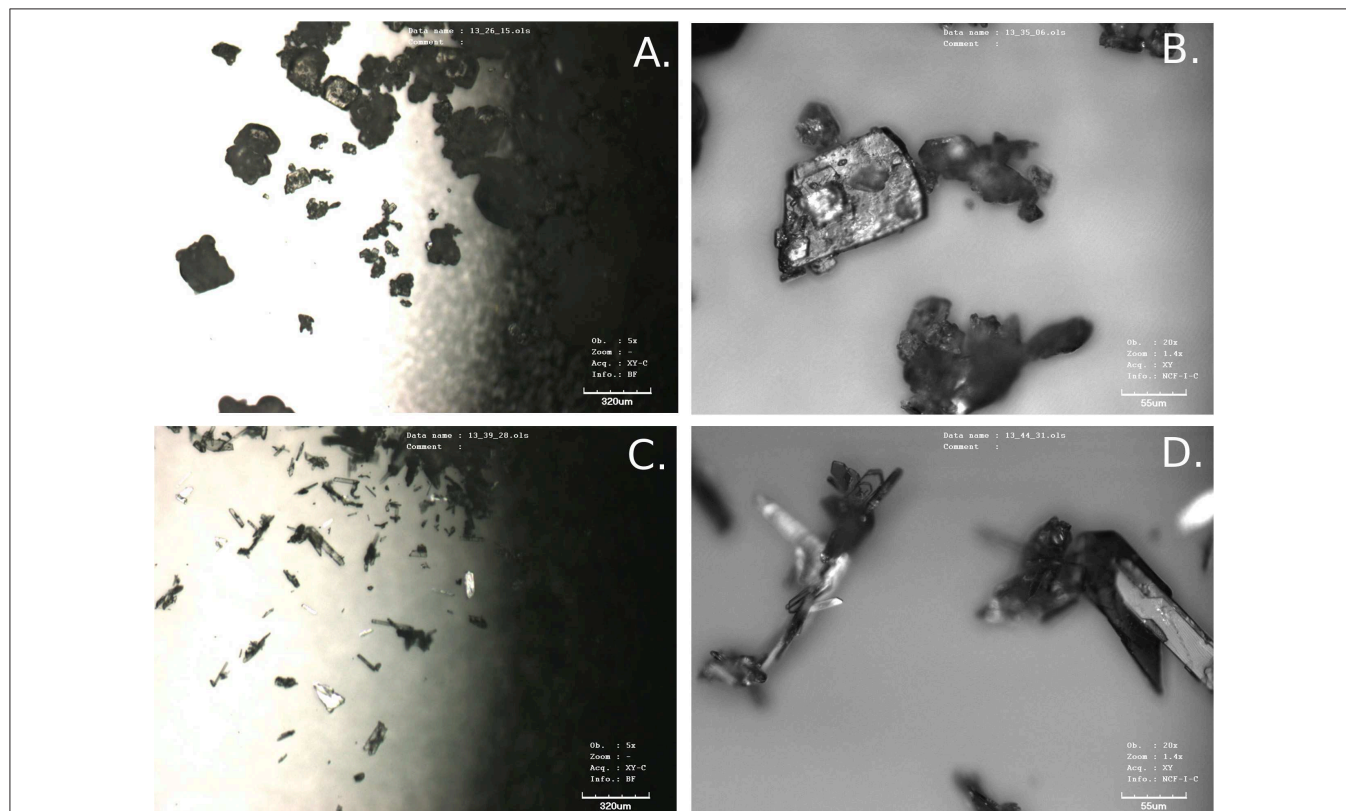


**FIGURE 2** | Confocal microscopy visualizations of JWH-073 standard (**A,B**—closer detail) and seized sample (**C,D**—closer detail).

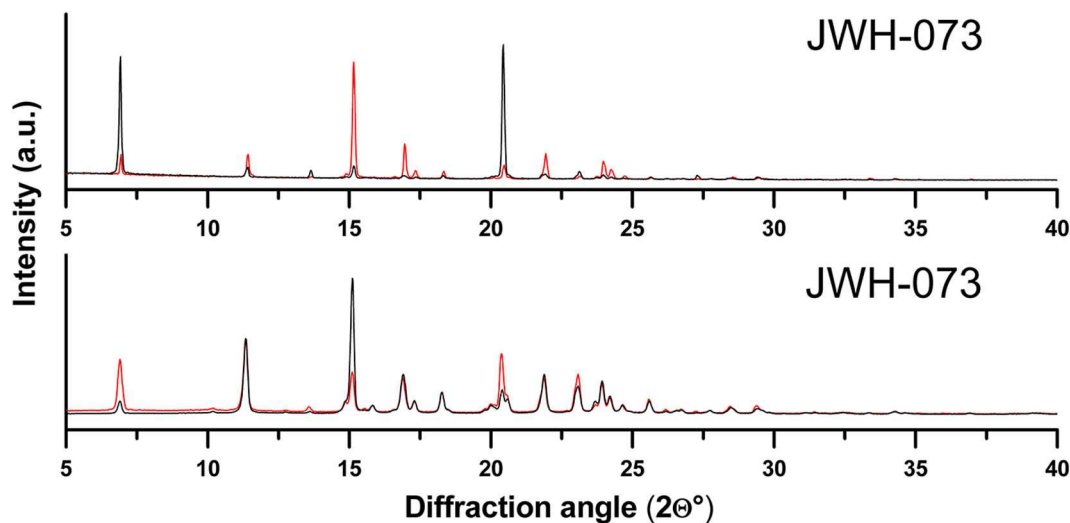


**FIGURE 3** | Diffraction patterns of JWH-073 sample and the respective standard remeasured after grinding in the agate mortar.

crystal shapes, they were subjected to a visual analysis by the optical confocal microscope (**Figure 2**). The crystal proportions of the seized sample were approximately the same in all three dimensions, but the standard formed needle-like shapes and so one dimension was significantly larger than the other two. This was presumably caused either by the type of crystallization or the synthetic process of the respective samples (Morris et al., 2000). Therefore, to reduce the differences in relative intensities both JWH-073 sample and the respective standard were extensively ground in an agate mortar and remeasured with the same setting of the goniometer (see **Figure 3**). The differences in the signal intensities did not have any effect regarding the identification of the compound in the seized sample as the peak positions did not change. The sample was successfully identified according to the peak positions and no other peaks were observed suggesting a high purity of the JWH-073 in the seized material.

Mephedrone, ephylone, naphyrone, and butylone were successfully identified in the seized material by comparison of the seized samples and respective standard diffraction patterns. Although the relative intensities of some peaks differed slightly in both samples, which was presumably caused again by different

crystal shapes, there were no other peaks at different positions suggesting that the seized materials were of high purity.

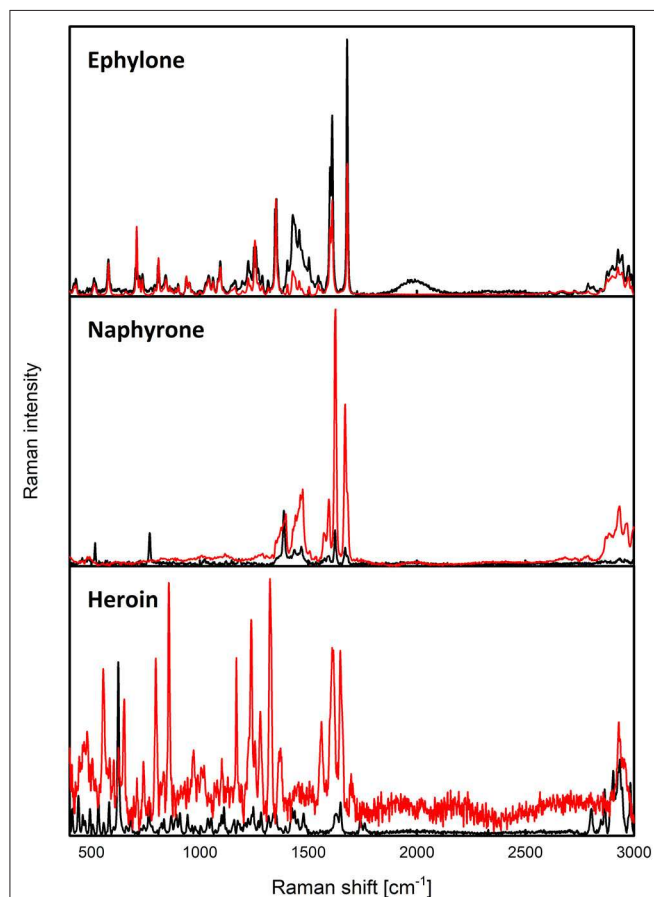


**FIGURE 4** | Raman spectra of ephylone, naphyrone, and heroin. The red line marks the seized samples and the black marks the standards.

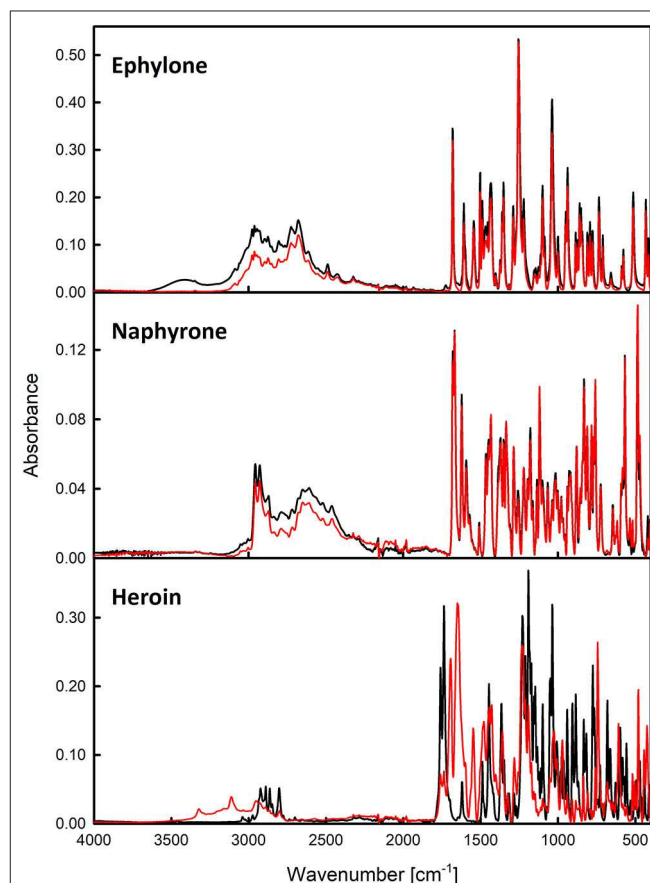


**FIGURE 5** | IR spectra of ephylone, naphyrone, and heroin. The red line marks the seized samples and the black marks the standards.

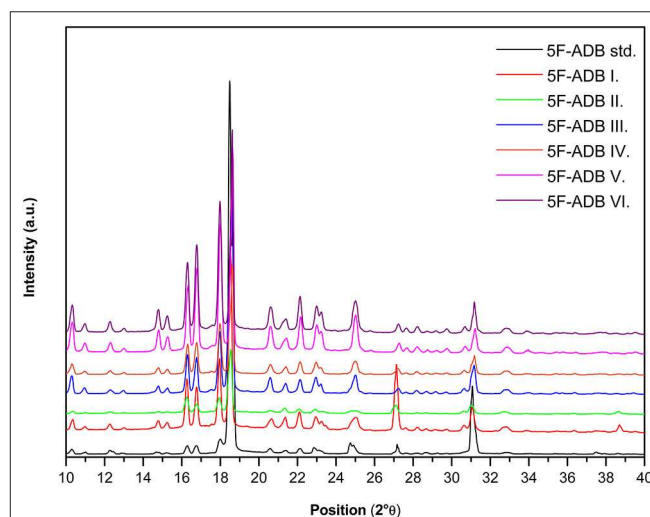


**FIGURE 6** | Diffraction patterns of 5F-ADB samples. The color lines marks the seized samples and the black marks the standards.

Although cocaine and heroin do not belong to the NPSs, the prevalence of these compounds on the drug market is high and therefore we have included these “classic” street drugs in the examination test of XRPD in a similar manner as in the case of the NPSs. Since cocaine and heroin have been already measured and their diffractograms were included in the database of PDFs (powder diffraction file), database cards were used for the identification instead of using the respective standards.

This approach was chosen mainly to prove that the samples could be identified without the need of a standard only by using a suitable database. The seized sample of heroin was successfully identified as diacetylmorphine with card PDF 00-033-1635 when most of the peaks belonged to the drug. The relatively intensive peaks 11.5 and 11.8 °2 $\theta$  might be attributed to possible diluting agents (e.g., caffeine, PDF 00-049-2058). However, the aim of this study was to prove that XRPD can be used for drug identification and therefore, these impurities were not further investigated. Cocaine was identified by XRPD in the last seized sample. All of the major peaks were attributed to cocaine hydrochloride (PDF 00-030-1629) with the exception of the less intensive peak 10.7 °2 $\theta$  and a few minor peaks, which might be attributed to specific adulterants in the future.

## Comparison With Vibrational Spectroscopy Measurements

To compare the efficiency of XRPD with other non-destructive methods that are often used in forensic practice, all of the samples and standards were measured by the IR and Raman spectroscopies. The differences of the results provided by these methods have been highlighted.

The Raman spectroscopy suffered from the high fluorescence level with the use of the 532 nm excitation wavelength, where only measurements of the real sample of JWH-073 provided an interpretable spectrum. After the application of the 780 nm excitation wavelength, the fluorescence level decreased in most

cases and the active substances were identified by a simple comparison with the spectra of the corresponding standards (**Figure 4** and **Supplementary Data**). However, the high level of fluorescence made the analysis of the naphyrone street sample impossible (**Supplementary Data**) and the high amount of the adulterants in the heroin sample did not allow a reliable identification of the active substance (**Figure 4**).

The IR spectroscopy performed slightly better, as it allowed the reliable identification of 6 of the 7 analyzed samples (**Figure 5** and **Supplementary Data**), but the identification of the active substance in the heroin street sample was not possible due to the presence of many interfering bands. Both IR and Raman spectroscopies can offer spectra within several minutes, whereas XRPD instrumentation is usually more time demanding (about 15–20 min). All the measured data can be found in the **Supplementary Data**.

Vibrational spectroscopy proved to be a powerful tool in the analysis of illicit drug samples as was expected. However, in the case of the heroin sample, both methods struggled in the identification of the active substance. On the other hand, heroin was easily identified by XRPD, we thus believe that its potential in the forensic practice is promising.

Although differences in relative intensities in the XRPD patterns may seem to complicate the identification of unknown substances, on the contrary, in some cases, it might further provide valuable data about the analyte (e.g., differences between the production procedures). To demonstrate this ability, six different samples of the 5F-ADB, which were obtained during our NPS survey in the Czech Republic, were analyzed and compared with the standard. The same peak positions in the diffraction patterns enabled the identification of the 5F-ADB in the samples. Two of the samples offered diffraction patterns with not only the same peak position but the relative intensities corresponded as well. The other samples exhibited differences in relative intensities (see **Figure 6**).

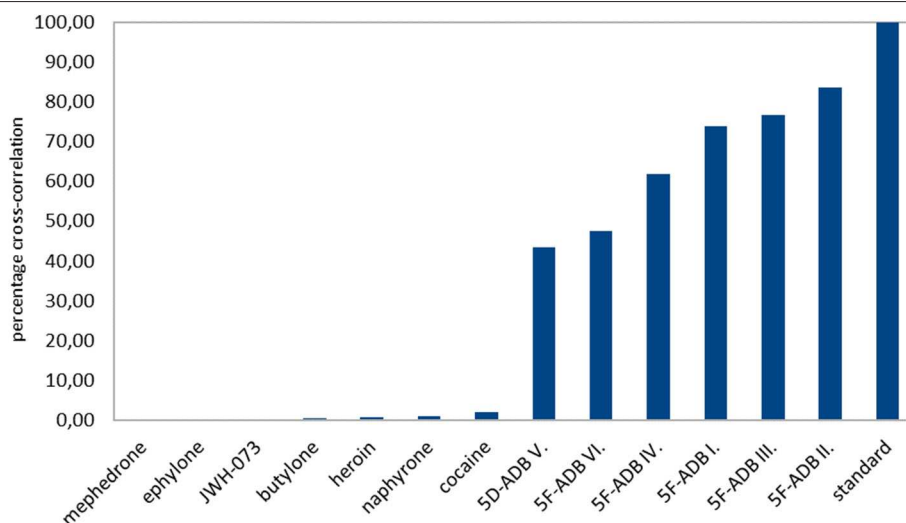


**FIGURE 7** | A cross-correlation score for the quantitative comparison of XRPD diffractograms.

This difference in relative intensities makes qualitative estimation of similarity by visual comparing and simple pattern subtracting suggestive but tricky and non-trivial. As a quantitative similarity approach, we proposed a cross-correlation score. This showed that the XRPD patterns of all seven different samples of 5F-ADB have a much higher score than the diffractograms of other, unrelated compounds (see **Figure 7**).

This suggests that peak positions are essential for the substance identification, whereas an exact match of the relative intensities is not needed, as is a well-known property of XRPD patterns (Pecharsky and Zavalij, 2009). A match of the relative intensities occur when the shape of the crystals and partly their size correspond. Interestingly, we observed a similar relative intensity pattern for sample V. and VI., which could be possibly attributed to their shared origin. If so, such information may be useful for investigators as samples with the same relative intensities could either be from the same source or possibly even from the same batch. Yet, drawing such conclusions based on the agreement of relative intensities may be unreliable, therefore the use of LC-MS remains the only reliable and generally powerful method for this purpose. In case a reliable correlation could be found generally, XRPD may be useful as a pre-screening method for this purpose. Notably, significant grinding of the samples undoubtedly affects the relative intensity pattern of the measured samples (see **Figure 3**), which unfortunately further complicates the option to compare “similarity of the samples” in a straightforward manner.

Nevertheless, it is essential to note that if it is not possible to assign all the signals in the diffraction pattern, then further analyses may be required. However, after creating a robust database of diffraction patterns of NPSs and cutting agents, such database would enable the identification of not only the main compound but also help with assigning all of the other signals in the pattern to other compounds.

## CONCLUSIONS

Seized samples of heroin, cocaine and 5 NPSs (mephedrone, ephylone, butylone, JWH-073, and 2-naphyrone) were analyzed by XRPD, IR, and Raman spectroscopies and compared to the standards of the respective substances. We have shown that XRPD detected all of the analyzed NPSs, as well as providing a reliable identification of the “traditional” drugs cocaine and heroin. In the latter case, the methods of

vibrational spectroscopy struggled with the identification of the active substance, while XRPD provided a convincing result, which documents its promising potential in the field of the forensic practice. This instrumentation is not omnipotent, (nor are any other instrumentation currently being used in forensics). However, further combination of XRPD with vibrational spectroscopic methods can effectively eliminate the shortcomings of each of the methods and thus increase the overall reliability of the analysis. Moreover, we believe that in the future, when an appropriate database becomes available, this technique will have the potential to become a strong forensic tool.

## DATA AVAILABILITY STATEMENT

The datasets generated for this study are available on request to the corresponding author.

## AUTHOR CONTRIBUTIONS

BJ and MK designed the experiment. FK measured the IR spectra and PF measured the Raman spectra. BJ, VB, and ŠH measured the XRPD. ŠH, VS, and PF evaluated the XRPD, IR, and Raman data. WD and DS developed, tested and applied Python script for cross-correlation calculations. BJ, VB, and FK prepared the manuscript. MK, VS, and DS proofread the manuscript. DS, BJ, and VB revised the manuscript.

## FUNDING

This work was supported by the project OPPC CZ.2.16/3.1.00/21537, grant NPU I LO1601 from the MEYS CR under the NPU I program, Ministry of the Interior of the Czech Republic (MV0/VI20172020056), UNMZ (M/VIII/3/18) and by the Ministry of Education, Youth and Sports of the Czech Republic – project numbers LM2018130 and MSM T No. 21 SVV/2020.

## SUPPLEMENTARY MATERIAL

The Supplementary Material for this article can be found online at: <https://www.frontiersin.org/articles/10.3389/fchem.2020.00499/full#supplementary-material>

## REFERENCES

- Apirakkan, O., Frinculescu, A., Shine, T., Parkin, M. C., Cilibrizzi, A., Frascione, N., et al. (2018). Analytical characterization of three cathinone derivatives, 4-MPD, 4F-PHP and bk-EPDP, purchased as bulk powder from online vendors. *Drug Test. Anal.* 10, 372–378. doi: 10.1002/dt.a.2218
- Cannaert, A., Vasudevan, L., Friscia, M., Mohr, A. L. A., Wille, S. M. R., and Stove, C. P. (2018). Activity-based concept to screen biological matrices for opiates and (synthetic) opioids. *Clin. Chem.* 64, 1221–1229. doi: 10.1373/clinchem.2018.289496
- Ciolino, L. A. (2015). Quantitation of synthetic cannabinoids in plant materials using high performance liquid chromatography with UV detection (validated method). *J. Forensic Sci.* 60, 1171–1181. doi: 10.1111/1556-4029.12795
- Correia, R. M., Domingos, E., Tosato, F., dos Santos, N. A., Leite, J., de, A., et al. (2018). Portable near infrared spectroscopy applied to abuse drugs and medicine analyses. *Anal. Methods* 10, 593–603. doi: 10.1039/C7AY02998E
- Croft, T. L., Huffines, R. A., Pathak, M., and Subedi, B. (2020). Prevalence of illicit and prescribed neuropsychiatric drugs in three communities in Kentucky using wastewater-based epidemiology and monte carlo simulation



- for the estimation of associated uncertainties. *J. Hazard Mater.* 384:121306. doi: 10.1016/j.jhazmat.2019.121306
- European Monitoring Centre for Drugs and Drug Addiction (2018). *European Drug Report 2018: Trends and Developments*. Luxembourg.
- European Monitoring Centre for Drugs and Drug Addiction and Europol (2019). *European Drug Report 2019: Trends and Developments*. Luxembourg.
- Fabresse, N., Larabi, I. A., Stratton, T., Mistrik, R., Pfau, G., Lorin de la Grandmaison, G., et al. (2019). Development of a sensitive untargeted liquid chromatography-high resolution mass spectrometry screening devoted to hair analysis through a shared MS2 spectra database: a step toward early detection of new psychoactive substances. *Drug Test. Anal.* 11, 697–708. doi: 10.1002/dta.2535
- Folen, V. A. (1975). X-ray powder diffraction data for some drugs, excipients, and adulterants in illicit samples. *J. Forensic Sci.* 20:10282J. doi: 10.1520/JFS10282J
- González-Mariño, I., Rodríguez, I., Quintana, J. B., and Cela, R. (2013). Investigation of the transformation of 11-nor-9-carboxy- $\Delta^9$ -tetrahydrocannabinol during water chlorination by liquid chromatography-quadrupole-time-of-flight-mass spectrometry. *J. Hazard Mater.* 261, 628–636. doi: 10.1016/j.jhazmat.2013.08.006
- Hvozdoch, J. A., Chronister, C. W., Logan, B. K., and Goldberger, B. A. (2020). Case report: synthetic cannabinoid deaths in state of florida prisoners. *J. Anal. Toxicol.* 44, 298–300. doi: 10.1093/jat/bkz092
- Jones, L. E., Stewart, A., Peters, K. L., McNaul, M., Speers, S. J., Fletcher, N. C., et al. (2016). Infrared and Raman screening of seized novel psychoactive substances: a large scale study of <200 samples. *Analyst* 141, 902–909. doi: 10.1039/C5AN02326B
- Jurásek, B., Bartuněk, V., Huber, Š., and Kuchar, M. (2019). X-Ray powder diffraction - a non-destructive and versatile approach for the identification of new psychoactive substances. *Talanta* 195, 414–418. doi: 10.1016/j.talanta.2018.11.063
- Kotrlý, M. (2006). "Application of X-ray diffraction in forensic science" in *Ninth European Powder Diffraction Conference* (München: Oldenbourg Wissenschaftsverlag), 35–40. doi: 10.1524/9783486992526-009
- Kyriakou, C., Pellegrini, M., García-Algar, O., Marinelli, E., and Zaami, S. (2017). Recent trends in analytical methods to determine new psychoactive substances in hair. *Curr. Neuropharmacol.* 15, 663–681. doi: 10.2174/1570159X1566616111112545
- Maheux, C. R., Alarcon, I. Q., Copeland, C. R., Cameron, T. S., Linden, A., and Grossert, J. S. (2016). Identification of polymorphism in ethylone hydrochloride: synthesis and characterization. *Drug Test. Anal.* 8, 847–857. doi: 10.1002/dta.1859
- Maryška, M., Fojtíková, L., Jurok, R., Holubová, B., Lapčík, O., and Kuchar, M. (2018). Use of novel haptens in the production of antibodies for the detection of tryptamines. *RSC Adv.* 8, 16243–16250. doi: 10.1039/C8RA02528B
- Mastroianni, N., Bleda, M. J., López de Alda, M., and Barceló, D. (2016). Occurrence of drugs of abuse in surface water from four Spanish river basins: Spatial and temporal variations and environmental risk assessment. *J. Hazard Mater.* 316, 134–142. doi: 10.1016/j.jhazmat.2016.05.025
- Mercieca, G., Odoardi, S., Cassar, M., and Strano Rossi, S. (2018). Rapid and simple procedure for the determination of cathinones, amphetamine-like stimulants and other new psychoactive substances in blood and urine by GC-MS. *J. Pharm. Biomed. Anal.* 149, 494–501. doi: 10.1016/j.jpba.2017.11.024
- Metternich, S., Zörntlein, S., Schönberger, T., and Huhn, C. (2019). Ion mobility spectrometry as a fast screening tool for synthetic cannabinoids to uncover drug trafficking in jail via herbal mixtures, paper, food, and cosmetics. *Drug Test. Anal.* 11, 833–846. doi: 10.1002/dta.2565
- Meyer, M. R., Bergstrand, M. P., Helander, A., and Beck, O. (2016). Identification of main human urinary metabolites of the designer nitrobenzodiazepines clonazepam, meclonazepam, and nifoxipam by nano-liquid chromatography-high-resolution mass spectrometry for drug testing purposes. *Anal. Bioanal. Chem.* 408, 3571–3591. doi: 10.1007/s00216-016-9439-6
- Morris, K. R., Schlam, R. F., Cao, W., and Short, M. S. (2000). Determination of average crystallite shape by X-ray diffraction and computational methods. *J. Pharm. Sci.* 89, 1432–1442. doi: 10.1002/1520-6017(200011)89:11<1432::AID-JPS6>3.0.CO;2-X
- Namera, A., Kawamura, M., Nakamoto, A., Saito, T., and Nagao, M. (2015). Comprehensive review of the detection methods for synthetic cannabinoids and cathinones. *Forensic Toxicol.* 33, 175–194. doi: 10.1007/s11419-015-0270-0
- Pasin, D., Cawley, A., Bidny, S., and Fu, S. (2017). Current applications of high-resolution mass spectrometry for the analysis of new psychoactive substances: a critical review. *Anal. Bioanal. Chem.* 409, 5821–5836. doi: 10.1007/s00216-017-0441-4
- Pecharsky, V., and Zavalij, P. (2009). *Fundamentals of Powder Diffraction and Structural Characterization of Materials*. 2nd Edn. Boston, MA: Springer.
- Pereira, L. S. A., Lisboa, F. L. C., Coelho Neto, J., Valladão, F. N., and Sena, M. M. (2018). Screening method for rapid classification of psychoactive substances in illicit tablets using mid infrared spectroscopy and PLS-DA. *Forensic Sci. Int.* 288, 227–235. doi: 10.1016/j.forsciint.2018.05.001
- Popovic, A., Morelato, M., Roux, C., and Beavis, A. (2019). Review of the most common chemometric techniques in illicit drug profiling. *Forensic Sci. Int.* 302:109911. doi: 10.1016/j.forsciint.2019.109911
- Rosi-Marshall, E. J., Snow, D., Bartelt-Hunt, S. L., Paspalof, A., and Tank, J. L. (2015). A review of ecological effects and environmental fate of illicit drugs in aquatic ecosystems. *J. Hazard Mater.* 282, 18–25. doi: 10.1016/j.jhazmat.2014.06.062
- Salomone, A., Palamar, J. J., Gerace, E., Di Corcia, D., and Vincenti, M. (2017). Hair testing for drugs of abuse and new psychoactive substances in a high-risk population. *J. Anal. Toxicol.* 41, 376–381. doi: 10.1093/jat/bkx020
- Šicho, M., Stork, C., Mazzolari, A., de Bruyn Kops, C., and Pedretti, A., Testa, B., et al. (2019). FAME 3: predicting the sites of metabolism in synthetic compounds and natural products for phase 1 and phase 2 metabolic enzymes. *J. Chem. Inf. Model.* 59, 3400–3412. doi: 10.1021/acs.jcim.9b00376
- Stewart, S. P., Bell, S. E. J., Fletcher, N. C., Bouazzaoui, S., Ho, Y. C., Speers, S. J., et al. (2012). Raman spectroscopy for forensic examination of  $\beta$ -ketophenethylamine "legal highs": reference and seized samples of cathinone derivatives. *Anal. Chim. Acta* 711, 1–6. doi: 10.1016/j.aca.2011.10.018
- Thatcher, P. J., and Briner, G. P. (1986). The application of X-Ray powder diffraction to forensic science. *Powder Diffr.* 1, 320–324. doi: 10.1017/S.0885715600011994
- UNODC - United Nations Office on Drugs and Crime (2013). *The Challenge of New Psychoactive Substances*. Vienna. Available online at: [https://www.unodc.org/documents/scientific/NPS\\_Report.pdf](https://www.unodc.org/documents/scientific/NPS_Report.pdf).
- Vikingsson, S., Josefsson, M., and Gréen, H. (2015). Identification of AKB-48 and 5F-AKB-48 metabolites in authentic human urine samples using human liver microsomes and time of flight mass spectrometry. *J. Anal. Toxicol.* 39, 426–435. doi: 10.1093/jat/bkv045
- Vikingsson, S., Wohlfarth, A., Andersson, M., Gréen, H., Roman, M., Josefsson, M., et al. (2017). Identifying metabolites of meclonazepam by high-resolution mass spectrometry using human liver microsomes, hepatocytes, a mouse model, and authentic urine samples. *AAPS J.* 19, 736–742. doi: 10.1208/s12248-016-0040-x
- Yu, B., Cao, C., Li, P., Mao, M., Xie, Q., and Yang, L. (2018). Sensitive and simple determination of zwitterionic morphine in human urine based on liquid-liquid micro-extraction coupled with surface-enhanced Raman spectroscopy. *Talanta* 186, 427–432. doi: 10.1016/j.talanta.2018.04.094

**Conflict of Interest:** The authors declare that the research was conducted in the absence of any commercial or financial relationships that could be construed as a potential conflict of interest.

Copyright © 2020 Jurásek, Bartuněk, Huber, Fagan, Setnička, Králík, Dehaen, Svoviz and Kuchar. This is an open-access article distributed under the terms of the Creative Commons Attribution License (CC BY). The use, distribution or reproduction in other forums is permitted, provided the original author(s) and the copyright owner(s) are credited and that the original publication in this journal is cited, in accordance with accepted academic practice. No use, distribution or reproduction is permitted which does not comply with these terms.



# High-Throughput Qualitative and Quantitative Drug Checking by MALDI HRMS

Timothée Joye<sup>1,2</sup>, Christèle Widmer<sup>1</sup>, Roxane Morger Mégevand<sup>3</sup>, Serge Longère<sup>3</sup>, Marc Augsburger<sup>1</sup> and Aurélien Thomas<sup>1,2\*</sup>

<sup>1</sup> Forensic Toxicology and Chemistry Unit, CURML, Lausanne University Hospital, Geneva University Hospitals, Geneva, Switzerland, <sup>2</sup> Faculty Unit of Toxicology, CURML, Faculty of Biology and Medicine, University of Lausanne, Lausanne, Switzerland, <sup>3</sup> Nuit Blanche?, Association Première Ligne, Geneva, Switzerland

## OPEN ACCESS

### Edited by:

Eugenia Gallardo,  
Faculty of Health Sciences, University  
of Beira Interior, Portugal

### Reviewed by:

Francesco Paolo Busardò,  
Sapienza University of Rome, Italy  
Jose Restolho,  
University of Beira Interior, Portugal

### \*Correspondence:

Aurélien Thomas  
aurelien.thomas@chuv.ch

### Specialty section:

This article was submitted to  
Analytical Chemistry,  
a section of the journal  
Frontiers in Chemistry

**Received:** 15 April 2020

**Accepted:** 06 July 2020

**Published:** 25 August 2020

### Citation:

Joye T, Widmer C,  
Morger Mégevand R, Longère S,  
Augsburger M and Thomas A (2020)  
High-Throughput Qualitative and  
Quantitative Drug Checking by MALDI  
HRMS. *Front. Chem.* 8:695.  
doi: 10.3389/fchem.2020.00695

Illicit drugs are a global health problem, since both their acute and chronic consumption have negative impacts on the drug user's health. Drug checking facilities are receiving growing interest as they allow drug users to chemically analyze their product prior to consumption to assess the presence of adulterants or other non-expected substances. Such harm reduction programs allow the reduction of the risks associated with drug consumption without encouraging it. In particular, the emergence of new psychoactive substances (NPS) emphasizes the risk for the population increasing the diversity and the lability of illicit drugs on the market. Analytical developments are required to catch up with this rapid evolution and reduce the potential harm caused by such consumption. In this study, we developed a matrix-assisted laser desorption/ionization (MALDI) high-resolution mass spectrometry (HRMS) strategy for the high-throughput qualitative and quantitative analysis of drug checking samples. The use of online-based m/z cloud library for untargeted compound search improved the ability to identify unknown compounds. Sixty-seven drug checking samples were analyzed using this analytical strategy, allowing the detection of 10 designer drugs and several classical drugs of abuse (mainly cocaine and MDMA) as well as adulterants and contaminants. The results were then compared with routine analyses of the same samples using conventional approaches showing similar performance while removing the use of chromatographic separation thus resulting in a significant reduction of the time required for sample preparation and analysis. This study enlightens the potential of MALDI-HRMS as a high-throughput approach allowing to speed-up up to six times the identification and quantification of substances enabling to catch the fast changes on the drug of abuse market. This strategy could be an interesting alternative analytical approach, allowing better prevention and harm reduction for drug users.

**Keywords:** MALDI, drug checking, qualitative, quantitative, HRMS, high throughput

## INTRODUCTION

The use of recreational drugs is widespread worldwide, and both the number of users and the diversity of substances are increasing. In Europe, for instance, almost 25% of adults reported at least one illicit drug consumption in their life (Liakoni et al., 2018). In Australia, the situation is more concerning, indeed, in 2016, more than 40% of the population over 14 years old reported a

drug use during their lifetimes and more than 15% during the month preceding the survey (Day et al., 2018). Illicit drugs are a global public health issue, since both their acute and chronic consumption have pernicious impacts on the consumer's health (Crowley et al., 2017; Joye et al., 2017; Vearrier, 2019). For instance, it is estimated that almost 10,000 overdose deaths occurred in Europe in 2017 (EMCDDA, 2019).

The risk associated with drug consumption has also increased with the emergence of new psychoactive substances (NPS) or designer drugs leading to a significantly growing number of emergency admissions and fatal overdoses (Miliano et al., 2016). NPS are a rapidly evolving class of substances with various physico-chemical properties and toxicological effects. This class of molecules can be defined as all the substances that are not controlled by the United Nations Single Convention on Narcotic Drugs or the United Nations Convention on Psychotropic substances but might pose public health issues and are often "classical" drugs of abuse derivatives (Khaled et al., 2016). Between 2012 and 2017, more than 400 NPS were monitored for the first time (Elliott et al., 2018). The risk with those substances is that only limited information is available regarding their toxicity for both the drug user and the healthcare professionals (Wood et al., 2016). Various analytical procedures have been published for NPS monitoring in classical and alternative matrices, especially regarding new synthetic opioids (Pichini et al., 2017; Zawilska, 2017; Marchei et al., 2018). For instance, screening procedures targeting a wide range of NPS and designer stimulants as well as studies focusing on designer benzodiazepines have been reported (Adamowicz and Tokarczyk, 2016, 2019; Zawilska and Wojcieszak, 2019). The development of those procedures alongside with the sharing of information through early warning systems is capital to reduce the risk of intoxications and fatalities associated with NPS consumption.

Various drug checking facilities have emerged in the past 20 years. Those facilities allow the drug users to chemically analyze their drugs to check for the presence of adulterants or other non-expected substances without encouraging drug consumption (Sande and Sabic, 2018). Such harm reduction programs provide several advantages such as gaining contact with hard-to-reach target group to provide information and counsel for an increased prevention (Hungerbuehler et al., 2011). The analysis of those substances also provides information regarding the prevalence of drug consumption including NPS arriving on the market and allows the monitoring of a potential altered substance presenting risks. Indeed, evidence also suggests the potential synergistic effect of certain toxic adulterants associated with the illicit drugs leading to overdoses, severe health consequences, and even deaths (Solimini et al., 2017; Singh et al., 2020).

On an analytical point of view, the continuous emergence of new drugs presents an ongoing challenge for clinical and forensic toxicology. Neither the serious toxicity or impairment caused by such substances, nor the analytical methods for their detection and identification is well-established (Peters and Martinez-Ramirez, 2010). To adapt to this constant apparition of new substances and the importance of controlling the substances consumed by drug users, it

is necessary to develop analytical tools enabling fast and reliable screening.

Among those analytical approaches, matrix-assisted laser desorption/ionization (MALDI) allows a quick and simple sample preparation. A wide range of use of MALDI technology has been reported for drug monitoring. For instance, MALDI ionization has been used for drug analysis in hair (Vogliardi et al., 2010; Porta et al., 2011; Flinders et al., 2017) and drug mapping in organs or whole-body tissue sections for pharmacodynamic or toxicodynamic studies (Lietz et al., 2013; Sun and Walch, 2013; Patel et al., 2015). Interestingly, an Austrian research group reported the successful use of MALDI combined with high-resolution (HR) MS for the qualitative analysis on drug checking samples focusing on designer drugs (Ostermann et al., 2014). Indeed, the introduction of HRMS analyzers and especially Orbitrap technology increases mass accuracy, allowing the facilitation of identification by reducing the number of possible chemical formulas (Jagerdeo and Schaff, 2016; Joye et al., 2020). Moreover, by improving the mass resolution power, HRMS increases the selectivity, therefore reducing the potential interferences (Chindarkar et al., 2014). Therefore, MALDI-HRMS technology seems to be an interesting alternative to classical GC and LC-MS/MS analyses providing a fast high-throughput complementary approach with a high identification power.

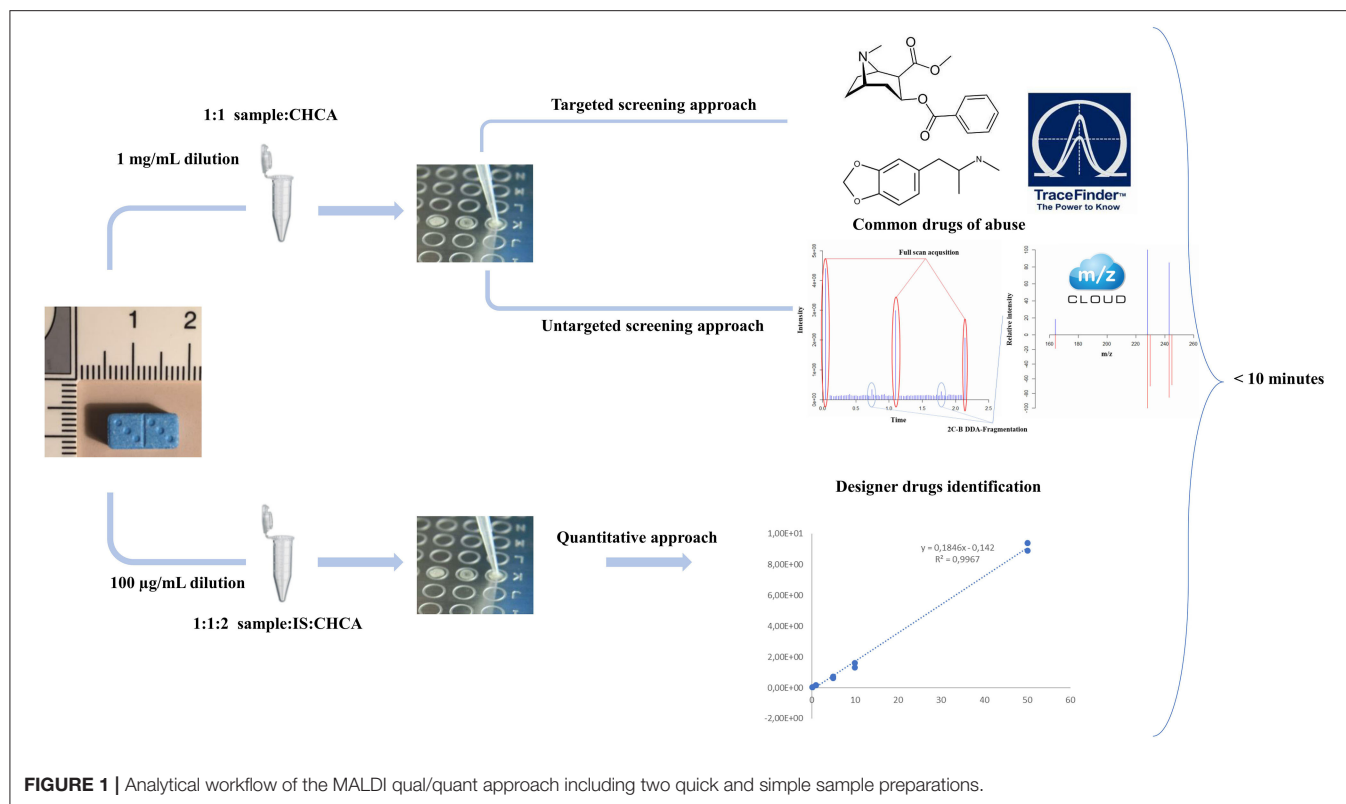
The present study was performed in collaboration with the association "Nuit Blanche" whose goal is to limit the risks associated with drug consumption in the nightlife context of the Swiss Canton of Geneva. This association collects drug checking samples on a weekly basis that are routinely analyzed by GC-MS regarding the screening approach and by LC-MS for the quantitative analyses focusing on 12 substances. Herein, we present a MALDI-HRMS procedure allowing the high-throughput identification of a wide range of drugs of abuse present in drug checking samples based on the online *m/z* cloud library for untargeted compound search.

The method was applied to 67 real drug checking cases revealing several NPS among the analyzed samples, as well as adulterants. Globally, the method resulted in similar performances than the conventional routine analyses with a significant reduction of the analysis time. In the meantime, the samples were quantified for the most detected drugs of abuse using a single and simple sample preparation. To demonstrate the potential of MALDI quantification in the context of drug checking samples, we further performed a validation according to the FDA (Food and Drug Administration) guidelines. The results of this high-throughput qualitative and quantitative approach were then compared with the classical methodology used in routine showing similar results.

## METHODS

### Standard and Reagents

Drug checking samples were provided by the harm reduction association "Nuit Blanche." LSD, methamphetamine, MDEA, MDMA, amphetamine, mephedrone, and cocaine, as well as their deuterated analogs, were purchased as standards at 1



mg/ml either from Cerilliant or Lipomed. Acetonitrile (ULC-MS 99.99%), methanol (ULC-MS 99.99%), water (ULC-MS), formic acid 99% (ULC-MS), trifluoroacetic acid, as well as the ammonium formate salt were purchased from Biosolve. Alpha-Cyano-4-hydroxycinnamic acid (CHCA) was purchased from Sigma-Aldrich.

## Sample Preparation

Regarding MALDI experiments, all samples were prepared at 1 mg/ml and 100 µg/ml for qualitative and quantitative analyses, respectively. For qualitative analysis, 10 µl of the sample solution was mixed with 10 µl of matrix solution (CHCA 1 mg/ml, 1:1 ACN: H<sub>2</sub>O + 0.1% TFA). Concerning quantitative analyses, 5 µl of sample solution was first mixed with 5 µl of internal standard (IS) solution. Ten microliters of matrix solution was then added to the mix. The IS solution was prepared containing deuterated LSD, methamphetamine, MDEA, MDMA, amphetamine, mephedrone, and cocaine at 10 µg/ml. Calibration samples were prepared by spiking MeOH at five concentration levels (six considering a blank) ranging from 0.1 to 50 µg/ml with the same undeuterated substances than in the IS solution; 1.5 µl of sample/matrix solution was then spotted on a MALDI stainless steel samples plate for analysis.

An experiment was conducted in order to evaluate the minimal number of acquire spectra to minimize the variability and, therefore, perform accurate quantification. Five samples were prepared using MDMA at 10 µg/ml with a 1:1 drug-to-IS ratio. Five replicates were used to determine intra-spot variability

and the relative standard deviation of the signal at 1, 10, 20, 50, 100, and 150 laser shots, respectively.

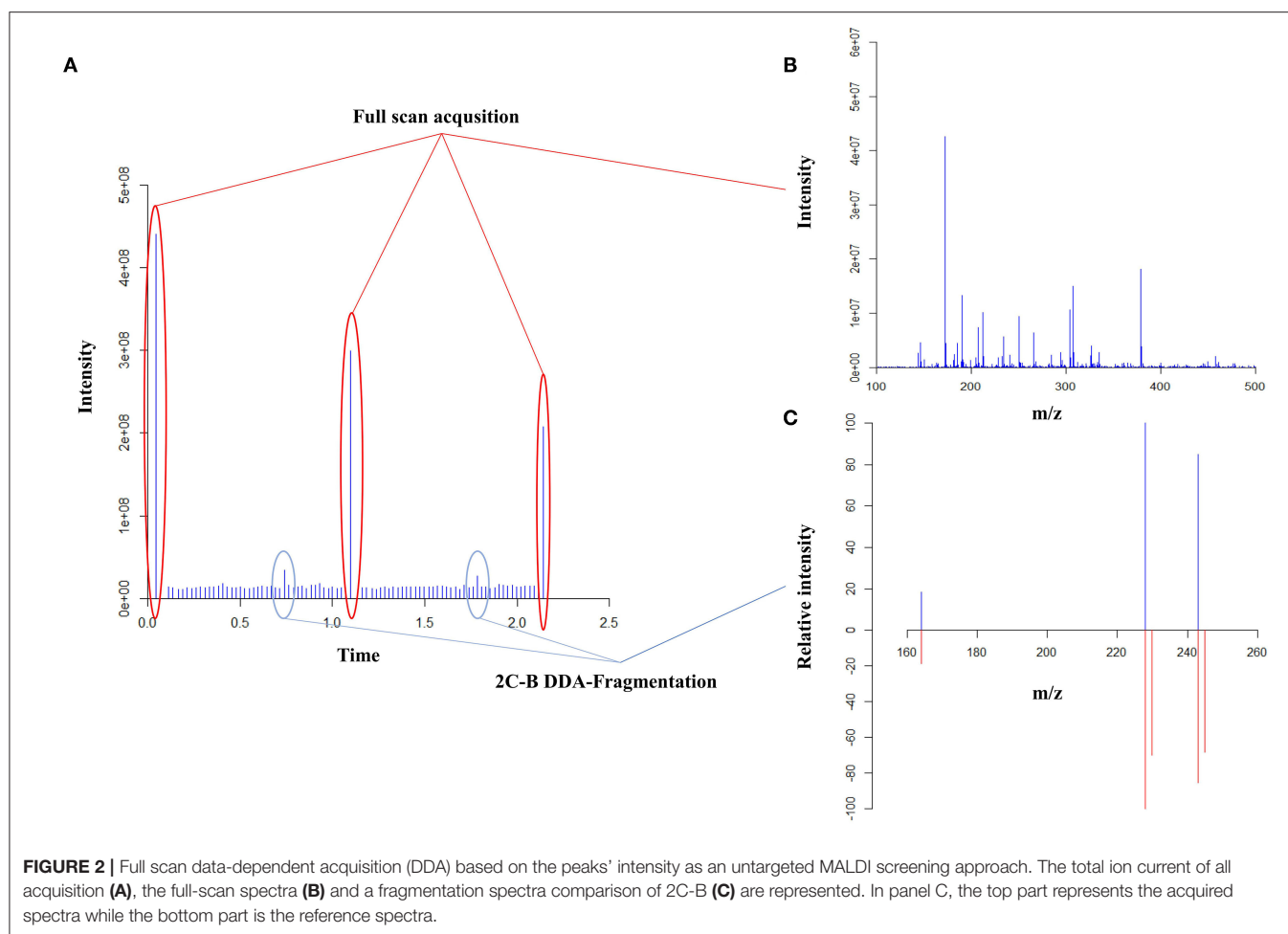
Routine analyses were performed using two different sample preparations including simple dilutions at 100 µg/ml and 200 ng/ml and a derivation step. Regarding GC-MS screening analyses, a first injection was performed with the diluted samples at 100 µg/ml. For the second injection, 100 µl of the 100 µg/ml sample solution was mixed with 100 µl of anhydric acetic acid and 100 µl of pyridine for derivation. After vortexing, the samples were incubated at 60°C for 30 min. Samples were then evaporated and reconstituted in 100 µl of MeOH. For the quantitative analyses, the dilution at 200 ng/ml was performed in a 50/50 mix of formate buffer 5 mM at pH 3 and MeOH containing IS at a final concentration of 10 ng/ml. Calibration samples were prepared by spiking MeOH at five concentration levels ranging from 1 to 500 ng/ml.

## MALDI Analyses

All samples were analyzed in a three-step process (**Figure 1**). A first targeted approach targeting the most common drugs of abuse and adulterant was processed, followed by a non-targeted data-dependent acquisition for the detection and identification of other drugs, adulterants, or dangerous contaminants. Then, a full-scan experiment was operated for quantitative analysis.

All MALDI-HRMS experiments were performed using a MALDI-LTQ-Orbitrap XL equipped with a 337-nm N<sub>2</sub> laser operating at 60 Hz (Thermo Scientific, Bremen, Germany) with a laser beam size of 60 × 50 µm. All analyses were performed





with a spectral resolution of 60,000 for full-scan experiments and 17,500 regarding fragmentation. Both the automatic spectral filtering (ASF) and the automatic gain control (AGC) were switched off. MALDI plate motion was set to survey CPS. MALDI laser energy was set to 5  $\mu\text{J}$  and the number of laser shot was set to five in positive polarity. The scan masses were ranging from 100 to 1,000  $m/z$ .

Regarding qualitative analyses, first, a full-scan data-dependant MS/MS approach was performed using an inclusion list of 41 substances containing the most frequent drugs of abuse and adulterants (**Table S1**). Fragmentation experiments were performed using higher-energy collisional dissociation (HCD) with normalized collision energy set between 30 and 100 eV depending on the compounds of interest. The second full-scan data-dependent approach was then performed for the detection of other drugs, adulterants or contaminants using a non-targeted approach (**Figure 2**). Based on the full-scan spectra, the 10 most intense ions were then fragmented using HCD with a normalized energy of 50 eV. A minimum signal threshold was set to 10,000 to avoid fragmenting noise. All fragmented compounds were then sent to an exclusion list already containing the targeted substances for 3 min to avoid fragmenting always the same substances. Quantitative analyses were performed averaging

120 acquired full-scan spectra. The validation criteria used to evaluate the analytical process was based on the directives of the FDA regarding bioanalytical methods and adapted to our specific requirements. The validation was performed over three non-consecutive days ( $p = 3$ ). The trueness and precision were evaluated using a variance analysis-based statistical treatment (ANOVA). Calibration (Cal) was performed in duplicate at five different concentration levels ( $k = 5$ ) (**Table 1**) while quality controls (QCs) were prepared in quadruplicate at the two lowest and highest concentration levels ( $k = 4$ ). Using the acquired data, trueness, precision, accuracy, and linearity were determined.

## Routine Analyses

GC screening analyses were performed using an existing published procedure on a similar instrument (Lefrancois et al., 2016). For the LC-MS/MS quantitative analyses, a Dionex UltiMate 3000 LC-system (Thermo Fischer Scientific, Germany) was used. Gradient elution was performed on a Chromolith Performance RP-C18 (100  $\times$  3 mm) column using a 5 mM formate ammonium buffer at pH 3 (mobile phase A) and acetonitrile (mobile phase B). The gradient and flow rate were programmed as follows: 0–0.2 min hold at 2% B; 0.2–8 min

**TABLE 1 |** Results for trueness, precision, and linearity ( $k$  is the number of concentration levels,  $n$  the number of repetitions by levels, and  $p$  is the number of non-consecutive days).

Trueness (%) ( $k = 4$ ; $n = 4$ ; $p = 3$ )				
Calibration level (ng/ml)	100	1,000	10,000	50,000
MDMA	102.7	103.3	109.0	100.7
Cocaine	97.3	103.9	114.4	99.6
Repeatability/Intermediate precision (RSD%) ( $k = 4$ , $n = 4$ , $p = 3$ )				
Calibration level (ng/ml)	100	1,000	10,000	50,000
MDMA	11.6/11.1	13.0/12.3	9.3/10.5	7.0/7.6
Cocaine	12.2/13.7	10.2/11.6	5.9/7.6	4.3/3.9
Linearity ( $k = 4$ , $n = 4$ , $p = 3$ )				
	Range (ng/ml)	Slope	$R^2$	Exact mass (m/z)
MDMA	100–50,000	1.0037	0.9913	194.1176
Cocaine	100–50,000	0.9909	0.9966	304.1543

linear increase to 70% B; 8–10 min linear increase to 95% of B; 10–11 min hold at 95% B; 11–14 min hold at 2% B at a constant flow rate of 0.6 ml/min. The injection volume was set to 1  $\mu$ l. The LC system was coupled with a QTRAP 5500 MS instrument (SCIEX, Netherlands). The mass spectrometer was operated with positive electrospray ionization in multiple reaction monitoring (MRM) mode. The ion spray voltage was set to 5,500 V and the source temperature was 500°C. The gas settings were as follows: Curtain gas: 20 psi, ion source gas 1: 60 psi, ion source gas 2: 40 psi.

## Data Analysis

Information regarding the suspected sample's composition was almost always provided by the drug user. Then, MALDI data were analyzed using Tracefinder (Thermo Scientific) and a database created for this specific drug checking application. Identification was based on the mass over charge ratio, the isotopic pattern, and the library search based on MS/MS spectra comparison. Regarding the samples containing a substance that was not indexed in the library, Xcalibur was used combined with different external library search such as Metlin or m/z cloud. The data were analyzed using MSD Enhanced ChemStation (Agilent Technologies) and compound characterization was performed using mass spectra computerized databases, such as NIST Version 2014 (National Institute of Standards and Technology), Wiley Edition 10, MPW Version 2011 (Maurer, Pfeleger, Weber, Drugs, Poisons, Pesticides, Pollutants, and Metabolites), DD Version 2014 (Drug Design and Discovery) and custom databases from the University Institutes of Legal Medicine of the Faculty of Medicine of Geneva (CURML). Quantitative results were treated using Analyst software version 1.6.2.

## RESULTS AND DISCUSSION

### MALDI Qualitative Analyses

Consumption of drugs of abuse is a global public health issue. In particular, the emergence of NPS including the classes of phenethylamine and tryptamine emphasizes the risk for the

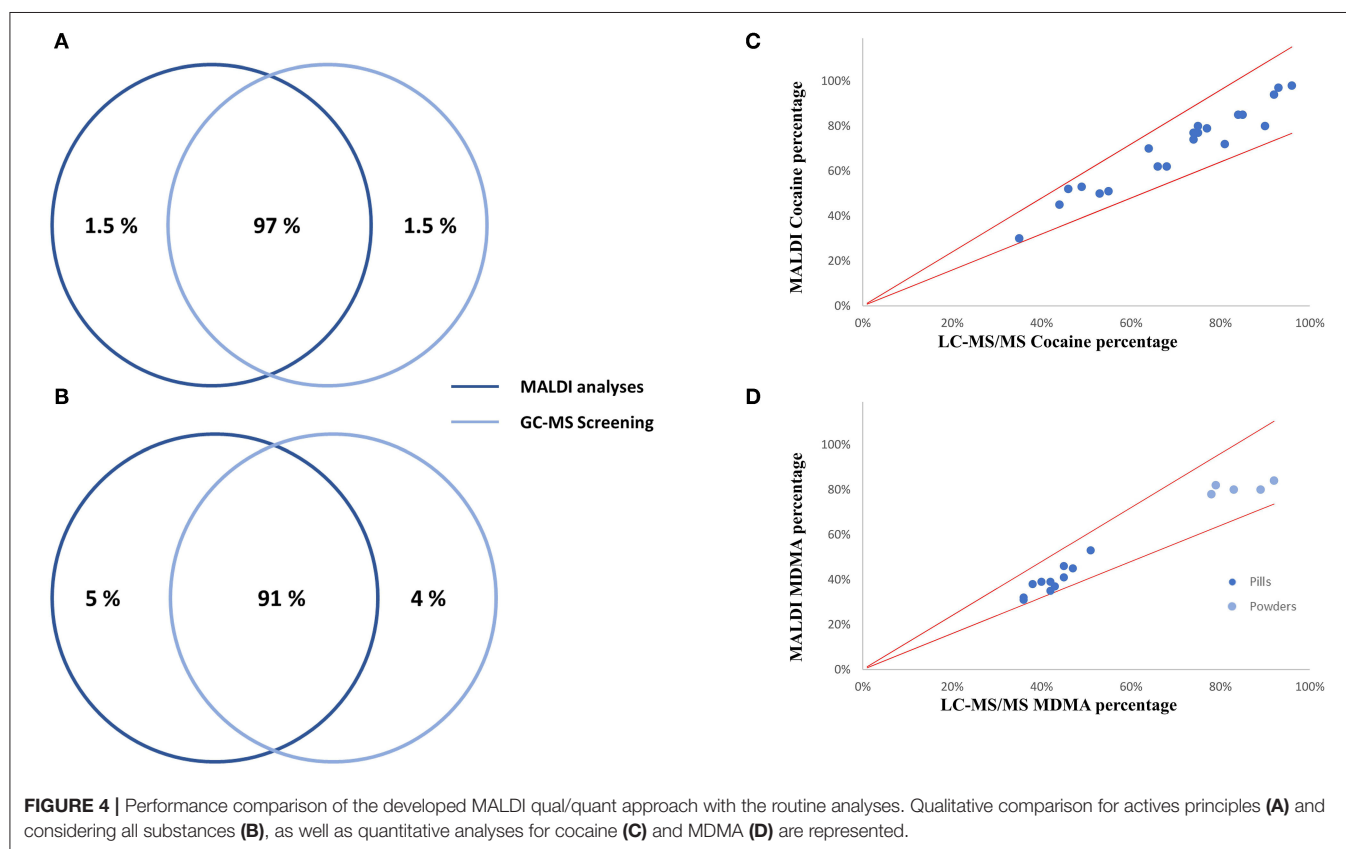
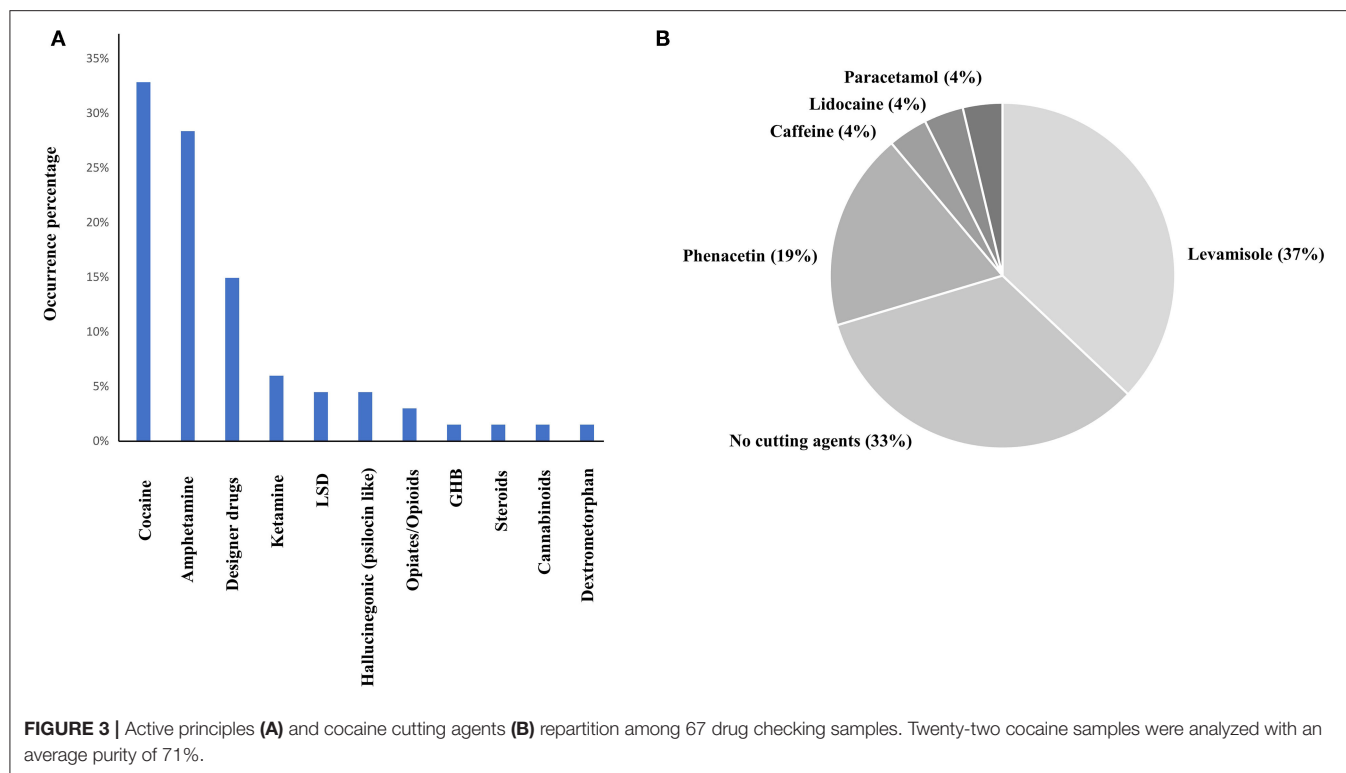
population. Therefore, the development of new fast screening procedures allowing the identification of known and unknown drugs of abuse is a priority to keep up with the ongoing developments on the illicit drug market. The association of highly concentrated analytes with the increased selectivity brought by HRMS technology allows the facilitation of high-throughput MALDI detection and identification of various unknown substances.

With the developed MALDI-HRMS method, several designer drugs were successfully identified including 2,5-dimethoxy-4-methylamphetamine (DOM), 2,5-dimethoxy-4-bromoamphetamine (DOB), 2,5-dimethoxy-4-chloroamphetamine (DOC), 2,5-dimethoxy-4-bromophenethylamine (2C-B) and its position isomer 2-Br-4,5-DMPEA, 2,5-dimethoxy-4-ethylphenethylamine (2C-E), methoxetamine, 4-hydroxy-N-methyl-N-ethyltryptamine (4-HO-MET), 6-(2-aminopropyl)benzofuran (6-APB), and clephedrone. Moreover, the MALDI analysis allowed the identification of various adulterants, contaminations, impurities, and synthesis precursors such as safrole, which is used for the synthesis of MDMA.

In total, 67 drug checking samples were analyzed with the developed procedure leading to 101 identifications including 36 different substances (Table S2). Despite the identification of several designer drugs, most samples contained classical drugs of abuse, with 22 samples positive to cocaine and 16 samples positive to MDMA. All the active principles detected using both approaches are represented in Figure 3A. On average, the cocaine purity detected in the 22 samples was high (71%), among them, 10 were containing levamisole, while 9 of them were not containing any cutting agents (Figure 3B). Only classical cocaine cutting agents were identified, yet the identification of such substances is of importance since evidence suggests the concomitant role of certain adulterants and illicit drugs on toxicity (Solimini et al., 2017). The GC-MS screening approach, which is the gold standard for qualitative analyses, showed similar performances to the developed MALDI procedure. Indeed, only one active principle (GHB) was not detected using MALDI-HRMS. Among the cutting agents, metabolites, precursors and alkaloids, one cocaine metabolite (tropacocaine in two samples), and one adulterant (phenacetine) were not detected by the developed approach. On the other hand, one active principle (clephedrone), one cocaine adulterant (levamisole in two samples), one cocaine alkaloid (cinnamoylcocaine), and one MDMA precursor (safrole) were not detected by the GC-MS approach (Figure 3). With a coverage of 98.5% regarding the active principles and 91% considering all the substances (see Figures 4A,B), the main difference between those two approaches was that the use of MALDI analyses allowed the reduction of the time spent for the sample preparation with the removal of the derivation process and the analysis by a six times factor reaching a total analysis times of around 10 min per sample.

### MALDI Quantitative Analyses

MALDI analyses are often associated with a relatively important variability regarding signal intensity. Therefore, MALDI



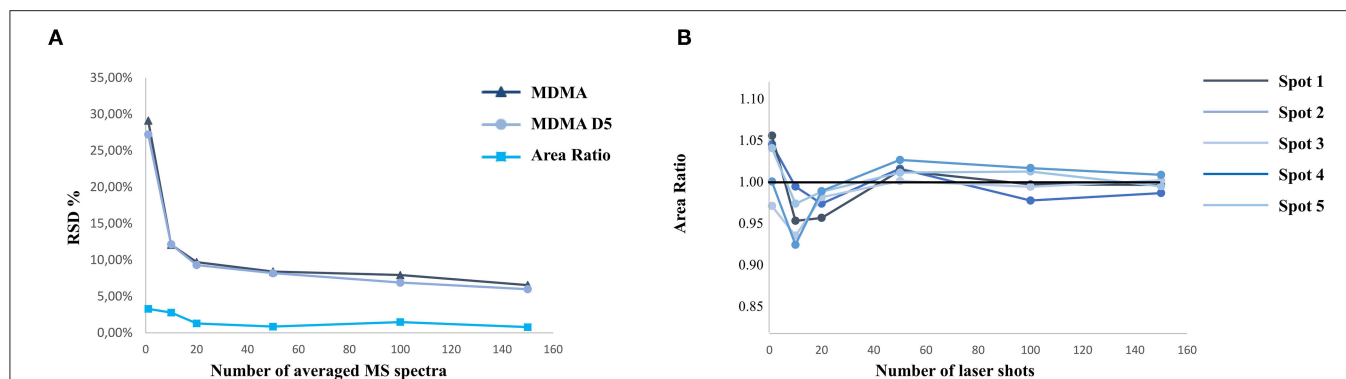


**FIGURE 5 |** Relative standard deviation (%) associated with MALDI analysis as a function of the number of averaged acquisition points (A). Intra-spot variability and accuracy depending on the number of laser shot averaged per acquisition (B).

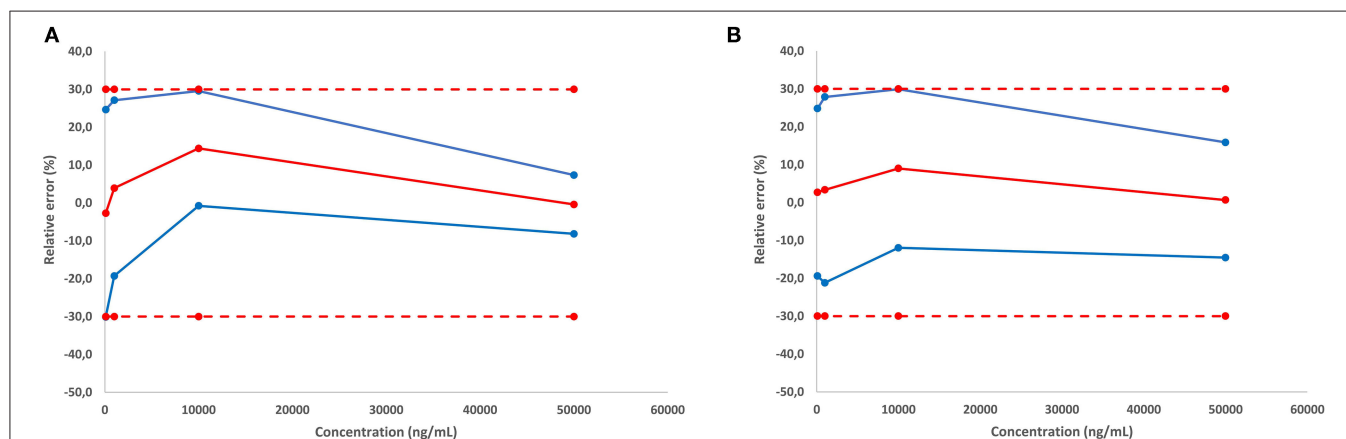


**FIGURE 6 |** Accuracy profile for cocaine (A), and MDMA (B).

quantification requires specific development to ensure good results in terms of accuracy, precision, and repeatability (Porta et al., 2015). One solution to limit this specific signal variability issue is to normalize the intensity obtained by averaging enough acquired pixels. One of the challenges is to find the right compromise between the time of acquisition associated with the number of averaged spectra and a good accuracy and precision. During this study, tests were performed to optimize the acquisition time with a limited variability. As demonstrated in the literature, our results enlightened the need for isotopically labeled IS and acquisition of a sufficient number of spectra to decrease relative standard deviation below 10% (Figure 5) (Ostermann et al., 2014; Porta et al., 2015). As demonstrated in Figure 5, the acquisition of more than 100 averaged spectra was thus necessary to obtain good repeatability and accuracy.

The validation of the quantitative approach was performed for cocaine and MDMA by analyzing independent QC samples in quadruplicates at four different calibration levels over three non-consecutive days for the determination of trueness, precision, and linearity. Accuracy represents the total error and can

be divided into two parameters including trueness (bias or systematic error) and precision (the standard deviation or random errors). Trueness is calculated using the percentage difference between the experimental and the expected values. In the present study, trueness was ranging from -2.7 to 14.4% (Table 1). Precision was divided into repeatability and the inter-day variability (intermediate precision). Repeatability represents the variability under similar conditions performed by the same operator while intermediate precision is the variability associated with the use of the same samples on different days with different reagents. Repeatability and intermediate precision were measured between 3.9 and 13.7% (Table 1). Accuracy profiles are visual representations of the uncertainty measurement combining the trueness and precision (Figure 6). Precision is represented by the calculated confidence limit at 95% for each concentration limit. Accuracy profiles also include the representation of acceptance limits of  $\pm 30\%$  suggested for method validation. Linearity is defined as the method capacity to provide a result proportional to the real sample concentration. Its determination requires linear regression model based on the least square method applied on the fit of the obtained concentrations

as a function of the expected concentrations. Slope values were calculated at 1.0037 and 0.9909 with coefficients of determination of 0.9913 and 0.9966 for MDMA and cocaine, respectively.

Overall, MALDI quantitative results showed a good correlation with the routine LC-MS/MS MRM experiments. Indeed, all MALDI results were in agreement with the routine analysis with a  $\pm 20\%$  tolerance window. The correlation between the two analytical strategies is represented in **Figure 4** for cocaine and MDMA, being the two most detected substances. Interestingly, among all MDMA-positive cases, two groups can be distinguished. Indeed, all the samples in the form of pills had an MDMA percentage between 31 and 52%, while this percentage was measured between 78 and 84% regarding powders (**Figure 4D**). MALDI quantitation analyses were performed in around 3 min per sample while one LC injection lasted for 14 min. With the HRMS quantification being based on full-scan spectra, the addition of new substances of interest can easily be performed without the need of any preliminary developments such as infusion processes.

## CONCLUSION

In this study, we enlighten the potential of MALDI-HRMS as a high-throughput analytical strategy in forensic and clinical toxicology. This technology can bring interesting applications despite the absence of chromatographic separation, which may be detrimental for the analysis of low-concentration analytes in complex matrices. Nevertheless, considering drug checking analysis where the analytes can be concentrated at will, MALDI-HRMS allows one to significantly speed up the detection, identification, and quantification of various drugs of abuse. With the development of bioinformatic tools and online shared libraries such as m/z cloud, the method can easily be adapted for any new substance appearing on the market being in agreement with the challenges brought by the continuous emergence of NPS.

## REFERENCES

- Adamowicz, P., and Tokarczyk, B. (2016). Simple and rapid screening procedure for 143 new psychoactive substances by liquid chromatography-tandem mass spectrometry. *Drug Test. Anal.* 8, 652–667. doi: 10.1002/dta.1815
- Adamowicz, P., and Tokarczyk, B. (2019). Screening analysis for designer stimulants by LC-MS/MS. *Methods Mol. Biol.* 1872, 165–180. doi: 10.1007/978-1-4939-8823-5\_16
- Chindarkar, N. S., Wakefield, M. R., Stone, J. A., and Fitzgerald, R. L. (2014). Liquid chromatography high-resolution TOF analysis: investigation of MSE for broad-spectrum drug screening. *Clin. Chem.* 60, 1115–1125. doi: 10.1373/clinchem.2014.222976
- Crowley, R., Kirschner, N., Dunn, A. S., Bornstein, S. S., and Health and Public Policy Committee of the American College of Physicians. (2017). Health, and public policy to facilitate effective prevention and treatment of substance use disorders involving illicit and prescription drugs: an american college of physicians position paper. *Ann. Intern. Med.* 166, 733–736. doi: 10.7326/M16-2953
- Day, N., Criss, J., Griffiths, B., Gujral, S. K., John-Leader, F., Johnston, J., et al. (2018). Music festival attendees' illicit drug use, knowledge and practices regarding drug content and purity: a cross-sectional survey. *Harm Reduct. J.* 15:1. doi: 10.1186/s12954-017-0205-7
- Elliott, S., Sedefov, R., and Evans-Brown, M. (2018). Assessing the toxicological significance of new psychoactive substances in fatalities. *Drug Test. Anal.* 10, 120–126. doi: 10.1002/dta.2225
- EMCDDA (2019). *Drug-Related Deaths and Mortality in Europe: Update From the EMCDDA Expert Network*. Lisbon: EMCDDA.
- Flinders, B., Cuypers, E., Porta, T., Varesio, E., Hopfgartner, G., and Heeren, R. M. A. (2017). Mass spectrometry imaging of drugs of abuse in hair. *Methods Mol. Biol.* 1618, 137–147. doi: 10.1007/978-1-4939-7051-3\_12
- Hungerbuehler, I., Buecheli, A., and Schaub, M. (2011). Drug checking: a prevention measure for a heterogeneous group with high consumption frequency and polydrug use—evaluation of zurich's drug checking services. *Harm Reduct. J.* 8:16. doi: 10.1186/1477-7517-8-16
- Jagerdeo, E., and Schaff, J. E. (2016). Rapid screening for drugs of abuse in biological fluids by ultra high performance liquid chromatography/Orbitrap mass spectrometry. *J. Chromatogr. B Analyt. Technol. Biomed. Life Sci.* 1027, 11–18. doi: 10.1016/j.jchromb.2016.05.010
- Joye, T., Bararpour, N., Augsburger, M., Boutrel, B., and Thomas, A. (2017). *In situ* metabolomic changes in rat hippocampus after acute cocaine administration. *Int. J. Mass Spectrom.* 437, 87–91. doi: 10.1016/j.jms.2017.12.001
- Joye, T., Widmer, C., Favrat, B., Augsburger, M., and Thomas, A. (2020). Parallel reaction monitoring-based quantification of cannabinoids in whole blood. *J. Anal. Toxicol.* 44, 541–548. doi: 10.1093/jat/bkz113

The developed approach showed similar qualitative and quantitative results for drug checking compared to those obtained from both LC-MS and GC-MS while reducing by six times the analytical procedure. The development of such rapid drug checking strategies would enable faster monitoring of changes in the drug market, providing an improved tool for prevention and harm reduction for drug users.

## DATA AVAILABILITY STATEMENT

The raw data supporting the conclusions of this article will be made available by the authors, without undue reservation.

## AUTHOR CONTRIBUTIONS

TJ developed the analytical method did the samples analyses and wrote the manuscript. CW and MA participated in the strategic choices toward the study and its design and critically revised the manuscript. RM and SL provided the samples and critically revised the manuscript. AT was the main contributor to the study design, supervised the project, and critically revised the manuscript. All authors contributed to the article and approved the submitted version.

## FUNDING

The authors acknowledge financial support from the Swiss Federal Office of Public Health (contract no. 14.013792.204.0001/1300).

## SUPPLEMENTARY MATERIAL

The Supplementary Material for this article can be found online at: <https://www.frontiersin.org/articles/10.3389/fchem.2020.00695/full#supplementary-material>



- Khaled, S. M., Hughes, E., Bressington, D., Zolezzi, M., Radwan, A., Badnapurkar, A., et al. (2016). The prevalence of novel psychoactive substances (NPS) use in non-clinical populations: a systematic review protocol. *Syst. Rev.* 5:195. doi: 10.1186/s13643-016-0375-5
- Lefrançois, E., Esseiva, P., Gervasoni, J. P., Lucia, S., Zobel, F., and Augsburg, M. (2016). Analysis of residual content of used syringes collected from low threshold facilities in Lausanne, Switzerland. *Forensic Sci. Int.* 266: 534–540. doi: 10.1016/j.forsciint.2016.07.021
- Liakoni, E., Yates, C., Dines, A. M., Dargan, P. I., Heyerdahl, F., Hovda, K. E., et al. (2018). Acute recreational drug toxicity: comparison of self-reports and results of immunoassay and additional analytical methods in a multicenter European case series. *Medicine* 97:e9784. doi: 10.1097/MD.00000000000009784
- Lietz, C. B., Gemperline, E., and Li, L. (2013). Qualitative and quantitative mass spectrometry imaging of drugs and metabolites. *Adv. Drug Deliv. Rev.* 65, 1074–1085. doi: 10.1016/j.addr.2013.04.009
- Marchei, E., Pacifici, R., Mannocchi, G., Marinelli, E., Busardo, F. P., and Pichini, S. (2018). New synthetic opioids in biological and non-biological matrices: a review of current analytical methods. *Trends Anal. Chem.* 102, 1–15. doi: 10.1016/j.trac.2018.01.007
- Milano, C., Serpelloni, G., Rimondo, C., Mereu, M., Marti, M., and De Luca, M. A. (2016). Neuropharmacology of new psychoactive substances (NPS): focus on the rewarding and reinforcing properties of cannabinimetics and amphetamine-like stimulants. *Front. Neurosci.* 10:153. doi: 10.3389/fnins.2016.00153
- Ostermann, K. M., Luf, A., Lutsch, N. M., Dieplinger, R., Mechtler, T. P., Metz, T. F., et al. (2014). MALDI orbitrap mass spectrometry for fast and simplified analysis of novel street and designer drugs. *Clin. Chim. Acta* 433, 254–258. doi: 10.1016/j.cca.2014.03.013
- Patel, E., Cole, L. M., Bradshaw, R., Batubara, A., Mitchell, C. A., Francese, S., et al. (2015). MALDI-MS imaging for the study of tissue pharmacodynamics and toxicodynamics. *Bioanalysis* 7, 91–101. doi: 10.4155/bio.14.280
- Peters, F. T., and Martinez-Ramirez, J. A. (2010). Analytical toxicology of emerging drugs of abuse. *Ther. Drug Monit.* 32, 532–539. doi: 10.1097/FTD.0b013e3181f33411
- Pichini, S., Pacifici, R., Marinelli, E., and Busardo, F. P. (2017). European drug users at risk from illicit fentanyl mix. *Front. Pharmacol.* 8:785. doi: 10.3389/fphar.2017.00785
- Porta, T., Grivet, C., Kraemer, T., Varesio, E., and Hopfgartner, G. (2011). Single hair cocaine consumption monitoring by mass spectrometric imaging. *Anal. Chem.* 83, 4266–4272. doi: 10.1021/ac200610c
- Porta, T., Lesur, A., Varesio, E., and Hopfgartner, G. (2015). Quantification in MALDI-MS imaging: what can we learn from MALDI-selected reaction monitoring and what can we expect for imaging? *Anal. Bioanal. Chem.* 407, 2177–2187. doi: 10.1007/s00216-014-8315-5
- Sande, M., and Sabic, S. (2018). The importance of drug checking outside the context of nightlife in Slovenia. *Harm Reduct. J.* 15:2. doi: 10.1186/s12954-018-0208-z
- Singh, V. M., Browne, T., and Montgomery, J. (2020). The emerging role of toxic adulterants in street drugs in the US illicit opioid crisis. *Public Health Rep.* 135, 6–10. doi: 10.1177/0033354919887741
- Solimini, R., Rotolo, M. C., Pellegrini, M., Minutillo, A., Pacifici, R., Busardo, F. P., et al. (2017). Adulteration practices of psychoactive illicit drugs: an updated review. *Curr. Pharm. Biotechnol.* 18, 524–530. doi: 10.2174/1389201018666170710184531
- Sun, N., and Walch, A. (2013). Qualitative and quantitative mass spectrometry imaging of drugs and metabolites in tissue at therapeutic levels. *Histochem. Cell Biol.* 140, 93–104. doi: 10.1007/s00418-013-1127-4
- Vearrier, L. (2019). The value of harm reduction for injection drug use: a clinical and public health ethics analysis. *Dis. Mon.* 65, 119–141. doi: 10.1016/j.disamonth.2018.12.002
- Vogliardi, S., Favretto, D., Frison, G., Maietti, S., Viel, G., Seraglia, R., et al. (2010). Validation of a fast screening method for the detection of cocaine in hair by MALDI-MS. *Anal. Bioanal. Chem.* 396, 2435–2440. doi: 10.1007/s00216-009-3387-3
- Wood, D. M., Ceronie, B., and Dargan, P. I. (2016). Healthcare professionals are less confident in managing acute toxicity related to the use of new psychoactive substances (NPS) compared with classical recreational drugs. *QJM* 109, 527–529. doi: 10.1093/qjmed/hcv208
- Zawilska, J. B. (2017). An expanding world of novel psychoactive substances: opioids. *Front. Psychiatry* 8:110. doi: 10.3389/fpsy.2017.00110
- Zawilska, J. B., and Wojcieszak, J. (2019). An expanding world of new psychoactive substances-designer benzodiazepines. *Neurotoxicology* 73, 8–16. doi: 10.1016/j.neuro.2019.02.015

**Conflict of Interest:** The authors declare that the research was conducted in the absence of any commercial or financial relationships that could be construed as a potential conflict of interest.

Copyright © 2020 Joye, Widmer, Morger Mégevand, Longère, Augsburg and Thomas. This is an open-access article distributed under the terms of the Creative Commons Attribution License (CC BY). The use, distribution or reproduction in other forums is permitted, provided the original author(s) and the copyright owner(s) are credited and that the original publication in this journal is cited, in accordance with accepted academic practice. No use, distribution or reproduction is permitted which does not comply with these terms.



# Driving Under the Influence of Drugs: A Single Parallel Monitoring-Based Quantification Approach on Whole Blood

Timothée Joye<sup>1,2</sup>, Katell Rocher<sup>1</sup>, Julien Déglon<sup>1</sup>, Jonathan Sidibé<sup>1</sup>, Bernard Favrat<sup>3,4</sup>, Marc Augsburger<sup>1</sup> and Aurélien Thomas<sup>1,2\*</sup>

<sup>1</sup> Forensic Toxicology and Chemistry Unit, CURML, Lausanne University Hospital, Geneva University Hospitals, Lausanne, Switzerland, <sup>2</sup> Faculty Unit of Toxicology, CURML, Faculty of Biology and Medicine, University of Lausanne, Lausanne, Switzerland, <sup>3</sup> Unit of Medicine and Traffic Psychology, CURML, Lausanne University Hospital, Geneva University Hospitals, Lausanne, Switzerland, <sup>4</sup> Center for Primary Care and Public Health (Unisanté), University of Lausanne, Lausanne, Switzerland

## OPEN ACCESS

### Edited by:

Ana de-Castro-Ríos,  
University of Santiago de  
Compostela, Spain

### Reviewed by:

Sarah M. R. Wille,  
National Institute for Criminalistics and  
Criminology (NICC), Belgium  
Marilyn A. Huestis,  
Thomas Jefferson University,  
United States

### \*Correspondence:

Aurélien Thomas  
aurelien.thomas@chuv.ch

### Specialty section:

This article was submitted to  
Analytical Chemistry,  
a section of the journal  
Frontiers in Chemistry

Received: 15 April 2020

Accepted: 15 June 2020

Published: 26 August 2020

### Citation:

Joye T, Rocher K, Déglon J, Sidibé J,  
Favrat B, Augsburger M and  
Thomas A (2020) Driving Under the  
Influence of Drugs: A Single Parallel  
Monitoring-Based Quantification  
Approach on Whole Blood.  
Front. Chem. 8:626.  
doi: 10.3389/fchem.2020.00626

Driving under the influence of psychoactive substances is a major cause of motor vehicle crashes. The identification and quantification of substances most frequently involved in impaired-driving cases in a single analytic procedure could be an important asset in forensic toxicology. In this study, a highly sensitive and selective liquid chromatography (LC) approach hyphenated with Orbitrap high-resolution mass spectrometry (HRMS) was developed for the quantification of the main drugs present in the context of driving under the influence of drugs (DUID) using 100  $\mu$ L of whole blood. This procedure involves a simple sample preparation and benefit from the selectivity brought by parallel reaction monitoring (PRM) allowing to solve most DUID cases using a single multi-analyte injection. The method was fully validated for the quantification of the major classes of psychoactive substances associated with impaired-driving (cannabinoids, cocaine and its metabolites, amphetamines, opiates and opioids, and the major benzodiazepines and z-drugs). The validation guidelines set by the “Société Française des Sciences et des Techniques Pharmaceutiques” (SFSTP) were respected for 22 psychoactive substances using 15 internal standards. Trueness was measured to be between 95.3 and 107.6% for all the tested concentrations. Precision represented by repeatability and intermediate precision was lower than 12% while recovery (RE) and matrix effect (ME) ranged from 49 to 105% and from -51 to 3%, respectively. The validated procedure provides an efficient approach for the simultaneous and simple quantification of the major drugs associated with impaired driving benefiting from the selectivity of PRM.

**Keywords:** parallel reaction monitoring, quantitative analysis, whole blood, driving under the influence of drugs, multi-analyte

## INTRODUCTION

Road crashes are a worldwide public health issue, causing a significant number of deaths and injuries each year. Indeed, 1.25 million people died and about 50 million were injured in road traffic crashes in 2015 according to the World Health Organization (2015). In addition, in Europe almost 25% of adults reported at least one instance of illicit drug consumption in their life

(Liakoni et al., 2018). These two issues are closely linked, since one of the major causes of road crashes is the consumption of psychotropic substances, including drugs and alcohol, resulting in driving impairment (Elliott et al., 2009; Favretto et al., 2018). For instance, in Norway, at least 21% of traffic crashes were related to either alcohol or drug use between 2005 and 2015 (Valen et al., 2019). The total number of victims of fatal crashes has significantly decreased in the past years in Western countries thanks to efficient prevention. Yet, the use of medicinal or illicit drug and/or alcohol is an increasing phenomenon in Europe (Snenghi et al., 2018; Pelletti et al., 2019), and the percentage of fatal crashes due to the driver's impairment remain constant (between 17 and 22% from 1995 to 2017) in Switzerland [Office Fédéral de la Statistique (OFS), 2018].

Due to the large variety of drugs and pharmaceuticals with various psychoactive effects, there is a need for medical experts to establish solid statement on a potential driving-impairment and for official quantification of drugs and alcohol levels in blood (Martin et al., 2017). In Switzerland, a zero tolerance with technical cut-offs is implemented regarding classical drugs of abuse (DoA) toward drivers (1.5 ng/ml for THC and 15 ng/ml for morphine, cocaine, amphetamine, methamphetamines, MDEA, and MDMA) (Walsh et al., 2004; Steuer et al., 2016). The situation is more complex regarding the consumption of medicinal drugs and the toxicological interpretation of their concentration (Ravera et al., 2012). With respect to the law, the driving capability under pharmaceuticals is concomitantly determined by a “three pillars expertise” including police assessment, medical expertise, and toxicological analysis in blood, being the biological matrix of reference regarding toxicological interpretation (Steuer et al., 2014). The Swiss Federal Roads Office (FEDRO) defines a list of controlled substances that the laboratories must be able to quantify in the context of external quality controls (EQCs) in whole blood regarding driving under the influence of drugs (DUID). Those recommendations, associated with the knowledge of drug prevalence among suspected drivers, were used to establish a list of substances of interest in the present study.

Improvements regarding instrumentation, notably brought on by the developments of Orbitrap technology, offer new opportunities in terms of analytical strategies (Hoffman et al., 2018; Joye et al., 2019). Indeed, various Orbitrap-based parallel reaction monitoring (PRM) applications have been reported, especially in the field of proteomics (Domon and Gallien, 2015; Rauniyar, 2015; Bourmaud et al., 2016). In a PRM acquisition, a precursor selected by a quadrupole is fragmented in a higher-energy collisional dissociation (HCD) cell (Ronsein et al., 2015). Following this experiment, all product ions are simultaneously acquired in the high-resolution Orbitrap analyzer. Up to now, the use of triple-quadrupole (QQQ) using Selected Reaction Monitoring (SRM) has been the gold standard regarding targeted quantitative analyses (Hopfgartner et al., 2004; Rauniyar, 2015). However, SRM and PRM have comparable sensitivity with similar linearities, dynamic ranges, precision, and repeatability (Domon and Gallien, 2015; Joye et al., 2020). Yet Orbitrap-based PRM offers further advantages, since the acquisition of all selected precursors' fragments is performed, thereby limiting the

*a priori* information required for method development. Indeed, the selection of quantifying ions is only necessary during the data processing step once the whole fragmentation spectra is acquired. Moreover, HRMS provides a higher specificity, allowing for the separation of the background ions from the targeted molecules (Ronsein et al., 2015).

Drug quantification can easily benefit from the PRM specificities that have been enlightened for proteomic applications. Even though this strategy is relatively recent regarding illicit drug and pharmaceuticals analyses in toxicology, it has received a growing interest. Indeed, PRM quantification has been reported for the quantitative analysis of abiraterone (Bhatnagar et al., 2018), beclabuvir (Jiang et al., 2017), anticoagulant rodenticides (Gao et al., 2018), and sterols (Schott et al., 2018). Regarding drugs of abuse, a first application has been described for the quantification of cannabinoids in whole blood (Joye et al., 2020).

Herein, we present a validated single multi-analyte procedure for the quantification of the main substances regarding DUID cases using 100  $\mu$ L of whole blood. The quantified substances were selected based on the FEDRO list and the prevalence of substances consumed by the drivers in Switzerland (Augsburger and Rivier, 1997; Augsburger et al., 2005; Senna et al., 2010). The validated approach uses the advantages provided by HRMS and especially PRM for the simultaneous quantification of 22 DoA and pharmaceuticals alongside 15 internal standards (IS), enabling the solving of most DUID cases with a single injection and a simple sample preparation.

## MATERIALS AND METHODS

### Standards and Reagents

Water, methanol, formic acid (FA), and ammonium formate were furnished by Biosolve. Drugs standard were purchased from Cerilliant or Lipomed, at either 1 mg/ml or 100  $\mu$ g/ml. External quality controls (ECQ) were purchased from Medidrug, ACQ Science, or Clincheck. Blank lyophilized whole blood was acquired from ACQ Science.

### Solution Preparation

Standard solutions containing tetrahydrocannabinol (THC), 11-Nor-9-carboxy-THC (THC-COOH), alprazolam, amphetamine, methamphetamine, 3,4-methylenedioxymethamphetamine (MDMA), 3,4-methylene dioxy-amphetamine (MDA), methylphenidate, cocaine, cocaethylene, lorazepam, bromazepam, zolpidem, benzoylcegonine, morphine, codeine, methadone, tramadol, O-desmethyltramadol, diazepam, nordiazepam, oxazepam were prepared for calibration curve and internal quality control (IQC) preparation. In parallel, solutions containing THC-D3, THC-COOH-D9, cocaine-D3, benzoylcegonine-D3, amphetamine-D8, MDMA-D5, methylphenidate-D10, morphine-D3, codeine-D3, methadone-D3, tramadol-<sup>13</sup>C-D3, O-desmethyltramadol-D6, nordiazepam-D5, alprazolam-D5, and zolpidem-D6 were prepared as internal standard (IS) solutions.

Calibration samples were prepared by spiking lyophilized whole blood at 5 concentration levels (Table 1). IS were added to



**TABLE 1 |** Calibration levels and quantification parameters (IS, polarity, parent ion m/z, and quantifier ions) for the substances of interest. The calibration ranges are in adequacy with the legal thresholds and the therapeutic ranges.

	Calibration levels (ng/ml)					Quantification parameters					
	Level 1	Level 2	Level 3	Level 4	Level 5	Polarity	Parent Ion (m/z) → quantifier ion	Qualifier ion for data processing (m/z)	IS	IS concentration (ng/ml)	IS parent ion → quantifier ion
THC	1	2	5	10	20	+	315.2319 → 193.1222	123.0440	THC-D3	10	318.2507 → 196.1413
THC-COOH	5	10	25	50	100	–	343.1915 → 245.1546	191.1068	THC-COOH-D9	100	352.2479 → 254.2108
Cocaine	10	20	50	100	200	+	304.1543 → 182.1177	82.0657	Cocaine-D3	100	307.1731 → 185.1364
Cocaeethylene	50	100	250	500	1,000	+	318.1699 → 196.1333	82.0651	Cocaine-D3	100	307.1731 → 185.1364
Benzoylecgonine	50	100	250	500	1,000	+	290.1387 → 168.1020	105.0338	Benzoylecgonine-D3	100	293.1575 → 171.1204
Amphetamine	10	20	50	100	200	+	136.1121 → 91.0547	119.0857	Amphetamine-D8	100	144.1623 → 97.0921
Methamphetamine	10	20	50	100	200	+	150.1277 → 91.0547	119.0857	Amphetamine-D8	100	144.1623 → 97.0921
MDA	10	20	50	100	200	+	180.1019 → 133.0648	105.0702	MDMA-D5	100	199.1489 → 165.0877
MDMA	10	20	50	100	200	+	194.1175 → 163.0753	135.0441	MDMA-D5	100	199.1489 → 165.0877
Methylphenidate	10	20	50	100	200	+	234.1488 → 84.0813	56.0503	Methylphenidate-D10	100	244.2116 → 93.1376
Morphine	5	50	500	1,000	2,000	+	286.1438 → 201.0908	229.0858	Morphine-D3	1,000	289.1626 → 201.0906
Codeine	5	50	500	1,000	2,000	+	300.1594 → 215.1061	58.0659	Codeine-D3	1,000	303.1783 → 215.1061
Methadone	5	50	500	1,000	2,000	+	310.2165 → 105.0339	219.1167	Methadone-D3	1,000	313.2354 → 105.0337
Tramadol	5	50	500	1,000	2,000	+	264.1958 → 58.0659	–	Tramadol- <sup>13</sup> C-D3	1,000	269.2287 → 58.0657
O-Desmethyltramadol	5	50	500	1,000	2,000	+	250.1801 → 58.0659	–	O-Desmethyltramadol-D6	1,000	256.2178 → 64.1033
Diazepam	100	200	500	1,000	2,000	+	285.0789 → 154.0417	193.0885	Nordiazepam-D5	1,000	276.0947 → 140.0258
Nordiazepam	100	200	500	1,000	2,000	+	271.0633 → 140.0262	165.0212	Nordiazepam-D5	1,000	276.0947 → 140.0258
Oxazepam	100	200	500	1,000	2,000	+	287.0582 → 241.0527	104.0498	Nordiazepam-D5	1,000	276.0947 → 140.0258
Lorazepam	20	50	100	150	300	+	321.0192 → 229.0527	163.0055	Alprazolam-D5	100	314.1215 → 286.1018
Bromazepam	20	50	100	150	300	+	316.0080 → 182.0839	209.0945	Alprazolam-D5	100	314.1215 → 286.1018
Alprazolam	5	10	25	50	100	+	309.0902 → 281.0707	274.1208	Alprazolam-D5	100	314.1215 → 286.1018
Zolpidem	40	100	200	300	600	+	308.1757 → 235.1230	263.1175	Zolpidem-D6	100	314.2134 → 235.1224

reach a final concentration of 10 (THC-D3), 100, or 1,000 ng/ml depending on the specific calibration range.

## Sample Pre-treatment

IS solutions were spiked in Eppendorfs and evaporated to dryness before adding 100  $\mu$ L of whole blood. The extraction was then performed by protein precipitation using 300  $\mu$ L of methanol. After centrifugation for 10 min at 14,000 rpm, the upper methanolic phase was transferred into a new Eppendorf and evaporated to dryness under a nitrogen flow. Reconstitution was performed using 100  $\mu$ L of 1:9 methanol: water and 10  $\mu$ L were injected into the LC-HRMS system (**Supplemental Figure 1**).

## LC-HRMS Method

A Thermo Scientific Ultimate 3000 LC system with a Phenomenex 2.6  $\mu$ m C18 (10 cm  $\times$  2.1 mm) maintained at 45°C was used for chromatographic separation. Mobile phases were composed of A, ammonium formate 10 mM at pH 3.3, and B, methanol with 0.1% FA. Phase B was ramped linearly from 2 to 98% over 7.5 min. The column was then washed at 98% of B for 3.5 min, followed by a 6 min re-equilibration at 2% of B at 300  $\mu$ L/min for a total analysis run of 17 min. The LC was coupled to a Q Exactive Plus system (Thermo Scientific, Bremen, Germany) via a heated electro spray ionization (ESI) source (H-ESI II probe, Thermo Scientific). The ionization spray voltage was set to 3 kV, sheath gas flowrate was set to 40, and auxiliary gas flowrate to 10 (both in arbitrary units). The method functioned in PRM, using an inclusion list containing the exact mass of the parent ion and the retention time windows for the different analytes. A polarity switch in negative was performed at 7.5 min for the

specific detection of THC-COOH with a switch back in positive polarity at 8.7 min for the detection of THC. Resolution was set to 17,500 for the HCD fragmentation performed using an NCE at 50 eV with an AGC target of 1e5 and a maximum IT of 100 ms.

## Method Validation

The validation criteria used to evaluate the analytical process was based on the directives of the “Société Française des Sciences et des Techniques Pharmaceutiques” (SFSTP) regarding bioanalytical methods and adapted to our specific requirements (Boulanger et al., 2003; Peters et al., 2007; Lynch, 2016). Two product ions (one quantifier and one qualifier) were used for data processing (**Table 1**) and full MS/MS spectra were compared with the online advanced mass spectral database *m/z cloud*. The validation was performed over 3 non-consecutive days ( $p = 3$ ). The trueness and precision were evaluated using a variance analysis-based statistical treatment (ANOVA). Calibration (Cal) was performed in duplicate at 5 different concentration levels ( $k = 5$ ) (**Table 1**) while quality controls (QCs) were prepared in quadruplicate at the two lowest and highest concentration levels ( $k = 4$ ). Using the acquired data, trueness, precision, accuracy, linearity, limits of detection (LOD), and quantification (LOQ) were determined. Six different blank bloods were analyzed for selectivity assessment investigating for potential interferences. The approach developed by Matuszewski et al. was used for recovery (RE) and matrix effect (ME) evaluation (Matuszewski et al., 2003). In this optic, three sample sets were prepared, including all the substances of interest at two concentration levels (low being level 2 and high being level 4 described in **Table 1**). Sample set 1 represented neat standards spiked after

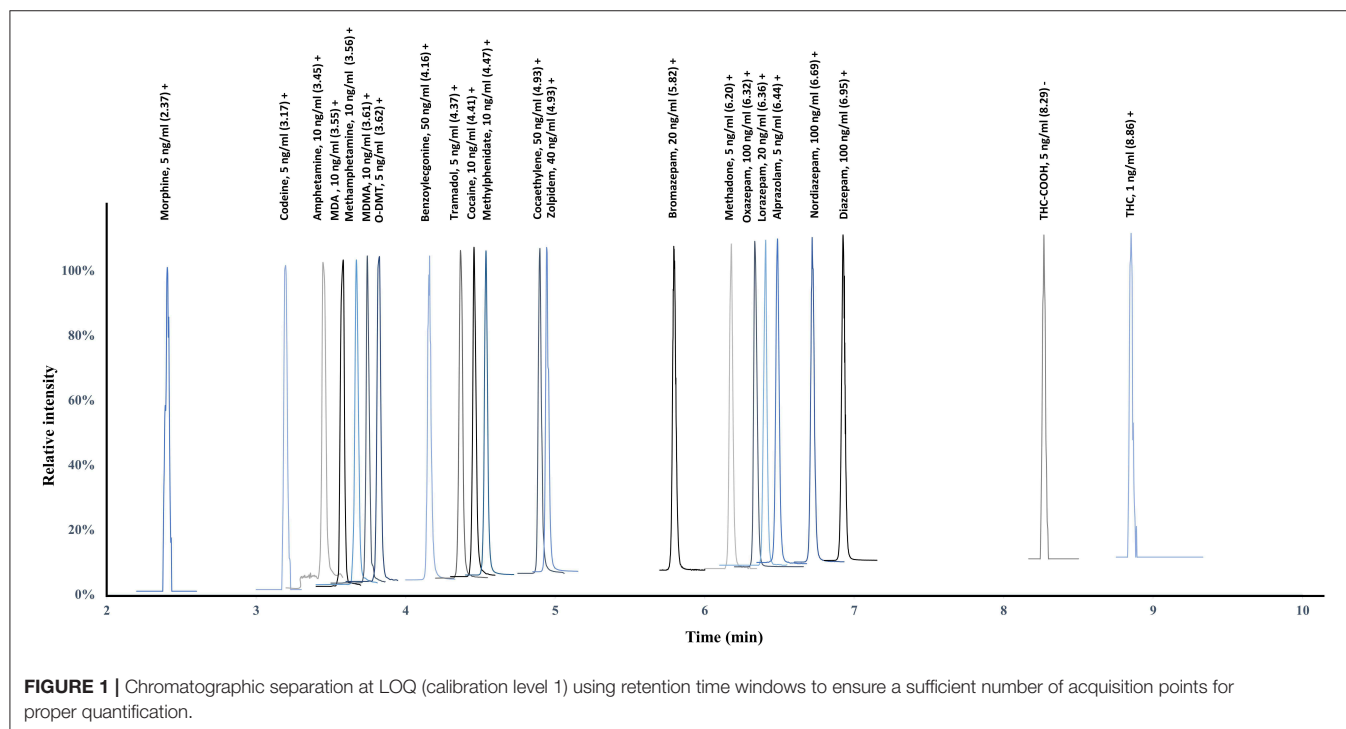


**FIGURE 1 |** Chromatographic separation at LOQ (calibration level 1) using retention time windows to ensure a sufficient number of acquisition points for proper quantification.

**TABLE 2 |** Results for trueness, precision, and linearity (k is the number of concentration levels, n the number of repetitions by levels, and p the number of non-consecutive days).

Trueness (%) (k = 4; n = 4; p = 3)				
Calibration level (ng/ml)	Level 1	Level 2	Level 4	Level 5
THC	107.3	98.4	101.8	106.2
THC-COOH	100.9	104.2	102.4	101.9
Cocaine	101.4	102.2	103.0	103.3
Cocaethylene	102.1	106.7	101.1	99.4
Benzoyllecgonine	101.8	103.6	100.6	99.8
Amphetamine	107.7	104.8	101.5	100.7
Methamphetamine	102.9	101.2	100.6	97.2
MDA	104.4	105.3	103.4	98.2
MDMA	107.2	102.2	97.6	98.3
Methylephenidate	104.8	103.4	102.4	100.6
Morphine	101.6	96.1	100.8	100.6
Codeine	103.5	107.6	103.2	102.4
Methadone	107.6	103.5	104.4	100.5
Tramadol	103.8	98.5	100.4	99.6
O-Desmethyltramadol	98.9	100.5	98.1	99.5
Diazepam	97.6	101.7	103.2	96.7
Nordazepam	98.4	102.6	103.0	99.6
Oxazepam	98.7	98.1	100.0	97.0
Lorazepam	101.0	99.5	99.3	102.2
Bromazepam	95.3	101.1	97.1	100.3
Alprazolam	100.9	105.1	101.8	97.2

Repeatability/intermediate precision (RSD %) (k = 4, n = 4, p = 3)				
Calibration level (ng/ml)	Level 1	Level 2	Level 4	Level 5
THC	5.6/5.6	3.1/3.9	3.9/4.0	3.2/7.1
THC-COOH	7.4/8.3	7.2/7.2	4.5/4.5	5.7/5.7
Cocaine	7.8/7.8	4.0/7.0	7.0/7.0	3.6/6.3
Cocaethylene	3.6/5.7	4.7/5.0	2.2/2.3	4.5/4.5
Benzoyllecgonine	5.0/5.0	2.4/3.3	2.2/2.2	3.1/3.5
Amphetamine	7.9/7.9	5.6/7.6	4.7/6.5	5.5/5.5
Methamphetamine	6.7/7.0	7.1/7.1	4.0/5.7	5.5/5.5
MDA	4.6/5.6	4.8/7.7	3.0/3.0	3.7/3.7
MDMA	5.2/6.9	6.8/6.8	4.8/4.8	6.4/4.7
Methylephenidate	3.6/4.1	4.1/5.6	3.1/3.7	3.8/3.8
Morphine	3.9/7.9	3.7/3.7	2.2/2.2	1.1/1.5
Codeine	7.2/8.4	5.3/6.3	5.0/6.2	2.8/4.8
Methadone	8.3/8.3	5.3/5.3	7.7/7.7	4.4/4.4
Tramadol	3.6/3.6	6.5/6.5	5.9/5.9	3.1/3.1
O-Desmethyltramadol	6.4/6.9	4.0/4.0	5.6/5.6	3.3/3.3
Diazepam	11.2/11.2	4.6/5.4	3.9/4.2	5.3/5.3
Nordazepam	3.8/4.2	3.1/3.2	2.2/2.2	1.9/2.2
Oxazepam	4.3/4.3	5.9/5.9	6.6/7.4	3.0/4.8
Lorazepam	8.4/11.0	5.5/5.5	9.4/9.8	4.6/6.5
Bromazepam	11.6/11.6	3.7/3.8	3.6/3.6	2.5/2.5
Alprazolam	9.0/9.0	5.2/5.6	7.0/7.0	3.8/4.2

(Continued)

**TABLE 2 |** Continued

Linearity (k = 4, n = 4, p = 3)				
	Range (ng/ml)	Slope	R <sup>2</sup>	LOQ (ng/ml)
THC	1–20	1.0623	0.9928	1
THC-COOH	5–100	1.0188	0.9946	5
Cocaine	10–200	1.0339	0.9933	10
Cocaethylene	50–1,000	0.9905	0.9970	50
Benzoyllecgonine	50–1,000	0.9959	0.9980	50
Amphetamine	10–200	1.0044	0.9937	10
Methamphetamine	10–200	0.9711	0.9944	10
MDA	10–200	0.9802	0.9967	10
MDMA	10–200	0.9779	0.9934	10
Methylephenidate	10–200	1.0046	0.9972	10
Morphine	5–2,000	1.0063	0.9995	5
Codeine	5–2,000	1.0237	0.9962	5
Methadone	5–2,000	1.0077	0.9951	5
Tramadol	5–2,000	0.9966	0.9978	5
O-Desmethyltramadol	5–2,000	0.9934	0.9977	5
Diazepam	5–2,000	0.9688	0.9936	5
Nordazepam	5–2,000	0.9969	0.9987	5
Oxazepam	5–2,000	0.9707	0.9945	5
Lorazepam	20–300	0.9921	0.9921	20
Bromazepam	20–300	1.0032	0.9980	20
Alprazolam	5–100	0.9697	0.9948	5
Zolpidem	40–600	1.0019	0.9983	40

the extraction, while sample set 2 represented blank blood spiked after extraction. Sample set 3 represented blank blood spiked before extraction. The absence of interfering peaks at the established retention times (RT) for the analytes and the IS was used to ensure the specificity. The chemical stability of all analytes was evaluated under sample handling and storage conditions at low and high concentrations in five replicates. Benchtop (6 h, room temperature), autosampler (24 h, 5°C), three cycles of freeze-thaw (–20°C), and short term (1 week, –20°C) conditions were used for stability determination.

In order to evaluate the method, 8 different EQCs were analyzed in duplicates using the exact same procedure.

## RESULTS AND DISCUSSION

### Method Development

In the present study, 22 analytes (15 IS) included in the main classes of drugs of abuse, as well as the major benzodiazepines, were analyzed using a single simultaneous multi-analyte quantitative approach. This list of substances was established based on the FEDRO recommendations and on the knowledge of the prevalence of psychoactive compounds among suspected impaired drivers. A nationwide study performed on 4,668 samples collected on suspected drivers in 2010 in Switzerland proved cannabinoids (48%), alcohol (35%), cocaine (25%), opiates (15%), amphetamines (7%), and benzodiazepines

(6%) to be the most detected substances (Senna et al., 2010). The use of such multi-analyte approaches is challenging due to the various physico-chemical properties of the substances of interest and requires specific care during method development. To ensure a proper quantification, retention time windows were set for the acquisition ensuring the acquisition of a sufficient number of acquisition points (Figure 1). For good-quality integration and reproducible quantification, a minimum of 10–15 points is necessary to define exactly the peak start, peak apex, and peak end. The method was designed to resolve the wide majority of DUID cases using a single procedure and a limited amount of biological sample (Supplemental Figure 1) (Senna et al., 2010). The method allows the successful PRM-based quantification of cannabinoids, amphetamines, cocaine and its metabolites, opiates and opioids, and the major benzodiazepines at the sensitivity necessary for legal thresholds and therapeutic ranges (OCCCR-OFROU, 2008; Schulz et al., 2012).

### Trueness and Precision

Independent QC samples at 4 different calibration levels were injected in 4 replicates over 3 non-consecutive days for the determination of trueness and precision. Accuracy represents the total error and is divided into trueness (representing the “bias” or the systematic error) and precision (referring as the standard deviation or random errors) (Gonzalez et al., 2010). The trueness can be evaluated by calculating the percentage difference between the experimental and the expected theoretical values. In the present study, the systematic error varied from −4.7 to 7.6% (Table 2). Precision was divided into two parameters:

**TABLE 3 |** Results for Recovery and Matrix Effect performed at low- and high-quality control concentrations.

	Matrix effect and recovery			
	ME low (CV %)	RE low (CV %)	ME high (CV %)	RE high (CV %)
THC	−51% (15)	78% (18)	−34% (16)	81% (12)
THC-COOH	−7% (9)	57% (10)	−4% (3)	49% (4)
Cocaine	−25% (8)	92% (8)	−26% (8)	94% (10)
Cocaehtylene	−27% (6)	91% (6)	−21% (6)	95% (9)
Benzoylcegonine	−22% (4)	91% (6)	−19% (8)	92% (8)
Amphetamine	−10% (12)	96% (12)	−13% (7)	86% (12)
Methamphetamine	−12% (11)	76% (10)	−18% (12)	75% (10)
MDA	−32% (8)	106% (8)	−22% (5)	89% (7)
MDMA	−35% (10)	96% (9)	−18% (8)	95% (7)
Methylephenidate	−30% (8)	82% (17)	−25% (16)	81% (10)
Morphine	−23% (9)	96% (5)	−12% (4)	86% (17)
Codeine	−27% (4)	96% (16)	−13% (6)	95% (7)
Methadone	−21% (11)	94% (8)	−13% (10)	97% (9)
Tramadol	−27% (10)	88% (17)	−15% (6)	82% (19)
O-Desmethyltramadol	−29% (14)	81% (12)	−15% (8)	95% (13)
Diazepam	−30% (5)	73% (5)	−10% (11)	67% (10)
Nordazepam	0% (11)	82% (9)	−4% (9)	86% (9)
Oxazepam	−13% (6)	86% (7)	−5% (10)	82% (9)
Lorazepam	−7% (7)	80% (6)	3% (13)	95% (6)
Bromazepam	−18% (9)	96% (8)	−15% (10)	105% (7)
Alprazolam	−4% (12)	81% (6)	−1% (7)	84% (9)
Zolpidem	−16% (7)	73% (15)	−11% (13)	86% (12)

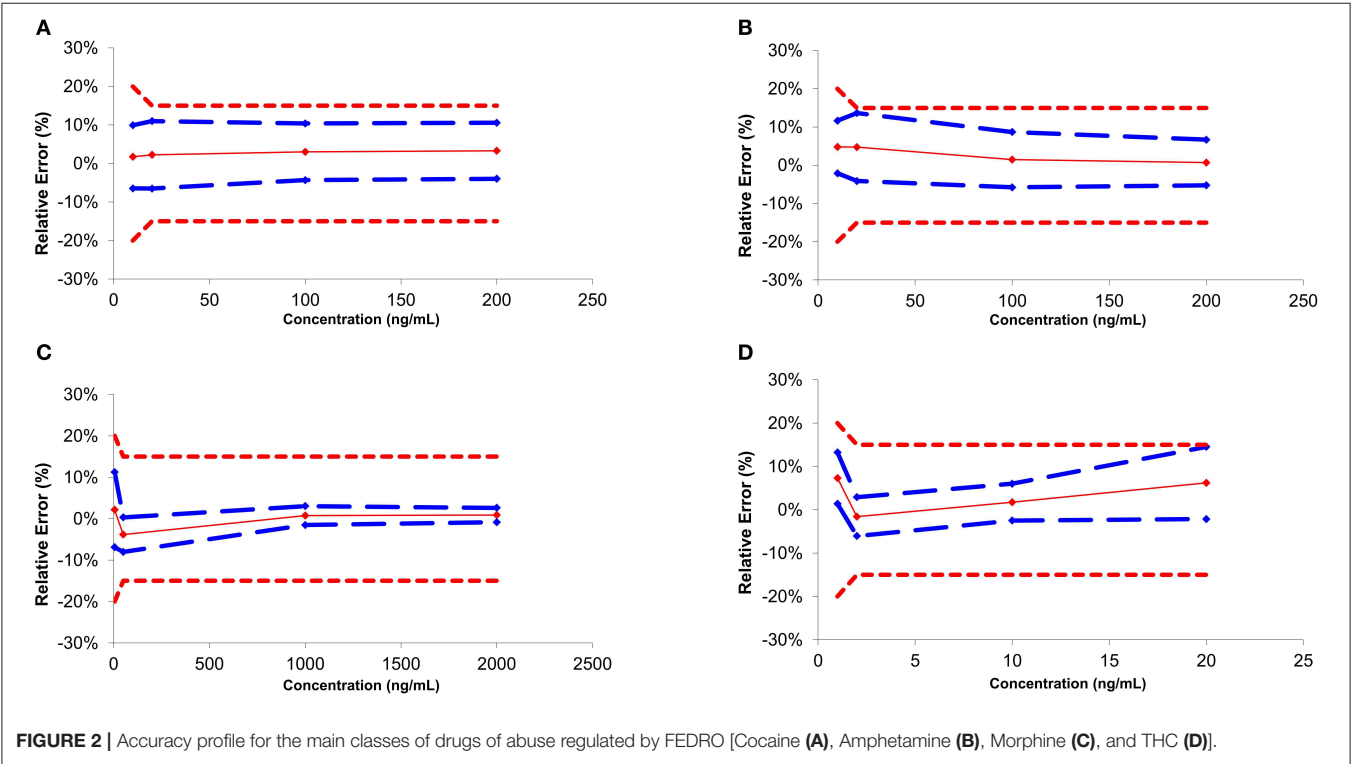
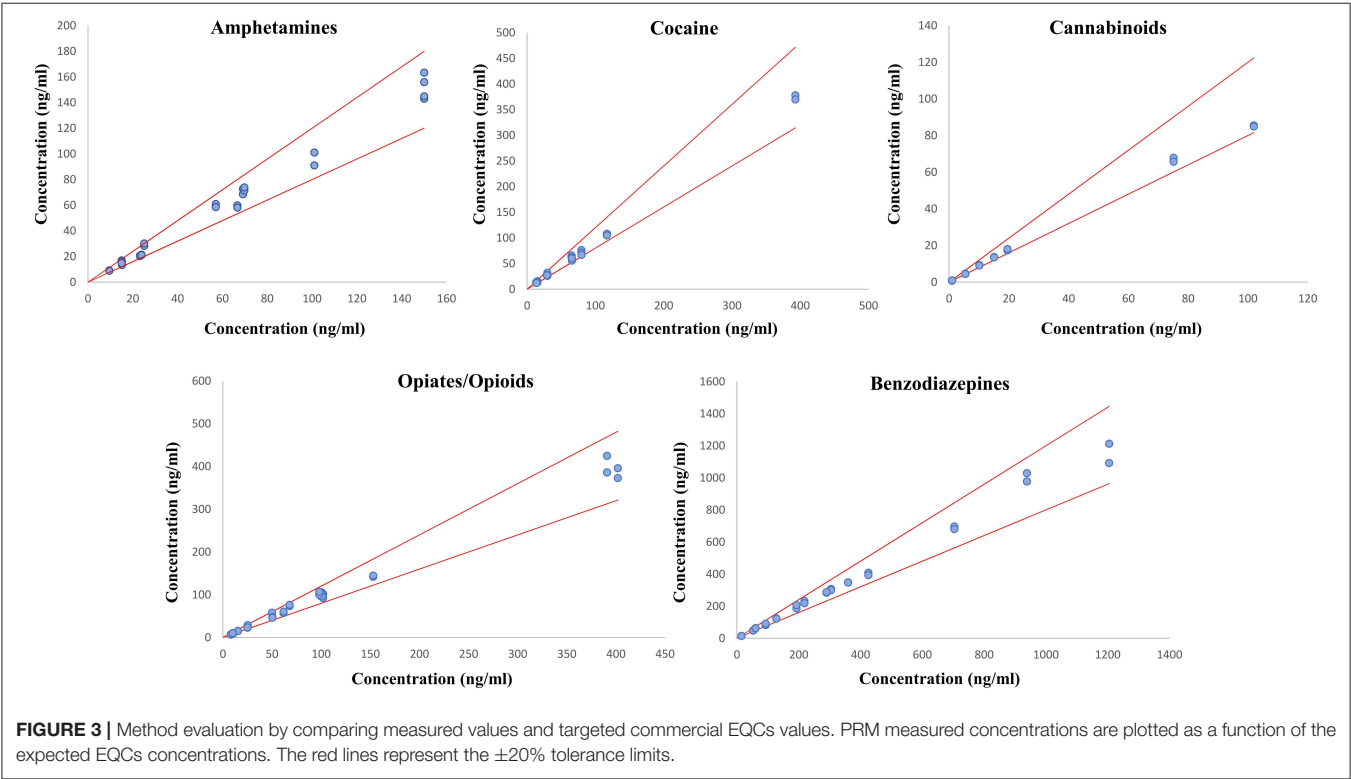


**TABLE 4 |** Three cycles of freeze-thaw (−20°C), benchtop (6 h, room temperature), autosampler (24 h, 5°C), and short-term (1 week, −20°C) conditions were performed in this stability assay at low- and high-quality control concentrations.

	Stability							
	Autosampler (5°C, 24 h)		Benchtop (Room Temp, 6 h)		Freeze-thaw (−20°C, 3 cycles)		Short term (−20°C, 1 week)	
	Low (CV %)	High (CV %)	Low (CV %)	High (CV %)	Low (CV %)	High (CV %)	Low (CV %)	High (CV %)
THC	100% (13)	93% (3)	92% (7)	95% (5)	108% (11)	98% (2)	99% (17)	98% (4)
THC-COOH	103% (7)	97% (4)	106% (8)	97% (8)	100% (11)	101% (5)	101% (7)	99% (2)
Cocaine	109% (7)	95% (6)	99% (12)	92% (7)	104% (10)	99% (6)	108% (12)	96% (7)
Cocaehtylene	107% (12)	96% (6)	99% (12)	92% (16)	93% (6)	95% (14)	88% (9)	94% (8)
Benzoylcegonine	102% (7)	95% (4)	97% (11)	97% (6)	99% (9)	98% (3)	104% (7)	95% (4)
Amphetamine	100% (3)	95% (11)	100% (6)	96% (8)	95% (2)	96% (8)	93% (2)	91% (6)
Methamphetamine	103% (15)	100% (9)	95% (11)	97% (14)	92% (7)	103% (5)	105% (21)	96% (12)
MDA	104% (13)	98% (6)	95% (5)	86% (8)	101% (11)	101% (7)	109% (21)	96% (7)
MDMA	108% (10)	98% (5)	101% (6)	97% (5)	106% (10)	104% (6)	108% (16)	96% (6)
Methylephenidate	109% (21)	106% (13)	106% (10)	92% (19)	105% (10)	106% (16)	109% (20)	108% (16)
Morphine	91% (2)	98% (4)	94% (8)	100% (14)	90% (7)	104% (4)	86% (8)	98% (3)
Codeine	108% (10)	104% (6)	97% (5)	106% (7)	104% (8)	110% (9)	103% (9)	105% (9)
Methadone	106% (6)	98% (17)	96% (6)	101% (14)	99% (6)	105% (5)	102% (4)	98% (3)
Tramadol	108% (11)	98% (7)	102% (6)	100% (7)	98% (9)	105% (8)	100% (10)	98% (9)
O-Desmethyltramadol	99% (10)	101% (6)	98% (9)	101% (9)	99% (6)	106% (11)	96% (9)	94% (7)
Diazepam	104% (6)	97% (6)	101% (8)	88% (7)	90% (6)	96% (9)	102% (5)	90% (9)
Nordazepam	107% (4)	103% (4)	105% (7)	104% (3)	94% (7)	102% (5)	99% (7)	97% (5)
Oxazepam	102% (4)	99% (3)	95% (9)	95% (6)	86% (9)	107% (5)	113% (8)	109% (10)
Lorazepam	97% (16)	98% (6)	85% (7)	93% (11)	94% (10)	108% (6)	110% (8)	106% (8)
Bromazepam	98% (10)	95% (4)	91% (3)	91% (6)	104% (17)	97% (3)	97% (7)	98% (4)
Alprazolam	106% (9)	97% (11)	96% (6)	90% (8)	99% (9)	95% (8)	104% (9)	100% (6)
Zolpidem	109% (10)	93% (9)	92% (8)	93% (10)	115% (10)	97% (6)	97% (7)	94% (6)



the relative standard deviation (repeatability or  $R_{R,S,D}$ ) and the inter-day variability (intermediate precision or  $IP_{R,S,D}$ ).  $R_{R,S,D}$  represents the variability under similar conditions, meaning that the analyses are performed by the same operator using the same reagents and samples. On the other hand,  $IP_{R,S,D}$  represented the variability associated with the use of the same samples on different days with different reagents. Precision parameters were evaluated to be between 1.1 and 11.6% (Table 2). Accuracy profiles are visual representations combining both the trueness and the precision to represent the uncertainty measurement (Figure 2). Precision is represented by the calculated confidence limit at 95% at each concentration level. Accuracy profiles also include the representation of acceptance limits of  $\pm 20\%$  at the LLOQ suggested for method validation ( $\pm 15\%$  at the other calibration levels). All analyzed QCs were within the acceptance limits.

### Linearity and LOQ

The definition of linearity stands as the method capacity to provide a result proportional to the actual sample concentration. To determine this parameter, a linear regression model based on the least square method was applied on the fit of the obtained concentration as a function of the theoretical concentration. Slopes values were comprised between 0.9688 and 1.0623 with coefficients of determination above 0.9921 for all the compounds confirming the method linearity within the concentration ranges of interest (Table 2). LOQs were fixed according to the lowest point of the calibration curve (Table 1).

### Selectivity, Recovery, and Matrix Effect

Selectivity is defined as the ability to differentiate the analyte of interest from potential interferences. To assess the good selectivity of the method, six different blank blood samples were analyzed using the complete extraction procedure. No compounds impairing the detection and quantification of the analytes of interest were observed. HRMS technology offers a high selectivity due to its resolving power, therefore reducing the number of potential interferences (Chindarkar et al., 2014). However, ME, including ion suppression or enhancement, are often associated with the use of ESI as ion source challenging the method selectivity. The determination of such ME is therefore crucial to ensure a proper detection and quantification of the substances of interest. ME ranged from  $-51\%$  (15% CV) of ion suppression for THC at low concentration and 3% (13% CV) of ion enhancement for lorazepam, being consistent with the existing literature (Table 3) (Simonsen et al., 2010; Fernandez Mdel et al., 2013; Montenarh et al., 2014; Steuer et al., 2014; Vaiano et al., 2016; De Boeck et al., 2017). All values concerning RE and ME are summarized in Table 3. To compensate for those undesirable ME, isotopically-labeled internal standards was used for normalization.

### Stability

Results regarding analytes' stability are listed in Table 4. Overall, stability ranged between 86 and 115%, assuring that the samples were stables within the tested conditions (auto-sampler, bench-top, 3 cycles of freeze-thaw and short-term stability).

### External Quality Control Analysis

Eight commercial EQCs were analyzed in duplicates to ensure the robustness of the developed method and procedure. In total, the quantification was performed on 28 samples of amphetamines, 24 samples of cocaine and its metabolites, 16 samples of cannabinoids, 36 samples of opioids and opiates, and 28 samples of benzodiazepines and z-drugs. Results comparison between the described method and the expected EQCs values are represented in Figure 3 for the different classes of molecules involved in DUID cases. A good correlation was observed between the expected and the obtained values. The relative standard deviation was lower than 20% for all tested substances, confirming the efficiency of the PRM quantitative acquisition mode for toxicological analyses. This method confirms the potential of PRM as a solid alternative to classical MRM approaches (Li et al., 2016; Lv et al., 2018; Joye et al., 2020).

### CONCLUSION

A quick and efficient multi-analyte procedure was successfully developed in whole blood for the simultaneous quantification of 37 substances of interest in DUID cases. PRM represents an interesting alternative to classical MRM quantitative analyses, with the capability of precisely quantifying a large panel of substances with similar performance in terms of linearity, dynamic range, precision, and repeatability (Rauniyar, 2015). PRM quantification does not require *a priori* selection of the fragments of interest, leading to a simplified method development and better control over the quantification experiment, especially regarding multi-analyte approaches. The quantitative PRM procedure presented herein benefits the increased selectivity and sensitivity brought by HRMS, offering a clear alternative for quantitative toxicological analyses.

### DATA AVAILABILITY STATEMENT

The raw data supporting the conclusions of this article will be made available by the authors, without undue reservation.

### AUTHOR CONTRIBUTIONS

TJ supervised the project, participated in the design of the study, did several analyses, and wrote the manuscript. KR did most of the analytical work and participated to the reflexion toward the project. JD participated in the strategic choices toward the study and its design and critically revised the manuscript. JS participated in the supervision and design of the project and critically revised the manuscript. BF participated in the design of the study and critically revised the manuscript. MA participated in the strategic choices toward the study and its design and critically revised the manuscript. AT is the main contributor to the study design, supervised the project, and critically revised the manuscript. All authors contributed to the article and approved the submitted version.



## FUNDING

The authors acknowledge financial support from the Swiss Federal Office of Public Health (contract no. 14.013792.204.0001/1300).

## REFERENCES

- Augsburger, M., Donze, N., Menetrey, A., Brossard, C., Sporkert, F., Giroud, C., et al. (2005). Concentration of drugs in blood of suspected impaired drivers. *Forensic Sci. Int.* 153, 11–15. doi: 10.1016/j.forsciint.2005.04.025
- Augsburger, M., and Rivier, L. (1997). Drugs and alcohol among suspected impaired drivers in Canton de Vaud (Switzerland). *Forensic Sci. Int.* 85, 95–104. doi: 10.1016/S0379-0738(96)02084-1
- Bhatnagar, A., McKay, M. J., Crumbaker, M., Ahire, K., Karuso, P., Gurney, H., et al. (2018). Quantitation of the anticancer drug abiraterone and its metabolite Delta(4)-abiraterone in human plasma using high-resolution mass spectrometry. *J. Pharm. Biomed. Anal.* 154, 66–74. doi: 10.1016/j.jpba.2018.03.012
- Boulanger, B., Chiap, P., Dewe, W., Crommen, J., and Hubert, P. (2003). An analysis of the SFSTP guide on validation of chromatographic bioanalytical methods: progress and limitations. *J. Pharm. Biomed. Anal.* 32, 753–765. doi: 10.1016/S0731-7085(03)00182-1
- Bourmaud, A., Gallien, S., and Domon, B. (2016). Parallel reaction monitoring using quadrupole-Orbitrap mass spectrometer: principle and applications. *Proteomics* 16, 2146–2159. doi: 10.1002/pmic.201500543
- Chindarkar, N. S., Wakefield, M. R., Stone, J. A., and Fitzgerald, R. L. (2014). Liquid chromatography high-resolution TOF analysis: investigation of MSE for broad-spectrum drug screening. *Clin. Chem.* 60, 1115–1125. doi: 10.1373/clinchem.2014.222976
- De Boeck, M., Missotten, S., Dehaen, W., Tytgat, J., and Cuyper, E. (2017). Development and validation of a fast ionic liquid-based dispersive liquid-liquid microextraction procedure combined with LC-MS/MS analysis for the quantification of benzodiazepines and benzodiazepine-like hypnotics in whole blood. *Forensic Sci. Int.* 274, 44–54. doi: 10.1016/j.forsciint.2016.12.026
- Domon, B., and Gallien, S. (2015). Recent advances in targeted proteomics for clinical applications. *Proteomics Clin. Appl.* 9, 423–431. doi: 10.1002/prca.201400136
- Elliott, S., Woolacott, H., and Braithwaite, R. (2009). The prevalence of drugs and alcohol found in road traffic fatalities: a comparative study of victims. *Sci. Justice* 49, 19–23. doi: 10.1016/j.scijus.2008.06.001
- Favretto, D., Visentin, S., Stocchero, G., Vogliardi, S., Sneghi, R., and Montisci, M. (2018). Driving under the influence of drugs: prevalence in road traffic accidents in Italy and considerations on per se limits legislation. *Traffic Inj. Prev.* 19, 786–793. doi: 10.1080/15389588.2018.1500018
- Fernandez Mdel, M., Wille, S. M., Kummer, N., Di Fazio, V., Ruyssinx, E., and Samyn, N. (2013). Quantitative analysis of 26 opioids, cocaine, and their metabolites in human blood by ultra performance liquid chromatography-tandem mass spectrometry. *Ther. Drug Monit.* 35, 510–521. doi: 10.1097/FTD.0b013e31828e7e6b
- Gao, X., Li, H., Li, H., Dong, S., Chu, J., Guo, H., et al. (2018). Sensitive determination of nine anticoagulant rodenticides in blood by high resolution mass spectrometry with supported liquid extraction pretreatment. *Forensic Sci. Int.* 292, 39–44. doi: 10.1016/j.forsciint.2018.09.009
- Gonzalez, A. G., Herrador, M. A., and Asuero, A. G. (2010). Intra-laboratory assessment of method accuracy (trueness and precision) by using validation standards. *Talanta* 82, 1995–1998. doi: 10.1016/j.talanta.2010.07.071
- Hoffman, M. A., Fang, B., Haura, E. B., Rix, U., and Koomen, J. M. (2018). Comparison of quantitative mass spectrometry platforms for monitoring kinase ATP probe uptake in lung cancer. *J. Proteome Res.* 17, 63–75. doi: 10.1021/acs.jproteome.7b00329
- Hopfgartner, G., Varesio, E., Tschappat, V., Grivet, C., Bourgoigne, E., and Leuthold, L. A. (2004). Triple quadrupole linear ion trap mass spectrometer for the analysis of small molecules and macromolecules. *J. Mass Spectr.* 39, 845–855. doi: 10.1002/jms.659
- Jiang, H., Titsch, C., Zeng, J., Jones, B., Joyce, P., Gandhi, Y., et al. (2017). Overcoming interference with the detection of a stable isotopically labeled microtracer in the evaluation of beclabuvir absolute bioavailability using a concomitant microtracer approach. *J. Pharm. Biomed. Anal.* 143, 9–16. doi: 10.1016/j.jpba.2017.04.030
- Joye, T., Sidibe, J., Deglon, J., Karmime, A., Sporkert, F., Widmer, C., et al. (2019). Liquid chromatography-high resolution mass spectrometry for broad-spectrum drug screening of dried blood spot as microsampling procedure. *Anal. Chim. Acta* 1063, 110–116. doi: 10.1016/j.aca.2019.02.011
- Joye, T., Widmer, C., Favrat, B., Augsburger, M., and Thomas, A. (2020). Parallel reaction monitoring-based quantification of cannabinoids in whole blood. *J. Anal. Toxicol.* 44, 541–548. doi: 10.1093/jat/bkz113
- Li, Y., Zhang, J., Jin, Y., Wang, L., Zhao, W., Zhang, W., et al. (2016). Hybrid quadrupole-orbitrap mass spectrometry analysis with accurate-mass database and parallel reaction monitoring for high-throughput screening and quantification of multi-xenobiotics in honey. *J. Chromatogr. A* 1429, 119–126. doi: 10.1016/j.chroma.2015.11.075
- Liakoni, E., Yates, C., Dines, A. M., Dargan, P. I., Heyerdahl, F., Hovda, K. E., et al. (2018). Acute recreational drug toxicity: comparison of self-reports and results of immunoassay and additional analytical methods in a multicenter European case series. *Medicine* 97:e9784. doi: 10.1097/MD.0000000000009784
- Lv, X. J., Sun, Z., Wang, P. L., Yang, J., Xu, T. Y., Jia, Q. Q., et al. (2018). Chemical profiling and quantification of Dan-Deng-Tong-Nao-capsule using ultra high performance liquid chromatography coupled with high resolution hybrid quadrupole-orbitrap mass spectrometry. *J. Pharm. Biomed. Anal.* 148, 189–204. doi: 10.1016/j.jpba.2017.09.034
- Lynch, K. L. (2016). CLSI C62-A: a new standard for clinical mass spectrometry. *Clin. Chem.* 62, 24–29. doi: 10.1373/clinchem.2015.238626
- Martin, J. L., Gadegbeku, B., Wu, D., Viallon, V., and Laumon, B. (2017). Cannabis, alcohol and fatal road accidents. *PLoS ONE* 12:e0187320. doi: 10.1371/journal.pone.0187320
- Matuszewski, B. K., Constanzer, M. L., and Chavez-Eng, C. M. (2003). Strategies for the assessment of matrix effect in quantitative bioanalytical methods based on HPLC-MS/MS. *Anal. Chem.* 75, 3019–3030. doi: 10.1021/ac020361s
- Montenarh, D., Hopf, M., Maurer, H. H., Schmidt, P., and Ewald, A. H. (2014). Detection and quantification of benzodiazepines and Z-drugs in human whole blood, plasma, and serum samples as part of a comprehensive multi-analyte LC-MS/MS approach. *Anal. Bioanal. Chem.* 406, 803–818. doi: 10.1007/s00216-013-7513-x
- Office Fédéral de la Statistique (OFS) (2018). *Accidents des Transports en 2017*. OOCR-OFROU (2008). *Ordonnance de l'OFROU concernant l'ordonnance sur le contrôle de la circulation routière (art. 34)*. Available online at: <https://www.admin.ch/opc/fr/classified-compilation/20080078/index.html#id-6-6> (accessed May 27, 2020).
- Pelletti, G., Verstraete, A. G., Reyns, T., Barone, R., Rossi, F., Garagnani, M., et al. (2019). Prevalence of therapeutic drugs in blood of drivers involved in traffic crashes in the area of Bologna, Italy. *Forensic Sci. Int.* 302:109914. doi: 10.1016/j.forsciint.2019.109914
- Peters, F. T., Drummer, O. H., and Musshoff, F. (2007). Validation of new methods. *Forensic Sci. Int.* 165, 216–224. doi: 10.1016/j.forsciint.2006.05.021
- Rauniyar, N. (2015). Parallel reaction monitoring: a targeted experiment performed using high resolution and high mass accuracy mass spectrometry. *Int. J. Mol. Sci.* 16, 28566–28581. doi: 10.3390/ijms161226120
- Ravera, S., Monteiro, S. P., de Gier, J. J., van der Linden, T., Gomez-Talegon, T., Alvarez, F. J., et al. (2012). A European approach to categorizing medicines for

## SUPPLEMENTARY MATERIAL

The Supplementary Material for this article can be found online at: <https://www.frontiersin.org/articles/10.3389/fchem.2020.00626/full#supplementary-material>

- fitness to drive: outcomes of the DRUID project. *Br. J. Clin. Pharmacol.* 74, 920–931. doi: 10.1111/j.1365-2125.2012.04279.x
- Ronsein, G. E., Pamir, N., von Haller, P. D., Kim, D. S., Oda, M. N., Jarvik, G. P., et al. (2015). Parallel reaction monitoring (PRM) and selected reaction monitoring (SRM) exhibit comparable linearity, dynamic range and precision for targeted quantitative HDL proteomics. *J. Proteomics* 113, 388–399. doi: 10.1016/j.jprot.2014.10.017
- Schott, H. F., Krautbauer, S., Horing, M., Liebisch, G., and Matysik, S. (2018). A validated, fast method for quantification of sterols and gut microbiome derived 5alpha/beta-stanols in human feces by isotope dilution LC-high-resolution MS. *Anal. Chem.* 90, 8487–8494. doi: 10.1021/acs.analchem.8b01278
- Schulz, M., Iwersen-Bergmann, S., Andresen, H., and Schmoldt, A. (2012). Therapeutic and toxic blood concentrations of nearly 1,000 drugs and other xenobiotics. *Crit. Care* 16:R136. doi: 10.1186/cc11441
- Senna, M. C., Augsburger, M., Aebi, B., Briellmann, T. A., Donze, N., Dubugnon, J. L., et al. (2010). First nationwide study on driving under the influence of drugs in Switzerland. *Forensic Sci. Int.* 198, 11–16. doi: 10.1016/j.forsciint.2010.02.014
- Simonsen, K. W., Hermansson, S., Steentoft, A., and Linnet, K. (2010). A validated method for simultaneous screening and quantification of twenty-three benzodiazepines and metabolites plus zopiclone and zaleplone in whole blood by liquid-liquid extraction and ultra-performance liquid chromatography-tandem mass spectrometry. *J. Anal. Toxicol.* 34, 332–341. doi: 10.1093/jat/34.6.332
- Snenghi, R., Pelletti, G., Frigo, A. C., Forza, G., Nalesso, A., Montisci, M., et al. (2018). The dangerous pattern of concurrent use of alcohol and cocaine among drunk-drivers of Northeast Italy. *Alcohol Alcohol* 53, 735–741. doi: 10.1093/alcalc/agy050
- Steuer, A. E., Eisenbeiss, L., and Kraemer, T. (2016). Blood alcohol analysis alone versus comprehensive toxicological analysis - systematic investigation of missed co-ingested other drugs in suspected alcohol-impaired drivers. *Forensic Sci. Int.* 267, 52–59. doi: 10.1016/j.forsciint.2016.08.009
- Steuer, A. E., Forss, A. M., Dally, A. M., and Kraemer, T. (2014). Method development and validation for simultaneous quantification of 15 drugs of abuse and prescription drugs and 7 of their metabolites in whole blood relevant in the context of driving under the influence of drugs-usefulness of multi-analyte calibration. *Forensic Sci. Int.* 244, 92–101. doi: 10.1016/j.forsciint.2014.08.022
- Vaiano, F., Busardo, F. P., Palumbo, D., Kyriakou, C., Fioravanti, A., Catalani, V., et al. (2016). A novel screening method for 64 new psychoactive substances and 5 amphetamines in blood by LC-MS/MS and application to real cases. *J. Pharm. Biomed. Anal.* 129, 441–449. doi: 10.1016/j.jpba.2016.07.009
- Valen, A., Bogstrand, S. T., Vindenes, V., Frost, J., Larsson, M., Holtan, A., et al. (2019). Driver-related risk factors of fatal road traffic crashes associated with alcohol or drug impairment. *Accid. Anal. Prev.* 131, 191–199. doi: 10.1016/j.aap.2019.06.014
- Walsh, J. M., de Gier, J. J., Christopherson, A. S., and Verstraete, A. G. (2004). Drugs and driving. *Traffic Inj. Prev.* 5, 241–253. doi: 10.1080/15389580490465292
- World Health Organization (2015). *Global Status Report on Road Safety*. Geneva: World Health Organization. Available online at: [https://www.who.int/violence\\_injury\\_prevention/road\\_safety\\_status/2015/en/](https://www.who.int/violence_injury_prevention/road_safety_status/2015/en/) (accessed May 27, 2020).

**Conflict of Interest:** The authors declare that the research was conducted in the absence of any commercial or financial relationships that could be construed as a potential conflict of interest.

Copyright © 2020 Joye, Rocher, Déglon, Sidibé, Favrat, Augsburger and Thomas. This is an open-access article distributed under the terms of the Creative Commons Attribution License (CC BY). The use, distribution or reproduction in other forums is permitted, provided the original author(s) and the copyright owner(s) are credited and that the original publication in this journal is cited, in accordance with accepted academic practice. No use, distribution or reproduction is permitted which does not comply with these terms.





# Fast Hollow Fiber Liquid-Phase Microextraction as a Greener Alternative for the Determination of N,N-Dimethyltryptamine and Harmala Alkaloids in Human Urine

Gabriela de Oliveira Silveira<sup>1\*</sup>, Felipe Rebello Lourenço<sup>2</sup>, Vitor Bruno<sup>1</sup> and Mauricio Yonamine<sup>1</sup>

<sup>1</sup> Department of Clinical and Toxicological Analyses, School of Pharmaceutical Sciences, University of São Paulo, São Paulo, Brazil, <sup>2</sup> Department of Pharmacy, School of Pharmaceutical Sciences, University of São Paulo, São Paulo, Brazil

## OPEN ACCESS

### Edited by:

Eugenia Gallardo,  
Universidade da Beira  
Interior, Portugal

### Reviewed by:

Wei-Lung Tseng,  
National Sun Yat-sen  
University, Taiwan  
José S. Câmara,  
Universidade da Madeira, Portugal

### \*Correspondence:

Gabriela de Oliveira Silveira  
silveirago@usp.br

### Specialty section:

This article was submitted to  
Analytical Chemistry,  
a section of the journal  
Frontiers in Chemistry

**Received:** 02 May 2020

**Accepted:** 08 September 2020

**Published:** 07 October 2020

### Citation:

Silveira GO, Lourenço FR, Bruno V  
and Yonamine M (2020) Fast Hollow  
Fiber Liquid-Phase Microextraction as  
a Greener Alternative for the  
Determination of  
N,N-Dimethyltryptamine and Harmala  
Alkaloids in Human Urine.  
Front. Chem. 8:558501.  
doi: 10.3389/fchem.2020.558501

Ayahuasca tea is an entheogen hallucinogenic beverage used for shamanic and spiritual purposes, prepared by the decoction of different Amazonian plants containing N,N-dimethyltryptamine (DMT) and harmala alkaloids. Since the therapeutic potential of this tea has been broadly studied in recent years, mainly for the treatment of psychiatric disorders, the determination of the ayahuasca tea components in human and animal matrices is of utmost importance. In order to avoid the use of large amounts of toxic solvents, typically employed in traditional sample preparation methods, hollow fiber liquid-phase microextraction (HF-LPME) presents a greener and time-saving alternative. The present study aims to fully develop and apply an HF-LPME method for the determination of DMT, harmine (HRM), harmaline (HRL), and tetrahydroharmine (THH) in human urine samples using liquid chromatography-tandem mass spectrometry (LC-MS/MS). Fractional factorial and Box-Behnken designs were used to identify and optimize significant method variables. Once optimized, validation has shown a limit of detection (LoD) of 1.0 ng/ml for DMT and 2.0 ng/ml for the harmala alkaloid. The limit of quantification (LoQ) was of 5.0 ng/ml for all analytes. The method has shown to be linear over a concentration range of 5–200 ng/ml ( $r^2 \geq 0.99$ ). Intra/inter-day precision and accuracy met the acceptance criteria at the three quality control (QC) levels studied (15.0, 90.0, and 170.0 ng/ml,  $n = 6$ , each). Matrix effect evaluation showed predominant ion enhancement and recovery values were above 80%. Dilution factors of 10- and 20-fold have shown acceptable values of accuracy. Selectivity studies showed no interferences. Analysis of eight authentic samples collected from four subjects proved method feasibility. A simple, time-saving and green alternative for the analysis of DMT and harmala alkaloids in human urine samples was developed, optimized using design of experiments, fully validated and applied to authentic samples.

**Keywords:** liquid-phase microextraction, green analytical chemistry, ayahuasca, DMT, harmala alkaloids, LC-MS/MS

## INTRODUCTION

Ayahuasca tea is an entheogen preparation historically used by the indigenous people from the Amazon Basin region for at least 1,000 years (Callaway et al., 1999; Miller et al., 2019; Orsolini et al., 2020). In the last decades, the use of ayahuasca has spread itself across the world via neoshamanic groups, which has caught the attention of the scientific community regarding its possible risks and benefits (Riba et al., 2003; Oliveira et al., 2010a,b; de Oliveira et al., 2011; Sánchez and Bouso, 2015; Palhano-Fontes et al., 2017; Estrella-Parra et al., 2019). The beverage is prepared by the decoction of the *Banisteriopsis caapi* vine and, typically, the *Psychotria viridis* leaves; while the former is rich in the  $\beta$ -carboline harmala alkaloids (harmine, harmaline, and tetrahydroharmine), the latter is the N,N-dimethyltryptamine (DMT)-containing plant and the main responsible for its hallucinogenic effects (Callaway et al., 1999; McKenna, 2004; Tupper, 2008). As DMT is orally inactive, a synergistic effect takes place when the harmala alkaloids, also present in the brew, act as reversible MAO-A inhibitors in the gastrointestinal tract and block the degradation of DMT, which allows for the psychoactive substance to reach its serotonergic receptors in the central nervous system (Riba et al., 2003; Tupper, 2008). In addition, it has been proven that tetrahydroharmine (THH) is a weak serotonin reuptake inhibitor (Callaway et al., 1999; McKenna, 2004; Frecska et al., 2016). Because of these unique features and the possible psychoplastogenic properties of DMT, several research groups have been studying the therapeutic potential of ayahuasca in the context of psychedelic therapy, mainly for the treatment of depression, anxiety, and drug dependence, as recently reviewed (Frecska et al., 2016; Muttoni et al., 2019; dos Santos and Hallak, 2020; Dunlap et al., 2020; Orsolini et al., 2020; Reiff et al., 2020).

As the relevance of using ayahuasca for both religious and scientific purposes expands continuously, the need for suitable analytical approaches rises accordingly. In fact, some methods for the analysis of ayahuasca alkaloids in plasma, whole blood, urine, hair, and sweat specimens have been published (Oliveira et al., 2012; de Moraes et al., 2018; Simão et al., 2019; Tavares et al., 2020). The traditional liquid–liquid extraction (LLE) and solid-phase extraction (SPE) were formerly employed for the analysis of DMT or harmine (HRM) and harmaline (HRL) in urine specimens (Ishii et al., 1997; Forsström et al., 2001; Frison et al., 2008; Wang et al., 2009). However, the methods employed then used significantly large amounts of organic solvents, such as chloroform, ethyl acetate, hexane, and dichloromethane (Ishii et al., 1997; Forsström et al., 2001; Frison et al., 2008; Wang et al., 2009). The improvement in the sensitivity of chromatographic and mass spectrometry techniques has resulted in the need for less laborious sample preparation methods, such as dilute-and-shoot (Bjornstad et al., 2009; McIlhenny et al., 2011; Pope et al., 2019) and protein precipitation (Zhao et al., 2012; Meyer et al., 2014; de Moraes et al., 2018) approaches, which use very small amounts of urine. These simple, faster, cheaper, and less hazardous methodologies have become prominent in the analysis of ayahuasca alkaloids. Nonetheless, it is important to note that the reported protein precipitation methods still required the

use of significant amounts of acetonitrile (Zhao et al., 2012; Meyer et al., 2014) and methyl *tert*-butyl ether (de Moraes et al., 2018).

Consequently, in order to fulfill the requirements from the Green Analytical Chemistry (GAC), once the sample preparation step can hardly be obviated, novel developed methods must focus on the reduction, replacement, or elimination of the use of toxic organic solvents and reagents, optimization of energy consumption, and adequate waste management, which in return may improve the safety of the operator and provide cost-effective alternatives (Gałuszka et al., 2013; Spietelun et al., 2014; Armenta et al., 2015; Silveira et al., 2019). Sample preparation based on GAC proves to be an even more challenging step for it must guarantee sensitivity, recovery, accuracy, and reproducibility as well as ensuring minimal environmental impact (Gałuszka et al., 2013; Turner, 2013; Silveira et al., 2019). Among the several available strategies, the miniaturization of extraction systems is one of the most remarkable alternatives as it proves to be able to drastically reduce the volumes of both solvents and samples, from milliliters used on classic extraction procedures (such as LLE and SPE) down to microliters, or even to completely eliminate the use of such solvents, as in hollow fiber liquid-phase microextraction (HF-LPME) and solid-phase microextraction (SPME) (Spietelun et al., 2014; Silveira et al., 2019).

HF-LPME is a successful microextraction technique first introduced by Pedersen-Bjergaard and Rasmussen (1999). This technique is based on the use of porous polypropylene hollow fibers that are impregnated with 15–20  $\mu$ l of an organic solvent within its pores to produce a supported liquid membrane (SLM) (Pedersen-Bjergaard and Rasmussen, 2005; Carasek and Merib, 2015). After that, the HF lumen is filled with an appropriate solution (acceptor phase), the SLM is introduced into the aqueous sample (donor phase), and the system is usually agitated in order to promote analyte transfer from the donor phase through the SLM into the acceptor phase, which is collected and submitted to further analysis (Pedersen-Bjergaard and Rasmussen, 2005; Silveira et al., 2019). If both the SLM and the acceptor solution are composed by the same organic solvent, the system is named two-phase LPME; on the contrary, the acceptor solution may be produced using an acidic or basic solution able to ionize the analytes—present in the donor phase mainly in its deionized form—which promotes analyte concentration within the fiber lumen by ion trapping (three-phase LPME) (Pedersen-Bjergaard and Rasmussen, 2005; Carasek and Merib, 2015).

The use of HF-LPME has been shown to offer a great performance and considering the importance of quantifying ayahuasca alkaloids in biological matrices, this study presents a fast HF-LPME method followed by ultra-high performance liquid chromatography-tandem mass spectrometry (UHPLC-MS/MS) for the determination of DMT, THH, HRL, and HRM in human urine samples. The current study has aimed to provide a simple miniaturized method in compliance with GAC requirements as an alternative to protein precipitation and dilute-and-shoot approaches which may not offer sufficient sensitivity, matrix clean-up, and sustainability. The HF-LPME method has been optimized through the use of design of experiments; it was then fully validated and its feasibility proof was achieved by the

**TABLE 1** | Mass spectrometry parameters for all analytes and the internal standard (quantifying transition marked with an asterisk).

Analyte	Retention time (min)	Precursor ion, Q1 ( <i>m/z</i> )	Product ion, Q3 ( <i>m/z</i> )	Cone voltage (V)	Collision energy (V)
DMT- <i>d</i> <sub>6</sub> (IS)	2.80	195.1	63.9*	15	14
			114.9		36
			143.8		22
DMT	2.80	188.9	57.8*	25	11
			116.7		29
			143.8		17
THH	4.12	217.1	172.8	25	29
			187.9*		17
			200.0		13
HRL	5.05	215.2	130.4	50	41
			171.7*		33
			199.9		25
HRM	5.32	213.2	143.8	50	41
			169.8*		33
			198.0		25

analysis of eight authentic samples donated by four individuals after a usual ayahuasca ceremony.

## MATERIALS AND METHODS

### Reagents, Standards, and Materials

N,N-Dimethyltryptamine was purchased from Cerilliant Corporation (Round Rock, Texas, USA). HRM and HRL were acquired from Sigma-Aldrich (Saint Louis, USA). The internal standard, deuterated dimethyltryptamine (DMT-*d*<sub>6</sub>), was synthesized as described by Oliveira and collaborators (Oliveira et al., 2012). THH was synthesized from HRL, according to the method described by Callaway et al. (1996). DMT stock solution was available at 1.0 mg/ml while DMT-*d*<sub>6</sub> [internal standard, (IS)], THH, HRL, and HRM powders were weighted out to produce methanolic stock solutions at that same concentration. When appropriate, standard solutions were simply diluted 10-, 100-, or 1,000-fold with methanol in volumetric glassware to obtain working solutions at concentrations of 100, 10.0, or 1.0 µg/ml. All standards solutions were stored in freezer at −20°C.

Methanol HPLC grade, n-octanol, n-non-anol, n-decanol, sodium bicarbonate, sodium carbonate, sodium borate, sodium chloride, ammonium formate, and formic acid (98–100% grade) were purchased from Merck KGaA (Darmstadt, Germany). A Milli-Q system was used to produce ultra-pure water (Millipore, Billerica, Massachusetts).

Hollow-fiber Q3/2 Accurel KM polypropylene (600-m i.d., 200-m wall thickness, and 0.2-m pore size) was purchased from Membrana (Wuppertal, Germany). Corning® gel-loading pipet tips (200-µl round and 0.5-mm thick) were obtained from Merck KGaA (Darmstadt, Germany).

### Instrumentation

Analyses were performed using a Waters UPLC Acquity System coupled to a Quattro Premier XE mass spectrometer (Waters

Corporation, Milford, MA) with an electrospray interface (ESI) operated in positive ion mode. Chromatographic separation was achieved with an Acquity UPLC BEH C18 column (2.1 mm × 100 mm, 1.7 µm) eluted with 2 mM ammonium formate buffer with 0.1% formic acid (mobile phase A) and 0.1% formic acid in methanol (mobile phase B) at a constant flow rate of 0.3 ml/min and column oven temperature at 40°C. The following elution gradient was used: 0–0.5 min, 0% B; 0.5–7 min, 10–50% B; 7.0–7.1 min, 50–10%B; and 7.1–8.0 min, 0% B. Total chromatographic run time was 8.0 min. The injection volume was 2 µl.

The mass spectrometer was operated under multiple-reaction monitoring mode (MRM), considering three transitions for each analyte. MS settings were established as follows: desolvation gas flow rate, 1,100 l/h; cone gas flow rate, 200 l/h; desolvation temperature, 350°C; source temperature, 100°C; capillary voltage, 1,000 V. The retention times, capillary voltage, collision energy, and *m/z* transitions used for quantification of each analyte are indicated in **Table 1**.

Chromatograms were designed after extracting raw data from MassLynx™ Software (Waters Corporation, Milford, MA) and plotting them on Microsoft Excel® 2010 to improve image resolution.

### Urine Specimens

Eight authentic samples were donated from four different subjects. The first and second urine samples were collected after the individuals had participated in a typical ayahuasca ceremony. The drug-free samples were obtained from 10 non-user volunteers, pooled, and used throughout the entire method optimization and validation. After collection, samples were stored untreated at −20°C until further analysis. The study protocol was approved by the Ethics Committee of School of Pharmaceutical Sciences, University of São Paulo (ethics protocol approval number 2.267.476). Informed consent was obtained from all individual participants included in the study.

**TABLE 2** | Experimental matrix for the fractional factorial design.

Experiment	Random order	SLM solvent	Buffer pH	Buffer volume ( $\mu$ l)	Stirring time (min)	Stirring rate (rpm)
1	14	Octanol	10.5	100	15	2,400
2	15	Octanol	9.5	500	15	2,400
3	9	Octanol	9.5	100	5	2,400
4	8	Octanol	10.5	500	15	1,200
5	5	Octanol	9.5	100	15	1,200
6	11	Decanol	9.5	500	5	2,400
7	1	Decanol	9.5	100	5	1,200
8	4	Decanol	10.5	500	5	1,200
9	6	Decanol	10.5	100	15	1,200
10	12	Octanol	10.5	500	5	2,400
11	16	Decanol	10.5	500	15	2,400
12	3	Octanol	9.5	500	5	1,200
13	10	Decanol	10.5	100	5	2,400
14	7	Decanol	9.5	500	15	1,200
15	13	Decanol	9.5	100	15	2,400
16	2	Octanol	10.5	100	5	1,200

## HF-LPME Procedure

A 500- $\mu$ l aliquot of urine was transferred into a 2-ml tube containing 80 mg ( $\pm$ 10 mg) of NaCl followed by the addition of 50  $\mu$ l of DMT-*d*<sub>6</sub> 1  $\mu$ g/ml (IS). The mixture's pH was adjusted using 200  $\mu$ l of 0.1 M carbonate-bicarbonate buffer pH 10.5. After that, an 8.0-cm polypropylene hollow fiber segment previously impregnated with n-decanol and filled with 2 mM ammonium formate buffer with 0.1% formic acid (mobile phase A) using gel-loading pipet tips was introduced into the sample solution. Both ends of the fiber were sealed by pressure using pliers. The LPME system was stirred for 5 min at 2,400 rpm using a multi-vortex. After agitation, the acceptor phase was collected from the fiber lumen, transferred into a vial, and dried under nitrogen stream at 50°C. Finally, the dried residue was re-suspended with 50  $\mu$ l of mobile phase A before injection (2  $\mu$ l) into the UPLC-MS/MS.

## Design of Experiments

Method optimization was accomplished by design of experiments (DoE) using the tools available on the Minitab® 18 software (LLC, State College, Pennsylvania, USA).

First, a screening step was performed taking into consideration five main parameters, selected during preliminary studies (not shown) included in a fractional factorial design, resolution V ( $2^{5-1}$ ): (a) SLM solvent (n-octanol and n-decanol), (b) buffer pH (borate buffer pH 9.5 and carbonate-bicarbonate buffer pH 10.5), (c) buffer volume (100 and 500  $\mu$ l), (d) stirring time (5 and 15 min), and (e) stirring rate (1,200 and 2,400 rpm). Sixteen random experiments were performed with a single replicate and the results were then evaluated according to the absolute response areas for all analytes.

Once these variables were screened and the significant ones were determined, a Box–Behnken design was performed with three variables at three different levels: (a) buffer pH (borate buffer pH 9.5, borate buffer pH 10.0, and carbonate-bicarbonate buffer pH 10.5), (b) buffer volume (100, 300, and 500  $\mu$ l), and

**TABLE 3** | Experimental matrix for the Box–Behnken design.

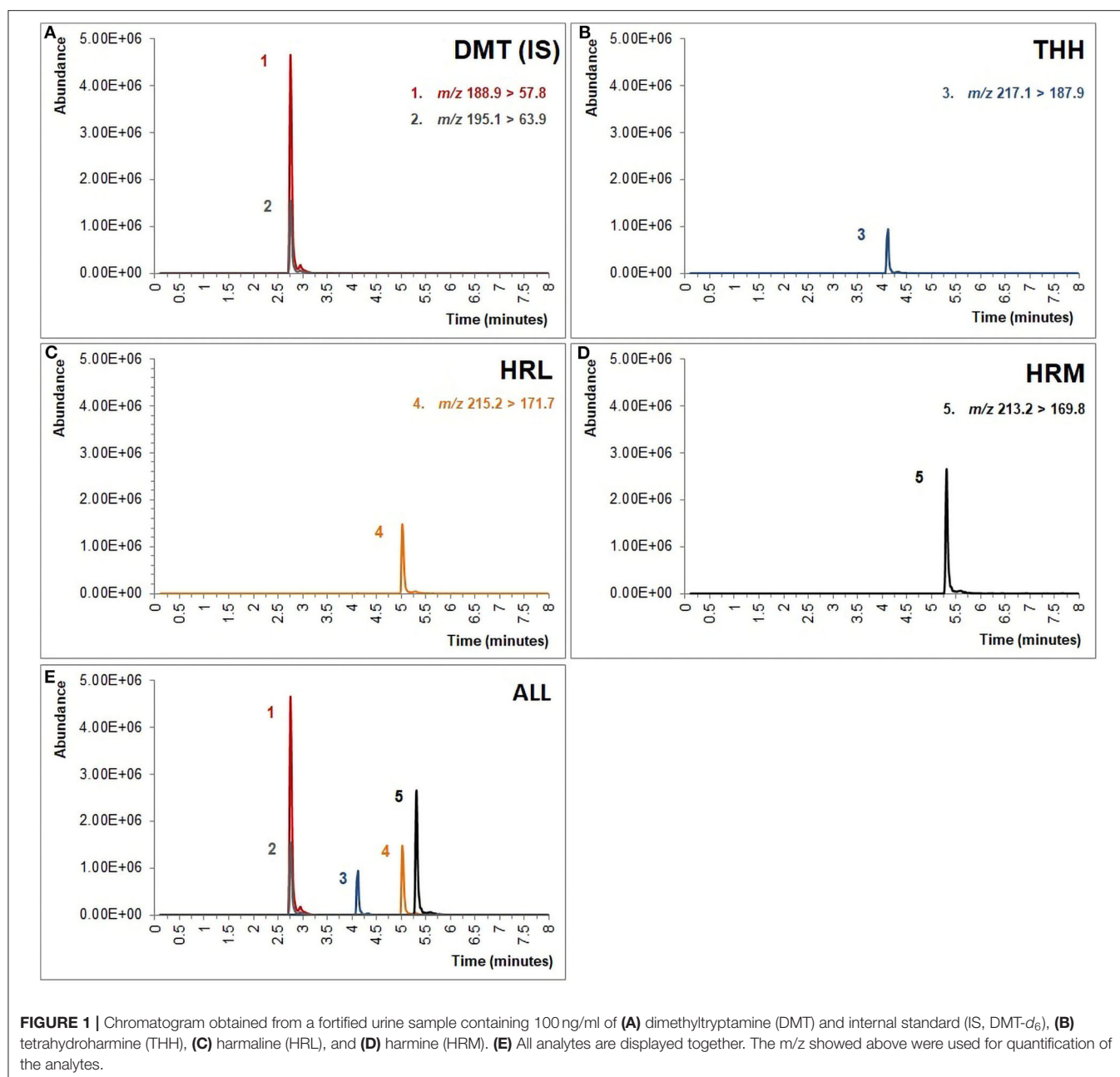
Experiment	Random order	Buffer pH	Buffer volume ( $\mu$ l)	Stirring time (min)
1	13	10.0	300	10
2	5	9.5	300	5
3	14	10.0	300	10
4	9	10.0	100	5
5	10	10.0	500	5
6	6	10.5	300	5
7	7	9.5	300	15
8	8	10.5	300	15
9	11	10.0	100	15
10	4	10.5	500	10
11	12	10.0	500	15
12	3	9.5	500	10
13	2	10.5	100	10
14	1	9.5	100	10
15	15	10.0	300	10

(c) stirring time (5, 10, and 15 min). Fifteen experiments were randomly performed with a replicate. Extraction parameters were optimized through response surface methodology (RSM) using absolute response areas.

Detailed description of experimental matrices is displayed in **Tables 2, 3**.

## Method Validation

Method validation was achieved in accordance to international recommendations (Matuszewski et al., 2003; Peters et al., 2007; United Nations Office On Drugs and Crime (UNODC), 2009). Limit of detection (LoD), limit of quantification (LoQ), selectivity, linearity, precision (intra- and inter-assay), accuracy, matrix effect (ME), recovery (RE), process efficiency (PE),



and dilution integrity studies were performed. The LoD was determined as the lowest concentration with a signal-to-noise ratio (S/N) of at least 3 showing all transitions and a relative standard deviation (RSD)  $\leq 20\%$ , while the LoQ was the lowest concentration presenting a S/N ratio of at least 10 and an RSD  $\leq 15\%$ .

Specificity was evaluated in 10 urine blank samples collected from different individuals and analyzed to attest the presence or absence of any endogenous interferences. The method was also assessed for potential exogenous interfering substances through the analysis of urine samples spiked at concentrations over the calibration range of 37 common drugs and metabolites:

caffeine, nicotine, cannabinoids, cocaine-related substances, amphetamines, opioids, barbiturates, antidepressants, and anxiolytics. Acceptance criteria were based on the absence of interfering peaks at the retention times of DMT, THH, HRL, HRM, and DMT- $d_6$ . IS possible interference was also assessed by analyzing a single urine sample fortified with DMT- $d_6$  and investigated for the presence of non-deuterated DMT as an impurity.

Linearity was evaluated over a wide concentration range, from LOQ to 200 ng/ml for all analytes of interest, at five different concentrations (5, 50, 100, 150, and 200 ng/ml) with each concentration value having six replicates. The peak area



ratios of the compounds to the IS were used for linear regression analysis, which was then expressed as the regression coefficients ( $r^2 \geq 0.99$ ).

Precision and accuracy studies were performed by analyzing negative urine specimens spiked with the analytes at three quality control (QC) levels: low (LQC, 15 ng/ml), medium (MQC, 90 ng/ml), and high (HQC, 170 ng/ml). QCs were evaluated over 3 consecutive days, through the analysis of six replicates for each QC level. These results were expressed as %RSD, calculated with one-way ANOVA. Acceptance criteria for both intra- and inter-assay precision were  $RSD \leq 20\%$  for the LQC and  $\leq 15\%$  for both MQC and HQC. Accuracy was determined through the quantification of six replicates at each QC level and was expressed as a percentage of the known concentration, i.e., acquired mean concentration/nominal concentration  $\times 100$ .

Blank samples were spiked with the analytes of interest at concentrations over the calibration range and then diluted 10- or 20-fold with 0.1 M carbonate-bicarbonate buffer pH 10.5 in order to evaluate dilution integrity. Both accuracy and precision parameters must remain within aforementioned acceptance criteria.

ME, RE, and PE experiments were assessed as described by Matuszewski et al. (2003). Three sets of experiments were prepared at LQC, MQC, and HQC with six replicates, given that each replicate was obtained from a different individual. Set

1: neat standards diluted in mobile phase; set 2: QC samples prepared by spiking blank urine samples after extraction, and set 3: represented by urine samples spiked before extraction. For RE calculation, absolute peak areas from set 3 were compared to those of set 2; for the ME, absolute peak areas from set 2 were compared to those of set 1; and for PE, absolute peak areas from set 3 were compared to those of set 1.

## RESULTS AND DISCUSSION

### Instrumental Analysis

The UPLC-MS/MS analysis, which has previously proven to be suitable for the analysis of ayahuasca tea samples (de Oliveira Silveira et al., 2020), has shown to be similarly adequate for the identification and quantification of all analytes in urine specimens using an 8-min chromatographic run as shown in **Figure 1**. Although chromatographic separation is not mandatory when using MRM, special attention was given to HRL and HRM separation since initial experimentation has demonstrated possible ion suppression for HRL when overlapped with HRM. Even though the focus of this study was to develop a green sample preparation method, it is clear that the greenness of this step is directly linked to the sensitivity of the subsequent chromatographic technique (Silveira et al., 2019). On the one

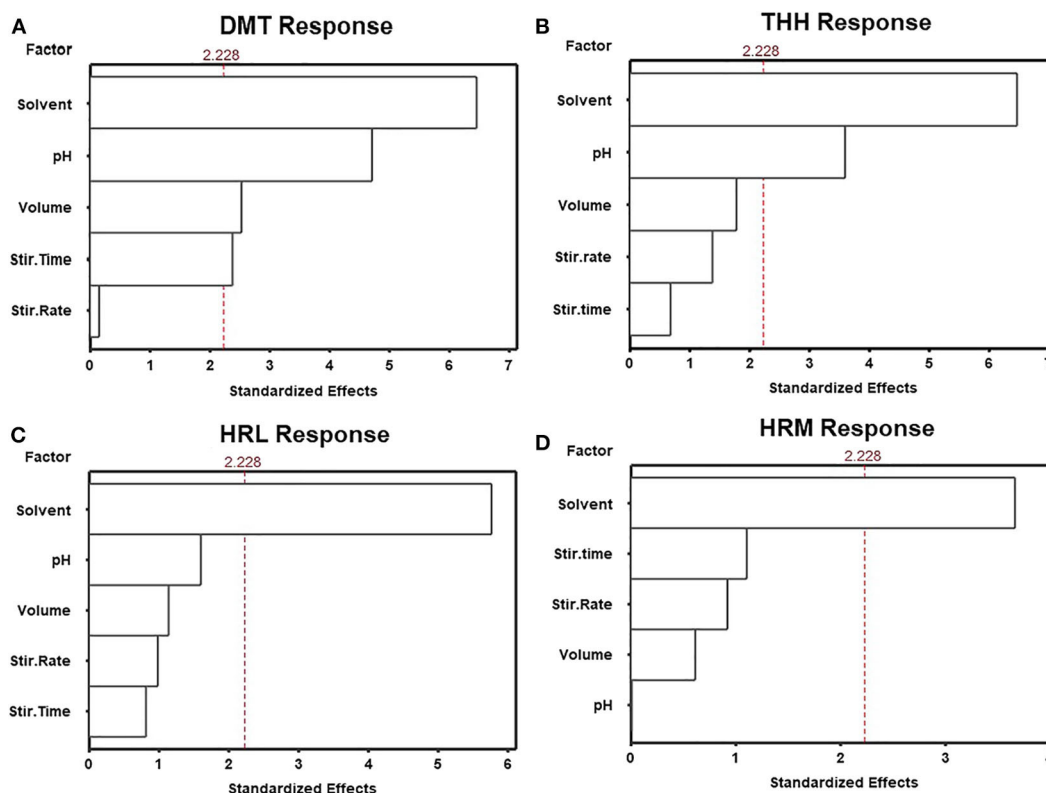
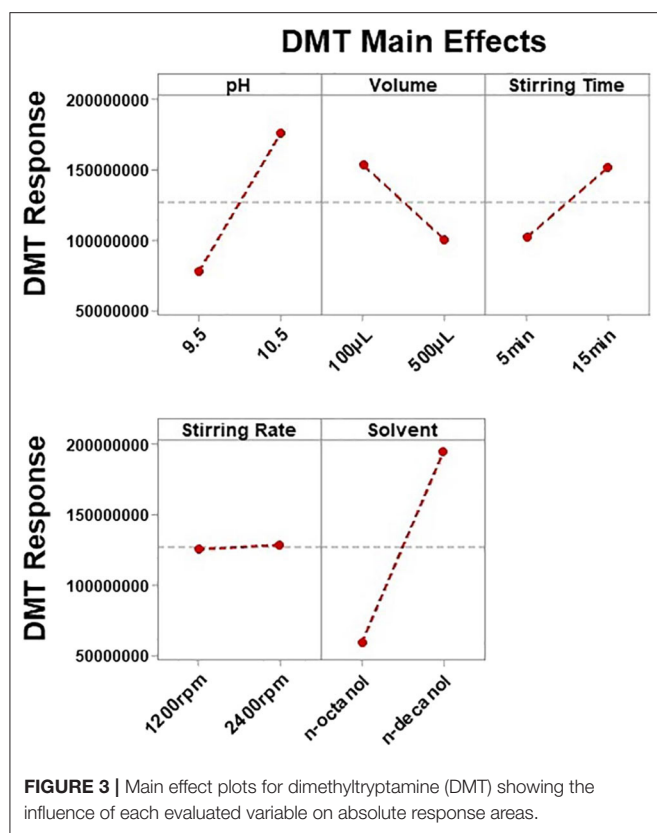


**FIGURE 2 |** Standardized main effect Pareto charts for the fractional factorial design of (A) dimethyltryptamine (DMT), (B) tetrahydroharmine (THH), (C) harmaline (HRL), and (D) harmine (HRM).



hand, gas chromatography (GC) is considered inherently eco-friendly once organic solvents are not necessary to achieve separation as in liquid chromatography (LC) (Ghosh, 2012), but on the other hand, some strategies may be used to reduce environmental impact of LC, such as shortening the run time by reducing column length and particle size leading to an overall decrease in solvent consumption which is readily achieved with ultra-high pressure liquid chromatography (UPLC) (Kaljurand and Koel, 2012; Korany et al., 2017). Nonetheless, the replacement of organic solvents used as mobile phases in LC is also a concern when dealing with GAC requirements given that the development of greener methods often depends on improving or modifying conventional procedures (Keith et al., 2007), and for this reason, the gradient elution was modified in order to guarantee significant satisfactory method performance when using methanol as mobile phase instead of acetonitrile as the former is considered less environmentally problematic than the latter, which makes acetonitrile substitution a main challenge in GAC (De La Guardia and Armenta, 2010; Korany et al., 2017; Silveira et al., 2019).

## Design of Experiments

HF-LPME performance may be influenced by several important parameters apart from those regarding the chemical characteristics of analytes, such as the following: sample volume, pH adjustment of donor phase, volume of the pH adjustment solution (sample dilution), type of organic solvent used as

SLM, agitation rate and time, acceptor solution composition, fiber segment length, and salting out (Psillakis and Kalogerakis, 2003). As urine is usually an abundant sample and of easy collection, method optimization was performed using 500 µl of the specimen, which lead to a fiber segment of 8.0 cm when using a 2.0-mL *Eppendorf* tube for optimum surface contact between phases. Considering that both LPME acceptor phase and LC mobile phase are required to have the same characteristics, i.e., a solution capable of ionizing the analytes, the acceptor solution used was composed of mobile phase A.

Consequently, among all above-mentioned variables, five were selected during preliminary studies (data not shown) for further investigation. SLM solvent, stirring time, stirring rate, buffer pH, and buffer volume were screened using a fractional factorial design (resolution V,  $2^{5-1}$ ) in order to determine variables significantly affecting method performance. Sixteen experiments were randomly performed and the results expressed as the mean of absolute response areas are displayed in Figures 2, 3. Figure 2 shows the Pareto charts for each analyte in which factors were considered of significance upon regression analysis if they revealed a  $p \leq 0.05$  (or standardized effect  $\geq 2.228$ ). According to this evaluation, only the organic solvent employed for the SLM influenced the extraction of all analytes. For this reason, the SLM composition must be carefully assessed when developing an LPME procedure since the solvent characteristics are directly associated to the extent of substance transfer through the membrane. Nonetheless, moderate polarity, viscosity, surface tensions, and boiling points are the features pursued in the search for an ideal LPME solvent (Kokosa, 2013). In this context, n-octanol and n-decanol were the solvents studied during method optimization.

THH's response was also determined by buffer pH, but only DMT's response was affected by more than three factors. Figure 3 shows how each variable influenced DMT's response. Once important parameters affecting method performance have been identified, based on the results obtained for DMT, a new optimization step was planned. Therefore, a Box–Behnken design was used to determine how these variables may be combined to promote maximum extraction response. Since n-decanol has shown to be the best solvent, not only for DMT but also for all analytes, it was incorporated in the HF-LPME procedure as well as the stirring rate of 2,400 rpm; thus, 15 Box–Behnken experiments were performed with the three remaining significant variables at three levels each (buffer pH, buffer volume, and stirring time).

Despite the response by THH not being affected by buffer volume or stirring time during the first optimization step, the Box–Behnken model results were evaluated according to the best combined response for both DMT and THH. Figure 4 shows how DMT and THH responded to different factor arrangements through response surface methodology after regression analysis. The pH of the donor phase (sample) may be adjusted by using an acidic/basic solution or a buffer; the latter is preferred since it guarantees pH maintenance during the whole extraction procedure. Also, pH value plays an important role because it is responsible for keeping the analyte in its uncharged form, so the substance is able to cross the SLM. Furthermore, the volume of

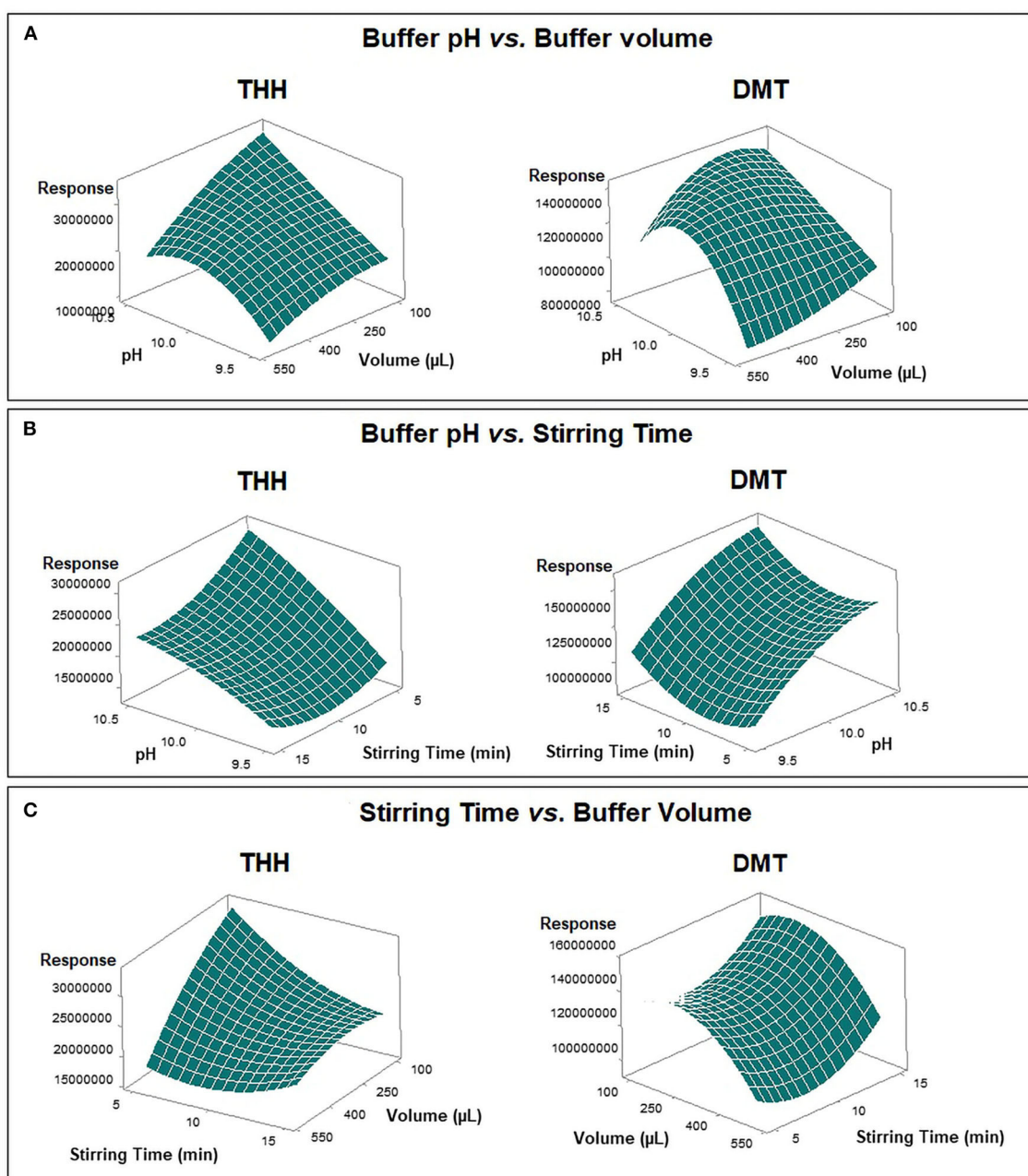


**FIGURE 4 |** Comparative response surface plots for absolute response areas of dimethyltryptamine (DMT) and tetrahydrocannabinol (THH) from Box-Behnken design. **(A)** Buffer pH vs. buffer volume. **(B)** Buffer pH vs. stirring time. **(C)** Stirring time vs. buffer volume.

the pH adjustment solution is responsible for sample dilution and influences the contact surface of the sample to the fiber segment, thus promoting extraction.

Optimum outcomes were found for both substances when using a carbonate-bicarbonate buffer pH 10.5; however, discrepancies were observed for buffer volume (300  $\mu$ l for DMT and 100  $\mu$ l for THH) and stirring time (15 min for DMT and 5 min for THH). In order to obtain the maximum response with the most economic combination of these variables for both

analytes, the optimization tool available on the Minitab software was applied to the acquired data; thus, a buffer volume of 200  $\mu$ l and a stirring time of 5 min were set as best extraction conditions (Figure 5).

Therefore, the use of a DoE strategy led to a less time-consuming and less laborious method development when compared to univariate methodologies in which only one factor is investigated at a time while keeping the remaining unchanged (Costa et al., 2010). In this case, interactions between different

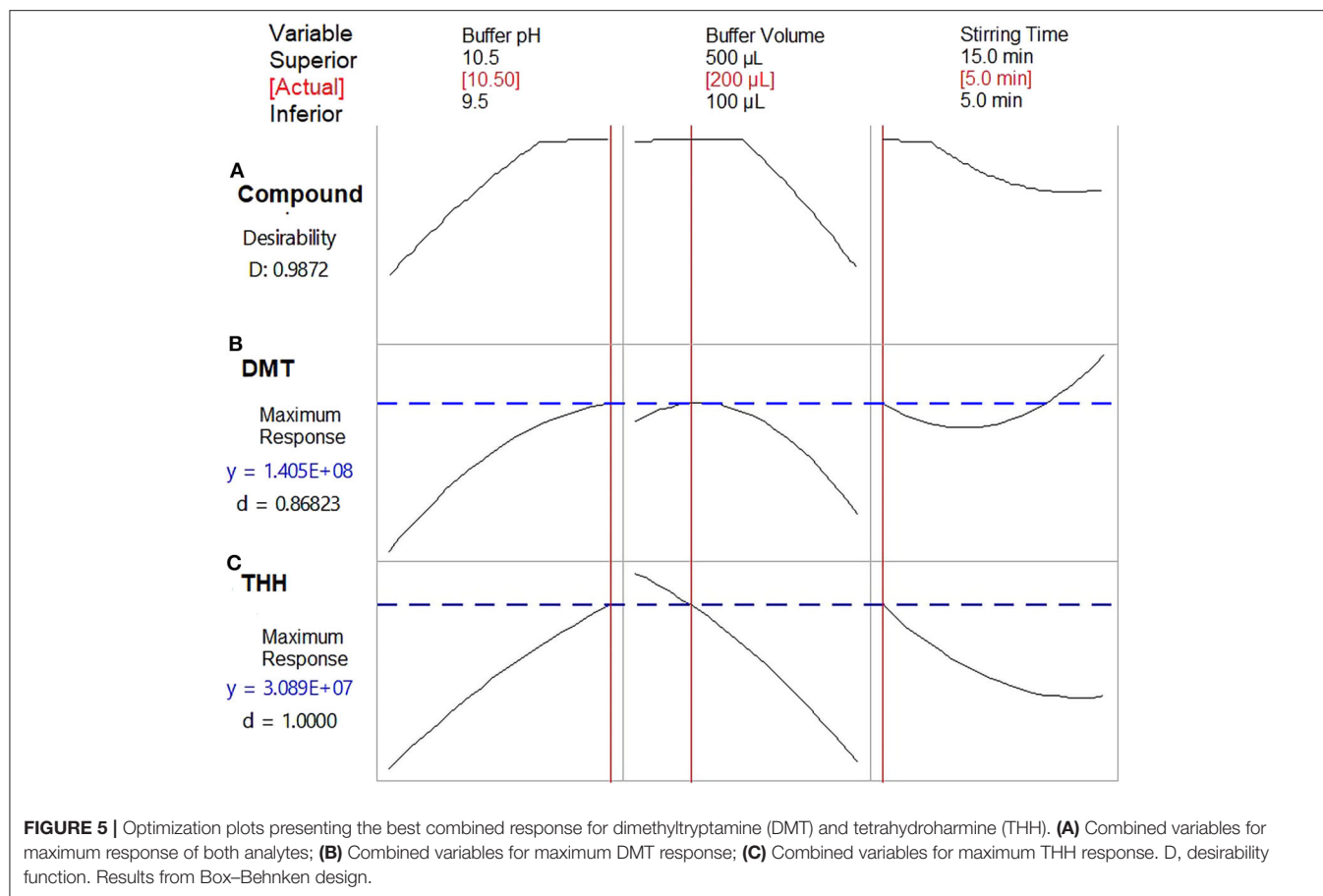


**TABLE 4 |** Limits of detection (LoD), limits of quantification (LoQ), linear regression equation, and determination coefficients for dimethyltryptamine (DMT), harmine (HRM), harmaline (HRL), and tetrahydroharmine (THH) in fortified urine samples.

Analyte	LoD (ng/ml)	LoQ (ng/ml)	Linear regression equation	Determination coefficient ( $r^2$ )
DMT	1.0	5.0	$y = 0.0613x - 0.0395$	0.9974
THH	2.0	5.0	$y = 0.0121x - 0.0183$	0.9923
HRL	2.0	5.0	$y = 0.0347x - 0.0855$	0.9913
HRM	2.0	5.0	$y = 0.0848x - 0.1024$	0.9921

parameters are not explored and the optimum arrangement may not be achieved (Costa et al., 2010). On the other hand, DoE allows for method optimization using a small number of experiments and combines the important variables in such a way that the maximum response can be obtained while minimal energy and materials are consumed, resulting in a greener extraction procedure. In our study, DoE resulted in an HF-LPME procedure using only 200  $\mu$ l of a carbonate-bicarbonate buffer pH 10.5 and a fast agitation step of 5 min at 2,400 rpm, minimizing energy consumption.

## Method Validation

Liquid microextraction may be defined as a sample preparation technique employing no more than 100  $\mu$ l of any organic solvent and promoting both extraction and analyte enrichment in the

final residue which leads to sensitive limits of detection (Spiegel et al., 2014). In the present study, LoD (1.0 or 2.0 ng/ml) and LoQ (5.0 ng/ml) values have shown to be fit-for-purpose for all analytes. These results can be seen in **Table 4** along with linearity parameters. This HF-LPME approach has proven to be linear over the range of 5.0–200 ng/ml and, since the *F*-test revealed that this method is heteroscedastic, the weighted least squares linear regression was applied resulting in a  $1/y$  weighting factor for HRL and  $1/x^2$  for DMT, THH, and HRM. All determination coefficients ( $r^2$ ) were above 0.99 and the relative error (RE%) of the weighted linear regression equations were never higher than 45.9% (HRL). Additionally, the least squares linear regression has resulted in negative intercept values that are not statistically different from zero, which means that the linear regression fits through the origin.



The evaluation of inter- and intra-assay precision was performed during 3 consecutive days, at three QC levels with six replicates for each level. **Table 5** shows that the RSD% values obtained after analysis of variance were according the acceptance criteria and ranged from 2.1% (DMT, LQC, and inter-assay) to 18% (HRL, LQC, an intra-assay). Likewise, the developed method revealed great accuracy performance ranging from 87.6% (THH and LQC) to 109.2% (THH and MQC) upon calculation using the resulting precision data.

After ingestion, the main compounds of the ayahuasca tea are partially excreted through the urine in their unmetabolized forms (Riba et al., 2012), and their concentrations may be 20 times above the highest calibration point of the abovementioned method. For this reason, dilution integrity was validated, considering both 10- and 20-fold in two different concentrations (300 and 3,200 ng/ml). Accuracy parameters remained acceptable for all analytes (87.0–110.5%), excluding HRL which when diluted 20-fold could neither maintain its accuracy nor detect analyte in some instances. Hence, HRL quantification in authentic samples was accomplished using only a 10-fold dilution factor as it provides sufficient accuracy (86.5%).

One of the main features of the HF-LPME approach rests in its clean-up potential as the pores within the fiber wall are able to separate the uncharged analytes from the endogenous matrix interferences (Sarafraz-Yazdi and Amiri, 2010; Ghambarian et al., 2012). Regardless of the simplicity provided by dilute-and-shoot and protein precipitation (PP) methods, these alternatives are not always suitable, especially when it comes to LC-MS instrumentation. The former is prone to rather large matrix effects and instrument contamination, while the latter hardly eliminates matrix interferences other than proteins, such as phospholipids, salts, cells, small peptides, and other organic molecules present in urine specimens that can bind to detector surfaces, which may reduce the LC column lifetime and lead to low sensitivity as well as additional drawbacks generated by matrix effects (Chiu et al., 2010; Rentsch, 2016; Peters et al., 2018). Although a previous PP approach published by de Moraes et al. (2018) has shown low ME, this may not be true to all LC systems with ESI interfaces, so we believe that HF-LPME may avoid these negative consequences. Additionally, PP methods previously published for the analysis of the analytes of interest in urine samples use large amounts of solvents, either acetonitrile or methyl *tert*-butyl ether ( $\geq 1.0$  ml) (Zhao et al., 2012; Meyer et al., 2014; de Moraes et al., 2018), to achieve sample clean-up, while the present method succeeded in accomplishing great ME and RE using volumes as low as 25  $\mu$ l of an organic solvent (n-decanol). ME, RE, and PE evaluation was developed by Matuszewski et al. (2003) protocols. As suggested by Bienvenu et al. (2017), samples were selected considering a large density range. Results are can be seen in **Table 6**. Although most analytes have revealed a small degree of ion enhancement which may super estimate recovery values, we concluded that our method has excellent ME, RE, and PE performances.

Interference studies showed no interfering peaks either by endogenous or exogenous substances at the retention times of DMT, THH, HRL, and HRM, nor was the deuterated internal standard contaminated with non-labeled DMT.

**TABLE 5 |** Inter-assay and intra-assay precision and accuracy for dimethyltryptamine (DMT), harmine (HRM), harmaline (HRL), and tetrahydroharmine (THH) in fortified urine samples.

Analyte	QC level (ng/ml)	Precision (n = 6)		Accuracy (% , n = 6)
		Inter-assay (RSD%)	Intra-assay (RSD%)	
DMT	15	2.1	10.2	98.5
	90	9.5	7.6	104.8
	170	8.9	7.4	103.7
THH	15	12.3	10.2	87.6
	90	9.6	10.8	109.2
	170	11.8	8.8	100.4
HRL	15	8.3	18.0	103.2
	90	11.8	11.1	99.1
	170	11.8	8.8	108.9
HRM	15	6.6	9.6	92.4
	90	5.5	11.3	95.8
	170	7.1	12.2	105.5

**TABLE 6 |** Percentage of matrix effect (ME%), recovery (RE%), and process efficiency (PE%) after submitting spiked urine samples to HF-LPME and UPLC-MS/MS analysis.

Analyte	QC level (ng/ml)	ME (%)	RE (%)	PE (%)
DMT	15	88.4	110.5	97.7
	90	107.1	124.8	133.7
	170	103.5	111.2	115.1
THH	15	108.7	79.2	86.1
	90	119.8	89.1	106.7
	170	112.4	97.7	109.8
HRL	15	111.7	94.8	105.8
	90	115.8	95.9	111.1
	170	112.5	99.9	112.4
HRM	15	96.0	117.9	113.2
	90	109.5	91.6	100.3
	170	101.0	102.0	103.0
DMT- <i>d</i> <sub>6</sub>	100	103.9	74.8	77.7

Finally, considering previously published articles on the analysis of ayahuasca alkaloids in urine specimens using LC-MS/MS, only three of them have provided detailed data regarding full validation protocols (Bjornstad et al., 2009; Mcilhenny et al., 2011; de Moraes et al., 2018). The present HF-LPME method has shown higher sensitivity than most of the referred methods, except by the dilute-and-shoot alternative given by Mcilhenny et al. (2011) that achieved LoD values below 1 ng/ml. However, both LoQ figures and linearity ranges were similar in all alternatives. Simply, the screening method by Bjornstad et al. (2009) has suggested a calibration range over 200 ng/ml. Additionally, reproducibility parameters are in compliance with both the aforementioned alternatives and current validation guidelines.



**TABLE 7 |** Concentrations (ng/ml) of ayahuasca alkaloids in authentic samples after quantification by HF-LPME and UPLC-MS/MS.

Subject	Sample	DMT	THH	HRL	HRM
01	1st	1,796.8	726.3	176.6	79.6
	2nd	67.5	129.1	45.9	33.7
02	1st	820.6	70.5	41.4	149.2
	2nd	253.5	174.2	56.9	72.9
03	1st	497.6	30.6	30.5	52.7
	2nd	4,120.3	908.6	334.0	859.4
04	1st	358.0	85.3	28.3	30.5
	2nd	1,559.2	658.7	68.9	101.0

## Authentic Samples

In order to prove method feasibility, eight samples were collected from four individuals. The subjects agreed in donating the specimens after having participated in a traditional ayahuasca ceremony. Three participants have ingested two different ayahuasca doses while one of them has drunk only a single dose. The first and second urine samples naturally produced by the individuals were analyzed. Information regarding the ingested amount of tea as well as the concentration of the alkaloids present in the beverage, time of consumption, and sample collection intervals were not assessed given that the alkaloid kinetics in humans is well-established, as previously published (McIlhenny et al., 2011; Riba et al., 2012, 2015).

As displayed in **Table 7**, DMT concentration ranged from 67.5 to 4,120.3 ng/ml. For this last sample, a 20-fold dilution was required in order to fit the validated calibration range. THH varied from 30.6 to 908.6 ng/ml, the second most abundant alkaloid, after DMT. HRL and HRM concentrations ranged from 28.3 to 334.0 ng/ml and 30.5 to 859.4 ng/ml, respectively. HRL was the less abundant compound quantified in these urine specimens. Both the calibration range and the dilution factors validated in our study proved to be suitable for the quantification of ayahuasca alkaloids.

## CONCLUSION

Given the imminent relevance of ayahuasca researches and the consequent importance and need for the quantification of its main compounds in biological samples, the present study has described a fast and simple HF-LPME method for the determination of DMT, THH, HRL, and HRM in urine samples of ayahuasca users. After effectively applying

a design-of-experiments approach, the significant factors influencing method performance were optimized to achieve the most time-, material- and energy-saving manner possible. The HF-LPME was fully validated showing excellent sensitivity, reproducibility, reduced matrix effect interferences, and outstanding recoveries. Therefore, we believe that given the fact that the sample preparation step in analytical chemistry can hardly be avoided, the eco-friendliest alternative that suits one's laboratory conditions (LC systems) must always be considered. In addition, our approach has proven to be a greener alternative when protein precipitation or dilute-and-shoot methods do not represent the most suitable option. Finally, eight authentic samples were successfully quantified by the developed method showing great applicability.

## DATA AVAILABILITY STATEMENT

The raw data supporting the conclusions of this article will be made available by the authors, without undue reservation.

## ETHICS STATEMENT

The studies involving human participants were reviewed and approved by the Ethics Committee of School of Pharmaceutical Sciences, University of São Paulo (ethics protocol approval number 2.267.476). The patients/participants provided their written informed consent to participate in this study.

## AUTHOR CONTRIBUTIONS

GS and MY contributed with the conception and design of the study. GS performed all experiments and wrote the first draft of the manuscript. FL performed the statistical analysis. VB was responsible for sample collection and consent from individuals. All authors contributed to manuscript revision, read, and approved the submitted version.

## FUNDING

This research was funded by Fundação de Amparo à Pesquisa do Estado de São Paulo (FAPESP, Grant Nos. 2016/06810-2 and 2018/24770-3).

## ACKNOWLEDGMENTS

Coordenação de Aperfeiçoamento de Pessoal de Nível Superior (CAPES) is gratefully acknowledged.

## REFERENCES

- Armenta, S., Garrigues, S., and de la Guardia, M. (2015). The role of green extraction techniques in green analytical chemistry. *TrAC Trends Anal. Chem.* 71, 2–8. doi: 10.1016/j.trac.2014.12.011
- Bienvenu, J. F., Provencher, G., Bélanger, P., Bérubé, R., Dumas, P., Gagné, S., et al. (2017). Standardized procedure for the simultaneous determination of

- the matrix effect, recovery, process efficiency, and internal standard association. *Anal. Chem.* 89, 7560–7568. doi: 10.1021/acs.analchem.7b01383
- Bjornstad, K., Beck, O., and Helander, A. (2009). A multi-component LC-MS/MS method for detection of ten plant-derived psychoactive substances in urine. *J. Chromatogr. B Anal. Technol. Biomed. Life Sci.* 877, 1162–1168. doi: 10.1016/j.jchromb.2009.03.004

- Callaway, J. C., McKenna, D. J., Grob, C. S., Brito, G. S., Raymon, L. P., Poland, R. E., et al. (1999). Pharmacokinetics of Hoasca alkaloids in healthy humans. *J. Ethnopharmacol.* 65, 243–256. doi: 10.1016/S0378-8741(98)00168-8
- Callaway, J. C., Raymon, L. P., Hearn, W. L., McKenna, D. J., Grob, C. S., Brito, G. S., et al. (1996). Quantitation of N,N-dimethyltryptamine and harmala alkaloids in human plasma after oral dosing with ayahuasca. *J. Anal. Toxicol.* 20, 492–497. doi: 10.1093/jat/20.6.492
- Carasek, E., and Merib, J. (2015). Membrane-based microextraction techniques in analytical chemistry: a review. *Anal. Chim. Acta* 880, 8–25. doi: 10.1016/j.aca.2015.02.049
- Chiu, M. L., Lawi, W., Snyder, S. T., Wong, P. K., Liao, J. C., and Gau, V. (2010). Matrix effects-A challenge toward automation of molecular analysis. *J. Assoc. Lab. Autom.* 15, 233–242. doi: 10.1016/j.jala.2010.02.001
- Costa, S., Barroso, M., Castañera, A., and Dias, M. (2010). Design of experiments, a powerful tool for method development in forensic toxicology : application to the optimization of urinary morphine 3-glucuronide acid hydrolysis. *Anal. Bioanal. Chem.* 396, 2533–2542. doi: 10.1007/s00216-009-3447-8
- De La Guardia, M., and Armenta, S. (2010). Green solvents for analytical separation and analyses. In: Meyers RA, editors. *Encyclopedia of Analytical Chemistry: Applications, Theory and Instrumentation* (Nova Jersey: John Wiley & Sons, Ltd), 1–20. doi: 10.1002/9780470027318.a9179
- de Moraes, D. R., Lanaro, R., Barbosa, I. L., Santos, J. M., Cunha, K. F., Hernandez, V. V., et al. (2018). Ayahuasca and Kambo intoxication after alternative natural therapy for depression, confirmed by mass spectrometry. *Forensic Toxicol.* 36, 212–221. doi: 10.1007/s11419-017-0394-5
- de Oliveira Silveira, G., Guimarães dos Santos, R., Rebello Lourenço, F., Novak Rossi, G., Hallak, J., and Yonamine, M. (2020). Stability evaluation of DMT and harmala alkaloids in ayahuasca tea samples. *Molecules* 25:2072. doi: 10.3390/molecules25092072
- de Oliveira, C. D. R., Moreira, C. Q., Spinosa, H., de, S., and Yonamine, M. (2011). Neurobehavioral, reflexological and physical development of wistar rat offspring exposed to ayahuasca during pregnancy and lactation. *Brazil. J. Pharmacogn.* 21, 1065–1076. doi: 10.1590/S0102-695X2011005000170
- dos Santos, R. G., and Hallak, J. E. C. (2020). Therapeutic use of serotonergic hallucinogens: a review of the evidence and of the biological and psychological mechanisms. *Neurosci. Biobehav. Rev.* 108, 423–434. doi: 10.1016/j.neubiorev.2019.12.001
- Dunlap, L. E., Azinfar, A., Ly, C., Cameron, L. P., Viswanathan, J., Tombari, R. J., et al. (2020). Identification of psychoplastogenic N, N-dimethylaminoisotryptamine (isoDMT) analogues through structure-activity relationship studies. *J. Med. Chem.* 63, 1142–1155. doi: 10.1021/acs.jmedchem.9b01404
- Estrella-Parra, E. A., Almanza-Pérez, J. C., and Alarcón-Aguilar, F. J. (2019). Ayahuasca: uses, phytochemical and biological activities. *Nat. Products Bioprospect.* 9, 251–265. doi: 10.1007/s13659-019-0210-5
- Forsström, T., Tuominen, J., and Kärkkäinen, J. (2001). Determination of potentially hallucinogenic N-dimethylated indoleamines in human urine by HPLC/ESI-MS-MS. *Scand. J. Clin. Lab. Invest.* 61, 547–556. doi: 10.1080/003655101753218319
- Frecka, E., Bokor, P., and Winkelman, M. (2016). The therapeutic potentials of Ayahuasca: possible effects against various diseases of civilization. *Front. Pharmacol.* 7:35. doi: 10.3389/fphar.2016.00035
- Frison, G., Favretto, D., Zancanaro, F., Fazzin, G., and Ferrara, S. D. (2008). A case of  $\beta$ -carboline alkaloid intoxication following ingestion of Peganum harmala seed extract. *Forensic Sci. Int.* 179, 37–43. doi: 10.1016/j.forsciint.2008.05.003
- Gałuszka, A., Migaszewski, Z., and Namieśnik, J. (2013). The 12 principles of green analytical chemistry and the SIGNIFICANCE mnemonic of green analytical practices. *TrAC Trends Anal. Chem.* 50, 78–84. doi: 10.1016/j.trac.2013.04.010
- Ghambarian, M., Yamini, Y., and Esrafil, A. (2012). Developments in hollow fiber based liquid-phase microextraction: principles and applications. *Microchim. Acta* 177, 271–294. doi: 10.1007/s00604-012-0773-x
- Ghosh, C. (2012). Green bioanalysis: Some innovative ideas towards green analytical techniques. *Bioanalysis* 4, 1377–1391. doi: 10.4155/bio.12.31
- Ishii, A., Seno, H., Suzuki, O., Hattori, H., and Kumazawa, T. (1997). A simple and sensitive quantitation of N,N-dimethyltryptamine by gas chromatography with surface ionization detection. *J. Anal. Toxicol.* 21, 36–40. doi: 10.1093/jat/21.1.36
- Kaljurand, M., and Koel, M. (2012). “Green bioanalytical chemistry,” in *Handbook of Green Analytical Chemistry* (Chichester: John Wiley & Sons, Ltd.), 425–447. doi: 10.4155/bio.12.70
- Keith, L. H., Gron, L. U., and Young, J. L. (2007). Green analytical methodologies. *Chem. Rev.* 107, 2695–2708. doi: 10.1021/cr068359e
- Kokosa, J. M. (2013). Advances in solvent-microextraction techniques. *TrAC Trends Anal. Chem.* 43, 2–13. doi: 10.1016/j.trac.2012.09.020
- Korany, M. A., Mahgoub, H., Haggag, R. S., Ragab, M. A. A., and Elmallah, O. A. (2017). Green chemistry : analytical and chromatography. *J. Liq. Chromatogr. Relat. Technol.* 40, 839–852. doi: 10.1080/10826076.2017.1373672
- Matuszewski, B. K., Constanzer, M. L., and Chavez-Eng, C. M. (2003). Strategies for the assessment of matrix effect in quantitative bioanalytical methods based on HPLC-MS/MS. *Anal. Chem.* 75, 3019–3030. doi: 10.1021/ac020361s
- McIlhenny, E. H., Riba, J., Barbanjo, M. J., Strassman, R., and Barker, S. A. (2011). Methodology for and the determination of the major constituents and metabolites of the amazonian botanical medicine ayahuasca in human urine. *Biomed. Chromatogr.* 25, 970–984. doi: 10.1002/bmc.1551
- McKenna, D. J. (2004). Clinical investigations of the therapeutic potential of ayahuasca: Rationale and regulatory challenges. *Pharmacol. Ther.* 102, 111–129. doi: 10.1016/j.pharmthera.2004.03.002
- Meyer, M. R., Caspar, A., Brandt, S. D., and Maurer, H. H. (2014). A qualitative/quantitative approach for the detection of 37 tryptamine-derived designer drugs, 5 -carbolines, ibogaine, and yohimbine in human urine and plasma using standard urine screening and multi-analyte approaches. *Anal. Bioanal. Chem.* 406, 225–237. doi: 10.1007/s00216-013-7425-9
- Miller, M. J., Albarracín-Jordan, J., Moore, C., and Capriles, J. M. (2019). Chemical evidence for the use of multiple psychotropic plants in a 1,000-year-old ritual bundle from South America. *Proc. Natl. Acad. Sci. U.S.A.* 166, 11207–11212. doi: 10.1073/pnas.1902174116
- Muttoni, S., Ardissino, M., and John, C. (2019). Classical psychedelics for the treatment of depression and anxiety: a systematic review. *J. Affect. Disord.* 258, 11–24. doi: 10.1016/j.jad.2019.07.076
- Oliveira, C. D., Okai, G. G., da Costa, J. L., de Almeida, R. M., Oliveira-Silva, D., and Yonamine, M. (2012). Determination of dimethyltryptamine and beta-carbolines (ayahuasca alkaloids) in plasma samples by LC-MS/MS. *Bioanalysis* 4, 1731–1738. doi: 10.4155/bio.12.124
- Oliveira, C. D. R., Moreira, C. Q., de Sá, L. R. M., de Souza Spinosa, H., and Yonamine, M. (2010a). Maternal and developmental toxicity of ayahuasca in wistar rats. *Dev. Reprod. Toxicol.* 89, 207–212. doi: 10.1002/bdrb.20244
- Oliveira, C. D. R., Moreira, C. Q., de Sá, L. R. M., de Souza Spinosa, H., and Yonamine, M. (2010b). The relevance of performing developmental toxicity studies about ayahuasca. *Dev. Reprod. Toxicol.* 89, 531–532. doi: 10.1002/bdrb.20271
- Orsolini, L., Volpe, U., Vellante, F., Chiappini, S., Papanti, D., Latini, R., et al. (2020). How does ayahuasca work from a psychiatric perspective? Pros and cons of the entheogenic therapy. *Hum. Psychopharmacol.* 35:e2728. doi: 10.1002/hup.2728
- Palhano-Fontes, F., Barreto, D., Onias, H., Andrade, K. C., Novaes, M., Pessoa, J., et al. (2017). Rapid antidepressant effects of the psychedelic ayahuasca in treatment-resistant depression: a randomised placebo-controlled trial. *Psychol. Med.* 49, 655–663. doi: 10.1017/S0033291718001356
- Pedersen-Bjergaard, S., and Rasmussen, K. E. (1999). Liquid-liquid-liquid microextraction for sample preparation of biological fluids prior to capillary electrophoresis. *Anal. Chem.* 71, 2650–2656. doi: 10.1021/ac990055n
- Pedersen-Bjergaard, S., and Rasmussen, K. E. (2005). Bioanalysis of drugs by liquid-phase microextraction coupled to separation techniques. *J. Chromatogr. B Anal. Technol. Biomed. Life Sci.* 817, 3–12. doi: 10.1016/j.jchromb.2004.08.034
- Peters, F. T., Drummer, O. H., and Musshoff, F. (2007). Validation of new methods. *Forensic Sci. Int.* 165, 216–224. doi: 10.1016/j.forsciint.2006.05.021
- Peters, F. T., Wissenbach, D. K., Busardo, F. P., Marchei, E., and Pichini, S. (2018). Method development in forensic toxicology. *Curr. Pharm. Des.* 23, 5455–5467. doi: 10.2174/1381612823666170622113331
- Pope, J. D., Choy, K. W., Drummer, O. H., and Schneider, H. G. (2019). Harmala alkaloids identify Ayahuasca intoxication in a urine drug screen. *J. Anal. Toxicol.* 43, e23–e27. doi: 10.1093/jat/bky105
- Psillakis, E., and Kalogerakis, N. (2003). Developments in liquid-phase microextraction. *TrAC Trends Anal. Chem.* 22, 565–574. doi: 10.1016/S0165-9936(03)01007-0

- Reiff, C. M., Richman, E. E., Nemeroff, C. B., Carpenter, L. L., Widge, A. S., Rodriguez, C. I., et al. (2020). Psychedelics and psychedelic-assisted psychotherapy. *Am. J. Psychiatry* 175, 391–410. doi: 10.1176/appi.ajp.2019.19010035
- Rentsch, K. M. (2016). Knowing the unknown – State of the art of LCMS in toxicology. *TrAC Trends Anal. Chem.* 84, 88–93. doi: 10.1016/j.trac.2016.01.028
- Riba, J., McIlhenny, E. H., Bouso, J. C., and Barker, S. A. (2015). Metabolism and urinary disposition of N,N-dimethyltryptamine after oral and smoked administration: a comparative study. *Drug Test. Anal.* 7, 401–406. doi: 10.1002/dta.1344
- Riba, J., McIlhenny, E. H., Valle, M., Bouso, J. C., and Barker, S. A. (2012). Metabolism and disposition of N,N-dimethyltryptamine and harmala alkaloids after oral administration of ayahuasca. *Drug Test. Anal.* 4, 610–616. doi: 10.1002/dta.1344
- Riba, J., Valle, M., Urbano, G., Yritia, M., Morte, A., and Barbanjo, M. J. (2003). Human pharmacology of ayahuasca: Subjective and cardiovascular effects, monoamine metabolite excretion, and pharmacokinetics. *J. Pharmacol. Exp. Ther.* 306, 73–83. doi: 10.1124/jpet.103.049882
- Sánchez, C., and Bouso, C. (2015). Ayahuasca: from the Amazon to the global village. *Drug Policy Briefings* 43, 1–24.
- Sarafraz-Yazdi, A., and Amiri, A. (2010). Liquid-phase microextraction. *TrAC Trends Anal. Chem.* 29, 1–14. doi: 10.1016/j.trac.2009.10.003
- Silveira, G. D. O., Pego, A. M. F., Pereira E Silva, J., and Yonamine, M. (2019). Green sample preparations for the bioanalysis of drugs of abuse in complex matrices. *Bioanalysis* 11, 295–312. doi: 10.4155/bio-2018-0208
- Simão, A. Y., Gonçalves, J., Duarte, A. P., Barroso, M., Cristóvão, A. C., and Gallardo, E. (2019). Toxicological aspects and determination of the main components of ayahuasca: a critical review. *Medicines* 6:106. doi: 10.3390/medicines6040106
- Spietelun, A., Marcinkowski, Ł., de La Guardia, M., and Namieśnik, J. (2014). Green aspects, developments and perspectives of liquid phase microextraction techniques. *Talanta* 119, 34–45. doi: 10.1016/j.talanta.2013.10.050
- Tavares, L., Monedeiro, F., Bordin, D. M., and de Martinis, B. S. (2020). Investigation of ayahuasca  $\beta$ -carboline alkaloids and tryptamine in sweat samples from religious community participants by GC-MS. *J. Anal. Toxicol.* 44, 601–609. doi: 10.1093/jat/bkz116
- Tupper, K. W. (2008). The globalization of ayahuasca: Harm reduction or benefit maximization? *Int. J. Drug Policy* 19, 297–303. doi: 10.1016/j.drugpo.2006.11.001
- Turner, C. (2013). Sustainable analytical chemistry—more than just being green. *Pure Appl. Chem.* 85, 2217–2229. doi: 10.1351/pac-con-13-02-05
- United Nations Office On Drugs and Crime (UNODC) (2009). *Guidance for the Validation of Analytical Methodology and Calibration of Equipment Used for Testing of Illicit Drugs in Seized Materials and Biological Specimens*.
- Wang, M. J., Tsai, C. H., Hsu, W. Y., Liu, J. T., and Lin, C. H. (2009). Optimization of separation and online sample concentration of N,N-dimethyltryptamine and related compounds using MEKC. *J. Sep. Sci.* 32, 441–445. doi: 10.1002/jssc.200800492
- Zhao, T., Zheng, S. S., Zhang, B. F., Li, Y. Y., Bligh, S. W. A., Wang, C. H., et al. (2012). Metabolic pathways of the psychotropic-carboline alkaloids, harmaline and harmine, by liquid chromatography/mass spectrometry and NMR spectroscopy. *Food Chem.* 134, 1096–1105. doi: 10.1016/j.foodchem.2012.03.024

**Conflict of Interest:** The authors declare that the research was conducted in the absence of any commercial or financial relationships that could be construed as a potential conflict of interest.

Copyright © 2020 Silveira, Lourenço, Bruno and Yonamine. This is an open-access article distributed under the terms of the Creative Commons Attribution License (CC BY). The use, distribution or reproduction in other forums is permitted, provided the original author(s) and the copyright owner(s) are credited and that the original publication in this journal is cited, in accordance with accepted academic practice. No use, distribution or reproduction is permitted which does not comply with these terms.



# Extended Stability Evaluation of Selected Cathinones

Heather L. Ciallella<sup>1</sup>, Lexus R. Rutter<sup>1</sup>, Lorna A. Nisbet<sup>2</sup> and Karen S. Scott<sup>1\*</sup>

<sup>1</sup> Forensic Science, Department of Chemistry and Physics, Arcadia University, Glenside, PA, United States, <sup>2</sup> Forensic and Investigative Science, School of Life Science, Anglia Ruskin University, Cambridge, United Kingdom

## OPEN ACCESS

### Edited by:

Marta Concheiro-Guisan,  
John Jay College of Criminal Justice,  
United States

### Reviewed by:

Rafael De La Torre,  
IMIM-Hospital del Mar Medical  
Research Institute, Spain  
Ana Miguel Fonseca Pego,  
Other, Maastricht, Netherlands  
Kayla Ellefsen,  
Travis County Medical Examiner's  
Office (TCMEO), United States

### \*Correspondence:

Karen S. Scott  
scottk@arcadia.edu

### Specialty section:

This article was submitted to  
Analytical Chemistry,  
a section of the journal  
Frontiers in Chemistry

Received: 21 August 2020

Accepted: 13 October 2020

Published: 13 November 2020

### Citation:

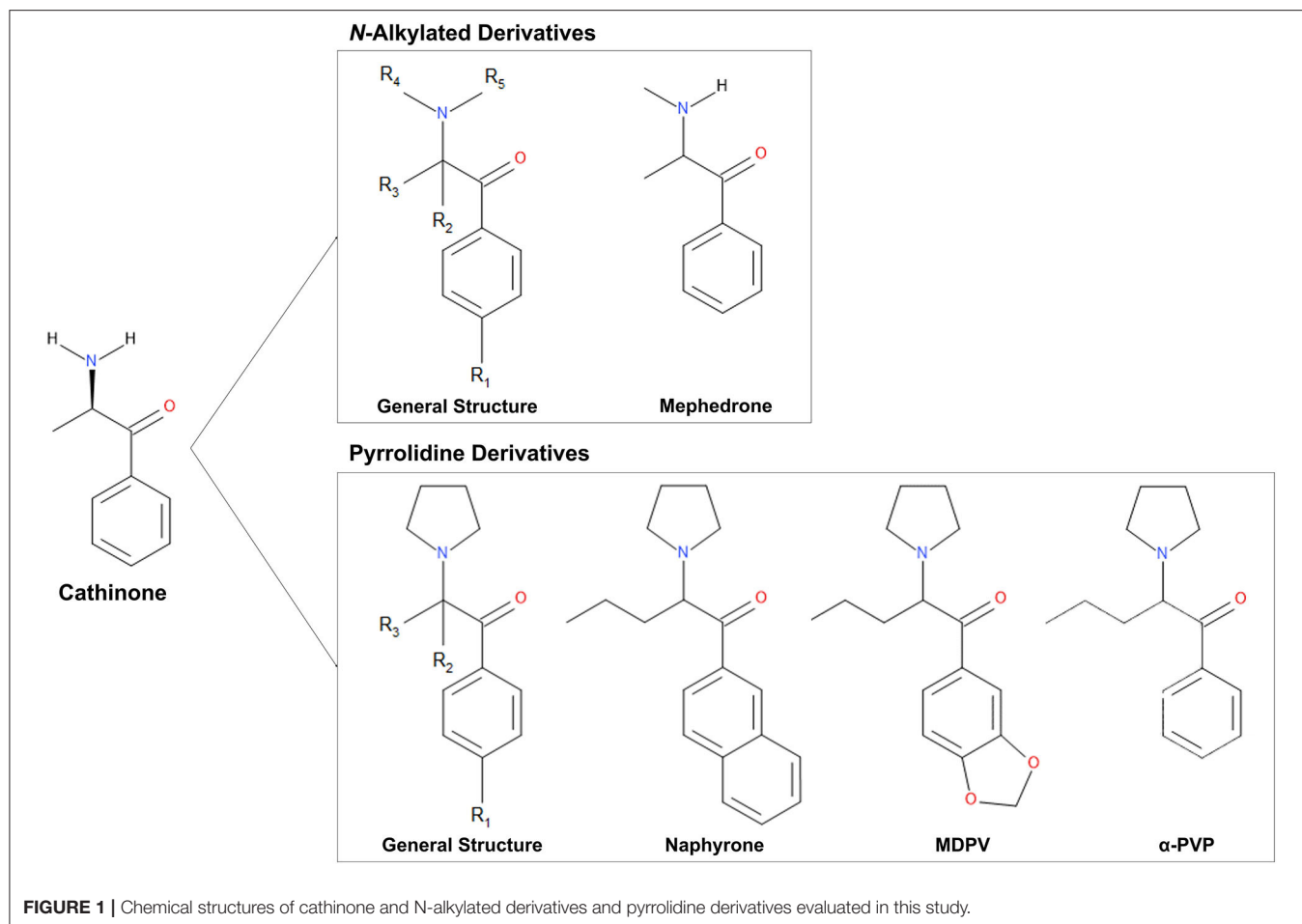
Ciallella HL, Rutter LR, Nisbet LA and  
Scott KS (2020) Extended Stability  
Evaluation of Selected Cathinones.  
Front. Chem. 8:597726.  
doi: 10.3389/fchem.2020.597726

Understanding the stability of drugs in a forensic toxicology setting is critical for the evaluation of drug concentrations. Synthetic cathinones are new psychoactive substances structurally derived from cathinone, the psychoactive component of *Catha edulis* ("khat"), a shrub that is indigenous to the Middle East and East Africa. Previous research has evaluated the stability of synthetic cathinones in biological matrices, including blood preserved with the combination of NaF and K<sub>2</sub>C<sub>2</sub>O<sub>4</sub> used in gray-top tubes. However, it does not assess their stability in blood preserved with Na<sub>2</sub>EDTA, used for some clinical samples. Further, stability in unpreserved urine samples was only studied for two weeks. This research evaluates the stabilities of four Schedule I synthetic cathinones: mephedrone, MDPV (3,4-methylenedioxypyrovalerone), naphyrone, and  $\alpha$ -PVP (alpha-pyrrolidinopentiophenone) at 20°C (room temperature), 4°C (refrigerator), and -20°C (freezer). Stability was assessed in methanolic and acetonitrile solutions, as well as in Na<sub>2</sub>EDTA-preserved blood and unpreserved urine. Solutions (1 mg/L) of each drug in each matrix stored in aliquots (100  $\mu$ L, solvents; 1.2 mL, biological samples;  $n = 12$ ) at each of the three temperatures for triplicate analysis on days 3, 7, 14, and 30. On day 0 of each study, three additional aliquots of each solution were analyzed. Biological samples underwent solid-phase extraction before analysis. All samples were analyzed in full-scan by gas chromatography-mass spectrometry (GC-MS). The results of this study show that under room temperature and refrigerator storage conditions, mephedrone, naphyrone, and MDPV will degrade in methanol. This degradation starts as early as day 3. Additionally, all four drugs will degrade in Na<sub>2</sub>EDTA-preserved human whole blood samples in at least one evaluated storage environment. However, when in acetonitrile-based working solutions and unpreserved urine samples, they proved to be more stable. Methanolic working solutions and samples of Na<sub>2</sub>EDTA-preserved blood containing these cathinones should be stored in the freezer and used or tested with urgency to ensure that quantitative sample analysis is as accurate as possible in forensic casework.

**Keywords:** stability, cathinone, GC/MS (gas chromatograph/mass spectrometry), solvents, blood, urine

## INTRODUCTION

Cathinone (**Figure 1**) is the naturally occurring psychoactive component of *Catha edulis* ("Khat"), a plant that is indigenous to the Middle East and East Africa (Halbach, 1972; Krikorian, 1984). The structure of cathinone is similar to that of amphetamines. However, it contains an additional carbonyl group at the  $\beta$  position, which decreases its ability to cross the blood-brain barrier and,



therefore, its potency (Gibbons and Zloh, 2010). As the structural similarities suggest, cathinone induces similar effects to amphetamines (Zelger et al., 1980; Kalix and Khan, 1984; Brenneisen et al., 1990). Cathinone is a mixed-acting sympathomimetic central nervous system stimulant (Halbach, 1972; Kalix and Khan, 1984). Its main effects likely result from increased bioavailability of certain neurotransmitters and include euphoria, increased alertness, hypertension, and tachycardia (Kalix and Khan, 1984; Bentur et al., 2008; Patel, 2009; Simmler et al., 2013).

The United Nations defines new psychoactive substances (NPS) as “substances of abuse, either in a pure form or a preparation, that are not controlled by the 1961 Single Convention on Narcotic Drugs or the 1971 Convention on Psychotropic Substances, but which may pose a public health threat” (United Nations Office on Drugs Crime, 2013). Standard colloquial terms for these drugs include “designer drugs” and “legal highs,” as they are sold online or in head shops, and their primary purpose is to circumvent international drug legislation (United Nations Office on Drugs Crime, 2013). This category of drugs includes a broad range of substances, including phenethylamines and piperazines (Rosenbaum et al., 2012). Synthetic cathinone derivatives are among the most

widely used new psychoactive substances (5). Although most NPS are newly available on the illicit drug market, many of these compounds were synthesized many years ago, such as the synthetic cathinone MDPV (3,4-methylenedioxypyrovalerone), for which the original synthesis dates back to 1969 (Yohannan and Bozenko, 2010).

Synthetic cathinones (Figure 1) are new psychoactive substances and structural derivatives of cathinone (Rosenbaum et al., 2012; Abdullah et al., 2014; Banks et al., 2014; Katz et al., 2014; Pieprzyc et al., 2020). The class of synthetic cathinones encompasses a large number of compounds because the cathinone molecule has several places at which the addition and modification of functional groups are possible. Synthetic cathinones pose a significant public health risk, mainly due to their inconsistent purity (Davies et al., 2010) and frequent co-administration with other drugs (Katz et al., 2014).

Head shops and Internet retailers sell synthetic cathinones under names such as “bath salts” and “plant food” and are often labeled “not for human consumption” to circumvent international legislation (Rosenbaum et al., 2012; Ross et al., 2012; Shanks et al., 2012; United Nations Office on Drugs Crime,



2013; Hohmann et al., 2014). In 2010, synthetic cathinone use spiked worldwide, likely due to a decrease in purity of cocaine and 3,4-methylenedioxymethamphetamine (MDMA), which rendered concerns about the relatively lower potency of synthetic cathinones less important to consumers (Measham et al., 2010; Prosser and Nelson, 2012). Unlike other commonly abused drugs such as methamphetamine, which were approved for therapeutic use and went through full clinical trials, synthetic cathinones were identified as dangerous before the completion of extensive clinical trials (Prosser and Nelson, 2012; Hohmann et al., 2014; Papaseit et al., 2017). Therefore, the reliable toxicological information available in the scientific literature regarding these compounds is limited (Prosser and Nelson, 2012; Rosenbaum et al., 2012). Like cathinone, synthetic cathinone users report effects that closely mimic the effects of amphetamines (Prosser and Nelson, 2012). Their hypothesized mechanism of action is a promotion of the release of neurotransmitters (dopamine, serotonin, and norepinephrine) with dose-dependent effects (Cozzi et al., 1999; Prosser and Nelson, 2012; Simmler et al., 2013). However, the use of these drugs appears to trigger additional adverse effects, namely delusions, hallucinations, and reckless behavior (Kasick et al., 2012; Murray et al., 2012; Prosser and Nelson, 2012).

Sunlight and heat are known to degrade the cathinone in *Catha edulis* into dimers or inactive metabolites (Chappell and Lee, 2010; Katz et al., 2014). Stability research on cathinone's synthetic derivatives tells a similar story, with many synthetic cathinones showing some degree of instability based on storage temperature and sample matrix (Sørensen, 2011; Tsujikawa et al., 2012; Al-Saffar et al., 2013; Concheiro et al., 2013; Johnson and Botch-Jones, 2013; Maskell et al., 2013; Soh and Elliott, 2014; Busardò et al., 2015; Glicksberg and Kerrigan, 2017, 2018; Miller et al., 2017; da Cunha et al., 2018; Glicksberg et al., 2018; Adamowicz and Malczyk, 2019; Czerwinska et al., 2019; Nowak et al., 2020). Understanding the consequences of this variability on subsequent interpretations of data derived from samples suspected to contain synthetic cathinones is crucial. Room temperature stability is often variable for synthetic cathinones, which does not pose a threat to most laboratories, as it is standard procedure to store samples in the refrigerator or freezer. However, room temperature instability does have a substantial impact on post-mortem toxicology, where the time between death and sample collection at room temperature could cause inaccurate results. Of additional concern is the conditions used to transport samples from the point of collection to the laboratory. These concerns about stability can become heightened if the drugs also exhibit variability in the refrigerator and freezer in both working solutions and biological matrices. The instability presented in refrigerator and freezer storage environments has an impact on the toxicological analysis of samples associated with post-mortem, driving under the influence (DUI), and drug-facilitated sexual assault (DFSA) casework.

This research aimed to determine the effects of storage temperature and matrix on the stability of four Schedule I synthetic cathinones (mephedrone, naphyrone, MDPV, and  $\alpha$ -PVP). Currently, the most cited relevant study evaluates only one derivative, mephedrone, in unpreserved equine blood

samples (Soh and Elliott, 2014). Previous synthetic cathinone stability studies primarily focus on blood samples preserved with the combination of sodium fluoride (NaF) and potassium oxalate ( $K_2C_2O_4$ ) in gray-top tubes. However, they do not assess their stability in blood preserved with  $Na_2EDTA$ , used for some clinical samples, or in unpreserved human urine. Further, no previous research provides insight into the stability of these compounds in solvent-based working solutions. The results of this study provide a more comprehensive overview of the stability of these compounds in biological matrices over a more extended period, with an alternative preservative as well as the inclusion of solvent-based working solutions.

## MATERIALS AND METHODS

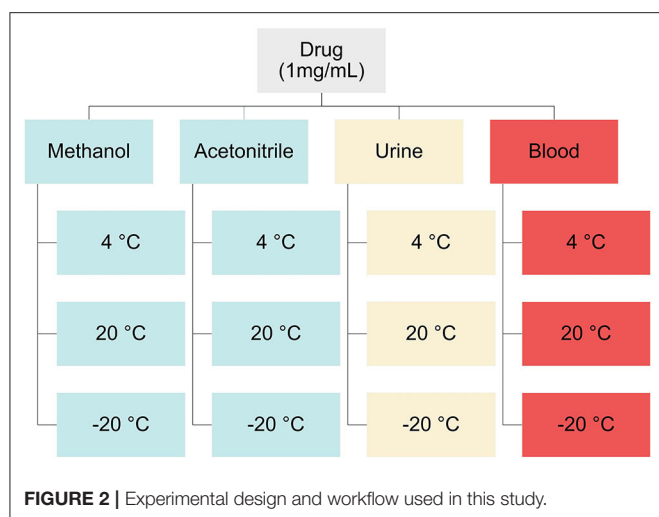
### Chemicals and Reagents

Mephedrone, naphyrone, and mephedrone- $D_3$  as 1 mg/mL solutions were purchased from Lipomed (Cambridge, Massachusetts, USA). Naphyrone- $D_5$  100  $\mu$ g/mL solution was purchased from Cerilliant (Round Rock, Texas, USA). MDPV and  $\alpha$ -PVP reference standards (5.0 mg) were purchased from Cayman Chemical Company (Ann Arbor, Michigan, USA) for the preparation of samples and calibrators. MDPV- $D_8$  and  $\alpha$ -PVP- $D_8$  reference standards (100  $\mu$ g/mL in methanol) were purchased from Cerilliant Corporation (Round Rock, Texas, USA). Methanol (MeOH), dichloromethane (DCM), ethyl acetate (EtOAc), ammonium hydroxide ( $NH_4OH$ ), isopropyl alcohol (IPA), and glacial acetic acid were all analytical grade and purchased from Pharmco by Greenfield Global (Brookfield, Connecticut, USA). Pentafluoropropionic anhydride (PFPA) was purchased from Sigma Aldrich (St Louis, MO, USA).

Blank human whole blood preserved with  $Na_2EDTA$  was purchased from Golden West Biologicals (Temecula, California, USA). Blank human urine was self-collected under Arcadia University Institutional Review Board (IRB) proposal #17-01-16 and was tested unpreserved. Blank human whole blood and urine were screened for the presence of any standard prescription, over-the-counter, and recreational drugs before their use in this study. CLEAN SCREEN<sup>®</sup> CSDAU506 solid-phase extraction (SPE) cartridges with a combination of  $C_8$  (reverse phase) and benzenesulfonic acid (ion exchange) sorbent were purchased from United Chemical Technologies (UCT) (Bristol, Pennsylvania, USA).

### Calibration Curves

Calibrators were prepared by spiking 1 mL of the matrix of interest with a 10 mg/L drug stock solution and a 1 mg/L internal standard stock solution. Calibration curves were prepared by plotting peak area ratio (PAR) vs. the concentration of the associated calibrators. ChemStation Enhanced Data Analysis E.02.02.1431 calculated linear regression equations and correlation coefficients. SWGTOX guidelines require a correlation coefficient ( $r^2$ ) of 0.99 for each calibration curve and quantitated values within  $\pm 20\%$  of their target values for suitable calibration models (Scientific Working Group for Forensic Toxicology, 2013).



## Sample Preparation and Analysis

Solvent samples for stability studies were prepared by pipetting 100  $\mu\text{L}$  of 1 mg/L solutions of mephedrone, naphyrone, MDPV, or  $\alpha$ -PVP into glass culture tubes ( $n = 48$ ). Human whole blood and urine samples for stability studies were prepared in 60 mL of the biological matrix of interest to a concentration of 1 mg/L. These solutions were then aliquoted into Eppendorf<sup>®</sup> polypropylene microcentrifuge tubes ( $n = 48$ , 1.2 mL). Fifteen samples spiked with each drug in each matrix were stored at 20°C (room temperature), 4°C (refrigerator), and -20°C (freezer) temperatures (Figure 2). On days 0, 3, 7, 14, and 30, samples from each temperature were extracted in triplicate. Fifty microliters of the corresponding deuterated internal standard (mephedrone- $\text{D}_3$  for mephedrone, naphyrone- $\text{D}_5$  for naphyrone, MDPV- $\text{D}_8$  for MDPV,  $\alpha$ -PVP- $\text{D}_8$  for  $\alpha$ -PVP) was added to the solvent samples on the day of their extraction. Samples were then evaporated at 37°C under compressed air.

Before SPE for the blood and urine studies, 100  $\mu\text{L}$  of the corresponding deuterated internal standard, 3 mL of 0.1 M pH 6 phosphate buffer, and 2 mL of  $\text{dH}_2\text{O}$  were added to 1 mL of each sample and calibrator. The samples were then vortexed for 5 s and centrifuged for 10 min at 3,000 rotations per minute (rpm). SPE cartridges were conditioned with 3 mL MeOH, 3 mL  $\text{dH}_2\text{O}$ , and 1 mL 0.1 M pH 6 phosphate buffer, and the supernatants from centrifuged samples were transferred into correspondingly labeled CLEAN SCREEN<sup>®</sup> CSDAU506 SPE cartridges. Cartridges were then washed with 3 mL  $\text{dH}_2\text{O}$ , 1 mL 1 M acetic acid, and 3 mL MeOH and then dried under a vacuum pressure of at least 5 mmHg. Samples and calibrators were eluted with 3 mL of a 78:20:2 mixture of DCM/IPA/ $\text{NH}_4\text{OH}$ , which was then evaporated at 37°C under compressed air. When using GC/MS to detect analytes, sample derivatization is often necessary before analysis. Derivatizing a compound changes a polar hydroxyl or amine group to a less polar functional group and increases the molecule's volatility, allowing for a better chromatogram. Derivatization often utilizes acylating agents. The polar N-H group of mephedrone was derivatized in this study using a 2:1 mixture of PFPA and EtOAc. After derivatization, the PFPA/EtOAc solution was evaporated to dryness. The dried

down solutions for all four drugs were then reconstituted in 100  $\mu\text{g/mL}$  of EtOAc and transferred to GC/MS vials for analysis.

## Instrumentation

Gas chromatography-mass spectrometry (GC-MS) analysis was carried out on an Agilent Technologies 7890 GC system/5973 EI-MS or Perkin Elmer Clarus<sup>®</sup> 680 GC system/SQ 8T MS. Equivalency between the two instruments was established based on calibration and controls. Once a stability study was started, the same instrument was used through the remainder of the 30 days. A Restek<sup>®</sup> Rtx<sup>®</sup>-5 fused silica column (30 m  $\times$  0.32 mm, 0.25  $\mu\text{m}$  film thickness) was used for separation by GC. The MS was operated in full scan mode so that the method could be used for future stability studies in which scanning for degradation products would be required. The GC-MS method used for this analysis method was previously validated for the detection of 23 NPS, including synthetic cathinones (Nisbet et al., 2019). Although the previous study did not include  $\alpha$ -PVP, the Nisbet et al. method was successfully validated for this analyte according to SWGTOX guidelines. Table 1 shows the retention times and ions used to monitor analyte stability throughout the study. Because the instrument was operated in full-scan, mass spectral matches were also made.

## Data Processing and Statistical Analysis

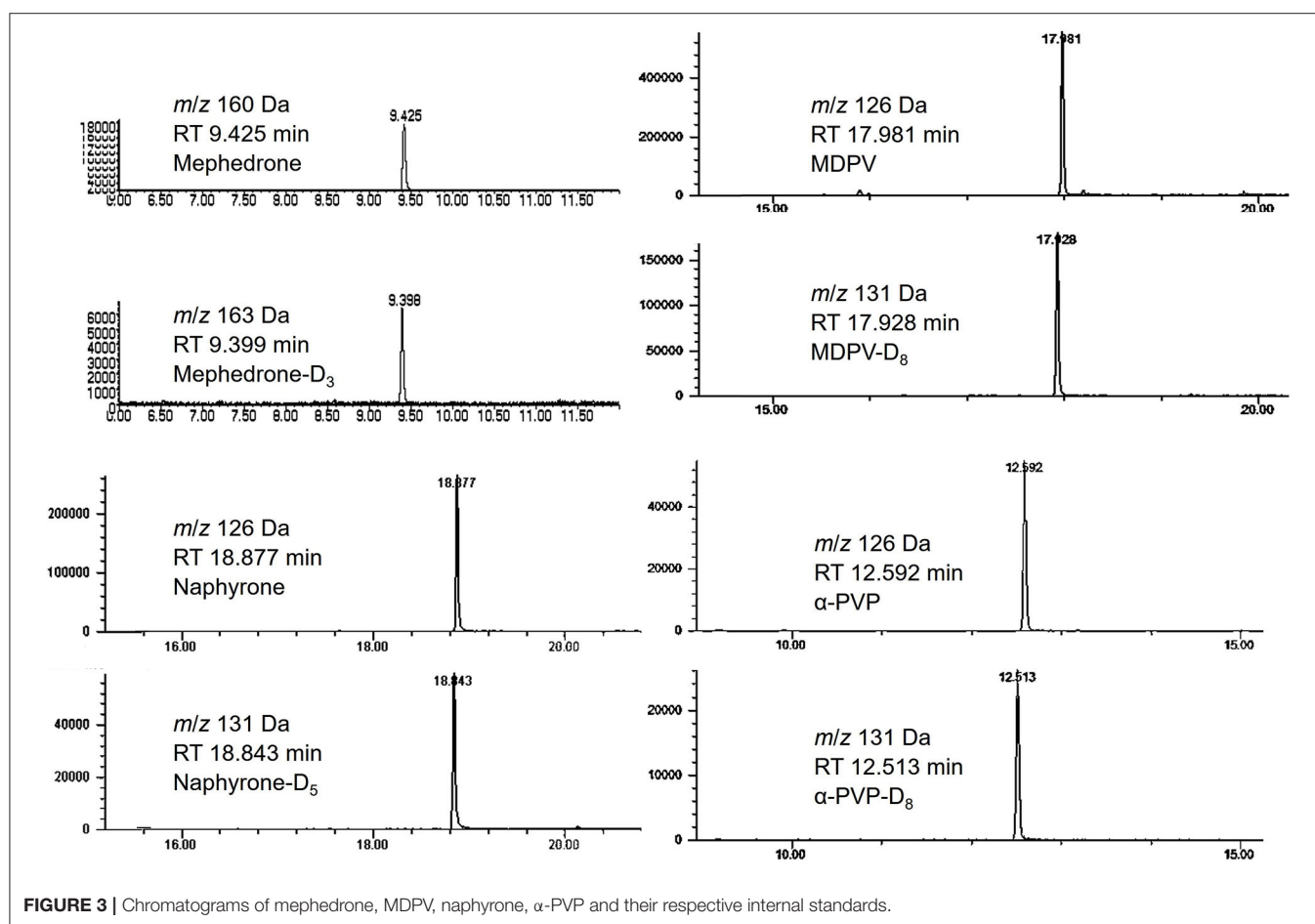
Peak area ratio and concentration were monitored to monitor the stability of the four drugs. Both peak area ratio (PAR) and linear regression are suitable methods for monitoring stability per SWGTOX validation guidelines (Scientific Working Group for Forensic Toxicology, 2013). At the appropriate retention times, peaks for each analyte and internal standard were present. Single-factor one-way analysis of variance (ANOVA) was performed on the data using Microsoft<sup>®</sup> Excel<sup>®</sup> Professional Plus 2013 to assess whether fluctuations in PAR or concentration were statistically significant throughout the 30-day studies. Performing an ANOVA evaluates whether variability in the data sets acquired in this analysis is attributed to differences in sample population means ( $\mu_x$ ) or within-sample population variability (Peck et al., 2015). This statistic evaluated acquired data based on the null hypothesis ( $H_0$ ) that the mean PAR, or concentration, for days 0, 3, 7, 14, and 30 at a specific storage temperature are all equal to each other (Equation 1) (Peck et al., 2015).  $H_0$  is rejected for the alternative hypothesis ( $H_1$ ) that the mean PAR, or concentration, is significantly different for at least one sample population when the fluctuations in PAR or concentration cannot fully be explained by within-sample population variability (Peck et al., 2015). The ANOVA performed on data sets for this study assumed a significance level ( $\alpha$ ) of 0.05, meaning that there is a 5% chance that the null hypothesis is rejected despite being true (Peck et al., 2015). A test statistic ( $p$ ) is calculated for the data, and if the  $p$ -value calculated for a data set falls below  $\alpha$ ,  $H_0$  is rejected. Values have been normalized as percent change from day 0 for ease of comparison among PARs in different matrices.

$$H_0 : \mu_{\text{Day } 0} = \mu_{\text{Day } 3} = \mu_{\text{Day } 7} = \mu_{\text{Day } 14} = \mu_{\text{Day } 30} \quad (1)$$

where  $\mu_x$  equals the sample PAR from day 0 to day  $x$ .

**TABLE 1** | Retention times and ions used for quantitation.

Analyte	Retention time (min)	Quantitation ion (m/z)	Qualifier ion 1 (m/z)	Qualifier ion 2 (m/z)
Mephedrone	9.43	160	204	323
Mephedrone-D <sub>3</sub>	9.40	163	207	326
Naphyrone	18.88	126	155	127
Naphyrone-D <sub>5</sub>	18.84	131	132	133
MDPV	17.98	126	149	110
MDPV-D <sub>8</sub>	17.93	134	133	135
$\alpha$ -PVP	12.59	126	124	127
$\alpha$ -PVP-D <sub>8</sub>	12.51	134	133	135

**FIGURE 3** | Chromatograms of mephedrone, MDPV, naphyrone,  $\alpha$ -PVP and their respective internal standards.

## RESULTS AND DISCUSSION

### Calibration

Calibration curves were run prior to the analysis of each stability batch. All calibration curves produced acceptable  $R^2$  ( $>0.99$ ) and consistent linear regression values across the expected concentration range. PAR was, therefore, acceptable to use for the determination of analyte loss during the studies. Extracted ion chromatograms for the quantification ion of each analyte and their respective internal standards are shown in **Figure 3**.

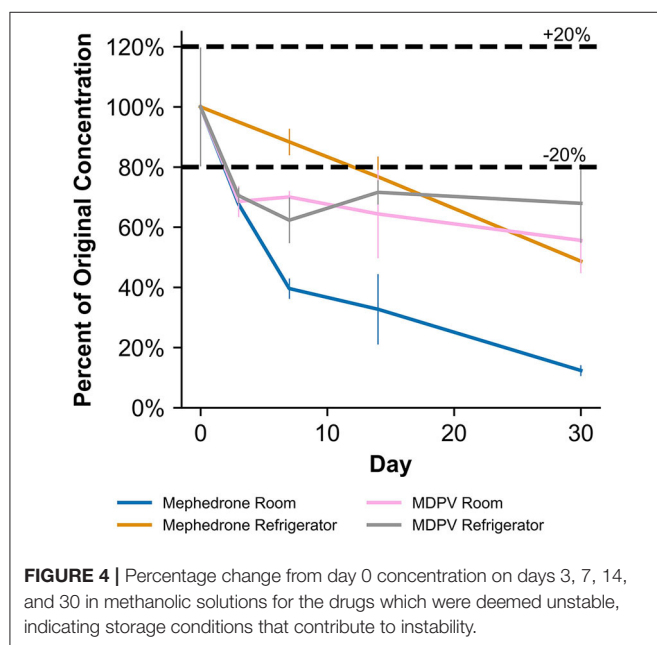
### Mephedrone Stability

**Table 2** shows that in MeOH, mephedrone was most stable when stored in the freezer and least stable when stored at room temperature. By day 3, samples of mephedrone in MeOH stored at room temperature showed a  $32.3 \pm 6.1\%$  loss of their initial concentration (**Figure 4**). After 30 days,  $87.6 \pm 3.9\%$  of the original mephedrone concentration had degraded (**Figure 4**, **Table 2**). By comparison, mephedrone samples in MeOH stored in the refrigerator first showed a significant loss of concentration after 14 days, indicating a  $23.3 \pm 9.0\%$  loss by this time (**Figure 4**).

**TABLE 2** | Cathinone stability in solvents.

Analyte	Solvent	Storage temperature (°C)	% Difference between days 0 and 30	p-value	Stability call	First unstable day of analysis
Mephedrone	MeOH	20	<b>87.6 ± 3.9%</b>	<b>3.27E-08</b>	<b>Unstable</b>	<b>Day 3</b>
		4	<b>51.3 ± 5.6%</b>	<b>1.44E-05</b>	<b>Unstable</b>	<b>Day 14</b>
		−20	8.7 ± 7.5%	8.41E-02	Stable	–
	ACN	20	<b>32.9 ± 9.7%</b>	<b>5.23E-05</b>	<b>Unstable</b>	<b>Day 30</b>
		4	7.2 ± 14.2%	3.77E-01	Stable	–
		−20	8.5 ± 3.3%	<b>5.04E-04</b>	Stable	–
Naphyrone	MeOH	20	<b>23.5 ± 30.3%</b>	8.84E-02	Stable	–
		4	<b>23.3 ± 2.7%</b>	1.65E-01	Stable	–
		−20	18.6 ± 4.6%	6.44E-02	Stable	–
	ACN	20	<b>26.0 ± 1.7%</b>	<b>1.94E-02</b>	<b>Unstable</b>	<b>Day 30</b>
		4	7.5 ± 3.8%	1.14E-01	Stable	–
		−20	6.6 ± 7.3%	4.80E-01	Stable	–
MDPV	MeOH	20	<b>44.4 ± 10.7%</b>	<b>1.84E-02</b>	<b>Unstable</b>	<b>Day 3</b>
		4	<b>32.1 ± 12.9%</b>	<b>2.51E-02</b>	<b>Unstable</b>	<b>Day 3</b>
		−20	<b>25.5 ± 9.5%</b>	4.80E-01	Stable	–
	ACN	20	18.6 ± 12.1%	6.79E-02	Stable	–
		4	12.1 ± 7.2%	6.70E-02	Stable	–
		−20	10.4 ± 8.7%	<b>1.00E-02</b>	Stable	–
α-PVP	MeOH	20	3.4 ± 39.7%	5.77E-01	Stable	–
		4	6.9 ± 12.2%	4.02E-01	Stable	–
		−20	2.9 ± 5.1%	<b>4.61E-02</b>	Stable	–
	ACN	20	15.1 ± 4.3%	<b>4.81E-06</b>	Stable	–
		4	7.5 ± 10.8%	<b>9.94E-06</b>	Stable	–
		−20	50.9 ± 63.5%	9.44E-01	Stable	–

Bold values indicate instability criteria were met (i.e., % change in concentration  $\geq 20$  and/or  $p < 0.05$ ).



After 30 days, samples stored in the refrigerator showed that  $51.3 \pm 5.6\%$  of the initial mephedrone concentration had degraded (Figure 4, Table 2). The most stable of these samples were those

stored in the freezer, which did not demonstrate a significant loss by day 30. Notably, mephedrone was less stable in MeOH than ACN. In ACN, mephedrone was most stable when stored in the refrigerator and freezer and least stable when stored at room temperature. The ACN solutions stored at room temperature had a  $32.9 \pm 9.7\%$  reduction in PAR by day 30, 10 times the amount of time than it took for MeOH samples to experience a similar loss (Figure 5, Table 2). A significant loss of PAR exceeding the method bias was not seen by the end of the study when storing mephedrone samples in ACN at refrigerator or freezer temperatures.

When stored at room temperature, mephedrone samples in blood showed a  $25.4 \pm 0.7\%$  reduction in PAR by day 7 (Figure 6). By day 30, mephedrone samples in blood showed a  $96.5 \pm 0.3\%$  loss of their initial concentration (Table 3). For samples stored in the fridge,  $21.2 \pm 3.3\%$  degraded after 14 days, and in the freezer,  $27.6 \pm 2.4\%$  degraded during the same period (Figure 6). By day 30, samples stored at refrigerator and freezer temperatures experienced similar losses of concentration of  $24.0 \pm 2.1\%$  and  $25.5 \pm 7.8\%$ , respectively (Figure 6, Table 3). When stored at room temperature, mephedrone samples in urine showed a  $41.7 \pm 11.5\%$  reduction after 14 days, which did not significantly change before day 30 (Figure 7, Table 3). After the duration of the study, samples stored in the refrigerator and freezer did not show a significant difference from day 0 that exceeded the method bias.

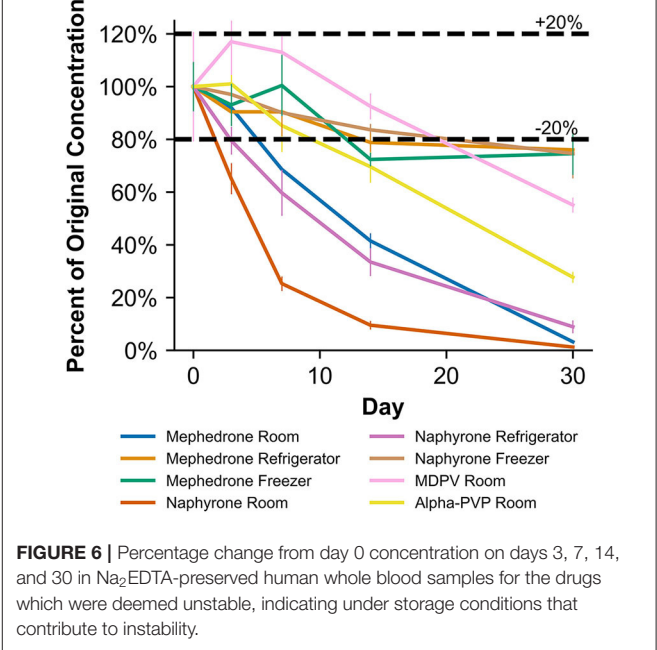
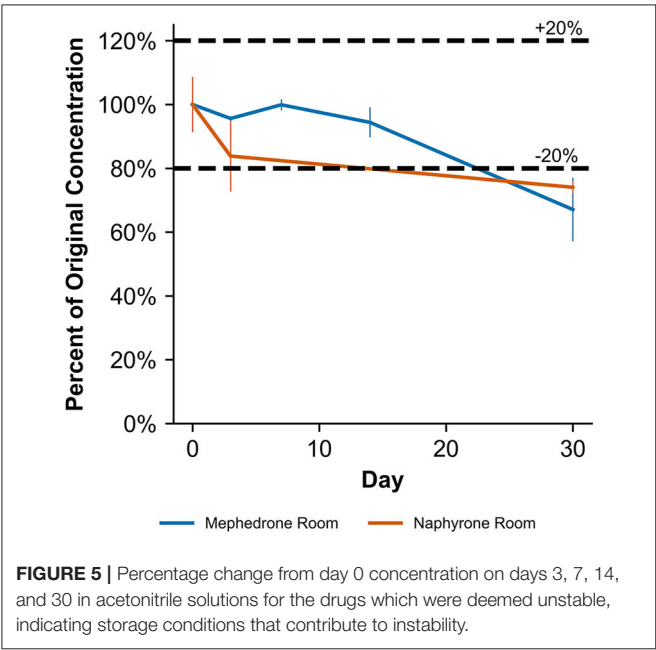
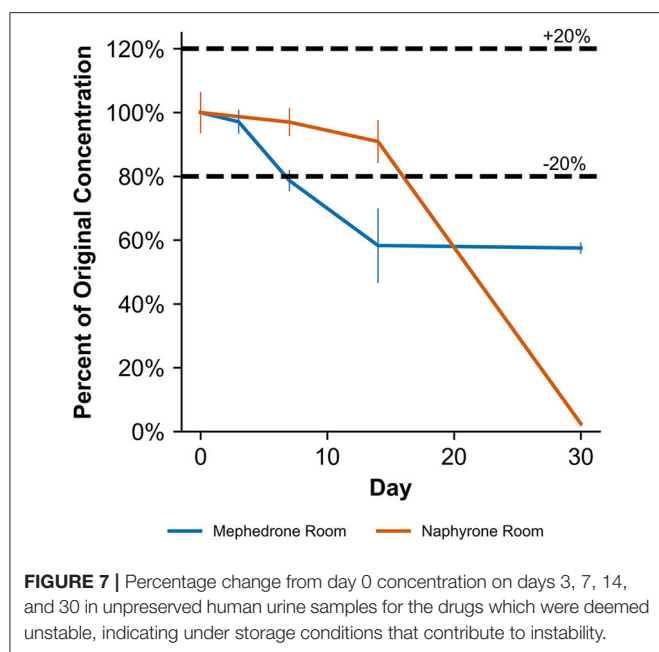


**TABLE 3 |** Cathinone stability in biological matrices.

Analyte	Solvent	Storage temperature (°C)	% Difference between days 0 and 30	p-value	Stability call	First unstable day of analysis
Mephedrone	Blood	20	<b>96.5 ± 0.3%</b>	<b>3.56E-09</b>	<b>Unstable</b>	<b>Day 7</b>
		4	<b>24.0 ± 2.1%</b>	<b>5.42E-03</b>	<b>Unstable</b>	<b>Day 14</b>
		-20	<b>25.5 ± 7.8%</b>	<b>3.33E-03</b>	<b>Unstable</b>	<b>Day 14</b>
	Urine	20	<b>40.8 ± 1.6%</b>	<b>5.24E-05</b>	<b>Unstable</b>	<b>Day 7</b>
		4	0.1 ± 5.2%	1.50E-01	Stable	–
		-20	7.0 ± 8.4%	<b>3.48E-02</b>	Stable	–
Naphyrone	Blood	20	<b>98.8 ± 0.2%</b>	<b>1.12E-09</b>	<b>Unstable</b>	<b>Day 3</b>
		4	<b>91.1 ± 2.2%</b>	<b>6.44E-08</b>	<b>Unstable</b>	<b>Day 3</b>
		-20	<b>25.4 ± 9.1%</b>	<b>7.65E-03</b>	<b>Unstable</b>	<b>Day 30</b>
	Urine	20	<b>97.6 ± 0.6%</b>	<b>2.44E-08</b>	<b>Unstable</b>	<b>Day 30</b>
		4	0.4 ± 3.1%	4.21E-01	Stable	–
		-20	2.7 ± 4.4%	2.65E-01	Stable	–
MDPV	Blood	20	<b>45.7 ± 3.2%</b>	<b>1.32E-03</b>	<b>Unstable</b>	<b>Day 30</b>
		4	4.9 ± 12.8%	3.72E-01	Stable	–
		-20	9.4 ± 3.2%	3.39E-01	Stable	–
	Urine	20	8.0 ± 5.8%	5.26E-01	Stable	–
		4	14.7 ± 8.3%	7.32E-02	Stable	–
		-20	8.6 ± 1.2%	8.23E-01	Stable	–
α-PVP	Blood	20	<b>72.3 ± 1.9%</b>	<b>6.75E-08</b>	<b>Unstable</b>	<b>Day 14</b>
		4	8.0 ± 1.2%	<b>9.16E-03</b>	Stable	–
		-20	6.6 ± 2.8%	<b>3.17E-03</b>	Stable	–
	Urine	20	12.4 ± 2.7%	<b>4.61E-05</b>	Stable	–
		4	12.4 ± 2.0%	<b>2.40E-02</b>	Stable	–
		-20	14.7 ± 4.6%	<b>9.14E-04</b>	Stable	–

Bold values indicate instability criteria were met (i.e., % change in concentration >= 20 and/or p < 0.05).





## Naphyrone Stability

When stored at room temperature, naphyrone samples in MeOH indicated a  $23.3 \pm 2.7\%$  loss of their original concentration by day 30 (Table 2). After the same amount of time, samples stored in the refrigerator and freezer experienced no significant change in concentration by day 30 (Table 2). When stored at room temperature, naphyrone samples in ACN showed a  $26.0 \pm 1.7\%$  loss of their initial concentration, indicating similar stability to storage in MeOH, unlike mephedrone. After the same amount of time, samples stored in the refrigerator and freezer remained stable.

When stored at room temperature, naphyrone samples in blood showed high instability, losing  $34.9 \pm 5.7\%$  of their original concentration by day 3 and  $98.8 \pm 0.2\%$  by day 30 (Figure 6, Table 3). Notably, refrigerator storage did not substantially improve naphyrone blood sample stability, still showing losses of  $20.5 \pm 5.1\%$  and  $91.1 \pm 2.2\%$  by days 3 and 30, respectively. Samples stored in the freezer, however, remained stable for longer, only losing  $25.4 \pm 9.1\%$  over the 30-day study (Figure 6, Table 3). Similarly, when stored at room temperature, naphyrone samples in urine showed  $97.6 \pm 0.6\%$  loss of their original concentration by day 30 (Figure 7, Table 3). After the same amount of time, however, samples stored in the refrigerator and freezer remained stable (Table 3).

## MDPV Stability

In MeOH, MDPV exhibited the highest stability under freezer storage temperatures and the least stability under room temperature storage temperatures (Table 2). Over the 30-day stability study, the PAR in MeOH samples stored at room temperature and in the refrigerator decreased by  $44.4 \pm 10.7\%$  and  $32.1 \pm 12.9\%$ , respectively. At both temperatures, samples began to show instability by day 3, losing  $31.5 \pm 4.9\%$

and  $29.5 \pm 2.5\%$ , respectively (Figure 4). However, at freezer temperatures, the samples showed no statistically significant loss of their initial concentration on day 0. Similarly to mephedrone, MDPV exhibited higher stability in ACN when compared to MeOH. MDPV exhibited stability when stored in ACN under room temperature, refrigerator, and freezer storage temperatures (Table 2). At the end of the 30-day stability study, none of the MDPV samples in ACN showed a statistically significant loss exceeding the method bias, regardless of their storage temperature.

In human whole blood preserved with  $\text{Na}_2\text{EDTA}$ , MDPV exhibited the highest stability under freezer storage temperatures and the least stability under room temperature storage temperatures (Table 3, Figure 6). Over the 30-day stability study, the concentration of MDPV in human whole blood samples that were stored at room temperature decreased by  $45.7 \pm 3.2\%$ . However, at refrigerator and freezer temperatures, the concentrations after 30 days remained stable. In unpreserved human urine, MDPV remained stable at all storage temperatures (Table 3).

## $\alpha$ -PVP Stability

$\alpha$ -PVP exhibited stability in both MeOH and ACN under room temperature, refrigerator, and freezer storage conditions (Table 2). In human whole blood preserved with  $\text{Na}_2\text{EDTA}$ ,  $\alpha$ -PVP exhibited stability under refrigerator and freezer storage temperatures (Table 3) but was found to be unstable at room temperature after day 14, when  $30.4 \pm 5.8\%$  was lost (Figure 6). Over the 30-day stability study, the concentration of  $\alpha$ -PVP in whole human whole blood samples that were stored at room temperature decreased by  $72.3 \pm 1.9\%$ . In urine,  $\alpha$ -PVP was found to be stable when stored at room temperature, refrigerator, and freezer conditions.

## Impact of Chemical Structure

Overall, mephedrone was found to be the most affected by storage temperature, followed by naphyrone and then MDPV and  $\alpha$ -PVP. Previous studies have shown that secondary amines are less stable than tertiary amines with, further substitutions such as a methylenedioxy group, present in MDPV, further increasing analyte stability (Tsujikawa et al., 2012; Glucksberg and Kerrigan, 2017). Our research has shown that a fused benzene ring reduces stability, which is a possible explanation for the difference in stability between naphyrone and  $\alpha$ -PVP, with the additional fused benzene ring contributing to the electrophilicity of the structure. This highlights the importance of evaluating the chemical structures of these compounds in order to identify those which are likely to be least stable as they appear on the recreational drugs market.

## Implications for Forensic Toxicology

Storage temperature plays a critical role in the stability of these four synthetic cathinones in all tested matrices (MeOH, ACN, human whole blood, and human urine). This information is essential in evaluating samples in forensic casework to give accurate results to aid in court cases, particularly those in blood and urine. Human whole blood samples thought to contain

mephedrone or naphyrone should be stored under freezer conditions and analyzed as quickly as possible to discourage degradation, as even at this storage temperature, there is a loss of drug over time. However, the human whole blood used in this study contained Na<sub>2</sub>EDTA as an anticoagulant. The long-term stability of these synthetic cathinones in blood has also been evaluated when containing sodium fluoride as a preservative and potassium oxalate as an anticoagulant (i.e., the combination in gray-top tubes) (Glicksberg and Kerrigan, 2017). However, no additional studies are published on the effects of other preservatives on the stability of this compound in blood samples. Additionally, special attention should be given when evaluating post-mortem toxicological samples suspected to contain mephedrone, naphyrone, or MDPV, particularly with regards to quantitative analysis, as before samples are collected for analysis, this blood contains neither preservatives nor anticoagulants and is at room temperature. Therefore, the stability may be affected even further, particularly in circumstances where there is a prolonged interval before sample collection.

When stored at freezer temperatures, mephedrone, naphyrone, MDPV, and  $\alpha$ -PVP were stable in both MeOH and ACN. In the refrigerator, these compounds remained stable in ACN. However, mephedrone, naphyrone, and MDPV showed instability in MeOH under refrigerator conditions, which is a significant finding. Currently, most suppliers of forensic reference material only offer these compounds in powdered form or MeOH solutions, and most recommend refrigerator storage upon arrival in the associated material safety data sheets (MSDS) and certificates of analysis (CoA). Laboratories without the proper United States Drug Enforcement Agency (US DEA) clearance must order solvent-based 1 mg/mL solutions of Schedule I compounds rather than as powders. Although the manufacturer's recommendations may hold true for unopened amber ampules with no internal exposure to air, previous research indicates that cathinones demonstrate instability with air exposure (Tsujikawa et al., 2015). The results of this study raise cause for concern once the manufacturer-supplied ampules have been opened and exposed to air. Consequently, even laboratories that follow the recommendations of the manufacturer from which they order their standards could experience detrimental effects from this instability when determining quantitative values. This is particularly relevant for substances such as synthetic cathinones, which may not be part of routine analysis, increasing the time period reference material may be in circulation within the laboratory.

The MSDS and CoA associated with cathinone standard solutions also often recommend storage in a dark location. This recommendation indicates that uncontrolled light exposure could also contribute to cathinone instability in solvents. The results presented here were acquired under uncontrolled light conditions, which may partially account for the high standard deviations sometimes associated with solvent instability over the 30 days. Although these high standard deviations did not show statistical significance indicating instability in all cases, minimizing the effects of light/dark cycles is expected to improve future analytical data. Making diluted working solutions in ACN

rather than MeOH and storing them in amber vials under freezer conditions rather than the refrigerator when laboratories receive these standards may be beneficial. Taking these precautionary steps can help to safeguard against reporting concentrations that are artificially raised by degrading standard solutions used for generating calibration curves and positive controls.

## Future Work

Although this paper examined the stability of mephedrone, naphyrone, MDPV, and  $\alpha$ -PVP in MeOH, ACN, human whole blood, and human urine it did so only for a period of 30-days. Due to the continual identification of new NPSs, it may be that retrospective analysis in samples for these analytes does not happen within a 30-day window. As a result, further work is needed to establish the long-term stability of these analytes within these matrices and solvents. This study did also not investigate the impact of freeze/thaw cycles on biological samples as this parameter is investigated during method development. Although reference material typically does not freeze, cold/warm cycles still occur when this material is removed from the fridge or freezer. This impact of this parameter should, therefore, be investigated when dealing with reference material in future work. Finally, it has been shown that pH also plays a significant role in analyte stability, particularly with urine samples. However, this parameter is being investigated as part of a larger study.

## CONCLUSIONS

Understanding the stability of reference material is fundamental within the field of forensic toxicology in order to ensure accurate and reliable results are reported. The use of unstable reference material can lead to the artificial inflation of results, which could have a significant impact upon the justice system and the individuals whose samples are being tested in casework. The stability of four synthetic cathinones, mephedrone, naphyrone, MDPV, and  $\alpha$ -PVP, were assessed over a 30-day period when stored in MeOH, ACN, human whole blood, and human urine, at room, fridge, and freezer temperatures.

Overall, increased stability was shown when samples were stored in ACN, as opposed to MeOH. Mephedrone was shown to be the least stable of the four cathinones monitored and  $\alpha$ -PVP the most. Samples showed the largest level of degradation when stored at room temperature and showed the greatest stability when stored in the freezer.

Although unopened reference material may be stable for a long period of time, this work highlights the importance of renewing reference material on a regular basis once opened.

When introducing new NPS drugs into the laboratory, analysts and reporting officers should be aware that these compounds may not be stable, and care should be taken when interpreting results. Where possible, extended stability studies should be carried out during validation to evaluate the stability of these compounds to determine the potential impact that instability may have upon casework.

## DATA AVAILABILITY STATEMENT

The original contributions presented in the study are included in the article/supplementary materials, further inquiries can be directed to the corresponding author.

## AUTHOR CONTRIBUTIONS

LN and KS contributed to the conception and design of the study. HC and LR acquired and analyzed experimental data. HC, LN, and KS drafted the manuscript. All authors were involved in the interpretation of experimental data and manuscript revision. All authors contributed to the article and approved the submitted version.

## REFERENCES

- Abdullah, A. F. L., Chang, K. H., Jayaram, S. K., and Sulaiman, M. (2014). A review on synthetic cathinone and its derivatives: prevalence and syntheses. *Malays. J. Forensic Sci.* 5, 46–52. Available online at: <http://forensics.org.my/mjofos/pdf/fssmVol.5No.2/Article%2009.pdf>
- Adamowicz, P., and Malczyk, A. (2019). Stability of synthetic cathinones in blood and urine. *Forensic Sci. Int.* 295, 36–45. doi: 10.1016/j.forsciint.2018.12.001
- Al-Saffar, Y., Stephanson, N. N., and Beck, O. (2013). Multicomponent LC-MS/MS screening method for detection of new psychoactive drugs, legal highs, in urine—experience from the Swedish population. *J. Chromatogr. B Analyt. Technol. Biomed. Life. Sci.* 930, 112–120. doi: 10.1016/j.jchromb.2013.04.043
- Banks, M. L., Worst, T. J., Rusyniak, D. E., and Sprague, J. E. (2014). Synthetic cathinones (“bath salts”). *J. Emerg. Med.* 46, 632–642. doi: 10.1016/j.jemermed.2013.11.104
- Bentur, Y., Bloom-Krasik, A., and Raikhlin-Eisenkraft, B. (2008). Illicit cathinone (“Hagigat”) poisoning. *Clin. Toxicol.* 46, 206–210. doi: 10.1080/15563650701517574
- Brenneisen, R., Fisch, H.-U., Koelbing, U., Geissshusler, S., and Kalix, P. (1990). Amphetamine-like effects in humans of the khat alkaloid cathinone. *Br. J. Clin. Pharmacol.* 30, 825–828. doi: 10.1111/j.1365-2125.1990.tb05447.x
- Busardò, F. P., Kyriakou, C., Tittarelli, R., Mannocchi, G., Pantano, F., Santurro, A., et al. (2015). Assessment of the stability of mephedrone in ante-mortem and post-mortem blood specimens. *Forensic Sci. Int.* 256, 28–37. doi: 10.1016/j.forsciint.2015.07.021
- Chappell, J. S., and Lee, M. M. (2010). Cathinone preservation in khat evidence via drying. *Forensic Sci. Int.* 195, 108–120. doi: 10.1016/j.forsciint.2009.12.002
- Concheiro, M., Anizan, S., Ellefsen, K., and Huestis, M. A. (2013). Simultaneous quantification of 28 synthetic cathinones and metabolites in urine by liquid chromatography-high resolution mass spectrometry. *Anal. Bioanal. Chem.* 405, 9437–9448. doi: 10.1007/s00216-013-7386-z
- Cozzi, N. V., Sievert, M. K., Shulgin, A. T., Jacob, P. III, and Ruoho, A. E. (1999). Inhibition of plasma membrane monoamine transporters by beta-ketoamphetamines. *Eur. J. Pharmacol.* 381, 63–69. doi: 10.1016/S0014-2999(99)00538-5
- Czerwinska, J., Parkin, M. C., Dargan, P. I., George, C., Kicman, A. T., and Abbate, V. (2019). Stability of mephedrone and five of its phase I metabolites in human whole blood. *Drug Test. Anal.* 11, 586–594. doi: 10.1002/dta.2525
- da Cunha, K. F., Eberlin, M. N., and Costa, J. L. (2018). Long-term stability of synthetic cathinones in dried blood spots and whole blood samples: a comparative study. *Forensic Toxicol.* 36, 424–434. doi: 10.1007/s11419-018-0418-9
- Davies, S., Wood, D. M., Smith, G., Button, J., Ramsey, J., Archer, R., et al. (2010). Purchasing “legal highs” on the Internet—is there consistency in what you get? *QJM* 103, 489–493. doi: 10.1093/qjmed/hcq056
- Gibbons, S., and Zloh, M. (2010). An analysis of the ‘legal high’ mephedrone. *Bioorg. Med. Chem. Lett.* 20, 4135–4139. doi: 10.1016/j.bmcl.2010.05.065

## FUNDING

The Arcadia University Forensic Science Program, Department of Chemistry and Physics, and Office of the Dean of Students financially supported this research.

## ACKNOWLEDGMENTS

The authors want to thank the CFSRE, Willow Grove for providing instrumentation and facilities for some of the experiments herein. The authors also gratefully acknowledge Stephanie Oddi, Meaghan Ringel, and Robert Hessler for thoughtful discussions related to this research.

- Glicksberg, L., and Kerrigan, S. (2017). Stability of synthetic cathinones in blood. *J. Anal. Toxicol.* 41, 711–719. doi: 10.1093/jat/bkx071
- Glicksberg, L., and Kerrigan, S. (2018). Stability of synthetic cathinones in urine. *J. Anal. Toxicol.* 42, 77–87. doi: 10.1093/jat/bkx091
- Glicksberg, L., Rana, S., and Kerrigan, S. (2018). Cathinone stability in authentic urine specimens. *Forensic Sci. Int.* 286, 54–60. doi: 10.1016/j.forsciint.2018.02.016
- Halbach, H. (1972). Medical aspects of the chewing of khat leaves. *Bull. World Health Organ.* 47, 21–29.
- Hohmann, N., Mikus, G., and Czock, D. (2014). Effects and risks associated with novel psychoactive substances: mislabeling and sale as bath salts, spice, and research chemicals. *Dtsch. Ärztebl. Int.* 111, 139–147. doi: 10.3238/arztebl.2014.0139
- Johnson, R. D., and Botch-Jones, S. R. (2013). The stability of four designer drugs: MDPV, mephedrone, BZP and TFMPP in three biological matrices under various storage conditions. *J. Anal. Toxicol.* 37, 51–55. doi: 10.1093/jat/bks138
- Kalix, P., and Khan, I. (1984). Khat: an amphetamine-like plant material. *Bull. World Health Organ.* 62, 681–686.
- Kasick, D. P., McKnight, C. A., and Klisovic, E. (2012). “Bath salt” ingestion leading to severe intoxication delirium: two cases and a brief review of the emergence of mephedrone use. *Am. J. Drug Alcohol Abuse* 38, 176–180. doi: 10.3109/00952990.2011.643999
- Katz, D. P., Bhattacharya, D., Bhattacharya, S., Deruiter, J., Clark, C. R., Suppiramaniam, V., et al. (2014). Synthetic cathinones: “A khat and mouse game.” *Toxicol. Lett.* 229, 349–356. doi: 10.1016/j.toxlet.2014.06.020
- Krikorian, A. D. (1984). Kat and its use: an historical perspective. *J. Ethnopharmacol.* 12, 115–178. doi: 10.1016/0378-8741(84)90047-3
- Maskell, P. D., Seetohul, L. N., Livingstone, A. C., Cockburn, A. K., Preece, J., and Pounder, D. J. (2013). Stability of 3,4-methylenedioxymethamphetamine (MDMA), 4-methylmethcathinone (Mephedrone) and 3-trifluoromethylphenylpiperazine (3-TFMPP) in formalin solution. *J. Anal. Toxicol.* 37, 440–446. doi: 10.1093/jat/bkt051
- Measham, F., Moore, K., Newcombe, R., and Welch, Z. (2010). Tweaking, bombing, dabbing and stockpiling: the emergence of mephedrone and the perversity of prohibition. *Drug Alcohol Today.* 10, 14–21. doi: 10.5042/daat.2010.0123
- Miller, B., Kim, J., and Concheiro, M. (2017). Stability of synthetic cathinones in oral fluid samples. *Forensic Sci. Int.* 274, 13–21. doi: 10.1016/j.forsciint.2016.11.034
- Murray, B. L., Murphy, C. M., and Beuhler, M. C. (2012). Death following recreational use of designer drug “Bath salts” containing 3,4-methylenedioxypyrovalerone (MDPV). *J. Med. Toxicol.* 8, 69–75. doi: 10.1007/s13181-011-0196-9
- Nisbet, L. A., Wylie, F. M., Logan, B. K., and Scott, K. S. (2019). Gas chromatography-mass spectrometry method for the quantitative identification of 23 new psychoactive substances in blood and urine. *J. Anal. Toxicol.* 43, 346–352. doi: 10.1093/jat/bky109

- Nowak, K., Szpot, P., and Zawadzki, M. (2020). The stability of 4-chloromethcathinone in blood and vitreous humor. *J. Forensic Sci.* 65, 1784–1790. doi: 10.1111/1556-4029.14454
- Papaseit, E., Moltó, J., Muga, R., Torrens, M., de la Torre, R., and Farré, M. (2017). “Clinical pharmacology of the synthetic cathinone mephedrone,” in *Neuropharmacology of New Psychoactive Substances (NPS)*, eds M. H. Baumann, R. A. Glennon, and J. L. Wiley (Cham: Springer), 313–331.
- Patel, N. (2009). Mechanism of action of cathinone: the active ingredient of khat (*Catha edulis*). *East Afr. Med. J.* 77, 329–332. doi: 10.4314/eamj.v77i6.46651
- Peck, R., Olsen, C., and Devore, J. L. (2015). *Introduction to Statistics and Data Analysis*. 5th ed. Boston, MA: Brooks/Cole; Cengage Learning.
- Pieprzyc, E., Skowronek, R., Nižnanský, L., and Czekaj, P. (2020). Synthetic cathinones – From natural plant stimulant to new drug of abuse. *Eur. J. Pharmacol.* 875:173012. doi: 10.1016/j.ejphar.2020.173012
- Prosser, J. M., and Nelson, L. S. (2012). The toxicology of bath salts: a review of synthetic cathinones. *J. Med. Toxicol.* 8, 33–42. doi: 10.1007/s13181-011-0193-z
- Rosenbaum, C. D., Carreiro, S. P., and Babu, K. M. (2012). Here today, gone tomorrow...and back again? A review of herbal marijuana alternatives (K2, Spice), synthetic cathinones (bath salts), kratom, *Salvia divinorum*, methoxetamine, and piperazines. *J. Med. Toxicol.* 8, 15–32. doi: 10.1007/s13181-011-0202-2
- Ross, E. A., Reisfield, G. M., Watson, M. C., Chronister, C. W., and Goldberger, B. A. (2012). Psychoactive “bath salts” intoxication with methylenedioxypyrovalerone. *Am. J. Med.* 125, 854–858. doi: 10.1016/j.amjmed.2012.02.019
- Scientific Working Group for Forensic Toxicology (2013). Scientific working group for forensic toxicology (SWGTOX) standard practices for method validation in forensic toxicology. *J. Anal. Toxicol.* 37, 452–474. doi: 10.1093/jat/bkt054
- Shanks, K. G., Dahn, T., Behonick, G., and Terrell, A. (2012). Analysis of first and second generation legal highs for synthetic cannabinoids and synthetic stimulants by ultra-performance liquid chromatography and time of flight mass spectrometry. *J. Anal. Toxicol.* 36, 360–371. doi: 10.1093/jat/bks047
- Simmler, L., Buser, T., Donzelli, M., Schramm, Y., Dieu, L.-H., Huwyler, J., et al. (2013). Pharmacological characterization of designer cathinones *in vitro*. *Br. J. Pharmacol.* 168, 458–470. doi: 10.1111/j.1476-5381.2012.02145.x
- Soh, Y. N. A., and Elliott, S. (2014). An investigation of the stability of emerging new psychoactive substances. *Drug Test. Anal.* 6, 696–704. doi: 10.1002/dta.1576
- Sørensen, L. K. (2011). Determination of cathinones and related ephedrine in forensic whole-blood samples by liquid-chromatography–electrospray tandem mass spectrometry. *J. Chromatogr. B Analyt. Technol. Biomed. Life. Sci.* 879, 727–736. doi: 10.1016/j.jchromb.2011.02.010
- Tsujikawa, K., Mikuma, T., Kuwayama, K., Miyaguchi, H., Kanamori, T., Iwata, Y. T., et al. (2012). Degradation pathways of 4-methylmethcathinone in alkaline solution and stability of methcathinone analogs in various pH solutions. *Forensic Sci. Int.* 220, 103–110. doi: 10.1016/j.forsciint.2012.02.005
- Tsujikawa, K., Yamamuro, T., Kuwayama, K., Kanamori, T., Iwata, Y. T., and Inoue, H. (2015). Instability of the hydrochloride salts of cathinone derivatives in air. *Forensic Sci. Int.* 248, 48–54. doi: 10.1016/j.forsciint.2014.12.016
- United Nations Office on Drugs and Crime (2013). *The Challenge of New Psychoactive Substances: A Report from the Global SMART Programme*. Available online at: [https://www.unodc.org/documents/scientific/NPS\\_Report.pdf](https://www.unodc.org/documents/scientific/NPS_Report.pdf) (accessed May 22, 2020).
- Yohannan, J. C., and Bozenko, J. S. (2010). The Characterization of 3,4-Methylenedioxypyrovalerone (MDPV). *Microgram J.* 7:4. Available online at: [https://www.dea.gov/sites/default/files/pr/microgram-journals/2010/mj7-1\\_12-15.pdf](https://www.dea.gov/sites/default/files/pr/microgram-journals/2010/mj7-1_12-15.pdf)
- Zelger, J. L., Schorno, H. X., and Carlini, E. A. (1980). Behavioural effects of cathinone, an amine obtained from *Catha edulis* Forsk: comparisons with amphetamine, norpseudoephedrine, apomorphine and nomifensine. *Bull. Narc.* 32, 67–81.

**Conflict of Interest:** The authors declare that the research was conducted in the absence of any commercial or financial relationships that could be construed as a potential conflict of interest.

Copyright © 2020 Ciallella, Rutter, Nisbet and Scott. This is an open-access article distributed under the terms of the Creative Commons Attribution License (CC BY). The use, distribution or reproduction in other forums is permitted, provided the original author(s) and the copyright owner(s) are credited and that the original publication in this journal is cited, in accordance with accepted academic practice. No use, distribution or reproduction is permitted which does not comply with these terms.





# Detection of a New Tert-Leucinate Synthetic Cannabinoid 5F-MDMB-PICA and Its Metabolites in Human Hair: Application to Authentic Cases

Yan Shi<sup>1†</sup>, Liying Zhou<sup>1,2†</sup>, Le Li<sup>1,2</sup>, Mengxi Liu<sup>1</sup>, Huosheng Qiang<sup>1</sup>, Min Shen<sup>1</sup>, Baohua Shen<sup>1</sup>, Hang Chen<sup>1</sup>, Olaf H. Drummer<sup>3</sup>, Wanhui Liu<sup>2</sup>, Hejian Wu<sup>1\*</sup> and Ping Xiang<sup>1\*</sup>

## OPEN ACCESS

### Edited by:

Marta Concheiro-Guisan,  
John Jay College of Criminal Justice,  
United States

### Reviewed by:

Alberto Salomone,  
University of Turin, Italy  
Elena Lendoiro,  
Universidade de Santiago de  
Compostela, Spain

### \*Correspondence:

Hejian Wu  
wuhj@ssjfd.cn  
Ping Xiang  
xiangping2630@163.com

<sup>†</sup>These authors have contributed  
equally to this work and share first  
authorship

### Specialty section:

This article was submitted to  
Analytical Chemistry,  
a section of the journal  
Frontiers in Chemistry

**Received:** 25 September 2020

**Accepted:** 30 October 2020

**Published:** 26 November 2020

### Citation:

Shi Y, Zhou L, Li L, Liu M, Qiang H,  
Shen M, Shen B, Chen H,  
Drummer OH, Liu W, Wu H and  
Xiang P (2020) Detection of a New  
Tert-Leucinate Synthetic Cannabinoid  
5F-MDMB-PICA and Its Metabolites in  
Human Hair: Application to Authentic  
Cases. *Front. Chem.* 8:610312.  
doi: 10.3389/fchem.2020.610312

<sup>1</sup> Department of Forensic Toxicology, Shanghai Key Laboratory of Forensic Medicine, Shanghai Forensic Science Platform, Academy of Forensic Science, Shanghai, China, <sup>2</sup> School of Pharmacy, Yantai University, Yantai, China, <sup>3</sup> Department of Forensic Medicine, Faculty of Medicine, School of Public Health and Preventive Medicine, Nursing and Health Sciences, Monash University, Southbank, VIC, Australia

Methyl 2-[[1-(5-fluoropentyl) indole-3-carbonyl] amino]-3,3-dimethyl-butanoate (5F-MDMB-PICA) is a new synthetic cannabinoid characterized by valinate or tert-leucinate moieties. In recent years, 5F-MDMB-PICA has been abused in the form of “spice-like” herbal incenses or electronic cigarette oil. A UHPLC-MS/MS method was developed to detect 5F-MDMB-PICA and its metabolites in human hair. Approximately 20 mg of hair was weighed and pulverized with methanol below 4°C. After ultrasonication, centrifugation and filtration, 200  $\mu$ L of supernatant was placed into an autosampler vial and analyzed on a Waters Acquity UPLC HSS T<sub>3</sub> column (100 mm  $\times$  2.1 mm, 1.8  $\mu$ m particle size) using an acetonitrile-20 mmol/L ammonium acetate (0.1% formic acid, 5% acetonitrile) gradient with a run time of 8 min. The limit of detection (LOD) ranged from 0.5 to 5 pg/mg, and the lower limit of quantitation (LLOQ) ranged from 1 to 5 pg/mg. The method was shown to be linear over a concentration range of 1–200 pg/mg. The linear correlation ( $R^2$ ) of the calibration curves for all analytes was >0.999. The accuracy varied from 95.4 to 107.4%, while the intra- and inter-day precision RSD values were 0.7–10.6% and 1.7–12.2%, respectively. Recoveries were within the range of 61.1–93.3%, and matrix effects were in the range of 19.1–102.6%. The validated method was successfully applied to the identification and quantification of 5F-MDMB-PICA and its metabolites in hair from authentic forensic cases.

**Keywords:** synthetic cannabinoid, 5F-MDMB-PICA, metabolites, UHPLC-MS/MS, hair analysis

## INTRODUCTION

Recently, new psychoactive substances (NPS) have surged at an alarming rate worldwide, which has severely impacted global health problems. Contrary to traditional drugs of abuse, the structures of NPS are diverse, and the pharmacokinetic and physiological properties of most of them have never been evaluated in controlled studies, which brings great challenges to their detection and



interpretation (Smith et al., 2015; Risseeuw et al., 2017). Among NPS, synthetic cannabinoids (SCs) are still the fastest-growing class of NPS monitored by the Early Warning System (EWS) of the European Monitoring Centre for Drugs and Drug Addiction (EMCDDA) (2017). As of 2017, according to EMCDDA data, 179 synthetic cannabinoids were reported (Truver et al., 2020). Illegal drug dealers and secret laboratories use the structural diversity of SCs to evade analysis and detection and to circumvent prohibition by international legislation (Debruyne and Le Boisselier, 2015; Banister and Connor, 2018a,b). Due to the illegal abuse of a large number of synthetic cannabinoids in recent years, many serious poisoning and death cases have occurred worldwide (Hess et al., 2015; Weaver et al., 2015; Chinnadurai and Srijan, 2016). At present, 5F-MDMB-PICA is relatively common in China and is mainly sold on the Internet or in retail stores in the form of shredded tobacco, tobacco leaves or e-liquid.

Methyl 2-[[1-(5-fluoropentyl)indole-3-carbonyl]amino]-3,3-dimethyl-butanolate (5F-MDMB-PICA) belongs to the class of synthetic cannabinoids. This compound was synthesized and described for the first time by Banister et al. for the purpose of pharmacological research on novel SCs characterized by valinate or tert-leucinate moieties (Banister et al., 2016). The structure of 5F-MDMB-PICA is similar to that of 5F-MDMB-PINACA, but the indazole moiety is replaced by an indole group. 5F-MDMB-PICA was first detected in herbal incense packages by Risseeuw et al. (2017). In biological matrices, the parent structure of synthetic cannabinoids is often difficult to detect, so metabolic studies are needed to improve the detection of emerging synthetic cannabinoids. To date, only the detection of 5F-MDMB-PICA and its metabolites in urine have been reported (Mogler et al., 2018; Truver et al., 2020).

The detection and quantitative analysis of NPS in different biomatrices has become a great challenge for forensic toxicology research, mainly due to the need for sensitive, reliable and specific analytical techniques. Synthetic cannabinoids are usually monitored by analyzing the parent drug and its metabolites in blood and urine samples (Presley et al., 2016; Krotulski et al., 2019). Currently, hair is one of the key sample matrices for determining drug abuse in the field of forensic science (Salomone et al., 2014). Compared with that of biological matrices such as blood and urine, hair testing has the advantages of stable target compounds, a larger detection window for drug detection, and the ability to reflect drug usage for a longer period of time (Baumgartner et al., 1989). However, few studies have examined synthetic cannabinoids and their metabolites in human hair.

To our knowledge, analytical data on 5F-MDMB-PICA and its metabolites in hair have not been published. According to reference reports, the five metabolites M2, M4, M7, M8, and M9 in urine are the main metabolites of 5F-MDMB-PICA, so these five metabolites were selected as the identification metabolites of 5F-MDMB-PICA in human hair (Mogler et al., 2018). In this study, a validated method is presented for the quantitative determination of 5F-MDMB-PICA and its five metabolites in human hair by liquid chromatography-tandem mass spectrometry (**Scheme 1**). The method was successfully applied to authentic hair samples from real cases.

## MATERIALS AND METHODS

### Reagents and Chemicals

A standard of 5F-MDMB-PICA was purchased from Cayman Chemical Company (Michigan, USA). Standards of metabolites M2, M4, M7, M8, and M9 were provided by Glpbio (California, USA). The deuterated internal standard (IS) JWH-018 4-hydroxypentyl metabolite-D5 was purchased from Cerilliant (Texas, USA). High-performance liquid chromatography-grade methanol and acetonitrile were obtained from Sigma-Aldrich (St. Louis, MO, USA). Analytical-grade isopropanol was provided by Shanghai Lingfeng Chemical Reagent Co. (Shanghai, China). Formic acid ( $\geq 98\%$ ) and ammonium acetate ( $\geq 98\%$ ) were obtained from Fluka (Buchs, Switzerland). Ultrapure water was prepared using a Millipore AFS-10 water purification system (Billerica, MA, USA).

### Hair Samples

Hair samples from healthy laboratory drug-free volunteers were used to prepare standard curves and quality control (QC) samples. Hair samples were obtained from suspected 5F-MDMB-PICA users. All individuals provided written informed consent.

### Preparation of Calibration Standards and Quality Control Samples

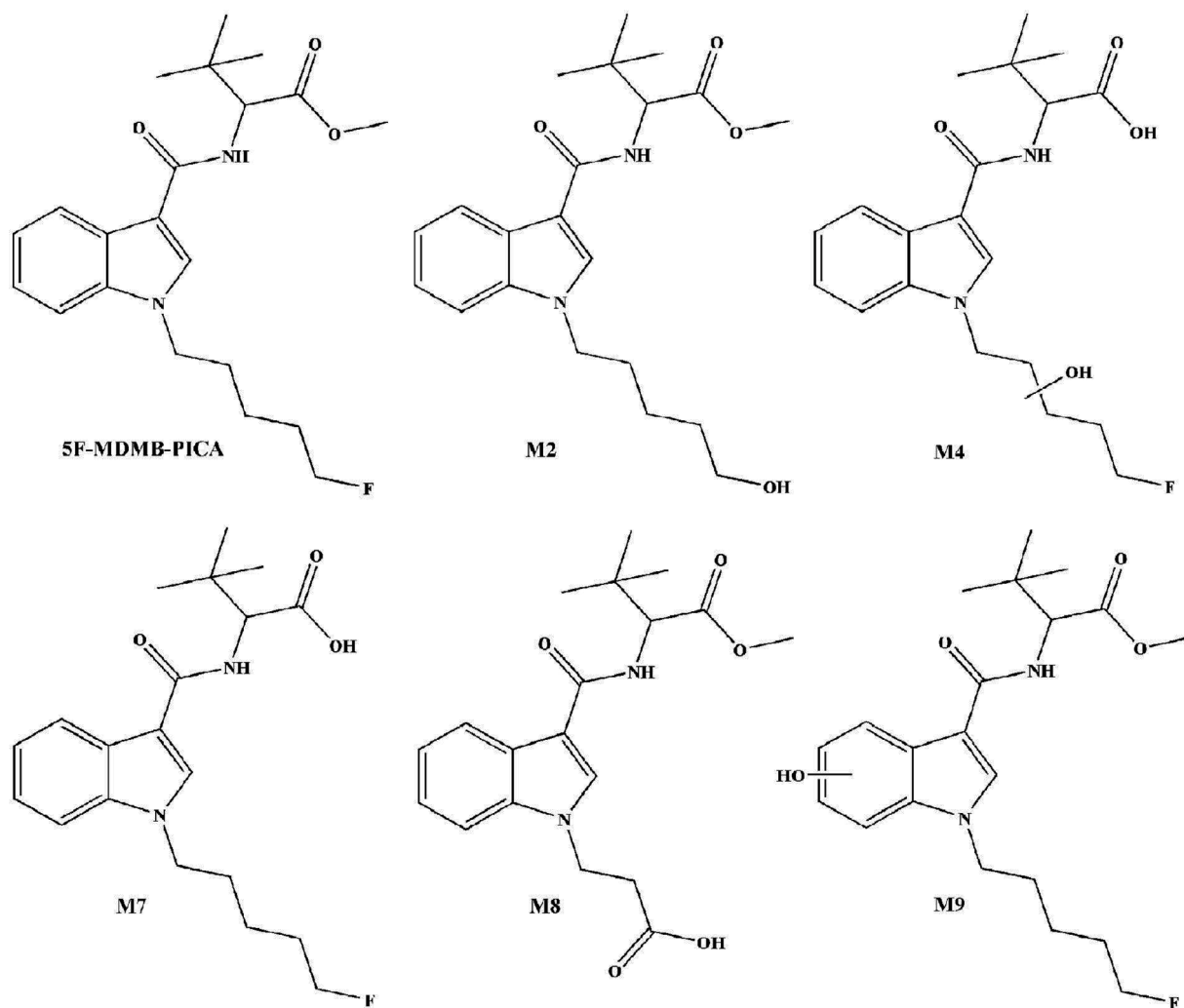
A  $1\text{ }\mu\text{g/mL}$  stock solution containing 5F-MDMB-PICA and its metabolites was prepared with methanol. From this stock solution, working solutions with concentrations of 200, 50, 10, 5, 1, and  $0.5\text{ ng/mL}$  were prepared with methanol. A  $10\text{ }\mu\text{g/mL}$  IS stock solution was diluted with methanol to provide the IS working solution with a concentration of  $100\text{ ng/mL}$ .

Calibration standards were prepared by spiking blank hair with the working solution to obtain final concentrations of 1, 2, 5, 10, 20, 50, 100, and  $200\text{ pg/mg}$  for 5F-MDMB-PICA, M2, and M9; 2, 5, 10, 20, 50, 100, and  $200\text{ pg/mg}$  for M4 and M7; and 5, 10, 20, 50, 100, and  $200\text{ pg/mg}$  for M8. Quality control (QC) samples were prepared at four concentrations, namely, the LLOQ and low, medium and high concentrations. The QC concentrations of 5F-MDMB-PICA, M2 and M9 were 1, 10, 50, and  $150\text{ pg/mg}$ ; the QC concentrations of M4 and M7 were 2, 10, 50, and  $150\text{ pg/mg}$ ; and the QC concentrations of M8 were 5, 20, 50, and  $200\text{ pg/mg}$ . All the standard stock solutions, working solutions and QC samples were stored at  $-20^\circ\text{C}$  before use.

### Instrumentation

LC-MS/MS analysis was performed using an Acquity™ Ultra performance LC I-CLASS (Waters, USA) coupled with a Sciex 6500 Plus Q-trap™ quadrupole mass spectrometer (Sciex, Foster City, USA) with electrospray ionization (ESI). Data acquisition and processing were performed by MultiQuant 3.0.2.

Chromatographic separation was performed with a Waters Acquity UPLC HSS T<sub>3</sub> column ( $100\text{ mm} \times 2.1\text{ mm}$ ,  $1.8\text{ }\mu\text{m}$  particle size) using linear gradient elution. Mobile phase A (MPA) consisted of 0.1% formic acid,  $20\text{ mmol/L}$  ammonium acetate and 5% acetonitrile. Mobile phase B (MPB) was acetonitrile. The gradient elution used was as follows: start at 0 min with 70% solvent A and 30% solvent B, held for 1 min; 1–2 min linear rate



**SCHEME 1** | Chemical structures of 5F-MDMB-PICA and its metabolites used for method validation.

to 85% B, 2–6 min linear rate to 90% B; 6–7 min with 90% B, held for 1 min; 7–7.1 min return to initial conditions, 30% B; 7.1–8 min with 30% B, held for 0.9 min. was programmed as shown in **Table 1**. The flow rate was 0.3 mL/min, and the total run time was 8 min. The injection volume was 5  $\mu$ L.

The mass spectrometer was operated in multiple reaction monitoring (MRM) mode. The ESI source settings were as follows: source mode, positive; source temperature, 500°C; curtain gas (CUR, nitrogen), 18 psi; ion spray voltage (ISV), 5,500 V; collision cell exit potential (CXP), 10 V; entrance potential (EP), 10 V; collision activation dissociation (CAD) gas, low; ion source gas 1 (GS1), 40 psi; and ion source gas 2 (GS2), 35 psi. A summary of the MRM parameters and retention times is shown in **Table 1**.

## Sample Preparation

Hair samples were consecutively washed once with isopropanol and twice with water and dried at room temperature. The hair samples were then cut into 1–2 mm pieces with scissors for

further study. Hair (20 mg) was weighed into 2 mL tubes. Mix the extraction solvent methanol solution with 1  $\mu$ g/mL IS working solution to prepare 20 pg/mg IS extraction solution. Ceramic beads (1 mm) were added before the addition of the mixture solution of methanol solution and the IS (20 pg/mg). Hair samples were then homogenized using the BeadRuptor system (OMNI, USA). The settings for pulverization were as follows: temperature, below 4°C; speed, 6 m/s; time, 20 s; dwell time 40 s; and cycles, 10. The samples were then sonicated in an ice bath for 15 min and centrifuged for 5 min at 13,500  $\times$  g. Approximately 200  $\mu$ L of the supernatant was removed and filtered through a 0.22  $\mu$ m filter membrane (Sinopharm Chemical Reagent Co., Ltd., China). The filtrate was transferred into the autosampler vial, and 5  $\mu$ L was injected into the LC-MS/MS system.

## Method Validation

Analytical method validation was carried out according to international guidelines (Peters et al., 2007; Scientific Working

**TABLE 1 |** MRM parameters and retention times for 5F-MDMB-PICA, its metabolites and the IS.

Analytes	Formula	Precursor ion ( <i>m/z</i> )	Product ion ( <i>m/z</i> )	DP (eV)	CE (eV)	Rt (min)
5F-MDMB-PICA	C <sub>21</sub> H <sub>29</sub> FN <sub>2</sub> O <sub>3</sub>	377.2	232.2*	50	25	3.35
			144.0	50	55	3.35
M2	C <sub>21</sub> H <sub>29</sub> FN <sub>2</sub> O <sub>3</sub>	375.3	230.0*	75	22	2.89
			144.0	75	48	2.89
M4	C <sub>20</sub> H <sub>27</sub> FN <sub>2</sub> O <sub>4</sub>	379.1	248.2*	60	18	2.44
			143.9	60	44	2.44
M7	C <sub>20</sub> H <sub>27</sub> FN <sub>2</sub> O <sub>3</sub>	363.1	232.0	55	23	2.85
			144.0*	55	51	2.85
M8	C <sub>19</sub> H <sub>24</sub> N <sub>2</sub> O <sub>5</sub>	361.1	216.0	40	20	2.69
			144.0*	40	55	2.68
M9	C <sub>21</sub> H <sub>29</sub> FN <sub>2</sub> O <sub>3</sub>	393.1	248.1*	60	21	2.88
			240.1	60	32	2.88
JWH-014 Hydroxypentyl metabolite-D5	C <sub>24</sub> H <sub>18</sub> D <sub>5</sub> NO <sub>2</sub>	363.3	155.0*	80	28	3.12
			127.0	80	60	3.12

\*quantifier ions; DP, declustering potential; CE, collision potential; Rt, retention time.

**TABLE 2 |** Linearity, LOD, and LLOQ for 5F-MDMB-PICA and its metabolites in hair.

Analytes	Linearity range (pg/mg) ( <i>n</i> = 2)	Regression equations	Correlation coefficients ( <i>R</i> <sup>2</sup> )	LOD (pg/mg)	LLOQ (pg/mg)
5F-MDMB-PICA	1–200	$y = 0.07073x + 0.01786$	0.9992	0.5	1
M2	1–200	$y = 0.08282x + 0.01135$	0.9991	0.5	1
M4	2–200	$y = 0.03617x - 0.00555$	0.9994	1	2
M7	2–100	$y = 0.04442x - 0.03089$	0.9992	1	2
M8	5–200	$y = 0.03365x - 0.00790$	0.9992	5	5
M9	1–200	$y = 0.08553x - 0.02541$	0.9989	0.5	1

Group for Forensic Toxicology, 2013; Desharnais et al., 2014). Validation parameters, such as selectivity, limit of detection (LOD), lower limit of quantification (LLOQ), linearity, accuracy, precision, recovery, matrix effect and stability, were evaluated.

### Selectivity

Selectivity was evaluated by analyzing 10 blank hair samples obtained from ten drug-free volunteers to check potential endogenous interferences from matrix components with the signals of analytes and the IS.

### LOD and LLOQ

The LOD was defined by evaluating the signal/noise (S/N) ratio of three replicates of spiked blank hair samples at decreasing concentrations. A S/N of at least 3:1 was selected as the LOD, while the LLOQ was determined as the concentration having a S/N ≥ 10, and both required accuracy and precision values < ±20%.

### Linearity, Accuracy, and Precision

Linearity was verified from six duplicates with concentrations of 1, 2, 5, 10, 20, 50, 100, and 200 pg/mg from the “in-house” certified drug-free hair. The deviation value of the LLOQ sample on the linearity does not exceed 20%, and the deviation

value of other samples does not exceed 15%. Accuracy refers to “the difference between the value of the test result and the acceptable reference value.” It is usually expressed as the percentage deviation of the average of the test results from the acceptable reference value. Precision refers to “the closeness of agreement (degree of scatter) between a series of the test results obtained from multiple sampling of the same homogenous sample under the prescribed conditions,” and is usually expressed in terms of relative standard deviation (RSD). Accuracy and precision were assessed for hair samples by measuring six replicates at the LLOQ and QC samples. Intra-day precision and accuracy were determined by analyzing six replicates on a single day, while inter-day precision and accuracy were evaluated by analyzing six replicates prepared daily for 4 days. The maximum acceptable accuracy for QC samples does not exceed 85–115%, and for LLOQ samples it does not exceed 80–120%. The CV value of intra-day precision and inter-day precision is not more than ±15% for QC samples and not more than ±20% for LLOQ samples.

### Recovery and Matrix Effect

The matrix effect and recovery experiments were designed according to the experimental scheme proposed by Matuszewski et al. (2003). Recovery and matrix effects were measured by

analyzing QC samples with six replicates. The samples were divided into three groups: pre-extraction spiked samples (A), post-extraction spiked samples (B) and neat solution (C). The matrix effect was calculated by B/C, and recovery was calculated by A/C.

### Dilution Integrity

Hair samples at concentrations of 1,000 and 2,000 pg/mg were prepared. Hair samples with concentrations of 1,000 pg/mg ( $n = 6$ ) and 2,000 pg/mg ( $n = 6$ ) were diluted 10 times and 100 times, respectively, after extraction. Dilution integrity was evaluated by determining the precision and accuracy.

### Stability

Three QC samples at low, medium and high concentrations were used from six batches and stored in the autosampler at 4°C for 24, 48, and 72 h to investigate the stability of 5F-MDMB-PICA and its metabolites in extracts.

### Application to Real Cases

The validated method was applied to four authentic forensic cases. All hair samples came from suspected drug users. The hair samples were washed, and 1–6 cm sections of the hair samples were cut and divided into 1–3 and 4–6 cm sections. Each section of hair was cut into ~1–2 mm pieces for analysis of the presence of drug of abuse. Four suspicious users provided written informed consent.

## RESULTS AND DISCUSSION

### Method Development

To obtain good chromatographic separation and symmetrical peak shape, the chromatographic conditions were optimized. After investigation, different gradient mobile phases were able to separate 5F-MDMB-PICA and its metabolites at a flow rate of 0.3 mL/min. The retention times of 5F-MDMB-PICA and its metabolites are shown in **Table 1**. The collision energy and declustering voltage were optimized to obtain suitable precursor and product ions.

There have been some reports in the literature on the choice of organic solvents to extract synthetic cannabinoids in hair (Hutter et al., 2012; Salomone et al., 2012, 2014; Gottardo et al., 2014), although methanol is the most common solvent for extracting drugs from hair. To optimize the extraction solvent of 5F-MDMB-PICA and its metabolites, methanol, an EM solution (a mixture of methanol, acetonitrile, and 2 mM ammonium formate) and *n*-hexane:ethyl acetate (9:1, v/v) were used as extraction solvents to evaluate their extraction recovery. The result shows the extraction recoveries of 5F-MDMB-PICA and its metabolites using these different extraction solvents. The extraction recoveries of the target analytes with methanol were significantly higher than those achieved with the other two extraction solvents; hence, methanol was chosen for subsequent analyses. To obtain a good extraction recovery and absence of a significant matrix effect, 5F-MDMB-PICA and its metabolites were filtered with different filter membranes.

This showed that the extraction recovery rates of 5F-MDMB-PICA and its metabolites on polyethersulfone ( $13 \times 0.22$  mm), nylon ( $13 \times 0.22$  mm), nylon ( $13 \times 0.45$  mm) and acrodisc ( $13 \times 0.2$  mm) filter membranes were high; however, because of their relative matrix effects, these filters were not selected. In addition, the material of polytetrafluoroethylene 1 ( $13 \times 0.22$  mm) and polytetrafluoroethylene 2 ( $13 \times 0.22$  mm) are the same, but the manufacturers of the two are different, which may cause different production processes. After investigating these two types of membranes, it was found that the extraction recoveries of polytetrafluoroethylene 1 ( $13 \times 0.22$  mm) and polytetrafluoroethylene 2 ( $13 \times 0.22$  mm) were essentially the same; both of them were higher than 85%, although the matrix effect of polytetrafluoroethylene 2 ( $13 \times 0.22$  mm) was better than that of polytetrafluoroethylene 1 ( $13 \times 0.22$  mm). Therefore, polytetrafluoroethylene 1 ( $13 \times 0.22$  mm) was chosen as the membrane for filtration.

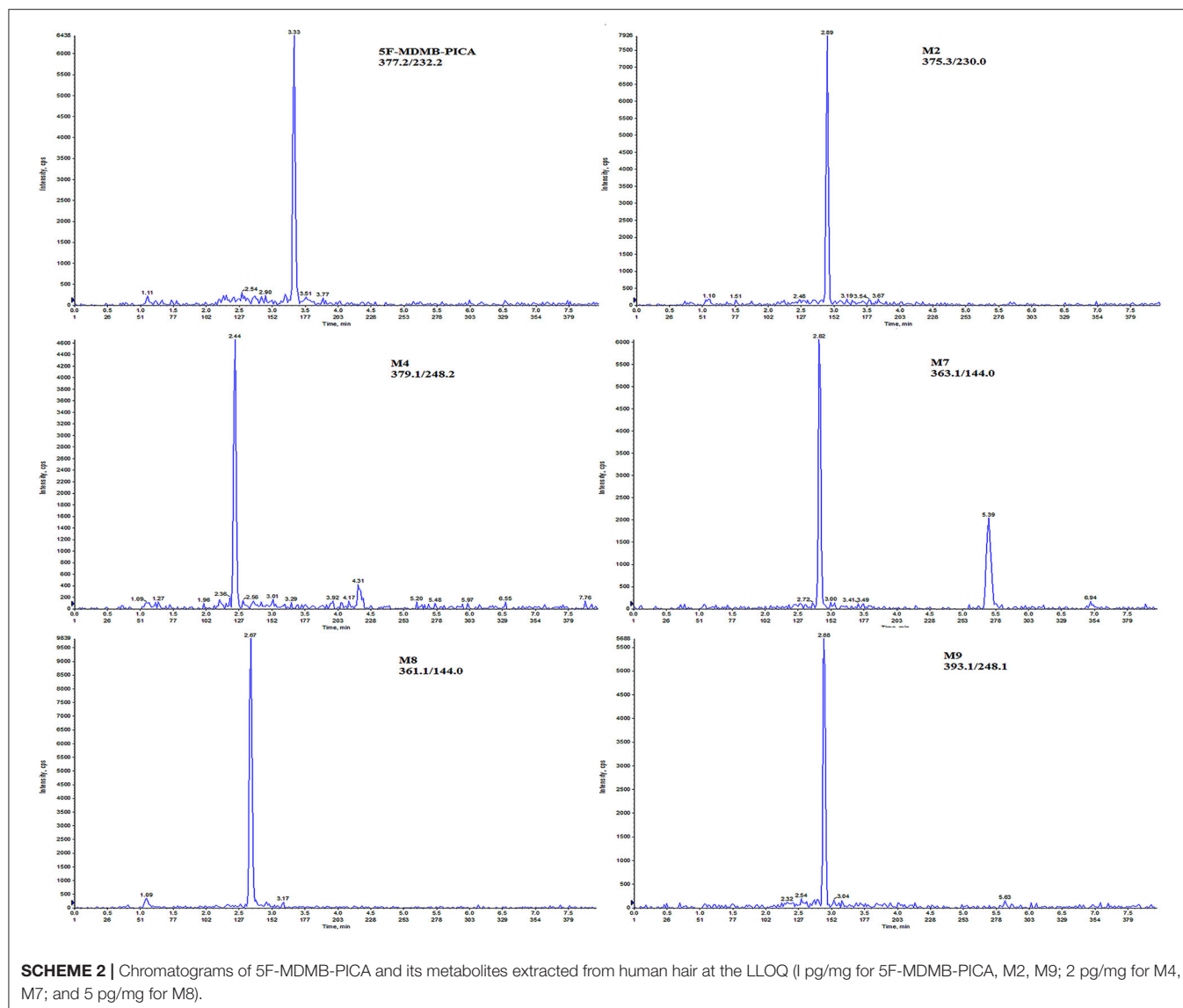
### Method Validation

No interference was observed with any of the analytes, including the IS, in the 10 hair samples obtained from drug-free volunteers.

The LOD and LLOQ of the analytes are shown in **Table 1**. The LOD ranged from 0.5 to 5 pg/mg, while the LLOQ ranged from 1 to 5 pg/mg (**Scheme 2**). According to the reference (Peters et al., 2007), for LLOQ, S/N is usually required to be equal to or >10; in contrast to the LLOQ determination, for LOD a S/N or *k*-factor equal to or greater than three is usually chosen. In our experiment, the S/N of 5F-MDMB-PICA, M2, M4, M7, M8, and M9 at LOD concentration are 3.1, 5.7, 3.8, 4.9, 5.6, and 3.6, respectively; while the S/N at LLOQ concentration are 10.8, 13.4, 11.2, 13.6, 12.7, and 10.9, respectively, and the precision and accuracy of LLOQ concentration meet criteria. In general, LLOQ concentration is 3 times the LOD concentration, but in some cases LLOQ concentration is not 3 times the LOD concentration. For example, according to the reference (Scientific Working Group for Forensic Toxicology, 2013), it is determined that the LOD concentration is 8.8 ng/mL and the LLOQ concentration is 10 ng/mL. Considering the reference literature and the experimental results of multiple compounds, it is determined that LLOQ concentration is twice the LOD concentration. This method had higher selectivity than those of other procedures published in the literature and exhibited improved sensitivity (Salomone et al., 2014). The linearity of each analyte is shown in **Table 2**, with correlation coefficients ( $R^2$ ) all higher than 0.999. The linear range of 5F-MDMB-PICA, M2 and M9 was 1–200 pg/mg; that of M4 and M7 was 2–200 pg/mg; and that of M8 was 5–200 pg/mg. The deviation value of the LLOQ concentration point on the linearity is <20%, while the deviation value of the other concentration points is <15%.

The intra- and inter-day precision and accuracy of all of the analytes at four levels are summarized in **Table 3**. The intra-day precision ranged from 0.7 to 10.8%, and the accuracy varied between 95.4 and 107.4% ( $n = 6$ ). The inter-day precision ranged from 1.7 to 12.2%, and the accuracy varied between 95.0 and 102.8% ( $n = 6$ ). In general, the RSD values of the intra- and inter-day precision and accuracy of the three QC samples were <15%, while the RSD values of the LLOQ samples were <20%.





Intra-day and inter-day precision and accuracy values met the acceptance criteria.

The results of the recovery and matrix effect are shown in **Table 3**. The matrix effect ranged from 19.1 to 102.6%. However, ion suppression occurred for 5F-MDMB-PICA and M8 in the hair matrix. Even at a low concentration, the matrix effect ranged from 19.7 to 33.6%. Whether this was indeed a systematic effect needs to be clarified; however, the relative standard deviation of the six different samples for each matrix was <5.8%. The recoveries of all the analytes were within a range of 61.1–93.3% for the three QC samples and for the LLOQ samples. According to the reference (Goebel et al., 2013), in hair matrix, however, only ion suppression was found. Even at a low concentration (5 pg/mg) absolute matrix values range from 15.4 to 71.5%. The matrix effect of compounds is easily affected by the concentration, and the lower the concentration, the higher the influence of the matrix effect. Affected by the

physical and chemical properties of the compound, the polarity of 5F-MDMB-PICA is small, while the polarity of its metabolites is relatively large. We speculated that a competitive relationship was formed during the ionization process of 5F-MDMB-PICA and its metabolites. The ionization efficiency of 5F-MDMB-PICA was reduced, resulting in ion suppression. In addition, 5F-MDMB-PICA and its metabolites should be considered at the same time during sample preparation, which may also affect the matrix effect of 5F-MDMB-PICA. In the method validation, the linearity, precision and accuracy all meet the requirements.

The effect of dilution on precision and accuracy was investigated. The accuracies were 93–109%, and the RSD values were within 3.7%, demonstrating no detrimental impact of dilution.

The RSD values of 5F-MDMB-PICA and its metabolites stored at 4°C for 24, 48, and 72 h were 97–104%, 97–103%, and 97–105%, respectively. The RSD values were all within 20%,



**TABLE 3 |** Intra-day and inter-day accuracy and precision, matrix effect and recovery for 5F-MDMB-PICA and its metabolites in hair.

Analytes	Concentrations (pg/mg)	Intra-day (n = 6)		Inter-day (n =24)		Matrix effect (n = 6)		Recovery (%) (n = 6)
		Precision (%)	Accuracy (%)	Precision (%)	Accuracy (%)	Mean (%)	CV (%)	
5F-MDMB-PICA	1	6.6	105.0	5.8	98.8	23.0	1.2	72.5
	10	1.2	102.6	2.5	100.9	19.7	0.8	78.1
	50	4.0	99.8	4.9	101.3	19.1	1.7	91.8
	150	2.8	99.4	5.6	96.8	20.2	1.1	93.3
M2	1	1.2	97.4	8.3	95.0	53.5	4.9	83.8
	10	4.3	104.2	6.5	101.3	43.0	2.5	80.8
	50	4.5	99.0	7.4	101.0	40.6	4.1	81.5
	150	6.1	100.1	10.0	95.4	41.0	2.8	77.2
M4	2	1.2	101.2	5.0	102.3	90.4	11.4	64.4
	10	4.2	103.7	4.2	97.6	102.6	6.9	60.7
	50	4.1	98.0	4.5	99.6	98.3	6.6	76.0
	150	2.4	99.9	7.3	98.7	93.9	7.7	81.5
M7	2	0.7	104.2	7.8	105.7	55.6	4.3	63.3
	10	1.6	100.4	6.0	97.0	59.7	6.1	61.1
	50	1.8	96.1	4.6	99.8	59.2	7.2	77.5
	150	6.0	101.3	8.5	98.3	58.9	2.5	83.3
M8	5	2.8	97.7	5.3	101.3	30.2	2.2	63.0
	20	1.2	101.8	1.7	99.5	33.6	2.0	76.1
	50	1.3	97.6	4.1	98.3	35.6	4.2	79.4
	150	5.0	100.5	7.7	100.1	36.8	2.0	85.6
M9	1	10.8	107.4	12.2	101.0	57.2	8.3	70.6
	10	1.1	98.8	6.5	101.2	46.2	3.6	71.6
	50	1.5	95.4	6.9	98.6	46.0	2.6	70.8
	150	2.4	101.7	11.5	94.7	48.4	4.0	72.2

indicating that these analytes were sufficiently stable in hair. The stability results are shown in **Table 4**.

### Application to Cases

The LC-MS/MS method was applied to the determination of 5F-MDMB-PICA and its metabolites in four authentic forensic cases (see **Table 5** and **Scheme 3**).

#### Case 1

A 23-year-old female with a history of smoking was introduced by a friend that smoking e-liquid is more fun than smoking regular tobacco cigarettes. She smoked e-liquids many times without knowing their composition. The individual developed hallucinations and euphoria after smoking and fell down a set of stairs. She was found by her family, who promptly sent her to the hospital. She recovered after rescue and 5F-MDMB-PICA and its metabolites were detected in her hair. The concentrations of 5F-MDMB-PICA were 77 and 283 pg/mg in the proximal 1–3 and 4–6 cm sections of her hair, respectively. Only metabolite M7 was detected in the 1–3 cm sections, and its concentration was lower than the LLOQ. The metabolites M2 and M7 were detected at 4–6 cm, and their concentrations were also lower than the LLOQ.

#### Case 2

A 53-year-old male with high blood pressure purchased e-liquids several times on the Internet. After the last inhalation, he developed tachycardia, convulsions and shock. Upon discovery, he was admitted to the hospital for treatment but died of cerebral hemorrhage. 5F-MDMB-PICA and its metabolites were detected in both 1–3 and 4–6 cm sections of the hair. Metabolites M4, M7, M8, and M9 were detected in the 1–3 cm hair section, and their concentrations were all lower than the LLOQ. All metabolites are detected in the 4–6 cm hair section and were lower than the LLOQ.

#### Case 3

A 25-year-old male with a long history of drug abuse attended a gathering of friends. He drank alcohol and smoked e-liquid and K powder at the party. During this period, he suddenly experienced shock, convulsions and tachycardia. This individual was seen by a doctor soon after and recovered without sequelae. The police found a large amount of e-liquid and K powder at the scene. According to the existing method of our forensic toxicology laboratory, the concentration of K powder in the hair was qualitatively and quantitatively determined to be 200 pg/mg (Zhuo et al., 2020). The concentrations of 5F-MDMB-PICA detected in the 1–3 and 4–6 cm hair sections were 275 and

1,025 pg/mg, respectively. The concentration of metabolite M7 was 2.8 pg/mg in the 1–3 cm hair section, and the concentrations of M2 and M8 were both lower than the LLOQ. In addition, the concentrations of metabolites M2 and M7 were detected in the 4–6 cm hair section at 3.0 and 5.6 pg/mg, respectively, and the concentrations of the remaining metabolites were lower than the LLOQ.

**TABLE 4 |** Stability of 5F-MDMB-PICA and its metabolites in human hair.

Analytes	Concentration (pg/mg)	Autosampler, 4°C, n = 6 (%)		
		24 h	48 h	72 h
5F-MDMB-PICA	1	100.6	100.8	105.0
	10	100.2	99.2	100.8
	50	99.7	100.4	99.1
	150	100.0	99.8	101.0
M2	1	102.2	103.4	103.7
	10	98.9	101.0	100.5
	50	97.4	98.2	99.7
	150	101.2	100.6	100.5
M4	2	103.7	101.8	96.8
	10	99.2	100.0	100.9
	50	94.7	96.7	99.6
	150	101.8	101.0	99.1
M7	2	101.7	104.4	105.3
	10	99.4	98.7	101.6
	50	99.7	96.8	99.8
	150	100.2	100.8	100.6
M8	5	100.6	103.4	102.5
	20	100.4	100.8	104.4
	50	98.7	95.0	94.3
	150	100.4	101.0	101.4
M9	1	97.1	105.8	102.2
	10	103.9	100.3	100.2
	50	100.2	98.0	97.0
	150	99.6	100.9	101.3

**Case 4**

A 36-year-old male was meeting with friends at an entertainment venue. The police received a report that someone in the crowd took drugs. A man and his friend were detained and found to have a large amount of suspicious white powder and liquid at the scene. The man said that he had smoked the e-liquid for the first time under unknown circumstances. After testing, the suspicious white powder and liquid at the scene were found to be fentanyl and 5F-MDMB-PICA. No fentanyl was detected in his hair (Qin et al., 2019). The 5F-MDMB-PICA concentration was 2 pg/mg, and its metabolites were lower than the LLOQ in the 1–3 cm hair section of the individual, while 5F-MDMB-PICA and its metabolites were negative in the 4–6 cm sections.

**Comparison With Previous Research**

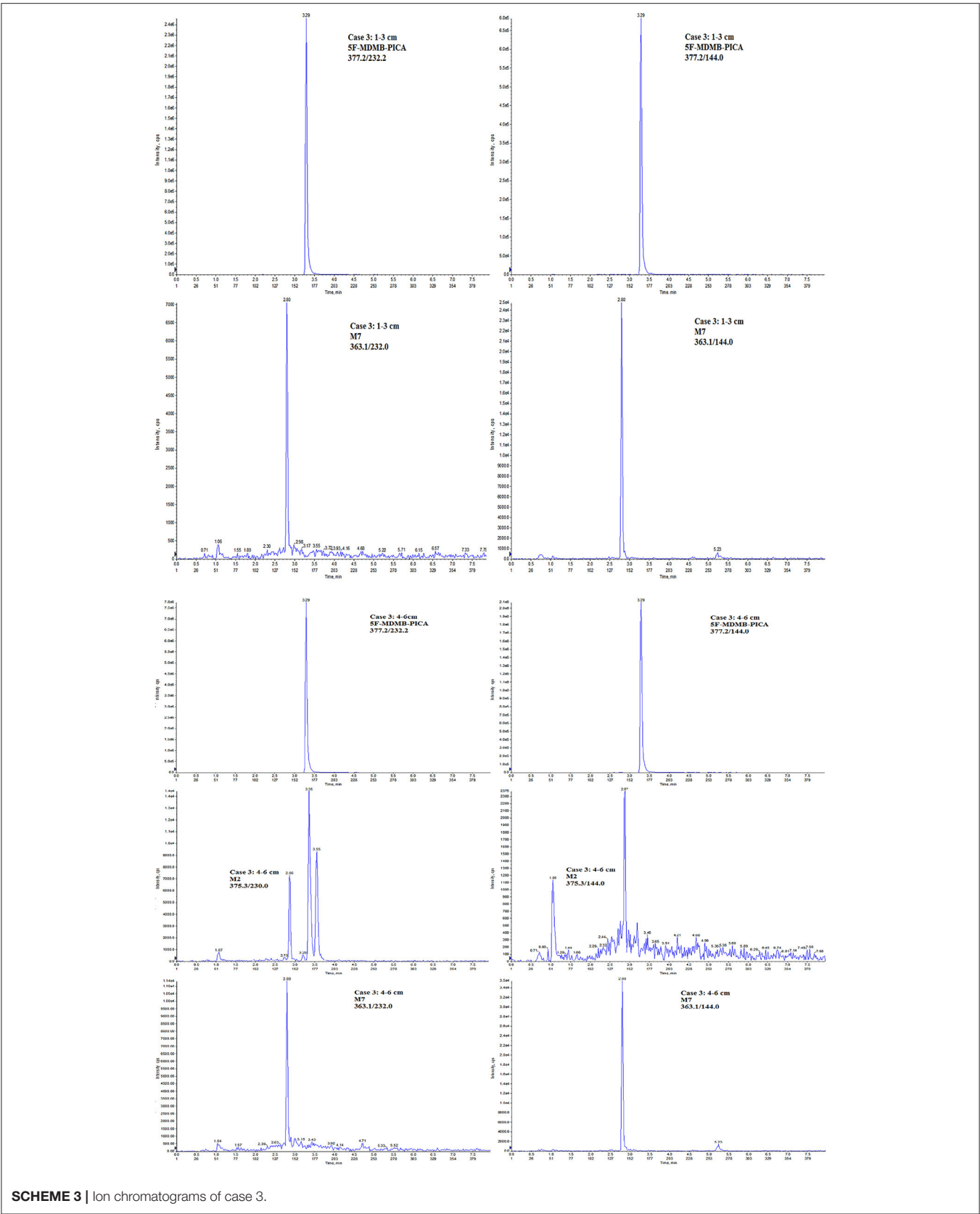
It has been reported in some studies that LC-MS/MS methods can be used to analyse other synthetic cannabinoids in human hair. The limit of detection of this study was the same as that of a previous study and reached the pg level (Arbouche et al., 2019; Cho et al., 2020). Chinese hair is similar to Korean and Japanese hair. Cho et al. (2020) studied the distribution of synthetic cannabinoids and metabolites in the hair of Korean drug users. The concentrations of AB-CHMINCA and its metabolite M2 were 2.5–13,500.0 and 0.5–35.1 pg/mg, respectively, and the concentration of the precursor drug was greater than the concentrations of metabolites in all cases. Moreover, Arbouche et al. (2019) detected a higher concentration of AB-PINACA in head hair than in pubic hair and detected a very low concentration of AB-PINACA in urine, which may be caused by rapid metabolism, and pubic hair is easily contaminated by urine.

The growth rate of human hair is ~0.7–1.4 cm per month, and hair can accurately reflect the medication history of an individual. Generally, a proximal 1 cm of hair can roughly reflect the medication history of an individual in the past month. We analyzed 5F-MDMB-PICA and its metabolites in the 1–6 cm section in four individuals suspected of drug use, reflecting the medication situation in the past 6 months. The individuals in cases 1 and 2 had 5F-MDMB-PICA in their 1–6 cm hair section samples, and the metabolite concentrations were low, below the LLOQ, indicating that the drug had been consumed

**TABLE 5 |** Case Information and toxicology results.

Case	Age	Sex	Hair section (cm)	Concentration (pg/mg)					
				5F-MDMB-PICA	M2	M4	M7	M8	M9
1	22	Female	1–3	77	nd	nd	<2*	nd	nd
			4–6	283	<1*	nd	<2*	nd	nd
2	53	Male	1–3	46	nd	<2*	2.7	<5*	<1*
			4–6	349	<1*	<2*	<2*	<5*	<1*
3	25	Male	1–3	275	<1*	nd	2.8	<5*	nd
			4–6	1025	3.0	<2*	5.6	<5*	<1*
4	36	Male	1–3	2	nd	<2*	<2*	<5*	<1*
			4–6	nd	nd	nd	nd	nd	nd

\*, detected below the LLOQ; nd, not detected.



within 6 months, but only a small amount of the drug was consumed. The individual from case 3 had higher concentrations of the precursor drug and its metabolites than the individuals from cases 1 and 2 in the 1–6 cm hair section, indicating that he had taken 5F-MDMB-PICA for a long time and had consumed a large amount of this drug in the past 6 months. In case 4, 5F-MDMB-PICA was only detected in the 1–3 cm hair section of the individual, the concentration was very low, and the concentrations of metabolites were lower than the LLOQ, supporting the idea that the individual had taken the drug for the first time. The concentration of 5F-MDMB-PICA detected in human hair samples is much higher than the concentration of its metabolites. 5F-MDMB-PICA undergoes metabolic reactions such as hydrolysis, hydroxylation or oxidation in the body to produce metabolites, which increase the polarity of metabolites (Mogler et al., 2018). Therefore, metabolites are not easily combined with the keratin matrix in human hair, which may result in lower levels of metabolites in human hair. In addition, studies have reported that some people have detected synthetic cannabinoids in hair samples of individuals that have not taken those drugs, which indicates that some drug powders or fumes can cause external contamination of hair samples or that an additional route of synthetic cannabinoid absorption by hair, such as sidestream smoke, may cause false positive results (Hutter et al., 2012; Saito et al., 2014). Therefore, analysis of the precursor drug and its metabolites in hair provides useful information for analysis. In this study, we detected metabolites of 5F-MDMB-PICA when analyzing 4 real hair samples. Metabolite M7 ( $m/z$  363.1) is the most abundant metabolite among the 4 real hair samples. According to previously reported data on SCs containing tert-leucine methyl ester substituents (such as MDMB-CHMICA), this metabolic step of ester hydrolysis is usually one of the main reactions *in vivo* (Grigoryev et al., 2016). In addition, we detected four other metabolites of 5F-MDMB-PICA in real human hair samples, M2, M4, M8, and M9. Previously, Mogler et al. (2018) detected 12 phase I metabolites of 5F-MDMB-PICA in the analysis of real urine samples. Compound M12 ( $m/z$  363), which is the same as metabolite M7 in human hair, is also the most abundant metabolite in all real urine samples and is formed by the hydrolysis of terminal methyl esters. As described in Table 4, it was found that 5F-MDMB-PICA was the main compound detected in the hair

samples, and its abundance was higher than that those of its metabolites M2, M4, M7, M8, and M9. The metabolites in this study are the same as the metabolites of 5F-MDMB-PICA detected in urine (Mogler et al., 2018). In addition, metabolite M7 is also formed as an artificial product through the hydrolysis of methyl esters during smoking. If M7 condenses on hair, it may be falsely determined as 5F-MDMB-PICA consumption when analyzing the metabolites of synthetic cannabinoids in hair. Therefore, the interpretation of metabolites should be treated with caution.

## CONCLUSION

This study describes the development and validation of an LC-MS/MS procedure for the identification and quantification of 5F-MDMB-PICA and its metabolites in human hair. The method was successfully applied to four individuals suspected of the use of a synthetic cannabinoid in which 5F-MDMB-PICA was detected.

## DATA AVAILABILITY STATEMENT

The raw data supporting the conclusions of this article will be made available by the authors, without undue reservation.

## AUTHOR CONTRIBUTIONS

LZ wrote the article and completed the experiment. YS revised the article and guided the experiment. HW and PX provided fund support and guidance for the experiment. WL and OD provided guidance for the experiment and instruments. HC, BS, and MS provided real materials. LL, ML, and HQ provided help for the experiment.

## FUNDING

This study was supported by grants from Shanghai Science and Technology Commission (19DZ1200600), National Natural Science Foundation of China (81971789 and 81871531), Research Institute Projects (2019G-4 and 2020Z-2), Shanghai Key Laboratory of Forensic Medicine (17DZ2273200), and Shanghai Forensic Service Platform (19DZ2292700).

## REFERENCES

- Arbouche, N., Raul, J. S., Garnier, D., Kintz, P., and Ameline, A. (2019). Testing for AB-PINACA in human hair: distribution in head hair versus pubic hair. *Drug Test. Anal.* 11, 610–616. doi: 10.1002/dta.2564
- Banister, S. D., and Connor, M. (2018a). The chemistry and pharmacology of synthetic cannabinoid receptor agonist new psychoactive substances: evolution. *Handb. Exp. Pharmacol.* 252, 191–226. doi: 10.1007/164\_2018\_144
- Banister, S. D., and Connor, M. (2018b). The chemistry and pharmacology of synthetic cannabinoid receptor agonists as new psychoactive substances: origins. *Handb. Exp. Pharmacol.* 252, 165–190. doi: 10.1007/164\_2018\_143
- Banister, S. D., Longworth, M., Kevin, R., Sachdev, S., Santiago, M., Stuart, J., et al. (2016). Pharmacology of valinate and tert-leucinate synthetic cannabinoids 5F-AMBICA, 5F-AMB, 5F-ADB, AMB-FUBINACA, MDMB-FUBINACA, MDMB-CHMICA, and their analogues. *ACS Chem. Neurosci.* 7, 1241–1254. doi: 10.1021/acschemneuro.6b00137
- Baumgartner, W. A., Hill, V. A., and Blahd, W. H. (1989). Hair analysis for drugs of abuse. *J. Forensic Sci.* 34, 1433–1453. doi: 10.1520/JFS12787J
- Chinnadurai, T. S., Srijan, and Ayinla, R. (2016). A curious case of inhalation fever caused by synthetic cannabinoid. *Am. J. Case Rep.* 17, 379–383. doi: 10.12659/AJCR.898500
- Cho, B., Cho, H. S., Kim, J., Sim, J., Seol, I., Baeck, S. K., et al. (2020). Simultaneous determination of synthetic cannabinoids and their metabolites in human hair using LC-MS/MS and application to human hair. *Forensic Sci. Int.* 306:110058. doi: 10.1016/j.forsciint.2019.110058
- Debruyne, D., and Le Boisselier, R. (2015). Emerging drugs of abuse: current perspectives on synthetic cannabinoids. *Subst. Abuse Rehabil.* 6, 113–129. doi: 10.2147/SAR.S73586

- Desharnais, B., Camirand-Lemyre, F., Mireault, P., and Skinner, C. D. (2014). *Validation of Calibration Models: Development and Testing of a Practical Procedure*. Grand Rapids, MI: ResearchGate.
- European Monitoring Centre for Drugs and Drug Addiction (EMCDDA) (2017). *European Drug Report 2016: Trends and Developments*. Lisbon: Publications Office of the European Union. Available online at: <https://www.emcdda.europa.eu/edr2016> (accessed November 16, 2017).
- Goebel, A., Boehm, M., Kirchherr, H., and Kühn-Velten, W. N. (2013). Simultaneous identification and quantification of synthetic cannabinoids (cannabimimetics) in serum, hair, and urine by rapid and sensitive HPLC tandem mass spectrometry screenings: overview and experience from routine testing. *J. Lab. Med.* 37, 167–180. doi: 10.1515/labmed-2012-0059
- Gottardo, R. S. D., Musile, G., Trapani, E., Seri, C., Serpelloni, G., and Tagliaro F. (2014). Screening for synthetic cannabinoids in hair by using LC-QTOF MS: a new and powerful approach to study the penetration of these new psychoactive substances in the population. *Med. Sci. Law* 54, 22–27. doi: 10.1177/0025802413477396
- Grigoryev, A., Kavanagh, P., and Pechnikov, A. (2016). Human urinary metabolite pattern of a new synthetic cannabimimetic, methyl 2-(1-(cyclohexylmethyl)-1H-indole-3-carboxamido)-3,3-dimethylbutanoate. *Forensic Toxicol.* 34, 316–328. doi: 10.1007/s11419-016-0319-8
- Hess, C. S. S., Kernbach-Wighton, G., and Madea, B. (2015). Death due to diabetic ketoacidosis: induction by the consumption of synthetic cannabinoids? *Forensic Sci. Int.* 257, e6–e11. doi: 10.1016/j.forsciint.2015.08.012
- Hutter, M., Kneisel, S., Auwärter, V., and Neukamm, M. A. (2012). Determination of 22 synthetic cannabinoids in human hair by liquid chromatography-tandem mass spectrometry. *J. Chromatogr. B* 903, 95–101. doi: 10.1016/j.jchromb.2012.07.002
- Krotulski, A. J., Mohr, A. L., Kacinko, S. L., Fogarty, M. F., Shuda, S. A., Diamond, F. X., et al. (2019). 4F-MDMB-BINACA: a new synthetic cannabinoid widely implicated in forensic casework. *J. Forensic Sci.* 64, 1451–1461. doi: 10.1111/1556-4029.14101
- Matuszewski, B. K., Constanzer, M. L., Chavez-Eng, C. M. (2003). Strategies for the assessment of matrix effect in quantitative bioanalytical methods based on HPLC-MS/MS. *Anal. Chem.* 75, 3019–3030. doi: 10.1021/ac020361s
- Mogler, L., Franz, F., Rentsch, D., Angerer, V., Weinfurtner, G., Longworth, M., et al. (2018). Detection of the recently emerged synthetic cannabinoid 5F-MDMB-PICA in 'legal high' products and human urine samples. *Drug Test. Anal.* 10, 196–205. doi: 10.1002/dta.2201
- Peters, F. T., Drummer, O. H., and Musshoff, F. (2007). Validation of new methods. *Forensic Sci. Inter.* 165, 216–224. doi: 10.1016/j.forsciint.2006.05.021
- Presley, B. C., Gurney, S. M., Scott, K. S., Kacinko, S. L., and Logan, B. K. (2016). Metabolism and toxicological analysis of synthetic cannabinoids in biological fluids and tissues. *Forensic Sci. Rev.* 28, 103–169.
- Qin, N., Xiang, P., Shen, B., Zhuo, X., Shi, Y., and Song, F. (2019). Application of a validated UHPLC-MS/MS method for 28 fentanyl-analogue and novel synthetic opioids in whole blood in authentic forensic cases. *J. Chromatogr. B* 1124, 82–99. doi: 10.1016/j.jchromb.2019.05.025
- Risseuw, M. D., Blanckaert, P., Coopman, V., Van Quekelberghe, S., Van Calenbergh, S., and Cordonnier, J. (2017). Identification of a new tert-leucinate class synthetic cannabinoid in powder and "spice-like" herbal incenses: Methyl 2-[[1-(5-fluoropentyl)indole-3-carbonyl]amino]-3,3-dimethyl-butanoate (5F-MDMB-PICA). *Forensic Sci. International* 273, 45–52. doi: 10.1016/j.forsciint.2017.01.023
- Saito, T., Sasaki, C., Namera, A., Kurihara, K., and Inokuchi, S. (2014). Experimental study on external contamination of hair by synthetic cannabinoids and effect of hair treatment. *Forensic Toxicol.* 33, 155–158. doi: 10.1007/s11419-014-0250-9
- Salomone, A., Gerace, E., D'Urso, F., Di Corcia, D., and Vincenti, M. (2012). Simultaneous analysis of several synthetic cannabinoids, THC, CBD and CBN, in hair by ultra-high performance liquid chromatography tandem mass spectrometry. Method validation and application to real samples. *J. Mass Spectrom.* 47, 604–610. doi: 10.1002/jms.2988
- Salomone, A., Luciano, C., Di Corcia, D., Gerace, E. N., and Vincenti, M. (2014). Hair analysis as a tool to evaluate the prevalence of synthetic cannabinoids in different populations of drug consumers. *Drug Test. Anal.* 6, 126–134. doi: 10.1002/dta.1556
- Scientific Working Group for Forensic Toxicology (2013). Scientific Working Group for Forensic Toxicology (SWGTOX) standard practices for method validation in forensic toxicology. *J. Anal. Toxicol.* 37, 452–474. doi: 10.1093/jat/bkt054
- Smith, J. P. S., Oliver, B., and Banks, C. E. (2015). An overview of recent developments in the analytical detection of new psychoactive substances (NPSs). *Analyst* 140, 4932–4948. doi: 10.1039/C5AN00797F
- Truver, M. T., Watanabe, S., Åstrand, A., Vikingsson, S., Green, H., Swortwood, M. J., et al. (2020). 5F-MDMB-PICA metabolite identification and cannabinoid receptor activity. *Drug Test. Anal.* 12, 127–135. doi: 10.1002/dta.2688
- Weaver, M. F., Hopper, J. A., and Gunderson, E. W. (2015). Designer drugs 2015: assessment and management. *Addict. Sci. Clin. Pract.* 10, 1–9. doi: 10.1186/s13722-015-0024-7
- Zhuo, Y., Wang, X., Wu, J., Zhang, S., Deng, H., Liu, W., et al. (2020). Simultaneous quantitative determination of amphetamines, opiates, ketamine, cocaine and metabolites in human hair: application to forensic cases of drug abuse. *J. Forensic Sci.* 65, 563–569. doi: 10.1111/1556-4029.14179

**Conflict of Interest:** The authors declare that the research was conducted in the absence of any commercial or financial relationships that could be construed as a potential conflict of interest.

Copyright © 2020 Shi, Zhou, Li, Liu, Qiang, Shen, Shen, Chen, Drummer, Liu, Wu and Xiang. This is an open-access article distributed under the terms of the Creative Commons Attribution License (CC BY). The use, distribution or reproduction in other forums is permitted, provided the original author(s) and the copyright owner(s) are credited and that the original publication in this journal is cited, in accordance with accepted academic practice. No use, distribution or reproduction is permitted which does not comply with these terms.





# Metabolic Profile of Four Selected Cathinones in Microsome Incubations: Identification of Phase I and II Metabolites by Liquid Chromatography High Resolution Mass Spectrometry

## OPEN ACCESS

### Edited by:

Marta Concheiro-Guisan,  
John Jay College of Criminal Justice,  
United States

### Reviewed by:

Svante Vikingsson,  
Swedish National Board of Forensic  
Medicine, Sweden  
Jose Luiz Costa,  
University of Campinas, Brazil

### \*Correspondence:

Helena Gaspar  
hmgaspar@ciencias.ulisboa.pt  
Alexandra M. M. Antunes  
alexandra.antunes@tecnico.ulisboa.pt

†These authors have contributed  
equally to this work

### Specialty section:

This article was submitted to  
Analytical Chemistry,  
a section of the journal  
Frontiers in Chemistry

**Received:** 22 September 2020

**Accepted:** 08 December 2020

**Published:** 12 January 2021

### Citation:

Lopes BT, Caldeira MJ, Gaspar H and  
Antunes AMM (2021) Metabolic  
Profile of Four Selected Cathinones in  
Microsome Incubations: Identification  
of Phase I and II Metabolites by Liquid  
Chromatography High Resolution  
Mass Spectrometry.  
Front. Chem. 8:609251.  
doi: 10.3389/fchem.2020.609251

Beatriz T. Lopes<sup>1,2</sup>, Maria João Caldeira<sup>3</sup>, Helena Gaspar<sup>2,4\*†</sup> and  
Alexandra M. M. Antunes<sup>1\*†</sup>

<sup>1</sup> Centro de Química Estrutural (CQE), Instituto Superior Técnico (IST), ULisboa, Lisboa, Portugal, <sup>2</sup> BioISI – Biosystems & Integrative Sciences, Faculty of Sciences, University of Lisbon, Lisboa, Portugal, <sup>3</sup> Laboratório de Polícia Científica da Polícia Judiciária (LPC/PJ), Novo edifício Sede da Polícia Judiciária, Lisboa, Portugal, <sup>4</sup> MARE - Marine and Environmental Sciences Centre - Polytechnic of Leiria, Peniche, Portugal

Consumption of synthetic cathinones, the second largest class of new psychoactive substances (NPS) reported worldwide, represents a serious public health risk. One of the biggest challenges created by the rapid spread of NPS on the illegal drug market is the discovery of selective biomarkers for their detection in biological matrices, which is only possible through the study of their metabolic profile. The synthetic cathinones 4'-methyl-N,N-dimethylcathinone (**4-MDMC**), 4'-methyl-N,N-diethylcathinone (**4-MDEC**), 4'-chloro- $\alpha$ -pyrrolidinovalerophenone (**4CI-PVP**), and 4'-chloroethylcathinone (**4-CEC**) are NPS recently seized in Europe, and, with the exception of **4-CEC**, no metabolism study was reported for these cathinones. With the ultimate goal of overcoming this gap, these cathinones were incubated *in vitro* in human and rat liver microsomes in the presence of Phase I and II (glucuronidation) co-factors, using  $\alpha$ -pyrrolidinovalerophenone ( $\alpha$ -PVP) as positive control. The metabolite identification was performed by liquid chromatography coupled to tandem high resolution mass spectrometry (LC-HRMS/MS). This allowed the identification of multiple Phase I and glucuronide metabolites of the selected cathinones. Additionally, a new glucuronide conjugate, derived from the recreational drug  $\alpha$ -PVP, was herein identified for the first time. Importantly, we have demonstrated that **4-MDMC** and **4-MDEC** can act as prodrugs of the controlled substances **4-MMC** and **4-MEC**, respectively. The metabolites herein identified are expected to play an important role not only by acting as potential selective biomarkers of the intake of the synthetic cathinones selected for this study but also to understand their potential adverse effects and link these causative agents to toxicities, thereby helping in the treatment of non-fatal intoxications.

**Keywords:** 4-CEC, 4CI-PVP, 4-MDEC, 4-MDMC, LC-HRMS, glucuronides, Phase I, metabolites

## INTRODUCTION

NPS are a range of substances, mostly synthetic, that have been emerging in the recreational drugs market with the purpose of mimicking the effects of classic drugs and circumvent legislation restrictions against illicit substances (German et al., 2014). The term NPS, according to the Directive (EU) 2017/2103 (EU, 2017) designates substances that are not covered by the Single Convention on Narcotic Drugs of 1961 neither by the Convention on Psychotropic Substances of 1971 but are likely to present health or social risks comparable to that posed by substances listed in those conventions. Despite the rapid spread of NPS over the last 10 years, the number of first detections of NPS, reported to the European Monitoring Center for Drugs and Drug Addiction (EMCDDA) through the European Union Early Warning System (EWS), has recently slowed-down, most likely due to changes in drug policies (EMCDDA and EUROPOL, 2019; EMCDDA, 2020). Nevertheless, the around 50 novel NPS that are still reported annually by EWS, together with the circulation in the market of about 400 previously reported NPS, pose serious health risks and constitute a great challenge for health and forensic institutions (EMCDDA, 2020). Importantly, until December 2019, a total of 790 NPS were monitored by EMCDDA (2017) overall, these represent more than three times the number of drugs currently controlled by international conventions.

Synthetic cathinones, the second largest group of NPS reported worldwide (UNODC, 2018; EMCDDA, 2020) are  $\beta$ -keto phenethylamines, structural analogs of cathinone, the major psychoactive alkaloid present in the leaves of *Catha edulis*. This plant, usually known as khat, is native from eastern Africa and southern Arabia, where it has been used, over centuries, due to its stimulant effects (Valente et al., 2014; Pieprzyc et al., 2020). In fact, synthetic cathinones are known to produce psychostimulant effects similar to methamphetamine, cocaine, or MDMA (ecstasy) by interacting with the plasma membrane transporters of the monoamine neurotransmitters, dopamine, norepinephrine, and serotonin, increasing their synaptic cleft concentration (German et al., 2014; Weinstein et al., 2017).

Synthetic cathinones were initially synthesized as an attempt to find new products with therapeutic applications due to their structural similarity with amphetamines (Kelly, 2011). Although some cathinones have been approved (FDA, 2020) and marketed as therapeutic agents, mainly as antidepressants or appetite suppressants (Arias et al., 2009; Kelly, 2011; Kang and Park, 2012; German et al., 2014; Onakpoya et al., 2016; FDA, 2020), most of them were banned or withdrawn from the market due

to serious adverse effects or their potential misuse. Nonetheless, some cathinones are still in clinical use. One representative example is bupropion, which is an uncontrolled drug and is clinically used, mainly in the treatment of depression (Carroll et al., 2014; Costa et al., 2019; FDA, 2020).

The increase of acute intoxication and deaths associated with the consumption of cathinones (and other NPS) (Weinstein et al., 2017; Zaami et al., 2018) has resulted in their continuous inclusion in the International Drug Control Convention (UNODC, 2020), based on their risk assessment. Since 2015, 11 synthetic cathinones were included in the Schedule II of the Convention on Psychotropic Substances of 1971 (UNODC, 2020): mephedrone (**4-MMC**), methylenedioxypyrovalerone (**MDPV**), and methylone (in 2015);  $\alpha$ -pyrrolidinopentiophenone ( **$\alpha$ -PVP**) (in 2016); 4'-methyl-*N*-ethylcathinone (**4-MEC**), pentadron and ethylone (in 2017); ephylone (in 2019); 4'-chloromethylcathinone (**4-CMC**), *N*-ethylhexedrone (**NEH**), and  $\alpha$ -pyrrolidinohexanophenone ( **$\alpha$ -PHP**) (in 2020).

Metabolic profiling of cathinones is crucial not only to understand potential adverse effects and link causative agents to toxicities but also to identify unique biomarkers of their intake, that will allow their unequivocal identification in biological matrices. Some cathinones undergo extensive metabolism *in vivo* (Uralets et al., 2014; Ellefsen et al., 2016), which is translated into low or even negligible urinary levels of the parent cathinone. Therefore, for these cases, the detection of cathinone's metabolites in biofluids, is the only possible way of proving the consumption of these NPS, in particular several hours after its intake. However, the metabolic profiles of most of the recently reported synthetic cathinones remain unknown. In fact, the large number of new substances that appear in the market makes it difficult for the authorities to respond with the needed analytical methodologies and metabolic studies for the identification and quantification of parent NPS and their metabolites in biofluids. In this regard, *in vitro* approaches, in particular liver microsome incubations, have proved their utility for studying the metabolic profile of cathinones (Meyer et al., 2010, 2012; Pedersen et al., 2013; Helfer et al., 2015; Negreira et al., 2015; Pozo et al., 2015).

With the ultimate goal of contributing for a proactive response in tackling the NPS problem, and within the scope of a protocol established between the Forensic Science Laboratory from Portuguese Criminal Police and the Lisbon University (Instituto Superior Técnico and Faculty of Sciences), the present work is aimed at determining the metabolite profile of four selected *para*-substituted cathinones: 4'-methyl-*N,N*-dimethylcathinone (**4-MDMC**), 4'-methyl-*N,N*-diethylcathinone (**4-MDEC**), 4'-chloro-  $\alpha$ -pyrrolidinovalerophenone (**4Cl-PVP**) and 4'-chloro-*N*-ethylcathinone (**4-CEC**) (**Figure 1**). The cathinone **4-MDMC** is a structural isomer of the controlled drug **4-MEC** and pentadron. **4-MDMC** is structurally-related to amfepramone (**DMC**) and **4-MDEC** is an isomeric structure of the recently scheduled drug **NEH**. Both these cathinones were seized for the first time during 2014 (EMCDDA, 2015) **4Cl-PVP** and **4-CEC** were reported in 2015 (EMCDDA, 2016) and 2016 (EMCDDA, 2017), respectively. Importantly, **4-MDEC** was the most cytotoxic cathinone tested in HepG2 cells, in our previous work (Gaspar et al., 2018) and **4-MDMC** was one of the five

**Abbreviations:** 4-CEC, 4'-chloro-*N*-ethylcathinone; 4Cl-PVP, 4'-chloro- $\alpha$ -pyrrolidinovalerophenone; 4-CMC, 4'-chloro-*N*-methylcathinone; ESI+, electrospray ionization in the positive mode; HLM, human liver microsomes; LC- HRMS/MS, Liquid chromatography coupled to tandem high-resolution mass spectrometry; 4-MDEC, 4-methyl-*N,N*-diethylcathinone; 4-MDMC, 4-methyl-*N,N*-dimethylcathinone; 4-MEC, 4'-methyl-*N*-ethylcathinone; MS, mass spectrometry; 4-MMC, 4'-methyl-*N*-methylcathinone; MS/MS, tandem mass spectrometry; *m/z*, mass-to-charge ratio; NADPH, 5'-phosphate adenosine 2,5'-bisphosphate in its reduced form; NEH, *N*-ethylhexedrone;  $\alpha$ -PHP,  $\alpha$ -pyrrolidinohexanophenone;  $\alpha$ -PVP,  $\alpha$ -pyrrolidinopentiophenone; RLM, rat liver microsomes; QTOF, hybrid quadrupole time-of-flight; UDPGA, uridine diphosphate glucuronic acid.

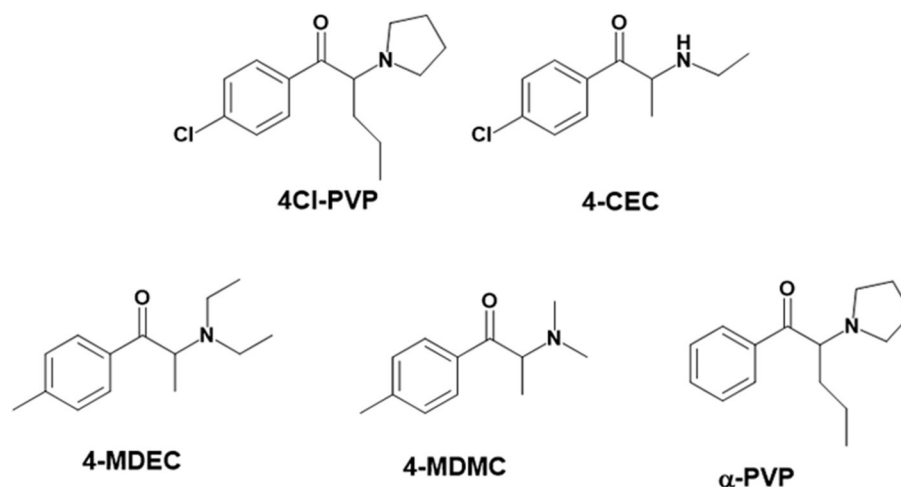


**FIGURE 1** | Structures of the synthetic cathinones used in the current study.

most seized cathinones in EU, during 2016, while 4-CEC was the second one with highest overall quantities of seized products (EMCDDA, 2017). All the four selected cathinones are controlled in Portugal (Decree Law 15/93 and Decree Law 54/2013) and only 4-CEC has already been subject of metabolism studies (Fabregat-Safont et al., 2020; Wagmann et al., 2020).

## MATERIALS AND METHODS

### Chemicals and Biochemicals

The analytical standards of the hydrochloride salts of the selected cathinones (purity >97%) used in this work were previously obtained and characterized within the scope of the protocol established between the Faculty of Sciences of the University of Lisbon (FCUL) and the Forensic Science Laboratory from Portuguese Criminal Police (LPC-PJ): 4-MDMC, 4-MDEC and α-PVP were synthesized at FCUL, as described by Gaspar et al. (2018), while 4Cl-PVP and 4-CEC were obtained from seized samples provided by LPC-PJ (Antunes et al., 2020). Rat and human liver microsomes were obtained from Thermo Fisher Scientific-Gibco. All other commercially available reagents were acquired from Sigma-Aldrich Química, S.A. and used as received.

### Incubation of Cathinones With Human and Rat Liver Microsomes

#### Generation of Phase I Metabolites

Cathinones, at a concentration of 10 μM (1 μL, 5 mM water solution), were incubated with human liver microsomes (HLM) and rat liver microsomes (RLM) (1 mg/mL), NADPH (20 mM, 1 μL), for a total incubation volume of 200 μL in 50 mM ammonium bicarbonate buffer at pH 7.4. Each incubation was run in duplicate. Control incubations were conducted in the same conditions: (1) using water as a negative control, in the absence of cathinone; (2) in the absence of the NADPH cofactor; and (3) using heat-denatured (90°C, 15 min) microsomes. Incubation of α-PVP, was run at the same conditions, as a positive control incubation. The mixtures were incubated

at 37°C and 100 μL aliquot was collected following 2 h of incubation. Acetonitrile (100 μL) was then added to quench the reactions. Following centrifugation at 10,000 g for 15 min at room temperature, the supernatants were collected and analyzed by liquid chromatography-tandem high resolution mass spectrometry (LC-HRMS/MS).

#### Generation of Phase II Metabolites

HLM and RLM (1 mg/mL) were preincubated for 15 min, in ice, with alamethicin (4 μL, 5 mg mL<sup>-1</sup>) in 50 mM ammonium bicarbonate buffer at pH 7.4, for a total incubation volume of 200 μL. Following the addition of MgCl<sub>2</sub> (400 mM; 1 μL) and cathinone (10 μM final concentration; 1 μL, 5 mM water solution), the resulting solution was incubated for 5 min at 37°C. NADPH (20 mM, 1 μL) and UDPGA (250 mM, 10 μL) were then added to start the Phase I and II reactions. Incubations were run in duplicate. Control incubations were conducted in the same conditions: (1) using water as a negative control, in the absence of cathinone; (2) in the absence of the NADPH and UDPGA cofactors; and (3) using heat-denatured (90°C, 15 min) microsomes. Incubation of α-PVP, was run at the same conditions, as a positive control incubation. The mixtures were incubated at 37°C and a 100 μL aliquot was collected following 2 h of incubation. Acetonitrile (100 μL) was then added to quench the reactions. Following centrifugation at 10,000 g for 15 min at room temperature, the supernatants were collected and analyzed by LC-HRMS/MS.

### Liquid Chromatography-Tandem High Resolution Mass Spectrometry (LC-HRMS/MS) Analyses

LC-HRMS/MS analyses were performed on a Bruker Impact II quadrupole time-of-flight mass spectrometer equipped with an ESI source (Bruker Daltonics, Bremen, Germany). Chromatographic separations were performed on: (1) an Ultimate 3000 RSLCnano system (ThermoFisher Scientific) using a Luna C18 column (3.0 μm, 2.0 × 150 mm; Phenomenex)

and an elution gradient of 0.1% formic acid in water (mobile phase A) and 0.1% formic acid in acetonitrile (mobile phase B) at a flow rate of 170  $\mu\text{L}/\text{min}$ . The elution conditions were as follows: 5–50% B for 6 min; 50–100% B for 4 min; isocratic elution with 100% B for 5 min; 100–5% B for 4 min; and finally, 5% B for 9 min; or (2) an Ultimate 3000 RSLCnano system (ThermoFisher Scientific) using a HypersilGold C18 column ( $2.1 \times 150 \text{ mm}$ ,  $1.9 \mu\text{m}$  particle size; ThermoFisher Scientific) at a flow rate of 200  $\mu\text{L}/\text{min}$ . The elution conditions were as follows: 5% B for 2.4 min; 5–25% B for 2.1 min; 25–70% B for 4.1 min; 70–100% B for 3 min; 100% B for 3 min; 100–5% B for 2 min; and finally 5% B for 6 min. In either instance, the injection volume was 10  $\mu\text{L}$ . The column and the autosampler were maintained at 40 and 8°C, respectively. The mass spectrometric parameters were set as follows: end plate offset, 500 V; capillary voltage, 4.5 kV; nebulizer, 40 psi; dry gas, 8 L/min; heater temperature, 200°C. Spectra were acquired in the positive electrospray ionization mode ESI (+). Internal calibration was performed for sodium formate cluster, with a sodium formate solution introduced to the ion source via a 20  $\mu\text{L}$  loop at the beginning of each analysis using a six-port valve. Calibration was then performed using high-precision calibration mode (HPC). Acquisition was performed in the  $m/z$  50–1,000 range and in a data-dependent MS/MS mode with an isolation window of 0.5, acquisition rate of 3 Hz and a fixed cycle time of 3 s. Precursor ions were selected for auto MS/MS at an absolute threshold of 153, with the active exclusion mode set at three spectra and released after 1 min, but precursor ions with intensities in the range of 5x the previous intensities were reconsidered.

## Data Processing

The acquired data were processed by DataAnalysis 4.1 software (Bruker Daltonics). Extracted ion chromatograms (EIC), with a mass window of  $\pm 5$  ppm, were performed for searching the protonated molecule of the expected metabolites in the full scan spectra. Isotope cluster analysis was also used to identify chlorinated metabolites. All spectra corresponding to metabolites were then manually checked. The mass deviation from the accurate mass of the identified cathinone metabolites remained below 5 ppm for the precursor and below 10 ppm for product ions. The MS/MS spectra of the four selected cathinones and their identified metabolites are displayed in the Supplementary Material (Supplementary Figures 1–20).

## RESULTS AND DISCUSSION

Taking into consideration that liver microsome incubations were already successfully used for the generation of metabolites that occur *in vivo* for other cathinones (Meyer and Maurer, 2010; Meyer et al., 2010, 2012; Strano-Rossi et al., 2010; Negreira et al., 2015), this *in vitro* model was used for the identification of the metabolite profile of the four *para*-substituted cathinones, 4-MDMC, 4-MDEC, 4CI-PVP, and 4-CEC, selected for this study. HLM and RLM incubations were run for each of these cathinones. This decision was made based on our previous work (Godinho et al., 2018), where considerably more metabolites were identified in the incubations of the anti-HIV drug

etravirine run in the rat liver S9 fraction when compared with the corresponding human liver S9 fraction incubations, due possibly to the higher enzymatic activity of the rodent fraction. Nonetheless, importantly, metabolites that were solely identified *in vitro* in the rat liver S9 incubations were also identified *in vivo* in the urine of HIV patients in etravirine therapy. Therefore, the fact that a specific metabolite is only detected in RLM does not necessarily mean that this metabolite cannot be formed *in vivo* in humans. However, in the current study, with very few exceptions, which will be conveniently mentioned, the metabolites were consistently identified in HLM and RLM incubations. This is particularly relevant since most *in vivo* toxicological studies are performed in rodent models (Prosser and Nelson, 2012).

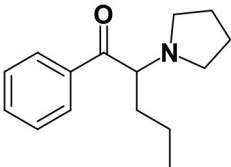
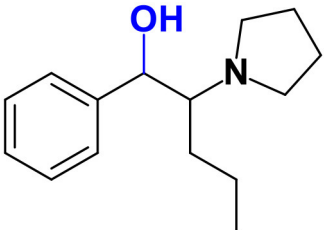
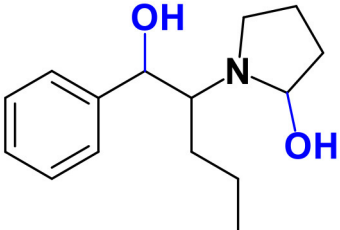
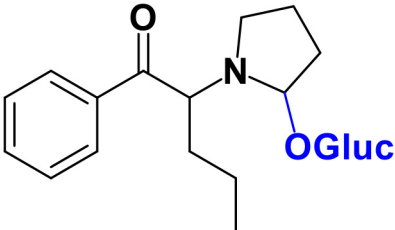
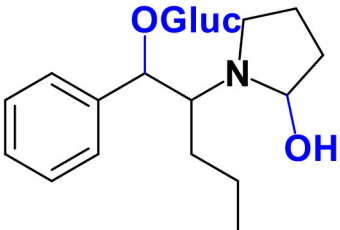
For the identification of Phase I metabolites, incubations were run in the presence of NADPH co-factor. Glucuronidation of Phase I metabolites, and urinary excretion of the glucuronide conjugates represent the primary routes of cathinones biotransformation and elimination in humans (Ellefsen et al., 2016). Therefore, toward the identification of glucuronic acid conjugates of the selected cathinones, additional incubations were run in the presence of Phase I and II cofactors, NADPH and UDPGA, respectively, using both HLM and RLM that were preincubated with the pore-forming peptide alamethicin. This procedure was already proved to increase considerably the rates of the Phase II glucuronidation, while not effecting the Phase I capacity (Fisher et al., 2000). Since the metabolite profile of the drug  $\alpha$ -PVP was already determined *in vivo* (Shima et al., 2014) and *in vitro* (Negreira et al., 2015),  $\alpha$ -PVP incubations were run in parallel with the incubations of selected cathinones, as positive controls.

LC-HRMS/MS, using hybrid quadrupole time-of-flight (QTOF) analyzer, was the method of choice for establishing the metabolic profile of the selected cathinones, since it constitutes one of the most useful analytical platforms for the identification of unknown metabolites. In fact, this methodology allows the direct and simultaneous detection of both Phase I and II metabolites, providing information about accurate mass and isotopic pattern not only of intact (de)protonated molecules, but also of fragment ions, which is of particular usefulness for metabolite identification.

As stated above,  $\alpha$ -PVP incubations were performed in this study as positive controls. The fragmentation pattern obtained for this cathinone (Table 1, Supplementary Figure 1) is in agreement with the one reported by Negreira et al. (2015). Likewise, all Phase I  $\alpha$ -PVP metabolites identified in current study (Table 1, Figure 2, Supplementary Figures 2–5) were also identified by these authors *in vitro*, including the product of  $\alpha$ -PVP ketone reduction (M1  $\alpha$ -PVP), which was the most abundant metabolite found in *in vivo* for this cathinone (Tyrkkö et al., 2013). This result attests the viability of the experimental conditions used in the current study for identifying the metabolites that are most likely to be found *in vivo*. Of note is the identification of the Phase II metabolite M4  $\alpha$ -PVP ( $m/z$  426.2118,  $-0.9$  ppm,  $\text{C}_{21}\text{H}_{32}\text{NO}_8$ ) that stems from glucuronic acid conjugation of M2  $\alpha$ -PVP, a Phase I metabolite formed upon  $\alpha$ -PVP keto reduction and hydroxylation of the pyrrolidine ring (Figure 2). The base peak of the tandem mass spectrum of this



**TABLE 1** | Structures of the  $\alpha$ -PVP metabolites identified in HLM and RLM incubations by LC-HRMS/MS (ESI+) analysis.

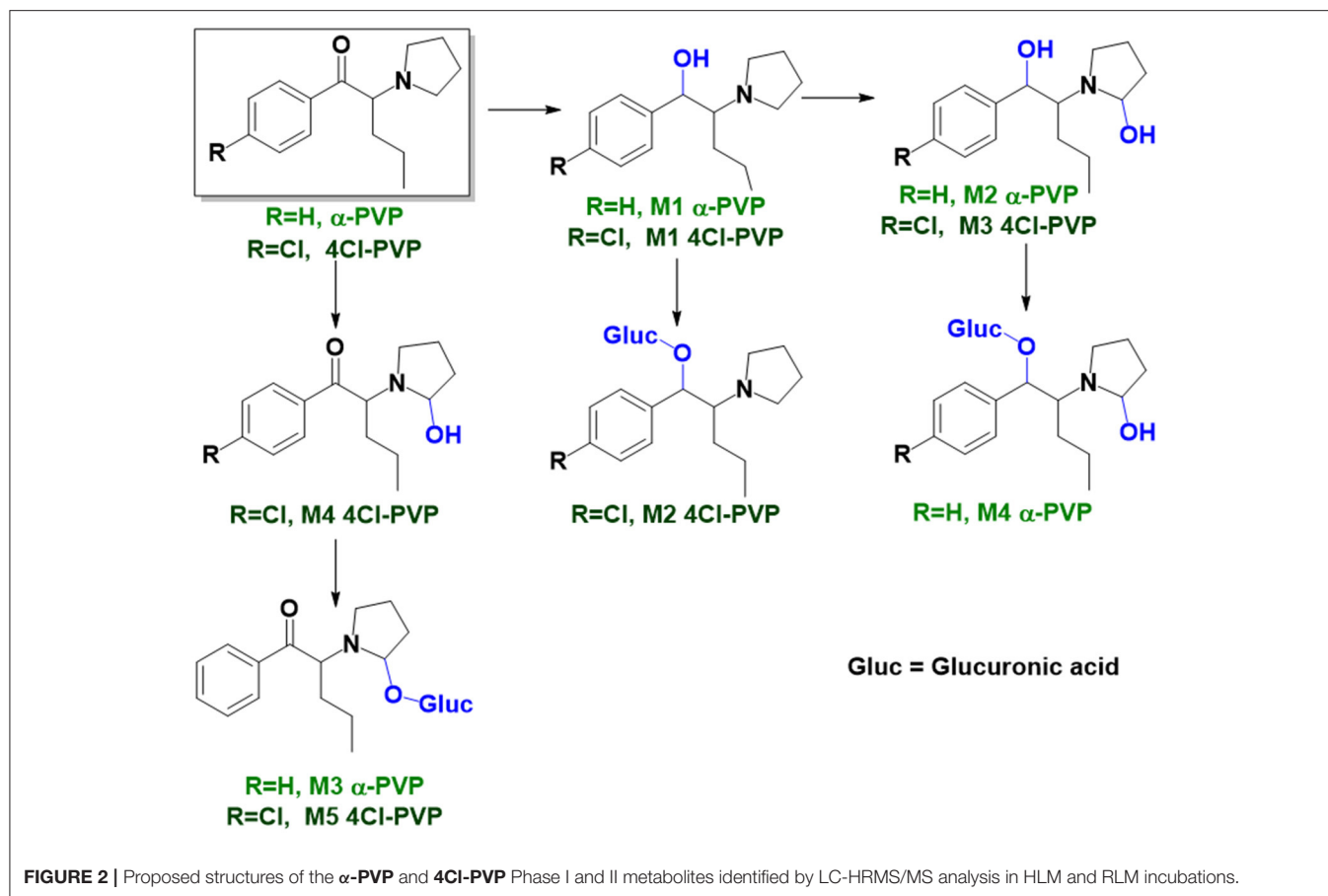
Compound	Structure	[M+H] <sup>+</sup> (m/z)	Elemental composition	Error (ppm)	Production (m/z)	Elemental composition	Error (ppm)	Identification
$\alpha$ -PVP		232.1685	C <sub>15</sub> H <sub>22</sub> NO	−4.7	161.0964	C <sub>11</sub> H <sub>13</sub> O	+2.5	–
					126.1281	C <sub>8</sub> H <sub>16</sub> N	+3.2	
					105.0343	C <sub>7</sub> H <sub>5</sub> N	+7.6	
					91.0541	C <sub>7</sub> H <sub>7</sub>	−1.9	
					70.0650	C <sub>4</sub> H <sub>8</sub> N	−1.4	
M1 $\alpha$ -PVP		234.1849	C <sub>15</sub> H <sub>24</sub> NO	−1.3	216.1736	C <sub>15</sub> H <sub>22</sub> N	−5.1	HLM
					173.1194	C <sub>12</sub> H <sub>15</sub> N	−2.8	RLM
					91.0539	C <sub>7</sub> H <sub>7</sub>	−3.3	
M2 $\alpha$ -PVP		250.1809	C <sub>15</sub> H <sub>24</sub> NO <sub>2</sub>	+2.8	232.1706	C <sub>15</sub> H <sub>22</sub> NO	−4.3	HLM
					214.1591	C <sub>15</sub> H <sub>20</sub> N	−0.5	
M3 $\alpha$ -PVP		424.1972	C <sub>21</sub> H <sub>30</sub> NO <sub>8</sub>	+1.4	48.1645	C <sub>15</sub> H <sub>22</sub> NO <sub>2</sub>	0	HLM RLM
					230.1538	C <sub>15</sub> H <sub>20</sub> NO	−0.4	
					161.0960	C <sub>11</sub> H <sub>13</sub> O	−0.6	
M4 $\alpha$ -PVP		426.2118	C <sub>21</sub> H <sub>32</sub> NO <sub>8</sub>	−0.9	250.1803	C <sub>15</sub> H <sub>24</sub> NO <sub>2</sub>	+0.8	HLM RLM
					232.1699	C <sub>15</sub> H <sub>22</sub> NO	+1.3	
					248.1653	C <sub>14</sub> H <sub>19</sub> NO <sub>2</sub>	+3.2	
					161.0953	C <sub>11</sub> H <sub>13</sub> O	+5.0	

Also shown the corresponding experimental *m/z* values and proposed elemental composition for the protonated molecule and characteristic fragment ions (presented with the associated error in ppm).

Phase II metabolite, at *m/z* 250.1803 (+0.8 ppm, C<sub>15</sub>H<sub>24</sub>NO<sub>2</sub>) (**Supplementary Figure 5**), corresponds to the typical neutral loss of 176.0315 u from the protonated molecule, corresponding to the glucuronide moiety. The occurrence of glucuronidation at the hydroxyl group resulting from the reduction of the keto group of the parent cathinone is suggested based on the observation of the product ion at *m/z* 161.0953 (+5.0 ppm, C<sub>11</sub>H<sub>13</sub>O). In fact, the formation of this product ion can only be explained on

basis of the loss of the hydroxylated pyrrolidine moiety from the fragment ion at *m/z* 248.1653 (+3.2 ppm, C<sub>14</sub>H<sub>19</sub>NO<sub>2</sub>), which is proposed to be formed via the neutral loss of 178.0465 u from the protonated molecule of **M4  $\alpha$ -PVP**. Whereas, the *in vivo* occurrence of the parent Phase I metabolite was already evidenced by Tyrkkö et al. (2013) to the best of our knowledge, this constitutes the first report on the identification of the glucuronic acid conjugate of this  $\alpha$ -PVP Phase I metabolite.





Coherently, the product ion displayed by metabolite **M4  $\alpha$ -PVP** is distinct from the one reported by Negreira et al. (2015) for its isomer, resulting from the glucuronidation of the hydroxyl group of the Phase I metabolite stemming from reduction of  $\alpha$ -PVP combined with a hydroxylation in the pyrrolidine ring and a subsequent oxidation. Interestingly whereas **M2  $\alpha$ -PVP** was only identified in HLM incubations, its Phase II metabolite was identified in both RLM and HLM, thereby suggesting that the parent Phase I metabolite was also formed in RLM.

### 4'-Chloro- $\alpha$ -pyrrolidinovalerophenone (4Cl-PVP)

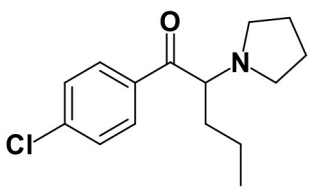
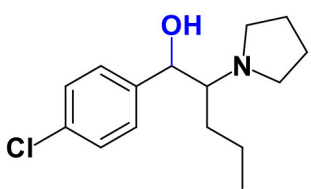
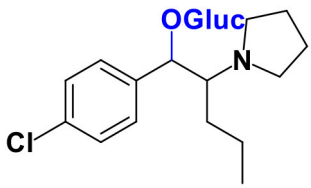
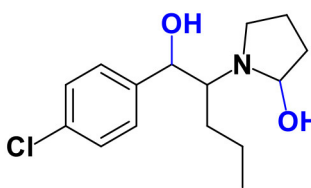
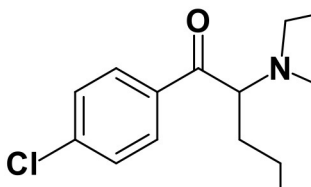
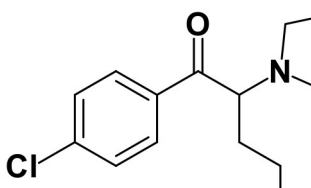
4Cl-PVP is a chlorinated derivative of  $\alpha$ -PVP and, as expected, these two cathinones present similar behaviors when analyzed by LC-HRMS/MS. Presenting the protonated molecule at  $m/z$  266.1311 (+1.9 ppm,  $C_{15}H_{21}ClNO$ ), with the chlorine isotopic pattern, the product ion of this cathinone displays at least three fragmentation pathways similar to the ones observed for  $\alpha$ -PVP (Supplementary Figure 1 vs. Supplementary Figure 6): (1) at  $m/z$  195.0568 (−1.5 ppm,  $C_{11}H_{13}ClO$ ) which is formed upon loss of the pyrrolidine moiety from the parent protonated molecule; (2) at  $m/z$  126.1304 (−4.7 ppm,  $C_8H_{16}N$ ), which corresponds to the loss of pyrrolidine and alkyl moieties from the protonated molecule; and (3) at  $m/z$  138.9957 (+8.6 ppm,  $C_7H_4ClO$ ) corresponding to the oxonium ion. Two additional product ions

are observed at  $m/z$  223.0753 (2.2 ppm,  $C_{12}H_{14}ClNO$ ), which corresponds to the loss of propyl radical from the protonated molecule, and  $m/z$  153.0102 (0 ppm,  $C_6H_6ClO$ ), stemming from the loss of the pyrrolidine and propyl moieties.

The recognition of the chlorine isotopic cluster was key for the identification of 4Cl-PVP metabolites. Two Phase I and two Phase II metabolites were consistently identified in the RLM and HLM incubations of this cathinone and a third Phase I metabolite, **M3 4Cl-PVP**, was only identified in HLM incubations (Table 2, Figure 2, Supplementary Figures 7–11).

The Phase I metabolite, **M1 4Cl-PVP**, exhibits the protonated molecule at  $m/z$  268.1463 (0 ppm,  $C_{15}H_{23}ClNO$ ), compatible with the reduction of the carbonyl group of 4Cl-PVP. This constitutes a metabolic transformation very frequent for cathinones (Zaitsu et al., 2014) and is also reported to occur for  $\alpha$ -PVP, *in vivo* (Shima et al., 2014). The tandem mass spectrum of this metabolite exhibits two main fragments (Supplementary Figure 7): (1) at  $m/z$  250.1359 (+0.8 ppm,  $C_{15}H_{21}ClN$ ) that stems from the loss of water from the protonated molecule; and (2) at  $m/z$  207.0806 (−1.4 ppm,  $C_{12}H_{14}ClN$ ), which results from the subsequent loss of the propyl radical from the previous fragment ion. This fragmentation pattern is consistent with the one described for the analog  $\alpha$ -PVP metabolite (Shima et al., 2014; Zaitsu et al., 2014). As stated above, ketone reduction is the major metabolic pathway

**TABLE 2** | Structures of the **4Cl-PVP** metabolites identified in HLM and RLM incubations by LC-HRMS/MS (ESI+) analysis.

Compound	Structure	[M+H] <sup>+</sup> (m/z)	Elemental composition	Error (ppm)	Productions (m/z)	Elemental composition	Error (ppm)	Identification
4Cl-PVP		266.1311	C <sub>15</sub> H <sub>21</sub> ClNO	+1.9	223.0753	C <sub>12</sub> H <sub>14</sub> ClNO	+2.2	
					195.0568	C <sub>11</sub> H <sub>13</sub> ClO	−1.5	
					153.0102	C <sub>8</sub> H <sub>6</sub> ClO	0	
					138.9957	C <sub>7</sub> H <sub>4</sub> ClO	+8.6	
					126.1304	C <sub>8</sub> H <sub>16</sub> N	−4.7	
M1 4Cl-PVP		268.1463	C <sub>15</sub> H <sub>23</sub> ClNO	0	250.1359	C <sub>15</sub> H <sub>21</sub> ClN	+0.8	HLM
					207.0806	C <sub>12</sub> H <sub>14</sub> ClN	−1.4	RLM
M2 4Cl-PVP		444.1786	C <sub>21</sub> H <sub>31</sub> ClNO <sub>7</sub>	+0.5	268.1469	C <sub>15</sub> H <sub>23</sub> ClNO	+2.2	HLM RLM
					250.1371	C <sub>15</sub> H <sub>20</sub> ClN	+5.6	
					207.0808	C <sub>12</sub> H <sub>14</sub> ClN	−0.5	
M3 4Cl-PVP		284.1413	C <sub>15</sub> H <sub>23</sub> ClNO <sub>2</sub>	+0.4	266.1302	C <sub>15</sub> H <sub>21</sub> ClNO	−1.5	HLM
					248.1201	C <sub>15</sub> H <sub>19</sub> ClN	0	
					206.0738	C <sub>12</sub> H <sub>13</sub> ClN	+0.5	
M4 4Cl-PVP		282.1256	C <sub>15</sub> H <sub>21</sub> ClNO <sub>2</sub>	+0.4	264.1155	C <sub>15</sub> H <sub>19</sub> ClNO	+1.9	HLM RLM
					142.1233	C <sub>8</sub> H <sub>16</sub> NO	+4.9	
					153.0109	C <sub>8</sub> H <sub>6</sub> ClO	+4.6	
M5 4Cl-PVP		458.1580	C <sub>21</sub> H <sub>29</sub> ClNO <sub>8</sub>	+0.9	282.1261	C <sub>15</sub> H <sub>21</sub> ClNO <sub>2</sub>	+2.1	HLM RLM
					264.1154	C <sub>15</sub> H <sub>19</sub> ClNO	+1.5	
					195.0568	C <sub>11</sub> H <sub>12</sub> ClO	−1.5	

Also shown the corresponding experimental m/z values and proposed elemental composition for the protonated molecule and characteristic fragment ions (presented with the associated error in ppm).

reported for other  $\alpha$ -pyrrolidinophenones in humans, thereby supporting the potential *in vivo* relevance of this metabolite for **4Cl-PVP**. The glucuronide conjugate of **M1 4Cl-PVP** was also identified. In fact, the neutral loss of 176.0317 u from

the protonated molecule of **M2 4Cl-PVP** ( $m/z$  444.1786, +0.5 ppm, C<sub>21</sub>H<sub>31</sub>ClNO<sub>7</sub>), observed in the tandem mass spectrum (**Supplementary Figure 8**), is indicative of glucuronidation. The observation of two fragment ions at  $m/z$  250.1371 (+5.6 ppm,

$C_{15}H_{20}ClN$ ) and 207.0808 (−0.5 ppm,  $C_{12}H_{14}ClN$ ), which are also observed in the tandem mass spectrum of **4Cl-PVP M1**, further substantiates the assigned structure of **M2 4Cl-PVP**. The fact that a structurally similar glucuronide derived from  $\alpha$ -PVP was identified as a urinary metabolite in humans, suggests that this might also be a metabolically relevant pathway for **4Cl-PVP in vivo** (Shima et al., 2014).

**M3 4Cl-PVP** is one additional Phase I metabolite that was identified in **4Cl-PVP** HLM incubations and results from the hydroxylation of **M1 4Cl-PVP**. Exhibiting the protonated molecule at  $m/z$  284.1413 (+0.4 ppm,  $C_{15}H_{23}ClNO_2$ ), **M3 4Cl-PVP** displays diagnostic product ions (Supplementary Figure 9), corresponding to two consecutive losses of water: at  $m/z$  266.1302 (−1.5 ppm,  $C_{15}H_{21}ClNO$ ) and 248.1201 (0 ppm,  $C_{15}H_{19}ClN$ ). The subsequent loss of the alkyl chain is also observed at  $m/z$  206.0738 (+0.5 ppm,  $C_{12}H_{13}ClN$ ). Whereas the product ion obtained does not allow the identification of the exact location of the hydroxyl group, the 2' position of the pyrrolidine is suggested, since it is a frequent hydroxylation site for other  $\alpha$ -pyrrolidinophenones, including  $\alpha$ -PVP (Tyrkkö et al., 2013; Negreira et al., 2015). A similar metabolic transformation was also reported for **PV8** ( $\alpha$ -pyrrolidinoheptaphenone) (Swortwood et al., 2016), a cathinone analog closely resembling  $\alpha$ -PVP.

The mass increase of 15.994 u from **4Cl-PVP** observed for the protonated molecule of **M4 4Cl-PVP**, at  $m/z$  282.1256 (−0.4 ppm,  $C_{15}H_{21}ClNO_2$ ), is indicative of direct hydroxylation of the parent cathinone. The observation of the product ion at  $m/z$  142.1233 (+4.9 ppm,  $C_8H_{16}NO$ ) (Supplementary Figure 10), suggests that this metabolite stems from the hydroxylation of the pyrodidine or alkyl moieties. Coherently, these hydroxylation locations are also reported for  $\alpha$ -PVP *in vivo* (Tyrkkö et al., 2013). Nonetheless, the consistent identification of the glucuronide **M5 4Cl-PVP** in HLM and RLM incubations suggests that the most probable location of hydroxylation in **M4 4Cl-PVP** is the pyrrolidine ring. In fact, the tandem mass spectrum of **M5 4Cl-PVP** protonated molecule, at  $m/z$  458.1580 (+ 0.9 ppm,

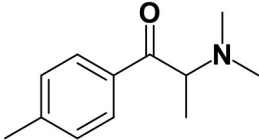
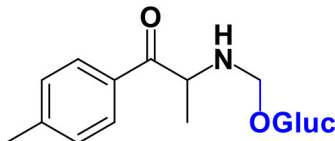
$C_{21}H_{29}ClNO_8$ ), exhibits a product ion at  $m/z$  195.0568 (−1.5 ppm,  $C_{11}H_{12}ClO$ ) (Supplementary Figure 11), which results from the loss of hydroxylated and glucuronidated pyrrolidine moiety from the protonated molecule, thereby evidencing that this Phase II metabolite stems from the glucuronidation of **M4 4Cl-PVP**, bearing the hydroxyl group in the pyrrolidine moiety (Figure 2). Of note is the fact that this metabolic pathway is also observed for  $\alpha$ -PVP.

### 4'-Methyl- *N,N*-dimethylcathinone (4-MDMC)

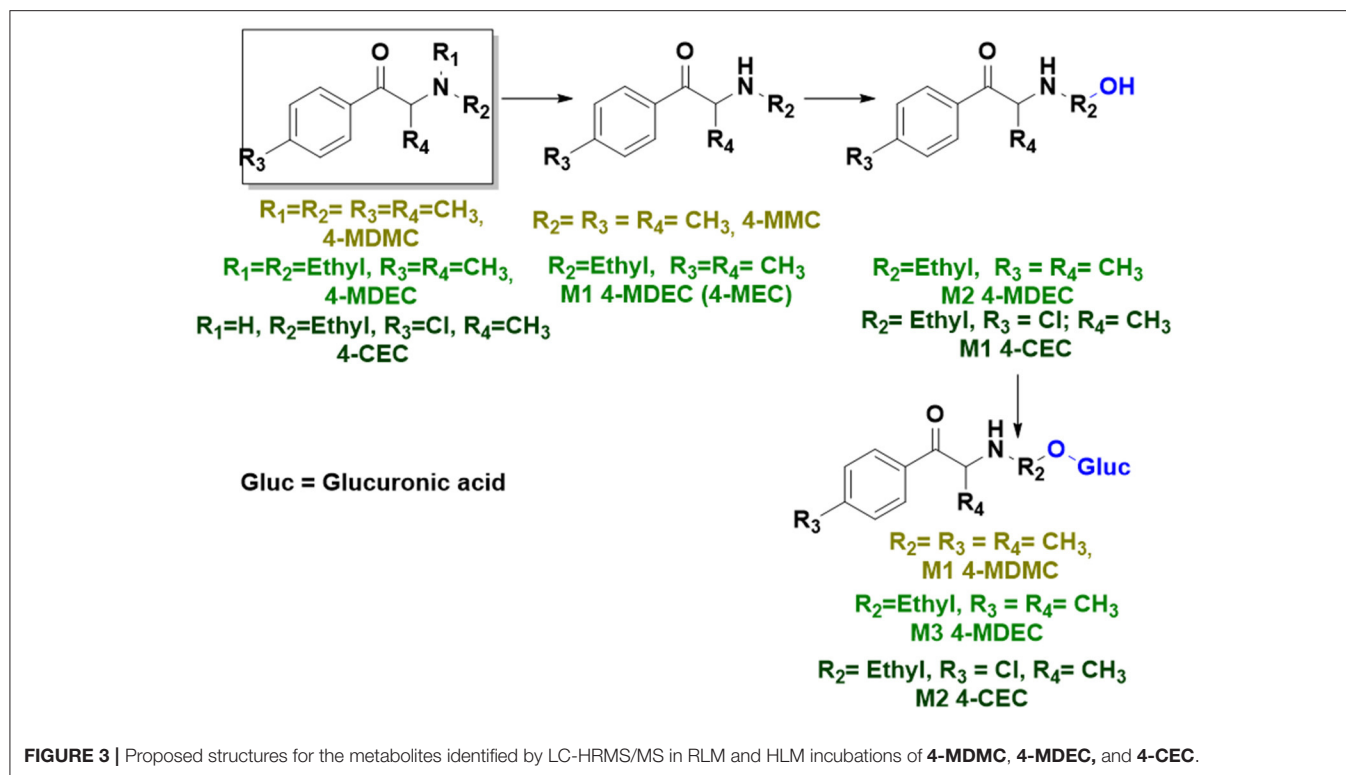
The protonated molecule of **4-MDMC** is observed at  $m/z$  192.1374 (−4.7 ppm,  $C_{12}H_{18}NO$ ) (Table 3) and its tandem mass spectrum presents a base peak at  $m/z$  119.0877 (+0.2 ppm,  $C_9H_{11}$ ) (Supplementary Figure 12). This fragment ion was already reported for mephedrone (**4-MMC**), when analyzed by LC-HRMS (Pozo et al., 2015), and may be explained on basis of a neutral loss containing the nitrogen after dissociation of the C-N bond from the protonated molecule, followed by CO loss. The possibility of subsequently undergoing rearrangement, with the formation of a seven-membered ring, may explain the conferred stability of this fragment (Zuba, 2012; Pedersen et al., 2013).

Whereas, no Phase I metabolites were identified in **4-MDMC** incubations run in the presence of Phase I cofactors, one signal at  $m/z$  370.1488 (−2.1 ppm,  $C_{17}H_{24}NO_8$ ), compatible with the glucuronide conjugate **M1 4-MDMC** (Table 3, Figure 3), was identified following LC-HRMS analysis of alamethicin-induced RLM incubations run in the presence of Phase I and II cofactors. **M1 4-MDMC** is compatible with the glucuronidation of a **4-MDMC** Phase I metabolite that stems from two consecutive metabolic transformations (Figure 3): **4-MDMC** demethylation, yielding mephedrone (**4-MMC**), which is subsequently hydroxylated in a methyl group. In fact, the tandem mass spectrum of **M1 4-MDMC** metabolite displays a very similar product ion profile to the one reported by Pozo et al. (2015) for a **4-MMC** Phase II metabolite, which was identified

**TABLE 3 |** Structures for **4-MDMC** and its Phase II metabolite identified in HLM and RLM incubations by LC-HRMS/MS (ESI+) analysis.

Compound	Structure	[M+H] <sup>+</sup> ( <i>m/z</i> )	Elemental composition	Error (ppm)	Product ions ( <i>m/z</i> )	Elemental composition	Error (ppm)	identification
4-MDMC		192.1374	$C_{12}H_{18}NO$	−4.7	119.0877	$C_9H_{11}$	+0.2	—
M1 4-MDMC		370.1488	$C_{17}H_{24}NO_8$	−2.1	194.1167 178.1229 160.1121	$C_{11}H_{16}NO_2$ $C_{11}H_{16}NO$ $C_{11}H_{14}N$	−4.6 +1.7 0	RLM

Also shown the corresponding experimental *m/z* values and proposed elemental composition for the protonated molecule and characteristic fragment ions (presented with the associated error in ppm).



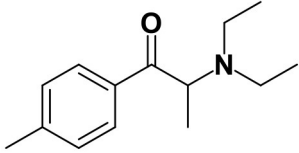
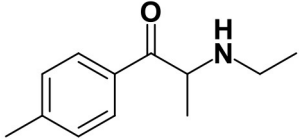
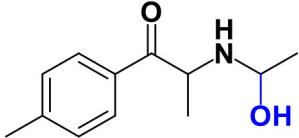
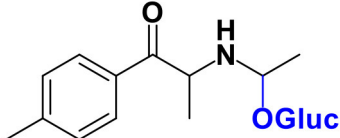
in the urine of two human volunteers that ingested 200 mg **4-MMC** orally (Pozo et al., 2015). However, whereas these authors suggest that C3 is the most probable hydroxylation site, the hydroxyl group is more likely to be at the *N*-methyl substituent. In fact, *N*-alkyl groups are considered hot spots for metabolic hydroxylation, which constitutes the first step of *N*-dealkylation that is a common metabolic pathway for substituted amines (Trager, 2007). Coherently, similarly to what was reported for this glucuronide metabolite of **4-MMC**, the tandem mass spectrum of the glucuronide **M1 4-MDMC** exhibits a base peak at  $m/z$  194.1167 ( $-4.6$  ppm,  $C_{11}H_{16}NO_2$ ) (**Supplementary Figure 13**) that results from the neutral loss of 176.0321 u from the protonated molecule, corresponding to typical the glucuronide loss. Two other minor product ions are observed at  $m/z$  178.1229 ( $+1.7$  ppm,  $C_{11}H_{16}NO$ ) and 160.1121 (0 ppm,  $C_{11}H_{14}N$ ), which can be explained by a mechanism similar to the one proposed by Pozo et al. (2015) (**Supplementary Figure 13**) for the glucuronide conjugate of the hydroxylated metabolite of **4-MMC**. Regardless of the exact location of hydroxylation of this phase I metabolite, our results suggest that **4-MDMC** may act as a prodrug of **4-MMC**. This constitutes an issue of concern taking into consideration the number of **4-MMC**-related fatalities (Busardò et al., 2015). In fact, with a very narrow safety window, **4-MMC** dosages that fall within the recreational use limits are suggested to be potentially fatal, in particular when combined with other drugs (Busardò et al., 2015). Additionally, the fact that no **4-MDMC** was identified in the incubation where **M1 4-MDMC** was identified, suggests that this might constitute an important metabolic pathway for **4-MDMC**.

### 4'-Methyl-*N,N*-diethylcathinone (**4-MDEC**)

The protonated molecule of **4-MDEC** was observed at  $m/z$  220.1697 ( $+0.5$  ppm,  $C_{14}H_{22}NO$ ) (**Table 4**) and whereas the fragment ion stemming from the loss of a first *N*-ethyl group is not observed in the tandem mass spectrum (**Supplementary Figure 14**), this constitutes the first loss undergone by this cathinone, at the experimental conditions used. In fact, the fragment ion at  $m/z$  174.1270 ( $-4.0$  ppm,  $C_{12}H_{16}N$ ) is formed water by loss from this first product ion, a fragmentation pathway which is characteristic of other cathinones (Namera et al., 2015). The subsequent loss of  $CH_3$  radical explains the formation of the fragment ion at  $m/z$  159.1044 ( $+0.6$  ppm,  $C_{10}H_{12}N$ ). Whereas the formation of radical ions is not a frequent mechanism when using ESI (Thurman et al., 2007), it seems to be particularly frequent on the LC-HRMS analysis of cathinones. In fact, this kind of fragmentation was already reported for **4-MMC** and was consistently observed in the fragmentation pattern of the glucuronide **M1 4-MDMC** (see above) (Namera et al., 2015). Likewise, the in-source rearrangement to a indole ring that was already used to explain **4-MMC** fragmentation (Pozo et al., 2015), followed by loss of the ethyl radical, can also be evoked to explain the formation of the product ion at 144.0813 ( $-3.5$  ppm,  $C_{10}H_{10}N$ ) observed in the **4-MDEC** tandem mass spectrum.

Two Phase I metabolites were consistently identified in **4-MDEC** HLM and RLM incubations (**Table 4**, **Figure 3**, **Supplementary Figures 15, 16**). The protonated molecule of **M1 4-MDEC** was observed at  $m/z$  192.1378 ( $-2.6$  ppm,  $C_{12}H_{18}NO$ ),

**TABLE 4 |** Structures of the **4-MDEC** metabolites identified in HLM and RLM incubations by LC-HRMS/MS (ESI+) analysis.

Compound	Structure	[M+H] <sup>+</sup> (m/z)	Elemental composition	Error (ppm)	Product ions (m/z)	Elemental composition	Error (ppm)	Identification
4-MDEC		220.1697	C <sub>14</sub> H <sub>22</sub> NO	+0.5	174.1270 159.1044 144.0813	C <sub>12</sub> H <sub>16</sub> N C <sub>10</sub> H <sub>12</sub> N C <sub>10</sub> H <sub>10</sub> N	4.0 +0.6 −3.5	—
M1 4-MDEC		192.1378	C <sub>12</sub> H <sub>18</sub> NO	−2.6	144.0812	C <sub>10</sub> H <sub>10</sub> N	+2.8	HLM RLM
M2 4-MDEC		208.1329	C <sub>12</sub> H <sub>18</sub> NO <sub>2</sub>	+1.4	172.1128 144.0813	C <sub>12</sub> H <sub>14</sub> N C <sub>10</sub> H <sub>10</sub> N	+4.1 +3.5	HLM RLM
M3 4-MDEC		384.1637	C <sub>18</sub> H <sub>26</sub> NO <sub>8</sub>	+4.1	208.1337 172.1124	C <sub>12</sub> H <sub>18</sub> NO <sub>2</sub> C <sub>12</sub> H <sub>14</sub> N	+2.4 +1.7	RLM

Also shown the corresponding experimental *m/z* values and proposed elemental composition for the protonated molecule and characteristic fragment ions (presented with the associated error in ppm).

which is compatible with the protonated molecule **4-MEC**. This product of deethylation of **4-MDEC** is also a controlled drug that have been linked with several overdose cases (Gil et al., 2013; Rojek et al., 2014). However, contrary to what was reported by Helfer et al. (2015), the initial fragmentation step of **4-MEC** was not the loss of water. In fact, at the experimental conditions used, the base peak of the tandem mass spectrum of **M1 4-MDEC (4-MEC)** was observed at *m/z* 144.0812 (−2.8 ppm, C<sub>12</sub>H<sub>18</sub>NO) which stems from the loss of 48.0566 u from the protonated molecule. In accordance with what was already discussed, the formation of a more stable indole system can be postulated for the formation of this product ion (**Supplementary Figure 15**). This suggests that **4-MDEC** is metabolically converted into the controlled psychotic substance **4-MEC**.

One additional Phase I metabolite, **M2 4-MDEC**, was observed at *m/z* 208.1329 (−1.4 ppm, C<sub>12</sub>H<sub>18</sub>NO<sub>2</sub>). The mass increment of 15.9944 u from **M1 4-MDEC (4-MEC)**, suggests that **M2 4-MDEC** was formed upon hydroxylation of **4-MEC**. A similar metabolite was identified by Helfer et al. (2015) upon GC-MS analysis of **4-MEC** incubations in HLM. Whereas the location for **4-MEC** hydroxylation is proposed to be the methyl substituent of the aromatic moiety (Helfer

et al., 2015), no LC-HRMS data is provided for this metabolite, thereby precluding any comparison with our data. Nonetheless, the fact that the base peak, at *m/z* 144.0823 (+3.5 ppm, C<sub>10</sub>H<sub>10</sub>N), of the **M2 4-MDEC** tandem mass spectrum is the same observed for **M1 4-MDEC (Supplementary Figure 16 vs. Supplementary Figure 15)**, suggests that this metabolite results from hydroxylation at the *N*-ethyl substituent. **M3 4-MDEC** is one additional Phase II metabolite that was identified in RLM incubations (**Table 4, Figure 3**). The protonated molecule of this glucuronide is displayed at *m/z* 384.1637 (+4.1 ppm, C<sub>18</sub>H<sub>26</sub>NO<sub>8</sub>) and the tandem mass spectrum of this ion (**Supplementary Figure 17**) shows the characteristic loss of the glucuronide moiety (176.0300 u) at *m/z* 208.1337 (+2.4 ppm, C<sub>12</sub>H<sub>18</sub>NO<sub>2</sub>). One additional fragment ion is observed at *m/z* 172.1124 (+1.7 ppm, C<sub>12</sub>H<sub>14</sub>N), stemming from two consecutive losses of water. Taking into consideration that the same fragment ion is also observed in the tandem spectrum of **M2 4-MDEC**, **M3 4-MDEC** is suggested to be the glucuronic acid conjugate of this Phase I metabolite. The fact that no parent cathinone was detected in the incubations where this Phase II metabolite was identified, suggests that this might constitute a relevant metabolic pathway of **4-MDEC**.



## 4'-Chloro-*N*-ethylcathinone (4-CEC)

The protonated molecule of **4-CEC** is observed at  $m/z$  212.0837 (0 ppm,  $C_{11}H_{15}ClNO$ ), exhibiting the chlorine isotope cluster. This isotopic pattern is also observed in the first product ion at  $m/z$  164.0252 (−5.5 ppm,  $C_9H_7ClN$ ), corresponding to the rearrangement product to an indole ring, following the loss of *N*-substituent and water from the protonated molecule (**Supplementary Figure 18**) (Nóbrega and Dinis-Oliveira, 2018). The fragment ion at  $m/z$  159.1036 (−3.8 ppm,  $C_{11}H_{13}N$ ) is formed from the consecutive loss of Cl radical and water from the protonated molecule. The subsequent loss of  $CH_3$  radical, explains the formation of the base peak, at  $m/z$  144.0813 (+3.5 ppm,  $C_{10}H_{10}N$ ).

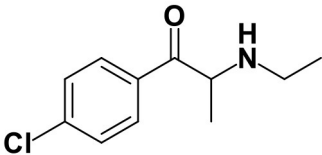
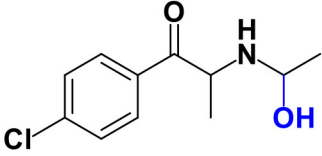
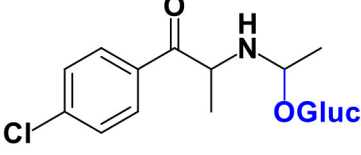
A first attempt to investigate the metabolic profile of **4-CEC** was performed in human hepatocytes (Fabregat-Safont et al., 2020). However, no metabolites were identified for this cathinone in this *in vitro* system. Nonetheless, Wagmann et al. (2020) reported the metabolic profile of this cathinone in liver microsome and S9 fraction incubations, thereby enabling the identification of several Phase I and Phase II metabolites. In the current work, the recognition of the chlorine isotopic cluster, and the use of the Data Analysis isotope Cluster analysis tool, were key for the identification of additional Phase I and Phase II metabolites of **4-CEC** that were identified in RLM incubations (**Table 5**, **Figure 3**, **Supplementary Figures 19, 20**). **M1 4-CEC** metabolite, presents a mass increase of 15.9942 u from **4-CEC**, exhibiting the protonated molecule at  $m/z$  228.0779 (−3.1 ppm,  $C_{11}H_{15}ClNO_2$ ) (**Supplementary Figure 19**). This mass increase is compatible

with a hydroxylation. The observation of the base fragment ion at  $m/z$  138.9947 (+1.4 ppm,  $C_7H_4ClO$ ), corresponding to the oxonium ion, suggests that hydroxylation occurred in one of the alkyl carbons of **4-CEC**. Therefore, taking into consideration the arguments presented for the hydroxylation location of **M2 4-MDMC**, the *N*-ethyl group of **M1 4-CEC** was suggested as the most likely hydroxyl location. The glucuronide conjugate of this Phase II metabolite, **M2 4-CEC**, was also identified. Coherently, the protonated molecule of **M2 4-CEC**,  $m/z$  404.1104 (+0.7 ppm,  $C_{17}H_{23}ClNO_8$ ), displays a product ion at  $m/z$  228.0780 (+2.6 ppm,  $C_{11}H_{15}ClNO_2$ ), corresponding to the loss of the glucuronic acid moiety from the protonated molecule (**Supplementary Figure 20**). Importantly, none of these metabolites were reported by Wagmann et al. (2020). As stated above, taking into consideration the group experience (Godinho et al., 2018), the fact that these metabolites were solely identified in RLM does not necessarily imply that they cannot be also formed in humans, *in vivo*.

## CONCLUSION

Using LC-HRMS/MS analysis of HLM and RLM incubations multiple Phase I and glucuronide metabolites were identified for the selected synthetic cathinones: **4-Cl-PVP**, **4-CEC**, **4-MDEC**, and **4-MDMC**. Specifically: (1) four Phase I and two Phase II metabolites were identified for the chlorinated derivative of  $\alpha$ -PVP, **4-Cl-PVP**; (2) one Phase I and one glucuronide conjugate were identified in RLM for **4-CEC**, which is among the most seized cathinones in 2017; (3) two Phase I and one

**TABLE 5** | Structures of the 4-CEC metabolites identified in RLM incubations by LC-HRMS/MS (ESI+) analysis.

Compound	Structure	[M+H] <sup>+</sup> ( $m/z$ )	Elemental composition	Error (ppm)	Fragmentions ( $m/z$ )	Elemental composition	Error (ppm)	Identification
4-CEC		212.0837	$C_{11}H_{15}ClNO$	0	164.0252 159.1036 144.0813	$C_9H_7ClN$ $C_{11}H_{13}N$ $C_{10}H_{10}N$	+5.5 −3.8 +3.5	–
M1 4-CEC		228.0779	$C_{11}H_{15}ClNO_2$	−3.1	138.9947	$C_7H_4ClO$	+1.4	RLM
M2 4-CEC		404.1104	$C_{17}H_{23}ClNO_8$	+0.7	228.0780	$C_{11}H_{15}ClNO_2$	−2.6	RLM

Also shown the corresponding experimental  $m/z$  values and proposed elemental composition for the protonated molecule and characteristic fragment ions (presented with the associated error in ppm).

Phase II metabolites were identified for **4-MDEC**; and (4) one Phase II metabolite was identified for **4-MDMC**. Additionally, a new Phase II conjugate, derived from the recreational drug  **$\alpha$ -PVP**, was herein identified for the first time. Of note is the fact that this metabolic pathway, consisting on hydroxylation of the alkyl nitrogen substituent, followed by glucuronidation, was consistently observed in all cathinones studied in the current work. The reduction of the carbonyl group constituted one additional metabolic pathway for pyrrolidinic cathinones. Whereas, the metabolic profiles of these cathinones were obtained *in vitro*, the identification of metabolites stemming from metabolic pathways frequently identified *in vivo* for this class of compounds, suggests the likelihood of a similar metabolic profile being observed *in vivo*. Also noteworthy is the fact that our results suggest that **4-MDMC** and **4-MDEC** might act as prodrugs of the controlled substances **4-MMC** and **4-MEC**, respectively. These findings constitute an important contribute not only for the unequivocal proof of the intake of these recently reported synthetic cathinones but also to understand their potential adverse effects and link causative agents to toxicities.

## DATA AVAILABILITY STATEMENT

The original contributions presented in the study are included in the article/**Supplementary Material**, further inquiries can be directed to the corresponding author/s.

## REFERENCES

- Antunes, M., Sequeira, M., de Caires Pereira, M., Caldeira, M. J., Santos, S., Franco, J., et al. (2020). Determination of selected cathinones in blood by solid-phase extraction and GC-MS. *J. Anal. Toxicol.* doi: 10.1093/jat/bkaa074. [Epub ahead of print].
- Arias, H. R., Santamaría, A., and Ali, S. F. (2009). Pharmacological and neurotoxicological actions mediated by bupropion and diethylpropion. *Int. Rev. Neurobiol.* 88, 223–255. doi: 10.1016/S0074-7742(09)88009-4
- Busardó, F. P., Kyriakou, C., Napoletano, S., Marinelli, E., and Zaami, S. (2015). Mephedrone related fatalities: a review. *Eur. Rev. Med. Pharmacol. Sci.* 19, 3777–3790.
- Carroll, F. I., Blough, B. E., Mascarella, S. W., Navarro, H. A., Lukas, R. J., and Damaj, M. I. (2014). Bupropion and bupropion analogs as treatments for CNS disorders. *Adv. Pharmacol.* 69, 177–216. doi: 10.1016/B978-0-12-420118-7.00005-6
- Costa, R., Oliveira, N. G., and Dinis-Oliveira, R. J. (2019). Pharmacokinetic and pharmacodynamic of bupropion: integrative overview of relevant clinical and forensic aspects. *Drug Metab. Rev.* 51, 293–313. doi: 10.1080/03602532.2019.1620763
- Ellefsen, K. N., Concheiro, M., and Huestis, M. A. (2016). Synthetic cathinone pharmacokinetics, analytical methods, and toxicological findings from human performance and postmortem cases. *Drug Metab. Rev.* 48, 237–265. doi: 10.1080/03602532.2016.1188937
- EMCDDA (2015). *EMCDDA-Europol 2014 Annual Report on the Implementation of Council Decision 2005/387/JHA*. Available online at: [https://www.emcdda.europa.eu/publications/implementation-reports/2014\\_en](https://www.emcdda.europa.eu/publications/implementation-reports/2014_en) (accessed September 15, 2020).
- EMCDDA (2016). *EMCDDA-Europol 2015 Annual Report on the Implementation of Council Decision 2005/387/JHA*. Available online at: [https://www.emcdda.europa.eu/publications/implementation-reports/2015\\_en](https://www.emcdda.europa.eu/publications/implementation-reports/2015_en) (accessed September 15, 2020).
- EMCDDA (2017). *EMCDDA-Europol 2016 Annual Report on the Implementation of Council Decision 2005/387/JHA*. Available online at: [https://www.emcdda.europa.eu/publications/implementation-reports/2016\\_el](https://www.emcdda.europa.eu/publications/implementation-reports/2016_el) (accessed September 15, 2020).
- EMCDDA (2020). *European Drug Report 2020: Trends and Developments*. Available online at: [https://www.emcdda.europa.eu/publications/edr/trends-developments/2020\\_en](https://www.emcdda.europa.eu/publications/edr/trends-developments/2020_en) (accessed September 15, 2020).
- EMCDDA and EUROPOL (2019). *EU Drug Markets Report 2019*. Available online at: [https://www.emcdda.europa.eu/publications/joint-publications/eu-drug-markets-report-2019\\_en](https://www.emcdda.europa.eu/publications/joint-publications/eu-drug-markets-report-2019_en) (accessed September 15, 2020).
- EU (2017). DIRECTIVE (EU) 2017/2103 Of The European Parliament and of the Council of 15 November 2017 amending Council Framework Decision 2004/757/JHA in order to include new psychoactive substances in the definition of “drug” and repealing Council Decision 2005/387. *Off. J. Euro. Union* 305, 12–18.
- Fabregat-Safont, D., Mardal, M., Sancho, J. V., Hernández, F., Linnet, K., and Ibáñez, M. (2020). Metabolic profiling of four synthetic stimulants, including the novel indanyl-cathinone 5-PPDi, after human hepatocyte incubation. *J. Pharm. Anal.* 10, 147–156. doi: 10.1016/j.jpba.2019.12.006
- FDA (2020). *Drugs@FDA: FDA-Approved Drugs*. Available online at: <https://www.accessdata.fda.gov/scripts/cder/daf/> (accessed September 15, 2020).
- Fisher, M. B., Campanale, K., Ackermann, B. L., Vandenbranden, M., and Wrighton, S. A. (2000). *In vitro* glucuronidation using human liver microsomes and the pore-forming peptide alamethicin. *Drug Metab. Dispos.* 28, 560–566.
- Gaspar, H., Bronze, S., Oliveira, C., Victor, B. L., Machuqueiro, M., Pacheco, R., et al. (2018). Proactive response to tackle the threat of emerging drugs: synthesis and toxicity evaluation of new cathinones. *Forensic. Sci. Int.* 290, 146–156. doi: 10.1016/j.forsciint.2018.07.001
- German, C. L., Fleckenstein, A. E., and Hanson, G. R. (2014). Bath salts and synthetic cathinones: an emerging designer drug phenomenon. *Life Sci.* 97, 2–8. doi: 10.1016/j.lfs.2013.07.023

## AUTHOR CONTRIBUTIONS

HG and AA planned the work, interpreted the data, and wrote the article. BL performed the experimental and data processing steps. MC critically revised the manuscript. All authors approved the final version of the manuscript.

## FUNDING

We thank FCT (Fundação para a Ciência e Tecnologia) for funding the strategic projects UIDB/00100/2020 and UIDP/00100/2020 to CQE - Centro de Química Estrutural, UIDB/04046/2020 and UIDP/04046/2020 to BioISI - Biosystems & Integrative Sciences Institute, UIDB/04292/2020 and UIDP/04292/2020 to MARE - Marine and Environmental Sciences Centre, and the research projects PTDC/QUIQAN/32242/2017, PTDC/QUI-QIN/28662/2017, PTDC/QUI-QOR/29664/2017, and POINT4PAC project (SAICTPAC/0019/2015-LISBOA-01-0145-FEDER-016405).

## SUPPLEMENTARY MATERIAL

The Supplementary Material for this article can be found online at: <https://www.frontiersin.org/articles/10.3389/fchem.2020.609251/full#supplementary-material>

- Gil, D., Adamowicz, P., Skulska, A., Tokarczyk, B., and Stanaszek, R. (2013). Analysis of 4-MEC in biological and non-biological material—three case reports. *Forensic Sci. Int.* 228, e11–15. doi: 10.1016/j.forsciint.2013.03.011
- Godinho, A. L. A., Martins, I. L., Nunes, J., Charneira, C., Grilo, J., Silva, D. M., et al. (2018). High resolution mass spectrometry-based methodologies for identification of Etravirine bioactivation to reactive metabolites: in vitro and in vivo approaches. *Eur. J. Pharm. Sci.* 119, 70–82. doi: 10.1016/j.ejps.2018.03.026
- Helfer, A. G., Turcant, A., Boels, D., Ferec, S., Lelièvre, B., Welter, J., et al. (2015). Elucidation of the metabolites of the novel psychoactive substance 4-methyl-N-ethyl-cathinone (4-MEC) in human urine and pooled liver microsomes by GC-MS and LC-HR-MS/MS techniques and of its detectability by GC-MS or LC-MSn standard screening approaches. *Drug Test. Anal.* 7, 368–375. doi: 10.1002/dta.1682
- Kang, J. G., and Park, C. Y. (2012). Anti-obesity drugs: a review about their effects and safety. *Diabetes Metab. J.* 36, 13–25. doi: 10.4093/dmj.2012.36.1.13
- Kelly, J. P. (2011). Cathinone derivatives: a review of their chemistry, pharmacology and toxicology. *Drug Test. Anal.* 3, 439–453. doi: 10.1002/dta.313
- Meyer, M. R., Du, P., Schuster, F., and Maurer, H. H. (2010). Studies on the metabolism of the  $\alpha$ -pyrrolidinophenone designer drug methylenedioxy-pyrovalerone (MDPV) in rat and human urine and human liver microsomes using GC-MS and LC-high-resolution MS and its detectability in urine by GC-MS. *J. Mass Spectrom.* 45, 1426–1442. doi: 10.1002/jms.1859
- Meyer, M. R., Vollmar, C., Schwaninger, A. E., Wolf, E. U., and Maurer, H. H. (2012). New cathinone-derived designer drugs 3-bromomethcathinone and 3-fluoromethcathinone: studies on their metabolism in rat urine and human liver microsomes using GC-MS and LC-high-resolution MS and their detectability in urine. *J. Mass Spectrom.* 47, 253–262. doi: 10.1002/jms.2960
- Meyer, R. M., and Maurer, H. H. (2010). Metabolism of designer drugs of abuse: an updated review. *Curr. Drug Metab.* 11, 468–482. doi: 10.2174/138920010791526042
- Namara, A., Kawamura, M., Nakamoto, A., Saito, T., and Nagao, M. (2015). Comprehensive review of the detection methods for synthetic cannabinoids and cathinones. *Forensic. Toxicol.* 33, 175–194. doi: 10.1007/s11419-015-0270-0
- Negreira, N., Erratico, C., Kosjek, T., van Nuijs, A. L. N., Heath, E., Neels, H., et al. (2015). In vitro phase I and phase II metabolism of  $\alpha$ -pyrrolidinoveralphenone ( $\alpha$ -PVP), methylenedioxy-pyrovalerone (MDPV) and methedrone by human liver microsomes and human liver cytosol. *Anal. Bioanal. Chem.* 407, 5803–5816. doi: 10.1007/s00216-015-8763-6
- Nóbrega, L., and Dinis-Oliveira, R. J. (2018). The synthetic cathinone  $\alpha$ -pyrrolidinoveralphenone ( $\alpha$ -PVP): pharmacokinetic and pharmacodynamic clinical and forensic aspects. *Drug Metab. Rev.* 50, 125–139. doi: 10.1080/03602532.2018.1448867
- Onakpoya, I. J., Heneghan, C. J., and Aronson, J. K. (2016). Post-marketing withdrawal of anti-obesity medicinal products because of adverse drug reactions: a systematic review. *BMC Med.* 14, 1–10. doi: 10.1186/s12916-016-0735-y
- Pedersen, A. J., Reitzel, L. A., Johansen, S. S., and Linnet, K. (2013). In vitro metabolism studies on mephedrone and analysis of forensic cases. *Drug Test. Anal.* 5, 430–438. doi: 10.1002/dta.1369
- Pieprzyca, E., Skowronek, R., Nižnanský, L., and Czekaj, P. (2020). Synthetic cathinones – from natural plant stimulant to new drug of abuse. *Eur. J. Pharmacol.* 875:173012. doi: 10.1016/j.ejphar.2020.173012
- Pozo, Ó. J., Ibáñez, M., Sancho, J. V., Lahoz-Beneytez, J., Farré, M., Papaseit, E., et al. (2015). Mass spectrometric evaluation of mephedrone in vivo human metabolism: Identification of phase I and phase II metabolites, including a novel succinyl conjugate. *Drug Metab. Dispos.* 43, 248–257. doi: 10.1124/dmd.114.061416
- Prosser, J. M., and Nelson, L. S. (2012). The toxicology of bath salts: a review of synthetic cathinones. *J. Med. Toxicol.* 8, 33–42. doi: 10.1007/s13181-011-0193-z
- Rojek, S., Klys, M., Maciów-Glab, M., Kula, K., and Strona, M. (2014). Cathinones derivatives-related deaths as exemplified by two fatal cases involving methcathinone with 4-methylmethcathinone and 4-methylethcathinone. *Drug Test. Anal.* 6, 770–777. doi: 10.1002/dta.1615
- Shima, N., Katagi, M., Kamata, H., Matsuta, S., Sasaki, K., Kamata, T., et al. (2014). Metabolism of the newly encountered designer drug  $\alpha$ -pyrrolidinoveralphenone in humans: Identification and quantitation of urinary metabolites. *Forensic. Toxicol.* 32, 59–67. doi: 10.1007/s11419-013-0202-9
- Strano-Rossi, S., Cadwallader, A. B., de la Torre, X., and Botrè, F. (2010). Toxicological determination and in vitro metabolism of the designer drug methylenedioxy-pyrovalerone (MPDV) by gas chromatography/mass spectrometry and liquid chromatography/quadrupole time-of-flight mass spectrometry. *Rapid Commun. Mass Spectrom.* 24, 2706–2714. doi: 10.1002/rcm.4692
- Swortwood, M. J., Ellefsen, K. N., Wohlfarth, A., Diao, X., Concheiro-Guisan, M., Kronstrand, R., et al. (2016). First metabolic profile of PV8, a novel synthetic cathinone, in human hepatocytes and urine by high-resolution mass spectrometry. *Anal. Bioanal. Chem.* 408, 4845–4856. doi: 10.1007/s00216-016-9599-4
- Thurman, E. M., Ferrer, I., Pozo, O. J., Sancho, J. V., and Hernandez, F. (2007). The even-electron rule in electrospray mass spectra of pesticides. *Rapid Commun. Mass Spectrom.* 21, 3855–3868. doi: 10.1002/rcm.3271
- Trager, W. F. (2007). “Principles of drug metabolism 1: redox reactions, in ADMETox Approaches,” in *Comprehensive Medicinal Chemistry, 2nd Edn*, eds J. B. Taylor and D. J. Triggle (Oxford: Elsevier), 87–132. doi: 10.1016/B0-08-045044-X/00119-X
- Tyrkkö, E., Pelander, A., Ketola, R. A., and Ojanperä, I. (2013). In silico and in vitro metabolism studies support identification of designer drugs in human urine by liquid chromatography/quadrupole-time-of-flight mass spectrometry. *Anal. Bioanal. Chem.* 405, 6697–6709. doi: 10.1007/s00216-013-7137-1
- UNODC (2018). *World Drug Report 2018*, Booklet 3. Available online at: [https://www.unodc.org/pdf/opioids-crisis/WDR18\\_Booklet\\_3\\_DRUG\\_MARKETS.PDF](https://www.unodc.org/pdf/opioids-crisis/WDR18_Booklet_3_DRUG_MARKETS.PDF) (accessed September 15, 2020).
- UNODC (2020). Drug-Related Resolutions and Decisions 2010 to 2019. Available online at: [https://www.unodc.org/unodc/en/commissions/CND/Resolutions\\_Decisions/Resolutions-Decisions\\_2010-2019.html](https://www.unodc.org/unodc/en/commissions/CND/Resolutions_Decisions/Resolutions-Decisions_2010-2019.html) (accessed September 15, 2020).
- Uralets, V., Rana, S., Morgan, S., and Ross, W. (2014). Testing for designer stimulants: Metabolic profiles of 16 synthetic cathinones excreted free in human urine. *J. Anal. Toxicol.* 38, 233–241. doi: 10.1093/jat/bku021
- Valente, M. J., Guedes De Pinho, P., De Lourdes Bastos, M., Carvalho, F., and Carvalho, M. (2014). Khat and synthetic cathinones: a review. *Arch. Toxicol.* 88, 15–45. doi: 10.1007/s00204-013-1163-9
- Wagmann, L., Manier, S. K., Eckstein, N., Maurer, H. H., and Meyer, M. R. (2020). Toxicokinetic studies of the four new psychoactive substances 4-chloroethcathinone, N-ethylnorpentylone, N-ethylhexedrone, and 4-fluoro- $\alpha$ -pyrrolidinohexiophenone. *Forensic. Toxicol.* 38, 59–69. doi: 10.1007/s11419-019-00487-w
- Weinstein, A. M., Rosca, P., Fattore, L., and London, E. D. (2017). Synthetic cathinone and cannabinoid designer drugs pose a major risk for public health. *Front. Psychiatry* 8:156. doi: 10.3389/fpsy.2017.00156
- Zaami, S., Giorgetti, R., Pichini, S., Pantano, F., Marinelli, E., and Busardò, F. P. (2018). Synthetic cathinones related fatalities: an update. *Eur. Rev. Med. Pharmacol. Sci.* 22, 268–274.
- Zaitsu, K., Katagi, M., Tsuchihashi, H., and Ishii, A. (2014). Recently abused synthetic cathinones,  $\alpha$ -pyrrolidinophenone derivatives: a review of their pharmacology, acute toxicity, and metabolism. *Forensic. Toxicol.* 32, 1–8. doi: 10.1007/s11419-013-0218-1
- Zuba, D. (2012). Identification of cathinones and other active components of “legal highs” by mass spectrometric methods. *Trends Anal. Chem.* 32, 15–30. doi: 10.1016/j.trac.2011.09.009

**Conflict of Interest:** The authors declare that the research was conducted in the absence of any commercial or financial relationships that could be construed as a potential conflict of interest.

Copyright © 2021 Lopes, Caldeira, Gaspar and Antunes. This is an open-access article distributed under the terms of the Creative Commons Attribution License (CC BY). The use, distribution or reproduction in other forums is permitted, provided the original author(s) and the copyright owner(s) are credited and that the original publication in this journal is cited, in accordance with accepted academic practice. No use, distribution or reproduction is permitted which does not comply with these terms.



# Challenges and Strategies of Chemical Analysis of Drugs of Abuse and Explosives by Mass Spectrometry

Ahsan Habib<sup>1,2\*</sup>, Lei Bi<sup>1,3</sup>, Huanhuan Hong<sup>1,3</sup> and Luhong Wen<sup>1,3\*</sup>

<sup>1</sup> The Research Institute of Advanced Technologies, Ningbo University, Ningbo, China, <sup>2</sup> Department of Chemistry, University of Dhaka, Dhaka, Bangladesh, <sup>3</sup> China Innovation Instrument Co., Ltd., Ningbo, China

## OPEN ACCESS

### Edited by:

Mário Barroso,  
Portuguese National Institute of Legal  
Medicine and Forensic  
Sciences, Portugal

### Reviewed by:

Hani Nasser Abdelhamid,  
Assiut University, Egypt  
Keyller Bastos Borges,  
Universidade Federal de São João  
del-Rei, Brazil

### \*Correspondence:

Ahsan Habib  
habibchem@du.ac.bd  
Luhong Wen  
wenluhong@nbu.edu.cn

### Specialty section:

This article was submitted to  
Analytical Chemistry,  
a section of the journal  
Frontiers in Chemistry

Received: 24 August 2020

Accepted: 04 December 2020

Published: 18 January 2021

### Citation:

Habib A, Bi L, Hong H and Wen L  
(2021) Challenges and Strategies of  
Chemical Analysis of Drugs of Abuse  
and Explosives by Mass Spectrometry.  
Front. Chem. 8:598487.  
doi: 10.3389/fchem.2020.598487

In analytical science, mass spectrometry (MS) is known as a “gold analytical tool” because of its unique character of providing the direct molecular structural information of the relevant analyte molecules. Therefore, MS technique has widely been used in all branches of chemistry along with in proteomics, metabolomics, genomics, lipidomics, environmental monitoring etc. Mass spectrometry-based methods are very much needed for fast and reliable detection and quantification of drugs of abuse and explosives in order to provide fingerprint information for criminal investigation as well as for public security and safety at public places, respectively. Most of the compounds exist as their neutral form in nature except proteins, peptides, nucleic acids that are in ionic forms intrinsically. In MS, ion source is the heart of the MS that is used for ionizing the electrically neutral molecules. Performance of MS in terms of sensitivity and selectivity depends mainly on the efficiency of the ionization source. Accordingly, much attention has been paid to develop efficient ion sources for a wide range of compounds. Unfortunately, none of the commercial ion sources can be used for ionization of different types of compounds. Moreover, in MS, analyte molecules must be released into the gaseous phase and then ionize by using a suitable ion source for detection/quantification. Under these circumstances, fabrication of new ambient ion source and ultrasonic cutter blade-based non-thermal and thermal desorption methods have been taken into account. In this paper, challenges and strategies of mass spectrometry analysis of the drugs of abuse and explosives through fabrication of ambient ionization sources and new desorption methods for non-volatile compounds have been described. We will focus the literature progress mostly in the last decade and present our views for the future study.

**Keywords:** drugs of abuse, explosives, ambient ionization source, hollow cathode discharge ionization, headspace method, non-thermal desorption, tribological effect, mechanism of ionization and desorption

## INTRODUCTION

Mass spectrometry (MS) is one of the most powerful and widely used modern physical-chemical methods for analyzing all types of compounds and most of the elements in the periodic table with high selectivity and sensitivity. In analytical science, MS is known as a “gold standard” because of its unique character of providing the direct molecular structural information of the compounds



of interest. Therefore, MS technique has been widely used in all branches of chemistry along in proteomics, metabolomics, genomics, lipidomics, environmental monitoring etc. and also in technology. MS-based techniques have already been proven as a versatile analytical tool for solving many analytical problems such as characterization of biomolecules such as proteins, peptides, nucleic acids and also analysis of polymers. MS has widely been used to elucidate the structure of the compounds of interest through fragmentation using tandem MS (MS<sup>2</sup>) as well. In fact, MS technique is the method of choice for industrial, clinical, biological, forensic, environmental monitoring, isotope etc. analyses. The development of the MS-imaging system is a milestone to the scientific world because of its precise medical diagnosis such as tumor, cancer etc. through characterization of complex biomolecules (Rohner et al., 2005; McDonnell and Heeren, 2007; Addie et al., 2015).

Furthermore, application of MS in space research that started in the 1950's by the US Naval Research Laboratory has already been proven its high-throughput as an indispensable analytical tool in science and technology (Robert, 2008; Arkin et al., 2010). Mass spectrometry has been used by the International Space Station for monitoring air quality, propellant leakage of the Space Shuttles etc. (NASA, 2007). Japan Aerospace Exploration Agency (JAXA) has already been taken a collaborative research with the Indian Space Research Organization (ISRO) to send the H3-launch vehicle and the rover called as lunar polar exploration mission that for searching the existence of water to the south pole region of the moon in 2024 (Hoshino et al., 2019, 2020; The Yomiuri Shimbun, 2019). It is noted that the outstanding analytical performance of MS-based techniques facilitated us to achieve adequate knowledge and understanding about the solar system as well as the universe.

Applications of the MS technique should be emphasized into two general types: (i) detection and characterization of compounds introduced into the MS where it can be considered as a powerful detector and (ii) investigation of physical and/or chemical transformations of the compounds being studied. In the former case, MS couples directly with an ionization source

for detection and quantification of the relevant analytes (Fenn et al., 1989; Gale and Smith, 1993; McLuckey et al., 1996; Feng and Smith, 2000; Byrdwell, 2001; Cody et al., 2005; Shiea et al., 2005; Takáts et al., 2005; Hiraoka et al., 2006, 2007, 2015; Song and Cooks, 2006; Ganev et al., 2007; Na et al., 2007a,b; Cotte-Rodríguez et al., 2008; Harper et al., 2008; Zhang et al., 2009; Chen et al., 2010, 2017; Nilles et al., 2010; Garcia-Reyes et al., 2011; Takada et al., 2011; Habib et al., 2013, 2014, 2015, 2020; Sekar et al., 2013; Su et al., 2013; Groeneveld et al., 2015; Castiglioni et al., 2016; Damon et al., 2016; Kumano et al., 2018; Tavares et al., 2018; Usmanov et al., 2018; Borges et al., 2019; Feider et al., 2019; Ng et al., 2019) and/or couple with a separation technique (chromatographic) such as gas chromatography (GC), liquid chromatography (LC), high performance liquid chromatography (HPLC), electrophoresis, paper chromatography etc. and then coupled with an ionization source for ionization (Horning et al., 1974; Carroll et al., 1975; Alexandrov et al., 1984; Whitehouse et al., 1985; Olivares et al., 1987; Smith et al., 1988a,b; Lee et al., 1989; Covey and Devanand, 2002; Sigman et al., 2006; Pizzolato et al., 2007; Khan et al., 2015; Gilbert-López et al., 2019). Mass spectrometer comprises an ion source, mass analyzer and a detector. In MS, ion source is considered as the heart of it because the sensitivity mostly depends on the ionization efficiency of the ion source. Since the discovery of MS in the 1950's, electron ionization (EI) (Dempster, 1918, 1921), chemical ionization (CI) (Fales et al., 1972; Harrison, 1992; Field, 2002), fast atom bombardment (FAB) ionization (Barber et al., 1981a,b, 1982), Panning ionization (Penning, 1927; Arango et al., 2006; Hiraoka et al., 2006) were widely used for ionization of the compounds of interest under vacuum condition. In the 1970s, Carroll and co-workers at the Baylor College of Medicine invented the atmospheric pressure chemical ionization (APCI) (Horning et al., 1973) that was applied to gas chromatography-mass spectrometry (GC-MS) (Carroll et al., 1975) and liquid chromatography-mass spectrometry (LC-MS) (Horning et al., 1974). In 1975, a corona discharge electrode developed that has widely been used as an APCI ion source for commercially available MS system (Byrdwell, 2001).

In the history of MS, development and application of electrospray ionization (ESI) opened a new research arena for the analysis of macromolecules and biological materials (Whitehouse et al., 1985; Meng et al., 1988; Smith et al., 1988a, 1990; Fenn et al., 1989, 1990, 1997; Lee et al., 1989; Loo et al., 1990; Cole, 1997; Kebarle, 2000). Electrospray ionization (ESI) is a technique that uses high voltage to generate ions from an aerosol of charged liquid droplets. Since its first discover by Rayleigh (1882) for theoretical estimation of maximum amount of charge of a liquid droplet could carry before throwing out fine jets of liquid that is known as a Rayleigh limit (Rayleigh, 1882) and has then extended by Zeleny (1914) to study the behavior of fluid droplets at the end of glass capillaries for knowing different electrospray modes (Zeleny, 1914). After that, Wilson and Taylor (Wilson and Taylor, 1925) and (Nolan and O'Keefe, 1932) investigated electrospray extensively in the 1920s. The electrospray cone was described by Sir Geoffrey Ingram Taylor (Taylor, 1964), accordingly, the cone later coined as Taylor cone (Wilm and Mann, 1994). Macky (1931) also studied the behavior of electrospray (Macky, 1931).

**Abbreviations:** MS, mass spectrometry; MS/MS, mass spectrometry/mass spectrometry; IMS, ion mobility spectrometry; GC, gas chromatography; LC, liquid chromatography; HPLC, high performance liquid chromatography; GC-MS, gas chromatography-mass spectrometry; LC-MS, liquid chromatography-mass spectrometry; HPLC-MS, high performance liquid chromatography-mass spectrometry; MSE, microfluidic surface extractor; DBDI, dielectric barrier discharge ionization; HCIDI, hollow cathode discharge ionization; ac/dc-APCI-ac/dc, atmospheric pressure chemical ionization; ESI, electrospray ionization; Nano-ESI, nano-electrospray ionization; PESI, probe electrospray ionization; MALDI, matrix assisted laser desorption/ionization; DESI, desorption electrospray ionization; DART, direct analysis in real time; EESI, extractive electrospray ionization; EI, electron ionization; CI, chemical ionization; FAB, fast atom bombardment; PI, Panning ionization; TB, tribodesorption; AM, amphetamine; MA, methamphetamine; MDA, 3,4-methylenedioxymphetamine; MDMA, 3,4-methylenedioxymphetamine; TATP, triacetone triperoxide; HMTD, hexamethylene triperoxide diamine; TNT, trinitrotoluene; TNB, 1,3,5-trinitrobenzene; AN, ammonium nitrate; RDX, hexahydro-1,3,5-trinitro-1,3,5-triazine; HMX, 1,3,5,7-tetranitro-1,3,5,7-tetrazoctane; NG, nitroglycerine; PETN, pentaerythritol tetranitrate; DFT, density functional theory; JAXA, Japan Aerospace Exploration Agency; ISRO, Indian Space Research Organization; NASA, National Aeronautics and Space Administration.



Dole et al. (1968) used the electrospray ionization with MS for the first time in 1968 (Dole et al., 1968; Pramanik et al., 2002) and finally Yamashita and Fenn (Yamashita and Fenn, 1984; Whitehouse et al., 1985; Meng et al., 1988; Fenn et al., 1989, 1990, 1997) as well as Alexandrov et al. (1984) and co-workers developed the electrospray ionization mass spectrometry in 1984. John B. Fenn was awarded the Nobel Prize for the development of ESI-MS in Chemistry in 2002 (Press Release, 2002).

In fact, commercial ESI utilizes high flow rates that keep within a range from 10.0  $\mu\text{L}/\text{min}$  to 1.0  $\text{mL}/\text{min}$  (Meng et al., 1988; Smith et al., 1988a,b, 1990; Fenn et al., 1989, 1990; Lee et al., 1989; Loo et al., 1990; Kebarle, 2000; Sekar et al., 2013; Abdelhamid and Wu, 2015, 2019a; Khan et al., 2015). The high flow rate is responsible for the formation of liquid droplets with large size that causes slow evaporation, thereby resulting in obtaining poor sensitivity of the relevant analyte compounds. The high flow rate system also consumes large sample volume that causes less stability of the spray. However, when the flow rate is reduced to nanoliters per minute ( $\text{nL}/\text{min}$ ) in case of nano-ESI, droplet formation occurs more readily, requiring only the applied voltage to the metal-coated nano-capillary (Olivares et al., 1987; Smith et al., 1988a; Gale and Smith, 1993; Wilm and Mann, 1996; Juraschek et al., 1999; Feng and Smith, 2000; Karas et al., 2000; Covey and Devanand, 2002; Ushijima et al., 2019). Accordingly, the spray achieves stability with relatively smaller size of the droplets that results in better sensitivity. Though nano-ESI exhibits better sensitivity than that by ESI, however, nano-ESI has been limited in its applications for biological fluids because of clogging problems by the presence of high salts and/or other biological. To overcome the clogging problem, Hiraoka and co-workers developed a needle-based ESI coined as a probe-electrospray (PESI) ion source for MS that can operate under ambient conditions (Hiraoka et al., 2007, 2015; Usmanov et al., 2018). In ambient mass spectrometry, ionization of neutral compounds of interest occurs under ambient conditions and then collected and analyzed by MS (Takáts et al., 2004; Cody et al., 2005; Cooks et al., 2006; Feider et al., 2019). The ambient ion sources allow the high-throughput analysis of sample of interest in their native state, often with minimal or no sample pre-treatment. The developed ambient ion sources such as desorption electrospray ionization (DESI) (Takáts et al., 2004; Justes et al., 2007), direct analysis in real time (DART) (Cody et al., 2005), matrix-assisted laser desorption/ionization (MALDI) (Karas et al., 1985; Abdelhamid and Wu, 2012, 2013, 2016, 2019a,b; Abdelhamid et al., 2017; Chen et al., 2017; Abdelhamid, 2018, 2019a,b), electrospray-assisted laser desorption/ionization (ELDI) (Shiea et al., 2005), desorption atmospheric pressure chemical ionization (DAPCI) (Takáts et al., 2005) have already been coupled to commercial MS. Beside these, ac-atmospheric pressure chemical ionization (ac-APCI) (Habib et al., 2013), He-flow dielectric barrier discharge ionization (DBDI) (Na et al., 2007a,b; Zhang et al., 2009; Habib et al., 2014, 2020; Gilbert-López et al., 2019), PESI (Hiraoka et al., 2007) have been fabricated as ambient ion sources and applied to analyze a wide range of compounds. Since the pioneering work of the DBD ion source by Zhang and co-workers (Na et al., 2007a,b; Zhang et al., 2009), it has widely been used in

mass/ion-mobility spectrometry (Usmanov et al., 2013; Habib et al., 2014, 2020; Gilbert-López et al., 2019). According to the design of the homemade He-DBDI,  $\text{H}_3\text{O}^+$  and  $\text{NO}_2^-$  and/or  $\text{NO}_3^-$  ions are formed as reagent ions in positive and negative ion modes, respectively and the gaseous neutral molecules of interest take part in ion-molecule reactions outside of the plasma. In the positive ion mode, the gaseous neutral analyte molecules ionized mainly by the  $\text{H}_3\text{O}^+$ , however, in the negative ion mode, the reagent ions  $\text{NO}_2^-$  and/or  $\text{NO}_3^-$  combine with the analyte molecules lead to cluster and/or adduct ions (Usmanov et al., 2013; Habib et al., 2014, 2020). In our fabricated DBDI, water forms its cluster ion,  $\text{H}_3\text{O}^+(\text{H}_2\text{O})_n$ , outside of the DBD ceramic tube, accordingly, it is regarded as an ambient ion source just mimic of APCI.

In analytical mass spectrometry, it is highly appealing that the investigated analytes should undergo minimal fragmentation during desorption/ionization in order to achieve better limits of detection (LODs). Among the developed ion sources, MALDI, DESI, ESI, and/or PESI have been proved as soft ionization methods for a wide range of compounds ranging from large molecules such as proteins, peptides, polymers, nucleic acids etc. to small molecules like amino acids, drugs of abuses, explosives and many of commonly naturally found compounds. As mentioned, an ionization method plays a vital role in quantifying the relevant analytes at ultra-trace level where efficient desorption of the investigated compounds is mandatory. In this regard, MALDI, DESI, or ESI function both as an efficient ion source and desorption method simultaneously. Since the pioneering work of MALDI by Franz Hillenkamp, Michael Karas, and their colleagues in 1985, much attention has been paid to develop matrices for efficient desorption and ionization of particularly biomolecules such as peptides, proteins, nucleic acids, lipids, oligosaccharides, amino acids etc. (Karas et al., 1985, 1987; Tanaka et al., 1988; Karas and Bahr, 1990; Fitzgerald et al., 1993; Tang et al., 1994; Abdelhamid and Wu, 2012, 2013, 2016, 2019a,b; Abdelhamid et al., 2017; Chen et al., 2017; Abdelhamid, 2018, 2019a,b). Organic compounds such as 2,5-dihydroxy benzoic acid, 3,5-dimethoxy-4-hydroxycinnamic acid, 4-hydroxy-3-methoxycinnamic acid,  $\alpha$ -cyano-4-hydroxycinnamic acid, picolinic acid, and/or 3-hydroxy picolinic acid etc. have widely been used as MALDI matrices for desorption/ionization of peptides, proteins, nucleotides, oligonucleotides, oligosaccharides, lipids etc. (Karas et al., 1985, 1987; Tanaka et al., 1988; Beavis et al., 1989, 1992; Karas and Bahr, 1990; Strupat et al., 1991; Fitzgerald et al., 1993; Wu et al., 1993), however, inorganic materials, particularly nanoparticles (NPs) have advanced applications in mass spectrometry as MALDI matrices (Abdelhamid and Wu, 2012, 2013, 2016, 2019a,b; Abdelhamid et al., 2017; Chen et al., 2017; Abdelhamid, 2018, 2019a,b). Besides the development of hybrid desorption/ionization system, attentions have also been taken to fabricate desorption method for non-volatile compounds from their solid state (Saha et al., 2013; Usmanov et al., 2013, 2016; Habib et al., 2014; Bi et al., 2021). Of them, Leidenfrost-assisted thermal desorption (LPTD) and ultrasonic-cutter blade-based desorption methods exhibited efficient desorption methods for gasification of mostly non-volatile compounds without and/or

with minimal fragmentation (Saha et al., 2013; Usmanov et al., 2013, 2016; Habib et al., 2014; Bi et al., 2021). Coupling of these noble desorption methods with homemade helium-DBDI-MS system exhibited as potential analytical techniques in detection and quantification of highly non-volatile drugs of abuse, explosives, carbohydrates, rhodamine B, ionic liquids, amino acids, spinosad etc. at ultra-trace levels to some extent (Saha et al., 2013; Habib et al., 2014, 2020; Bi et al., 2021).

The direct structural information of compounds of interest using mass spectrometry has given golden opportunity to the scientists and researchers of its versatile applications in various fields in science and technology. Accordingly, MS technique in forensic laboratories as well as for explosive detection has been increased significantly in the last few decades from criminal investigation and public security and safety point of views. The sensitivity, rapid analysis, selectivity and simple sample pretreatment requirements have led to MS-based methods being adopted as the choice to analyze illicit drugs (Pizzolato et al., 2007; Habib et al., 2014, 2020; Groeneveld et al., 2015; Damon et al., 2016; Brettell and Lum, 2018; Tavares et al., 2018; Borges et al., 2019; Ng et al., 2019; Filho et al., 2020) and explosives (Chen et al., 2009; Takada et al., 2011, 2012a,b, 2016; Habib et al., 2013, 2014; Hashimoto et al., 2014; Kumano et al., 2018). Besides these applications, MS-based technique has also been used in analysis of complex biological samples through coupling with micro-chips, microfluidic surface extractor (MSE) and/or single drop microextraction device (He et al., 2014; Chen et al., 2017; Liu et al., 2020; Zhang et al., 2020).

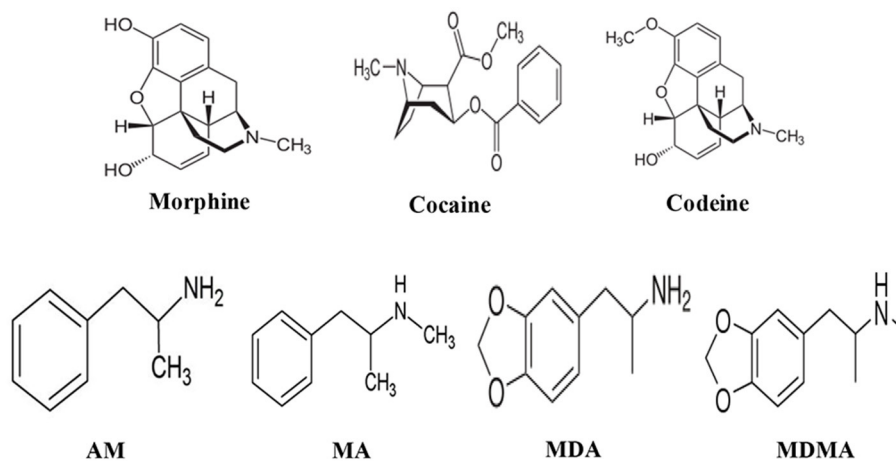
In this review article, challenges and strategies of mass spectrometry analysis of the illicit drugs and explosives through fabrication of new ionization sources and new desorption methods for non-volatile compounds have been described. As illicit drugs, morphine, cocaine, codeine, amphetamine (AM), methamphetamine (MA), 3,4-methylenedioxyamphetamine (MDA), and 3,4-methylenedioxymethamphetamine (MDMA) (**Scheme 1**) and as explosives, triacetone triperoxide (TATP), hexamethylene triperoxide diamine (HMTD), trinitrotoluene (TNT), 1,3,5-trinitrobenzene (TNB), ammonium nitrate (AN), hexahydro-1,3,5-trinitro-1,3,5-triazine (RDX), 1,3,5,7-tetranitro-1,3,5,7-tetrazoctane (HMX), nitroglycerine (NG), and pentaerythritol tetranitrate (PETN) (**Scheme 2**) were taken as model compounds. In view of this, firstly, the following ionization sources: dielectric barrier discharge ionization (DBDI), hollow cathode discharge ionization (HCDI), ac/dc-atmospheric pressure chemical ionization (APCI) secondly, thermal/non-thermal desorption methods for non-volatile compounds such as solid/solid friction and flash heating/rapid cooling have been described. The developed DBDI and ac/dc-APCI ion sources function well under ambient conditions while the HCDI works well at much below atmospheric (ranging from 1 to 28 Torr) pressure from sensitivity and selectivity point of views. Mechanisms of ion formation and desorption of non-volatile drug and explosive compounds by using the developed ion sources and solid/solid-based desorption method are also discussed.

## TRIBODESORPTION-DIELECTRIC BARRIER DISCHARGE (DBD) IONIZATION-MS SYETM

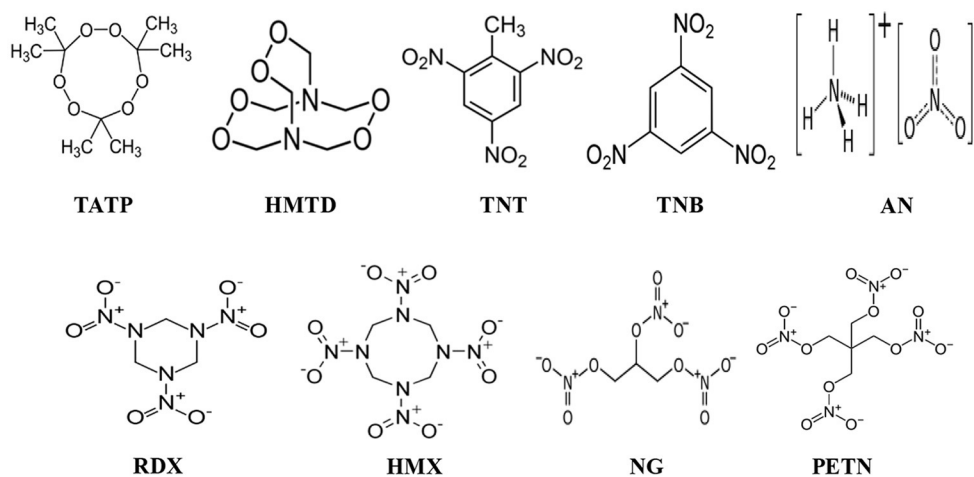
### Concept of Desorption of Non-volatile Compounds by Tribological Effect

**Figure 1** shows a homemade helium dielectric barrier discharge (DBD) ion source fabricated using a ceramic tube as a dielectric barrier tube where a stainless steel wire was inserted into the ceramic tube and grounded that acted as an inner electrode (Usmanov et al., 2013; Habib et al., 2014, 2020; Bi et al., 2021). The DBD plasma was generated inside the ceramic tube by flowing He gas (99.9999%) with a flow rate ranging from 0.25 to 0.30 L/min through applying 2.4 kV<sub>PTP</sub> (peak-to-peak) ac high voltage to the outer electrode (copper strip). A function generator was used to generate 15 kHz sinusoidal signal and then amplified by a power generator in order to generate the ac high voltage. The inner grounded wire electrode was protruded from the exit of the ceramic tube, thereby resulting in confinement of the DBD plasma inside the ceramic tube. As a result, the desorbed gaseous analyte molecules were not exposed directly by the plasma but ionized by reacting with mainly H<sub>3</sub>O<sup>+</sup> ion and/or with NO<sub>2</sub><sup>+</sup>/NO<sub>3</sub><sup>+</sup> in the positive and negative modes of ionization, respectively. Under the ambient condition, water forms its cluster ion, H<sub>3</sub>O<sup>+</sup>(H<sub>2</sub>O)<sub>n</sub>, outside of the DBD ceramic tube. The present DBD ion source is thus regarded as an atmospheric pressure chemical ionization (APCI) (Usmanov et al., 2013; Habib et al., 2014, 2020; Bi et al., 2021).

Prior to discussing the mass spectral results, it is better to focus on the mechanism of desorption of the non-volatile analyte compounds by the ultrasonic cutter-based desorption method. In this desorption method, exactly 2 μL of the sample solution was deposited on a flat perfluoroalkoxy (PFA) substrate and diameter of the sample spot was found to be 2 mm. After dried in air, the deposited sample on the PFA substrate was desorbed through very gentle touching with an ultrasonic cutter by applying an oscillation frequency of 40 kHz to the cutter blade (20 W, Honda Electronics, Toyohashi, Japan). The gaseous molecules were then ionized using a homemade He-DBDI and detected by an ion trap mass spectrometer. The solid/solid friction of the ultrasonic cutter with the PFA substrate has been coined as a tribological event (Habib et al., 2014; Bi et al., 2021). In another study, we found enhanced sensitivity of the relevant compounds when the compounds were deposited on the ultrasonic blade instead of the substrate and then gently touch with the substrate's surface for rubbing (Bi et al., 2021). Such an experimental setup is shown in **Figure 2**. This is because the oscillation/vibrational energy from the ultrasonic cutter blade directly transfer to the deposited solid molecules as an additional kinetic energy that causes the intermolecular force of attraction to weaken before touching the substrate. During the touching/rubbing process, the deposited molecules on the blade also gain mechanical/frictional energy in terms of tribological event as an extra energy in order to amplify the desorption process before penetrating and/or remaining into/on the substrate. This synergistic effect, caused by gaining the vibrational/oscillation and frictional/mechanical



**SCHEME 1** | Molecular structures of the illicit drug compounds.



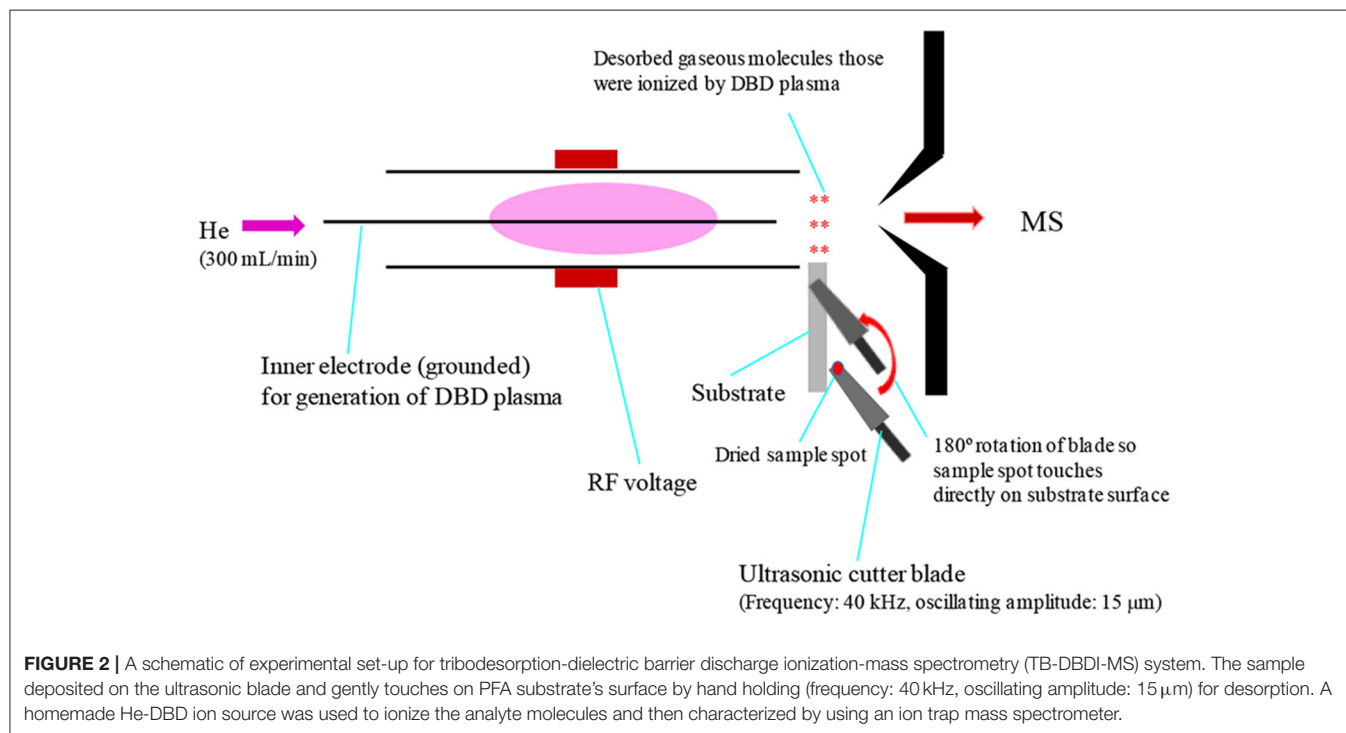
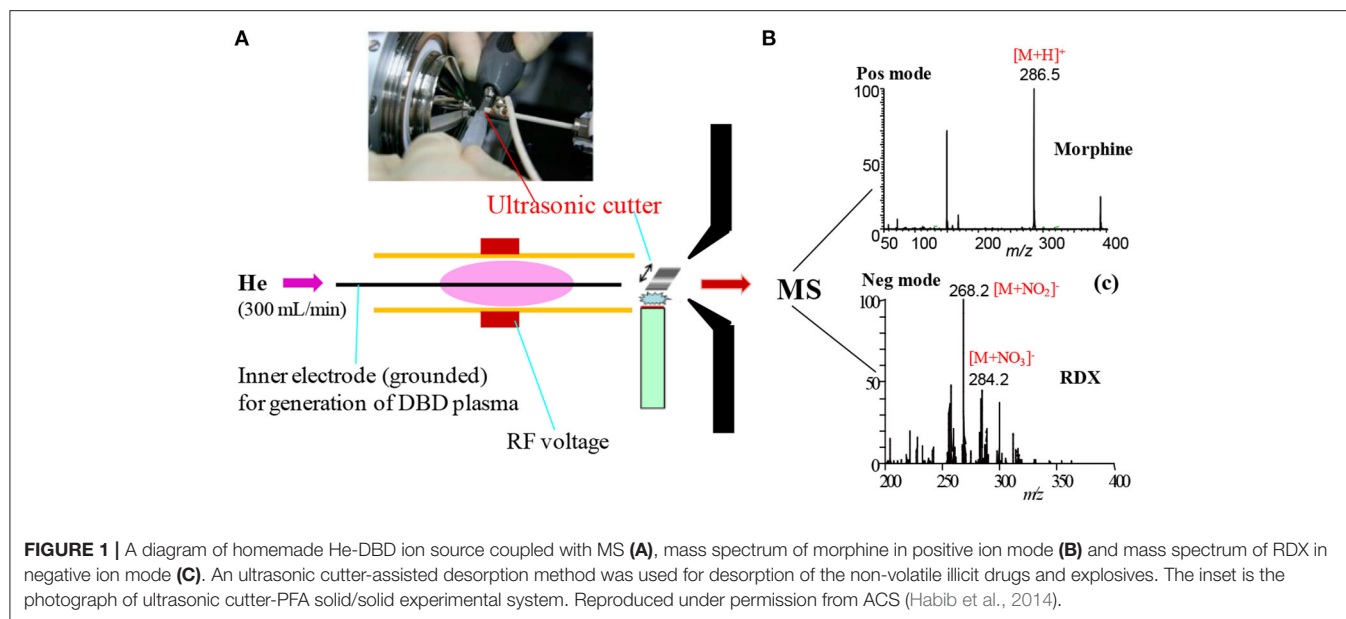
**SCHEME 2** | Molecular structures of the explosive compounds.

energy, enhances the desorption process of the non-volatile solid molecules into the gaseous phase that provides better sensitivity, realizing ultra-trace level detection.

The term tribology means the interface of moving matters. Friction of moving bodies also plays a vital role in the interface. In MS, analytes in gaseous phase is mandatory consequently, thermal energy has long been used for desorption of solid molecules into the gaseous phase, however, thermal energy may cause fragmentation of the analyte compounds that is not expected in analytical mass spectrometry. This is because fragmentation may not provide better limits of detection in most of the MS experiments while that is highly desirable in analytical MS. Mechanical energy in terms of tribological event is commonly found in nature as well as in many scientific and technological areas. However, thermal energy and mechanical energy are inherently different. The former is a scalar quantity with random energy while the latter is a vector quantity where

all the atoms and molecules of the moving matters have the same direction. Therefore, it may conclude that mechanical energy is regarded as the high-quality energy with coherency. The macroscopic mechanical energy is transferred to non-thermal energy by the nano- and/or microscopic contact with the moving bodies, thus it seems very difficult to recognize molecular-level information by the conventional analytical techniques (Nevshupa, 2009). Mass spectrometry is a highly appealing analytical tool because of its direct structural information of the generated molecules and/or ions during moving bodies, ultimately interface mechanism will be achieved.

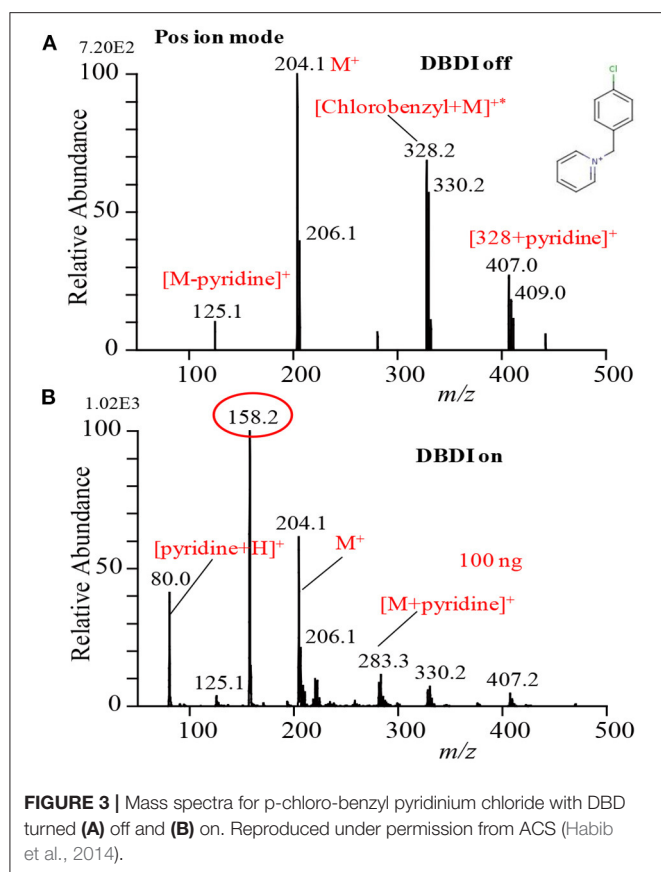
In order to investigate whether the ultrasonic cutter-based desorption method is non-thermal or thermal, p-chloro-benzyl pyridinium chloride was taken as a model thermometer compound to obtain direct information about desorption (Habib et al., 2014). The p-chloro-benzyl pyridinium chloride is a highly non-volatile ionic compound. **Figure 3** shows the mass



spectrum of the p-chloro-benzyl pyridinium chloride in the positive mode of ionization. The compound gave molecular ion,  $M^+$ , as the major ion that appeared at  $m/z$  204.1 along with a much weaker signal from the fragment ion  $[M-\text{pyridine}]^+$  (i.e., p-chlorobenzyl cation,  $\text{ClC}_6\text{H}_4\text{CH}_2^+$ ,  $m/z$  125.1) as the DBDI was turned off condition. Therefore, it is concluded that the fabricated ultrasonic cutter-based desorption method can efficiently gasify highly non-volatile compounds as their monomer with a very minimal fragmentation. It has also been

reported that the temperature of effused gases just outside of the dielectric ceramic tube was to be  $\sim 49^\circ\text{C}$  that was slightly elevated from room temperature (Habib et al., 2014). The radiofrequency heating of the dielectric tube causes such elevation of the gas temperature. On the other hand, the direct analysis in real time (DARD) fabricated by Cody and co-workers used quite high gas temperature in order to gasify the solid analyte compounds for ionization (Cody et al., 2005).





In conclusion, the soft mechanical frictional energy generated by the ultrasonic cutter in combination with a substrate can be used as an efficient desorption process for gasification of non-volatile compounds. The developed method, especially deposition of the relevant compound on the cutter blade instead of the substrate (Bi et al., 2021), is reasonably sensitive and may be applied for quick analysis of contaminants, such as narcotics, explosives, and/or any other non-volatile compounds, deposited on substrates' surfaces.

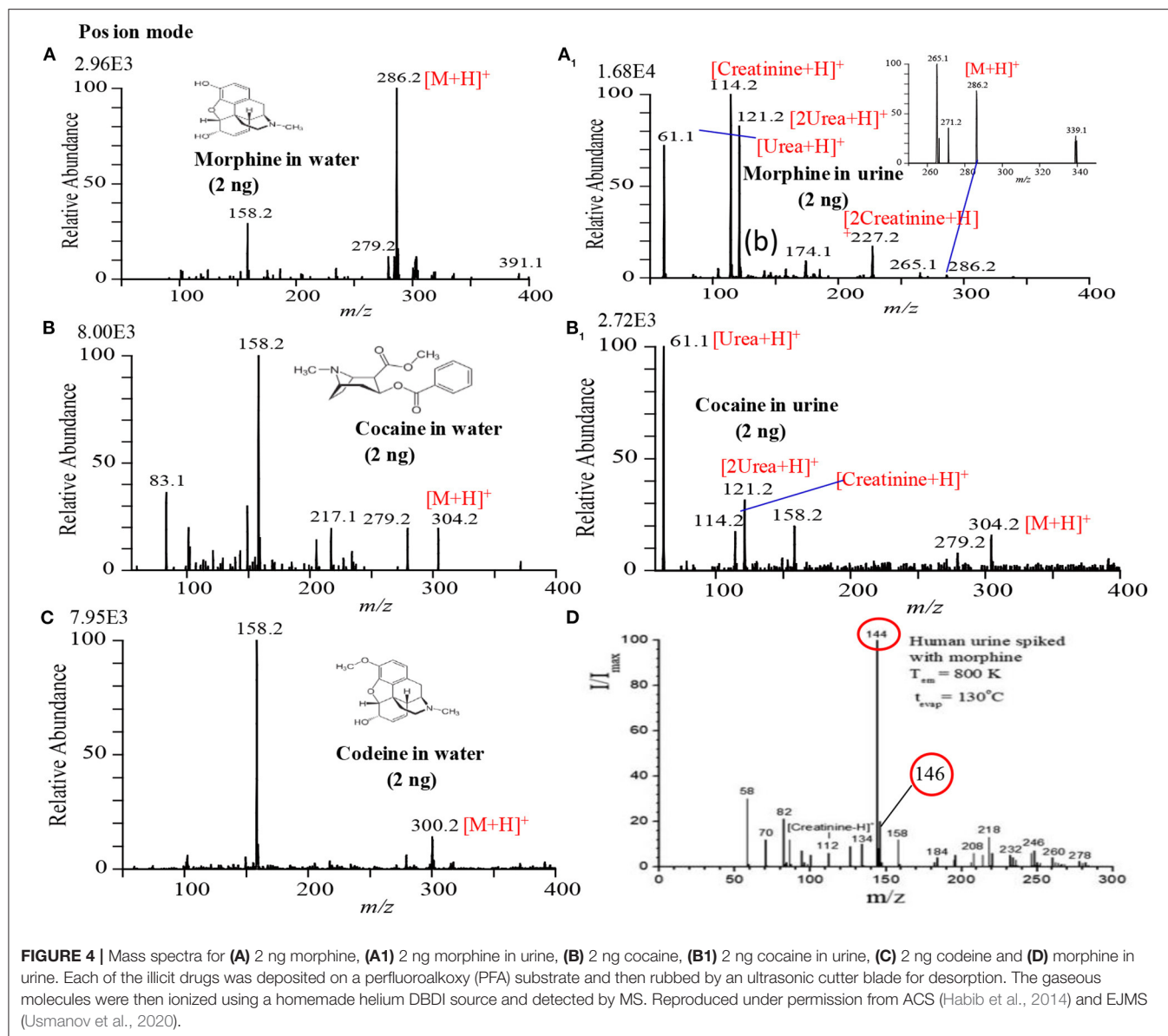
## Analysis of Drugs of Abuse

**Figure 4** shows the mass spectra of morphine, cocaine and codeine. Exactly 2  $\mu$ L sample solution containing 2 ng of each illicit drug compound was deposited on the PFA substrate and then dried in air. The dried spot was gently touched using the ultrasonic cutter for gasification. A homemade He-DBDI coupled with a MS was used for ionization/detection of the illicit drug compounds. As seen from **Figure 4**, morphine, cocaine, and codeine were detected in their protonated forms,  $[M+H]^+$ , at  $m/z$  286, 304, and 300, respectively without any fragmentation. However, Usmanov et al. (2020) reported that morphine underwent severe fragmentation by using surface-ionization mass spectrometry and the major fragment ions appeared at  $m/z$  144, 146 when detected from human urine spiked (**Figure 4D**) (Usmanov et al., 2020).

**Figures 4A<sub>1</sub>,B<sub>1</sub>** show the raw urine sample spiked with 2 ng of morphine and cocaine, respectively. Both the morphine and codeine display their protonated ions at  $m/z$  286 and 304, respectively without any fragmentation along with the protonated urea, creatinine, and their protonated dimmers. The developed desorption method exhibited its potentiality for gasification of the non-volatile illicit drug compounds from complex body fluids as well. As mentioned in the previous section, the homemade DBD ion source acts as an ambient atmospheric pressure chemical ionization (APCI). In the positive ion mode, hydronium ion,  $H_3O^+$ , comes from the DBD ion source as a reagent ion and takes part in ion-molecule reactions with the gaseous analyte molecules under the ambient condition, thereby resulting in the formation of protonated molecular ion,  $[M+H]^+$  of analytes of interest. The limits of detection (LODs) for the morphine, cocaine and codeine from water/methanol and spiked in urine are tabulated in **Table 1**. The values of LODs for morphine, cocaine and codeine in water/methanol were smaller than that spiked in urine and the values were 0.30, 0.50, and 0.60 ng in water/methanol and 0.50, 0.80, and 0.90 ng from spiked in urine, respectively (**Table 1**). The elevated values of LOD for the illicit drugs spiked in urine are due to ion suppression effects by the constituents of urine such as urea, creatinine etc. As seen from **Figures 4A<sub>1</sub>,B<sub>1</sub>**, protonated creatinine and/or urea,  $[M+H]^+$ , exhibit as base peaks because of higher proton affinity of these urine constituents than that of the illicit drugs of interest. The low molar mass of the urine's constituents also causes efficient desorption of creatinine, urea etc. from the sample spot during rubbing by the ultrasonic cutter with the substrate. In our another study, however, we found enhanced sensitivity of the amphetaminic drug compounds such as amphetamine (AM), methamphetamine (MA), 3,4-Methylene dioxy amphetamine (MDA) and 3,4-Methyl enedioxy methamphetamine (MDMA) from spiked urine by an alkaline treated headspace method (**Table 1**) (Habib et al., 2020). The amphetaminic drug compounds contain either amine or imine groups, thus they exhibit volatile and/or semi-volatile in nature at room temperature. Accordingly, these nitrogenous compounds make their pills through treating with hydrochloric acid in order to provide stability. So, alkali treatment causes evaporation of the free base amphetaminic compounds into the gaseous phase from solution. Ammoniated carbonated alkali solutions such as sodium carbonate, potassium carbonate etc. provide better limits of detection even from spiked urine (**Table 1**) (Habib et al., 2020). Addition of alkali solution into the HCl-amphetaminic drug evolves gaseous carbon dioxide that acts as a carrier gas to bring the free base amphetaminic molecules from the liquid to the gaseous phase. Presence of trace level ammonia also enhances the sensitivity of the amphetaminic drug compounds using the headspace-DBDI-MS system (Habib et al., 2020).

As mentioned above, we found enhanced sensitivity for the relevant non-volatile drugs of abuse by using the ultrasonic cutter blade-based desorption method coupled with the same He-DBDI-MS system where the relevant analyte was deposited on the cutter blade instead of the PFA substrate and then rubbed (**Figure 2** and **Table 1**) (Bi et al., 2021). The values of the limit of detections (LODs) for the morphine, cocaine and codeine were





40.38 ± 1.55, 20.00 ± 0.91, and 50.25 ± 1.85 pg, respectively, that were at least 8–10 time lower than that obtained for the cutter blade-based desorption method where the analyte compounds were deposited on the PFA substrate (Table 1). As described above, the enhanced sensitivity is due to synergistic effect caused by gaining the vibrational/oscillation and frictional/mechanical energy by the ultrasonic cutter when the analyte compounds deposited on the blade (Bi et al., 2021). By using the similar homemade He-DBDI and ion trap MS, Usmanov et al. (2013) reported quite high LOD values for morphine, cocaine and codeine by a heated filament (154°C) as a desorption means and these were 25.0, 7.0, and 3.0 ng, respectively (Usmanov et al., 2013). A brief description of this system has been elaborated in Figures 5, 6. A homemade ac-APCI ion source has also been fabricated by Usmanov and Hiraoka (2016) for characterization of morphine, cocaine and codeine and the LOD values were

found to be 5.0, 5.0, 0.5 ng, respectively (Usmanov and Hiraoka, 2016). However, Jackson et al. (2010) reported only 15, 150 pg for cocaine and codeine, respectively where that for morphine was quite high, 3,000 pg, by using a heated substrate coupled to the DBDI-MS/MS system. The low LOD values for the cocaine and codeine using the tandem mass spectrometry (MS/MS) system is desirable, however, the high LOD value (3,000 pg) for morphine is suggesting the difficulties to analyze morphine at ultra-trace level using the heated substrate as a desorption process is challenging.

A heated filament-based desorption method has been used in order to desorb solid drug of abuse compounds and ionized/detected by a homemade He-DBDI coupled with a MS system. Such an experimental setup is shown in Figure 5 (Usmanov et al., 2013). Results show that a significant fragmentation for cocaine was observed using the

**TABLE 1** | Limits of detection (LODs) for drugs of abuse and explosives measured by tribodesorption-helium-DBDI-MS and other MS techniques.

Target Compounds	Characteristic ion ( <i>m/z</i> )	LOD (pg) Mean $\pm$ SD	RSD (%)
Morphine (285.34)	<b>[M+H]<sup>+</sup> (286)</b>	(40.38 $\pm$ 1.55) <sup>a*</sup> , (59.63 $\pm$ 5.39) <sup>a**</sup> , (300) <sup>b</sup> , (25 $\times$ 10 <sup>3</sup> ) <sup>c</sup> , (5 $\times$ 10 <sup>3</sup> ) <sup>d</sup> (3 $\times$ 10 <sup>3</sup> ) <sup>e</sup>	(3.83) <sup>a*</sup> , (9.04) <sup>a**</sup>
Morphine (285.34) spiked in human urine	<b>[M+H]<sup>+</sup> (286)</b>	(500) <sup>b*</sup> (1 $\times$ 10 <sup>3</sup> ) <sup>b**</sup>	-
Cocaine (303.35)	<b>[M+H]<sup>+</sup> (304)</b>	(20.00 $\pm$ 0.91) <sup>a*</sup> , (500) <sup>b</sup> , (7 $\times$ 10 <sup>3</sup> ) <sup>c</sup> , (5 $\times$ 10 <sup>3</sup> ) <sup>d</sup> , (15) <sup>e</sup>	(4.56) <sup>a*</sup>
Cocaine (303.35) spiked in human urine	<b>[M+H]<sup>+</sup> (304)</b>	(39.88 $\pm$ 1.65) <sup>a*</sup> (800) <sup>b*</sup> (500) <sup>d</sup>	(4.14) <sup>a*</sup>
Codeine (299.36)	<b>[M+H]<sup>+</sup> (300)</b>	(50.25 $\pm$ 1.85) <sup>a*</sup> , (600) <sup>b</sup> , (3 $\times$ 10 <sup>3</sup> ) <sup>c</sup> , (500) <sup>d</sup> , (150) <sup>e</sup>	(3.68) <sup>a*</sup>
Codeine (299.36) spiked in human urine	<b>[M+H]<sup>+</sup> (300)</b>	(900) <sup>b*</sup>	-
AM (135.21)	<b>[M+H]<sup>+</sup> (136)</b>	(0.10) <sup>ht</sup> (0.60) <sup>htt</sup>	(7.89) <sup>ht</sup>
AM (135.21) spiked in human urine	<b>[M+H]<sup>+</sup> (136)</b>	(0.05) <sup>ht</sup>	(6.23) <sup>ht</sup>
MA (149.24)	<b>[M+H]<sup>+</sup> (150)</b>	(0.10) <sup>ht</sup> (0.60) <sup>htt</sup>	(6.67) <sup>ht</sup>
MA (149.24) spiked in human urine	<b>[M+H]<sup>+</sup> (150)</b>	(1 $\times$ 10 <sup>3</sup> ) <sup>d</sup> , (0.04) <sup>ht</sup>	(5.73) <sup>ht</sup>
MDA (179.22)	<b>[M+H]<sup>+</sup> (180)</b>	(0.80) <sup>ht</sup> (3.00) <sup>htt</sup>	(14.05) <sup>ht</sup>
MDA (179.22) spiked in human urine	<b>[M+H]<sup>+</sup> (180)</b>	(0.40) <sup>ht</sup>	(8.56) <sup>ht</sup>
MDMA (193.25)	<b>[M+H]<sup>+</sup> (194)</b>	(0.60) <sup>ht</sup> (1.00) <sup>htt</sup>	(11.72) <sup>ht</sup>
MDMA (193.25) spiked in human urine	<b>[M+H]<sup>+</sup> (194)</b>	(0.20) <sup>ht</sup>	(7.92) <sup>ht</sup>
HMTD (208.17)	<b>[M+H]<sup>+</sup> (209)</b>	(19.38 $\pm$ 0.85) <sup>a*</sup> , (30.25 $\pm$ 2.72) <sup>a**</sup> , (200) <sup>b</sup> , (3 $\times$ 10 <sup>3</sup> ) <sup>d</sup>	(4.41) <sup>a*</sup> , (9.00) <sup>a**</sup>
RDX (222.12)	<b>[M+NO<sub>2</sub>]<sup>-</sup> (268)</b> <b>[M+NO<sub>3</sub>]<sup>-</sup> (284)</b>	(29.63 $\pm$ 1.31) <sup>a*</sup> , (50.75 $\pm$ 4.29) <sup>a**</sup> , (200) <sup>b</sup> , (5 $\times$ 10 <sup>3</sup> ) <sup>c</sup> , (50) <sup>d</sup> , (2 $\times$ 10 <sup>3</sup> ) <sup>f</sup> , (30) <sup>g</sup>	(4.44) <sup>a*</sup> , (8.46) <sup>a**</sup>
HMX (296.16)	<b>[M+NO<sub>2</sub>]<sup>-</sup> (342)</b> <b>[M+NO<sub>3</sub>]<sup>-</sup> (358)</b>	(100.13 $\pm$ 4.66) <sup>a*</sup> , (900) <sup>b</sup>	(4.66) <sup>a*</sup>
AN (80.05)	<b>[HNO<sub>3</sub>+NO<sub>3</sub>]<sup>-</sup> (125)</b>	(200.25 $\pm$ 9.04) <sup>a*</sup> , (2 $\times$ 10 <sup>3</sup> ) <sup>b</sup> , (10 $\times$ 10 <sup>3</sup> ) <sup>c</sup>	(4.52) <sup>a*</sup>

Reproduced under permission from ACS (Habib et al., 2014) and Elsevier (Bi et al., 2021).

<sup>a</sup>Bi et al. (2021) (Limits of detection in the present study (LODs: S/N = 3:1) and relative standard deviation (RSD %) using PFA\* and wooden\*\* substrate). <sup>b</sup> Habib et al. (2014). <sup>c</sup> Usmanov et al. (2013). <sup>d</sup> Usmanov and Hiraoka (2016). <sup>e</sup> Jackson et al. (2010). <sup>f</sup> Justes et al. (2007). <sup>g</sup> Garcia-Reyes et al. (2011). <sup>h</sup> Habib et al. (2020) (Limits of detection in the present study (LODs: S/N = 3:1) and relative standard deviation (RSD %) using (K<sub>2</sub>CO<sub>3</sub>+NH<sub>3</sub>)<sup>†</sup> and (K<sub>2</sub>CO<sub>3</sub>)<sup>††</sup> solutions).

The limits of detection (LODs) of the compounds of interest have been estimated on the basis of the bold underlined peaks.

heated filament-based desorption method (154°C) and the fragmented peak appeared as a protonated at *m/z* 182, [M+H-C<sub>6</sub>H<sub>5</sub>COOH]<sup>+</sup> (Figure 6C) while morphine (Figure 6A) and/or codeine (Figure 6B) did not show any considerable fragmentation using the same desorption system at 154°C (Usmanov et al., 2013). However, morphine underwent fragmentation as the filament temperature increased from 154 to 200°C and appeared at *m/z* 268, [morphine-H<sub>2</sub>O+H]<sup>+</sup> (Usmanov et al., 2013). They also found poor levels of LODs for the drugs of abuse using the heated filament-based desorption method coupled with the homemade He-DBDI-MS system (Table 1).

Therefore, it is concluded that coupling the cutter blade-based desorption method with the homemade He-DBDI-MS system will be a dignified analytical tool for detection of the non-volatile illicit drugs such as morphine, cocaine, codeine etc. at ultra-trace levels even from body fluids.

## Analysis of Explosives

Exactly, 2  $\mu$ L of the explosive compound of interest in acetonitrile solution was deposited on PFA substrate and dried in air.

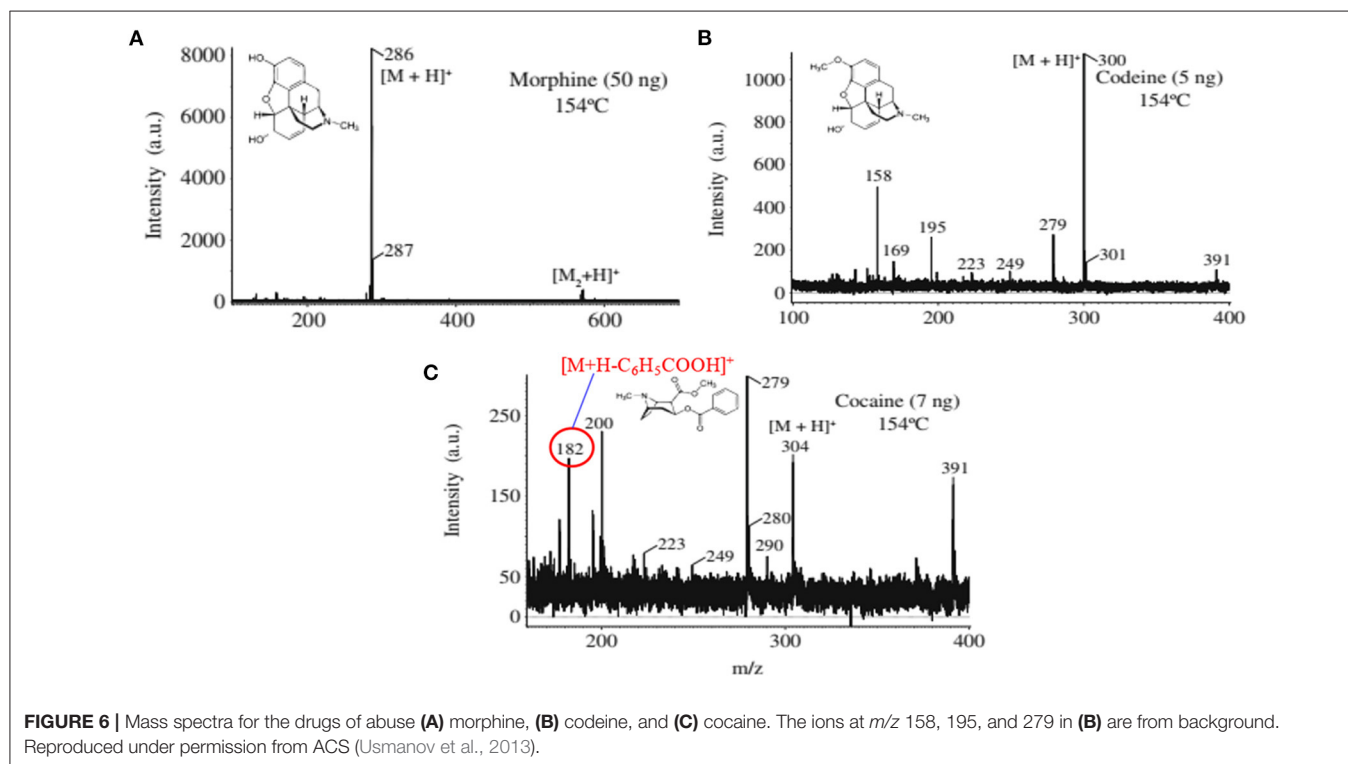
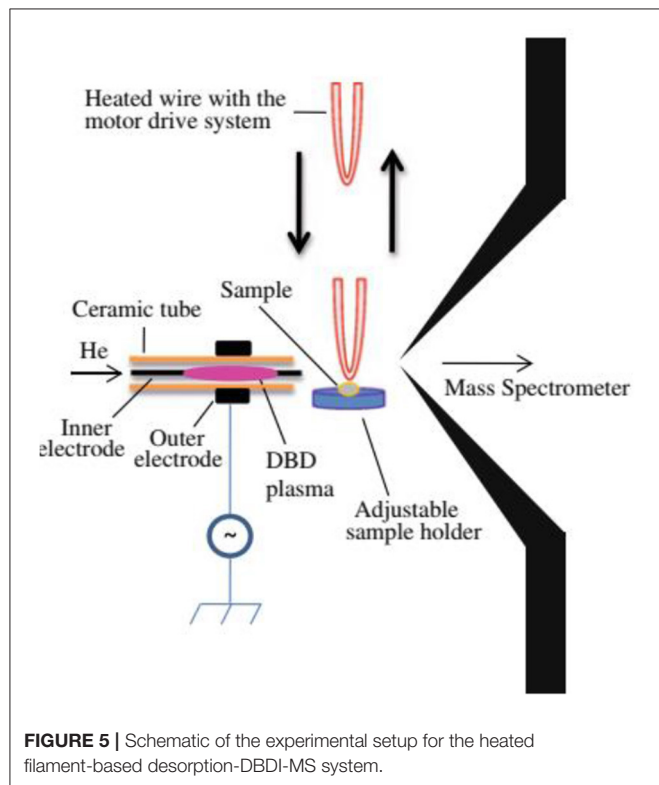
An ultrasonic cutter blade was used to desorb the deposited molecules into the gaseous phase by gentle touches with the PFA's surface. The gaseous analyte molecules were then ionized using a homemade He-DBDI and detected by an ion trap MS. Figure 7A shows the positive mass spectrum for 2 ng HMTD and Figures 7B–D show the negative mass spectra for 10 ng AN, 2 ng RDX, and 2 ng HMX, respectively. As seen from Figure 7A, HMTD gave the protonated ion, [M+H]<sup>+</sup>, that appeared at *m/z* 209. The origin of the peak that appeared at *m/z* 158 has been confirmed with and without laboratory hand gloves. It was confirmed that laboratory hand gloves is the origin of the peak that appeared at *m/z* 158 (Habib et al., 2013, 2014, 2015, 2020). The other peaks in Figure 7A were not identified.

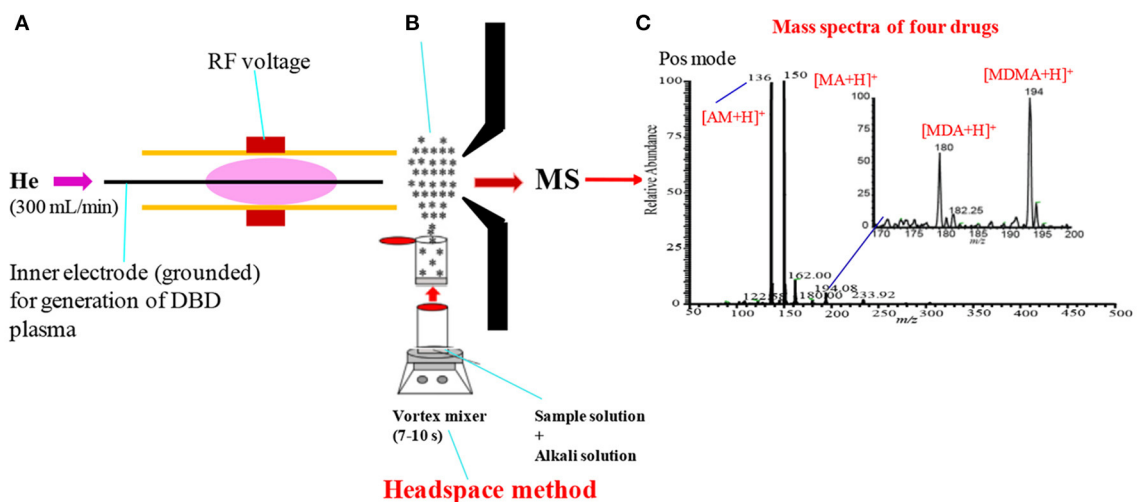
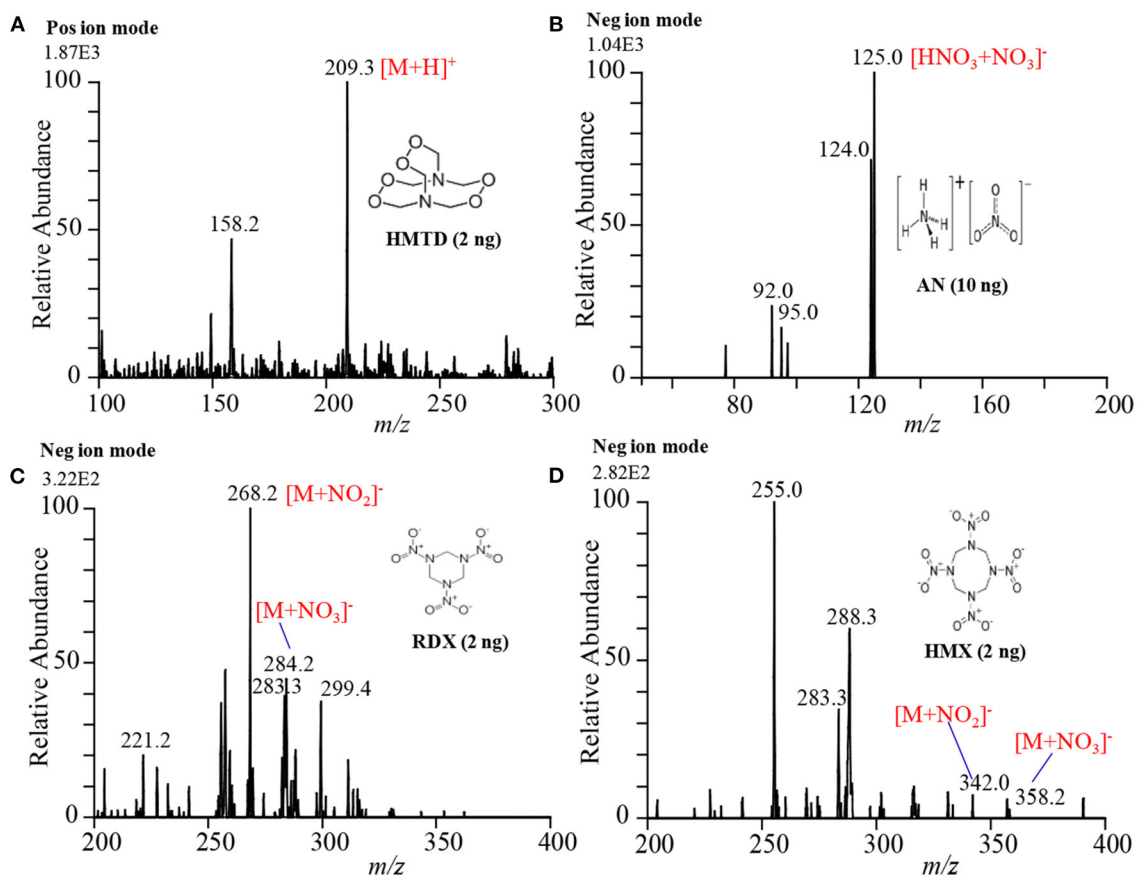
In contrast, RDX and HMX were detected as adduct ions with NO<sub>2</sub><sup>-</sup> and NO<sub>3</sub><sup>-</sup> such as [RDX+NO<sub>2</sub>]<sup>-</sup> (*m/z* 268), [HMX+NO<sub>2</sub>]<sup>-</sup> (*m/z* 342), [RDX+NO<sub>3</sub>]<sup>-</sup> (*m/z* 284), [HMX+NO<sub>3</sub>]<sup>-</sup> (*m/z* 358) in the negative mode ionization as shown in Figures 7C,D, respectively. Ammonium nitrate (AN), however, was detected as a cluster ion of HNO<sub>3</sub> with NO<sub>3</sub><sup>-</sup>, [HNO<sub>3</sub>+NO<sub>3</sub>]<sup>-</sup>, (see Figure 7B). It is noted that the reactant ions NO<sub>3</sub><sup>-</sup> and NO<sub>2</sub><sup>-</sup> were the major background ions formed

by the present ambient He-DBD ion source under the ambient conditions. The presence of the plenty of  $\text{NO}_2^-$  and  $\text{NO}_3^-$  ions was facilitating the formation of the adduct/cluster ions of RDX

and HMX and also the adduct ion of  $\text{HNO}_3$  with the  $\text{NO}_3^-$  for AN. Both the  $\text{NO}_2^-$  and  $\text{NO}_3^-$  ions have trigonal planar geometry and the oxygen atoms of each ion are highly negatively charged. The nitrogen atoms of the nitro ( $\text{NO}_2$ ) groups in the RDX and HMX molecules carry highly electropositive charge, thus they must form multidentate electrostatic bonds with the negatively  $\text{NO}_2^-$  and  $\text{NO}_3^-$  ions, thereby resulting in the formation of the cluster/adduct ions for RDX and HMX with these nitroxo anions (Usmanov et al., 2013; Habib et al., 2014; Bi et al., 2021). However, AN directly doesn't form any cluster ion with the  $\text{NO}_2^-$  and/or  $\text{NO}_3^-$  ion, rather it forms a cluster ion of  $\text{HNO}_3$  with the  $\text{NO}_3^-$  ion. Ammonium nitrate dissociates into  $\text{NH}_3$  and  $\text{HNO}_3$  in the DBD plasma as follows:  $\text{NH}_4\text{NO}_3 \rightarrow \text{NH}_3 + \text{HNO}_3$  (Usmanov et al., 2013; Habib et al., 2014). The formed  $\text{HNO}_3$  then forms cluster/adduct ion with the  $\text{NO}_3^-$  ion,  $[\text{HNO}_3 + \text{NO}_3]^-$ , that appeared at  $m/z$  125 (Usmanov et al., 2013; Habib et al., 2014; Bi et al., 2021).

It is suggested that the proton of the  $\text{HNO}_3$  molecule acts as a bridge between the two  $\text{NO}_3^-$  ions. Analytical curves for the explosives of interest were made in order to evaluate the performance of the developed tribological desorption as well as the homemade He-DBDI methods. The values of limit of detection (LODs) are shown in Table 1. Other ambient ionization methods such as DESI (Takáts et al., 2005), EESI (Chen et al., 2009), DBDI (Zhang et al., 2009; Garcia-Reyes et al., 2011) have also been used for the detection and quantification of explosive compounds. It seems that the developed ultrasonic cutter-based tribodesorption (TD) method can work for efficient non-thermal desorption of the non-volatile drugs of abuse as well as explosives. The coupling of the tribodesorption with DBDI





must have potentiality for trace-level detection of non-volatile drugs of abuse and explosives from analytical point of view.

Among the MS systems, ultrasonic cutter blade-based desorption process coupled with the He-DBDI-MS system exhibited as a promising analytical tool for analysis of highly non-volatile explosive compounds at ultra-trace levels (Habib et al., 2014; Bi et al., 2021). Further attempts have already been taken to fabricate a commercial hybrid MS system through combination of the ultrasonic cutter blade, He-DBD ion source and an ion trap MS for analysis of highly non-volatile compounds such as drugs of abuse, explosives etc. at ultra-trace levels.

## HEADSPACE-DIELECTRIC BARRIER DISCHARGE (DBD) IONIZATION-MS SYSTEM

Amphetamines belong to an amine group under the aliphatic compounds and they can significantly stimulate the central nervous system. Of them, amphetamine (AM) and methamphetamine (MA) and their methylenedioxy derivatives such as 3,4-methylenedioxyamphetamine (MDA) and 3,4-methylenedioxy methamphetamine (MDMA) are the main amphetaminic compounds that have been commonly used by athletes, drug addicts and recreational users as stimulants (Perez-Reyes et al., 1991; Ropero-Miller and Goldberger, 1998). Therefore, rapid detection of illicit drugs such as amphetaminic compounds in urine is very much needed in order to examine the consumption of these illicit drugs by the athletes as well as the young population in developing countries like Bangladesh, Myanmar, India, Thailand, China etc.

**Figure 8** shows an experimental setup of the headspace-He-DBDI coupled with MS system for gasification of amphetaminic drugs of abuse through headspace method. The presence of amine and/imine groups in the amphetaminic compounds causes their volatility, thus these compounds treat with hydrochloric acid (HCl) in order to provide their stability. The addition of hydrochloric acid causes the formation of the quaternary cationic nitrogen centered where chloride ( $\text{Cl}^-$ ) acts as a counter ion, thereby resulting in gaining stability of the amphetaminic compounds. Thus, alkali treatment of the quaternary amphetaminic compounds ceases the free base amphetaminic compounds into gaseous phase that is called as a headspace method. In the present section, the headspace method was applied for the gasification of the amphetaminic compounds spiked raw urine. Herein, MA, MA, 3,4-methylenedioxyamphetamine (MDA) and 3,4-methylenedioxymethamphetamine (MDMA) were taken as model compounds to evaluate the analytical performance of the headspace-DBDI-MS system. These amphetaminic compounds were spiked in raw urine and treated with non-carbonated (e.g., NaOH, KOH etc.) and carbonated ( $\text{Na}_2\text{CO}_3$ ,  $\text{K}_2\text{CO}_3$  etc.) alkali solutions (Habib et al., 2020). **Figure 5B** shows such an example of headspace method. **Figure 5C** shows positive headspace-DBDI mass spectra for a mixture of AM, MA, MDA, and MDMA in aqueous solution. As seen from **Figure 5C**, both the AM and MA show their protonated ions,  $[\text{AM}+\text{H}]^+$ ,  $[\text{MA}+\text{H}]^+$ , as the

major ions, and MDA and MDMA also provide their protonated ions,  $[\text{MDA}+\text{H}]^+$ ,  $[\text{MDMA}+\text{H}]^+$ , but with much weaker ion signals. This is because of the difference in vapor pressures of the amphetaminic compounds as described in the following section (Habib et al., 2020).

As mentioned above, amphetamine compounds are aliphatic amines, thus they are either volatile and/or semi-volatile in nature. According to the literature, the vapor pressures of AM, MA, MDA, and MDMA are  $310.0 \times 10^{-3}$ ,  $5.4 \times 10^{-3}$ ,  $1.0 \times 10^{-3}$ , and  $1.6 \times 10^{-3}$  mm of Hg at  $25^\circ\text{C}$ , respectively (Habib et al., 2020). Amphetamine compounds are mainly aliphatic amines thus, they have positive proton affinity. Accordingly, they convert into quaternary amines just mixing with hydrochloric acid where chloride ( $\text{Cl}^-$ ) ion acts as a counter ion. Formation of the quaternary amines prevents the volatility of the amphetamines that provides their better stability. Addition of alkali solution to the quaternary amines evolves gaseous free base amines because of their considerable vapor pressures at room temperature. The homemade He-DBDI seems as an atmospheric pressure chemical ionization (APCI) because of formation of hydronium ion,  $\text{H}_3\text{O}^+$ , in the positive mode of operation (Habib et al., 2014, 2020). In addition, the proton affinity (PA) of this group of compounds is quite high i.e., PA for MA is 965 kJ/mol, and follows the increasing order:  $\text{AM} < \text{MDA} < \text{MA} < \text{MDMA}$  (Matsumura et al., 2003). Thus, these compounds efficiently form their protonated molecular ion,  $[\text{M}+\text{H}]^+$ , in the positive ion mode.

**Figures 9A–D<sub>1</sub>** show the positive headspace-DBDI mass spectra for AM, MA, MDA, and MDMA, respectively. The values at the top-left corner in each spectrum indicate the intensities of the ions of interest. **Figures 9A, A<sub>1</sub>** show the positive mass spectra for AM in water and spiked raw urine, respectively. As seen from **Figures 9A, A<sub>1</sub>**, the ion intensity for the  $[\text{AM}+\text{H}]^+$  ion is relatively higher for AM spiked urine than that for water, however, the presence of urea, creatinine in raw urine suppress the ion signals of the analytes of interest (Habib et al., 2020). Similar observation was also observed for MA (see **Figures 9B, B<sub>1</sub>**), MDA (see **Figures 9C, C<sub>1</sub>**) and MDMA (see **Figures 9D, D<sub>1</sub>**). The volatile components of the raw urine (e.g., urea, creatinine etc.) play crucial roles for the better sensitivity of these amphetaminic compounds. Addition of NaOH and/or KOH to the solution of the relevant compound, the quaternary nitrogen converts to free base amine where the volatile urine components act as carrier gas to bring the free base amine to the gas phase. However, urine's components must cause ion suppression of the analytes of interest. In this study, non-carbonated and carbonated alkali solutions were used for the ceasing amphetaminic compounds in the headspace method (Habib et al., 2020).

It is noted that carbonated alkali solution enhances the sensitivity for these amphetaminic compounds. The quaternary nitrogen containing amine compounds are acidic in nature, thus, a reaction might occur between the acidic amphetaminic compounds and the alkali  $\text{Na}_2\text{CO}_3$  or  $\text{K}_2\text{CO}_3$ , thereby resulting in the formation of gaseous  $\text{CO}_2$  as well as free base amines. The generation of gaseous  $\text{CO}_2$  in *in-situ* acts as a carrier gas for the free base amines. A trace amount of ammonia solution



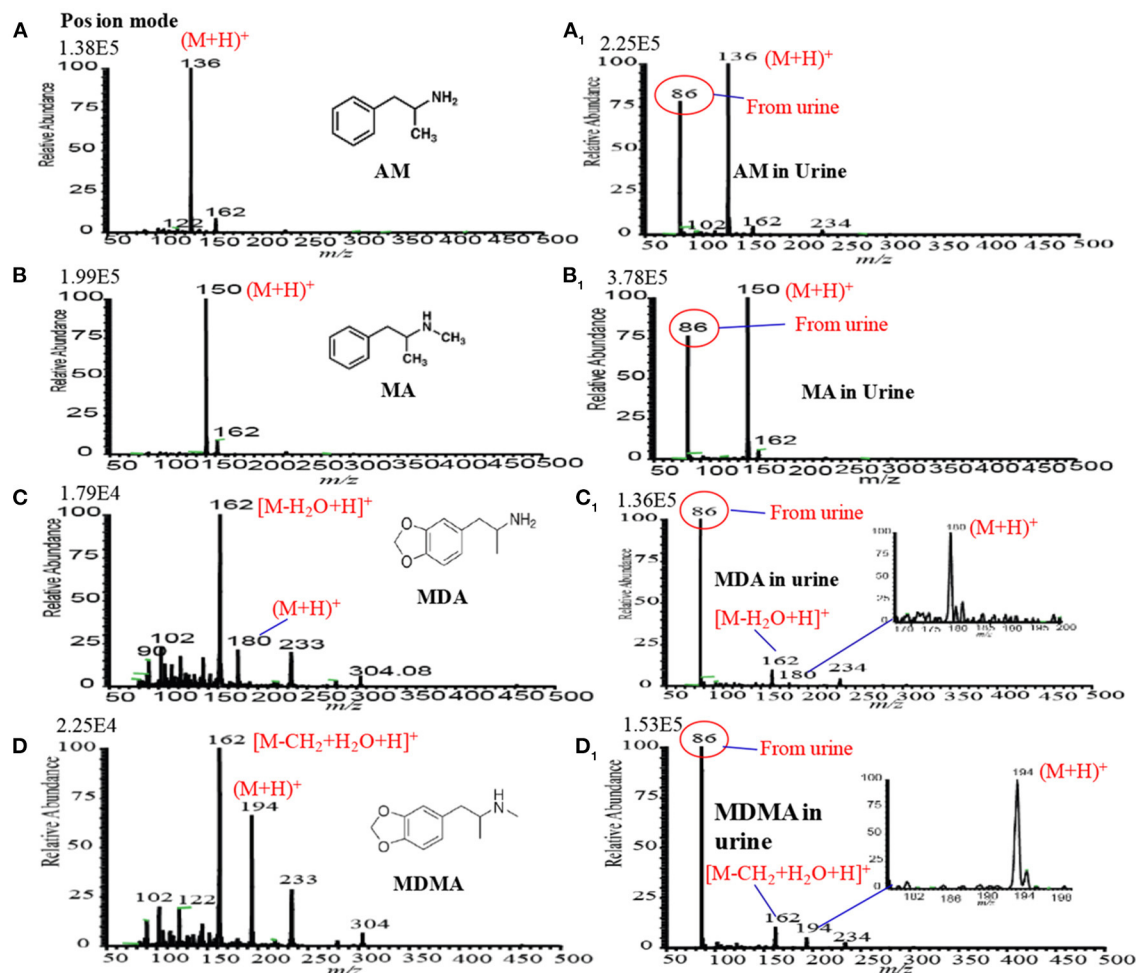


**FIGURE 9 |** Mass spectra for (A) amphetamine (AM), (A<sub>1</sub>) amphetamine in urine, (B) methamphetamine (MA), (B<sub>1</sub>) methamphetamine (MA) in urine, (C) 3,4-methylenedioxymphetamine (MDA), (C<sub>1</sub>) 3,4-methylenedioxymphetamine (MDA), (D) 3,4-methylenedioxymethamphetamine (MDMA) and (D<sub>1</sub>) (D) 3,4-methylenedioxymethamphetamine (MDMA) measured by headspace-DBDI-MS system. Amount of each amphetamine compound was 1 ng/mL in water as standard and spiked in raw urine and then treated by equal volume of ammoniated K<sub>2</sub>CO<sub>3</sub> solution [85% K<sub>2</sub>CO<sub>3</sub> (4 M) + 15% NH<sub>3</sub> (28%)]. Reproduced under permission from Elsevier (Habib et al., 2014).

with the alkali solution also causes better sensitivity for the amphetaminic compounds. To find the quantitative capabilities of the headspace-DBDI-MS system, analytical validation such as LOD, precision, linear range correlation coefficient ( $R^2$ ) and analyte recovery rate were investigated with three replicates ( $n = 3$ ). Peak intensities, with the signal-to-noise ratio (S/N) of at least 3, the protonated molecular ion,  $[M+H]^+$ , of the analyte of interest were used to construct the analytical calibration curves. Each of the points in the calibration curve was at least three in replication. The minimum amount of the calibration curve has been considered as the LOD of the analyte of interest. It is noteworthy to mention that amphetamine compounds spiked in raw urine exhibited better LOD compared to the corresponding standard solutions. The values of LOD for the AM, MA, MDA, and MDMA from standard and spiked in urine are tabulated in Table 1 (Habib et al., 2020). Therefore, it is concluded that the developed headspace-DBDI system can be applied for trace level detection of amphetaminic compounds even from biological

samples like urine, but the method may not be suitable for the non-volatile drugs of abuse such as morphine, cocaine, codeine, heroin etc.

In summary, the presence of amine and/or imine groups in the amphetaminic compounds makes them suitable for the headspace method in order to desorb into the gaseous phase which is the mandatory step for ionization in MS. On the other hand, morphine, cocaine, codeine, heroin etc. are rather non-volatile compounds and they do not have any amine and/or imine groups, thus these drugs of abuse compounds need mechanical and/or thermal desorption method rather than chemical treatment as described in the preceding section.

## HOLLOW CATHODE DISCHARGE (HCD) IONIZATION-MS SYSTEM

In mass spectrometry, ion source plays a vital role for detection and quantification of analytes of interest at trace to ultra-trace

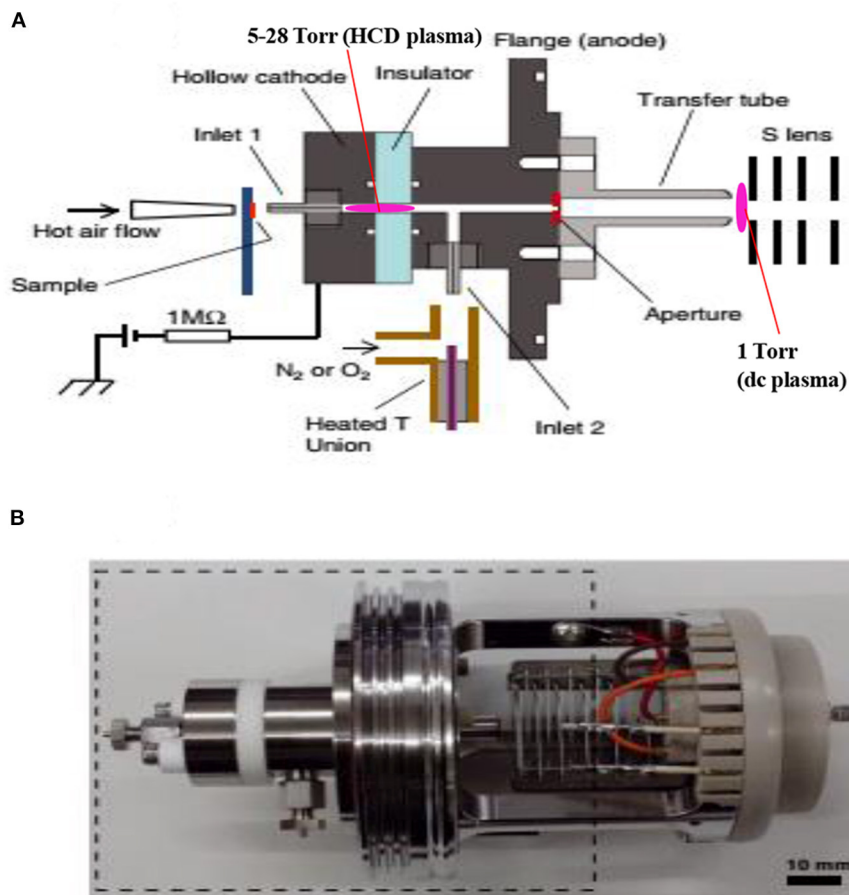


**FIGURE 10 |** A schematic of the fabricated hollow cathode discharge (HCD) ion source **(A)**. The length of cathode electrode is 5 mm and its inner diameter is 2 mm. An insulator made of aluminum oxide (5 mm thick) is for separation of the cathode and anode. An aperture with 1 mm diameter is for getting ions into the 1 Torr vacuum stage is 1 mm. A stainless steel capillary (ion transfer tube) with an i.d. of 4 mm is used to transfer ions from the ion source to the S-lens. The difference between the aperture and the exit of the transfer tube is 24 mm. There is a ~3 mm gap between the edge of the transfer tube and the first electrode of the S-lens. A photograph for the HCD ion source **(B)**. The dotted-line box around the portion of the photograph shows part **(A)**. Reproduced under permission from Wiley (Habib et al., 2015).

levels. Hence, much attention has been paid to fabricate new ion sources for MS that can efficiently ionize the compounds of interest, thereby resulting in realizing ultra-trace level detection. Herein, a hollow cathode discharge (HCD) ion source has been fabricated for the detection of mainly explosives. A schematic of the HCD ion source is shown in **Figure 10A** where **Figure 10B** stands for its photograph. The salient feature of the developed HCD ion source is air its carrier gas instead of rare gases like He or Ar, thus HCDI-MS system can deploy at public places such as airports, railway stations, cultural sites etc. for characterization of explosives. The use of air as a carrier gas in the HCD ion source can also ensure no need for periodic change of reagent gas. The HCD ion source was kept as turned on condition at 5 Torr using air as a carrier gas for a month in order to evaluate its robustness and found no severe corrosion inside of the electrodes or insulators with naked eye.

As seen from **Figure 10A**, the ion source has two inlets for introducing samples under ambient conditions. The inlets made

of stainless steel capillary with the length and inner diameter (i.d.) are 10 and 0.25 mm, respectively. The HCD ion source consists of two metallic electrodes made of stainless steel. The two electrodes are separated by an insulator made of ceramic with 5 mm thick. The inlet-1 is connected to the cathode while inlet-2 is connected to the flange of the ion source that acts as an anode (**Figure 10A**). Inlet-1 is used for ambient sampling throughout the experiments while the inlet-2 closed. A high-voltage power supply (Pulse Electronic Engineering Co. Ltd, Chiba, Japan) was connected to the cathode (length: 2 mm; i.d.: 2 mm) while the flange of the ion source (stainless steel) that acted as an anode was kept at ground potential.

According to the design of the HCD ion source, the ion source pressure can be varied using an aperture of 1 mm diameter by placing it between the flange and the transfer tube (**Figure 10A**). The gas pressure in the HCD ion source was measured through installing a pressure gauge (SMC, Tokyo, Japan) at the port of inlet-2. The pressure gauge showed a gas pressure of 28 Torr

by placing the aperture between the flange and the transfer tube while that was 5 Torr when the aperture was removed. The flow rate of air through the inlet-1 was calculated in order to know an empirical flow rate of the analyte of interest and the calculated flow rate was found to be  $\sim 360$  mL/min. The ions formed in the HCD ion source were transferred using a transfer tube made of stainless steel to the S-lens of a linear ion trap mass spectrometer (LTQ XL, Thermo Scientific, San Jose, CA, USA). A rotary vane pump was used to keep the pressure at 1 Torr in the first pumping stage in the MS. It is noted that an ion trap mass spectrometer requires high vacuum conditions in order to run the MS properly.

A high-voltage power was applied to the cathode to generate HCD plasma. The potential was just above the threshold of the gaseous breakdown voltage to stabilize the HCD glow. The potential and current were kept constant at  $-1.30$  kV ( $0.3$  mA) and  $-1.62$  kV ( $0.3$  mA) for the ion source pressures 5 and 28 Torr, respectively. Herein, the discharge current was kept relatively at low in order to facilitate soft ionization of the labile explosives while Ganeev et al. (2007) reported that the HCD ion source can be operated within a wide range from a few mA to several hundreds of mA (Ganeev et al., 2007).

As seen from **Figure 10A**, a dc plasma was generated between the transfer tube and the S-lens by applying  $+0.85$  kV ( $0.12$  mA) and  $-0.85$  kV ( $0.15$  mA) to the transfer tube in the positive and negative ion modes, respectively under 1 Torr ion source pressure in order to investigate the ionization mechanism of the relevant explosives with ion source pressure. A linear ion trap mass spectrometer was used to monitor the ions generated by the HCD ion source for the explosives of interest through adjusting the instrumental settings as follows:  $150$ – $200^\circ\text{C}$  for ion transport tube;  $80\%$  for S-lens and  $600$ – $800$  V for RF ion guide voltage. The auto gain control was enabled with a maximum ion injection time of  $2$  ms, and the number of micro scans was  $1$ . A tandem mass spectrometry (MS/MS) mode was used for characterization of the ions formed from the explosive compounds. Herein, the collision-induced dissociation (CID) mode with the collision energy within a range from  $20$  to  $50\%$  was used where helium was used for collision (Habib et al., 2015).

A microscopic glass slide was used as a sample holder. Exactly  $2$   $\mu\text{L}$  solution of the relevant explosive was deposited on the slide and kept for air drying. The sample spot diameter was  $\sim 2$  mm. An air heater (ranging from  $150$  to  $225^\circ\text{C}$ ) attached with a quartz nozzle (i.d.  $2$  mm) was used to vaporize the solid compounds through heating from the backside of the sample spot. A thermocouple was used to observe the heater temperature. The solid explosives were gasified by using the hot air except TATP. This explosive was kept in a glass vial like a headspace because of its high vapor pressure at room temperature and then introduced into the ion source for ionization through the inlet-1 (**Figure 10A**).

To evaluate the quantitative capabilities of the fabricated HCD ion source, analytical validation, for example, limit of detection (LOD), precision and linear range of coefficient of determination ( $R^2$ ) were investigated with at least four replications ( $n = 4$ ). Peak areas for the relevant ions, as shown underlined in **Table 1**, were used to construct the analytical calibration curves for HMTD,

RDX, PETN, and TNT. The values of the LOD for the explosive compounds of interest were based on a signal-to-noise ratio (S/N) of at least  $3$  (Habib et al., 2015). The constructed calibration curves exhibited about two orders of magnitude of their linear range with reproducible signal intensities.

The hollow cathode discharge (HCD) ion source has been fabricated in order to analyze the explosive compounds as shown in **Table 2**. Mass spectra for TATP and HMTD in the positive ion mode and that for RDX, PETN, TNT, and NG in the negative ion mode were measured through adjusting the ion source pressures at  $1$ ,  $5$ , and  $28$  Torr. The ion source temperatures for analysis of the explosives are also tabulated in **Table 2** (Habib et al., 2015).

**Figures 11A,B** show the background mass spectra for the HCD ion source recorded at  $5$  Torr in the positive and negative ion modes, respectively. As seen from **Figures 11A,B**, oxygen molecular ion,  $\text{O}_2^+$  ( $m/z$   $32$ ), and protonated acetone,  $[(\text{CH}_3)_2\text{CO}+\text{H}]^+$  ( $m/z$   $59$ ), are the major ions in the positive ion mode while  $\text{NO}_2^-$  ( $m/z$   $46$ ),  $\text{CO}_3^-$  ( $m/z$   $60$ ), and  $\text{NO}_3^-$  ( $m/z$   $62$ ) ions are observed as the major ions in the negative mode of operation. In the positive ion mode, protonated acetone,  $[(\text{CH}_3)_2\text{CO}+\text{H}]^+$  ( $m/z$   $59$ ), as the base peak is reasonable. This is because laboratory air is commonly contaminated with organic solvent such as acetone, ethanol, methanol, ammonia etc. The formation of the protonated acetone,  $[(\text{CH}_3)_2\text{CO}+\text{H}]^+$ , ion acts as the major reagent ion for the protonation of TATP and HMTD in the positive ion mode. The ambient air molecules became excited by the HCD plasma that causes the formation of the  $\text{NO}_2^-$ ,  $\text{CO}_3^-$  and  $\text{NO}_3^-$  ions and appeared in the negative ion mode as shown in **Figure 11B**. Sekimoto and Takayama (2010) described the mechanism of formation of the  $\text{NO}_2^-$ ,  $\text{CO}_3^-$  and  $\text{NO}_3^-$  ions in the plasma-excited air as well (Sekimoto and Takayama, 2010). Other background signals in **Figure 11** were not identified.

In conclusion, the fabricated HCD ion source was applied to analyze explosives such as TATP, HMTD, RDX, PETN, TNT, and NG at different ion source pressures in order to investigate ion formation mechanisms. The formation of protonated acetone,  $[(\text{CH}_3)_2\text{CO}+\text{H}]^+$ , as a reagent ion in the positive ion mode facilitates the formation of the protonated compounds of interest such as  $[\text{HMTD}+\text{H}]^+$ ,  $[\text{TATP}+\text{H}]^+$ , and its protonated fragment ion,  $[\text{C}_3\text{H}_6\text{O}_3+\text{H}]^+$  ( $m/z$   $91$ ) etc. while the formation of  $\text{NO}_2^-$ ,  $\text{NO}_3^-$  in the negative ion mode causes the formation of cluster ions of RDX, PETN and also dehydrogenated of TNT,  $[\text{TNT}-\text{H}]^-$  ( $m/z$   $226$ ) etc.

## Mass Spectra of Explosives by HCD Ion Source in Positive Ion Mode

**Figures 12A,A<sub>1</sub>** show the mass spectra for the headspace TATP measured by the HCD ion source in the positive ion mode at  $5$  and  $28$  Torr ion source pressure, respectively. As seen from **Figures 12A,A<sub>1</sub>**, TATP showed the protonated fragment ion,  $[\text{C}_3\text{H}_6\text{O}_3+\text{H}]^+$ , that appeared at  $m/z$   $91$  as the major ion along with another protonated fragment ion,  $[\text{C}_3\text{H}_6\text{O}_2+\text{H}]^+$  ( $m/z$   $75$ ) and protonated molecular ion,  $[\text{TATP}+\text{H}]^+$  ( $m/z$   $223$ ) as the minor ions, however, a new peak for the ammoniated TATP,  $[\text{TATP}+\text{NH}_4]^+$ , was observed at  $m/z$   $240$  when the ion source pressure was kept at  $28$  Torr. In a blank experiment by

**TABLE 2 |** Limits of detection (LODs) (pg) and observed ions ( $m/z$  values in parentheses) for the explosives examined at three ion source pressures.

Ions observed at three ion source pressures with $m/z$ values in the ion source parentheses				LOD (pg) at three ion source pressures (Torr)		
Compounds (molecular mass)	Temperature 1 Torr (°C)	5 Torr	28 Torr	1	5	28
TATP (222)	150	$[\text{C}_3\text{H}_6\text{O}_2+\text{H}]^+$ (75) <b><math>[\text{C}_3\text{H}_6\text{O}_3+\text{H}]^+</math> (91)</b>	$[\text{C}_3\text{H}_6\text{O}_2+\text{H}]^+$ (75) <b><math>[\text{C}_3\text{H}_6\text{O}_3+\text{H}]^+</math> (91)</b> $[\text{M}+\text{NH}_4]^+$ (240)	-	-	-
HMTD (208)	180	<b><math>[\text{M}+\text{H}]^+</math> (209)</b> $[\text{M}-\text{CH}_2\text{O}]^+$ (179)	<b><math>[\text{M}+\text{H}]^+</math> (209)</b> $[\text{M}-\text{CH}_2\text{O}]^+$ (179)	-	100	20
TNT (227)	150 <b><math>\text{M}^-</math> (227)</b> $[\text{M}-\text{NO}]^-$ (197) $[\text{M}-\text{OH}]^-$ (210)	$\text{M}^-$ (227) <b><math>[\text{M}-\text{H}]^-</math> (226)</b> $[\text{M}-\text{NO}]^-$ (197) $[\text{M}-2\text{NO}]^-$ (167) $[\text{M}-3\text{NO}]^-$ (137) $[\text{M}-\text{H}+\text{O}]^-$ (242)	$[\text{M}-\text{H}]^-$ (226) $[\text{M}+\text{H}]^-$ (228) <b><math>[\text{M}-\text{H}+\text{O}]^-</math> (242)</b>	2	50	70
NG (227)	150		<b><math>[\text{M}+\text{NO}_3]^-</math> 289</b>	-	-	300
PETN (316)	180	<b><math>[\text{M}-\text{CH}_2\text{ONO}_2]^-</math> (240)</b> $[\text{M}+\text{NO}_3]^-$ (378)	<b><math>[\text{M}-\text{CH}_2\text{ONO}_2]^-</math> (240)</b> $[\text{M}+\text{NO}_2]^-$ (362) <b><math>[\text{M}+\text{NO}_3]^-</math> (378)</b>	1000	1000	800
RDX (222)	180	$[\text{M}-\text{NO}_2-\text{CH}_2\text{NNO}_2]^-$ (102) <b><math>[\text{M}-\text{NO}_2-\text{HNO}_2]^-</math> (129)</b> $[\text{M}-\text{NO}_2]^-$ (176)	<b><math>[\text{M}-\text{NO}_2-\text{HNO}_2]^-</math> (129)</b> $[\text{M}+\text{NO}_2]^-$ (268) $[\text{M}+\text{NO}_3]^-$ (284)		30	40

Bold type indicates the major ion. The ions used to obtain analytical curves are underlined.

Reproduced under permission from Wiley (Habib et al., 2015).

introduction of methanol to the ion source, however, there were no ions observed at  $m/z$  91 and 75. By using the ac/dc-APCI, we also found the ammoniated TATP,  $[\text{TATP}+\text{NH}_4]^+$  ( $m/z$  240), ion in the positive mode of operation (Habib et al., 2013). This is because of the contamination of laboratory air by the ammonia used in chemical laboratories for different purposes. The presence of ammonia in the laboratory air causes the formation of the adduct ion of the TATP with ammonia,  $[\text{TATP}+\text{NH}_4]^+$  ( $m/z$  240). The appearance of the adduct ion at 28 Torr is logical because of presence of requisite level of ammonia at high ion source pressure, 28 Torr, that facilitates the formation of the  $[\text{TATP}+\text{NH}_4]^+$  ion. The formation of the adduct ion passes through its transition state complex,  $[\text{TATP}\cdots\text{NH}_4]^{+*}$  and according to transition state theory, a third-body collision is required to stabilize the intermediate transition state in order to obtain the product,  $[\text{TATP}+\text{NH}_4]^+$  ion that can be ascribed by the following equation (Laidler, 1987):



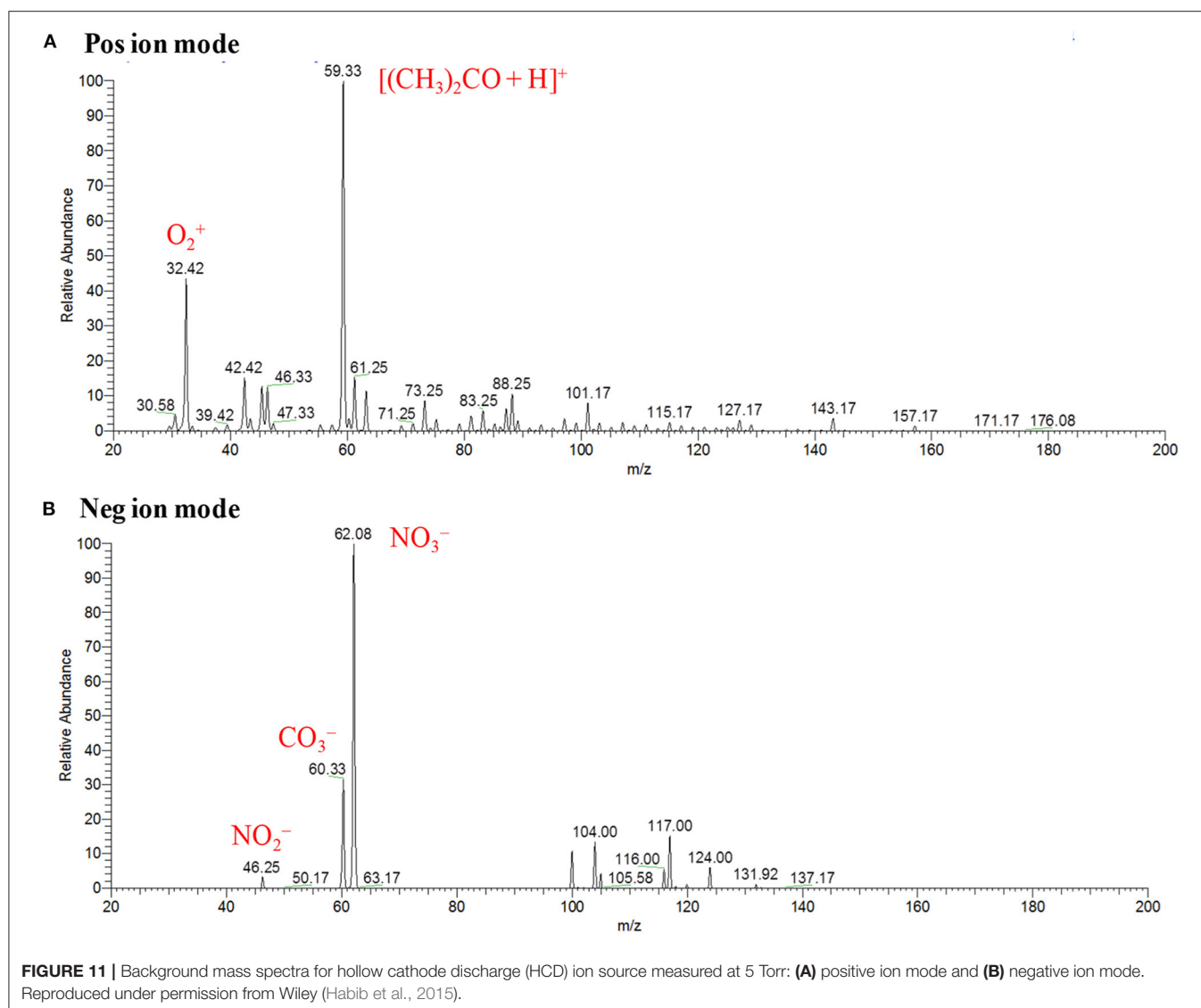
where  $\text{T}_3$  represents the third body.

Peak intensities of the relevant ion signals are shown at the upper left hand corner of the spectra. As shown in **Figure 12A**<sub>1</sub>, the intensities for the ions appeared at  $m/z$  91, 223 were enhanced by a factor 2 compared to that as shown in **Figure 12A**. It is noted that high ion source pressure assists the formation of protonated acetone,  $[(\text{CH}_3)_2\text{CO}+\text{H}]^+$  ( $m/z$  59) and/ or hydronium ion,  $\text{H}_3\text{O}^+$ , as reagent ions in the positive ion mode. The relatively high level of the reagent ions,  $[(\text{CH}_3)_2\text{CO}+\text{H}]^+/\text{H}_3\text{O}^+$ , at high ion source pressure enhances the formation of the protonated ion of the relevant compounds. Therefore, it is concluded that

plasma-based ionization methods facilitate the formation of protonated fragment ion,  $[\text{C}_3\text{H}_6\text{O}_3+\text{H}]^+$ , of the TATP that appeared at  $m/z$  91. Takada et al. (2012b) also found the protonated fragment ion for TATP,  $[\text{C}_3\text{H}_6\text{O}_3+\text{H}]^+$  ( $m/z$  91), by using counter-flow dc corona APCI (Takada et al., 2012b), however, electrospray-based ionization methods such as DESI (Cotte-Rodríguez et al., 2008), extractive electrospray ionization (EESI) (Chen et al., 2009) facilitate the formation of protonated, sodiated, and ammoniated TATP. Sigman et al. (2006) analyzed TATP by the chemical ionization, and performed a theoretical calculation using the density functional theory (DFT) in order to investigate the fragmentation pathway of the  $[\text{TATP}+\text{H}]^+$  ( $m/z$  223) ion (Sigman et al., 2006). They also reported the formation of the protonated fragment ion for the TATP,  $[\text{C}_3\text{H}_6\text{O}_3+\text{H}]^+$  ( $m/z$  91), as well.

**Figures 12B**<sub>1</sub> show the mass spectra of HMTD measured by HCD ion source at 5 and 28 Torr in the positive ion mode, respectively. Results show that HMTD appeared as its protonated molecular ion,  $[\text{HMTD}+\text{H}]^+$  ( $m/z$  209), as the major with a protonated fragment ion,  $[\text{HMTD}+\text{H}-\text{CH}_2\text{O}]^+$ , as a minor ion that appeared at  $m/z$  179 (Habib et al., 2015). It has also been reported that HMTD detected as its protonated form,  $[\text{HMTD}+\text{H}]^+$ , by using discharge-based ion sources (Chen et al., 2010; Hiraoka et al., 2010; Garcia-Reyes et al., 2011; Habib et al., 2014). As seen from **Figure 12B**<sub>1</sub>, intensity of the protonated molecular ion,  $[\text{HMTD}+\text{H}]^+$ , increased by a factor of 7 as the ion source pressure increases from 5 to 28 Torr and the ratio of  $[\text{HMTD}-\text{CH}_2\text{O}]^+ / [\text{HMTD}+\text{H}]^+$  decreased. Hiraoka (2013) also reported that the higher ion source pressure stabilizes of a nascent protonated molecular ion by a third-body collision. It is noted that electrons generated in the HCD plasma gain relatively low





kinetic energy under high gas pressure (Mavrodineanu, 1984). Therefore, it is concluded that high ion source pressure facilitates the detection of HMTD as its protonated form. The other peaks shown in **Figures 12B,B<sub>1</sub>** were not assigned.

The high ion source pressure in the HCD plasma facilitates the formation of protonated molecular and/or protonated fragment ion in the positive ion mode. This is the reason for finding the enhanced intensity for the protonated ions at higher ion source pressure for HMTD and TATP. In conclusion, the high gas pressure is desirable in the positive HCD ion source in order to detect the explosive compounds at trace levels.

## Mass Spectra of Explosives by HCD Ion Source in Negative Ion Mode

**Figures 13A,A<sub>1</sub>** show the negative mode mass spectra for 1 ng RDX measured by the HCD ion source at 5 and 28 Torr ion source pressure, respectively. As seen from **Figure 13A**, RDX

exhibited severe fragmentation at 5 Torr, thus its fragment ion,  $[RDX-NO_2-HNO_2]^-$  ( $m/z$  129), appeared as a base peak while its adduct ions,  $[RDX+NO_2]^-$  ( $m/z$  268) and  $[RDX+NO_3]^-$  ( $m/z$  284), appeared as minor ion signals. Contrary to the higher ion source pressure (28 Torr), the adduct ion of RDX with the reagent ion  $NO_3^-$ ,  $[RDX+NO_3]^-$  ( $m/z$  284), appeared as a major ion where the ion intensity of the  $[RDX+NO_3]^-$  ion was 8 times higher than that for 5 Torr. It is reasonable that the higher ion source pressure enhances the formation of the adduct ion of RDX,  $[RDX+NO_3]^-$  ( $m/z$  284). This is because the rate of formation of the reagent ions i.e.,  $NO_2^-$  and  $NO_3^-$ , in the negative ion mode increases with the ion source pressure. The presence of plenty of the reagent ions under the higher gas pressure acts as a third body that enhances the collisional probability between the RDX and  $NO_3^-$ , thus the transition state complex of RDX with  $NO_3^-$ ,  $[RDX \cdots NO_3]^{-*}$  gains adequate stabilization energy. By dc glow discharge ionization, RDX gave mostly fragment ions under 0.8 Torr of air pressure (McLuckey et al., 1996), however, adduct



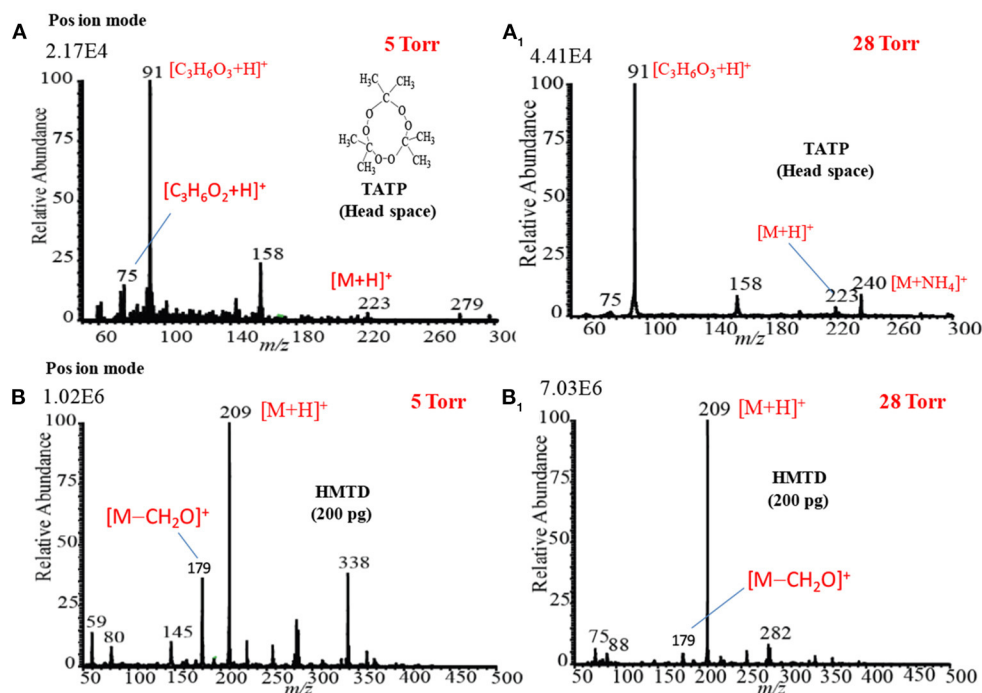


**FIGURE 12** | Positive ion mode hollow cathode discharge (HCD) mass spectra for **(A)** TATP (headspace) measured at 5 Torr, **(A1)** TATP (headspace) measured at 28 Torr, **(B)** HMTD (200 pg) measured at 5 Torr, and **(B1)** HMTD (200 pg) measured at 28 Torr. Reproduced under permission from Wiley (Habib et al., 2015).

ions of RDX,  $[\text{RDX}+\text{NO}_2]^-$  and  $[\text{RDX}+\text{NO}_3]^-$ , were observed as major ions using atmospheric-pressure DBD ion source (Na et al., 2007b; Garcia-Reyes et al., 2011; Habib et al., 2014; Bi et al., 2021).

**Figures 13B,B1** show the mass spectra for 10 ng of PETN measured by HCD in negative ion mode at 5 and 28 Torr of ion source pressures, respectively. As shown in **Figure 13B**, the intensity of the fragment ion,  $[\text{PETN}-\text{CH}_2\text{ONO}_2]^-$  ( $m/z$  240), for PETN is higher than that of the adduct ion with  $\text{NO}_3^-$ ,  $[\text{PETN}+\text{NO}_3]^-$  ( $m/z$  378) at 5 Torr. The intensity of the adduct ion,  $[\text{PETN}+\text{NO}_3]^-$ , increases with ion source pressure and ultimately became as the major ion at 28 Torr. McLuckey et al. (1996) found only the fragment ion for PETN,  $[\text{PETN}-\text{CH}_2\text{ONO}_2]^-$  ( $m/z$  240), in the negative ion mode using dc glow discharge through adjusting the ion source pressure at 0.8 Torr with air (McLuckey et al., 1996). However, by using the atmospheric pressure DBD ionization, PETN gave the adduct ion,  $[\text{PETN}+\text{NO}_3]^-$  ( $m/z$  378), as the major ion (Zhang et al., 2009; Habib et al., 2014), that was also found for the RDX (**Figure 13A1**).

Among the explosives, TNT has widely been studied through fabrication of various ion sources for mass spectrometry including  $\text{MS}^n$  system (Harper et al., 2008; Zhang et al., 2009; Nilles et al., 2010; Garcia-Reyes et al., 2011; Habib et al., 2013). **Figures 13C,C1** show the negative mode mass spectra for 2 ng TNT measured by HCD ion source at 5 and 28 Torr, respectively. As seen from **Figure 13C**, the fragment ion,  $[\text{TNT}-\text{H}]^-$  ( $m/z$  226), is the major ion at 5 Torr along with other fragment

ions such as,  $[\text{TNT}-\text{NO}]^-$  ( $m/z$  197),  $[\text{TNT}-2\text{NO}]^-$  ( $m/z$  167,  $[\text{TNT}-3\text{NO}]^-$  ( $m/z$  137) as the minor ions, however, TNT usually gives its molecular ion,  $[\text{TNT}]^-$ , as the major ion even in the ambient conditions (Habib et al., 2013). Furthermore, TNT gave an adduct ion,  $[\text{TNT}-\text{H}+\text{O}]^-$  ( $m/z$  242), as the minor ion at 5 Torr. The adduct ion,  $[\text{TNT}-\text{H}+\text{O}]^-$  ( $m/z$  242), became as the major ion at 28 Torr (**Figure 13C1**). On the basis of the mass spectra of TNT at 5 and 28 Torr, it may conclude that the TNT molecules suffered from complicated ion-molecule reactions in the HCD ion source.

To investigate the formation of the fragment and adduct ions from TNT molecules using the HCD ion source, tandem mass spectrometry ( $\text{MS}^2$ ) was applied to monitor the collision induced dissociation (CID) products. Herein, the adduct ion,  $[\text{TNT}-\text{H}+\text{O}]^-$  ( $m/z$  242), was taken as a precursor ion to monitor the  $\text{MS}^2$  CID product ions. The inset in **Figure 13C1** shows the  $\text{MS}/\text{MS}$  product ion spectrum for the precursor ion,  $[\text{TNT}-\text{H}+\text{O}]^-$  ( $m/z$  242). As seen from  $\text{MS}/\text{MS}$  spectrum (inset in **Figure 13C1**), the first product ion,  $m/z$  225, is due to elimination of OH from the precursor ion,  $[\text{TNT}-\text{H}+\text{O}]^-$  ( $m/z$  242), ion at  $m/z$  210 is due to elimination of NO from  $[\text{TNT}]^-$  ( $m/z$  227), ion at  $m/z$  167 is for elimination of NO from  $[\text{TNT}-\text{NO}]^-$  ( $m/z$  197), ion at  $m/z$  137 is for elimination of NO from  $[\text{TNT}-2\text{NO}]^-$  ( $m/z$  167) and ion at  $m/z$  107 is for elimination of NO from  $[\text{TNT}-3\text{NO}]^-$  ( $m/z$  137).

Nitroglycerine (NG) an explosive compound was also analyzed by the HCD ion source in the negative mode of operation at 1, 5, and 28 Torr of ion source pressures (data not

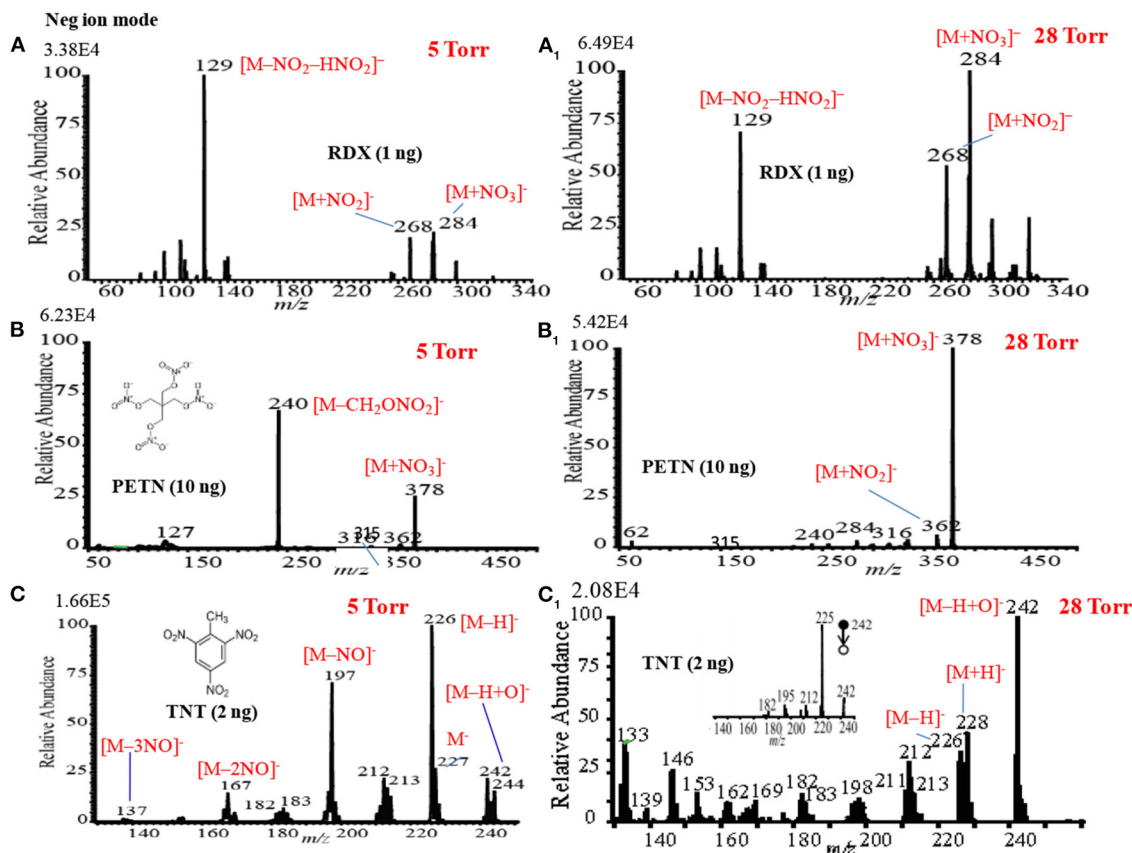


**FIGURE 13** | Mass spectra for (A) RDX (5 Torr), (A<sub>1</sub>) RDX (28 Torr), (B) PETN (5 Torr), (B<sub>1</sub>) PETN (28 Torr), (C) TNT (5 Torr), and (C<sub>1</sub>) TNT (28 Torr) measured by the HCD ion source in the negative ion mode. The MS/MS spectrum of [TNT-H+O]<sup>-</sup> (*m/z* 242) is shown in the inset (CID: 25%). Reproduced under permission from Wiley (Habib et al., 2015).

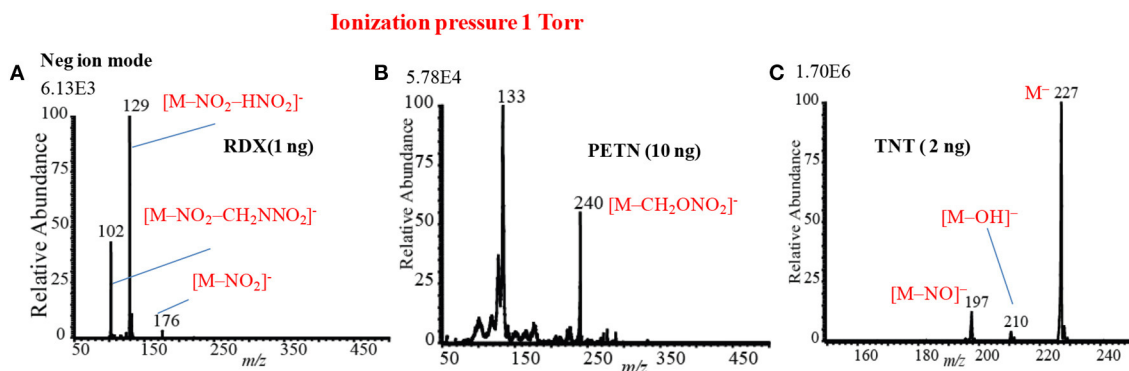


**FIGURE 14** | Mass spectra for (A) RDX (1 ng), (B) PETN (10 ng), and TNT (2 ng) at 1 Torr using the HCD ion source in the negative ion mode. Reproduced under permission from Wiley (Habib et al., 2015).

shown). Unlike RDX and PETN, NG did not show any ion signal at low ion source pressure such as 1 and 5 Torr even though the amount of NG was increased up to 10 ng, however, the adduct ion for NG with  $\text{NO}_3^-$ ,  $[\text{NG}+\text{NO}_3]^-$  (*m/z* 289), was observed at 28 Torr (Habib et al., 2015). In the negative ion mode, NG may

provide  $\text{NO}_3^-$  as a fragment ion (McLuckey et al., 1996; Hiraoka et al., 2010) that hampers the analysis of NG at low ion source pressure. This is because  $\text{NO}_3^-$  is one of the reagent ions of the HCD ion source (see Figure 11B). Thermal instability of NG causes poor detection sensitivity as its adduct ion with the  $\text{NO}_3^-$ ,

[NG+NO<sub>3</sub>]<sup>−</sup>. Yinon et al. (1997) also found the formation of the adduct ion of NG with NO<sub>3</sub><sup>−</sup> reagent ion, [NG+NO<sub>3</sub>]<sup>−</sup> (Yinon et al., 1997). To investigate the stability of NG, a preliminary experiment was done through depositing a considerable amount on a metal substrate and found it decomposed above ~100°C.

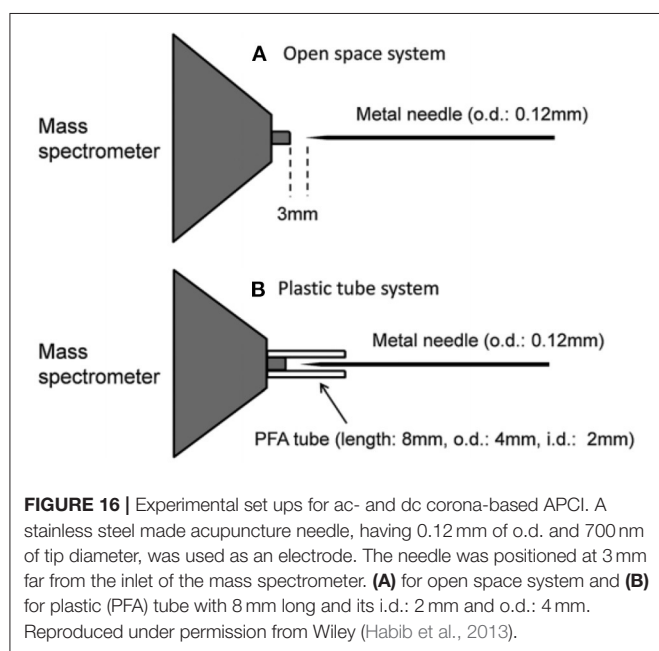
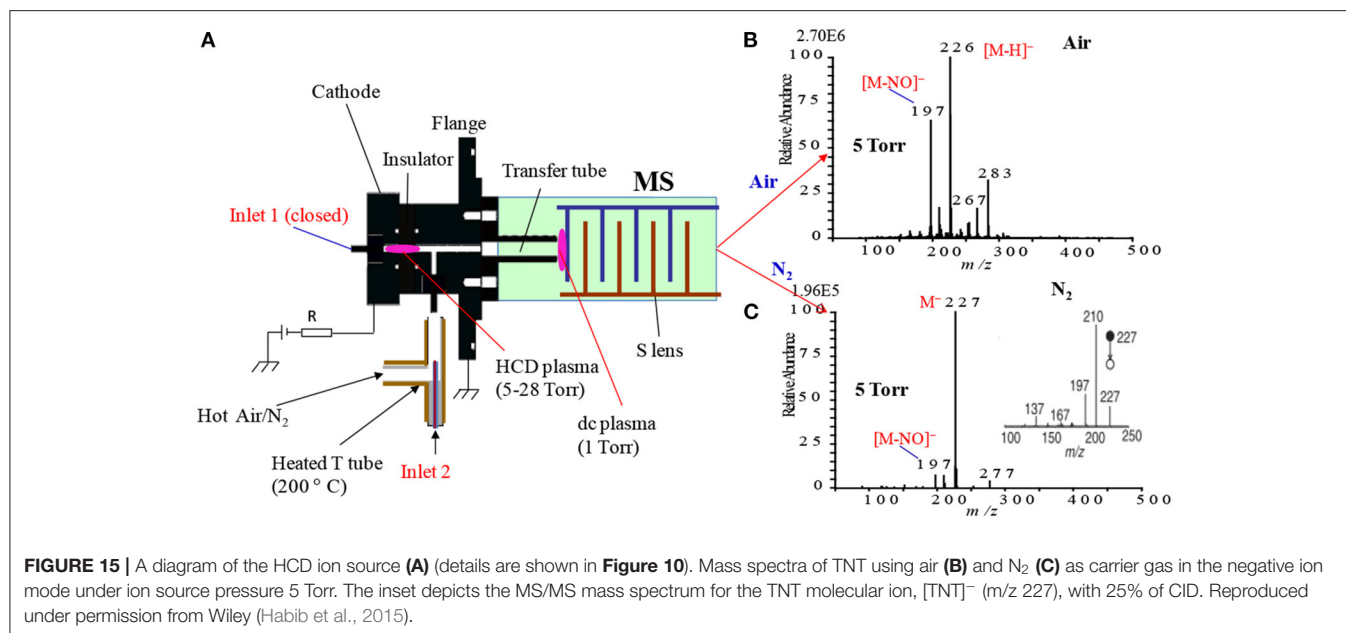
As seen from **Figures 12, 13**, the mass spectra for the explosive compounds remarkably depend on the ion source pressures. Thus, additional experiments for the explosives were performed at relatively lower ion source pressure (1 Torr) in order to investigate the ionization mechanism of the explosives with the ion source pressures. At 1 Torr, a dc plasma was generated between the transfer tube and S-lens by applying +0.85 kV and −0.85 kV in the positive and negative ion modes, respectively. In the both positive and negative ion modes, TATP and HMTD did not give any ion signals under 1 Torr ion source pressure, on the other hand, RDX, PETN, and TNT exhibited strong ion signals in the negative mode of operation (see **Figures 14A–C**). As seen from **Figure 14A**, RDX gave the fragment ion, [RDX-NO<sub>2</sub>-HNO<sub>2</sub>]<sup>−</sup> (*m/z* 129) that found as the major ion along with the other fragment ions such as, [RDX-NO<sub>2</sub>-CH<sub>2</sub>NNO<sub>2</sub>]<sup>−</sup> (*m/z* 102) and [RDX-NO<sub>2</sub>]<sup>−</sup> (*m/z* 176) as the minor ions at 1 Torr. The results were in good agreement with the results obtained by McLuckey et al. (1996) where they used low pressure glow discharge ion source (0.8 Torr of air pressure) (McLuckey et al., 1996). **Figure 14B** shows the mass spectrum for 10 ng of PETN in the negative ion mode. Herein, PETN only gave the fragment ion, [PETN-CH<sub>2</sub>ONO<sub>2</sub>]<sup>−</sup> (*m/z* 240) in the negative mode. McLuckey et al. (1996) also found the appearance of the fragment ion, [PETN-CH<sub>2</sub>ONO<sub>2</sub>]<sup>−</sup>, as the major ion at 0.8 Torr of air pressure (McLuckey et al., 1996). It is noted that RDX and/or PETN did not give an adduct ions such as [M+NO<sub>2</sub>]<sup>−</sup> or [M+NO<sub>3</sub>]<sup>−</sup> when the ion source pressure was kept at 1 Torr, however, these adduct ions were appeared in abundance at 5 and/or 28 Torr. **Figure 14C** shows the mass spectrum of TNT (2 ng) in the negative ion mode at 1 Torr. As seen from **Figure 10C**, TNT gave the molecular ion, [TNT]<sup>−</sup> (*m/z* 227) as the major ion with very high ion intensity (1.70E6) under 1 Torr ion source pressure along with the [M-NO]<sup>−</sup> (*m/z* 197) and [M-OH]<sup>−</sup> (*m/z* 210) ions as the minor ions. The other fragment ions such as [M-H]<sup>−</sup> (*m/z* 226), [M-2NO]<sup>−</sup> (*m/z* 167) and also the adduct ion, [M-H+O]<sup>−</sup> (*m/z* 242) were completely absent at 1 Torr (see **Figure 14C**). The major ions observed under different ion source pressures such as 1, 5 and 28 Torr are tabulated in **Table 2**. The limits of detection (LODs) with S/N ≥ 3 for the explosives of interest are also summarized in **Table 2**. It is noted that the explosive compounds did not give any dimer ions by using the fabricated HCD ion source.

On the basis of the analytical calibration curves, the values of LOD for HMTD, RDX, PETN, and TNT were 20, 40, 800, and 2 pg, respectively. These values are comparable to those obtained by DESI (Takáts et al., 2005; Cotte-Rodríguez et al., 2008), EESI (Chen et al., 2009), DBDI (Harper et al., 2008; Zhang et al., 2009; Garcia-Reyes et al., 2011), and ac-APCI (Habib et al., 2013). The LOD value for PETN was 800 pg measured by the HCD (**Table 2**) while Zhang et al. (2009) found only 500 fg using DBD ion source that is 16 times lower than that observed by the HCD ion source (Zhang et al., 2009). This is logical because the ions generated by the DESI, EESI and DBDI under ambient

conditions and introduced directly into the mass spectrometer, thus, the compounds of interest and their ions do not suffer from thermal decomposition. On the other hand, in the HCD ion source, the formed ions might be suffering from the thermal decomposition because of the high temperature (150°C) of the ion source that was observed in this study (**Table 2**). The compact size of the HCD ion source also causes the neutralization of the formed ions by hitting walls of the ion source under reduced pressure. As seen from **Figures 13, 14**, the intensities (digits at left top in each spectrum) of the observed ions were increased with increased the ion source pressure except for TNT at 1 Torr where TNT was observed as its molecular ion, [TNT]<sup>−</sup>, with the strongest ion signal (ion intensity 1.70E6). Under low ion source pressure, the electron capturing process became more favorable for TNT molecules because of their positive electron affinity (Habib et al., 2014). As described above, lower ion source pressure is suitable to detect TNT with better sensitivity in the negative mode of operation, however, RDX, PETN, and NG in the negative ion mode and TATP and HMTD in the positive mode exhibited better sensitivity with low values of LOD under the higher ion source pressures. In the previous study, ion formation mechanism for the explosive compounds by using the HCD ion source has been significantly discussed (Habib et al., 2015).

Nitro- and nitro-groups containing compounds exhibit positive electron affinity, thus electron affinity for NO<sub>3</sub> is 3.92 eV (Lias et al., 1988) while that for TNT is only 2.50 (Habib et al., 2015). Cooper et al. (2012) performed ab initio calculations in order to obtain the values of the electron affinities for RDX, HMX, TNT, and PETN and they found positive electron affinities for these explosive compounds. However, these explosive compounds did not give the molecular ion, M<sup>−</sup>, except TNT in the negative mode of operation (Habib et al., 2015). The results suggest that RDX, PETN and NG prefer adduct/cluster ion formation with the reagent ions i.e., NO<sub>2</sub><sup>−</sup>/NO<sub>3</sub><sup>−</sup> rather than electron capturing process in the HCD ion source. The results were in good agreement by the other groups where they used plasma-based ionization methods (Na et al., 2007b; Zhang et al., 2009; Garcia-Reyes et al., 2011; Habib et al., 2014). It has been reported that NO<sub>x</sub> is one of the major products in plasma-excited air (Nagato et al., 2006; Sekimoto et al., 2012). The nitro-species (NO<sub>x</sub>) formed in the plasma-excited air capture electrons preferably because of their higher electron affinity than that of the relevant explosives, thereby resulting in decreasing the signal intensity of the [TNT]<sup>−</sup> ion with pressure (Habib et al., 2015).

As described above, ionization of TNT is strongly dependent on the ion source pressure (see **Figures 13C, C<sub>1</sub>, 14C**). To investigate the ion formation mechanism of the TNT molecules with ion source pressure, additional experiments were performed using air and nitrogen as carrier gas. **Figure 15A** shows a schematic of the fabricated HCD ion source in which there are two inlets: inlet-1 for introduction of the analytes with air into the ion chamber while inlet-2 was closed (see **Figure 7**). To confirm the ionization of TNT with different ion source pressures, a sample was introduced through inlet-2 while the inlet-1 was closed as shown in **Figure 15A**. **Figures 15B,C** show the negative HCD mass spectra of TNT for air and N<sub>2</sub> as carrier gas, respectively. As seen from **Figures 15B**, there is no



molecular ion of TNT,  $[TNT]^-$ , as air was the carrier gas, but the fragment ions,  $[TNT-H]^-$  ( $m/z$  226) and  $[TNT-NO]^-$  ( $m/z$  197) are appeared with strong intensities where  $[TNT-H]^-$  is the major ion. In contrast, by using  $N_2$  as a carrier gas, the molecular ion for TNT,  $[TNT]^-$  ( $m/z$  227) appeared as the major ion with a strong intensity where the fragment ion,  $[TNT-H]^-$  ( $m/z$  226) has been completely disappeared (see **Figure 15C**). However, another fragment ion for TNT,  $[TNT-NO]^-$  ( $m/z$  197) appeared as the minor ion with a much weaker intensity.

The explosive compound TNT has also been investigated by using different atmospheric pressure ion sources such as DBDI (Na et al., 2007b; Harper et al., 2008; Zhang et al., 2009; Chen et al., 2010; Usmanov et al., 2013), dc-corona APCI (Takada et al., 2002), electrospray-based techniques (Yinon et al., 1997; Takáts et al., 2005; Chen et al., 2009), and ac-corona APCI (Habib et al., 2013). By using the electrospray-based ionization methods, TNT usually gave its molecular ion,  $[TNT]^-$ , as the major ion where the fragment ion,  $[TNT-H]^-$ , rarely observed (Yinon et al., 1997; Takáts et al., 2005; Chen et al., 2009).

However, discharge-based ionization methods provided the strong ion signals of the fragment ion,  $[TNT-H]^-$ , and molecular ion,  $[TNT]^-$  for TNT. Song and Cooks (2006) reported that TNT gave strong ion signals of the  $[TNT-H]^-$  and  $[TNT]^-$  using the desorption atmospheric pressure chemical ionization (DAPCI) (Song and Cooks, 2006). Dielectric barrier discharge ionization (DBDI) also produced the strong signals of the  $[TNT-H]^-$  and  $[TNT]^-$  (Na et al., 2007b; Zhang et al., 2009; Usmanov et al., 2013). Thus, it is concluded that ionization methods play a vital role in the relative ratio of  $[TNT]^-$  and  $[TNT-H]^-$ . The presence of air in the plasma also causes the variation of the relative ratios of the  $[TNT]^-$  and  $[TNT-H]^-$  ions (Na et al., 2007b; Zhang et al., 2009; Usmanov et al., 2013; Habib et al., 2015). The direct analysis in real time (DART) exhibited a strong signal of the  $[TNT]^-$  ion because of use of helium plasma in DART (Cody et al., 2005; Nilles et al., 2010). The presence or absence of air in the plasma/glow causes the relative abundances of  $[TNT]^-$  and  $[TNT-H]^-$ . It is, therefore, concluded that the analysis of explosives at trace-level is really a challenging task from the analytical point of view.

In summary, the developed HCD ion source exhibited better sensitivity for the explosives such as HMTD, TATP, RDX, PETN etc. both in the positive and negative ion modes under high ion source pressures, e.g., 5 and 28 Torr, however, ultra-trace



level detection was achieved for TNT (LOD  $\sim 2$  pg) at lower pressure (1 Torr) in the HCD plasma in the negative ion mode. At 1 Torr, no cluster ions were observed from the RDX and PETN through ion-molecule reactions while these two explosive compounds gave fragment ions with better sensitivity, particularly RDX at lower ion source pressure (1 Torr). It is noted that density of electrons goes to the maximum levels under low ion source pressure (e.g., 1 Torr) in the HCD plasma, thus compounds having positive electron affinity take part in electron attachment reactions. Accordingly, TNT exhibited its molecular ion,  $[\text{TNT}]^-$  ( $m/z$  227), as the major ion through electron attachment reactions while RDX and PETN took part in electron capture dissociation in the negative ion mode at 1 Torr. The estimated value of electron affinity for TNT was found to be 0.6–0.7 eV (Batley and Lyons, 1962; Foster, 1969). While the electron capture dissociation reactions of RDX and PETN gave their fragment ions as the major ion signals under low ion source pressure (1 Torr). RDX and PETN gave cluster ions with the reagent ions i.e.,  $\text{NO}_2^-$ ,  $\text{NO}_3^-$  at higher ion source pressure such as 5 and 28 Torr while AN showed cluster ion of  $\text{HNO}_3$  with  $\text{NO}_3^-$ ,  $[\text{HNO}_3 + \text{NO}_3]^-$  ( $m/z$  125). This is because AN decomposes to  $\text{HNO}_3$  in the plasma-excited air and the formed  $\text{HNO}_3$  forms cluster ion with the predominantly present  $\text{NO}_3^-$  ion in the HCD ion source. Among the explosive compounds, TNT showed significant pressure dependence mass spectra. At 1 Torr, the major ion signal for TNT was its molecular ion,  $[\text{TNT}]^-$  ( $m/z$  227), however, fragment ions became major ions such as  $[\text{TNT-H}]^-$ ,  $[\text{TNT}-n\text{NO}]^-$  ( $n = 1-3$ ), and  $[\text{TNT-H+O}]^-$  with increasing ion source pressure from 1 to 28 Torr. It has been proposed that the predominant presence of  $\text{NO}_2^-$ ,  $\text{NO}_3^-$  as well as  $\text{O}_3$  in the HCD ion source causes the formation of these fragment ions. The limits of detection for the explosives examined were a bit higher than those reported by DESI, DBDI and/or DAPCI, however, the present HCD ion source showed as robust, compact and easy to operation. Moreover, the use of air as a carrier gas in the HCD ion source is its merit to deploy at public places in order to detect explosives along drugs of abuse.

## ALTERNATING CURRENT CORONA DISCHARGE/ATMOSPHERIC PRESSURE CHEMICAL IONIZATION (AC-APCI)

In the atmospheric pressure chemical ionization (APCI), direct current (dc) has long been used since its pioneering work by Horning and co-workers in the 1970s (Horning et al., 1973). In 1975, Carroll and co-workers developed a corona discharge electrode, which had a larger dynamic response range (Carroll et al., 1975). The APCI has already been coupled to mass spectrometry and has widely been used to the commercial GC/MS (Horning et al., 1973) as well as to LC/MS (Horning et al., 1974; Byrdwell, 2001).

An ac-corona-based ambient atmospheric pressure chemical ionization (ac-APCI) was fabricated using an acupuncture needle (stainless steel made) with o.d. (outer diameter); 0.12 mm and tip diameter: 700 nm (Seirin, Shizuoka, Japan). For comparison, the same acupuncture needle was used to generate dc-corona as well.

**Figure 16** shows the experimental setup for ac- and dc corona-based APCI. As seen from **Figure 16**, the distance between the needle and inlet of the MS was only 3 mm. **Figures 16A,B** show open space and closed system plastic tube (perfluoroalkoxy, PFA), respectively.

In the fabrication of ac corona-based APCI, a function generator was used to generate 15 kHz radio frequency (RF) in order to apply ac voltage to the needle. Exactly 2.6 kV<sub>PTP</sub> (peak-to-peak) ac voltage was applied to the needle without plastic tube while 2.7 kV<sub>PTP</sub> (peak-to-peak) was for the needle with the plastic tube. In the dc corona-based APCI, a range of voltage from +2.5 to –1.5 kV was applied to the needle without plastic in the positive and negative ion modes while that ranging from +3.4 to –2.3 kV was applied to the needle with plastic, respectively through 4  $\mu\text{A}$  discharge current kept constant. Due to the charging effect inside the plastic tube, the dc discharge voltage was fluctuated and found relatively higher values than that for ac corona with plastic. The voltages for the ac and dc corona were adjusted just above the threshold levels of gas discharge in order to obtain stable glow/plasma. The high voltage causes arc or spark discharge that leads to generation of extremely high discharge currents ( $\geq 200$   $\mu\text{A}$ ) (Akishev et al., 2005). The generation of arc between the needle and the counter electrode (metallic flange of MS) may cause damage to the MS through creating a short circuit.

Triacetone triperoxide (TATP) and TNT were taken as model explosive compounds to evaluate the performance of the developed ac-APCI as an ambient ion source for trace-level detection of explosives. Herein, the developed ac-APCI was compared with a dc-APCI using the TATP and TNT in positive and negative ion mode, respectively in order to investigate its potentiality as an alternative to commercial dc-APCI (Habib et al., 2013). The electric field created by the plasma at the tip of the needle is radially diffused along the electric field for the open system as shown in **Figure 16A**, however, in the closed system (with plastic tube), the plasma was confined in the plastic tube (**Figure 16B**). In fact, the charging effect created inside the plastic tube causes it to confine the plasma inside the tube. The different characters of the dc plasmas without and with plastic tube led characteristics spectral pattern from the relevant explosive compounds.

## Positive Ion Mode AC- and DC Corona-Based APCI

**Figure 17** shows the mass spectra of TATP in positive ion mode by using ac/dc open and plastic tube systems. As seen from **Figure 17**, TATP showed an adduct ion with ammonium,  $[\text{TATP} + \text{NH}_4]^+$ , as the base peak for all the systems along with many background signals originated from the laboratory air. This result suggests that ac corona (**Figures 17B,D**) can be used in the development of APCI ion source for mass spectrometry because of similar performance to the dc corona discharge (**Figures 17A,C**).

Sigman et al. (2006) reported that TATP also forms adduct ion with ammonium,  $[\text{TATP} + \text{NH}_4]^+$  by using electron and chemical ionization coupled to GC-MS and/or GC-MS/MS systems,



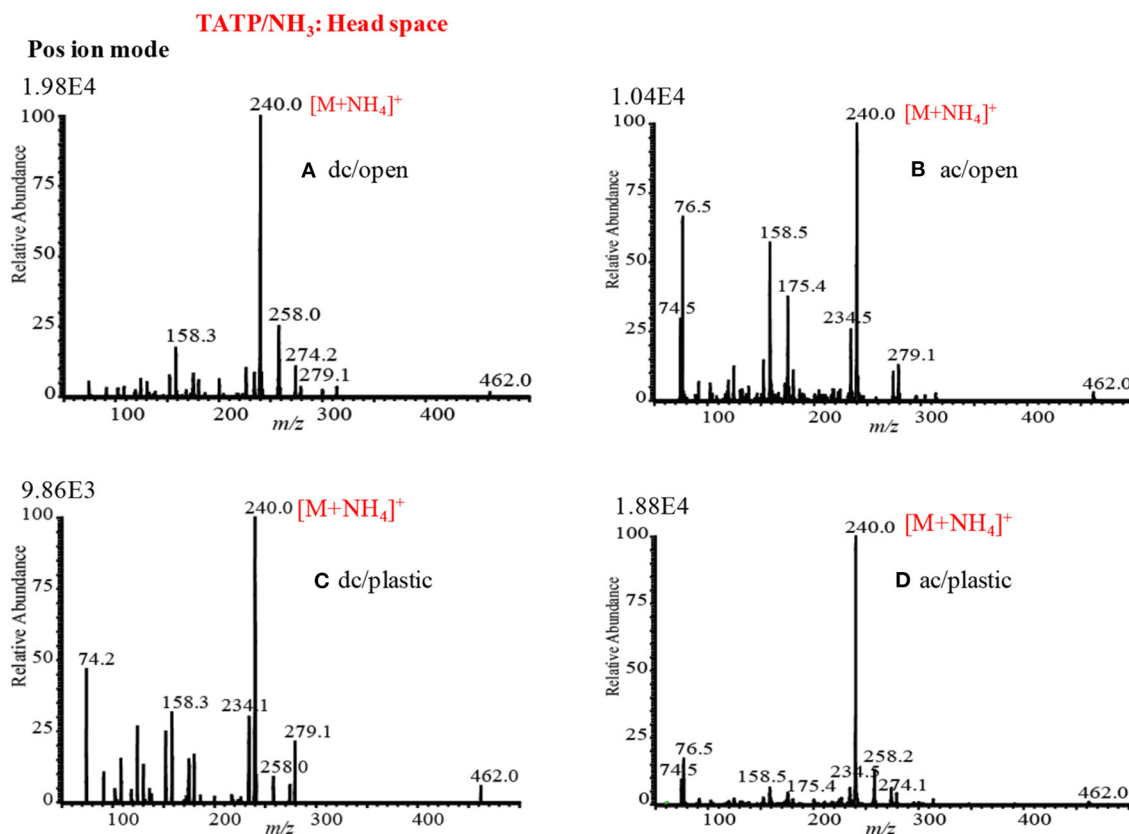


**FIGURE 17 |** Mass spectra of TATP (head-space gas) in the positive ion mode (A) dc-APCI without plastic tube (applied voltage: +2.5 kV dc), (B) ac-APCI without plastic tube (applied voltage: 2.6 kVptp ac), (C) dc-APCI with plastic tube (applied voltage: +3.4 kV dc), and (D) ac-APCI with plastic tube (applied voltage: 2.7 kVptp ac). Reproduced under permission from Wiley (Habib et al., 2013).

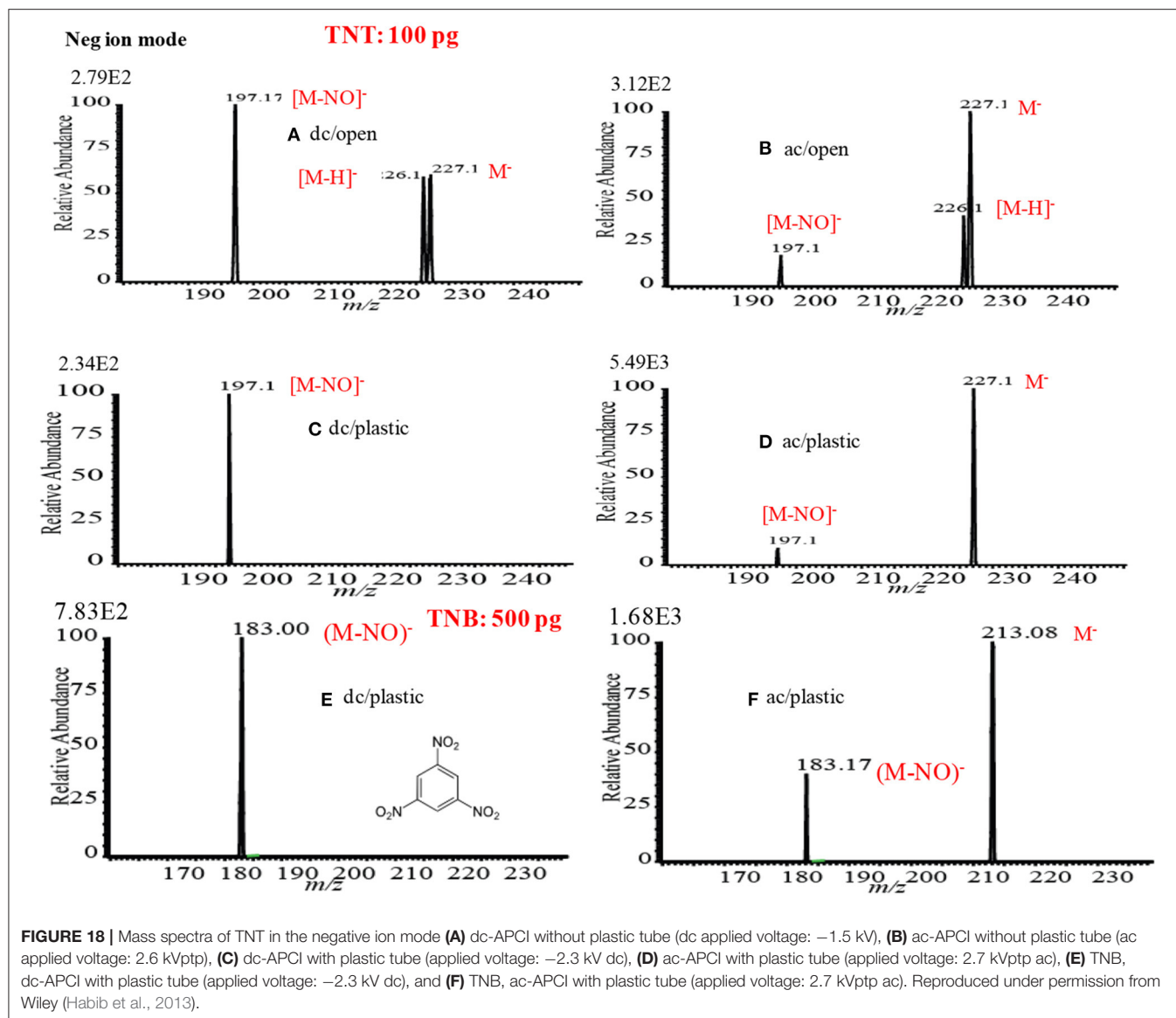
however, they did not observe both the fragment ions (having  $m/z$  values higher than 60) and protonated molecular ion,  $[TATP+H]^+$  ( $m/z$  223), through applying subsequent collision-induced dissociation (CID) (Sigman et al., 2006). The binding energy for the  $[TATP-NH_4]^+$  was calculated using DFT (basis set: B88LYP/DVZP level) calculation and found to be 25 kcal/mol.

As seen from **Figures 17A–D**, TATP gave strong ion signal as its ammoniated adduct ion,  $[TATP+NH_4]^+$  ( $m/z$  240), in all types of ac/dc and open/plastic system in the positive ion mode. The appearance of the adduct ion,  $[TATP+NH_4]^+$  ( $m/z$  240), as the major ion would be used as a better diagnostic ion at trace-level detection of TATP at public places in order to provide public security and safety. In the open system, the intensity of the adduct ion was about two times higher in dc/open than that in ac/open. Contrast to the closed system (with plastic tube), the intensity of the adduct ion was about two times higher for ac/closed compared to that for dc/closed system. The creation of static charge inside the plastic tube traps the positive adduct ion,  $[TATP+NH_4]^+$ , that leads to the lower value of the ion intensity. It is expected that the value of the static potential (wall potential) would be higher than that of plasma, thus the adduct ion,  $[TATP+NH_4]^+$ , suffered from fragmentation. This could be the reason for observing the low value of the intensity of the adduct ion in the dc/plastic system (Habib et al., 2013).

## Negative Ion Mode AC- and DC Corona-Based APCI

As mentioned above, TNT was taken as a model explosive compound to investigate the performance of the fabricated ac- and dc corona-based APCI. **Figures 18A,B** show the mass spectra of TNT by using dc/open-APCI and ac/open-APCI, respectively. As seen from **Figure 18A**, TNT gave the fragment ion,  $[TNT-NO]^-$  ( $m/z$  197), as the major ion while the molecular ion,  $[TNT]^-$  ( $m/z$  227), and/or fragment ion,  $[TNT-H]^-$  ( $m/z$  226), appeared as the minor ions. Contrast to the ac/open APCI, TNT rather gave its molecular ion,  $[TNT]^-$ , as the major ion where the fragment ion,  $[TNT-NO]^-$ , along with the adduct ion,  $[TNT-H]^-$ , appeared as the minor ions (**Figure 18B**). These results suggest that the ion-molecule reactions for TNT molecules took place rather softer in the ac/open APCI.

As seen from **Figure 18C**, TNT gave only the fragment ion,  $[M-NO_2]^-$  ( $m/z$  197), in the dc/plastic APCI system. However, TNT exhibited its molecular ion,  $[TNT]^-$ , as the major ion while the only fragment ion,  $[TNT-NO]^-$ , appeared as the minor ion with a much weaker intensity in the ac/plastic APCI system. But it was expected to observe the fragment ion,  $[TNT-H]^-$ , under the ambient condition for the ac/plastic system. This result suggests that TNT took place in an electron capturing reaction



in the ac-corona that leads to the formation of its molecular ion,  $[TNT]^-$ . It is, therefore, concluded that the ac/plastic-based APCI showed as a much softer ion source than the dc/plastic-APCI. In order to confirm this phenomenon, 1,3,5-trinitrobenzene (TNB), which is structurally similar to TNT, was investigated using the dc/plastic and ac/plastic systems and its mass spectra are shown in **Figures 18E,F**, respectively. As seen from **Figure 15E**, TNB gave only the fragment ion,  $[M-NO]^-$  ( $m/z$  183) that is just mimic of TNT in the dc/plastic system while TNB showed its molecular ion,  $[TNB]^-$  ( $m/z$  213), as the major ion where the fragment ion,  $[TNB-NO]^-$  ( $m/z$  183) as the minor ion in the ac/plastic system.

The developed dc/plastic-APCI and ac/plastic-APCI ion sources were examined in order to evaluate their analytical validation in quantification of explosives at trace level. Herein, TNT was taken as a model explosive compound. In the dc/plastic

system, signal intensities for the fragment ion,  $[M-NO]^-$  ( $m/z$  197) were used to construct the analytical calibration curve while that for the molecular ion,  $[TNT]^-$  ( $m/z$  227), were used for the calibration curve in the ac/plastic system. A good dynamic range up to  $2$  ng was observed for both the cases with a correlation coefficient  $R^2$  of  $\sim 0.99$  (Habib et al., 2013). The values of limits of detection (LODs) for TNT (S/N: 3) were 50 and 30 pg in the dc/plastic and ac/plastic systems, respectively. The low values of standard deviations with five replications demonstrate the good reproducibility in the dc/plastic and ac/plastic systems.

As seen from **Figures 18C,E**, the ions were underwent severe fragmentation in the dc/plastic compared to that in the ac/plastic for TNT and TNB, respectively while dc/open system exhibited moderate and ac/open showed less fragmentation in the negative mode of ionization. The PFA plastic surface acts as perfectly an insulator, thus the applied high voltage creates static charging

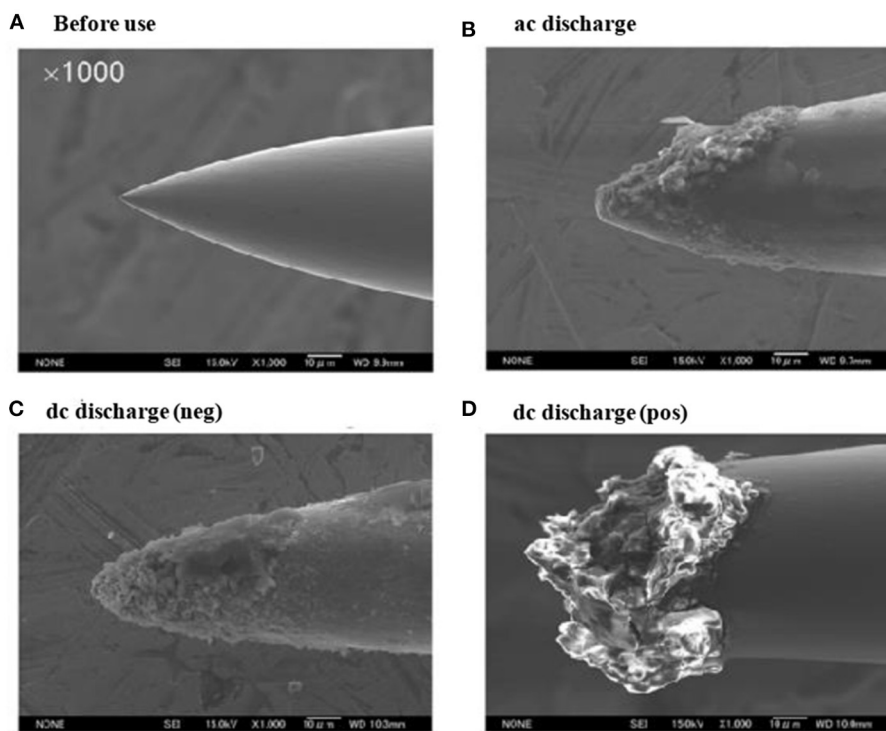


**FIGURE 19** | Scanning electron microscope (SEM) images of acupuncture needles made of stainless steel: **(A)** before use, **(B)** ac corona discharge in open space for 20 h (applied voltage: 2.6 kVtp ac), **(C)** –dc corona discharge in open space for 20 h (applied voltage: 1.5 kV dc), and **(D)** +dc corona discharge in open space for 20 h (applied voltage: +2.5 kV dc at the start and +2.8 kV dc after 20 h). Reproduced under permission from Wiley (Habib et al., 2013).

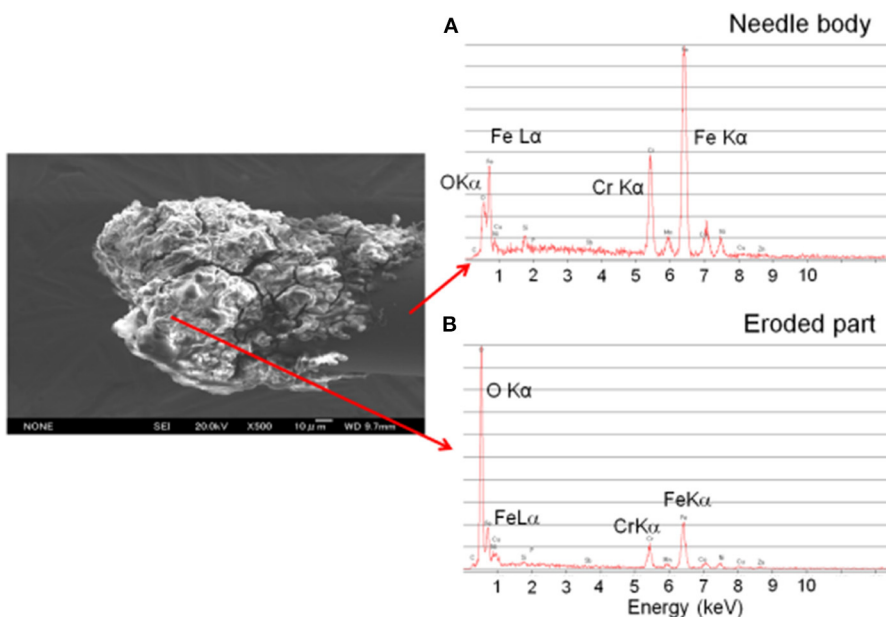


**FIGURE 20** | Energy dispersive X-ray spectroscopy (EDX) spectra for the stainless steel acupuncture needle: **(A)** needle body and **(B)** eroded part. Reproduced under permission from Wiley (Habib et al., 2013).

in the inner wall of the plastic tube (Akishev et al., 2005). It is expected that the plasma developed inside the plastic tube distributed uniformly and becomes convex at the tip of the needle that causes the plasma to be diffusive toward the radial direction in the dc/open system. Under this circumstance, the formed primary ions in the plasma have less chance to undergo secondary decomposition (Habib et al., 2013). On the contrary, a concave shape of the equipotential surface is formed at the tip of the needle because of the inner wall static charging. The formation of the concave shape allows the confinement of the plasma within a narrow space, thus the ions generated must undergo further severe secondary fragmentation. The ac corona, however, should be different from the dc corona from their origin point of views. The ac corona plasma generated in the plastic (PFA) tube must have some characteristic features compared to that generated in the open system. The inner insulating wall has a strong effect on the local field distortion caused by a surface charge accumulation on the dielectric (Akishev et al., 2005; Habib et al., 2013). The charge accumulation developed on the dielectric surface controls the discharge current, thus the initially formed plasma ceases before the transition from glow discharge to arc-like hot plasma. The wall charging causes the occurrence of a non-equilibrium cold plasma that is responsible for the better performance in the ac/plastic system as shown in **Figures 18D,F**.

As described above, dc corona in positive as well as in negative ion modes showed some different features. In our previous study, we found that the applied voltage for the negative mode (-1.5 kV) was lower than that for the positive mode (+2.5 kV) in the open system in order to keep a constant current of 4  $\mu$ A (Habib et al., 2013). It is noted that a 4  $\mu$ A current was kept constant throughout the dc mode experiments. The low value of the applied voltage in the negative mode of operation than that of the positive mode is needed to maintain stable plasma in the negative mode. It is highly expected that the value of the applied voltage in the negative mode of dc corona would be low because of gaining additional electrons by the photoelectron emission and the value was found to be -1.5 kV (Akishev et al., 2003; Habib et al., 2013). Contrary to the dc in positive mode, the applied voltage to the needle tip varied from the initial value of +2.5 kV to the higher values up to +2.8 kV to maintain the constant discharge current. To compare the ac corona-APCI as a soft ionization with the dc corona-APCI ion source, the used acupuncture needles in the open system were examined for erosion by using scanning electron microscope (SEM) and energy dispersive X-ray spectroscopy (EDS) spectra. **Figures 19A–D** show the SEM images of the used acupuncture needles for ac and dc discharges in the open system. The SEM image for the pristine acupuncture needle is shown in **Figure 19A** while **Figures 19B–D** stand for the SEM images of the used in the ac corona, dc negative and dc positive corona after 20 h of continuous discharge operation, respectively. As seen from **Figures 19B,C**, the tip of the needles was corroded slightly, but the original shape of the needles was reasonably maintained while the tip of the needle was completely eroded and some rugged product was formed at the tip in the positive dc mode of operation (**Figure 19D**). In the dc positive mode, the voltage was applied to a point electrode but extended to a much longer distance from the point toward the gap than for the negative

corona (Lowke and Morrow, 1994). This is because the discharge is streamer discharge and it has two modes such as diffusive and filamentary streamer mode. In the filamentary streamer mode, the surface of the electrode gains the joule energy, thus the tip of the needle becomes heated (Akishev et al., 2003). The heating effect causes severe erosion of the needle rather in the positive dc corona (Bárdos and Baránková, 2009). Therefore, it is concluded that the streamer discharge leads to the melting of the tip of the needle at the filamentary discharge spot in the positive dc corona. However, a thicker needle has widely been used to commercial dc corona APCI.

**Figures 20A,B** show the EDX spectra for non-eroded and eroded part of the used acupuncture needle, respectively. As seen from **Figure 20A**, the signal intensity of the iron  $K\alpha$  from the body part was much stronger than that of the oxygen  $K\alpha$ . However, the  $K\alpha$  for the oxygen was found as the highest intensity from the eroded part as shown in **Figure 20B**. This result is confirming the formation of oxides at the tip of the acupuncture needle for the dc positive mode of operation. The appearance of the second highest intensity for chromium  $K\alpha$  is reasonable. This is because stainless steel is an alloy of iron with mostly chromium (~18%). When chrome alloy exposes to air, its surface metallic chromium converts to  $Cr_2O_3$  and forms a very thin layer. The formation of a thin layer of the  $Cr_2O_3$  prevents the oxidation of iron in steel, however, the tip of the acupuncture needle becomes melted in the positive dc corona discharge mode. This is because the high energetic ejected electrons return back to the needle in the positive dc polarity and heated up the tip of the needle and then melted. The melted part of the needle is readily exposed to air, thereby resulting in formation of oxides of Fe and Cr. Therefore, it is reasonable to observe the very high intensity of oxygen  $K\alpha$  from the eroded part of the needle.

An atmospheric pressure chemical ionization (APCI) ion source has been fabricated with the means of point-to-plane ac corona discharge in order to detect explosives. Here, TATP and TNT were taken as model compounds for positive and negative modes of operation, respectively. The developed ac corona APCI gave ion signals that were as strong as in the usual dc corona-based APCI. A perfluorinated plastic tube (PFA) was used as an insulation tube to investigate the ionization mechanism for the explosive compounds. The ac and dc type corona discharges were examined with and without the plastic insulation tube in order to investigate the fragmentation mechanisms of the relevant explosives. Static charging was developed in the insulator wall and that causes fragmentation of the primary ions in the negative dc corona, however, this effect was minor in the ac corona discharge. The ac/plastic system was found to be the best for the APCI ion source. The needle for the ac corona was less eroded than that for positive mode dc corona and was found to be suitable for long-term operation.

## CONCLUDING REMARKS

In this review article, fabrication of new ion sources such as homemade helium-dielectric barrier discharge ionization (DBDI), hollow cathode discharge ionization (HCDI), ac-atmospheric pressure chemical ionization (APCI) for mass spectrometry has been taken into account in order to analyze



drugs of abuse and explosives at trace to ultra-trace levels. Ultrasonic cutter blade-based desorption method for desorption of solid non-volatile drugs of abuse and explosives has also been discussed. The developed ultrasonic cutter blade-based desorption method showed as a non-thermal method for desorption of non-volatile compounds such as drugs of abuse, explosives etc. The desorption method is also exhibited as a soft desorption process for non-volatile compounds. This is because of the generation of mechanical frictional energy from the cutter blade that is much coherent compared to thermal energy. The developed desorption method is reasonably sensitive and may be applied for quick analysis of contaminants, such as narcotics, explosives and/ or any other non-volatile compounds, deposited on substrates' surfaces. The fabricated homemade He-DBDI ion source was found to ionize a wide range of drugs of abuse and explosives without and/or with minimal fragmentation. The pressure dependent HCD ion source exhibited as a suitable ion source for MS to detect the explosive compounds at trace to ultra-trace levels. The beauty of the fabricated HCD ion source is its carrier gas is air, thus this ion source may be commercialized through coupling with an MS in order to detect explosives at public places. The headspace method has been proven its versatile use in detection of amphetaminic drug compounds even from body fluids at ultra-trace levels. The ac corona-based APCI exhibited as a promising new ion source for MS in detection of explosives.

Despite profuse prospects in the field of MS-based analytical science, there are still some challenges in exploring the remarkable effectiveness of the developed new ion sources and new desorption methods for non-volatile compounds in future:

1. A single ion source should not be suitable for all types of the drugs of abuse and explosives.
2. Investigation of the coupling of the ultrasonic cutter blade-based desorption process with the homemade DBDI-MS system.
3. Fabrication of air-based DBD ion source for ultra-trace levels detection of the drugs of abuse and explosives.

## REFERENCES

- Abdelhamid, H. N. (2018). Nanoparticle assisted laser desorption/ionization mass spectrometry for small molecule analytes. *Microchim. Acta* 185:200. doi: 10.1007/s00604-018-2687-8
- Abdelhamid, H. N. (2019a). Nanoparticle-based surface assisted laser desorption ionization mass spectrometry: a review. *Microchim. Acta* 186:682. doi: 10.1007/s00604-019-3770-5
- Abdelhamid, H. N. (2019b). "Nanoparticles assisted laser desorption/ionization mass spectrometry," in *Chapter 23: Handbook of Smart Materials in Analytical Chemistry* (Chichester: John Wiley & Sons, Ltd), 729–755.
- Abdelhamid, H. N., Chen, Z. Y., and Wu, H. F. (2017). Surface tuning laser desorption/ionization mass spectrometry (STLDI-MS) for the analysis of small molecules using quantum dots. *Anal. Bioanal. Chem.* 409, 4943–4950. doi: 10.1007/s00216-017-0433-4
- Abdelhamid, H. N., and Wu, H.-F. (2019a). "Graphene and its derivatives as platforms for MALDI-MS," in *Handbook of Graphene 2, Vol 2: Physics, Chemistry and Biology*, eds S. Tobias (Beverly, MA: Scrivener Publishing).
- Abdelhamid, H. N., and Wu, H. F. (2012). A method to detect metal-drug complexes and their interactions with pathogenic bacteria via graphene

4. Exploration of the developed ion sources for other compounds should be investigated
5. Development of hybrid ion source for MS in order to analyze a wide range of compounds.
6. The developed ultrasonic cutter blade-based desorption method needs further investigation in order to make it as a versatile desorption method for non-volatile compounds.

## AUTHOR CONTRIBUTIONS

AH: conceptualization, writing original draft-review, and final review & editing. LB and HH: conceptualization and funding acquisition. LW: conceptualization, supervision, final review & editing, and funding acquisition. All the authors have read and agreed to the published version of the manuscript.

## FUNDING

We acknowledge the financial support for this work by the National Key Research and Development Program of China (2018YFC0807404), and the National Key Research and Development Program of China (2018YFC1603504). We also acknowledge the financial support by the Zhejiang Provincial Key Research and Development Program of China (2020C02023), the Yunnan Provincial Key Research and Development Program of China (2018BC011), and the K. C. Wong Magna Fund in Ningbo University.

## ACKNOWLEDGMENTS

AH would like to thanks to Prof. Kenzo Hiraoka, University of Yamanashi, Japan for hiring as a postdoctoral fellow for the development of new ion sources for mass spectrometry and new desorption methods for non-volatile compounds (2011–2013). This is a short text to acknowledge the contributions of specific colleagues, institutions, or agencies that aided the efforts of the authors.

- nanosheet assist laser desorption/ionization mass spectrometry and biosensors. *Anal. Chim. Acta* 751, 94–104. doi: 10.1016/j.aca.2012.09.012
- Abdelhamid, H. N., and Wu, H. F. (2013). Furoic and mefenamic acids as new matrices for matrix assisted laser desorption/ionization-(MALDI)-mass spectrometry. *Talanta* 115, 442–450. doi: 10.1016/j.talanta.2013.05.050
- Abdelhamid, H. N., and Wu, H. F. (2015). Soft ionization of metallo-mefenamic using electrospray ionization mass spectrometry. *Mass Spectrom. Lett.* 6, 43–47. doi: 10.5478/MSL.2015.6.2.43
- Abdelhamid, H. N., and Wu, H. F. (2016). Gold nanoparticles assisted laser desorption/ionization mass spectrometry and applications: from simple molecules to intact cells. *Anal. Bioanal. Chem.* 408, 4485–4502. doi: 10.1007/s00216-016-9374-6
- Abdelhamid, H. N., and Wu, H. F. (2019b). A new binary matrix for specific detection of mercury(II) using matrix-assisted laser desorption ionization mass spectrometry. *J. Am. Soc. Mass Spectrom.* 30, 2617–2622. doi: 10.1007/s13361-019-02324-1
- Addie, R. D., Balluff, B., Bové, J. V. M. G., Morreau, H., and McDonnell, L. A. (2015). Current state and future challenges of mass spectrometry imaging for clinical research. *Anal. Chem.* 87, 6426–6433. doi: 10.1021/acs.analchem.5b00416



- Akishev, Y. S., Dem'yanov, A. V., Karal'nik, V. B., Monich, A. E., and Trushkin, N. I. (2003). Comparison of the ac barrier corona with dc positive and negative coronas and barrier discharge. *Plasma Phys. Rep.* 29, 82–91. doi: 10.1134/1.1538505
- Akishev, Y. S., Grushin, M., Kochetov, I., Karal'nik, V., Napartovich, A., and Trushkin, N. (2005). Negative corona, glow and spark discharges in ambient air and transitions between them. *Plasma Sources Sci. Technol.* 14:S18. doi: 10.1088/0963-0252/14/2/S03
- Alexandrov, M. L., Gall, L. N., Krasnov, N. V., Nikolaev, V. I., Panvlenko, V. A., Shkurov, V. A., et al. (1984). Direct interfacing of a micro-column liquid chromatograph with a mass spectrometer. *Bioorg. Khim.* 10, 710–712.
- Arango, C. A., Shapiro, M., and Brumer, P. (2006). Cold atomic collisions: coherent control of penning and associative ionization. *Phys. Rev. Lett.* 97:193202. doi: 10.1103/PhysRevLett.97.193202
- Arkin, C. R., Griffin, T. P., Hoffman, J. H., and Limero, T. (2010). Space Applications of Mass Spectrometry. *Ch.* 31, 3–5. Available online at: <https://ntrs.nasa.gov/citations/2010003943>
- Barber, M., Bordoli, R., Elliott, G., Sedgwick, R. D., and Tyler, A. N. (1982). Fast atom bombardment mass spectrometry. *Anal. Chem.* 54, 645A–657A. doi: 10.1021/ac00241a817
- Barber, M., Bordoli, R. S., Sedgwick, R. D., and Tyler, A. N. (1981b). Fast atom bombardment of solids (FAB): a new ion source for mass spectrometry. *J. Chem. Soc. Chem. Commun.* 1981, 325–327. doi: 10.1039/c39810000325
- Barber, M., Bordoli, R. S., Sedgwick, R. D., and Tyler, A. N. (1981a). Fast atom bombardment of solids as an ion source in mass spectrometry. *Nature* 293, 270–275. doi: 10.1038/293270a0
- Bárdos, L., and Baránková, H. (2009). Plasma processes at atmospheric and low pressures. *Vacuum* 83, 522–527. doi: 10.1016/j.vacuum.2008.04.063
- Batley, M., and Lyons, L. (1962). Electron affinities of organic molecules. *Nature* 196, 573–574. doi: 10.1038/196573a0
- Beavis, R. C., Chait, B. T., and Fales, H. M. (1989). Cinnamic acid derivatives as matrices for ultraviolet laser desorption mass spectrometry of proteins. *Rapid Commun. Mass Spectrom.* 3, 432–435. doi: 10.1002/rcm.1290031207
- Beavis, R. C., Chaudhary, T., and Chait, B. T. (1992).  $\alpha$ -Cyano-4-hydroxycinnamic acid as a matrix for matrix-assisted laser desorption mass spectrometry. *Org. Mass Spectrom.* 27, 156–158. doi: 10.1002/oms.1210270217
- Bi, L., Habib, A., Chen, L., Xu, T., and Wen, L. (2021). Ultra-trace level detection of nonvolatile compounds studied by ultrasonic cutter blade coupled with dielectric barrier discharge ionization-mass spectrometry. *Talanta* 222:121673. doi: 10.1016/j.talanta.2020.121673
- Borges, M. M. C., Santos, H., Vasconcelos, G. A., Nascimento, T. A., Dutra, F. V. A., Pires, B. C., et al. (2019). The use of conductive polymers as a substrate for paper spray ionization mass spectrometry. *Anal. Methods* 11, 3388–3400. doi: 10.1039/C9AY00484J
- Brettell, T. A., and Lum, B. J. (2018). Analysis of drugs of abuse by Gas Chromatography-Mass Spectrometry (GC-MS). *Methods Mol. Biol.* 1810, 29–42. doi: 10.1007/978-1-4939-8579-1\_3
- Byrdwell, W. C. (2001). Atmospheric pressure chemical ionization mass spectrometry for analysis of lipids. *Lipids* 36, 327–346. doi: 10.1007/s11745-001-0725-5
- Carroll, D. I., Dzidic, I., Stillwell, R. N., Haegle, K. D., and Horning, E. C. (1975). Atmospheric pressure ionization mass spectrometry corona discharge ion source for use in a liquid chromatograph-mass spectrometer-computer analytical system. *Anal. Chem.* 47, 2369–2373. doi: 10.1021/ac60364a031
- Castiglioni, S., Bijlsma, L., Covaci, A., Emke, E., Harman, C., Hernández, F., et al. (2016). “Estimating community drug use through wastewater-based epidemiology,” in *Assessing Illicit Drugs in Wastewater, Ch. 1*, ed S. Castiglioni (Lisbon: European Monitoring Centre for Drugs and Drug Addiction).
- Chen, H., Hu, B., Hu, Y., Huan, Y., Zhou, Z., and Qiao, X. (2009). Neutral desorption using a sealed enclosure to sample explosives on human skin for rapid detection by EESI-MS. *J. Am. Soc. Mass. Spectrom.* 20, 719–722. doi: 10.1016/j.jasms.2008.12.011
- Chen, L. C., Yu, Z., Furuya, H., Hashimoto, Y., Takekawa, K., Suzuki, H., et al. (2010). Development of ambient sampling chemi/chemical ion source with dielectric barrier discharge. *J. Mass Spectrom.* 45, 861–869. doi: 10.1002/jms.1772
- Chen, Y.-C., Abdelhamid, H. N., and Wu, H.-F. (2017). Simple and direct quantitative analysis for quinidine drug in fish tissues. *Mass Spectrom. Lett.* 8, 8–13. doi: 10.5478/MSL.2017.8.1.8
- Cody, R. B., Laramée, J. A., and Durst, H. D. (2005). Versatile new ion source for the analysis of materials in open air under ambient conditions. *Anal. Chem.* 77, 2297–2302. doi: 10.1021/ac050162j
- Cole, R. B. (1997). *Electrospray Ionization Mass Spectrometry: Fundamentals, Instrumentation, and Applications*. Hoboken, NJ: Wiley.
- Cooks, R. G., Ouyang, Z., Takats, Z., and Wiseman, J. M. (2006). Ambient mass spectrometry. *Science* 311, 1566–1570. doi: 10.1126/science.1119426
- Cooper, J., Grant, C. D., and Zhang, J. (2012). An initio calculation of ionization potential and electron affinity of six common explosive compounds. *Rep. Theoret. Chem.* 1, 11–19. doi: 10.2147/RTC.S36686
- Cotte-Rodríguez, I., Hernandez-Soto, H., Chen, H., and Cooks, R. G. (2008). *In situ* trace detection of peroxide explosives by desorption electrospray ionization and desorption atmospheric pressure chemical ionization. *Anal. Chem.* 80, 1512–1519. doi: 10.1021/ac7020085
- Covey, T. R., and Devanand, P. (2002). “Nanospray electrospray ionization development: LC/MS, CE/MS application,” in *Practical Spectroscopy Series, Volume 32: Applied Electrospray Mass Spectrometry*, eds B. N. Pramanik, A. K. Ganguly, M. L. Gross (New York, NY: Marcel Dekker).
- Damon, D. E., Davis, K. M., Moreira, C. R., Capone, P., Cruttenden, R., and Badu-Tawiah, A. K. (2016). Direct biofluid analysis using hydrophobic paper spray mass spectrometry. *Anal. Chem.* 88, 1878–1884. doi: 10.1021/acs.analchem.5b04278
- Dempster, A. J. (1918). A new method of positive ray analysis. *Phys. Rev.* 11, 316–325. doi: 10.1103/PhysRev.11.316
- Dempster, A. J. (1921). Positive ray analysis of lithium and magnesium. *Phys. Rev.* 18, 415–422. doi: 10.1103/PhysRev.18.415
- Dole, M., Mack, L. L., Hines, R. L., Mobley, R. C., Ferguson, L. D., and Alice, M. B. (1968). Molecular beams of macroions. *J. Chem. Phys.* 49, 2240–2249. doi: 10.1063/1.1670391
- Fales, H. M., Milne, G. W., Pisano, J. J., Brewer, H. B., Blum, M. S., MacConnell, J. G., et al. (1972). Biological applications of electron ionization and chemical ionization mass spectrometry. *Recent Prog. Horm. Res.* 28, 591–626.
- Feider, C. L., Krieger, A., DeHoog, R. J., and Eberlin, L. S. (2019). Ambient ionization mass spectrometry: recent developments and applications. *Anal. Chem.* 7, 4266–4290. doi: 10.1021/acs.analchem.9b00807
- Feng, B., and Smith, R. D. (2000). A simple nanoelectrospray arrangement with controllable flowrate for mass analysis of submicroliter protein samples. *J. Am. Soc. Mass Spectrom.* 11, 94–99. doi: 10.1016/S1044-0305(99)00124-5
- Fenn, J. B., Mann, M., Meng, C. K., Wong, S. F., and Whitehouse, C. M. (1989). Electrospray ionization for mass spectrometry of large biomolecules. *Science* 246, 64–71. doi: 10.1126/science.2675315
- Fenn, J. B., Mann, M., Meng, C. K., Wong, S. F., and Whitehouse, C. M. (1990). Electrospray ionization-principles and practice. *Mass Spectrom. Rev.* 9, 37–70. doi: 10.1002/mas.1280090103
- Fenn, J. B., Roswell, J., and Meng, C. K. (1997). In electrospray ionization, how much pull does an ion need to escape its droplet prison? *J. Am. Soc. Mass Spectrom.* 8, 1147–1157. doi: 10.1016/S1044-0305(97)00161-X
- Field, F. H. (2002). Chemical ionization mass spectrometry. *Accounts Chem. Res.* 1, 42–49. doi: 10.1021/ar50002a002
- Filho, J. F. A., dos Santos, N. A., Borges, K. B., Lacerda, V. Jr., Pelição, F. S., and Romão, W. (2020). Fiber spray ionization mass spectrometry in forensic chemistry: a screening of drugs of abuse and direct determination of cocaine in urine. *Rapid Commun. Mass Spectrom.* 34:e8747. doi: 10.1002/rcm.8747
- Fitzgerald, M. C., Parr, G. R., and Smith, L. M. (1993). Basic matrixes for the matrix-assisted laser desorption/ionization mass spectrometry of proteins and oligonucleotides. *Anal. Chem.* 65, 3204–3211. doi: 10.1021/ac00070a007
- Foster, R. (1969). *Organic Charge-Transfer Complexes*. New York, NY: Academic Press.
- Gale, D. C., and Smith, R. D. (1993). Small volume and low flow-rate electrospray ionization mass spectrometry of aqueous samples. *Rapid Commun. Mass Spectrom.* 7, 1017–1021. doi: 10.1002/rcm.1290071111
- Ganeev, A. A., Kuz'menkov, M. A., Lyubimov, V. A., Potapov, S. V., Drobyshev, A. I., Potemkin, S. S., et al. (2007). Pulsed discharge in a hollow cathode with the detection of ions in a time-of-flight mass spectrometer: analytical

- capabilities in the analysis of solid samples. *J. Anal. Chem.* 62, 444–453. doi: 10.1134/S1061934807050097
- Garcia-Reyes, J. F., Harper, J. D., Salazar, G. A., Charipar, N. A., Ouyang, Z., and Cooks, R. G. (2011). Detection of explosives and related compounds by low-temperature plasma ambient ionization mass spectrometry. *Anal. Chem.* 83, 1084–1092. doi: 10.1021/ac1029117
- Gilbert-López, B., Lara-Ortega, F. J., Robles-Molina, J., Brandt, S., Schütz, A., Moreno-González, D., et al. (2019). Detection of multiclass explosives and related compounds in soil and water by liquid chromatography-dielectric barrier discharge ionization-mass spectrometry. *Anal. Bioanal. Chem.* 411, 4785–4796. doi: 10.1007/s00216-019-01627-2
- Groeneveld, G., de Puit, M., Bleay, S., Bradshaw, R., and Francese, S. (2015). Detection and mapping of illicit drugs and their metabolites in fingerprints by MALDI MS and compatibility with forensic techniques. *Sci. Rep.* 5:11716. doi: 10.1038/srep11716
- Habib, A., Chen, L. C., Usmanov, D. T., Yu, Z., and Hiraoka, K. (2015). Detection of explosives using a hollow cathode discharge ion source. *Rapid Commun. Mass Spectrom.* 29, 601–610. doi: 10.1002/rcm.7142
- Habib, A., Nargis, A., Bi, L., Zhao, P., and Wen, L. (2020). Analysis of amphetamine drug compounds in urine by headspace- dielectric barrier discharge ionization-mass spectrometry. *Arab. J. Chem.* 13, 2162–2170. doi: 10.1016/j.arabj.2018.04.001
- Habib, A., Ninomiya, S., Chen, L. C., Usmanov, D. T., and Hiraoka, K. (2014). Desorption mass spectrometry for nonvolatile compounds using an ultrasonic cutter. *J. Am. Soc. Mass Spectrom.* 25, 1177–1180. doi: 10.1007/s13361-014-0899-7
- Habib, A., Usmanov, D. T., Ninomiya, S., Chen, L. C., and Hiraoka, K. (2013). Alternative current corona discharge/atmospheric pressure chemical ionization (APCI) for mass spectrometry. *Rapid Commun. Mass Spectrom.* 27, 2760–2766. doi: 10.1002/rcm.6744
- Harper, J. D., Charipar, N. A., Mulligan, C. C., Zhang, X., Cooks, R. G., and Ouyang, Z. (2008). Low-temperature plasma probe for ambient desorption ionization. *Anal. Chem.* 80, 9097–9104. doi: 10.1021/ac801641a
- Harrison, A. G. (1992). *Chemical Ionization Mass Spectrometry, 2nd Edn.* Florida: CRC Press.
- Hashimoto, Y., Nagano, H., Takada, Y., Kashima, H., Sugaya, M., Terada, K., et al. (2014). Real-time explosive particle detection using a cyclone particle concentrator. *Rapid Commun. Mass Spectrom.* 28, 1376–1380. doi: 10.1002/rcm.6915
- He, X., Chen, Q., Zhang, Y., and Lin, J.-M. (2014). Recent advances in microchip-mass spectrometry for biological analysis. *TrAC Trends Anal. Chem.* 53, 84–97. doi: 10.1016/j.trac.2013.09.013
- Hiraoka, K. (2013). “Gas-phase ion/molecule reactions,” in *Fundamentals of Mass Spectrometry*, ed K. Hiraoka (Berlin: Springer).
- Hiraoka, K., Chen, L. C., Iwama, T., Mandal, M. K., Ninomiya, S., Suzuki, H., et al. (2010). Development of a remote-from-plasma dielectric barrier discharge ion source and its application to explosives. *J. Mass Spectrom.* 45, 215–220. doi: 10.5702/massspec.58.215
- Hiraoka, K., Furuya, H., Kambara, S., Suzuki, S., Hashimoto, Y., and Takamizawa, A. (2006). Atmospheric-pressure penning ionization of aliphatic hydrocarbons. *Rapid Commun. Mass Spectrom.* 20, 3213–3222. doi: 10.1002/rcm.2706
- Hiraoka, K., Nishidate, K., Mori, K., Asakawa, D., and Suzuki, S. (2007). Development of probe electrospray using a solid needle. *Rapid Commun. Mass Spectrom.* 21, 3139–3144. doi: 10.1002/rcm.3201
- Hiraoka, K., Usmanov, D. T., Chen, L. C., Ninomiya, S., Mandal, M. K., and Saha, S. (2015). Probe electrospray ionization (PESI) mass spectrometry with discontinuous atmospheric pressure interface (DAPI). *Eur. J. Mass Spectrom.* 21, 327–334. doi: 10.1255/ejms.1309
- Horning, E. C., Carroll, D. I., Dzidic, I., Haegele, K. D., Horning, M. G., and Stillwell, R. N. (1974). Atmospheric pressure ionization (API) mass spectrometry. *solvent-mediated ionization of samples introduced in solution and in a liquid chromatography effluent stream.* *J. Chromatograph. Sci.* 12, 725–729. doi: 10.1093/chromsci/12.11.725
- Horning, E. C., Horning, M. G., Carroll, D. I., Dzidic, I., and Stillwell, R. N. (1973). New picogram detection system based on a mass spectrometer with an external ionization source at atmospheric pressure. *Anal. Chem.* 45, 936–943. doi: 10.1021/ac60328a035
- Hoshino, T., Wakabayashi, S., Ohtake, M., Karouji, Y., Hayashi, T., Morimoto, H., et al. (2020). Lunar polar exploration mission for water prospecting-JAXA's current status of joint study with ISRO. *Acta Astronautica* 176, 52–58. doi: 10.1016/j.actaastro.2020.05.054
- Hoshino, T., Ohtake, M., Karouji, Y., and Shiraishi, H. (2019). *Current Status of a Japanese Lunar Polar Exploration Mission.* Japan Geoscience Union Meeting 2019. Makuhari Messe, Chiba, Japan.
- Jackson, A. U., Garcia-Reyes, J. F., Harper, J. D., Wiley, J. S., Molina-Diaz, A., Ouyang, Z., et al. (2010). Analysis of drugs of abuse in biofluids by low temperature plasma (LTP) ionization mass spectrometry. *Analyst* 135, 927–933. doi: 10.1039/b920155f
- Juraschek, R., Dülcks, T., and Karas, M. (1999). Nanoelectrospray-more than just a minimized-flow electrospray ionization source. *J. Am. Soc. Mass Spectrom.* 10, 300–308. doi: 10.1016/S1044-0305(98)00157-3
- Justes, D. R., Talaty, N., Cotte-Rodriguez, I., and Cooks, R. G. (2007). Detection of explosives on skin using ambient ionization mass spectrometry. *Chem. Commun.* 21, 2142–2144. doi: 10.1039/b703655h
- Karas, M., Bachmann, D., Bahr, U., and Hillenkamp, F. (1987). Matrix-assisted ultraviolet laser desorption of non-volatile compounds. *Inter. J. Mass Spectrom. Ion Proc.* 78, 53–68. doi: 10.1016/0168-1176(87)87041-6
- Karas, M., Bachmann, D., and Hillenkamp, F. (1985). Influence of the wavelength in high-irradiance ultraviolet laser desorption mass spectrometry of organic molecules. *Anal. Chem.* 57, 2935–2939. doi: 10.1021/ac00291a042
- Karas, M., and Bahr, U. (1990). Laser desorption/ionization mass spectrometry of large biomolecules. *Trends Anal. Chem.* 9, 321–325. doi: 10.1016/0165-9936(90)85065-F
- Karas, M., Bahr, U., and Dülcks, T. (2000). Nano-electrospray ionization mass spectrometry: addressing analytical problems beyond routine. *Fresenius J. Anal. Chem.* 366, 669–676. doi: 10.1007/s002160051561
- Kebarle, P. (2000). A brief overview of the present status of the mechanisms involved in electrospray mass spectrometry. *J. Mass Spectrom.* 35, 804–817. doi: 10.1002/1096-9888(200007)35:7<804::AID-JMS22>3.0.CO;2-Q
- Khan, N., Abdelhamid, H. N., Yan, J. Y., Chung, F. T., and Wu, H. F. (2015). Detection of flutamide in pharmaceutical dosage using higher electrospray ionization mass spectrometry (ESI-MS) tandem mass coupled with Soxhlet apparatus. *Anal. Chem. Res.* 3, 89–97. doi: 10.1016/j.ancr.2015.01.001
- Kumano, S., Nagano, H., Takada, Y., Sugiyama, M., Mizuno, H., Ito, T., et al. (2018). Development of evaluation method for explosives trace detection with non-contact sampling. *Sci. Tech. Energetic Mater.* 79, 124–130. <http://www.jes.or.jp/mag/stem/Vol.79/documents/Vol.79,No.4,p.124-130.pdf>
- Laidler, K. J. (1987). *Chemical Kinetics. 3rd Edn.* Pearson.
- Lee, E. D., Henion, J. D., and Covey, T. R. (1989). Microbore high performance liquid chromatography-ion spray mass spectrometry for the determination of peptides. *J. Microcol. Sep.* 1, 14–18. doi: 10.1002/mcs.1220010105
- Lias, S. G., Bartmess, J. E., Liebman, J. F., Holmes, J. L., Levin, R. D., and Mallard, W. G. (1988). Gas-phase ion and neutral thermochemistry. *J. Phys. Chem. Ref. Data* 17(Suppl. 1), 1–861.
- Liu, P., Huang, Q., Khan, M., Xu, N., Yao, H., and Lin, J. M. (2020). Microfluidic probe for in-situ extraction of adherent cancer cells to detect heterogeneity difference by electrospray ionization mass spectrometry. *Anal. Chem.* 92, 7900–7906. doi: 10.1021/acs.analchem.0c01200
- Loo, J. A., Edmonds, C. G., and Smith, R. D. (1990). Primary sequence information from intact proteins by electrospray ionization tandem mass spectrometry. *Science* 248, 201–204. doi: 10.1126/science.2326633
- Lowke, J. J., and Morrow, R. (1994). Theory of electric corona including the role of plasma chemistry. *Pure Appl. Chem.* 66, 1287–1294. doi: 10.1351/pac199466061287
- Mackay, W. A. (1931). Some investigations on the deformation and breaking of water drops in strong electric fields. *Proc. Royal Soc. A* 133, 565–587. doi: 10.1098/rspa.1931.0168
- Matsumura, S., Takezawa, H., and Isa, K. (2003). The fragmentation of amine cluster ion including HCl-Proton affinities of drugs of abuse. *J. Mass Spectrom. Soc. Jpn.* 51, 196–200. doi: 10.5702/massspec.51.196
- Mavrodineanu, R. (1984). Hollow cathode discharge. *J. Res. NBS* 89, 143–185. doi: 10.6028/jres.089.009
- McDonnell, L. A., and Heeren, R. M. (2007). Imaging mass spectrometry. *Mass Spectrom. Rev.* 26, 606–643. doi: 10.1002/mas.20124

- McLuckey, S. A., Goeringer, D. E., Asano, K. G., Vaidyanathan, G. Jr., and Stephenson, J. L. (1996). High explosives vapor detection by glow discharge ion trap mass spectrometry. *Rapid Commun. Mass Spectrom.* 10, 287–298. doi: 10.1002/(SICI)1097-0231(199602)10:3<287::AID-RCM429>3.0.CO;2-H
- Meng, C. K., Mann, M., and Fenn, J. B. (1988). Of protons or proteins. *Z. Phys. D Atoms Mol. Clusters* 10, 361–368. doi: 10.1007/BF01384871
- Na, N., Zhang, C., Zhao, M., Zhang, S., Yang, C., Fang, X., et al. (2007b). Direct detection of explosives on solid surfaces by mass spectrometry with an ambient ion source based on dielectric barrier discharge. *J. Mass Spectrom.* 42, 1079–1085. doi: 10.1002/jms.1243
- Na, N., Zhao, M., Zhang, S., Yang, C., and Zhang, X. (2007a). Development of a dielectric barrier discharge ion source for ambient mass spectrometry. *J. Am. Soc. Mass Spectrom.* 18, 1859–1862. doi: 10.1016/j.jasms.2007.07.027
- Nagato, K., Matsui, Y., Miyama, T., and Yamauchi, T. (2006). An analysis of the evolution of negative ions produced by a corona ionizer in air. *Int. J. Mass Spectrom.* 248, 142–147. doi: 10.1016/j.ijms.2005.12.001
- NASA. (2007). *Final Report of the International Space Station Independent Safety Task Force*. Washington, DC: IISTF, 1–107.
- Nevshupa, R. A. (2009). The role of a thermal mechanisms in the activation of tribodesorption and triboluminescence in miniature and lightly loaded friction unit. *J. Frict. Wear* 30, 118–126. doi: 10.3103/S1068366609020081
- Ng, T. T., So, P. K., Hu, B., and Yao, Z. P. (2019). Rapid detection and quantitation of drugs-of-abuse by wooden-tip electrospray ionization mass spectrometry. *J. Food Drug Anal.* 27, 428–438. doi: 10.1016/j.jfda.2018.09.002
- Nilles, J. M., Connell, T. R., Stokes, S. T., and Durst, H. D. (2010). Explosive detection using direct analysis in real time (DART) mass spectrometry. *Propellants Explos. Pyrotech.* 35, 446–451. doi: 10.1002/prep.200900084
- Nolan, J. J., and O'Keeffe, J. G. (1932). Electric discharge from water drops. *Proc. Royal Ir. Acad. Sec A Math. Phys. Sci.* 40, 86–98.
- Olivares, J. A., Nguyen, N. T., Yonker, C. R., and Smith, R. D. (1987). On-line mass spectrometric detection for capillary zone electrophoresis. *Anal. Chem.* 59, 1230–1232. doi: 10.1021/ac00135a034
- Penning, F. M. (1927). Über Ionisation durch metastabile atome (on the ionization of metastable atoms). *Naturwissenschaften* 15:818. doi: 10.1007/BF01505431
- Perez-Reyes, M., White, W. R., McDonald, S. A., Hill, J. M., Jeffcoat, A. R., and Cook, E. (1991). Clinical effects of methamphetamine vapor inhalation. *Life Sci.* 49, 953–959. doi: 10.1016/0024-3205(91)90078-p
- Pizzolato, T. M., de Alda, M. J. L., and Barceló, D. (2007). LC-based analysis of drugs of abuse and their metabolites in urine. *TrAC Trends Anal. Chem.* 26, 609–624. doi: 10.1016/j.trac.2007.04.005
- Pramanik, B. N., Ganguly, A. K., and Gross, M. L. (2002). *Applied Electrospray Mass Spectrometry: Practical Spectroscopy Series*. Florida: CRC Press.
- Press Release. (2002). *The Nobel Prize in Chemistry 2002*. Sweden: The Nobel Foundation.
- Rayleigh, L. (1882). On the equilibrium of liquid conducting masses charged with electricity. *Philos. Magazine* 14, 184–186. doi: 10.1080/14786448208628425
- Robert, S. (2008). “Space sciences (Mass Spectroscopy applications),” in *Mass Spectrometry: Instrumentation, Interpretation, and Applications*, eds. R. Ekman, J. Silberring, A. Westman-Brinkmalm, and A. Kraj (Hoboken, NJ: Wiley). 253–266.
- Rohner, T., Staab, D., and Stoeckli, M. (2005). MALDI mass spectrometric imaging of biological tissue sections. *Mechanisms Ageing Develop.* 126, 177–185. doi: 10.1016/j.mad.2004.09.032
- Ropero-Miller, J. D., and Goldberger, B. A. (1998). Recreational drugs: Current trends in the 90s. *Clin. Lab. Med.* 18, 727–746. doi: 10.1016/S0272-2712(18)30148-3
- Saha, S., Chen, L. C., Mandal, K. M., and Hiraoka, K. (2013). Leidenfrost Phenomenon-assisted Thermal Desorption (LPTD) and its application to open ion sources at atmospheric pressure mass spectrometry. *J. Am. Soc. Mass Spectrom.* 24, 341–347. doi: 10.1007/s13361-012-0564-y
- Sekar, R., Kailasa, S. K., Abdelhamid, H. N., Chen, Y. C., and Wu, H. F. (2013). Electrospray ionization tandem mass spectrometric studies of copper and iron complexes with tobramycin. *Inter. J. Mass Spectrom.* 338, 23–29. doi: 10.1016/j.ijms.2012.12.001
- Sekimoto, K., Sakai, M., and Takayama, M. (2012). Specific interaction between negative atmospheric ions and organic compounds in atmospheric pressure corona discharge ionization mass spectrometry. *J. Am. Soc. Mass Spectrom.* 23, 1109–1119. doi: 10.1007/s13361-012-0363-5
- Sekimoto, K., and Takayama, M. (2010). Negative ion formation and evolution in atmospheric pressure corona discharges between point-to-plane electrodes with arbitrary needle angle. *Eur. Phys. J. D* 60, 589–599. doi: 10.1140/epjd/e2010-10449-7
- Shiea, J., Huang, M. Z., Hsu, H. J., Lee, C. Y., Yuan, C. H., Beech, I., et al. (2005). Electrospray-assisted laser desorption/ionization mass spectrometry for direct ambient analysis of solids. *Rapid Commun. Mass Spectrom.* 19, 3701–3704. doi: 10.1002/rcm.2243
- Sigman, M. E., Clark, C. D., Fidler, R., Geiger, C. L., and Clausen, C. A. (2006). Analysis of triacetone triperoxide by gas chromatography/mass spectrometry and gas chromatography/tandem mass spectrometry by electron and chemical ionization. *Rapid Commun. Mass Spectrom.* 20, 2851–2857. doi: 10.1002/rcm.2678
- Smith, R. D., Barinaga, C. J., and Udseth, H. R. (1988a). Improved electrospray ionization interface for capillary zone electrophoresis-mass spectrometry. *Anal. Chem.* 60, 1948–1952. doi: 10.1021/ac00169a022
- Smith, R. D., Olivares, J. A., Nguyen, N. T., and Udseth, H. R. (1988b). Capillary electrophoresis-electrospray mass spectra of the herbicides paraquat and diquat. *Anal. Chem.* 60, 436–441. doi: 10.1021/ac00156a013
- Smith, R. D., Loo, J. A., Edmonds, C. G., Barinaga, C. J., and Udseth, H. R. (1990). New developments in biochemical mass spectrometry: electrospray ionization. *Anal. Chem.* 62, 882–899. doi: 10.1021/ac00208a002
- Song, Y., and Cooks, R. G. (2006). Atmospheric pressure ion/molecule reactions for the selective detection of nitroaromatic explosives using acetonitrile and air as reagents. *Rapid Commun. Mass Spectrom.* 20, 3130–3138. doi: 10.1002/rcm.2714
- Strupat, K., Karas, M., and Hillenkamp, F. (1991). 2,5-dihydroxybenzoic acid: a new matrix for laser desorption–ionization mass spectrometry. *Inter. J. Mass Spectrom. Ion Proc.* 72, 89–102. doi: 10.1016/0168-1176(91)85050-V
- Su, Y., Wang, H., Liu, J., Wei, P., Cooks, R. G., and Zheng, O. (2013). Quantitative paper spray mass spectrometry analysis of drugs of abuse. *Analyst* 138, 4443–4447. doi: 10.1039/c3an00934c
- Takada, Y., Kawaguchi, Y., Nagano, H., and Suzuki, Y. (2012b). Evaluation of false alarm rates of a walkthrough detection portal designed for detecting triacetone triperoxide (TATP) vapour from field test results and receiver operating characteristic (ROC) curves. *Int. J. Safety Secur. Eng.* 2, 25–264. doi: 10.2495/SAFE-V2-N3-256-264
- Takada, Y., Nagano, H., Kawaguchi, Y., Kashima, H., Sugaya, M., Terada, K., et al. (2016). Automated trace-explosives detection for passenger and baggage screening. *IEEE Sensors J.* 16, 1119–1129. doi: 10.1109/JSEN.2015.2499760
- Takada, Y., Nagano, H., Suga, M., Hashimoto, Y., Yamada, M., Sakairi, M., et al. (2002). Detection of military explosives by atmospheric pressure chemical ionization mass spectrometry with counter-flow introduction. *Propellants Explos. Pyrotech.* 27, 224–228. doi: 10.1002/1521-4087(200209)27:4<224::AID-PREP224>3.0.CO;2-V
- Takada, Y., Nagano, H., Suzuki, Y., Sugiyama, M., Nakajima, E., Hashimoto, Y., et al. (2011). High-throughput walkthrough detection portal for counter terrorism: detection of triacetone triperoxide (TATP) vapor by atmospheric-pressure chemical ionization ion trap mass spectrometry. *Rapid Commun. Mass Spectrom.* 25, 2448–2452. doi: 10.1002/rcm.5147
- Takada, Y., Suzuki, Y., Nagano, H., and Sugiyama, M. (2012a). High-throughput walkthrough detection portal as a measure for counter terrorism: design of a vapor sampler for detecting triacetone triperoxide vapor by atmospheric-pressure chemical ionization ion-trap mass spectrometry. *IEEE Sensors J.* 12, 1673–1680. doi: 10.1109/JSEN.2011.2176929
- Takáts, Z., Wiseman, J. M., Gologan, B., and Cooks, R. G. (2004). Mass spectrometry sampling under ambient conditions with desorption electrospray ionization. *Science* 306, 471–473. doi: 10.1126/science.1104404
- Takáts, Z., Cotte-Rodriguez, I., Talaty, N., Chena, H., and Cooks, R. G. (2005). Direct, trace level detection of explosives on ambient surfaces by desorption



- electrospray ionization mass spectrometry. *Chem. Commun.* 1950–1952. doi: 10.1039/B418697D
- Tanaka, K., Waki, H., Ido, Y., Akita, S., Yoshida, Y., Yoshida, T., et al. (1988). Protein and polymer analyses up to  $m/z$  100000 by laser ionization time-of flight mass spectrometry. *Rapid Commun. Mass Spectrom.* 2, 151–153. doi: 10.1002/rcm.1290020802
- Tang, K., Taranenko, N. I., Allman, S. L., Cháng, L. Y., Chen, C. H., and Lubman, D. M. (1994). Detection of 500-nucleotide DNA by laser desorption mass spectrometry. *Rapid Commun. Mass Spectrom.* 8, 727–730. doi: 10.1002/rcm.1290080913
- Tavares, L. S., Carvalho, T. C., Romão, W., Vaz, B. G., and Chaves, A. R. (2018). Paper spray tandem mass spectrometry based on molecularly imprinted polymer substrate for cocaine analysis in oral fluid. *J. Am. Soc. Mass Spectrom.* 29, 566–572. doi: 10.1007/s13361-017-1853-2
- Taylor, G. (1964). Disintegration of water droplets in an electric field. *Proc. Royal Soc. A* 280, 383–397. doi: 10.1098/rspa.1964.0151
- The Yomiuri Shimbun. (2019). *Japan, India to team up in race to discover water on moon.* *The Japan News.*
- Ushijima, H., Maekawa, R., Igarashi, E., and Akashi, S. (2019). Rapid and definitive analysis of *in vitro* DNA methylation by nano-electrospray ionization mass spectrometry. *J. Am. Soc. Mass Spectrom.* 30, 2335–2346. doi: 10.1007/s13361-019-02304-5
- Usmanov, D. T., Akhunov, S. D., Khasanov, U., Rotshteyn, V. M., and Kasimov, B. S. (2020). Direct detection of morphine in human urine by surface-ionization mass spectrometry. *Eur. J. Mass Spectrom.* 26, 153–157. doi: 10.1177/1469066719875655
- Usmanov, D. T., and Hiraoka, K. (2016). Discontinuous atmospheric pressure interface for mass spectrometry using a solenoid pulse valve. *Rapid Commun. Mass Spectrom.* 30, 1870–1874. doi: 10.1002/rcm.7654
- Usmanov, D. T., Hiraoka, K., Wada, H., Morita, S., and Nonami, H. (2016). Desorption of low-volatility compounds induced by dynamic friction between microdroplets and an ultrasonically vibrating blade. *Analyst* 141, 1398–1404. doi: 10.1039/C5AN02215K
- Usmanov, D. T., Mandal, M. K., Hiraoka, K., Ninomiya, S., Wada, H., Matsumura, M., et al. (2018). Dipping probe electrospray ionization/mass spectrometry for direct on-site and low-invasive food analysis. *Food Chem.* 260, 53–60. doi: 10.1016/j.foodchem.2018.04.003
- Usmanov, D. T., Ninomiya, S., and Hiraoka, K. (2013). Flash desorption/mass spectrometry for the analysis of less- and nonvolatile samples using a linearly driven heated metal filament. *J. Am. Soc. Mass Spectrom.* 24, 1727–1735. doi: 10.1007/s13361-013-0711-0
- Whitehouse, C. M., Dreyer, R. N., Yamashita, M., and Fenn, J. B. (1985). Electrospray interface for liquid chromatographs and mass spectrometers. *Anal. Chem.* 57, 675–679. doi: 10.1021/ac00280a023
- Wilm, M., and Mann, M. (1994). Electrospray and Taylor-cone theory, does the beam of macromolecules at last? *Int. J. Mass Spectrom. Ion Processes* 137, 167–180. doi: 10.1016/0168-1176(94)04024-9
- Wilm, M., and Mann, M. (1996). Analytical properties of the nanoelectrospray ion source. *Anal. Chem.* 68, 1–8. doi: 10.1021/ac9509519
- Wilson, C. T., and Taylor, G. I. (1925). The bursting of soap bubbles in a uniform electric field. *Proc. Cambridge Philos. Soc.* 22, 728–730. doi: 10.1017/S0305004100009609
- Wu, K. J., Steding, A., and Becker, C. H. (1993). Matrix-assisted laser desorption time-of-flight mass spectrometry of oligonucleotides using 3-hydroxypicolinic acid as an ultraviolet-sensitive matrix. *Rapid Commun. Mass Spectrom.* 7, 142–146. doi: 10.1002/rcm.1290070206
- Yamashita, M., and Fenn, J. B. (1984). Electrospray ion source. another variation on the free-jet theme. *J. Phys. Chem.* 20, 4451–4459. doi: 10.1021/j150664a002
- Yinon, J., McClellan, J. E., and Yost, R. A. (1997). Electrospray ionization tandem mass spectrometry collision-induced dissociation study of explosives in an ion trap mass spectrometry. *Rapid Commun. Mass Spectrom.* 11, 1961–1970. doi: 10.1002/(SICI)1097-0231(199712)11:18<1961::AID-RCM999>3.0.CO;2-K
- Zeleny, J. (1914). The electrical discharge from liquid points, and a hydrostatic method of measuring the electric intensity at their surfaces. *Phys. Rev.* 3, 69–91. doi: 10.1103/PhysRev.3.69
- Zhang, H., Lu, H., Huang, K., Li, J., Wei, F., Liu, A., et al. (2020). Selective detection of phospholipids in human blood plasma and single cells for cancer differentiation using dispersed solid-phase microextraction combined with extractive electrospray ionization mass spectrometry. *Analyst* 145, 7330–7339. doi: 10.1039/D0AN01204A
- Zhang, Y., Ma, X., Zhang, S., Yang, C., Ouyang, Z., and Zhang, X. (2009). Direct detection of explosives on solid surfaces by low temperature plasma desorption mass spectrometry. *Analyst* 134, 176–181. doi: 10.1039/B816230A

**Conflict of Interest:** HH was employed by company China Innovation Instrument Co., Ltd, Ningbo 315000, Zhejiang, China.

The remaining authors declare that the research was conducted in the absence of any commercial or financial relationships that could be construed as a potential conflict of interest.

Copyright © 2021 Habib, Bi, Hong and Wen. This is an open-access article distributed under the terms of the Creative Commons Attribution License (CC BY). The use, distribution or reproduction in other forums is permitted, provided the original author(s) and the copyright owner(s) are credited and that the original publication in this journal is cited, in accordance with accepted academic practice. No use, distribution or reproduction is permitted which does not comply with these terms.



# Analytical Characterization of 3-MeO-PCP and 3-MMC in Seized Products and Biosamples: The Role of LC-HRAM-Orbitrap-MS and Solid Deposition GC-FTIR

Giampietro Frison<sup>1</sup>, Flavio Zancanaro<sup>1</sup>, Samuela Frasson<sup>1</sup>, Laura Quadretti<sup>2</sup>, Michele Agnati<sup>2</sup>, Francesca Vlassich<sup>3</sup>, Giuseppe Gagliardi<sup>4</sup>, Tania Maria Grazia Salerno<sup>5</sup>, Paola Donato<sup>6\*</sup> and Luigi Mondello<sup>5,7,8,9</sup>

<sup>1</sup>Laboratory of Environmental Hygiene and Forensic Toxicology, DMPO Department, AULSS 3, Venice, Italy, <sup>2</sup>Emergency Department Unit, Madonna della Salute Hospital, AULSS 5, Porto Viro (Rovigo), Italy, <sup>3</sup>Intensive Care Unit, Madonna della Salute Hospital, AULSS 5, Porto Viro (Rovigo), Italy, <sup>4</sup>Department of Anesthesiology and Intensive Care, AULSS 5, Porto Viro (Rovigo), Italy, <sup>5</sup>BeSep S.r.l., c/o Department of Chemical, Biological, Pharmaceutical and Environmental Sciences, University of Messina, Messina, Italy, <sup>6</sup>Department of Biomedical, Dental, Morphological and Functional Imaging Sciences, University of Messina, Messina, Italy, <sup>7</sup>Department of Chemical, Biological, Pharmaceutical and Environmental Sciences, University of Messina, Messina, Italy, <sup>8</sup>Chromaleont S.r.l., c/o Department of Chemical, Biological, Pharmaceutical and Environmental Sciences, University of Messina, Messina, Italy, <sup>9</sup>Research Unit of Food Science and Nutrition, Department of Science and Technology for Humans and the Environment, Campus Bio-Medico University of Rome, Rome, Italy

## OPEN ACCESS

### Edited by:

Marta Concheiro-Guisan,  
John Jay College of Criminal Justice,  
United States

### Reviewed by:

Larabi Islam Amine,  
Hôpital Raymond-Poincaré, France  
Gabriella Massolini,  
University of Pavia, Italy

### \*Correspondence:

Paola Donato  
padonato@unime.it

### Specialty section:

This article was submitted to  
Analytical Chemistry,  
a section of the journal  
Frontiers in Chemistry

**Received:** 16 October 2020

**Accepted:** 22 December 2020

**Published:** 08 February 2021

### Citation:

Frison G, Zancanaro F, Frasson S, Quadretti L, Agnati M, Vlassich F, Gagliardi G, Salerno TMG, Donato P and Mondello L (2021) Analytical Characterization of 3-MeO-PCP and 3-MMC in Seized Products and Biosamples: The Role of LC-HRAM-Orbitrap-MS and Solid Deposition GC-FTIR.  
Front. Chem. 8:618339.  
doi: 10.3389/fchem.2020.618339

Among the phencyclidine (PCP) and synthetic cathinone analogs present on the street market, 3-methoxyphencyclidine (3-MeO-PCP) is one of the most popular dissociative hallucinogen drugs, while 3-methylmethcathinone (3-MMC) is a commonly encountered psychostimulant. Numerous 3-MeO-PCP- and 3-MMC-related intoxication cases have been reported worldwide. Identification of the positional isomers of MeO-PCP and MMC families are particularly challenging for clinical and forensic laboratories; this is mostly due to their difficult chromatographic separation (particularly when using liquid chromatography–LC) and similar mass spectrometric behaviors. 3-MeO-PCP and 3-MMC were identified in two powders, detained by two subjects and seized by the police, by different analytical techniques, including liquid chromatography-high-resolution accurate-mass Orbitrap mass spectrometry (LC-HRAM-Orbitrap-MS), and solid deposition gas chromatography-Fourier transform infrared spectroscopy (sd-GC-FTIR). LC-HRAM-Orbitrap-MS allowed us to assign the elemental formulae  $C_{18}H_{27}NO$  (MeO-PCP) and  $C_{11}H_{15}NO$  (MMC) through accurate mass measurement of the two  $MH^+$  ions, and the comparison of experimental and calculated  $MH^+$  isotopic patterns. However,  $MH^+$  collision-induced product ions spectra were not conclusive in discriminating between the positional isomers [(3-MeO-PCP vs. 4-MeO-PCP) and (3-MMC vs. 4-MMC and 2-MMC)]. Likewise, sd-GC-FTIR easily allowed us to differentiate between the MeO-PCP and MMC positional isomers unambiguously, confirming the presence of 3-MeO-PCP and 3-MMC, due to the high-quality match factor of the experimental FTIR spectra against the target FTIR spectra of MeO-PCP and MMC isomers in a dedicated library. 3-MeO-PCP (in contrast to 3-MMC) was also detected in blood and urine samples of both subjects and



analyzed in the context of routine forensic casework by LC-HRAM-Orbitrap-MS following a simple deproteinization step. In addition, this untargeted approach allowed us to detect dozens of phase I and phase II 3-MeO-PCP metabolites in all biological specimens. Analysis of the extracted samples by sd-GC-FTIR revealed the presence of 3-MeO-PCP, thus confirming the intake of such specific methoxy-PCP isomer in both cases. These results highlight the effectiveness of LC-HRAM-Orbitrap-MS and sd-GC-FTIR data in attaining full structural characterization of the psychoactive drugs, even in absence of reference standards, in both non-biological and biological specimens.

**Keywords:** 3-methoxyphencyclidine, 3-methylmethcathinone, non-fatal intoxication, forensic toxicology, liquid chromatography-high-resolution mass spectrometry, gas chromatography, fourier transform infrared spectroscopy, solid deposition GC-FTIR interface

## INTRODUCTION

The new psychoactive substances (NPS) phenomenon, characterized by peculiar features as opposed to the traditional drug phenomena (Peacock et al., 2019; Zamengo et al., 2019), has emerged as a global threat that challenges public health and institutions (UNODC, 2020). Psychoactive and physical effects, toxicity, addiction potential, and potency may vary dramatically among specific NPS. Furthermore, individual products may contain multiple psychoactive ingredients, adulterants, or by-products in extremely variable concentrations, exposing consumers to unpredictable doses of multiple NPS with serious health-related consequences, especially in young people (Zamengo et al., 2014; Orsolini et al., 2019; Larabi et al., 2020). According to their effects, dissociatives, sedatives/hypnotics, synthetic opioids, hallucinogens, synthetic cannabinoid receptor agonists, and psychostimulants are the NPS that most frequently appear on the recreational drug market (UNODC, 2020).

Synthetic cathinones include a very large number of substances with psychostimulant effects, elicited by augmenting central monoamine transmission through release facilitation and/or presynaptic transport inhibition (Simmons et al., 2018). 3-methylmethcathinone (3-MMC) is a commonly encountered synthetic cathinone, introduced in the NPS market to replace mephedrone (4-methylmethcathinone, 4-MMC), and it has seen rapid spread among drug users (Ferreira et al., 2019; Larabi et al., 2019a). 2-methylmethcathinone (2-MMC) has also been reported, albeit more rarely (Nycz et al., 2016). Several 3-MMC-related non-fatal and fatal intoxication cases have been described (Bäckberg et al., 2015b; Jamey et al., 2016; Ameline et al., 2019a; Margasińska-Olejak et al., 2019).

Phencyclidine (PCP)-based compounds are a group of dissociative hallucinogen NPS that exert their primary pharmacologic effect through blockade of excitatory N-methyl-D-aspartate (NMDA) receptors. Additional effects, as relatively weak opioid and dopamine receptor agonists and on serotonergic and noradrenergic pathways, have been described (Morris and Wallach, 2014; Wallach et al., 2014; Wallach and Brandt, 2018). Among the PCP analogs present on the street market, 3-methoxyphencyclidine (3-MeO-PCP) is one of the most popular ones. Even 4-methoxyphencyclidine (4-MeO-PCP)

and 2-methoxyphencyclidine (2-MeO-PCP) have been synthesized (Maddox et al., 1965). 4-MeO-PCP is less potent than 3-MeO-PCP, while 2-MeO-PCP is very weak (Kalir, 1981; Wallach and Brandt, 2018), probably explaining why the latter is almost absent from the recreational market. Instead, the relatively large worldwide diffusion of the most potent 3-MeO-PCP represents the cause of many non-fatal and fatal intoxication cases (Stevenson and Tuddenham, 2014; Bäckberg et al., 2015a; Bakota et al., 2016; Bertol et al., 2017; Johansson et al., 2017; Mitchell-Mata et al., 2017; Zidkova et al., 2017; Ameline et al., 2019b; Ameline et al., 2019c; Berar et al., 2019; de Jong et al., 2019; Grossenbacher et al., 2019; Kintz et al., 2019).

Widespread approaches to identification of NPS rely on gas chromatography (GC) or liquid chromatography (LC) separation coupled to mass spectrometry (MS) detection. A major challenge is thus posed by discrimination between regioisomers, in cases where the compounds show identical retention behavior, as well as fragmentation patterns. The combined use of different techniques may be required to gather complementary data supporting the submitted case. In a very recent report on a fatal intoxication case, the simultaneous combination of nuclear magnetic resonance ( $^1\text{H}$  NMR), ultra-high-performance liquid chromatography-tandem mass spectrometry (UHPLC-MS/MS), and GC-MS was deemed as necessary to discriminate the structural isomers of MeO-PCP in the biological specimens of the victim (Berar et al., 2019).

Likewise, Fourier Transform Infrared Spectroscopy (FTIR) can be very specific to the determination of functional groups within unknown samples by measuring small energy differences based on rotational and vibrational amplitudes between individual molecular bonds. In this regard, GC-FTIR data may well complement the information afforded by GC-MS and LC-MS in discriminating between regioisomeric compounds (Lee et al., 2019). Especially on-line techniques relying on the use of direct deposition interfaces enable sensitivity of at least two orders of magnitude more (at the ng scale) than the gas phase devices. Moreover, the sharper IR absorption bands arising from analytes in the solid state result in a significant gain in resolution with respect to spectra acquired from gas molecules (down to  $4\text{ cm}^{-1}$ ) affected by centrifugal distortion (Schneider and Demigian, 1986). The usefulness of solid deposition GC-FTIR (sd-GC-FTIR) in forensic laboratories has been demonstrated already for a number of different drug categories contained in

seized drugs (Lanzarotta et al., 2017; Cheng and Wong, 2019; Salerno et al., 2020); however the characterization of unknown molecules in biological specimens has never been attempted.

In this paper, we describe the analytical characterization, following two non-fatal intoxication cases, of 3-MMC and 3-MeO-PCP in seized products, and 3-MeO-PCP and its metabolites in biosamples. Different analytical techniques were employed, i.e., GC-MS with electron impact ionization (GC-EI MS), liquid chromatography-high-resolution accurate-mass Orbitrap mass spectrometry (LC-HRAM-Orbitrap-MS), and sd-GC-FTIR. The role of the two latter techniques in attaining full structural characterization of the psychoactive drugs and related metabolites, in both non-biological and biological samples, is highlighted.

## MATERIALS AND METHODS

### Chemicals

Water, acetonitrile, formic acid, ethyl acetate, methanol, and 3,4-Methylenedioxy-N-propylamphetamine (MDPA, internal standard, IS) were purchased from Sigma-Aldrich (Milan, Italy); ammonium formate, potassium dihydrogen phosphate, sodium hydroxide, and Bond Elute Certify 130 mg Solid Phase Extraction (SPE) columns were obtained from Agilent Technologies (Santa Clara, CA, United States).

### Sample Preparation

#### Seized Powders

Two white powders, contained in small bags, were seized by the police from two subjects later admitted to two nearby emergency departments because of neurological impairment. Bag labels indicated 3-MMC and 3-MeO-PCP as active ingredients. Police investigations found that both powders were purchased online. For analytical determination, 1 mg of each seized products were dissolved in 1 mL of methanol. About 1  $\mu$ L of a one-tenth-fold diluted methanol solution was injected into the GC-MS and sd-GC-FTIR systems, whereas 10  $\mu$ L of a 100-fold diluted methanol:LC mobile phase A (water with 0.05% formic acid and 10 mM ammonium formate) (10:90, v/v) solution were injected in the LC-HRAM-Orbitrap-MS system.

#### Biological Fluids

An immunoassay toxicological screening for common drugs of abuse and an enzymatic ethanol test were performed in urine and serum samples of both subjects upon hospital admission. For further toxicological tests, whole blood and urine samples were collected from subject A on admission, while plasma and urine samples were collected from subject B when admitted, and whole blood and urine the day after. For LC-HRAM-Orbitrap-MS analysis, 50  $\mu$ L aliquots of a 2  $\mu$ g/mL MDPA methanolic solution were poured in conical bottom tubes and evaporated to dryness by gently blowing nitrogen at an ambient temperature. Whole blood, plasma, and urine samples (250  $\mu$ L each) were subjected to protein precipitation by adding 750  $\mu$ L of acetonitrile/methanol 2:1 (v/v), previously stored at 4°C, drop

by drop while vortexing for 20 s. Precipitated samples were centrifuged at 2,800 rpm for 5 min and the supernatants taken to dryness. The residues were reconstituted with 50  $\mu$ L aliquots of methanol:LC mobile phase A (10:90, v/v) and transferred to glass inserts contained in 2 mL autosampler vials. Ten  $\mu$ L aliquots of the obtained solutions were injected onto the LC-HRAM-Orbitrap-MS system. For sd-GC-FTIR analysis, urine samples (0.5 mL each) were diluted with 6 mL of 0.1 M phosphate buffer and extracted on Bond Elute Certify 130 mg SPE columns. The obtained eluates were taken to dryness by gently blowing nitrogen at ambient temperature. The residues were reconstituted with 15  $\mu$ L of methanol and transferred to glass inserts contained in 2 mL autosampler vials. One  $\mu$ L aliquots of the methanolic solutions were injected into the sd-GC-FTIR system.

### GC-EI MS

GC-EI MS analyses of the seized powders were carried out as previously published (Frison et al., 2016b). Briefly, an Agilent 7890 series II/5975 GC/MS quadrupole mass spectrometer operating with electron ionization (EI, 70 eV) in full scan ( $m/z$  40–600) acquisition mode (Agilent Technologies, Cernusco sul Naviglio, Italy) was used. The capillary column was an Agilent HP-5MS UI (ultra inert, 30 m  $\times$  0.25 mm, 0.25  $\mu$ m film thickness), and the oven temperature was programmed from 50 to 300°C. Compounds were identified by comparison within the SWGDRUG MS Library version 3.6 (available at <http://www.swgdrug.org/ms.htm>), containing over 3,000 EI mass spectra of drugs and drug-related compounds.

### LC-HRAM-Orbitrap-MS

LC-HRAM-Orbitrap-MS analyses of both non-biological and biological specimens were carried out employing the analytical conditions previously published for the characterization of several NPS (Frison et al., 2015; Frison et al., 2016a; Frison et al., 2016b; Papa et al., 2019). Briefly, powder solutions and biosample extracts were analyzed using a Thermo Scientific Accela 1250 UHPLC system equipped with a Hypersil Gold PFP analytical column (2.1 mm  $\times$  100 mm, 1.9  $\mu$ m particle size), coupled to a Thermo Scientific single-stage Exactive HCD MS system, interfaced with an HESI-II source. Mobile phase A was water with 0.05% formic acid and 10 mM ammonium formate, and mobile phase B was acetonitrile with 0.05% formic acid. The flow rate was set to 400  $\mu$ L/min. The mobile phase gradient was as follows: 99% A for 1 min, linear gradient to 70% B in 6.5 min, linear gradient to 100% B in 1 min, held for 5.0 min, and column re-equilibration was performed with linear gradient to 99% A in 0.5 min, held for 3.0 min. MS was performed in positive-ion mode with a scan range from  $m/z$  50 to 800, alternating full scan (HCD off, resolution of 100,000 FWHM at  $m/z$  200) and “all-ion fragmentation” (AIF) (HCD on, collision energies 10, 25, and 50 eV, resolution of 25,000 FWHM at  $m/z$  200) acquisition. External mass calibration was performed, according to the guidelines provided by the instrument supplier, every 2 days over the mass range  $m/z$  130–2,000. Data were acquired and processed using Thermo Scientific Excalibur software version 2.1.0.

## sd-GC-FTIR

GC separations of seized powders and biological specimens were performed on a Nexis GC-2030 gas chromatograph equipped with an AOC-20i autosampler (Shimadzu, Kyoto, Japan) coupled to a DiscovIR solid deposition FTIR detector (Spectra-Analysis Instrument Inc., Marlborough, MA, United States). A Supelco SLB-5ms column (30 m × 0.25 mm, 0.25 μm film thickness) was employed for the separation (Merck KGaA, Darmstadt, Germany), using helium (purity 99.99%) as a carrier gas, at a constant linear velocity of 30 cm/s. The 1 μL samples were injected in splitless mode (1.50 min sampling time) at an injector temperature of 280°C. The oven temperature program was set to 100°C for 2 min before being ramped to 350°C at 15°C/min. The final temperature was held for 5.0 min, resulting in total analysis times of 24.0 min.

The end of the column was connected to a deactivated fused silica capillary through a micro Siltite μ-union (Trajan Scientific and Medical, Milton Keynes, United Kingdom) and inserted into a heated transfer line connected to the IR interface. The transfer line and restrictor temperatures were set at 280°C. Blanks were run in between samples to assure that the liner and column were free of contamination. The restrictor was positioned directly above a ZnSe disk, which was chilled down to −50°C by means of liquid nitrogen, and cleaned daily with acetone. The DiscovIR FTIR instrument was equipped with a Mercury-Cadmium-Telluride (MCT) cryogenically cooled detector. Solid-phase IR spectra of the GC eluted compounds were recorded in real time from 100 μm × 100 μm spots in the 650–4,000 cm<sup>−1</sup> range, with a resolution of 4 cm<sup>−1</sup> and a scan rate of 2 Hz, at a disc rotation speed of 3 mm/min. GC-FTIR data acquisition and processing were performed using the Thermo Galactic GRAMS/AI (version 9.3) spectroscopy and chromatography software. Compounds were identified through the library search program (Spectral ID), using a first derivative correlation algorithm, by comparison within a homemade solid deposition IR spectral library containing IR spectral data of around 600 NPS (namely, Controlled and Prohibited Substances version 1.0).

## RESULTS AND DISCUSSION

Identification of synthetic cathinone and PCP analogs, and in particular identification of positional isomers of the MMC and MeO-PCP families, may be particularly challenging for clinical and forensic laboratories. MMC and MeO-PCP analogs may show quite similar chromatographic and, especially, mass spectrometric behaviors, which may hinder their full characterization in the case of unavailability of reference standards for all isomers, and/or their metabolites in case of biosample analysis. These analytical challenges have been addressed by several authors by means of different analytical approaches, for the discrimination of 2-MMC, 3-MMC, and 4-MMC (Power et al., 2011; Power et al., 2012; Jamey et al., 2016; Maas et al., 2017; Zuba and Adamowicz, 2017; Nowak et al., 2018; Kranenburg et al., 2019; Kranenburg et al., 2020a; Kranenburg et al., 2020b) and 3-MeO-PCP and 4-MeO-PCP (Bäckberg et al.,

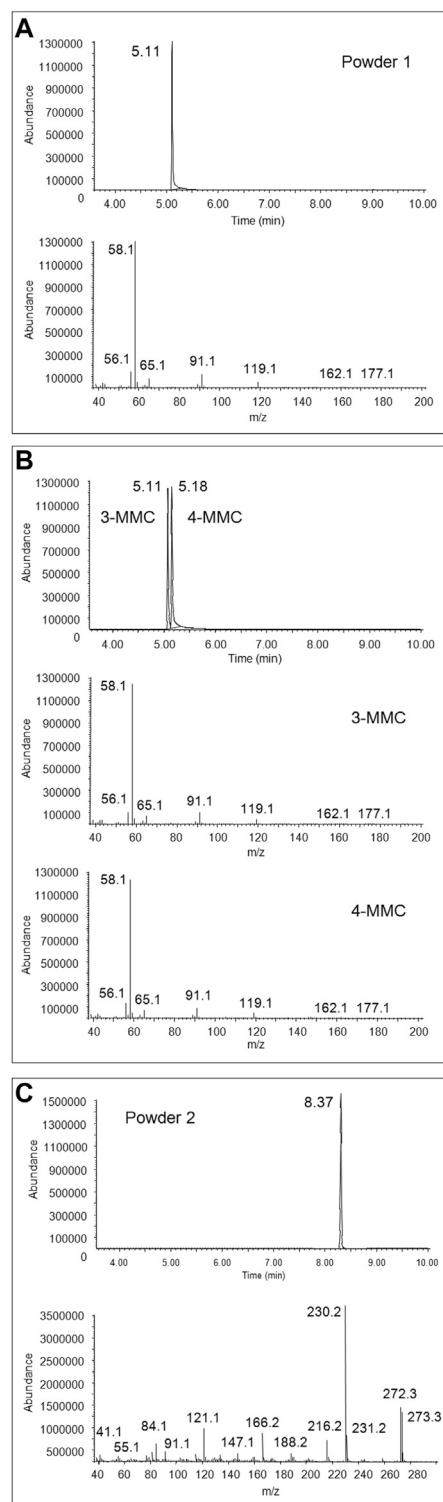


**FIGURE 1** | Full scan chromatogram and EI mass spectrum of the peak at 5.11 min obtained from GC-MS analysis of the first seized powder (A), full scan chromatogram and EI mass spectra, obtained from GC-MS analysis of 3-MMC and 4-MMC standards (B), and full scan chromatogram and EI mass spectrum of the peak at 8.37 min, obtained from GC-MS analysis of the second seized powder (C).

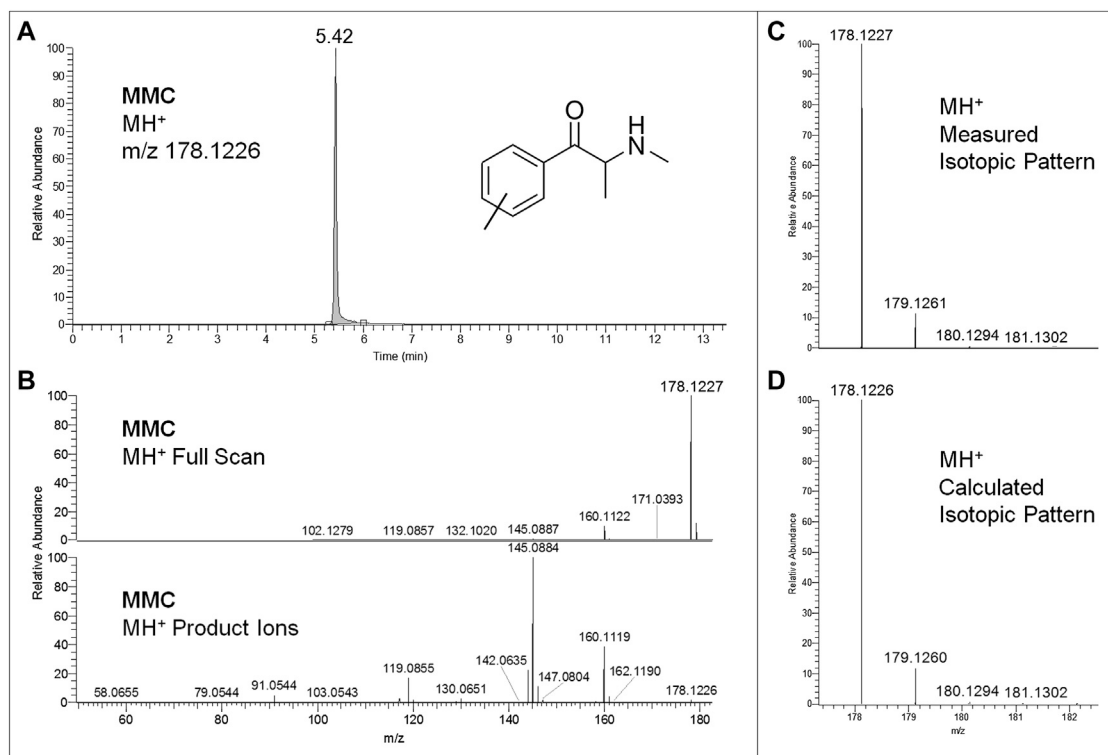


**FIGURE 2** | Extracted ion chromatogram at  $m/z$  178.1226 (MMC  $MH^+$  ions) of the full scan ion trace without fragmentation (A), corresponding MMC full scan mass spectrum and  $MH^+$  collision-induced product ion spectrum (collision energy 25 eV) (B), and experimental (C) and calculated (D) isotopic patterns of MMC  $MH^+$  ions, all obtained from LC-HRAM-Orbitrap-MS analysis of the first seized powder.

2015a; Bakota et al., 2016; Bertol et al., 2017; Johansson et al., 2017; Mitchell-Mata et al., 2017; Zidkova et al., 2017; Ameline et al., 2019b; Berar et al., 2019; de Jong et al., 2019; Kintz et al., 2019). However, such discriminative analyses were in most cases carried out with all the necessary reference standards available. We attained the full identification of the two NPS under study, in both non-biological (3-MMC and 3-MeO-PCP) and biological (3-MeO-PCP) specimens, through a combination of GC-EI MS, LC-HRAM-Orbitrap-MS, and sd-GC-FTIR, without resorting to specific reference standards. In particular, reliable results obtained from searching into dedicated spectral libraries allow for confident compound identification to be attained even if the reference material is not at hand.

## Analysis of Seized Powders

3-MMC and 3-MeO-PCP were putatively identified in the two seized powders through comparison of their GC-EI MS spectra with those of the SWGDRUG library and 3-MMC and 4-MMC reference standards, as, at the time of case processing, no 2-MMC and MeO-PCP standards were available (Figure 1). As a matter of fact, the identification of MMC and MeO-PCP positional isomers was not conclusive by GC-MS alone. Actually, isomers of the two chemical families may show similar EI spectra. For instance, 4-MMC, 3-MMC, and 2-MMC EI spectra are hardly distinguishable due to their extreme similarity (Power et al., 2011; Zuba and Adamowicz, 2017); they are in all cases

characterized by the barely visible molecular ions at  $m/z$  177, not abundant fragment ions at  $m/z$  162, 119, 91, 65, and 56 and the unspecific base peak at  $m/z$  58, caused by the well-known formation of the immonium ion via the amine-initiated alpha-cleavage of the benzylic bond, characteristic of all N-methyl phenethylamines (Frison et al., 2011). Also, 3-MeO-PCP and 4-MeO-PCP are hardly distinguishable by their EI spectra (Bertol et al., 2017; Mitchell-Mata et al., 2017; Kintz et al., 2019).

Regarding LC-HRAM-Orbitrap-MS analysis of the two seized powders, Figures 2, 3 show the extracted ion chromatograms at  $m/z$  178.1226 (MMC  $MH^+$  ions) and 274.2165 (MeO-PCP  $MH^+$  ions) of the full scan ion traces without fragmentation, the corresponding MMC and MeO-PCP full scan mass spectra and related  $MH^+$  collision-induced product ion spectra obtained in AIF conditions (HCD on, 25 eV), as well as the experimental and calculated isotopic patterns of MMC and MeO-PCP  $MH^+$  ions, obtained from the LC-HRAM-Orbitrap-MS analysis of the first and the second seized powder, respectively. Accurate mass measurements of the two  $MH^+$  ions had a mass accuracy [ $\Delta m = (\text{accurate mass} - \text{exact mass})/\text{exact mass} \times 10^6$ ] of +0.56 and -0.36 ppm for MMC and MeO-PCP, respectively. Fully superimposable experimental and calculated  $MH^+$  isotopic patterns were obtained for the two substances, with relative isotopic abundance (RIA,  $M+1/M+0$  ion abundances) error values (expressed as experimental RIA-calculated RIA)/calculated RIA $\times 100$ ) of -4.11 and -2.18% for MMC and



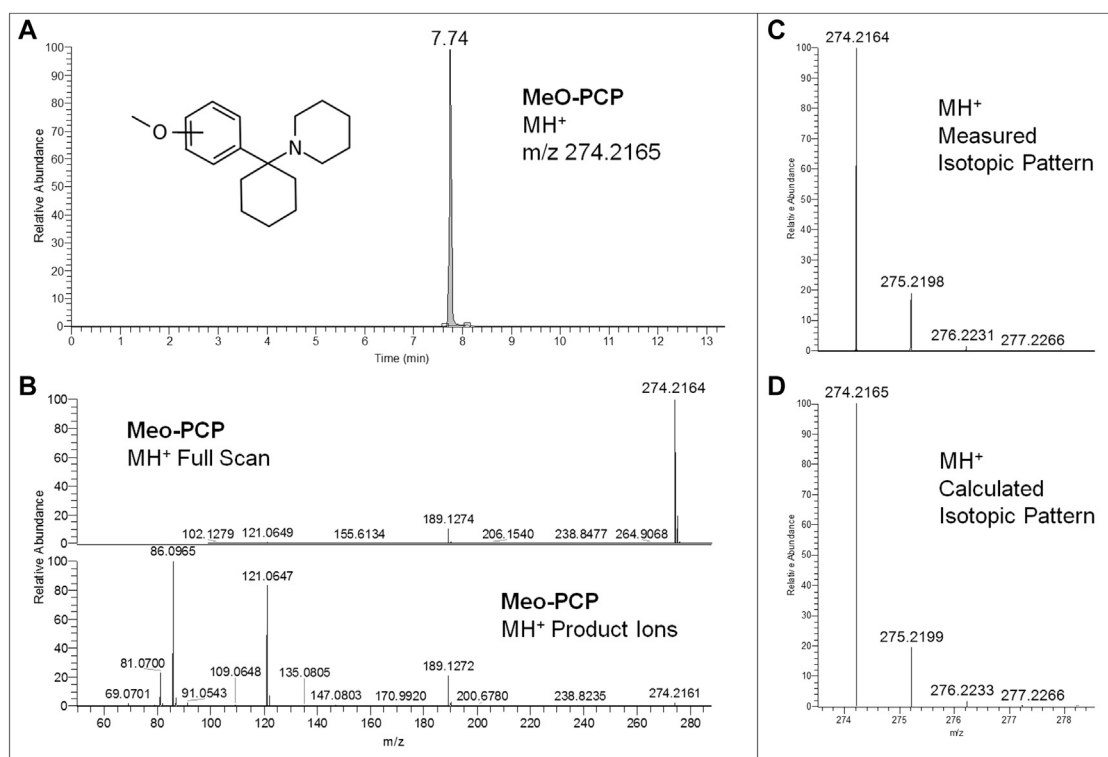


**FIGURE 3** | Extracted ion chromatogram at  $m/z$  274.2165 (MeO-PCP  $MH^+$  ions) of the full scan ion trace without fragmentation **(A)**, corresponding MeO-PCP full scan mass spectrum and  $MH^+$  collision-induced product ion spectrum (collision energy 25 eV) **(B)**, and experimental **(C)** and calculated **(D)** isotopic patterns of MeO-PCP  $MH^+$  ions, all obtained from LC-HRAM-Orbitrap-MS analysis of the second seized powder.

MeO-PCP, respectively. Hence, LC-HRAM-Orbitrap-MS measurements allowed us to assign the elemental formulae  $C_{11}H_{15}NO$  (MMC) and  $C_{18}H_{27}NO$  (MeO-PCP) for the two  $MH^+$  ions. However,  $MH^+$  collision-induced product ions spectra, although in agreement with those already described (Bakota et al., 2016; Frison et al., 2016a; Michely et al., 2017; Zidkova et al., 2017), were once again not conclusive in discriminating between the positional isomers [(3-MMC vs. 4-MMC and 2-MMC) and (3-MeO-PCP vs. 4-MeO-PCP)] without using reference standards, as even in these analytical conditions fragment ions sporting the same mass and similar abundances may be obtained from  $MH^+$  ions of individual MMC (Maas et al., 2017; Zuba and Adamowicz, 2017) and MeO-PCP (Bakota et al., 2016; Bertol et al., 2017; Zidkova et al., 2017) analogs.

Conversely, sd-GC-FTIR allowed us to identify MMC and MeO-PCP positional isomers unambiguously, confirming the presence of 3-MMC in the first seized powder and 3-MeO-PCP in the second seized powder. Confident discrimination of the positional isomers was possible based on the high quality match factor (QMF) of the experimental FTIR spectra against the target FTIR spectra upon searching in a dedicated solid-phase GC-FTIR library. The sharp absorption bands in FTIR spectra obtained from solid deposited analytes allow us to easily differentiate between very similar compounds, as shown in **Figure 4** for 3-MMC, 4-MMC, and 2-MMC. For identification purposes, the experimental GC-FTIR spectrum obtained for the

cathinone compound contained in the first seized powder was searched into a solid-phase GC-FTIR library containing IR spectral data of NPS (supplied by the vendor). A QMF criterion was adopted, based on quantitative evaluation of IR spectral data, as an unbiased criterion to achieve unambiguous compound identification. Thus, 3-MMC could be identified in the sample, ranking as Hit #1 in the library search result, with a QMF of 91.6%. Noticeably, much lower QMF values were obtained for the two incorrect matches, *viz.* 14.2% for the 4-substituted cathinone (4-MMC) and 11.0% for the 2-substituted isomer (2-MMC). It is also worth underlining that 4-MMC did not rank in the second hit position, as one could expect, but showed up as Hit #21, after a long list of candidates, and isomer 2-MMC was Hit #33.

In a similar way, the great specificity of molecule/bond-related information contained in the GC-FTIR spectrum allowed for a definite identification of the illicit drug constituent of the second seized powder, *i.e.*, 3-MeO-PCP. Again, a high QMF differential was obtained between the correct and the (closest) incorrect match, *i.e.*, the 3-methoxy-substituted phencyclidine and the 4-substituted isomer, thanks to distinctive spectral features especially in the fingerprint region to the right hand side of **Figure 5** (below  $1,500\text{ cm}^{-1}$ ). In detail, 3-MeO-PCP was found as Hit #1, with a QMF of 96.1%, while 4-MeO-PCP showed up as Hit #8, and with only 14.6% of a QMF. The significant gap in library search



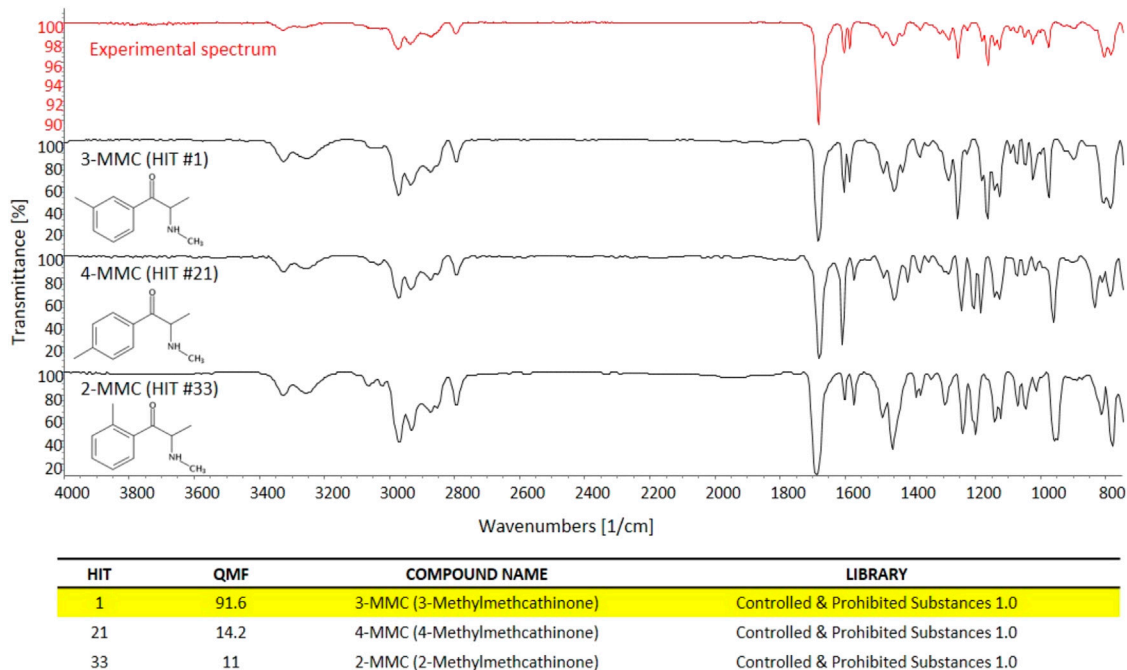


**FIGURE 4 |** The experimental GC-FTIR spectrum of 3-MMC, compared to the library GC-FTIR spectra of 3-MMC, 2-MMC, and 4-MMC isomers. Based on the library search results for 3-MMC FTIR spectral data, the following QMF values were obtained against correct and incorrect matches: Hit #1, 91.6%; Hit #21, 14.2%; Hit #33, 11.0%.

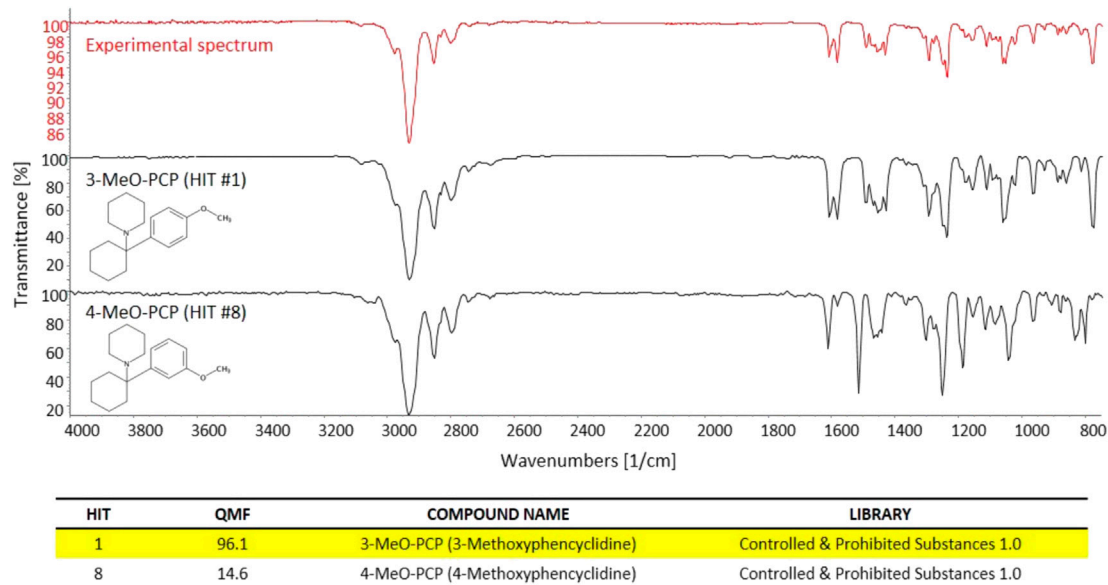


**FIGURE 5 |** The experimental GC-FTIR spectrum of 3-MeO-PCP, compared to the library GC-FTIR spectrum of 3-MeO-PCP and 4-MeO-PCP isomers. Based on the library search results for 3-MMC FTIR spectral data, the following QMF values were obtained against correct and incorrect match: Hit #1, 96.1%; Hit #8, 14.6%.

results would in turn reduce the likelihood for false positives and increase confidence in the identification. In more detail, the compounds that match in the library search between the 1st

and 21st hit for MMC were as follows: 3-Methylmethcathinone (Hit 1), 3-Methylethcathinone (Hit 2), 3-Ethylmethcathinone (Hit 3), Pentadron (Hit 4), N-Methylbenzedrone (Hit 5), 4-

Chloropentedrone (Hit 6), Ethcathinone (Hit 7), N-Ethylbuphedrone (Hit 8), 4-Methylcathinone (Hit 9), Cathinone (Hit 10), 3',4'-Tetramethylene- $\alpha$ -pyrrolidinovalerophenone (Hit 11), 4-Bromomethcathinone (Hit 12),  $\alpha$ -Isopropylamino-valerophenone (Hit 13), 4-Ethylmethcathinone (Hit 14), 3-Fluoromethcathinone (Hit 15), N-Ethylhexedrone (Hit 16), 4-Methyldiethcathinone (Hit 17), 3',4'-Tetramethylene- $\alpha$ -pyrrolidinobutiophenone (Hit 18), 4-Fluorobuphedrone (Hit 19), 4-Chloroethcathinone (Hit 20), and 4-Methylmethcathinone (Hit 21). The compounds that match in the library search between the first and eighth hit for MeO-PCP were as follows: 3-Methoxyphencyclidine (Hit 1), 3-Methoxyeticyclidine (Hit 2), Cannabicyclohexanol (Hit 3), Diphenidine (Hit 4), 4-[1-(3-Methoxyphenyl)cyclohexyl]morpholine (Hit 5), 5b-Androstane-3 $\alpha$ ,17b-diol (Hit 6), 4'-Methyl-2-piperidinopropiophenone (Hit 7), and 4-Methoxyphencyclidine (Hit 8).

## Analysis of Biological Fluids

All immunoassay toxicological screening for common drugs of abuse (not including PCP) performed in urine and serum samples were negative, which is the same as what occurred in other cases (Berar et al., 2019). If the immunoassay screening had included the PCP test (not a routine test in most European toxicology laboratories), a positive result would probably have been obtained considering the cross-reactivity of MeO-PCP analogs in several PCP immunoassay systems (Bäckberg et al., 2015a; Bakota et al., 2016; Chang and Smith, 2017; Mitchell-Mata et al., 2017; Gomila et al., 2019; Larabi et al., 2019b). Enzymatic ethanol tests were also negative in both cases.

Whole blood and urine samples collected from subject A, as well as whole blood, plasma, and urine samples collected from subject B on two consecutive days, were subjected to LC-HRAM-Orbitrap-MS analysis following a simple and rapid deproteinization step. 3-MeO-PCP was detected in all biosamples of both subjects, while no 3-MMC nor its metabolites dihydro-3-MMC (3-methylephedrine), nor-dihydro-3-MMC (3-methylnorephedrine), nor-3-MMC, hydroxytolyl-3-MMC, nor-hydroxytolyl-3-MMC, carboxy-3-MMC, carboxy-dihydro-3-MMC (Pedersen et al., 2013; Frison et al., 2016a) were detected in the samples from both subjects. This suggests that, of the two powders seized by police, only the one containing 3-MeO-PCP had been taken. No other NPS, traditional illicit drugs, or medications (other than those administered at the hospitals) were detected in both cases.

In addition, the comprehensive, untargeted, and sensitive analytical approach, consisting of generic sample preparation (a simple deproteinization step) and full scan MS detection in the high-resolution mode, allowed us to detect more than 20 phase I and 10 phase II 3-MeO-PCP metabolites in all biological specimens. Identification of metabolites was based on the following: 1) evaluation of their chromatographic behavior compared to the parent compound; 2) accurate mass measurements of their  $MH^+$  ions in full scan conditions; 3) evaluation of their  $MH^+$  isotopic patterns, including mass accuracy of  $MH^+$  ( $M+0$ ,  $M+1$ ,  $M+2$ ,  $M+3$ ) isotopic peaks; 4) accurate mass measurements of  $MH^+$  collision-induced productions (at three collision energies, 10, 25, 50 eV); and,

above all, 5) comparison with analytical results obtained with similar LC-HRAM-Orbitrap-MS instruments, reported in recently published papers dealing with 3-MeO-PCP metabolic studies on rat urine and human liver preparations (Michely et al., 2017), and a molecular networking approach application in a case of 3-MeO-PCP intoxication (Allard et al., 2019). In these studies, numerous phase I metabolites (related to 3-MeO-PCP multiple aliphatic hydroxylations at the cyclohexyl ring and the heterocyclic ring, single aromatic hydroxylation, carboxylation after ring opening, O-demethylation) and corresponding phase II glucuronide metabolites have been identified.

All equivalent analytical data from the present study are listed in detail in **Table 1**, as they may become supposedly helpful to other toxicologists in case of further 3-MeO-PCP intoxication cases. All phase I and phase II metabolites, being more hydrophilic and polar, elute at shorter retention times than the parent compound under the reported LC conditions, as previously described (Michely et al., 2017; Zidkova et al., 2017; Allard et al., 2019; Ameline et al., 2019c). Experimental isotopic patterns of each metabolite were in total agreement with the theoretical ones [ $MH^+$  ( $M+0$ )  $\Delta m$  values range from 0 to 1.37 ppm; ( $M+1$ ) values from 0 to 1.19 ppm; ( $M+2$ ) values from 0 to 2.76 ppm; ( $M+3$ ) values from  $-0.82$  to 4.20 ppm], and  $MH^+$  fragment ions, identified in variable numbers for each metabolite, mirrored those described in the above papers. Some values, mainly related to fragment ions, are missing due to the very low abundance of the specific metabolites. Typical full scan mass spectra,  $MH^+$  collision-induced product ion spectra obtained applying the three different (10, 25, 50 eV) collision energies, as well as experimental and calculated isotopic patterns, related to one phase I [piperidine-di-OH- ( $M1h$ )] and one phase II [O-demethyl-glucuronide- ( $M2a$ )] urinary metabolites, are shown in **Figures 6** and **7**. Similar results are shown in the **Supplementary Figures S1 and S2** for the O-demethyl- ( $M1a$ ), O-demethyl-piperidine-OH- ( $M1b$ ), and O-demethyl-piperidine-di-OH- ( $M1g$ ) phase I metabolites as well as the O-demethyl-piperidine-OH-glucuronide- ( $M2c$ ) phase II metabolite.

Although a great number of metabolites have been identified and listed in **Table 1**, a selection of compounds can be chosen to represent the main targets for an LC-(HR)MS screening of biofluids in case of suspected 3-MeO-PCP intoxication. Therefore, a specific instrumental layout covering the seven most abundant analytes for urine (and whole blood, barring the  $M1g$  metabolite) samples was arranged. Urinary metabolites other than the seven chosen all had minor abundances. **Figures 8** and **9** show the application of this layout, displaying the corresponding ion chromatograms of 3-MeO-PCP, the chosen phase I ( $M1a$ ,  $M1b$ ,  $M1g$ , and  $M1h$ ) and phase II ( $M2a$  and  $M2c$ ) metabolites, and the IS MDPA, obtained from whole blood and urine extracts, respectively, which were collected at the same time from the same subject (subject A in this case). Judging by the absolute and percent area values of compound peaks shown in the Figures, the relative abundances of both whole blood and urine 3-MeO-PCP and metabolite  $M1h$  (piperidine-di-OH-) were consistent with corresponding results reported by Allard et al. (2019). Roughly the same, as far as urine is concerned, for the abundance ratio of

**TABLE 1** | Chromatographic and mass spectrometric data of 3-MeO-PCP and its phase I and phase II metabolites identified in the biological specimens under study.

3-MeO-PCP Metabolite(s)	Acronym	MH <sup>+</sup> elemental composition	t <sub>R</sub> (min)	Exact mass, accurate mass, mass accuracy				MH <sup>+</sup> product ions						
				M+0 (MH <sup>+</sup> )	M+1	M+2	M+3	n. 1	n. 2	n. 3	n. 4	n. 5	n. 6	n. 7
3-MeO-PCP	3- MeO-PCP	C <sub>18</sub> H <sub>28</sub> NO	7.74	274.2165 274.2164 −0.36 ppm	275.2199 275.2198 −0.36 ppm	276.2233 276.2231 −0.72 ppm	277.2266 277.2266 0 ppm	189.1272	121.0647	95.0492	91.0543	86.0965	81.0700	-
O-demethyl-	M1a	C <sub>17</sub> H <sub>26</sub> NO	6.42	260.2009 260.2008 −0.38 ppm	261.2042 261.2041 −0.38 ppm	262.2076 262.2074 −0.76 ppm	263.2110 263.2109 −0.38 ppm	175.1115	107.0491	95.0492	91.0542	86.0965	81.0700	79.0544
O-demethyl-piperidine-OH-	M1b	C <sub>17</sub> H <sub>26</sub> NO <sub>2</sub>	5.49	276.1958 276.1956 −0.72 ppm	277.1992 277.1990 −0.72 ppm	278.2025 278.2023 −0.72 ppm	279.2059 279.2061 0.72 ppm	175.1113	107.0490	102.0912	95.0491	84.0808	81.0699	77.0388
O-demethyl-cyclohexyl-HO-	M1c	C <sub>17</sub> H <sub>26</sub> NO <sub>2</sub>	4.55	276.1958 5.01* 276.1958 5.09 0 ppm	277.1992 277.1992 277.1992 0 ppm	278.2025 278.2025 278.2025 −0.72 ppm	279.2059 279.2057 279.2057 −0.72 ppm	173.0959	107.0491	86.0966	79.0544	77.0387	-	-
O-demethyl-cyclohexyl-HO- dehydro-oxo-piperidine-	M1d	C <sub>17</sub> H <sub>22</sub> NO <sub>3</sub>	5.30	288.1594 288.1592 −0.69 ppm	289.1628 289.1625 −1.04 ppm	290.1661 290.1653 −2.76 ppm	-	98.0601	-	-	-	-	-	-
Piperidine-HO-	M1e	C <sub>18</sub> H <sub>28</sub> NO <sub>2</sub>	6.68	290.2115 290.2112 −1.03 ppm	291.2148 291.2146 −0.69 ppm	292.2182 292.2180 −0.68 ppm	293.2215 293.2211 −1.36 ppm	189.1274	121.0648	102.0914	91.0543	84.0809	81.0701	-
Cyclohexyl-HO- isomers	M1f	C <sub>18</sub> H <sub>28</sub> NO <sub>2</sub>	5.62* 6.18 6.34	290.2115 290.2112 −1.03 ppm	291.2148 291.2146 −0.69 ppm	292.2182 292.2179 −1.03 ppm	293.2215 293.2211 −1.36 ppm	205.1221	187.1116	121.0647	91.0543	86.0965	79.0544	77.0387
O-demethyl-piperidine-di-HO-	M1g	C <sub>17</sub> H <sub>26</sub> NO <sub>3</sub>	5.88	292.1907 292.1903 −1.37 ppm	293.1941 293.1938 −1.02 ppm	294.1974 294.1971 −1.02 ppm	295.1983 295.1977 −2.03 ppm	175.1114	118.0860	107.0490	101.0597	81.0699	79.0544	77.0387
Piperidine-di-HO-	M1h	C <sub>18</sub> H <sub>28</sub> NO <sub>3</sub>	6.95	306.2064 306.2061 −0.98 ppm	307.2097 307.2094 −0.98 ppm	308.2131 308.2129 −0.65 ppm	309.2140 309.2136 −1.29 ppm	189.1270	121.0646	118.0861	101.0597	100.0757	91.0543	81.0700
Cyclohexyl-HO-piperidine-HO- isomers	M1i	C <sub>18</sub> H <sub>28</sub> NO <sub>3</sub>	4.45* 5.15 5.33	306.2064 306.2063 −0.33 ppm	307.2097 307.2096 −0.33 ppm	308.2131 308.2131 0 ppm	309.2140 309.2127 −4.20 ppm	187.1114	121.0647	102.0914	84.0808	-	-	-
O-demethyl-cyclohexyl-HO- piperidine-di-HO-	M1k	C <sub>17</sub> H <sub>26</sub> NO <sub>4</sub>	4.72	308.1856 308.1856 0 ppm	309.1890 309.1889 −0.32 ppm	310.1923 310.1921 −0.64 ppm	-	191.1064	173.0958	118.0861	101.0597	-	-	-
Carboxy- methyl artifact	M1m	C <sub>19</sub> H <sub>30</sub> NO <sub>3</sub>	7.86	320.2220 320.2217 −0.94 ppm	321.2254 321.2251 −0.93 ppm	322.2287 322.2285 −0.62 ppm	323.2296 323.2297 0.31 ppm	189.1271	132.1017	115.0753	-	-	-	-
O-(demethyl-carboxy-cyclohexyl- HO-) methyl artifact	M1n	C <sub>18</sub> H <sub>28</sub> NO <sub>4</sub>	5.73	322.2013 322.2010 −0.93 ppm	323.2046 323.2044 −0.62 ppm	324.2080 324.2075 −1.54 ppm	-	-	-	-	-	-	-	-
Cyclohexyl-OH-piperidine-di-OH-	M1o	C <sub>18</sub> H <sub>28</sub> NO <sub>4</sub>	5.04	322.2013 322.2012 −0.31 ppm	323.2046 323.2045 −0.31 ppm	324.2080 324.2081 0.31 ppm	325.2089 325.2079 −3.07 ppm	187.1115	118.0860	100.0756	-	-	-	-
Carboxy-cyclohexyl-HO- methyl artifact isomers or Carboxy-alkyl-OH-	M1p	C <sub>19</sub> H <sub>30</sub> NO <sub>4</sub>	7.52 7.69* 8.23	336.2169 336.2166 −0.89 ppm	337.2203 337.2199 −1.19 ppm	338.2236 338.2230 −1.77 ppm	-	-	-	-	-	-	-	-

(Continued on following page)

**TABLE 1 |** (Continued) Chromatographic and mass spectrometric data of 3-MeO-PCP and its phase I and phase II metabolites identified in the biological specimens under study.

3-MeO-PCP Metabolite(s)	Acronym	MH <sup>+</sup> elemental composition	t <sub>R</sub> (min)	Exact mass, accurate mass, mass accuracy				MH <sup>+</sup> product ions						
				M+0 (MH <sup>+</sup> )	M+1	M+2	M+3	n. 1	n. 2	n. 3	n. 4	n. 5	n. 6	n. 7
O-demethyl- glucuronide	M2a	C <sub>23</sub> H <sub>34</sub> NO <sub>7</sub>	4.47	436.2330 436.2326 -0.92 ppm	437.2363 437.2359 -0.91 ppm	438.2397 438.2398 0.23 ppm	439.2406 439.2398 -1.82 ppm	175.1114	107.0490	95.0128	86.0964	81.0700	79.0544	-
O-demethyl-aryl-OH glucuronide	M2b	C <sub>23</sub> H <sub>34</sub> NO <sub>8</sub>	3.41	452.2279 452.2274 -1.11 ppm	453.2312 453.2310 -0.44 ppm	454.2346 454.2346 0 ppm	455.2355 455.2344 -2.42 ppm	191.1063	173.0958	107.0490	86.0964	79.0543	-	-
O-demethyl-piperidine-OH- glucuronide	M2c	C <sub>23</sub> H <sub>34</sub> NO <sub>8</sub>	4.07	452.2279 452.2275 -0.88 ppm	453.2312 453.2310 -0.44 ppm	454.2346 454.2346 0 ppm	455.2355 455.2346 -1.98 ppm	175.1114	107.0490	102.0913	84.0808	81.0699	-	-
O-demethyl-aryl-OH- dihydropyridine-OH- glucuronide	M2d	C <sub>23</sub> H <sub>30</sub> NO <sub>9</sub>	4.20	464.1915 464.1914 -0.22 ppm	465.1949 465.1947 -0.43 ppm	466.1982 466.1982 0 ppm	467.1991 467.1987 -0.86 ppm	173.0958	98.0601	79.0545	-	-	-	-
Piperidine-OH glucuronide	M2e	C <sub>24</sub> H <sub>36</sub> NO <sub>8</sub>	5.54	466.2435 466.2429 -1.29 ppm	467.2469 467.2465 -0.86 ppm	468.2503 468.2501 -0.43 ppm	469.2511 469.2501 -2.13 ppm	278.1227	189.1270	121.0646	102.0913	85.0284	84.0808	81.0700
O-demethyl-cyclohexyl-HO- piperidine-HO- glucuronide	M2f	C <sub>23</sub> H <sub>34</sub> NO <sub>9</sub>	3.77	468.2228 468.2226 -0.43 ppm	469.2262 469.2258 -0.85 ppm	470.2295 470.2294 -0.21 ppm	471.2304 471.2298 -1.27 ppm	-	-	-	-	-	-	-
O-demethyl-piperidine-di-OH- glucuronide	M2g	C <sub>23</sub> H <sub>34</sub> NO <sub>9</sub>	4.44	468.2228 468.2225 -0.64 ppm	469.2262 469.2259 -0.64 ppm	470.2295 470.2293 -0.43 ppm	471.2304 471.2295 -1.91 ppm	145.0657	107.0490	84.0808	79.0543	-	-	-
Cyclohexyl-HO-piperidine-HO- glucuronide	M2h	C <sub>24</sub> H <sub>36</sub> NO <sub>9</sub>	4.53	482.2385 482.2382 -0.62 ppm	483.2418 483.2416 -0.41 ppm	484.2452 484.2449 -0.62 ppm	485.2461 485.2465 0.82 ppm	187.1115	159.0802	121.0647	102.0914	84.0809	-	-
Piperidine-di-OH- glucuronide	M2i	C <sub>24</sub> H <sub>36</sub> NO <sub>9</sub>	5.93	482.2385 482.2379 -1.24 ppm	483.2418 483.2414 -0.83 ppm	484.2452 484.2449 -0.62 ppm	485.2461 485.2460 -0.21 ppm	121.0646	118.0861	-	-	-	-	-

Mass accuracy ( $\Delta m$ ) = (accurate mass – exact mass)/exact mass  $\times 10^6$ .

In case of isomers MS data refer to the most abundant one (\*).

Missing values (-) in some "isotopic pattern" or "product ion" columns are due to the very low abundance of some metabolites.

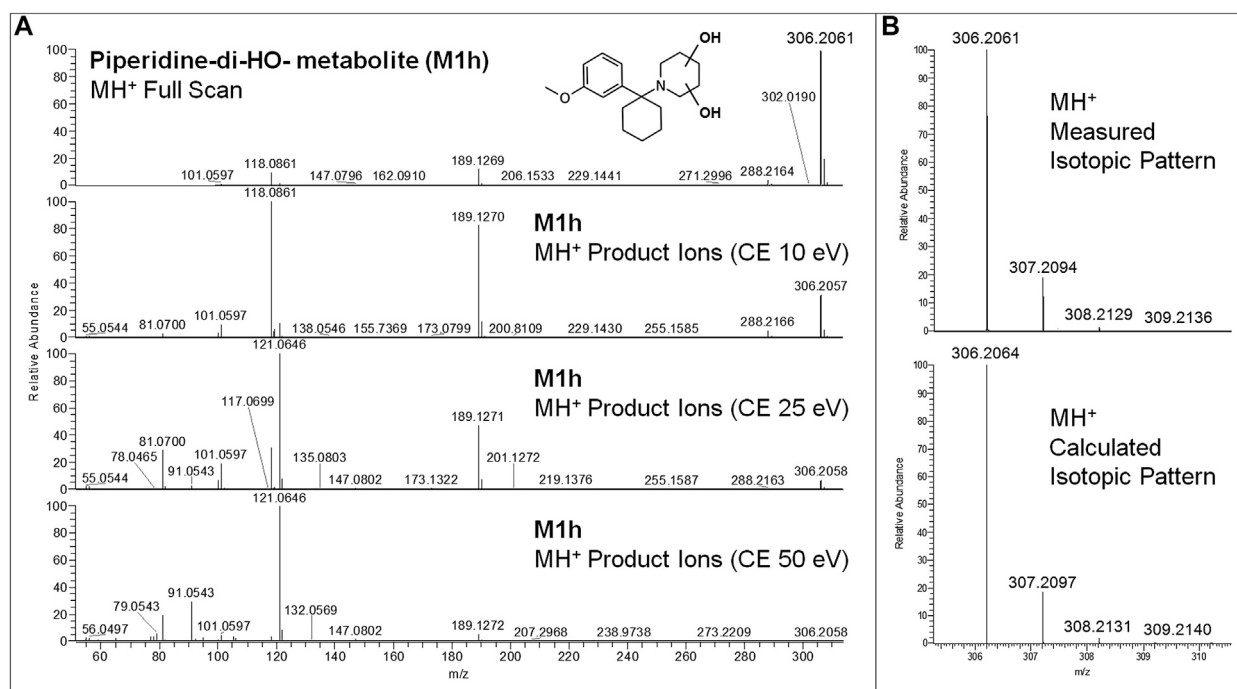


**FIGURE 6 |** 3-MeO-PCP piperidine-di-OH-metabolite (M1h) LC-HRAM-Orbitrap-MS full scan mass spectrum and MH<sup>+</sup> collision-induced product ion spectra (collision energies 10, 25, and 50 eV) **(A)**, experimental and calculated isotopic patterns of M1h MH<sup>+</sup> ions **(B)**, all obtained from LC-HRAM-Orbitrap-MS analysis of urine samples.

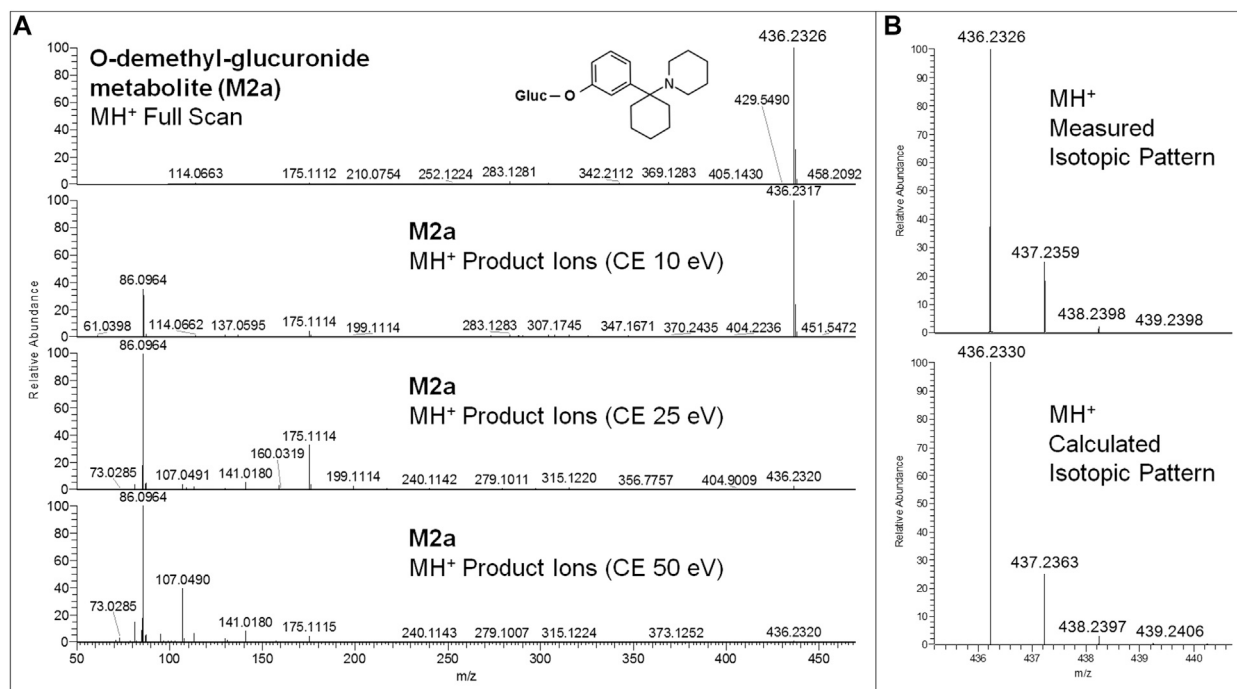


**FIGURE 7 |** 3-MeO-PCP O-demethyl-glucuronide-metabolite (M2a) LC-HRAM-Orbitrap-MS full scan mass spectrum and MH<sup>+</sup> collision-induced product ion spectra (collision energies 10, 25, 50 eV) **(A)**, and experimental and calculated isotopic patterns of M2a MH<sup>+</sup> ions **(B)**, all obtained from LC-HRAM-Orbitrap-MS analysis of urine samples.



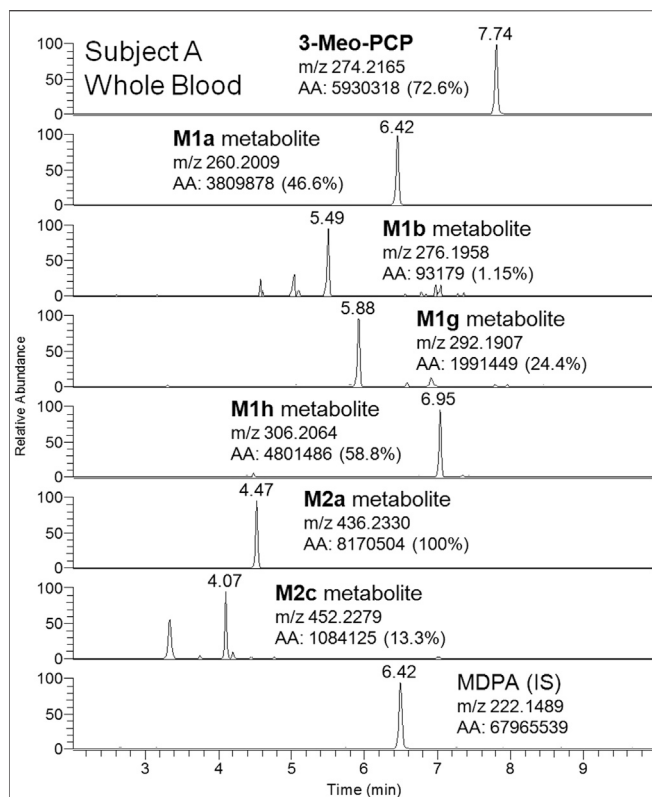


**FIGURE 8** | LC-HRAM-Orbitrap-MS ion chromatograms of 3-MeO-PCP, main phase I (M1a, M1b, M1g, and M1h) and phase II (M2a and M2c) metabolites, and the IS MDPA, obtained from whole blood collected at the same time of urine from the same subject.

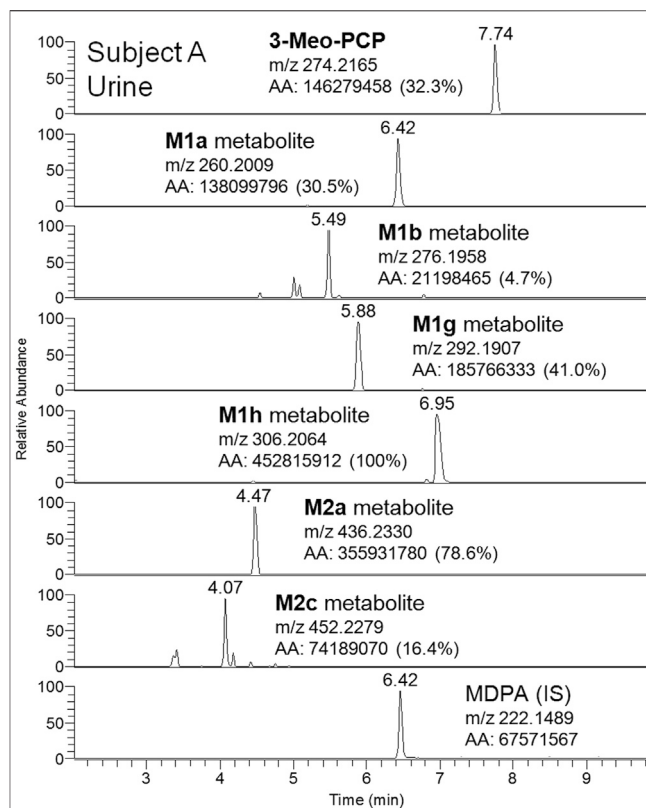


**FIGURE 9** | LC-HRAM-Orbitrap-MS ion chromatograms of 3-MeO-PCP, main phase I (M1a, M1b, M1g, and M1h) and phase II (M2a and M2c) metabolites, and the IS MDPA, obtained from urine collected at the same time of whole blood from the same subject.

M1a (O-demethyl-) to M1h (piperidine-di-OH-) metabolites, as well as abundance ratio of M2a (O-demethyl-glucuronide) to M2c (O-demethyl-piperidine-OH-glucuronide) metabolites. Moreover, differently from what is reported by Ameline et al. (2019c), elevated urinary metabolite-to-parent drug ratios were found here for some metabolites (M1g, M1h, and M2a), and this may be considered advantageous to increase the detection windows in intoxication cases. However, this was not the case with subject B, whose day 1 urine showed a higher abundance of parent compound compared to most metabolites. Hence, in these two cases, among other variables, different drug intake times may be hypothesized for the two subjects since, as widely known and already pointed out (Ameline et al., 2019c), metabolite ratios change during the parent drug excretion curve. Also, it should be considered that results from autopsy samples (Ameline et al., 2019c) may not be comparable with results from non-fatal cases, as those described here. As expected, analyte concentrations of biosamples collected from subject B were higher on hospital admission than on day 2 (data not shown). Whole blood 3-MeO-PCP quantitative analysis was not carried out due to 3-MeO-PCP reference standard unavailability at the time of case processing.

As further identification means, sd-GC-FTIR was applied for the analysis of SPE-extracted urine samples from both subjects. The presence of 3-MeO-PCP was revealed in both cases, thus proving, in conjunction with LC-HRAM-Orbitrap-MS, the intake

of such specific methoxy-PCP isomer by both subjects. A first GC-FTIR analysis of urine samples from both subjects did not yield satisfactory results, given the presence of a high number of different metabolites of the parent drug, all showing up as peaks of much higher abundance with respect to the compound under investigation (data shown in **Supplementary Figure S3**). In accordance with the results from LC-HRAM-Orbitrap-MS, the GC-FTIR peak corresponding to 3-MeO-PCP in a urine sample from patient B revealed much higher intensity than the corresponding one in subject A urine sample, with absorption intensities in the mid-IR region of 0.01 and 0.0032, respectively (data shown in **Supplementary Figure S3**). In both cases, the amount of analyte being deposited on the IR-transparent disc after GC separation was not sufficient to provide a full informative FTIR spectrum for identification purposes. This was reflected in the low QMF value obtained from searching the experimental spectra in a home-made solid-phase GC-FTIR library, which was equal to 13 for identification of 3-MeO-PCP in a urine sample from subject A. In order to enhance analyte detectability and further obtain confident identification of the target compound, concentrated deposits were obtained through multiple sample deposition. As expected, multiple deposits of the GC-eluted analyte from consecutive runs overlaid on the disc, afforded an increase in the signal-to-noise ratio, as shown in **Figure 10**. The similarity score, in terms of QMF, has increased to 80 after five consecutive

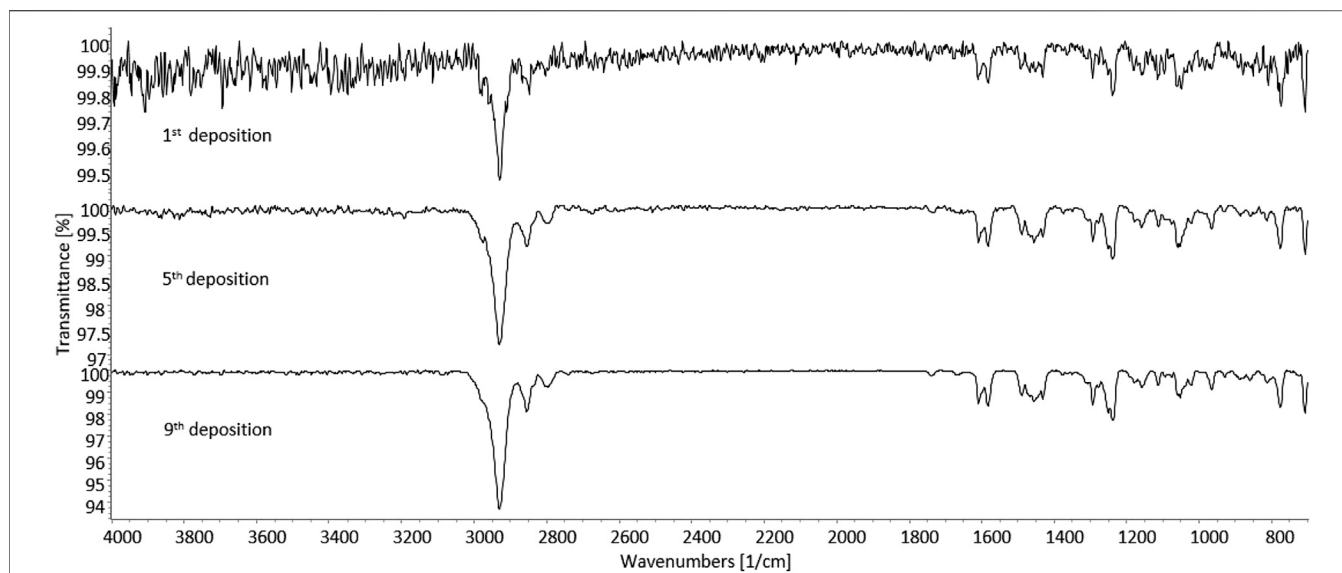


**FIGURE 10 |** Solid-phase GC-FTIR spectrum of 3-methoxyphenylcyclidine (3-MeO-PCP) in SPE-extracted human urine sample at  $4\text{ cm}^{-1}$  resolution. Top to bottom: increase in the signal-to-noise ratio resulting from multiple deposits of the GC-eluted analyte from consecutive runs overlaid on the disc. Column: Supelco SLB-5ms ( $30\text{ m} \times 0.25\text{ mm}$ ,  $0.25\text{ }\mu\text{m}$  film thickness).

depositions of the analyte, and progressively reached a value  $>90$  after the ninth deposition was accomplished (data shown in **Supplementary Figure S4**). This is related to a key validation parameter in spectroscopic measurements, defined as the limit of identification (LOI), and representing the lowest analyte concentration that yields a library searchable IR spectrum. Beyond the more common concept of Limit of Detection (LOD), LOI ultimately defines quantitatively the possibility for reliable identification of an unknown compound, contained at a certain amount in a given sample, and often in the presence of a noisy background (Salerno et al., 2020). As the result, 3-MeO-PCP was identified in the urine sample from subject A, with a QMF of 90.4 (Hit #1, correct match) vs. a QMF of 18 for the 4-MeO-PCP isomer (Hit #7, incorrect match).

Due to the higher concentration of the target 3-MeO-PCP analyte, only two consecutive depositions were sufficient in the case of a urine sample from subject B, for a QMF increase from 70 (first GC-FTIR analysis) to  $>90$  (second deposition). As for the previous case, a high QMF differential was obtained here too, between the correct (3-MeO-PCP) and the incorrect (4-MeO-PCP) match, viz. 92.9 vs. 12.2.

## CONCLUSION

The results described in this paper highlight the effectiveness of LC-HRAM-Orbitrap-MS and sd-GC-FTIR in attaining the full structural characterization of 3-MMC and 3-MeO-PCP in seized products, the identification of 3-MeO-PCP and numerous phase I and phase II metabolites in blood, plasma, and urine samples of both cases, and the discrimination between the MMC and MeO-PCP positional isomers [(3-MMC vs. 4-MMC and 2-MMC) and (3-MeO-PCP vs. 4-MeO-PCP)] in both non-biological and biological specimens.

Advanced MS techniques, such as LC-HRAM-Orbitrap-MS, represent valuable analytical tools in forensic toxicology, allowing for highly specific and sensitive untargeted or targeted drug detection in both seized materials and biological fluids. An outstanding analytical specificity is currently attainable; it is allowable through the accurate mass measurement of ionic species, the comparison of experimental and calculated isotopic patterns, and the study of collision-induced product ions obtained in high-resolution conditions. Furthermore, the application of HRMS measurements in full scan conditions avoids the drawbacks of the pre-selection of ions, as in Selected Ion Monitoring (SIM) or Multiple Reaction Monitoring (MRM) acquisition modes. Also, full-scan data may be always retrospectively processed, without resorting to new sample preparation and analytical runs.

Solid-phase GC-FTIR has proven to be an effective tool to widespread MS-based approaches, for achieving unequivocal identification of NPS, even in the case of regioisomers, having identical nominal masses, and yielding the same fragments upon dissociation. Noticeably, confident discrimination between 3-MeO-PCP and related isomers could be achieved from much lower analyte amounts ( $1\text{ }\mu\text{g}$  powder containing the molecule) compared to NMR approaches, which typically require mg-level quantities (Ameline et al., 2019b). Apart from the seized sample analysis, the application of sd-GC-FTIR to human urine samples demonstrated the usefulness of the technique for the investigation of biosamples of clinical and forensic toxicological concern. Thus, even in the absence of the powder, sd-GC-FTIR analysis of biological samples would have been sufficient to clarify the existence of a specific MeO-PCP positional isomer. Compared to the application of single GC, LC, and MS techniques for the discrimination of MMC and MeO-PCP analogs in non-biological drug samples, which can be problematic due to their quite similar

chromatographic and, especially, mass spectrometric, behaviors (Berar et al., 2019), the application of sd-GC-FTIR affords unambiguous identification of positional isomers.

## DATA AVAILABILITY STATEMENT

Due to legal reasons (analytical investigations requested by police for forensic purposes) the raw analytical data supporting the conclusions of this article are not publicly and indiscriminately available. They will be made available by the authors to qualified researchers only, on strictly specific and motivated instances. Any requests to access the raw data should be directed to the corresponding author.

## ETHICS STATEMENT

Ethical review and approval was not required for the study on human participants in accordance with the local legislation and institutional requirements. Written informed consent for participation was not required for this study in accordance with the national legislation and the institutional requirements.

## REFERENCES

- Allard, S., Allard, P. M., Morel, I., and Gicquel, T. (2019). Application of a molecular networking approach for clinical and forensic toxicology exemplified in three cases involving 3-MeO-PCP, doxylamine, and chlormequat. *Drug Test. Anal.* 11, 669–677. doi:10.1002/dta.2550
- Ameline, A., Dumestre-Toulet, V., Raul, J.-S., and Kintz, P. (2019a). Abuse of 3-MMC and forensic aspects: about 4 cases and review of the literature. *Toxicol. Anal. et Clin.* 31, 251–257. doi:10.1016/j.toxac.2018.11.001
- Ameline, A., Garnier, D., Gheddar, L., Richeval, C., Gaulier, J. M., Raul, J. S., et al. (2019b). Identification and analytical characterization of seven NPS, by combination of <sup>1</sup>H NMR spectroscopy, GC-MS and UPLC-MS/MS®, to resolve a complex toxicological fatal case. *Forensic Sci. Int.* 298, 140–148. doi:10.1016/j.forsciint.2019.03.003
- Ameline, A., Greney, H., Monassier, L., Raul, J. S., and Kintz, P. (2019c). Metabolites to parent 3-MeO-PCP ratio in human urine collected in two fatal cases. *J. Anal. Toxicol.* 43, 321–324. doi:10.1093/jat/bky097
- Bäckberg, M., Beck, O., and Helander, A. (2015a). Phencyclidine analog use in Sweden-intoxication cases involving 3-MeO-PCP and 4-MeO-PCP from the STRIDA project. *Clin. Toxicol.* 53, 856–864. doi:10.3109/15563650.2015.1079325
- Bäckberg, M., Lindeman, E., Beck, O., and Helander, A. (2015b). Characteristics of analytically confirmed 3-MMC-related intoxications from the Swedish STRIDA project. *Clin. Toxicol.* 53, 46–53. doi:10.3109/15563650.2014.981823
- Bakota, E., Arndt, C., Romoser, A. A., and Wilson, S. K. (2016). Fatal intoxication involving 3-MeO-PCP: a case report and validated method. *J. Anal. Toxicol.* 40, 504–510. doi:10.1093/jat/bkw056
- Berar, A., Allain, J. S., Allard, S., Lefevre, C., Baert, A., Morel, I., et al. (2019). Intoxication with 3-MeO-PCP alone: a case report and literature review. *Medicine* 98, e18295. doi:10.1097/MD.00000000000018295
- Bertol, E., Pascali, J., Palumbo, D., Catalani, V., Di Mili, M. G., Fioravanti, A., et al. (2017). 3-MeO-PCP intoxication in two young men: first *in vivo* detection in Italy. *Forensic Sci. Int.* 274, 7–12. doi:10.1016/j.forsciint.2016.12.028
- Chang, B. N., and Smith, M. P. (2017). A case of unusual drug screening results. *Clin. Chem.* 63, 958–961. doi:10.1373/clinchem.2016.264507
- Cheng, W. C., and Wong, W. C. (2019). Forensic drug analysis of chloro-N,N-dimethylcathinone (CDC) and chloroethcathinone (CEC): identification of 4-CDC and 4-CEC in drug seizures and differentiation from their ring-

## AUTHOR CONTRIBUTIONS

GF, PD, and LM: conception and design. FZ, SF, LQ, MA, FV, GG, and TS: acquisition of data. GF, FZ, SF, LQ, MA, FV, GG, TS, and PD: analysis and interpretation of data. GF and PD: drafting the article. All authors: contributed to the article and approved the submitted version.

## ACKNOWLEDGMENTS

The Laboratory of Environmental Hygiene and Forensic Toxicology, DMPO Department, AULSS 3 (Venice, Italy) gratefully acknowledges the invaluable help of Arianna Negro in analytical data processing and manuscript revision.

## SUPPLEMENTARY MATERIAL

The Supplementary Material for this article can be found online at: <https://www.frontiersin.org/articles/10.3389/fchem.2020.618339/full#supplementary-material>.

- substituted positional isomers. *Forensic Sci. Int.* 298, 268–277. doi:10.1016/j.forsciint.2019.03.002
- de Jong, L. A. A., Olyslager, E. J. H., and Duijst, W. L. J. M. (2019). The risk of emerging new psychoactive substances: the first fatal 3-MeO-PCP intoxication in The Netherlands. *J. Forensic Leg. Med.* 65, 101–104. doi:10.1016/j.jflm.2019.05.011
- Ferreira, B., Dias da Silva, D., Carvalho, F., de Lourdes Bastos, M., and Carmo, H. (2019). The novel psychoactive substance 3-methylmethcathinone (3-MMC or metaphedrone): a review. *Forensic Sci. Int.* 295, 54–63. doi:10.1016/j.forsciint.2018.11.024
- Frison, G., Gregio, M., Zamengo, L., Zancanaro, F., Frasson, S., and Sciarrone, R. (2011). Gas chromatography/mass spectrometry determination of mephedrone in drug seizures after derivatization with 2,2,2-trichloroethyl chloroformate. *Rapid Commun. Mass Spectrom.* 25, 387–390. doi:10.1002/rcm.4842
- Frison, G., Odoardi, S., Frasson, S., Sciarrone, R., Ortari, G., Romolo, F. S., et al. (2015). Characterization of the designer drug bk-2C-B (2-amino-1-(bromodimethoxyphenyl)ethan-1-one) by gas chromatography/mass spectrometry without and with derivatization with 2,2,2-trichloroethyl chloroformate, liquid chromatography/high-resolution mass spectrometry, and nuclear magnetic resonance. *Rapid Commun. Mass Spectrom.* 29, 1196–1204. doi:10.1002/rcm.7211
- Frison, G., Frasson, S., Zancanaro, F., Tedeschi, G., and Zamengo, L. (2016a). Detection of 3-methylmethcathinone and its metabolites 3-methylephedrine and 3-methylnorephedrine in pubic hair samples by liquid chromatography-high resolution/high accuracy orbitrap mass spectrometry. *Forensic Sci. Int.* 265, 131–137. doi:10.1016/j.forsciint.2016.01.039
- Frison, G., Zamengo, L., Zancanaro, F., Tisato, F., and Traldi, P. (2016b). Characterization of the designer drug deschloroketamine (2-methylamino-2-phenylcyclohexanone) by gas chromatography/mass spectrometry, liquid chromatography/high-resolution mass spectrometry, multistage mass spectrometry, and nuclear magnetic resonance. *Rapid Commun. Mass Spectrom.* 30, 151–160. doi:10.1002/rcm.7425
- Gomila, I., Lecifena, M. Á., Elorza, M. Á., Pastor, Y., Sahuquillo, L., Servera, M., et al. (2019). Detectability of dissociative psychoactive substances in urine by five commercial phencyclidine immunoassays. *J. Anal. Toxicol.* 43, 497–503. doi:10.1093/jat/bkz026
- Grossenbacher, F., Cazaubon, Y., Feliu, C., Ameline, A., Kintz, P., Passouant, O., et al. (2019). About 5 cases with 3 Meo-PCP including 2 deaths and 3 non-fatal cases seen in France in 2018. *Toxicol. Anal. et Clin.* 31, 332–336. doi:10.1016/j.toxac.2019.10.004

- Jamey, C., Kintz, P., Martrille, L., and Raul, J. S. (2016). Fatal combination with 3-methylmethcathinone (3-MMC) and gamma-hydroxybutyric acid (GHB). *J. Anal. Toxicol.* 40, 546–552. doi:10.1093/jat/bkw058
- Johansson, A., Lindstedt, D., Roman, M., Thelander, G., Nielsen, E. I., Lennborn, U., et al. (2017). A non-fatal intoxication and seven deaths involving the dissociative drug 3-MeO-PCP. *Forensic Sci. Int.* 275, 76–82. doi:10.1016/j.forsciint.2017.02.034
- Kalir, A. (1981). "Structure activity relationships of phencyclidine derivatives." in *PCP (phencyclidine), historical and current perspectives*. Editor E. F Domino (Arbor, MI: NPP Books), 31–46.
- Kintz, P., Ameline, A., Walch, A., Farrugia, A., and Raul, J. S. (2019). Murdered while under the influence of 3-MeO-PCP. *Int. J. Leg. Med.* 133, 475–478. doi:10.1007/s00414-018-1901-x
- Kranenburg, R. F., Garcia-Cicourel, A. R., Kukurin, C., Janssen, H. G., Schoenmakers, P. J., and van Asten, A. C. (2019). Distinguishing drug isomers in the forensic laboratory: GC-VUV in addition to GC-MS for orthogonal selectivity and the use of library match scores as a new source of information. *Forensic Sci. Int.* 302, 109900. doi:10.1016/j.forsciint.2019.109900
- Kranenburg, R. F., Peroni, D., Affourtit, S., Westerhuis, J. A., Smilde, A. K., and van Asten, A. C. (2020a). Revealing hidden information in GC-MS spectra from isomeric drugs: chemometrics based identification from 15 EV and 70 EV EI mass spectra. *Forensic Chem.* 18, 100225. doi:10.1016/j.forc.2020.100225
- Kranenburg, R. F., van Geenen, F. A. M. G., Berden, G., Oomens, J., Martens, J., and van Asten, A. C. (2020b). Mass-spectrometry-based identification of synthetic drug isomers using infrared ion spectroscopy. *Anal. Chem.* 92, 7282–7288. doi:10.1021/acs.analchem.0c00915
- Lanzarotta, A., Lorenz, L., Voelker, S., Falconer, T. M., and Batson, J. (2017). Forensic drug identification, confirmation, and quantification using a fully integrated gas chromatography-fourier transform infrared-mass spectrometer (GC-FT-IR-MS). *Appl. Spectrosc.* 72, 750–756. doi:10.1177/0003702817746964
- Larabi, I. A., Fabresse, N., Etting, I., Nadour, L., Pfau, G., Raphalen, J. H., et al. (2019a). Prevalence of New Psychoactive Substances (NPS) and conventional drugs of abuse (DOA) in high risk populations from Paris (France) and its suburbs: a cross sectional study by hair testing (2012–2017). *Drug Alcohol Depend.* 204, 107508. doi:10.1016/j.drugalcdep.2019.06.011
- Larabi, I. A., Fabresse, N., Etting, I., Abe, E., and Alvarez, J. C. (2019b). Rapid and simultaneous screening of new psychoactive substances and conventional drugs of abuse. a comparative study of Biochip Array Technology versus LC-MS/MS in whole blood and urine. *TIAFT Bull.* 2, 16–22.
- Larabi, I. A., Martin, M., Fabresse, N., Etting, I., Edel, Y., Pfau, G., et al. (2020). Hair testing for 3-fluorofentanyl, furanylfentanyl, methoxyacetylfentanyl, carfentanyl, acetylfentanyl and fentanyl by LC-MS/MS after unintentional overdose. *Forensic Toxicol.* 38, 277–286. doi:10.1007/s11419-019-00502-0
- Lee, H. Z. S., Koh, H. B., Tan, S., Goh, B. J., Lim, R., Lim, J. L. W., et al. (2019). Identification of closely related new psychoactive substances (NPS) using solid deposition gas-chromatography infra-red detection (GC-IRD) spectroscopy. *Forensic Sci. Int.* 299, 21–33. doi:10.1016/j.forsciint.2019.03.025
- Maas, A., Sydow, K., Madea, B., and Hess, C. (2017). Separation of ortho, meta and para isomers of methylmethcathinone (MMC) and methylethcathinone (MEC) using LC-ESI-MS/MS: application to forensic serum samples. *J. Chromatogr. B Analyt. Technol. Biomed. Life Sci.* 1051, 118–125. doi:10.1016/j.jchromb.2017.01.046
- Maddox, V. H., Godefroi, E. F., and Parcell, R. F. (1965). The synthesis of phencyclidine and other 1-arylcyclohexylamines. *J. Med. Chem.* 8, 230–235. doi:10.1021/jm00326a019
- Margasińska-Olejka, J., Celiński, R., Fischer, A., and Stojko, J. (2019). A fatal case of poisoning of a 19-year-old after taking 3-MMC. *Forensic Sci. Int.* 300, e34–e37. doi:10.1016/j.forsciint.2019.02.040
- Michely, J. A., Manier, S. K., Caspar, A. T., Brandt, S. D., Wallach, J., and Maurer, H. H. (2017). New psychoactive substances 3-methoxyphencyclidine (3-MeO-PCP) and 3-methoxyrolyclidine (3-MeO-PCPy): metabolic fate elucidated with rat urine and human liver preparations and their detectability in urine by GC-MS, "LC-(high resolution)-MSn" and "LC-(high resolution)-MS/MS". *Curr. Neuropharmacol.* 15, 692–712. doi:10.2174/1570159X14666161018151716
- Mitchell-Mata, C., Thomas, B., Peterson, B., and Couper, F. (2017). Two fatal intoxications involving 3-methoxyphencyclidine. *J. Anal. Toxicol.* 41, 503–507. doi:10.1093/jat/bkx048
- Morris, H., and Wallach, J. (2014). From PCP to MXE: a comprehensive review of the non-medical use of dissociative drugs. *Drug Test. Anal.* 6, 614–632. doi:10.1002/dta.1620
- Nowak, P. M., Olesek, K., Woźniakiewicz, M., and Kościelniak, P. (2018). Simultaneous enantioseparation of methcathinone and two isomeric methylmethcathinones using capillary electrophoresis assisted by 2-hydroxyethyl-β-cyclodextrin. *Electrophoresis* 39, 2406–2409. doi:10.1002/elps.201800142
- Nycz, J. E., Pazdziorek, T., Malecki, G., and Szala, M. (2016). Identification and derivatization of selected cathinones by spectroscopic studies. *Forensic Sci. Int.* 266, 416–426. doi:10.1016/j.forsciint.2016.06.034
- Orsolini, L., Chiappini, S., Corkery, J. M., Guirguis, A., Papanti, D., and Schifano, F. (2019). The use of new psychoactive substances (NPS) in young people and their role in mental health care: a systematic review. *Expert Rev. Neurother.* 19, 1253–1264. doi:10.1080/14737175.2019.1666712
- Papa, P., Valli, A., Di Tuccio, M., Frison, G., Zancanaro, F., Buscaglia, E., et al. (2019). Analytically confirmed intoxication by 4-fluoromethylphenidate, an analog of methylphenidate. *J. Anal. Toxicol.* 43, e1–e7. doi:10.1093/jat/bkz001
- Peacock, A., Bruno, R., Gisev, N., Degenhardt, L., Hall, W., Sedefov, R., et al. (2019). New psychoactive substances: challenges for drug surveillance, control, and public health responses. *Lancet* 394, 1668–1684. doi:10.1016/S0140-6736(19)32231-7
- Pedersen, A. J., Reitzel, L. A., Johansen, S. S., and Linnet, K. (2013). *In vitro* metabolism studies on mephedrone and analysis of forensic cases. *Drug Test. Anal.* 5, 430–438. doi:10.1002/dta.1369
- Power, J. D., McDermott, S. D., Talbot, B., O'Brien, J. E., and Kavanagh, P. (2012). The analysis of amphetamine-like cathinone derivatives using positive electrospray ionization with in-source collision-induced dissociation. *Rapid Commun. Mass Spectrom.* 26, 2601–2611. doi:10.1002/rcm.6383
- Power, J. D., McGlynn, P., Clarke, K., McDermott, S. D., Kavanagh, P., and O'Brien, J. (2011). The analysis of substituted cathinones. Part 1: chemical analysis of 2-, 3- and 4-methylmethcathinone. *Forensic Sci. Int.* 212, 6–12. doi:10.1016/j.forsciint.2011.04.020
- Salerno, T. M. G., Donato, P., Frison, G., Zamengo, L., and Mondello, L. (2020). Gas chromatography-Fourier transform infrared spectroscopy for unambiguous determination of illicit drugs: a proof of concept. *Front. Chem.* 8, 624. doi:10.3389/fchem.2020.00624
- Schneider, J. F., Demigian, J. C., and Stickler, J. C. (1986). A comparison of GC/IR interfaces: the light pipe versus matrix isolation. *J. Chromatogr. Sci.* 24, 330–335. doi:10.1093/chromsci/24.8.330
- Simmons, S. J., Leyrer-Jackson, J. M., Oliver, C. F., Hicks, C., Muschamp, J. W., Rawls, S. M., et al. (2018). DARK classics in chemical neuroscience: cathinone-derived psychostimulants. *ACS Chem. Neurosci.* 9, 2379–2394. doi:10.1021/acschemneuro.8b00147
- Stevenson, R., and Tuddenham, L. (2014). Novel psychoactive substance intoxication resulting in attempted murder. *J. Forensic Leg Med.* 25, 60–61. doi:10.1016/j.jflm.2014.04.007
- United Nations Office on Drugs and Crime (UNODC) (2020). *World drug report 2020. Booklet 4—cross-cutting issues: evolving trends and new challenges*. New York, NY: United Nations Publication, Sales No. E.20.XI.6.
- Wallach, J., and Brandt, S. D. (2018). "Phencyclidine-based new psychoactive substances," in *New psychoactive substances—pharmacology, clinical, forensic and analytical toxicology—handbook of experimental pharmacology*. Editors H. H. Maurer and S. D. Brandt (Cham, Switzerland: Springer International Publishing AG), Vol. 252, 261–303. doi:10.1007/164\_2018\_124
- Wallach, J., De Paoli, G., Adejare, A., and Brandt, S. D. (2014). Preparation and analytical characterization of 1-(1-phenylcyclohexyl)piperidine (PCP) and 1-(1-phenylcyclohexyl)pyrrolidine (PCPy) analogues. *Drug Test. Anal.* 6, 633–650. doi:10.1002/dta.1468
- Zamengo, L., Frison, G., Bettin, C., and Sciarone, R. (2014). Understanding the risks associated with the use of new psychoactive substances (NPS): high variability of active ingredients concentration, mislabelled preparations, multiple psychoactive substances in single products. *Toxicol. Lett.* 229, 220–228. doi:10.1016/j.toxlet.2014.06.012
- Zamengo, L., Frison, G., and Zwitter, G. (2019). Understanding and managing the new psychoactive substances phenomenon: a holistic approach. *J. Publ. Health Pol.* 40, 217–235. doi:10.1057/s41271-018-0156-6

Zidkova, M., Hlozek, T., Balik, M., Kopecky, O., Tesinsky, P., Svanda, J., et al. (2017). Two cases of non-fatal intoxication with a novel street hallucinogen: 3-methoxy-phencyclidine. *J. Anal. Toxicol.* 41, 350–354. doi:10.1093/jat/bkx009

Zuba, D., and Adamowicz, P. (2017). Distinction of constitutional isomers of mephedrone by chromatographic and spectrometric methods. *Aust. J. Forensic Sci.* 49, 637–649. doi:10.1080/00450618.2016.1167240

**Conflict of Interest:** Author TS was Technical Director of the company BeSep S.r.l. Author LM was Member of the Scientific Committee of the company BeSep S.r.l. and Scientific Member of the Board of Directors of Chromaleont S.r.l.

The remaining authors declare that the research was conducted in the absence of any commercial or financial relationships that could be construed as a potential conflict of interest.

Copyright © 2021 Frison, Zancanaro, Frasson, Quadretti, Agnati, Vlassich, Gagliardi, Salerno, Donato and Mondello. This is an open-access article distributed under the terms of the Creative Commons Attribution License (CC BY). The use, distribution or reproduction in other forums is permitted, provided the original author(s) and the copyright owner(s) are credited and that the original publication in this journal is cited, in accordance with accepted academic practice. No use, distribution or reproduction is permitted which does not comply with these terms.





# Evaluation of Illicit Drug Consumption by Wastewater Analysis Using Polar Organic Chemical Integrative Sampler as a Monitoring Tool

Roberta Zilles Hahn<sup>1</sup>, Carlos Augusto do Nascimento<sup>2</sup> and Rafael Linden<sup>1,3\*</sup>

<sup>1</sup>Laboratory of Analytical Toxicology, Universidade Feevale, Novo Hamburgo, Brazil, <sup>2</sup>Department of Production Engineering, Faculdades Integradas De Taquara, Taquara, Brazil, <sup>3</sup>National Institute of Forensic Science and Technology (INCT Forense), Porto Alegre, Brazil

## OPEN ACCESS

### Edited by:

Eugenia Gallardo,  
Universidade Da Beira Interior,  
Covilhã, Portugal

### Reviewed by:

André R. T. S. Araujo,  
Instituto Politécnico Da Guarda,  
Guarda, Portugal  
Paola Ondarza,  
Universidad Nacional De Mar Del  
Plata, Mar Del Plata, Argentina

### \*Correspondence:

Rafael Linden  
rafael.linden@feevale.br

### Specialty section:

This article was submitted to  
Analytical Chemistry,  
a section of the journal  
Frontiers in Chemistry

**Received:** 20 August 2020

**Accepted:** 25 January 2021

**Published:** 30 March 2021

### Citation:

Hahn RZ, Augusto do Nascimento C  
and Linden R (2021) Evaluation of Illicit  
Drug Consumption by Wastewater  
Analysis Using Polar Organic Chemical  
Integrative Sampler as a  
Monitoring Tool.  
Front. Chem. 9:596875.  
doi: 10.3389/fchem.2021.596875

Illicit drug abuse is a worldwide social and health problem, and monitoring illicit drug use is of paramount importance in the context of public policies. It is already known that relevant epidemiologic information can be obtained from the analysis of urban residual waters. This approach, named wastewater-based epidemiology (WBE), is based on the measurement of specific markers, resulting from human biotransformation of the target drugs, as indicators of the consumption of the compounds by the population served by the wastewater treatment installation under investigation. Drug consumption estimation based on WBE requires sewage sampling strategies that express the concentrations along the whole time period of time. To this end, the most common approach is the use of automatic composite samplers. However, this active sampling procedure is costly, especially for long-term studies and in limited-resources settings. An alternative, cost-effective, sampling strategy is the use of passive samplers, like the polar organic chemical integrative sampler (POCIS). POCIS sampling has already been applied to the estimation of exposure to pharmaceuticals, pesticides, and some drugs of abuse, and some studies evaluated the comparative performances of POCIS and automatic composite samplers. In this context, this manuscript aims to review the most important biomarkers of drugs of abuse consumption in wastewater, the fundamentals of POCIS sampling in WBE, the previous application of POCIS for WBE of drugs of abuse, and to discuss the advantages and disadvantages of POCIS sampling, in comparison with other strategies used in WBE. POCIS sampling is an effective strategy to obtain a representative overview of biomarker concentrations in sewage over time, with a small number of analyzed samples, increased detection limits, with lower costs than active sampling. Just a few studies applied POCIS sampling for WBE of drugs of abuse, but the available data support the use of POCIS as a valuable tool for the long-term monitoring of the consumption of certain drugs within a defined population, particularly in limited-resources settings.

**Keywords:** wastewater-based epidemiology, passive sampling, polar organic chemical integrative sampler, drug consumption, residual water

## INTRODUCTION

Abuse of licit and illicit drugs is an issue of global concern, with significant adverse impacts on human health and social welfare. Of particular concern is the abuse of illicit drugs, which are substances with prohibited or controlled nonmedical use, according to national laws (EMCDDA, 2019; UNODC, 2019). The nonmedical consumption of these controlled drugs (like cocaine, amphetamines, and Cannabis, among others) is usually associated with criminal activities, with severe social impacts (EMCDDA and Europol, 2019).

According to the World Drug Report, from the United Nations Office on Drugs and Crime (UNODC, 2019), 271 million people (5.5% of the World population between 15 and 64 years old) used illicit drugs at least once in 2017. Moreover, the same report estimates 35 million people suffering from illnesses due to drug consumption, with only one in each seven affected individuals receiving adequate treatment.

In this context, knowledge of the consumption behavior of these compounds is of utmost importance to develop damage reduction strategies and also to guide law enforcement strategic actions (Gao et al., 2018). Classical strategies to evaluate drug consumption behavior at the population level are based on epidemiological, sociological, and criminological indicators (EMCDDA, 2016). These strategies have several limitations, being intrinsically imprecise and inaccurate (Hernández et al., 2018). A novel and potentially sensitive way to detect emerging tendencies on drug abuse at a given population is the analysis of biomarkers of drug use in residual waters of a defined region, served by a wastewater treatment plant (WWTP) (van Wel et al., 2016). This evaluation approach is named wastewater-based epidemiology (WBE), which is defined as an analytical strategy to estimate drug consumption in a given population based on back-calculations, from concentrations of biomarkers measured in residual water (Devault et al., 2017b).

WBE is based on the principle that consumed drugs are excreted, either unaltered or as a mixture of metabolites, in urban wastewater networks and that the concentration of these chemical markers can be used to estimate the amount of drug consumed by the population served by the WWTP (van Wel et al., 2016; Hernández et al., 2018). WBE has the benefit of being able to detect changes in drug consumption patterns in a very sensitive and almost immediate way, being considered complementary to classical epidemiological tools (Gracia-Lor et al., 2017a).

A challenge to overcome in WBE is to obtain representative samples from residual waters. Single point sample collections (e.g., grab sampling) provide limited information due to the lack of temporal representativeness. A frequently used strategy is the use of automatic samplers, which allows the obtaining of composite samples, representative of a fixed period of time. Despite its value, automatic composite samplers are high-cost equipment and its use requires adequate facilities, including a power supply and environmental protection, which can be a limitation in resource-limited settings (Allan et al., 2006). Differently from the active sampling options, previously

mentioned, passive samplers such as the polar organic chemical integrative sampler (POCIS) are a more affordable and flexible option to obtain representative samples for WBE (Alvarez et al., 2007).

This manuscript aims to review the most important biomarkers of drug consumption in wastewater, the fundamentals of POCIS sampling in WBE, the previous application of POCIS for WBE of drugs of abuse, and to discuss the advantages and disadvantages of POCIS sampling, in comparison with other strategies in WBE. To this end, the PubMed database was searched considering articles published between the years 2000 and 2020, using the following keywords, both isolated or in combination: wastewater-based epidemiology, illicit drugs, passive sampling, and POCIS. The following filters were applied: full text, journal article, review, systematic review, English, and from 2000 to 2020. The combination of the keywords wastewater-based epidemiology and illicit drugs resulted in 116 hits, whereas POCIS and illicit drugs resulted in ten hits and POCIS and wastewater-based epidemiology resulted in only one hit. After checking for duplication of data, 99 published manuscripts were reviewed, with the addition of five online documents from national and international recognized agencies.

## WASTEWATER-BASED EPIDEMIOLOGY

Illicit drugs and its metabolites are emerging pollutants, and these compounds are frequently detected in environmentally relevant specimens, such as surface and residual waters (Boleda et al., 2009). As feces and urine contain amounts of ingested products, such as food, pharmaceuticals, and abused drugs, along with their metabolites, residual waters are an important source of information about the health conditions of a given population (Gracia-Lor et al., 2017a). It is also important to note that drugs can be found in residual waters as a result of accidental or intentional discharge from consumers of clandestine laboratories, making particularly relevant the use of metabolites as markers of human consumption (Pal et al., 2013). The evaluation of the presence of drugs and metabolites in environmental waters became feasible with the development of highly sensitive analytical methods (Gogoi et al., 2018). In this context, the use of biomarker concentrations in residual waters to estimate human consumption of drugs is named WBE (Causanilles et al., 2017).

The first report of the use of WBE for the estimation of illicit drug consumption dates from almost 20 years (Daughton, 2001). WBE requires knowledge of the size of the population served by the WWTP, the flow rate of the influent in the WWTP, and the metabolic rate of the parent drug with respect to the measured metabolite, along with the measured concentrations (Daughton, 2001). Recently, the European Drug Report included the use of WBE as a recommended method for monitoring illicit drug use at the population level, mainly due to the possibility of fast result reporting, almost in real-time, which allows immediate actions from the public authorities (EMCDDA, 2019).

**TABLE 1 |** Target compounds, biomarkers, excretion rates, and correction factors used in retrospective consumption calculations on the context of WBE.

Compound	Biomarker	Excretion rate of the biomarker (%)	Molecular weight ratio between drug and biomarker	Correction factor (f)	References
Cocaine	BZE	45	1.05	2.33	Daglioglu et al. (2019), Devault et al. (2014), Fallati et al. (2020), Foppe et al. (2018), Maldaner et al. (2012), Postigo et al. (2010), Postigo et al. (2011), van Nuijs et al. (2009a), Zuccato et al. (2005), Zuccato et al. (2008)
		38	1.05	2.77	Thomas et al. (2012), Mackulak et al. (2014), Mackulak et al. (2019)
		35	1.05	3.0	van Nuijs et al. (2011)
		35	1.10	3.14	Lai et al. (2011), Lai et al. (2013)
		30.07	1.05	3.49	Baker et al. (2014)
		30	1.05	3.50	Zhang et al. (2019)
		29	1.05	3.59	Castiglioni et al. (2013), Causanilles et al. (2017), Mercan et al. (2019), Ort et al. (2014b), van Wel et al. (2016)
	Cocaine	29	1.05	3.62	Archer et al. (2018)
		7.5	1.00	13.33	Lai et al. (2011)
		1.53	1.00	65.36	Baker et al. (2014)
	EME	15	1.52	10.20	van Nuijs et al. (2011)
	NBZE	0.95	1.10	115.79	Baker et al. (2014)
	Norcocaine	0.037	1.05	2,837.84	Baker et al. (2014)
Crack	AEME	0.19	1.67	878.95	Baker et al. (2014)
Amphetamine	Amphetamine	36	1	2.77	Krizman-Matasic et al. (2019), Mercan et al. (2019)
		30	1	3.33	Baker et al. (2014), Daglioglu et al. (2019), Devault et al. (2014), Emke et al. (2014), Fallati et al. (2020), Foppe et al. (2018), Postigo et al. (2010), Postigo et al. (2011), van Nuijs et al. (2011), van Wel et al. (2016), Zuccato et al. (2008)
Metamphetamine	Metamphetamine	43	1	2.33	Archer et al. (2018), Baker et al. (2014), Daglioglu et al. (2019), Fallati et al. (2020), Foppe et al. (2018), Postigo et al. (2010), Postigo et al. (2011), van Nuijs et al. (2011), Zhang et al. (2019), Zuccato et al. (2008)
		39	1	2.56	Lai et al. (2011)
		33	1	4.06	Lai et al. (2013)
		22.7	1	4.41	Mercan et al. (2019)
	Amphetamine	5.5	1.1	20.1	Lai et al. (2011), Archer et al. (2018)
	Norephedrine	5.0	0.99	19.7	Archer et al. (2018)
MDMA	MDMA	65	1	1.54	Zuccato et al. (2008), Postigo et al. (2010), Devault et al. (2014), van Wel et al. (2016), Daglioglu et al. (2019), Fallati et al. (2020)
		26	1	3.85	Postigo et al. (2011), Foppe et al. (2018)
		22.5	1	4.44	Archer et al. (2018), Krizman-Matasic et al. (2019), Mercan et al. (2019)
		20.3	1	4.93	Baker et al. (2014)
	HMMA	20	1	5.0	van Nuijs et al. (2011), Zhang et al. (2019)
		15	1	6.67	Lai et al. (2011), Emke et al. (2014)
		18.2	0.99	5.0	Archer et al. (2018)
		19	1	5.26	Baker et al. (2014), Foppe et al. (2018)
		0.025	1	4,000	Baker et al. (2014)
		55	1.29	2.35	Baker et al. (2014)
MDEA	MDEA	42.5	1.29	3.04	Daglioglu et al. (2019)
Heroin	Morphine	42	1.29	3.07	Zuccato et al. (2008), Boleda et al. (2009), Postigo et al. (2010), Fallati et al. (2020)
		4.2	1.29	30.71	Foppe et al. (2018)
		1.3	1.13	86.92	Postigo et al. (2011), van Nuijs et al. (2011), Foppe et al. (2018), Krizman-Matasic et al. (2019), Fallati et al. (2020)
	6-MAM	0.5	1.13	226	Baker et al. (2014)
		5	1.05	21.0	Baker et al. (2014)
Morphine	Normorphine	63.8	1	1.57	Baker et al. (2014)
Codeine	Codeine	30	1	3.33	Zhang et al. (2019)
		5.1	1.05	20.59	Baker et al. (2014)
		2.5	0.91	36.4	Postigo et al. (2011)
	THCCOOH	0.6	0.91	100	van Wel et al. (2016), Daglioglu et al. (2019)
		0.6	0.91	152	Zuccato et al. (2008), Boleda et al. (2009), Postigo et al. (2010), Lai et al. (2011), Devault et al. (2014), Mercan et al. (2019), Fallati et al. (2020)
THC		0.5	0.91	182	Causanilles et al. (2017), Foppe et al. (2018), Krizman-Matasic et al. (2019)

(Continued on following page)

**TABLE 1 |** (Continued) Target compounds, biomarkers, excretion rates, and correction factors used in retrospective consumption calculations on the context of WBE.

Compound	Biomarker	Excretion rate of the biomarker (%)	Molecular weight ratio between drug and biomarker	Correction factor (f)	References
Ketamine	Ketamine	20	1	5.0	Du et al. (2020)
		2.3	1	43.48	Baker et al. (2014)
	Norketamine	4	1.06	26.50	Du et al. (2020)
		1.6	1.06	65	Lai et al. (2013)
		1.6	1.06	66.25	Baker et al. (2014), Zhang et al. (2019)
Phencyclidine	Phencyclidine	10	1	10	Baker et al. (2014)
Methadone	Methadone	27.8	1	3.60	Baker et al. (2014)
		27.5	1	3.64	Postigo et al. (2011)
	EDDP	55	1.06	1.93	Du et al. (2019), Zhang et al. (2019)
		25	1.12	3.6	Krizman-Matasic et al. (2019)
		25	0.82	3.28	Boleda et al. (2009)
		24.6	1.06	4.31	Baker et al. (2014)
		23	1.12	4.87	van Nuijs et al. (2011)
		13	0.82	6.31	Devault et al. (2014)
Mephedrone	Mephedrone	15.4	1	6.5	Archer et al. (2018)
Mescaline	Mescaline	57.5	1	1.74	Baker et al. (2014)
Ephedrine	Ephedrine	75	1	1.33	Postigo et al. (2010), Postigo et al. (2011)

6-MAM, 6-monoacetylmorphine; AEME, anhydroecgonine methyl ester; BZE, benzoylecgonine; EDDP, 2-ethylidene-1,5-dimethyl-3,3-diphenylpyrrolidine; EME, ecgonine methyl ester; HMMA, 4-hydroxy-3-methoxymethamphetamine; MDEA, methyldiethanolamine; MDMA, 3,4-methylenedioxy-N-methylamphetamine; NBZE, norbenzoylecgonine; THC,  $\Delta^9$ -tetrahydrocannabinol; THCCOOH, 11-nor-9-carboxy-THC; WBE, wastewater-based epidemiology.

Classical strategies to evaluate drug consumption at the population level are based on information gathered from questionnaires, drug seizing statistics, and criminal and medical records (EMCDDA, 2016). These classical approaches are dependent on the self-report of the participants of the survey. However, the reliability of the self-report is affected by moral and social restraints, which can significantly impact the quality of the data (van Wel et al., 2016). Additionally, population surveys are expensive and complex to perform (Hernández et al., 2018). The benefits of WBE resulted in the publication of studies in many countries of the world (Archer et al., 2018; Bannwarth et al., 2019; Banta-Green et al., 2016; Bartelt-Hunt et al., 2009; Baz-Lomba et al., 2016; Benaglia et al., 2020; Boleda et al., 2009; Burgard et al., 2019; Foppe et al., 2018; Kankaanpää et al., 2016; Mackulak et al., 2014; Maldaner et al., 2012; Metcalfe et al., 2010; van Nuijs et al., 2009b; Zhang et al., 2019; Zuccato et al., 2008). In fact, since 2011, the Europe-wide network (Sewage analysis CORE Group Europe (SCORE)) performs the systematic monitoring of consumption biomarkers of four priority drugs (cocaine, methylenedioxymethamphetamine (MDMA), amphetamine, and methamphetamine) in WWTPs, covering 68 cities from 23 European countries in 2019 (EMCDDA, 2020).

However, WBE cannot provide information on the most common administration route, profile of the consumers, or purity and quality of the used drugs. Other challenges on the application of WBE include the uncertainties on the representativeness of the sampling procedure, lack of knowledge about the stability and chemical behavior of the measured biomarkers on the residual waters, variable analytical reliability of the measurements, availability of strategies to estimate the population size served by the WWTP, and the uncertainties on the calculation procedure to

retrospective estimate drug consumption by the population (Thomas et al., 2012; Castiglioni et al., 2013).

The estimation of the daily drug consumption per inhabitant ( $C$ ,  $\text{mg day}^{-1} 1,000 \text{ inh}^{-1}$ ) using WBE is based on a retrospective calculation, as presented in Eq. 1. First, the raw daily drug consumption of the drug at the population served by the WWTP is estimated by multiplying the concentration of the biomarker ( $c$ ,  $\text{ng L}^{-1}$ ) in a representative sample by the daily influent flow at the WWTP ( $Q_v$ ,  $\text{L day}^{-1}$ ) and by a correction factor ( $f$ ), which accounts for the average excretion rate of the biomarker and for the ratio between the molecular weight of the parent drug and its metabolite (van Nuijs et al., 2011; Zuccato et al., 2008). Afterward, the daily drug consumption per inhabitant ( $\text{inh}$ ) is obtained dividing by the number of individuals served by the WWTP. The value is multiplied by 1,000 to normalize for 1,000 inhabitants. Table 1 presents an overview of  $f$  values described in previous studies. Important to note is that these calculations require that the measured biomarker is specific and unique for a certain drug (Zuccato et al., 2008).

$$C = \left[ \frac{c \cdot Q_v \cdot f}{\text{inh}} \right] \cdot 1000 \quad [1]$$

Besides the correction applied in Eq. 1, the measured concentrations can also be multiplied by a correction factor that takes the biomarker stability on residual waters into account. van Nuijs et al., 2011 considered that ecgonine methyl ester (EME), amphetamine, and 6-monoacetyl morphine (6-MAM) had a degradation percentage of 20, 30, and 30%, respectively, during their residence time in the wastewater. Then, the authors used a stability correction factor

of 1.25, 1.43, and 1.43 for EME, amphetamine, and 6-MAM, respectively. Compounds presenting minimal degradation, like benzoylecgonine (BZE), methamphetamine, MDMA, and 2-ethylidene-1,5-dimethyl-3,3-diphenylpyrrolidine (EDDP), did not require the use of a stability correction factor (van Nuijs et al., 2011).

## BIOMARKERS OF DRUG CONSUMPTION IN RESIDUAL WATERS

The measured biomarkers in WBE are preferentially specific metabolites of the drug of interest with elimination mainly by the renal route, with wastewater concentrations in the range of ng L<sup>-1</sup> or higher (Gracia-Lor et al., 2017a; Vazquez-Roig et al., 2013). In addition to these characteristics, the biomarkers must have acceptable stability in wastewater since their entrance into the sewage system until sampling for analysis, storage, and processing (McCall et al., 2016). The removal of the biomarkers from wastewater can be attributed to chemical modifications on the water environment, as well as to microbiological biotransformation (Mardal and Meyer, 2014) and adsorption to particulate matter present in the sewage system and in the WWTP (Daughton, 2012; McCall et al., 2016). In fact, the knowledge of the stability of a certain biomarker at their environmental exposure conditions is mandatory before the use of concentration data in WBE, with a significant impact on the overall uncertainty of drug consumption estimation (Castiglioni et al., 2013). Laboratory simulation studies are often used to evaluate the stability of the biomarkers at different pH and temperature conditions, which also can modify microbiological activity, trying to simulate the actual conditions (Devault et al., 2017a). Adsorption to particulate matter present at the sewage and WWTP can be simulated using fortified residual waters and also evaluated at a realistic range of pH values and temperatures (Devault et al., 2017a).

## COCAINE

COC is the main psychoactive alkaloid present in *Erythroxylum coca* leaves. After intake, COC is hydrolyzed in the liver mainly to BZE and EME, which are excreted in urine at an average of 45 and 40% of the administered dose, respectively (Baselt, 2000). Cocaethylene (CE) is also formed by biotransformation when COC is used in combination with ethanol. Norcocaine (NCOC) is a minor oxidative metabolite. COC is used mainly as its chloridrate, by intravenous and intranasal routes, or as the free base (crack cocaine), by the respiratory route. When the free base is smoked, pyrolytic metabolites are formed, such as anidroecgonidine and anidroecgonidine methyl ester (Feitosa et al., 2013). The biomarker of COC most frequently used in WBE studies is BZE. Differently from COC, BZE is highly stable in residual waters. However, it is important to note that BZE can also be formed from COC degradation at residual waters, which can result in an overestimation of COC consumption if this conversion is not taken into account (Plósz et al., 2013). The

literature reported COC excretion rates in the range of 1–9% for the parent drug and about 45% for BZE (Baselt, 2000). Considering these average excretion rates, COC to BZE concentration ratios in residual waters in the range of 0.02–0.2 are an indication of drug consumption in the population served by the WWTP, whereas higher ratios can be suggestive of other COC sources, like leakages from clandestine laboratories (Castiglioni et al., 2011). However, as the COC to BZE ratio can also be affected by the temperature, complementary studies are needed to establish a cut-off ratio for the classification of the source of COC in the sewage system (van Nuijs et al., 2009b). In fact, the possible presence of COC in residual waters from nonhuman sources limits its use of a marker of drug consumption (van Nuijs et al., 2011).

Both BZE and EME concentrations in residual waters can be used for the estimation of COC consumption, usually resulting in similar results. However, the use of BZE is preferred due to its higher stability in water (van Nuijs et al., 2011). The most frequently reported correction factor for the estimation of COC consumption using BZE concentrations in residual waters is 2.33, which considers that BZE mounts to 45% of excreted COC (Daglioglu et al., 2019). This correction factor does not consider the simultaneous consumption of COC with other substances, particularly ethanol. The fraction of COC excreted as BZE and EME is significantly reduced when the drug is used along with ethanol due to the formation of CE (Harris et al., 2003). As the simultaneous use of COC and ethanol is common, van Nuijs et al., 2011 employed a correction factor of 3.0 for BZE concentrations, estimating that 35% of COC is excreted as BZE in this condition. If EME concentrations in residual waters are used for the estimation of COC consumption, a correction factor of 10.2 was proposed, which considers that 15% of the COC dose is excreted as EME (van Nuijs et al., 2011).

Castiglioni et al. (2006) evaluated the stability of illicit drugs and metabolites in residual water by analyzing laboratory prepared solutions in amber vials stored at 4°C for three days. In these conditions, the concentrations of COC, CE, and NCOC were reduced on 36, 15, and 13%, respectively. These concentration reductions were in parallel with the increase in the concentrations of the metabolites BZE and norbenzoylecgonine (NBZE).

## OPIATES

The opiate group of drugs includes not only prescription pharmaceuticals, like fentanyl, oxycodone, morphine, codeine, and tramadol, but also illicit compounds like heroin. The majority of the opiate drugs and metabolites are rapidly decomposed at residual waters. Additionally, several opiates are decomposed or metabolized to morphine, which presents some level of stability on the sewage. Therefore, by measuring morphine levels only, it is not possible to estimate the drug consumption (Werschler and Andrew, 2019).

Morphine is excreted in the urine mainly as morphine-3-βD-glucuronide. As this compound is usually found at a very low concentration in residual water, deconjugation is likely to happen



due to the enzymatic activity of bacteria present on sewage (Castiglioni et al., 2006). The contribution of codeine consumption to the morphine levels found on residual water is considered to be insignificant, once morphine is a minor metabolite of codeine (Baselt, 2000). The estimation of heroin consumption by WBE using morphine as a biomarker must consider the potential contribution of therapeutic drugs to the measured concentrations (Zuccato et al., 2008). Alternatively, 6-MAM can be used as the biomarker of heroin consumption in residual water due to the higher specificity. However, the high value of the correction factor can lead to significant uncertainties (van Nuijs et al., 2011).

## CANNABIS

The main psychoactive compound from the marijuana plant, *Cannabis sativa*, is tetrahydrocannabinol (THC). THC is metabolized by hydroxylation, forming the main active metabolite 11-hydroxy-tetrahydrocannabinol (11-OH-THC) and the minor metabolite 8-beta-hydroxy-tetrahydrocannabinol (8- $\beta$ -OH-THC). The further oxidation of 11-OH-THC produces the main inactive metabolite 11-nor-9-carboxy-tetrahydrocannabinol (THC-COOH) (Baselt, 2000). As the conversion of 11-OH-THC to THC-COOH is very fast, the latter is the most commonly used biomarker for the retrospective calculation of THC exposure in WBE. THC-COOH is excreted in urine and feces as a glucuronide conjugate, being hydrolyzed by  $\beta$ -glucuronidases present on fecal bacteria present in untreated residual water (Castiglioni et al., 2006). However, only a small amount of THC is excreted in the form of THC-COOH, requiring sensitive analytical methods for its detection. THC-COOH is a specific metabolite of THC, and the concentration of this biomarker is not affected by the use of other drugs in the population of the study (Werschler and Andrew, 2019).

Variable values of  $f$  were reported for the estimation of THC consumption from THC-COOH concentrations in WBE studies, as presented in **Table 1**. Gracia-Lor et al. (2016) and Huestis et al. (1996) established excretion rates of 0.5–0.6% considering the consumption of smoked marijuana. Alternatively, Postigo et al., 2011 used a higher excretion rate, of 2.5%, considering that all excreted 11-OH-THC was oxidized *in situ* to THC-COOH. Currently, the partition behavior of THC-COOH between water and particulate matter, present on the sewage system and WWTP, is not completely known, which can result in significant errors on the estimation of the mass of THC used by a given population (Causanilles et al., 2017).

## AMPHETAMINE STIMULANTS

The amphetamine stimulant group includes amphetamine itself and its derivatives, like methamphetamine, and ecstasy-like compounds, like 3,4-methylenedioxyamphetamine (MDA), 3,4-methylenedioxy-N-ethylamphetamine (MDEA), and MDMA, among others. Differently of COC, amphetamine-type drugs are excreted mainly as the parent drugs. This characteristic of the consumption biomarkers in residual water can be a limitation to the

identification of the presence of the raw drugs on the sewage system. However, most of the amphetamine compounds are racemic compounds, and the result of chemical synthesis has equal proportion of both enantiomers. However, the molecules formed after biotransformation will result in a particular enantiomeric proportion (Kasprzyk-Hordern and Baker, 2012; Emke et al., 2014). In this context, the characterization of the enantiomeric profile of the biomarkers can be used to differentiate between population consumption of the drug and disposal of the raw material on the sewage (Archer et al., 2018). A correction factor of 1.5 was originally proposed by Zuccato et al., 2008 for the estimation of MDMA consumption after measuring the concentration of the parent drug in residual water. This correction factor considers an excretion rate of 65% of the used dose as the parent compound. However, a more recent study showed that only 15% of the used dose is actually excreted as MDMA, and a correction factor of 6.67 should be used (Abraham et al., 2009).

A laboratory study of the stability of amphetamine, methamphetamine, MDA, MDEA, and MDMA found a maximum degradation rate of 5% (Castiglioni et al., 2006).

## OTHER COMPOUNDS EVALUATED IN PREVIOUS STUDIES

Methadone, a synthetic opioid drug used as an analgesic and heroin-substitution treatment, was already studied in WBE. The used biomarker is EDDP (Du et al., 2019). Ketamine, abusively used due to its dissociative and hallucinogenic effects, was also evaluated in WBE studies, using both ketamine and the metabolite norketamine as biomarkers (Baker et al., 2014). These authors reported the use of excretion rates of 1.6% and 2.3% for ketamine and norketamine, respectively. Recently, Du et al., 2020 concluded that excreted rates estimated based on pharmacokinetic studies were not appropriate for ketamine and suggested a much higher excretion factor, of 20%, relying on data from local drug seizures. Other compounds like mephedrone, mescaline, and ephedrine were also evaluated.

## BIOMARKERS OF POPULATION SIZE IN RESIDUAL WATERS

The estimation of drug consumption by a population served by a WWTP requires knowledge of the size of this population (**Eq. 1**). Census data can be outdated, leading to erroneous estimations. Different strategies were proposed to estimate the size of a population served by a WWTP, and the combination of estimation approaches is recommended to avoid deviations associated with a given method. Classical approaches include the designed capacity of the WWTP, census data, and hydrochemical measurement parameters (Castiglioni et al., 2014). The design capacity of the WWTP is usually not reliable to estimate the population size once the plant can operate either above or below its projected capacity. Census data are not adjusted over time and do not take into account seasonal population changes, as a result of tourism and other population movements. Population

size estimations can also be made using hydro-chemical parameters such as chemical oxygen demand (COD), biological oxygen demand (BOD), total nitrogen (N), and total phosphorus (P) (van Nuijs et al., 2011). Another valuable strategy is to measure concentrations of anthropogenic markers in residuals waters, like human endogenous compounds or metabolites of widely consumed products, caffeinated beverages, and tobacco cigarettes, among others.

The number of inhabitants served by a WWTP can be estimated using phosphorus, nitrogen, BOD, and COD levels on the residual waters, considering that a single person releases the equivalent to 1.7 g day<sup>-1</sup> of phosphorus, 12.5 g day<sup>-1</sup> of nitrogen, 59 g day<sup>-1</sup> of BOD, and 128 g day<sup>-1</sup> of COD (van Nuijs et al., 2011). This approach was applied to a WWTP located at Brussels, Belgium, and a wide range of served inhabitants was estimated along two consecutive months, between March 2009 and January 2010, with values in the range of 77.831 to 1.670.562, contrasting to the WWTP capacity of 1.1 million inhabitants. It is important to note that some variation in the number of served inhabitants is expected, once it is affected by several factors, like holiday periods and the occurrence of large public events. These results demonstrate that the use of WWTP capacity as the number of inhabitants served in the sewage epidemiology does not reflect the actual number of inhabitants served and should be replaced by real-time calculations of these parameters (van Nuijs et al., 2011). However, these hydro-chemical parameters do not only reflect human metabolism but also the presence of other biodegradable substances in the sewage system, being affected by industrial leakages, agricultural activities, and disposal of food residues, among others (Daughton, 2012).

Anthropogenic markers of population size in residuals waters must fulfill some requisites: present a predictable and constant elimination in urine, high stability in residual water, and be of exclusive human origin. Several potential candidate anthropogenic biomarkers were proposed, particularly creatinine, cotinine, and coprostanol (Daughton, 2012).

Senta et al. (2015) employed nicotine metabolites as population size biomarkers and found a good agreement with census data in Como, Italy. However, a limitation of the use of these markers is the need for a constant number of smokers throughout the investigated populations. Rico et al. (2017) evaluated twelve different urinary biomarkers as indicators of population size and found a similar population size when the estimation was made using either cotinine, 5-hydroxyindoleacetic acid, and caffeine compared with the hydro-chemical parameters (Rico et al., 2017).

Other alternative approaches for the estimation of the size of a population served by a WWTP have been described. Thomas et al. (2017), in a study performed in Norway, used data from a local mobile phone provider to estimate the population present in a given service area and used this population size to estimate the drug consumption in a dynamic way, particularly during the holiday period (Thomas et al., 2017).

A variety of urinary markers, derived from pharmaceuticals and personal care products, were evaluated in residual water in Australia, along with the population census of 2011 and with the per capita consumption of selected products, provided by the Australian Government through the Pharmaceutical Benefit

Scheme (O'Brien et al., 2014). The concentration of the makers atenolol, carbamazepine, codeine, furosemide, gabapentin, hydrochlorothiazide, ibuprofen, naproxen, norfloxacin, paracetamol, acesulfame, and caffeine presented high correlation ( $r^2 > 0.8$ ) with the population size.

Caffeine itself is considered to be a potentially biased biomarker of population size, once it comes not only from drinking coffee but also from other sources like coffee grounds spilled in the sink drain. However, 1,7-dimethyluric acid is a specific human caffeine metabolite, formed from paraxanthine (Gracia-Lor et al., 2017b). Then, considering the widespread human consumption of caffeine, 1,7-dimethyluric acid could be used as a biomarker to chemically estimate the population size of a population served by a WWTP.

The size of the population (*inh*) served by the WWTP can be estimated using Eq. 2, using the concentration of anthropogenic biomarkers in residual water. In this equation,  $C_{ab}$  is the concentration of the anthropogenic biomarker,  $Q_v$  is the daily influent flow at the WWTP ( $Q_v$ , L day<sup>-1</sup>),  $ER$  is the excretion rate of the biomarker, and  $DDD$  is the defined daily dose of the parent compound of the biomarker (mg per 1,000 inhabitants) (Rico et al., 2017).  $DDD$  data can be obtained from average selling data of the parent drug in the region served by the studied WWTP.

$$inh = (C_{ab} \cdot Q_v \cdot ER) / DDD \quad [2]$$

An important methodological advantage of the use of anthropogenic biomarkers for the estimation of population size is that biases at influent flow measurements are neutralized at the retrospective calculation of drug consumption, using Eq. 1 (Lai et al., 2011).

## SAMPLING STRATEGIES FOR THE ESTIMATION OF DRUG CONSUMPTION BIOMARKERS IN RESIDUAL WATER

Residual water collection at a WWTP in the context of drug consumption estimation must be representative of the 24 h of the day (Ort, 2014). One of the limitations of the use of WBE for drug consumption estimation is associated with the limited temporal representativeness, which must be taken into consideration during data interpretation (Baz-Lomba et al., 2016).

Many previous studies of WBE were limited to one-week sampling schemes (Ort et al., 2014b). However, stratified random sampling schemes (56 specimens per year) are recommended to estimate a representative average annual consumption of drugs (Ort et al., 2014a). Ort et al. (2014a) reported an annual average estimation error of COC consumption of 60% when only seven consecutive day samples of residual water were analyzed. This difference was attributed to the temporal variation of the drug consumption behavior by the population served by the WWTP. However, when 56 stratified random collected samples were tested, the deviation is expected to be around 10%. Increasing sampling frequency can lead to higher costs, also requiring a continuous supply of energy and availability of physical space for the sampling equipment. A higher sampling frequency will not be

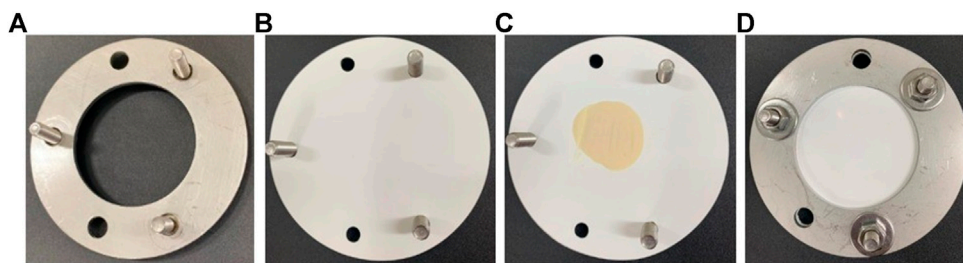


**FIGURE 1 |** POCIS assembly. **(A)** The bottom compression washer is assembled with screws. **(B)** PES membrane placed over the lower compression washer. **(C)** The amount of 200 mg of the sorbent is placed in the center of the PES membrane. **(D)** A second PES membrane is placed over the sorbent and the upper compression support washer is added. The screws and nuts are tightened to secure the support and prevent the loss of the solid sorbent.

adequate when the patterns of drug use are rapidly changing or the concentrations are affected in the short term by external factors, as rain precipitation (Ort et al., 2014a). Automatic sampling devices are programmed to collect several sample aliquots during the 24 h of the day, keeping the aliquoted specimens in a refrigerated compartment. The representativeness of the composite samples obtained with this kind of device is dependent on the minimal sample volume that can be collected, the storage capacity of the device, and its incapacity to account for high flow events, such as abundant rain. Usually, the composite sample has a 1–20 L volume, and a subsample can be directly analyzed or submitted to an extraction procedure (Ort et al., 2010).

Passive sampling devices (PSDs) are an alternative sampling strategy used to overcome some of the limitations described above. Particularly, PSDs are useful tools for screening and long-term monitoring of the use of drugs in WBE (Baz-Lomba et al., 2017), in a more straightforward and economical way when compared with spot or composite sampling (Allan et al., 2006; Magi et al., 2018). Additionally, PSDs are less affected by short-term variations in the concentration of drug consumption biomarkers (Harman et al., 2011; Kaserzon et al., 2014). As described by Baz-Lomba et al., 2017, annual drug monitoring in wastewater can be estimated using a relatively small number of passive samplers ( $n = 24$ ). Passive sampling combines both sampling and preconcentration of the compounds of interest in a single step (Magi et al., 2018). This characteristic allows the achievement of lower limits of detection than classical spot sampling or active sampling, once the *in situ* exposure occurs for several days (Morin et al., 2013). As an example, Fedorova et al., 2014 found several drug biomarkers in a PSD extract (BZE, ketamine, methadone, and midazolam) which were not detected in spot samples. PSD allows the estimation of time-weighted average (TWA) concentrations, in an economical and robust way, being of easy implementation at the point of collection, without the need for specific and sophisticated equipment and energy source (Alvarez et al., 2004).

## POLAR ORGANIC CHEMICAL INTEGRATIVE SAMPLER

Among the available PSD, the POCIS has been used for monitoring concentration of hydrophilic compounds, such as pesticides,

pharmaceutical, and personal care products (Kaserzon et al., 2014). POCIS was introduced by Alvarez et al., 2004 and consists of sorbent material sandwiched between two polyethersulphone (PES) membranes. POCIS is usually built using physically resistant materials as a structural basis, like stainless steel or aluminum. Two structural washers are used to compress two PES membranes, with the sorbent material being sandwiched between the membranes. The whole structure of the device is fixed with screws. The original study of Alvarez et al., 2004 employed washers and PES membranes of 90 mm of diameter, resulting in a membrane chemical exchange area of  $\approx 41 \text{ cm}^2$ . The structure of a laboratory-made POCIS is presented in Figure 1.

Usually, the POCIS is immersed for more than one week in water and accumulates the sampled compound by passive diffusion (Morin et al., 2013). The microporous PES membrane acts as a semipermeable barrier between the sorbent and the external environment, allowing the diffusion of organic polar solutes to the sorbent while avoiding that particulate matter, colloids, and microorganisms (with diameters higher than the membrane pore, usually  $0.1 \mu\text{m}$ ) pass through the membrane (Alvarez et al., 2004).

The original study of Alvarez et al., 2004 evaluated different membrane composition and selected PES due to the combination of high analyte uptake rates, minimal biological incrustation, and high durability on the sewage environment. The composition of the sorbent in POCIS depends on the target compounds to be sampled, and the most commonly used are named pesticide POCIS (Pest-POCIS) and pharmaceutical POCIS (Pharm-POCIS). Pest-POCIS sorbent is a mixture of three solid-phase sorbents: Isolute ENV+, polystyrene divinylbenzene, and Ambersorb 1,500 carbon. Pest-POCIS is used for monitoring concentrations of most pesticides, hormones, and several other chemicals. The Pharm-POCIS sorbent contains only the solid-phase extraction sorbent Oasis HLB® and is used for the sampling of pharmaceutical compounds and its metabolites in water. Oasis HLB® is a copolymer of [(poly [divinylbenzene]-co-N-vinylpyrrolidone)] and provides analyte retention based on hydrophilic-lipophilic balance retention, with the capacity of retaining compounds with a wide range of polarities (Alvarez et al., 2004). Both Pest-POCIS and Pharm-POCIS are commercially available and can also be prepared in house.

POCIS sampling is usually performed over several weeks, allowing the concentration of a large volume of water and accumulates the effects of periodic events that can be missed with grab sampling (Morin et al., 2013). As a result of the long exposure time of POCIS to the residual water, a TWA concentration can be obtained (Alvarez et al., 2004). The amount of the compounds at the sorbent of the POCIS after the sampling time is related to the concentration present in the water along the sampling period and is dependent of the sampling rate ( $R_s$ ), which represents the volume of water cleared of the compound by the POCIS over a given time (Magi et al., 2018).

Criquet et al. (2017) compared POCIS and composite automatic sampling for the determination of 46 pesticides and 19 pharmaceuticals in an urban river, with 2-week sampling campaigns. The authors reported a good agreement between both sampling methods, with 75% of measurements presenting ratios between 0.33 and 3. Concentrations measured with POCIS were, in general, between the maximum and minimum levels measured in the composite samples. Bishop et al. (2020) compared POCIS and composite automatic sampling for the measurement of the concentrations of drugs of abuse and pharmaceuticals in the influent of a WWTP. These authors reported a subestimation of concentrations using POCIS when compared with the median concentration of the composite sampling, with only 48% of the concentrations within a three-fold difference. However, the occlusion of the POCIS membrane, reported by the authors, could have affected the performance of the sampling device. When compared with composite automatic sampling, POCIS allows similar findings with a smaller number of samples, with cleaner sample extracts and easier handling, once large volumes of water are not needed. Besides, POCIS sampling can avoid missing a peak concentration event, which can happen if composite automatic sampling is used.

To calculate TWA concentrations,  $R_s$  of the analytes of interest must be established in calibration studies, which can be performed both *in situ* or in laboratory conditions (Harman et al., 2012; Morin et al., 2012). The lack of standardized  $R_s$  and the use of proper exposure corrections due to the influence of environmental factors are the main issues related to the estimation of TWA concentrations using POCIS (Baz-Lomba et al., 2017).

Other than POCIS, alternative PSDs were described, like those based on diffusive gradients in thin films (DGT) (Guo et al., 2017) and microporous polyethylene tubes (MPTs) (McKay et al., 2020). While these reports described the measurement of drugs of abuse concentrations, no WBE estimation was made.

## ACCUMULATION KINETICS IN POLAR ORGANIC CHEMICAL INTEGRATIVE SAMPLER AND DETERMINATION OF SAMPLING RATES

The accumulation of target compounds at the sorbent phase of the POCIS obeys the first-order kinetics, with an initial linear

stage, followed by curvilinear and equilibrium regime (Morin et al., 2012). The accumulation of a chemical in the POCIS is described by Eq. 3, where  $C_s$  ( $\text{ng g}^{-1}$ ) is the concentration of the compound on the sorbent phase,  $C_w$  ( $\text{ng L}^{-1}$ ) is the average concentration of the compound at the residual water,  $K_u$  is the uptake rate of the analyte in the sorbent phase ( $\text{L g}^{-1} \text{day}^{-1}$ ),  $K_e$  is the elimination rate constant of the chemical from the sorbent phase, and  $t$  (days) is the exposure time (Morin et al., 2013).

$$C_s = C_w * \frac{K_u}{K_e} * (1 - e^{-K_e t}) \quad [3]$$

POCIS is considered as an infinite collector of contaminants and, assuming constant concentrations, the compounds are accumulated linearly within time (Alvarez et al., 2007). In this context,  $K_e$  is insignificant when comparing with  $K_u$ , allowing the simplification of Eq. 3, which relates the concentration of the compound on the sorbent phase of the POCIS to the TWA concentration on the water ( $C_w$ ,  $\text{ng L}^{-1}$ ) through the value of the sampling rate ( $R_s$ ,  $\text{L day}^{-1}$ ), as presented in Eq. 4. In this equation,  $M_s$  (g) is the mass of sorbent present on the POCIS and  $t$  (days) is the exposure time (Baz-Lomba et al., 2017).

$$R_s = \frac{(C_s * M_s)}{(C_w * t)} \quad [4]$$

When  $C_s * M_s$  (the amount of contaminant accumulated in POCIS, ng) is plotted as a function of  $t$  (day), the slope of the obtained curve is  $C_w * R_s$ . Thus,  $R_s$  can be determined by dividing the slope by  $C_w$  (Jacquet et al., 2012).

Some authors rewrote Eq. 4 and used a concentration factor (CF,  $\text{L g}^{-1}$ ) to neutralize the effect of  $C_w$  variations, dividing the concentrations in the sorbent and in water ( $C_s/C_w$ ), as presented in Eq. 5 (Morin et al., 2013; Baz-Lomba et al., 2017).

$$CF = \left( \frac{C_s}{C_w} \right) = \left( \frac{R_s * t}{M_s} \right) \quad [5]$$

The time to achieve half of the equilibrium concentration (half-time,  $t_{1/2}$ ) reflects the limit between the linear and curvilinear regimen (Alvarez et al., 2007). This time can be estimated through the first-order curves adjusted to the calibration data in order to confirm adsorption linearity during the exposure time (Baz-Lomba et al., 2017). Therefore,  $R_s$  values must be calculated during a time equal or smaller to  $t_{1/2}$  for better accuracy (Morin et al., 2013). Half-time values are calculated using Eq. 6. The value of  $k_e$  is usually estimated by fitting exponential curves, using specialized statistical software.

$$t_{1/2} = \frac{0.693}{K_e} \quad [6]$$

Morin et al. (2013) evaluated the adsorption kinetics of 56 organic micropollutants to Pharm-POCIS. Among the tested compounds, 43 have curvilinear adsorption kinetics, allowing the use of Eq. 5 to calculate  $R_s$  values, if exposure time was lower than  $t_{1/2}$ . For these compounds, CF was calculated using  $C_s$  and  $C_w$  values obtained at different adsorption times. Afterward, the



plot of CF vs. time allowed the obtention of a straight line, whose slope was  $R_s/M_s$ . From this slope value, accurate  $R_s$  values could be calculated, using the average weight of the POCIS sorbent exposed at the water until  $t_{1/2}$ .

Half-time is an important parameter to estimate the ideal sampling time of the POCIS to obtain TWA concentrations of a given chemical. TWA ( $C_w$ ) concentrations can be calculated rearranging Eq. 4, as presented in Eq. 7, for analytes presenting  $t_{1/2}$  higher than the sampling time, once these compounds are linearly accumulated during *in situ* sampling (Morin et al., 2013).

$$C_w = \frac{(C_s * M_s)}{(R_s * t)} \quad [7]$$

Equation 7 is valid to estimate  $C_w$  when sampling is performed during the linear adsorption period. To this end, the duration of the linear regimen must be established for each monitored compound (Fedorova et al., 2014). The POCIS device should not be immersed in the sampled water for a time longer than  $t_{1/2}$ . Otherwise, nonreliable estimations of TWA will be calculated (Morin et al., 2013).

POCIS is usually used in a linear regimen for the estimation of TWA concentrations with acceptable accuracy. Alternatively, POCIS can be immersed in residual water only for the screening of micropollutants, independently from the regimen, once only qualitative information is desired (Morin et al., 2012).

## POLAR ORGANIC CHEMICAL INTEGRATIVE SAMPLER CALIBRATION

TWA concentrations can be calculated using  $R_s$  values obtained *in situ*. However, this approach requires that field calibrations are performed in each sampling campaign (Jacquet et al., 2012). Moreover, in this particular case, the contaminants must be present in the aquatic environment in a relatively constant concentration. The *in situ* calibration allows the obtention of  $R_s$  values specific of a certain collection location and takes into account the physicochemical conditions of the local environment (Harman et al., 2011).

Another alternative for the determination of  $R_s$  values is the laboratory calibration of the POCIS devices, which can be performed only once for a given compound. Laboratory calibration is more cost-effective. A potential disadvantage of laboratory calibration is that environmental conditions are not taken into consideration, which can lead to biased TWA estimations (Fedorova et al., 2014; Miller et al., 2016). Besides, it is also important to control important physicochemical parameters in water that may influence  $R_s$  values, such as temperature, flow, pH, conductivity, dissolved organic carbon (DOC), and the expected concentration of the compounds of interest on the water (Morin et al., 2012). Laboratory calibration is more commonly applied due to its simplicity and can be performed in both static or recirculation approaches (Arditsoglou and Voutsas, 2008; Harman et al., 2009).

The *in situ* calibration of  $R_s$  values of POCIS was applied to illicit drugs by Baz-Lomba et al. (2017). Accumulation curves, relating CF ( $C_s/C_w$ ) of the compound (y axis) to the POCIS exposure time to the investigated residual water environment (x axis, in days), were fitted for exposure times of 14, 21, and 28 days. From these curves,  $R_s$  values were calculated as the slope of the linear part of the fitted curves for the compound of interest, forcing this curve through the origin. The average coefficient of variation (CV%) for the different *in situ* calibration sets was smaller when using the results from the first 14 days of exposure, with an average CV% lower than 17.1% for the investigated compounds. COC, BZE, morphine, and methamphetamine presented linear incorporation profiles. However, the *in situ* calibration required a parallel composite collection of water samples for the estimation of  $R_s$ , which is required for the establishment of CF values ( $C_s/C_w$ ,  $L\ g^{-1}$ ), as presented in Eq. 5.

Laboratory calibration can be performed using static calibration procedures or continuous flow systems. Static calibration (closed system, with analyte spiking at the beginning of the experiment) is considered to be appropriate when the compounds of interest are not rapidly degraded or adsorbed and the calibration time is smaller than one week, to reduce the influence of other processes affecting dissipation (Magi et al., 2018). The  $R_s$  value in laboratory calibration is calculated similarly to *in situ* calibration, but, as the water concentration of the compounds is controlled, there is no need for active composite sampling during these experiments. Another way to estimate  $R_s$  of a compound is to measure the decrease in the analyte concentration in water along time in a static calibration, as applied by Yargeau et al. (2014). These authors calculated  $R_s$  using a linear regression describing the loss of the compound from water as the result of the adsorption into the POCIS during the 8 days of the calibration experiment. In this regression, the natural logarithm of the concentrations (y axis) was plotted against the adsorption time (x axis). At the end of the calibration experiment, the POCIS was removed from the testing vessel and analyzed to compare the accumulation of the compound at the sorbent with the  $R_s$  calculated considering the loss of the analyte in the water. The results of this evaluation concluded that the adsorption of the compound by the PES membrane has a negligible effect on the  $R_s$  (Yargeau et al., 2014).

If the concentration of the measured compound is sufficiently high, direct injection of the water being sampled in the analytical system is possible, simplifying the calibration procedure (Morin et al., 2013). Additionally, all interfering conditions, as pH, temperature, and conductivity, can be controlled during the calibration experiments. Laboratory calibration for drugs of abuse analysis using POCIS was already described by Yargeau et al., 2014.

Only a few studies reported  $R_s$  values for drugs of abuse, either obtained by *in situ* or laboratory calibration, as presented in Table 2. Also, the lack of standardization of the calibration procedures can result in significantly different  $R_s$  values for the same compound, as can be observed in the current literature.



**TABLE 2 |** Target compounds, POCIS calibration, and sampling rates used to estimate water concentration of drug consumption biomarkers from POCIS

Compound	Sampling rates, $R_s$ ( $L\ d^{-1}$ ) (days or average)	POCIS calibration	POCIS type	POCIS sampling time	Estimation of drug use using POCIS	Sampling site	References
Cocaine	0.096 (av. 14 days); 0.087 (av. 28 days)	<i>In situ</i>	Pharm-POCIS (HLB 220 mg)	POCIS ( $n = 3$ ) was replaced every 2 weeks during a 2 year-long period monitoring	Yes	WWTP in Oslo, Norway	Baz-Lomba et al. (2017)
BZE	0.039 (av. 14 days); 0.033 (av. 28 days)						
Methamphetamine	0.026 (av. 14 days); 0.026 (av. 28 days)						
Morphine	0.023 (av. 14 days); 0.021 (av. 28 days)						
Morphine	0.044 (14 days); 0.035 (av. 31 days)	<i>In situ</i>	Pharm-POCIS (HLB 200 mg)	POCIS ( $n = 3$ ) was replaced every 2 weeks over a year-long period monitoring	Yes	WWTP in Oslo, Norway	Harman et al. (2011)
Amphetamine	0.125 (14 days); 0.094 (av. 31 days)						
MDMA	<0.097 (14 days); <0.118 (av. 31 days)						
Methamphetamine	0.128 (14 days); 0.102 (av. 31 days)						
OH-Meth	0.070 (14 days); 0.053 (av. 31 days)						
Cocaine	0.186 (14 days); 0.150 (av. 31 days)						
BZE <sup>a</sup>	0.083 (14 days)						
Cocaethylene	0.137 (14 days); 0.112 (av. 31 days)						
Cocaine	0.130 ± 0.036	Static laboratory-based calibration experiment, for 8 days	Pharm-POCIS (HLB 200 mg)	POCIS was deployed over a two-week period	No	WWTPs in Ontario and Quebec, Canada	Yargeau et al. (2014)
BZE	0.134 ± 0.011						
Amphetamine	0.201 ± 0.038						
MDA	0.288 ± 0.021						
Methamphetamine	0.231 ± 0.025						
MDMA	0.222 ± 0.013						
Ephedrine	0.123 ± 0.039						
Codeine	0.394 ± 0.049						
Dihydrocodeine	0.110 ± 0.041						
Morphine	0.261 ± 0.036						
Methadone	0.408 ± 0.147						
EDDP	0.532 ± 0.193						
Ketamine	0.197 ± 0.007	Bench-scale experiments with static exposure, for 3 days	Pharm-POCIS (HLB 200 mg)	POCIS ( $n = 3$ , per location) was deployed over a 2-week period	No	WWTP, at sites in the Grand River and in the DWTP in Ontario, Canada	Rodayan et al. (2016)
Fentanyl	0.390 ± 0.051						

(Continued on following page)

**TABLE 2 |** (Continued) Target compounds, POCIS calibration, and sampling rates used to estimate water concentration of drug consumption biomarkers from POCIS

Compound	Sampling rates, $R_S$ ( $L\ d^{-1}$ ) (days or average)	POCIS calibration	POCIS type	POCIS sampling time	Estimation of drug use using POCIS	Sampling site	References
Cocaine	0.13	Laboratory experiments	Pharm-POCIS (HLB)	POCIS ( $n = 3$ ) was retrieved 28–32 days after deployment (depending on the site)	No	5 sites in flooded cave systems along the Caribbean coast of the Yucatan Peninsula in Mexico	Metcalfe et al. (2011)
BZE	0.13	conducted at water temperatures close to those in the cave systems (i.e., 26–28°C)					
Amphetamine	0.26	Calculated theoretical uptake rates	Pharm-POCIS (HLB 200 mg)	POCIS was deployed for a 7-day exposure period, at each sampling location	No	WWTPs at Lincoln, Grand Island, Columbus, Hastings, and Omaha, in Nebraska, USA	Bartelt-Hunt et al. (2009)
Methamphetamine	0.22						

BZE, benzoylcegonine; DWTP, drinking water treatment plant; EDDP, 2-ethylidene-1,5-dimethyl-3,3-diphenylpyrrolidine; MDMA, 3,4-methylenedioxy-N-methylamphetamine; OH-Meth, hydroxymethamphetamine; THC-COOH, 11-nor-9-carboxy-THC; WBE, wastewater-based epidemiology; WWTP, wastewater treatment plant.

<sup>a</sup>Uptake not linear after 14 days.

## EFFECT OF POLAR ORGANIC CHEMICAL INTEGRATIVE SAMPLER EXPOSURE CONDITIONS ON $R_S$ VALUES

The  $R_S$  of a certain POCIS device is significantly affected by environmental conditions, like water flow (Alvarez et al., 2004; Bailly et al., 2013; Guibal et al., 2020), water temperature (Li et al., 2010), pH (Li et al., 2011), and biofouling (Harman et al., 2009).

The effect of water flow during POCIS sampling was evaluated by Guibal et al., 2020, for 44 pharmaceutical drugs, in a wide range of polarities. The calibration was performed at four different water flows: 0 ( $v_0$ ), 2–3 ( $v_1$ ), 6–7 ( $v_2$ ), and 20 ( $v_3$ )  $cm\ s^{-1}$ . Sampling rates were in the range of 0.040–0.218, 0.063–0.375, 0.062–0.408, and 0.075–0.539  $L\ d^{-1}$  for  $v_0$ ,  $v_1$ ,  $v_2$ , and  $v_3$ , respectively. The authors concluded that an increase in water flow results in a decrease in the effective thickness of the water boundary layer at the POCIS membrane surface and, as a consequence, the increase in  $R_S$ . A similar observation was previously described by Alvarez et al. (2004) that evaluated  $R_S$  of six micropollutants under quiescent (nonstirred) and turbulent (stirred) conditions. The adsorption of the evaluated chemicals was considered under aqueous boundary layer control, as shown by the increase in 4–9 times in  $R_S$  when water was agitated. The effect of water flow on  $R_S$  is dependent on the physicochemical properties of the investigated compounds. Bailly et al., 2013 found that an increase in water flow from 0.11 to 0.29  $m\ s^{-1}$  did not affect  $R_S$  of sulfamethoxazole. Di Carro et al. (2014) evaluated  $R_S$  of several pesticides, pharmaceuticals, and chemicals by Pharm-POCIS and did not found differences at water flow rates in the range of 2–15.3  $cm\ s^{-1}$ .

The increase in water temperature influenced  $R_S$  of pharmaceuticals, personal care products, and endocrine disruptors adsorbed by POCIS, with an increase of up to two times when the temperature changed from 5 to 25°C (Li et al., 2010). Djomte et al. (2018) described a linear increase in  $R_S$  when increased in the range of 8–39°C in a constant water flow.

Li et al. (2011) studied the effect of pH on the  $R_S$  values on POCIS sampling. The  $R_S$  values of acidic pharmaceutical were

reduced with the increase in pH from 3 to 9, whereas basic compounds presented the opposite trend. However, the observed  $R_S$  changes were with a three-fold range for the majority of the compounds. The dissolved organic matter (DOM) did not affect  $R_S$  in a relatively narrow range of value DOM values, from 3 to 5  $mg\ L^{-1}$ . The authors concluded that expected values of pH and DOM in natural water sources will result in small changes in  $R_S$  values.

Harman et al. (2009) fouled the POCIS before exposure to water containing the chemicals of interest. The fouling ranged from 0.2 to 2.8 g of dry weight  $dm^{-2}$ , and exposure lasted for 6 weeks. Fouled POCIS adsorbed up to 55% more alkyl phenolic compounds than nonfouled POCIS.

Fouling can modify the mass transfer of the analyte, by increasing the thickness of the barrier or decreasing the size of membrane pores. Considering this possibility, Bailly et al., 2013 suggested that  $R_S$  values must be calculated using a matrix with organic content similar to the expected field conditions.

On the other hand, Rosen et al., 2018 did not found a relevant effect of biofouling on  $R_S$  of explosive compounds (2,4,6-trinitrotoluene and hexahydro-1,3,5-trinitro-1,3,5-triazine) when sampling was performed for up to 28 days. This behavior, different from the one observed for alkyl phenolic compounds, could be attributed to the higher polarity of the investigated chemicals.

Complementary studies are needed to clarify the impact of biofouling at POCIS adsorption of chemicals.

## ANALYTICAL METHODS FOR THE MEASUREMENTS OF DRUGS OF ABUSE IN POLAR ORGANIC CHEMICAL INTEGRATIVE SAMPLER

The measurement of drug consumption biomarkers in residual water requires the availability of sensitive analytical methods, usually after a concentration step. The concentration can be

performed by a variety of extraction approaches, being solid-phase extraction the most commonly used strategy. When using POCIS, the sampling device can concentrate the analytes of interest in a very effective way. Oasis HLB<sup>®</sup> is the more common sorbent used on POCIS for the determination of concentrations of drugs of abuse and its metabolites. This sorbent is highly versatile, being able to retain compounds with a wide range of polarities and acid-base properties, at variable pH ranges (Vazquez-Roig et al., 2013). After disassembling the device, the POCIS sorbent is usually transferred to an empty solid-phase extraction cartridge, washed with 10–20% methanol, and eluted using organic solvents (Harman et al., 2011; Baz-Lomba et al., 2017).

After extraction of the compounds of interest from the POCIS sorbent, analysis is usually performed using methods with mass spectrometric detection, particularly liquid-chromatography coupled to tandem mass spectrometry (LC-MS/MS) (Zuccato et al., 2005; van Nuijs et al., 2009a). LC-MS/MS is usually preferred once analytes in water are polar compounds, being amenable to liquid chromatographic separations without derivatization steps, and the technique also presents high sensitivity (Vazquez-Roig et al., 2013). Among the mass detector used in LC-MS/MS, triple quadrupoles are the most used due to its quantitative performance and robustness (Ort et al., 2014b; Thomas et al., 2012). The use of LC-MS/MS for the measurement of drug concentration in residual water requires the use of the deuterated internal standard to minimize matrix effects, which are usually significant when electrospray ionization sources are used (Castiglioni et al., 2006).

The uncertainty of the TWA concentrations estimated using POCIS was evaluated by Baz-Lomba et al. (2017). Two different confidence intervals were calculated, considering the precision of the  $R_s$  values obtained during *in situ* calibration and that  $R_s$  values could vary with a two-fold interval. The uncertainty ( $U$ ) was estimated for five pharmaceutical compounds, using the following equation:

$$U = \frac{CV}{\sqrt{n}} \quad [8]$$

The uncertainty ranged from  $\pm 35.4\%$  for atenolol to  $\pm 43.1\%$  for metoprolol. The uncertainties were attributed mainly due to the variability during the *in situ* calibration of the POCIS.

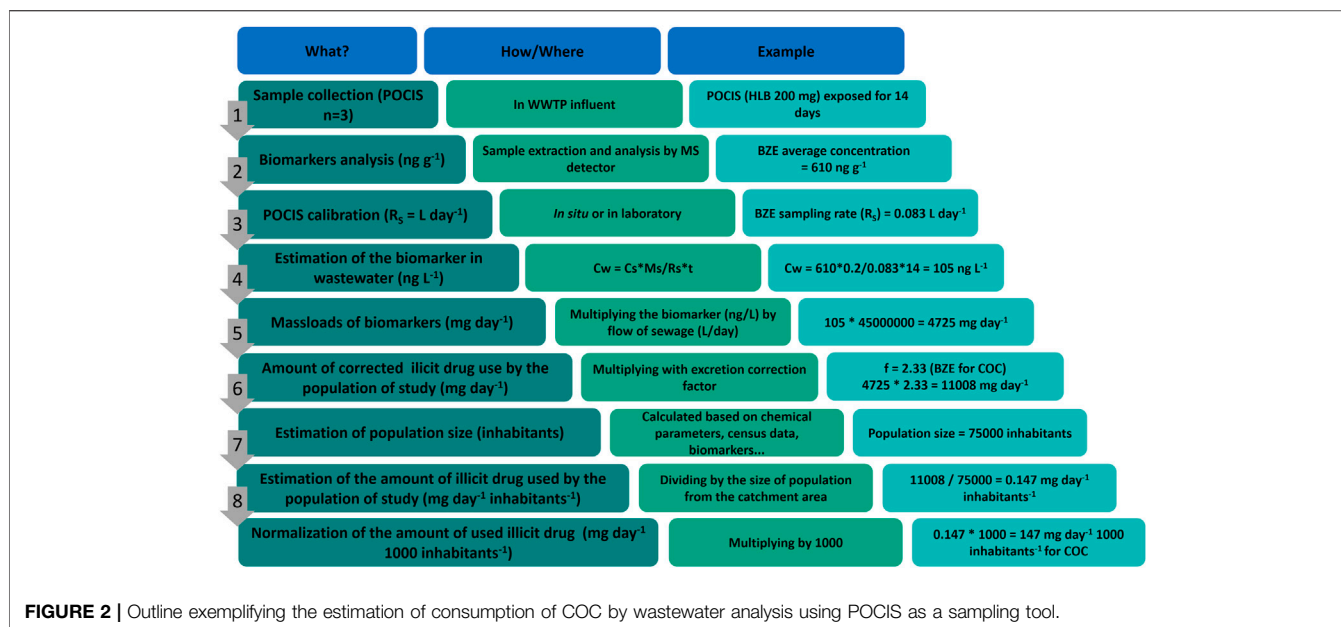
## PREVIOUS REPORTS OF POLAR ORGANIC CHEMICAL INTEGRATIVE SAMPLER USE FOR WASTEWATER-BASED EPIDEMIOLOGY OF DRUGS OF ABUSE

Despite the attractiveness of POCIS use in terms of cost and versatility, once a few studies had used this sampling strategy in WBE studies for drugs of abuse. **Table 2** presents an overview of studies that employed POCIS for the measurement of drugs of abuse concentrations. However, in the text below, only reports that used POCIS measurements for WBE of drugs of abuse will be discussed.

An early report applied POCIS for the evaluation of drug consumption in the city of Oslo, in Norway (Harman et al., 2011). In this study, the sampling campaign lasted for a whole year, and several temporal trends in drug consumption in the evaluated population were identified. Besides drugs of abuse, authors also monitored concentrations of cetirizine, an antihistaminic drug mostly used during spring months. In fact, cetirizine concentrations in POCIS samples collected during spring, when a high incidence of seasonal rhinitis is observed, were more than two-fold the levels measured in POCIS collected during the winter. Authors considered this finding as an indication of the POCIS capability of detecting time-related patterns of drug use in a monitored population. The same study reported peaks of MDMA consumption during a popular student celebration in Norway, as well as fluctuations in the consumption of COC and amphetamine over the year, with prominent peaks on summer and winter, usually associated with holidays. Variation in the estimated drug consumption over the year can also be associated to the variable availability of the different drugs. The authors estimated COC consumption based on the TWA concentrations of BZE, resulting in consumed amounts of  $20\text{--}70 \text{ mg day}^{-1} 1.000 \text{ inh}^{-1}$ . When using TWA concentration of COC for the estimation of the drug consumption, values were in the range of  $310\text{--}2,800 \text{ mg day}^{-1} 1.000 \text{ inh}^{-1}$ . The authors of this study concluded that consumption based on COC concentrations was more accurate when compared with studies performed in other European cities using active sampling. Measuring BZE in relation to COC is the preferred approach since COC can be present in wastewater without having been used and because COC exhibits significant degradation. However, due to the nonlinear absorption kinetics of BZE presented in their work, measuring COC may be more appropriate when using POCIS. In the case of amphetamine and methamphetamine, average daily consumption was estimated to be in the range of  $190 \text{ mg day}^{-1} 1.000 \text{ inh}^{-1}$  and  $400 \text{ mg day}^{-1} 1.000 \text{ inh}^{-1}$ , respectively.

Baz-Lomba et al. (2017) also made a WBE study in Oslo, with POCIS sampling being performed continuously for two years. Using BZE concentrations, the average COC consumption during the years of 2012 and 2013 was  $120 \text{ mg day}^{-1} 1.000 \text{ inh}^{-1}$ , which was considered as adequately concordant with estimations made using BZE levels obtained after an active composite sampling campaign, of  $152 \text{ mg day}^{-1} 1.000 \text{ inh}^{-1}$ , reported by SCORE group in 2015. Average methamphetamine consumption during the years of 2012 and 2013 was estimated as  $263 \text{ mg day}^{-1} 1.000 \text{ inh}^{-1}$ , also in concordance with the active sampling estimations.

There are a few report of POCIS  $R_s$  of illicit drugs in the literature. As summarized in **Table 2**, reported  $R_s$  is very variable even for the same compound. *In situ* determined  $R_s$  for COC was reported in the range of  $0.096\text{--}0.186 \text{ L d}^{-1}$  and laboratory calibration reports presented the value of  $0.13 \text{ L d}^{-1}$ . Also for BZE, a similar pattern is observed, with *in situ* determined  $R_s$  of  $0.039$  and  $0.083 \text{ L d}^{-1}$ , and laboratory calibration reports described  $R_s$  value of  $0.13 \text{ L d}^{-1}$ . Considerable differences can also be noted for morphine (*in situ*  $R_s$  of  $0.023\text{--}0.044 \text{ L d}^{-1}$ ; laboratory  $R_s$  of  $0.261 \text{ L d}^{-1}$ ) and methamphetamine (*in situ*  $R_s$  of  $0.026$  and  $0.128 \text{ L d}^{-1}$ ; laboratory  $R_s$  of  $0.231 \text{ L d}^{-1}$ ). The widely



variable of POCIS  $R_s$  values shows that these values are highly dependent of the experimental calibration conditions and also characterize the semiquantitative nature of the drug consumption estimation using POCIS in WBE. Baz-Lomba et al. (2017) performed a WBE study in the same location than Harman et al., 2011, using POCIS sampling, which were calibrated *in situ*. The  $R_s$  values described by Baz-Lomba et al., 2017 were almost the half for cocaine, BZE, and morphine and about five times lower for methamphetamine. One possible explanation for these differences could be the impact of the water flow rate around the passive samplers, with higher turbulence leading to increased  $R_s$  values due to the reduction of the water boundary layer over the POCIS membrane (Guibal et al., 2020).

Detailed analytical data are not available in several manuscripts summarized in Table 2. Liquid chromatography coupled to mass spectrometry was used in all studies, either with tandem quadrupole (Bartelt-Hunt et al., 2009; Harman et al., 2011; Metcalfe et al., 2011; Yargeau et al., 2014), ion trap (Rodayan et al., 2016), or time-of-flight (Baz-Lomba et al., 2017) detectors. Bartelt-Hunt et al. (2009) estimated a limit of detection lower than 1 ng mL<sup>-1</sup>, which relates to an absolute amount of 1 ng recovered from the POCIS. Also, recovery of target compounds was checked by analysis of fortified blanks spiked with known amounts of each compound, averaging 123 ± 30%. Rodayan et al. (2016) measured drug concentrations in wastewater, with limits of quantification between 0.48 and 8.4 ng L<sup>-1</sup>, according to the measured analyte. The analyte recovery from POCIS was higher than 80%. The concentrations of some analytes measured in grab samples were lower than TWA estimated from POCIS. In some cases, analytes were detected or quantifiable in POCIS but not in the corresponding grab samples, such as which illustrates the value of passive sampling for concentrating trace contaminants to detectable levels and the importance of effective sampling strategies. Yargeau et al. (2014) collected wastewater specimens both using POCIS and automatic composite sampling. Authors

reported that methamphetamine, dihydrocodeine, and oxycodone were detected on POCIS but not in all composite samples. These findings support previous studies showing that POCIS may accumulate drugs to detectable levels when these compounds are not detectable in grab or composite samples of wastewater. Harman et al. (2011) reported quantification limits for target compounds in POCIS 0.5 and 5 ng POCIS<sup>-1</sup> (morphine and methamphetamine were exceptions with limits of 10 and 50 ng POCIS<sup>-1</sup>, respectively). Baz-Lomba et al. (2017) reported recovery for all tested compounds in their study from the HLB POCIS sorbent in the range of 72–118%.

Figure 2 outlines all steps for a WBE study for drugs of abuse consumption using POCIS, from sampling to consumption estimation. In this example, an estimate of COC consumption after BZE concentration measurement is exemplified.

## CONCLUSION

Wastewater-based epidemiology is a useful tool to detect illicit drug use of a population in real-time, allowing effective health and law-enforcement actions. The application of wastewater-based epidemiology requires that representative samples are obtained in practical and effective way. An attractive, adaptable, and low-cost alternative for sampling of biomarkers of drug consumption in residual water is the use of POCIS. Average biomarkers concentration in residual water can be estimated using POCIS, particularly for compounds presenting linear accumulation kinetics on the sorbent. To date, only few studies applied POCIS in WBE and more studies are required before the use of this sampling strategy can be considered as standard. However, considering the cost of composite active samplers and also the operational requirements of these equipment, the use of POCIS is very

attractive to allow WBE long-term studies in limited resources settings, even considering its semiquantitative nature.

## AUTHOR CONTRIBUTIONS

RH reviewed the literature and prepared the draft of the manuscript. CN contributed to the draft preparation and reviewed the manuscript. RL designed the manuscript, contributed to the draft preparation, and reviewed the final version.

## REFERENCES

- Abraham, T. T., Barnes, A. J., Lowe, R. H., Kolbrich Spargo, E. A., Milman, G., Pirnay, S. O., et al. (2009). Urinary MDMA, MDA, HMMA, and HMA excretion following controlled MDMA administration to humans. *J. Anal. Toxicol.* 33 (8), 439–446. doi:10.1093/jat/33.8.439
- Allan, I. J., Vrana, B., Greenwood, R., Mills, G. A., Knutsson, J., Holmberg, A., et al. (2006). Strategic monitoring for the European water framework directive. *Trac Trends Anal. Chem.* 25 (7), 704–715. doi:10.1016/j.trac.2006.05.009
- Alvarez, D. A., Petty, J. D., Huckins, J. N., Jones-Lepp, T. L., Getting, D. T., Goddard, J. P., et al. (2004). Development of a passive, *in situ*, integrative sampler for hydrophilic organic contaminants in aquatic environments. *Environ. Toxicol. Chem.* 23 (7), 1640–1648. doi:10.1897/03-603
- Alvarez, D. A., Huckins, J. N., Petty, J. D., Jones-Lepp, T., Stuer-Lauridsen, F., Getting, D. T., et al. (2007). Chapter 8 Tool for monitoring hydrophilic contaminants in water: polar organic chemical integrative sampler (POCIS). *Compr. Anal. Chem.* 48 (06), 171–197. doi:10.1016/S0166-526X(06)48008-9
- Archer, E., Castrignanò, E., Kasprzyk-Hordern, B., and Wolfaardt, G. M. (2018). Wastewater-based epidemiology and enantiomeric profiling for drugs of abuse in South African wastewaters. *Sci. Total Environ.* 625, 792–800. doi:10.1016/j.scitotenv.2017.12.269
- Arditsoglou, A., and Voutsas, D. (2008). Passive sampling of selected endocrine disrupting compounds using polar organic chemical integrative samplers. *Environ. Pollut.* 156 (2), 316–324. doi:10.1016/j.envpol.2008.02.007
- Bailly, E., Levi, Y., and Karolak, S. (2013). Calibration and field evaluation of polar organic chemical integrative sampler (POCIS) for monitoring pharmaceuticals in hospital wastewater. *Environ. Pollut.* 174, 100–105. doi:10.1016/j.envpol.2012.10.025
- Baker, D. R., Barron, L., and Kasprzyk-Hordern, B. (2014). Illicit and pharmaceutical drug consumption estimated via wastewater analysis. Part A: chemical analysis and drug use estimates. *Sci. Total Environ.* 487 (1), 629–641. doi:10.1016/j.scitotenv.2013.11.107
- Bannwarth, A., Morelato, M., Benaglia, L., Been, F., Esseiva, P., Delemont, O., et al. (2019). The use of wastewater analysis in forensic intelligence: drug consumption comparison between Sydney and different European cities. *Forensic Sci. Res.* 4 (2), 141–151. doi:10.1080/20961790.2018.1500082
- Banta-Green, C. J., Brewer, C. J., Ort, C., Helsel, D. R., Williams, J. R., and Field, J. A. (2016). Using wastewater-based epidemiology to estimate drug consumption-Statistical analyses and data presentation. *Sci. Total Environ.* 568, 856–863. doi:10.1016/j.scitotenv.2016.06.052
- Bartelt-Hunt, S. L., Snow, D. D., Damon, T., Shockley, J., and Hoagland, K. (2009). The occurrence of illicit and therapeutic pharmaceuticals in wastewater effluent and surface waters in Nebraska. *Environ. Pollut.* 157 (3), 786–791. doi:10.1016/j.envpol.2008.11.025
- Baselt, R. C. (2000). “Disposition of toxic drugs and chemicals in man,” in *Chemical toxicology institute vol. 1*. Editors Randall C. Baselt. 5th Edn. Foster City, California: Chemical Toxicology Institute.
- Baz-Lomba, J. A., Harman, C., Reid, M., and Thomas, K. V. (2017). Passive sampling of wastewater as a tool for the long-term monitoring of community exposure: illicit and prescription drug trends as a proof of concept. *Water Res.* 121, 221–230. doi:10.1016/j.watres.2017.05.041
- Baz-Lomba, J. A., Salvatore, S., Gracia-Lor, E., Bade, R., Castiglioni, S., Castrignanò, E., et al. (2016). Comparison of pharmaceutical, illicit drug, alcohol, nicotine and caffeine levels in wastewater with sale, seizure and consumption data for 8 European cities. *BMC Public Health* 16 (1), 1035. doi:10.1186/s12889-016-3686-5
- Benaglia, L., Udrisard, R., Bannwarth, A., Gibson, A., Béen, F., Lai, F. Y., et al. (2020). Testing wastewater from a music festival in Switzerland to assess illicit drug use. *Forensic Sci. Int.* 309, 1–8. doi:10.1016/j.forsciint.2020.110148
- Bishop, N., Jones-Lepp, T., Margetts, M., Sykes, J., Alvarez, D., and Keil, D. E. (2020). Wastewater-based epidemiology pilot study to examine drug use in the Western United States. *Sci. Total Environ.* 745, 140697. doi:10.1016/j.scitotenv.2020.140697
- Boleda, M. A., Galceran, M. A., and Ventura, F. (2009). Monitoring of opiates, cannabinoids and their metabolites in wastewater, surface water and finished water in Catalonia, Spain. *Water Res.* 43 (4), 1126–1136. doi:10.1016/j.watres.2008.11.056
- Burgard, D. A., Williams, J., Westerman, D., Rushing, R., Carpenter, R., LaRock, A., et al. (2019). Using wastewater-based analysis to monitor the effects of legalized retail sales on cannabis consumption in Washington State, USA. *Addict. Res. Rep.* 114, 1582–1590. doi:10.1111/add.14641
- Castiglioni, S., Bagnati, R., Melis, M., Panawennage, D., Chiarelli, P., Fanelli, R., et al. (2011). Identification of cocaine and its metabolites in urban wastewater and comparison with the human excretion profile in urine. *Water Res.* 45(16), 5141–5150. doi:10.1016/j.watres.2011.07.017
- Castiglioni, S., Zuccato, E., Crisci, E., Chiabrando, C., Fanelli, R., and Bagnati, R. (2006). Identification and measurement of illicit drugs and their metabolites in urban wastewater by liquid chromatography-tandem mass spectrometry. *Anal. Chem.* 78 (24), 8421–8429. doi:10.1021/ac061095b
- Castiglioni, S., Bijlsma, L., Covaci, A., Emke, E., Hernández, F., Reid, M., et al. (2013). Evaluation of uncertainties associated with the determination of community drug use through the measurement of sewage drug biomarkers. *Environ. Sci. Technol.* 47 (3), 1452–1460. doi:10.1021/es302722f
- Castiglioni, S., Thomas, K. V., Kasprzyk-Hordern, B., Vandam, L., and Griffiths, P. (2014). Testing wastewater to detect illicit drugs: state of the art, potential and research needs. *Sci. Total Environ.* 487 (1), 613–620. doi:10.1016/j.scitotenv.2013.10.034
- Causanilles, A., Ruepert, C., Ibáñez, M., Emke, E., Hernández, F., and de Voogt, P. (2017). Occurrence and fate of illicit drugs and pharmaceuticals in wastewater from two wastewater treatment plants in Costa Rica. *Sci. Total Environ.* 599–600, 98–107. doi:10.1016/j.scitotenv.2017.04.202
- Criquet, J., Dumoulin, D., Howsam, M., Mondamert, L., Goossens, J. F., Prygiel, J., et al. (2017). Comparison of POCIS passive samplers vs. composite water sampling: a case study. *Sci. Total Environ.* 609, 982–991. doi:10.1016/j.scitotenv.2017.07.227
- Daglioglu, N., Guzel, E. Y., and Kilercioglu, S. (2019). Assessment of illicit drugs in wastewater and estimation of drugs of abuse in Adana Province, Turkey. *Forensic Sci. Int.* 294, 132–139. doi:10.1016/j.forsciint.2018.11.012
- Daughton, C. G. (2001). Illicit drugs in municipal sewage: proposed new noninvasive tool to heighten public awareness of societal use of illicit-abused drugs and their potential for ecological consequences. Available at: <http://www.scopus.com/inward/record.url?eid=s2.0-0041903551&partnerID=MN8TOARS> (Accessed April 23, 2020).

## FUNDING

RH is recipient of an academic scholarship from the Coordenação de Aperfeiçoamento de Pessoal de Nível Superior (CAPES), Ministry of Education, Brazil. RL is recipient of a research scholarship from the National Council for Scientific and Technological Development in Brazil (CNPq). This research was supported by the National Institute of Science and Technology in Forensic Sciences (MCTI/CNPQ/CAPES/FAPS 16/2014–INCT program, CNPQ 465450/2014-8). This work was also part of another project financially supported by CNPq (427723/2018-3).



- Daughton, C. G. (2012). Real-time estimation of small-area populations with human biomarkers in sewage. *Sci. Total Environ.* 414, 6–21. doi:10.1016/j.scitotenv.2011.11.015
- Devault, D. A., Lévi, Y., and Karolak, S. (2017a). Applying sewage epidemiology approach to estimate illicit drug consumption in a tropical context: bias related to sewage temperature and pH. *Sci. Total Environ.* 584–585, 252–258. doi:10.1016/j.scitotenv.2017.01.114
- Devault, D. A., Néfau, T., Levi, Y., and Karolak, S. (2017b). The removal of illicit drugs and morphine in two waste water treatment plants (WWTPs) under tropical conditions. *Environ. Sci. Pollut. Res. Int.* 24 (33), 25645–25655. doi:10.1007/s11356-015-6032-z
- Devault, D. A., Néfau, T., Pascaline, H., Karolak, S., and Levi, Y. (2014). First evaluation of illicit and licit drug consumption based on wastewater analysis in Fort de France urban area (Martinique, Caribbean), a transit area for drug smuggling. *Sci. Total Environ.* 490, 970–978. doi:10.1016/j.scitotenv.2014.05.090
- Di Carro, M., Bono, L., and Magi, E. (2014). A simple recirculating flow system for the calibration of polar organic chemical integrative samplers (POCIS): effect of flow rate on different water pollutants. *Talanta* 120, 30–33. doi:10.1016/j.talanta.2013.11.088
- Djomte, V. T., Taylor, R. B., Chen, S., Booij, K., and Chambliss, C. K. (2018). Effects of hydrodynamic conditions and temperature on polar organic chemical integrative sampling rates. *Environ. Toxicol. Chem.* 37 (9), 2331–2339. doi:10.1002/etc.4225
- Du, P., Thai, P. K., Bai, Y., Zhou, Z., Xu, Z., Zhang, X., et al. (2019). Monitoring consumption of methadone and heroin in major Chinese cities by wastewater-based epidemiology. *Drug Alcohol Depend.* 205, 107532. doi:10.1016/j.drugalcdep.2019.06.034
- Du, P., Zheng, Q., Thomas, K. V., Li, X., and Thai, P. K. (2020). A revised excretion factor for estimating ketamine consumption by wastewater-based epidemiology - utilising wastewater and seizure data. *Environ. Int.* 138, 105645. doi:10.1016/j.envint.2020.105645
- EMCDDA and Europol (2019). EU Drug Markets Report 2019. Luxembourg: . Publications Office of the European Union, 2019 (Accessed May 15, 2020).
- EMCDDA (2016). Assessing illicit drugs in wastewater: advances in wastewater-based drug epidemiology, insights 22. Luxembourg: . Publications Office of the European Union, 2016 (Accessed May 15, 2020).
- EMCDDA (2019). European drug report 2019: trends and developments. Luxembourg: . Publications Office of the European Union, 2019 (Accessed May 15, 2020).
- EMCDDA (2020). Wastewater analysis and drugs: a European multi-city study. Luxembourg: . Publications Office of the European Union, 2020 (Accessed May 15, 2020).
- Emke, E., Evans, S., Kasprzyk-Hordern, B., and de Voigt, P. (2014). Enantiomer profiling of high loads of amphetamine and MDMA in communal sewage: a Dutch perspective. *Sci. Total Environ.* 487 (1), 666–672. doi:10.1016/j.scitotenv.2013.11.043
- Fallati, L., Castiglioni, S., Galli, P., Riva, F., Gracia-Lor, E., González-Mariño, I., et al. (2020). Use of legal and illegal substances in Malé (Republic of Maldives) assessed by wastewater analysis. *Sci. Total Environ.* 698, 134207. doi:10.1016/j.scitotenv.2019.134207
- Fedorova, G., Randak, T., Golovko, O., Kodes, V., Grabicova, K., and Grabic, R. (2014). A passive sampling method for detecting analgesics, psycholeptics, antidepressants and illicit drugs in aquatic environments in the Czech Republic. *Sci. Total Environ.* 487 (1), 681–687. doi:10.1016/j.scitotenv.2013.12.091
- Feitosa, R. S., Sodr , F. F., and Maldaner, A. O. (2013). Drogas de abuso em  guas naturais e residu rias urbanas: ocorr ncia, determina  o e aplica  es forenses. *Quim. Nova* 36 (2), 291–305. doi:10.1590/S0100-40422013000200016
- Foppe, K. S., Hammond-Weinberger, D. R., and Subedi, B. (2018). Estimation of the consumption of illicit drugs during special events in two communities in Western Kentucky, USA using sewage epidemiology. *Sci. Total Environ.* 633, 249–256. doi:10.1016/j.scitotenv.2018.03.175
- Gao, J., Li, J., Jiang, G., Yuan, Z., Eaglesham, G., Covaci, A., et al. (2018). Stability of alcohol and tobacco consumption biomarkers in a real rising main sewer. *Water Res.* 138, 19–26. doi:10.1016/j.watres.2018.03.036
- Gogoi, A., Mazumder, P., Tyagi, V. K., Tushara Chaminda, G. G., An, A. K., and Kumar, M. (2018). Occurrence and fate of emerging contaminants in water environment: a review. *Groundw. Sustain. Dev.* 6, 169–180. doi:10.1016/j.gsd.2017.12.009
- Gracia-Lor, E., Zuccato, E., and Castiglioni, S. (2016). Refining correction factors for back-calculation of illicit drug use. *Sci. Total Environ.* 573, 1648–1659. doi:10.1016/j.scitotenv.2016.09.179
- Gracia-Lor, E., Castiglioni, S., Bade, R., Been, F., Castrignan , E., Covaci, A., et al. (2017a). Measuring biomarkers in wastewater as a new source of epidemiological information: current state and future perspectives. *Environ. Int.* 99, 131–150. doi:10.1016/j.envint.2016.12.016
- Gracia-Lor, E., Rousis, N. I., Zuccato, E., Bade, R., Baz-Lomba, J. A., Castrignan , E., et al. (2017b). Estimation of caffeine intake from analysis of caffeine metabolites in wastewater. *Sci. Total Environ.* 609, 1582–1588. doi:10.1016/j.scitotenv.2017.07.258
- Guibal, R., Lissalde, S., and Guibaud, G. (2020). Experimental estimation of 44 pharmaceutical polar organic chemical integrative sampler sampling rates in an artificial river under various flow conditions. *Environ. Toxicol. Chem.* 39 (6), 1186–1195. doi:10.1002/etc.4717
- Guo, C., Zhang, T., Hou, S., Lv, J., Zhang, Y., Wu, F., et al. (2017). Investigation and application of a new passive sampling technique for *in situ* monitoring of illicit drugs in waste waters and rivers. *Environ. Sci. Technol.* 51 (16), 9101–9108. doi:10.1021/acs.est.7b00731
- Harman, C., Allan, I. J., and Vermeirssen, E. L. (2012). Calibration and use of the polar organic chemical integrative sampler—a critical review. *Environ. Toxicol. Chem.* 31 (12), 2724–2738. doi:10.1002/etc.2011
- Harman, C., Boyum, O., Thomas, K. V., and Grung, M. (2009). Small but different effect of fouling on the uptake rates of semipermeable membrane devices and polar organic chemical integrative samplers. *Environ. Toxicol. Chem.* 28 (11), 2324–2332. doi:10.1897/09-090.1
- Harman, C., Reid, M., and Thomas, K. V. (2011). *In situ* calibration of a passive sampling device for selected illicit drugs and their metabolites in wastewater, and subsequent year-long assessment of community drug usage. *Environ. Sci. Technol.* 45 (13), 5676–5682. doi:10.1021/es201124j
- Harris, D. S., Everhart, E. T., Mendelson, J., and Jones, R. T. (2003). The pharmacology of cocaethylene in humans following cocaine and ethanol administration. *Drug Alcohol Depend.* 72 (2), 169–182. doi:10.1016/S0376-8716(03)00200-X
- Hern ndez, F., Castiglioni, S., Covaci, A., de Voigt, P., Emke, E., Kasprzyk-Hordern, B., et al. (2018). Mass spectrometric strategies for the investigation of biomarkers of illicit drug use in wastewater. *Mass Spectrom. Rev.* 37 (3), 258–280. doi:10.1002/mas.21525
- Huestis, M. A., Mitchell, J. M., and Cone, E. J. (1996). Urinary excretion profiles of 11-nor-9-carboxy- elta 9-tetrahydrocannabinol in humans after single smoked doses of marijuana. *J. Anal. Toxicol.* 20 (6), 441–452. doi:10.1093/jat/20.6.441
- Jacquet, R., Mi ge, C., Bados, P., Schiavone, S., and Coquery, M. (2012). Evaluating the polar organic chemical integrative sampler for the monitoring of beta-blockers and hormones in wastewater treatment plant effluents and receiving surface waters. *Environ. Toxicol. Chem.* 31 (2), 279–288. doi:10.1002/etc.737
- Kankaanp  , A., Ariniemi, K., Heinonen, M., Kuoppasalmi, K., and Gunnar, T. (2016). Current trends in Finnish drug abuse: wastewater based epidemiology combined with other national indicators. *Sci. Total Environ.* 568, 864–874. doi:10.1016/j.scitotenv.2016.06.060
- Kaserzon, S. L., Hawker, D. W., Kennedy, K., Bartkow, M., Carter, S., Booij, K., et al. (2014). Characterisation and comparison of the uptake of ionizable and polar pesticides, pharmaceuticals and personal care products by POCIS and Chemcatchers. *Environ. Sci. Process. Impacts* 16 (11), 2517–2526. doi:10.1039/c4em00392f
- Kasprzyk-Hordern, B., and Baker, D. R. (2012). Estimation of community-wide drugs use via stereoselective profiling of sewage. *Sci. Total Environ.* 423, 142–150. doi:10.1016/j.scitotenv.2012.02.019
- Krizman-Matasic, I., Senta, I., Kostanjevecki, P., Ahel, M., and Terzic, S. (2019). Long-term monitoring of drug consumption patterns in a large-sized European city using wastewater-based epidemiology: comparison of two sampling schemes for the assessment of multiannual trends. *Sci. Total Environ.* 647, 474–485. doi:10.1016/j.scitotenv.2018.07.441
- Lai, F. Y., Ort, C., Gartner, C., Carter, S., Prichard, J., Kirkbride, P., et al. (2011). Refining the estimation of illicit drug consumptions from wastewater analysis: Co-analysis of prescription pharmaceuticals and uncertainty assessment. *Water Res.* 45, 4437–4448. doi:10.1016/j.watres.2011.05.042
- Lai, F. Y., Bruno, R., Leung, H. W., Thai, P. K., Ort, C., Carter, S., et al. (2013). Estimating daily and diurnal variations of illicit drug use in Hong Kong: a pilot

- study of using wastewater analysis in an Asian metropolitan city. *Forensic Sci. Int.* 233, 126–132. doi:10.1016/j.forsciint.2013.09.003
- Li, H., Helm, P. A., and Metcalfe, C. D. (2010). Sampling in the great lakes for pharmaceuticals, personal care products, and endocrine-disrupting substances using the passive polar organic chemical integrative sampler. *Environ. Toxicol. Chem.* 29 (4), 751–762. doi:10.1002/etc.104
- Li, H., Helm, P. A., Paterson, G., and Metcalfe, C. D. (2011). The effects of dissolved organic matter and pH on sampling rates for polar organic chemical integrative samplers (POCIS). *Chemosphere* 83 (3), 271–280. doi:10.1016/j.chemosphere.2010.12.071
- Mackulak, T., Brandeburová, P., Grenčíková, A., Bodík, I., Staňová, A. V., Golovko, O., et al. (2019). Music festivals and drugs: wastewater analysis. *Sci. Total Environ.* 659, 326–334. doi:10.1016/j.scitotenv.2018.12.275
- Mackulak, T., Skubák, J., Grabic, R., Ryba, J., Birošová, L., Fedorova, G., et al. (2014). National study of illicit drug use in Slovakia based on wastewater analysis. *Sci. Total Environ.* 494–495, 158–165. doi:10.1016/j.scitotenv.2014.06.089
- Magi, E., Di Carro, M., Mirasole, C., and Benedetti, B. (2018). Combining passive sampling and tandem mass spectrometry for the determination of pharmaceuticals and other emerging pollutants in drinking water. *Microchem. J.* 136, 56–60. doi:10.1016/j.microc.2016.10.029
- Maldaner, A. O., Schmidt, L. L., Locatelli, M. A. F., Jardim, W. F., Sodré, F. F., Almeida, F. V., et al. (2012). Estimating cocaine consumption in the Brazilian federal district (FD) by sewage analysis. *J. Braz. Chem. Soc.* 23 (5), 861–867. doi:10.1590/S0103-50532012000500011
- Mardal, M., and Meyer, M. R. (2014). Studies on the microbial biotransformation of the novel psychoactive substance methylenedioxypyrovalerone (MDPV) in wastewater by means of liquid chromatography-high resolution mass spectrometry/mass spectrometry. *Sci. Total Environ.* 493, 588–595. doi:10.1016/j.scitotenv.2014.06.016
- McCall, A. K., Bade, R., Kinyua, J., Lai, F. Y., Thai, P. K., Covaci, A., et al. (2016). Critical review on the stability of illicit drugs in sewers and wastewater samples. *Water Res.* 88, 933–947. doi:10.1016/j.watres.2015.10.040
- McKay, S., Tschärke, B., Hawker, D., Thompson, K., O'Brien, J., Mueller, J. F., et al. (2020). Calibration and validation of a microporous polyethylene passive sampler for quantitative estimation of illicit drug and pharmaceutical and personal care product (PPCP) concentrations in wastewater influent. *Sci. Total Environ.* 704, 135891. doi:10.1016/j.scitotenv.2019.135891
- Mercan, S., Kuloglu, M., Tekin, T., Turkmen, Z., Dogru, A. O., Safran, A. N., et al. (2019). Wastewater-based monitoring of illicit drug consumption in Istanbul: preliminary results from two districts. *Sci. Total Environ.* 656, 231–238. doi:10.1016/j.scitotenv.2018.11.345
- Metcalfe, C., Tindale, K., Li, H., Rodayan, A., and Yargeau, V. (2010). Illicit drugs in Canadian municipal wastewater and estimates of community drug use. *Environ. Pollut.* 158 (10), 3179–3185. doi:10.1016/j.envpol.2010.07.002
- Metcalfe, C. D., Beddows, P. A., Bouchot, G. G., Metcalfe, T. L., Li, H., and Van Lavieren, H. (2011). Contaminants in the coastal karst aquifer system along the Caribbean coast of the Yucatan Peninsula, Mexico. *Environ. Pollut.* 159 (4), 991–997. doi:10.1016/j.envpol.2010.11.031
- Miller, T. H., Baz-Lomba, J. A., Harman, C., Reid, M. J., Owen, S. F., Bury, N. R., et al. (2016). The first attempt at non-linear in silico prediction of sampling rates for polar organic chemical integrative samplers (POCIS). *Environ. Sci. Technol.* 50 (15), 7973–7981. doi:10.1021/acs.est.6b01407
- Morin, N., Miège, C., Coquery, M., and Randon, J. (2012). Chemical calibration, performance, validation and applications of the polar organic chemical integrative sampler (POCIS) in aquatic environments. *Trac - Trends Anal. Chem.* 36, 144–175. doi:10.1016/j.trac.2012.01.007
- Morin, N., Camilleri, J., Cren-Olivé, C., Coquery, M., and Miège, C. (2013). Determination of uptake kinetics and sampling rates for 56 organic micropollutants using “pharmaceutical” POCIS. *Talanta* 109, 61–73. doi:10.1016/j.talanta.2013.01.058
- O'Brien, J. W., Thai, P. K., Eaglesham, G., Ort, C., Scheidegger, A., Carter, S., et al. (2014). A model to estimate the population contributing to the wastewater using samples collected on census day. *Environ. Sci. Technol.* 48 (1), 517–525. doi:10.1021/es403251g
- Ort, C., Lawrence, M. G., Reungtoot, J., and Mueller, J. F. (2010). Sampling for PPCPs in wastewater systems: comparison of different sampling modes and optimization strategies. *Environ. Sci. Technol.* 44 (16), 6289–6296. doi:10.1021/es100778d
- Ort, C., Eppler, J. M., Scheidegger, A., Rieckermann, J., Kinzig, M., and Sörgel, F. (2014a). Challenges of surveying wastewater drug loads of small populations and generalizable aspects on optimizing monitoring design. *Addiction* 109 (3), 472–481. doi:10.1111/add.12405
- Ort, C., van Nuijs, A. L., Berset, J. D., Bijlsma, L., Castiglioni, S., Covaci, A., et al. (2014b). Spatial differences and temporal changes in illicit drug use in Europe quantified by wastewater analysis. *Addiction* 109 (8), 1338–1352. doi:10.1111/add.12570
- Ort, C. (2014). Quality assurance/quality control in wastewater sampling. *Qual. Assur. Qual. Control. Environ. F. Samples* 146–168. doi:10.4155/EBO.13.476
- Pal, R., Megharaj, M., Kirkbride, K. P., and Naidu, R. (2013). Illicit drugs and the environment—a review. *Sci. Total Environ.* 463–464, 1079–1092. doi:10.1016/j.scitotenv.2012.05.086
- Plósz, B. G., Reid, M. J., Borup, M., Langford, K. H., and Thomas, K. V. (2013). Biotransformation kinetics and sorption of cocaine and its metabolites and the factors influencing their estimation in wastewater. *Water Res.* 47 (7), 2129–2140. doi:10.1016/j.watres.2012.12.034
- Postigo, C., López de Alda, M. J., and Barceló, D. (2010). Drugs of abuse and their metabolites in the Ebro River basin: occurrence in sewage and surface water, sewage treatment plants removal efficiency, and collective drug usage estimation. *Environ. Int.* 36 (1), 75–84. doi:10.1016/j.envint.2009.10.004
- Postigo, C., de Alda, M. L., and Barceló, D. (2011). Evaluation of drugs of abuse use and trends in a prison through wastewater analysis. *Environ. Int.* 37 (1), 49–55. doi:10.1016/j.envint.2010.06.012
- Rico, M., Andrés-Costa, M. J., and Picó, Y. (2017). Estimating population size in wastewater-based epidemiology. Valencia metropolitan area as a case study. *J. Hazard. Mater.* 323, 156–165. doi:10.1016/j.jhazmat.2016.05.079
- Rodayan, A., Afana, S., Segura, P. A., Sultana, T., Metcalfe, C. D., and Yargeau, V. (2016). Linking drugs of abuse in wastewater to contamination of surface and drinking water. *Environ. Toxicol. Chem.* 35 (4), 843–849. doi:10.1002/etc.3085
- Rosen, G., Lotufo, G. R., George, R. D., Wild, B., Rabalais, L. K., Morrison, S., et al. (2018). Field validation of POCIS for monitoring at underwater munitions sites. *Environ. Toxicol. Chem.* 37 (8), 2257–2267. doi:10.1002/etc.4159
- Senta, I., Gracia-Lor, E., Borsotti, A., Zuccato, E., and Castiglioni, S. (2015). Wastewater analysis to monitor use of caffeine and nicotine and evaluation of their metabolites as biomarkers for population size assessment. *Water Res.* 74, 23–33. doi:10.1016/j.watres.2015.02.002
- Thomas, K. V., Bijlsma, L., Castiglioni, S., Covaci, A., Emke, E., Grabic, R., et al. (2012). Comparing illicit drug use in 19 European cities through sewage analysis. *Sci. Total Environ.* 432, 432–439. doi:10.1016/j.scitotenv.2012.06.069
- Thomas, K. V., Amador, A., Baz-Lomba, J. A., and Reid, M. (2017). Use of mobile device data to better estimate dynamic population size for wastewater-based epidemiology. *Environ. Sci. Technol.* 51 (19), 11363–11370. doi:10.1021/acs.est.7b02538
- UNODC (2019). World drug report 2019 (United Nations publication, Sales No. E.19.XI.8) (Accessed May 15, 2020).
- van Nuijs, A. L., Pecceu, B., Theunis, L., Dubois, N., Charlier, C., Jorens, P. G., et al. (2009a). Cocaine and metabolites in waste and surface water across Belgium. *Environ. Pollut.* 157 (1), 123–129. doi:10.1016/j.envpol.2008.07.020
- van Nuijs, A. L., Pecceu, B., Theunis, L., Dubois, N., Charlier, C., Jorens, P. G., et al. (2009b). Spatial and temporal variations in the occurrence of cocaine and benzoylecgonine in waste- and surface water from Belgium and removal during wastewater treatment. *Water Res.* 43 (5), 1341–1349. doi:10.1016/j.watres.2008.12.020
- van Nuijs, A. L., Mougél, J. F., Tarcomnicu, I., Bervoets, L., Blust, R., Jorens, P. G., et al. (2011). Sewage epidemiology—a real-time approach to estimate the consumption of illicit drugs in Brussels, Belgium. *Environ. Int.* 37 (3), 612–621. doi:10.1016/j.envint.2010.12.006
- van Wel, J. H., Kinyua, J., van Nuijs, A. L., Salvatore, S., Bramness, J. G., Covaci, A., et al. (2016). A comparison between wastewater-based drug data and an illicit drug use survey in a selected community. *Int. J. Drug Pol.* 34, 20–26. doi:10.1016/j.drugpo.2016.04.003
- Vazquez-Roig, P., Blasco, C., and Picó, Y. (2013). Advances in the analysis of legal and illegal drugs in the aquatic environment. *Trac Trends Anal. Chem.* 50, 65–77. doi:10.1016/j.trac.2013.04.008
- Werschler, T., and Andrew, B. (2019). *Wastewater-based Estimates of cannabis and drug use in Canada: pilot test detailed results*. Ottawa: Stat. Canada, 368.
- Yargeau, V., Taylor, B., Li, H., Rodayan, A., and Metcalfe, C. D. (2014). Analysis of drugs of abuse in wastewater from two Canadian cities. *Sci. Total Environ.* 487, 722–730. doi:10.1016/j.scitotenv.2013.11.094

- Zhang, X., Huang, R., Li, P., Ren, Y., Gao, J., Mueller, J. F., et al. (2019). Temporal profile of illicit drug consumption in Guangzhou, China monitored by wastewater-based epidemiology. *Environ. Sci. Pollut. Res. Int.* 26 (23), 23593–23602. doi:10.1007/s11356-019-05575-3
- Zuccato, E., Chiabrando, C., Castiglioni, S., Bagnati, R., and Fanelli, R. (2008). Estimating community drug abuse by wastewater analysis. *Environ. Health Perspect.* 116 (8), 1027–1032. doi:10.1289/ehp.11022
- Zuccato, E., Chiabrando, C., Castiglioni, S., Calamari, D., Bagnati, R., Schiarea, S., et al. (2005). Cocaine in surface waters: a new evidence-based tool to monitor community drug abuse. *Environ. Health* 4 (14), 14–17. doi:10.1186/1476-069X-4-14

**Conflict of Interest:** The authors declare that the research was conducted in the absence of any commercial or financial relationships that could be considered as a potential conflict of interest.

Copyright © 2021 Hahn, Augusto do Nascimento and Linden. This is an open-access article distributed under the terms of the Creative Commons Attribution License (CC BY). The use, distribution or reproduction in other forums is permitted, provided the original author(s) and the copyright owner(s) are credited and that the original publication in this journal is cited, in accordance with accepted academic practice. No use, distribution or reproduction is permitted which does not comply with these terms.

# Advantages of publishing in Frontiers



## OPEN ACCESS

Articles are free to read for greatest visibility and readership



## FAST PUBLICATION

Around 90 days from submission to decision



## HIGH QUALITY PEER-REVIEW

Rigorous, collaborative, and constructive peer-review



## TRANSPARENT PEER-REVIEW

Editors and reviewers acknowledged by name on published articles

## Frontiers

Avenue du Tribunal-Fédéral 34  
1005 Lausanne | Switzerland

Visit us: [www.frontiersin.org](http://www.frontiersin.org)

Contact us: [frontiersin.org/about/contact](http://frontiersin.org/about/contact)



## REPRODUCIBILITY OF RESEARCH

Support open data and methods to enhance research reproducibility



## DIGITAL PUBLISHING

Articles designed for optimal readership across devices



## FOLLOW US

@frontiersin



## IMPACT METRICS

Advanced article metrics track visibility across digital media



## EXTENSIVE PROMOTION

Marketing and promotion of impactful research



## LOOP RESEARCH NETWORK

Our network increases your article's readership